THERMOLUMINESCENCE AND $^{234}U/^{230}Th$ DATING INVESTIGATIONS OF HELLENIC MATERIALS

Thesis

Submitted by

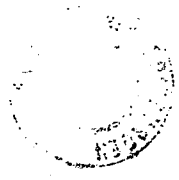
YIANNIS LIRITZIS B.Sc. (Patras)

For the degree of

DOCTOR OF PHILOSOPHY

Department of Physics
University of Edinburgh

JULY 1979



D E C L A R A T I O N

I hereby declare that the work presented in this thesis is my own, unless otherwise stated in the text, and that the thesis has been composed by myself.

P R O L E G O M E N A

"Nature is an artistically working fire, going on its way to create, ..."

STOICS

"..... Thus nothing remains of the Now, nor is there left any part of the present, but what is said to exist now is partly spread over the future and partly over the past."

CHRYSIPPOS

Αφιερωμα Ολοψυχα στους Θαυμαστους, Οντας Μεγαλους Γονεις μου.

Dedicated Heartily to my Wonderful, Indeed Great, Parents.

A C K N O W L E D G E M E N T S

I wish to express my sincere gratitude to:

My supervisors, Dr R B Galloway, for his contributory discussions and his continuous care and attention in the writing of my thesis and Dr H McKerrell, for initiating me in the field of archaeometric studies and for guiding my work by stimulating discussions and suggestions;

Prof. R Rigopoulos (Patras Univ), for his primary initiation, continuous encouragement, care and guidance on the subject of this thesis and for supporting me in various aspects of its completion;

Prof. H Schwarcz (McMaster Univ), for offering the facilities to study the U/Th Method, his critical evaluation of my work and the warmth and hospitality he extended to me during my stay in Canada;

Ada Dixon (McMaster Univ), who passed on to me the methodology of the U/Th Method with care and sincerity;

Dr. V Mejdahl (Risø), for his illuminating discussions and suggestions on the dosimetric aspects of my thesis and for his irradiation facilities;

Dr R Harmon (SSRC, East Kilbride), for his useful discussions and suggestions particularly on the alternative Thorium extraction method;

Dr A Wintle, for her liberal encouragement and her critical remarks on certain aspects of my work;

Dr J Dixon (Geol. Dept. Edinburgh Univ), for doing the Thin Section Analyses, his valuable comments and his helpful discussions on certain geological aspects;

Mr P Aspen (Geol. Dept. Edinburgh Univ), for doing the X-Ray Diffraction Analyses and his continual readiness to help by means of discussion;

Prof. K Creer (Geophys. Dept. Edinburgh University), for his general guidance and care and for making typing facilities available;

Prof W Cochran (Phys. Dept. Edinburgh Univ), for his helpful discussions on the variation of beta attenuation on grains and clays;

Mr A Murray (Oxford Univ), for his interesting discussions and useful correspondence;

Profs. C Renfrew (Southampton Univ) and G Chourmouziades (Volos Museum), for their invaluable advice on certain related archaeological aspects and also for making samples available;

Prof. N Platon (Athens) and Dr C Davaras (Ag. Nicolaos Museum, Crete), for giving archaeological permission and for helpful correspondence;

Prof A Poulianos (Athens), for providing me with important samples, valuable discussions on the Petralona skull and the interest and encouragement he showed in my subject;

Misses V Adrini and A Moundrea (Volos Museum), for their help in providing me with pottery their hospitality and helpful discussions;

Mrs C Orr (Stud. Accom. Office), for her help in accommodation facilities, and encouragement on difficulties during this thesis;

Mr P Tuffy (Physics Dept Edinburgh Univ) for his help and contribution towards the "artistic"photography;

Dr A Mackenzie (SSRC, East Kilbride), for the Fission Track Analysis;

Dr A Hall, for his great help in Nuclear Instrumentation aspects at the commencement of my thesis;

Mrs C McKerrell, for her help and encouragement on certain aspects of my projects;

Ruth Thomas (Geophys. Dept. Edinburgh Univ), for doing the X-Ray Fluorescence preparation;

Dr J G Fitton (Geol. Dept. Edinburgh Univ), for doing the X-Ray Fluorescence Analyses;

Mrs F Dumpstey (Nat Mus Antiq Scot) and Miss Sandra Mathieson (Edin Univ), for their contributions in administrative problems;

My colleagues, V Lagios (Geophys Dept Edinburgh Univ), for his kind assistance with computing;

Dr S Papamarinopoulos (Athens), Mr G Hennig, (Köln Univ) and Miss U Bangert (Köln Univ) for their helpful discussions on the Petralona fossil debate;

Mr J Stevens, Mr T Ryan, Mr T Montgomery, Mr J Howels, and Mr E Davidson (Phys Dept Edinburgh Univ), for their occassional technical assistance; National Hellenic Research Foundation and Royal Society of London, Schillizi Foundation, Dr D F O Russell (Russell Trust) and the University of Edinburgh Studentship, for their financial support which was most appreciated and valued and without which this thesis would not have been possible;

Last,but not least,I am mostly grateful to Miss Veronica McGeehan for her moral support and invaluable encouragements during the most difficult moments which contributed to the success of this project; and who undertook the monumental task of typing the final manuscript.

S Y N O P S I S

Chronological investigations of certain Hellenic archaeological problems have been undertaken with illuminative results with regard to their implications and possible consequences.

Part I - IV deal with the Thermoluminescence (TL) dating which has been applied to pottery and kiln materials from Neolithic and Bronze age sites. The "quartz inclusion" method was used.

When applied to the famous Minoan palaces, the dates ranged from c1300 yrs BC to c1900 yrs BC. In particular, the palaces of Kato Zakros, Agia Triada and Faistos were dated to 1313±2%, 1558±4% and 1516±6% BC, respectively, which dates are related to the destruction of these palaces by local paroxysmal earthquakes and possible influence of the Santorini volcanic eruption. Further, a coherent sequence in the dating was found for two Neolithic settlements, Dimini and Sesklo, (Thessaly, Greece), which allows the time span in question to be classified into a number of periods starting from the aceramic, c6800 yrs BC, to Late Neolithic, c3000 yrs BC. Analytical techniques suggested a degree of cultural intercommunication during the Late/Middle Neolithic period. Particular emphasis is given to the comparison between TL and C-14 dates for the same sites.

Part V deals with the application of Uranium disequilibrium dating technique to Petralona cave speleothems in order to resolve the age of the controversial skull found there and the question of whether it was Homo Neanderthal or Homo Erectus. Calcitic samples related to the former burial position (the "Mausoleum alcove") of the "Archanthropos Petraloniensis", as well as from various other places in the cave, were

dated. The method was that of Th-230/U-234, based on the principle that the calcium carbonate is deposited initially along with U, free from any Th, radioisotopes.

Due to the detritus state of the carbonates, eg., stalagmites, flowstones, certain methods were applied to correct for Thorium and Uranium detrital activities.

It is concluded that the age of this early fossil is definitely greater than 270,000 yrs BP, which sways opinion that this early hominid belongs to the species Homo Erectus. Due to the inexact knowledge of the original position of the "mysteriously missing" skeleton and that of the skull, suggested time ranges, related to other human artefacts are forwarded. From these, this skull could have existed between 300 - 350,000 yrs BP or c700,000 yrs BP.

CONTENTS

		PAGE
	PART I	
CHAPTER 1	INTRODUCTION TO THERMOLUMINESCENCE	
1.1	Dating Techniques in Archaeology	1
1.2	Thesis Objective	1
1.3	Theory of Thermoluminescence	10
1.4	Electron Traps and Mineral Inclusions of Pottery	10
1.5	Principles of TL Dating of Ceramics	13
1.6	Review of the Development of TL Dating Techniques	14
1.7	Errors Associated with the Inclusion Technique	17
1.8	Why Choose the Inclusion Technique?	19
1.9	Experimental TL Apparatus	21
1.9.1	Vacuum Glow Oven	21
1.9.2	Thermal Radiation	23
1.10	Non-Linear TL Response of Quartz Feldspar Grains: Some Annealing Experiments	24
1.10.2	Natural and Artificial TL Acquisition	26
1.11	Experiment(1): Annealing of Quartz at Different Temperatures	29
1.11.1	Results of Experiment (1)	32
1.12	Experiment(2): Testing the "Additive Procedure"	34
1.13	Experiment(3): Annealing Effects on Intercepts	36
1.13.5	Discussion on Experiment(3)	40
1.14	Correlations Between Annealing Experiments and TL Dated Samples	41
1.15	General Conclusions on the Above Three Experiments	48
1.16	Review of Mechanisms on Supralinearity	48
1.16.1	Some Possible Mechanisms Responsible for the Non-Linear TL Response	49
	PART II	
II.1	Introduction to the Contents	53
II.2	A Brief Outline on Dose Rates: Their Meaning and Significance to TL Dating	53
CHAPTER 2	BETA DOSIMETRY OF CERAMICS	
2.1	Review of Beta Dose Rate Evaluation	56
2.2	Review of Previous TLD Systems	56
2.3	Microdosimetry of Quartz: A New Practical Approach	61
2.4	Experimental Arrangements	61
2.4.1	Procedure of Firing the Clay	61

		PAGE
2.5	Background Reading	62
2.5.1	Read-Out Manner of the Phosphor	62
2.6	Measurement of Beta Dose with Quartz Grains and $CaSO_4$:Mn Phosphor. Experiment(1)	64
2.7	Results and Discussion of Experiment (1)	66
2.8	Fading of 110°C Peak at 0°	71
2.9	Quartz Etching at 0° and at Room Temperature	73
2.10	Fading of 110° Quartz Peak at Room Temperature	74
2.11	Measurement of Beta Dose on Simulated Potsherds. Experiment(2)	78
2.12	Results and Discussion of Experiment(2)	78
2.13	Increased Beta Dose due to Clay Densification	87
2.14	Discussion on Water Uptake Corrections of Solid Rings	91
2.15	Conclusions and Suggestions	92
CHAPTER 3	MEASUREMENT OF BETA DOSE RATE BY MEANS OF ALPHA COUNTING AND POTASSIUM DETERMINATION((α+K) METHOD)	
3.1	Introduction	95
3.2	Radioisotopes Embedded in Ceramics	96
3.3	Description of the Alpha Counting Method	100
3.4	Comparison of "Sealed" Alpha Counts within 24 Hours and after 15 Days	102
3.5	Radon Emanation in Ceramics	104
3.6	Alpha Counter Calibration	112
3.7	Alpha Counter Description	113
3.8	Alpha Counting Results	113
3.9	Potassium Determination	117
CHAPTER 4	ALPHA COUNTING AND GRAIN SIZE DISTRIBUTION	
4.1	Experimental Procedure and Results	120
4.2	Interpretation of the Results	120
4.3	Discussion	127
4.4	Conclusions	128
CHAPTER 5	MEASUREMENT OF BETA DOSE RATE BY TLD	
5.1	Introduction	129
5.2	Measurement of Beta Radiation by $CaSO_4$:Mn	129
5.3	TLD Results	133
5.4	Comparisons of Alpha Counting and TLD Techniques	136
5.5	Discussion on Alpha Counting and $CaSO_4$:Mn Methods	136
5.5.1	Discussion the Problems Associated with the $CaSO_4$:Mn Method	137
5.5.2	Discussion on Problems Associated with (α+K) Method	139
5.6	Tests on Choice of the Most Appropriate Technique	143
5.7	Conclusions	149

		PAGE
CHAPTER 6	VARIATIONS OF BETA DOSE ATTENUATION IN DIFFERENT CLAYS	
6.1	Introduction	150
6.2	Distance Scaling Factor and Its Theory (Some Aspects on β-Interaction with Low Z Materials)	151
6.3	Procedure for Calculating Stopping Powers and Relative Attenuation in Clays	153
6.4	Actual Correction of Beta Dose Rates due to Water Uptake	155
6.5	Discussion of the Results on Relative Attenuation and Stopping Powers of Beta Particles in Clays	155
6.6	Conclusions	164
	P A R T III ENVIRONMENTAL DOSIMETRY	
CHAPTER 7	EVALUATION OF GAMMA DOSE RATES IN ARCHAEOLOGICAL SITES	
7.1	Introduction - Contents	165
7.2	Aim of These Investigations	165
7.3	Review of the Techniques	167
7.4	Physical Aspects of Terrestrial Radiation	171
7.5	Fluctuation and Distribution of Soil Gamma Rays	172
7.5.1	Fluctuation	172
7.5.2	Distribution	174
7.6	NaI Calibration: Experimental Arrangements	177
7.7	About $CaSO_4$:Dy and Lif Phosphors	185
7.8	The Mass-Energy Absorption Coefficient of Mixtures and Compounds	190
7.9	Discussion of the Calibration Curves Obtained	192
7.10	Results: Comparison of Dose Rates with PPM Values	195
7.11	Discussion	195
CHAPTER 8	GAMMA SOIL FLUCTUATIONS DUE TO METEOROLOGICAL FACTORS	
8.1	Introduction	201
8.2	Results	201
8.3	Annual and Monthly Gamma Variations	205
8.4	Threshold Drift	207
8.5	Interpretation of Seasonal Gamma Soil Fluctuations	210
8.6	Conclusions	216
	P A R T IV	
CHAPTER 9	THERMOLUMINESCENCE DATING RESULTS AND DISCUSSION	
9.1	Introduction	217
9.2	Sample Preparation	218
9.3	Glow Curves from Pottery	219

		PAGE
9.3.1	Glow Curve Shapes	219
9.3.2	Classification of Glow Curves	222
9.4	Thermoluminescence Measurements	223
9.4.1	Measurement of First Radiation Sensitivity	223
9.4.2	Measurement of Second Radiation Sensitivity	224
9.5	Aspects of Pre-Dose and Sensitivity Effects	225
9.6	Water Uptake Values	229
9.7	Beta Dose Values	235
9.8	Evaluation of Gamma Dose Rates	240
9.9	Fading and Spurious TL Checks	243
9.10	Plateau Tests	243
9.11	C-14 Dating and Calibration	246
9.12	Thermoluminescence and C-14	251
9.13	Results and Discussions	251
	TL Dating Programmes and their Archaeological Interpretation	
9.13.1	Glozel	251
9.13.2	Phallus Object	254
9.14	Crete in Bronze Age	254
9.14.1	Description of a Typical Kiln	256
9.14.2	Up-to-date Archaeological Evidence of Minoan Chronology and their Correlation with Thermoluminescence Dates	258
9.14.3	Conclusions	262
9.15	Aegean Neolithic Settlements	262
9.15.1	Sesklo and Dimini	262
9.16	Comparison of TL and C-14 Dates for the Sesklo and Dimini Neolithic Settlements	266
9.17	Sitagroi Neolithic Site	270
9.18	Conclusions	272
	Intended Future Work	273
CHAPTER 10	APPLICATION OF ANALYTICAL TECHNIQUES TO SESKLO AND DIMINI	
10.1	Neutron Activation Analysis, X-Ray Fluorescence and Thin Section Analysis on Artefacts from Sesklo-Dimini Neolithic Settlements	274
10.2	Some Introductory Aspects Concerning NAA	274
10.3	Archaeology of the Context	276
10.4	NAA Procedure	277
10.4.1	Results and Discussion	279
10.5	X-Ray Fluorescence Analysis	286
10.6	Thin Section Analysis	286
10.6.1	Differences and Similarities	288
10.7	Conclusions	293

		PAGE
	PART V URANIUM/THORIUM SPELEOCHRONOLOGY (Nuclear Instrumentation, Chemical Procedures and Dating Method)	295
CHAPTER 11	NUCLEAR INSTRUMENTATION AND CHEMICAL PROCEDURES OF U/TH DATING METHOD	
11.1	Speleothem Deposits - Description and Mechanisms	296
11.2	Geochemistry of Uranium/Thorium	299
11.3	Th-230/U-234 Dating Method	302
11.4	Suitability of a Speleothem of Archaeological Significance for Dating Purposes	303
11.5	Epilogue	307
11.6	α Spectrometer	307
11.7	Counter Calibration and Spectral Resolution	310
11.7.1	Alpha Spectra	312
11.8	Spike Activity Ratio	312
11.9	Measurement of Uranium Concentration	313
11.10	Detector Calibration and Yield Determination	316
11.11	Determination of Constants	317
11.12	Alternative Measurement of Uranium Concentrations	318
11.13	Errors	318
11.14	Determination of Approximate Ages Greater Than 350,000 years	320
11.15	Th-230/U-234 Age Programme	320
11.16	Radiochemical Procedure	322
11.16.1	Interiors of Carbonates	322
11.16.2	U/Th Isotopic Analysis	323
11.17	Chemical Procedure for Extraction of Uranium and Thorium	324
CHAPTER 12	U/TH DATING OF PETRALONA CAVE	
12.1	Archaeological Context of the Cave	329
12.2	Sample Provenance	332
12.3	An Appraisal of Former Dating Results	335
12.4	Corrections Applied in the Case of Detrital Speleothems: A Reappraisal of the Two-Component Mode	340
12.4.1	Determination of Thorium and Uranium in Petralona Cave Sediments	341
12.4.2	Some Aspects on Leaching Studies	343
12.4.3	Discussion of the Radiochemical Analysis of Clays	344
12.5	A Reappraisal of the Two-Component Method	350
12.5.1	Some Theoretical and Experimental Considerations	350
12.5.2	Determination of U and Th Detrital Component ((U,Th) Correction Mode)	352
12.5.3	Th-230/Th-232 Decay Scheme (Initial Th only Correction)	354
12.5.4	Total Detrital Th-230 as Inferred from Detrital Th-232	355

		PAGE
12.6	Variations of the Initial Uranium Ratios	355
12.7	Radiometric Data from Petralona Cave	357
12.8	Thin Section Analysis	386
12.9	Fission Track Andlysis	388
12.10	Possible Correlations Between Radiometric Data and Palaeoclimatic Changes	391
12.10.1	From Wilderness to Metropolis in 15,000,000 years: The Unfolding Story of Human Evolution and the Human Conditions (A Resume)	393
12.11	Critical Interpretation of the Age of Archanthropus Petraloniensis	397
12.12	Epilogue	403
	Intended Future Work	404
APPENDIX A	Provinance of the Samples for TL Dating and Neutron Activation Analysis	405
APPENDIX B	Beta Source Calibration	408
APPENDIX C	Statistical Error as Derived from Build-Up Curves - A Typical Example	413
BIBLIOGRAPHY		415

FIGURES

Figure		PAGE
1.1	Hellenic Archaeological Sites	2
1.2	Egypt/Crete/S Greece, Chronological Links	6
1.3	TL Process	11
1.9	TL Apparatus	22
1.9.3	TL Linear Heating Circuit	25
1.10.2	Additive Procedure	27
1.11	Sensitivity Variations Under Different Annealing Procedures	30-31
1.12	Glow Curves of KZ2/5	35
1.12.1	First & Second Build-Up Curves for KZ2/5	35
1.13.1	First & Second Build-Up Curve for KZ2/5 with Simulation dose of 300 rads after Draining out the NTL to 500°C	37
1.13.2	First & Second Build-Up Curves for KZ2/5 with simulation dose of 300 and 600 rads after Heating to 1000°C	37
1.13.5	Glow Curve of Quartz fired at 900°C, 600°C and 1250°C	39
1.13.6	X-Ray Powder Photograph of Quartz annealed at three different Temperatures	43-44
1.14a,b1-7	First & Second Build-Up Curves of some TL Dated Samples	46-47
2.4.1a	Shrinkage of Clay after Firing	63
2.4.1b	Final Size of Solid Ring made by the Fired Clay	63
2.5	Geometrical Situation of Beta Irradiated Quartz and Phosphor inside the Ring	63
2.9	Sand Etched at two Temperatures	75
2.10a,b	TL Signal Decay as a Function of Time at 0° and 18°C	77
2.12	Beta Dose Against Thickness of Powder of Solid Rings	80
2.12.1	Beta Doses against % Deviation from 1cm and 2cm Powder Ring Doses	81
2.11	Schematic Representation of Solid Cylindrical Rings with Phosphors at the Centre	83
2.12.2	Geometrical Arrangement of the Phosphor Inside the Clay Ring	83
3.2.2	Decay Scheme of K-40	99
3.3	Assemblage of the Alpha Cell and PM in Alpha Counting	101
3.7	Alpha Counting System	114
4.1	No of Alphas vs Grain Size of Ground Down Potsherd	121-122
4.1.1	Electron Scanning Microscope Photos	124
4.2	Thin Section Photomicrographs	126

		PAGE
5.6a,b	Beta Dose Rate *vs* K_2O and Th *vs* K, for Geological Materials	144
5.6.1,2	Beta Dose Rate (α+K) *vs* K_2O and Beta Dose Rate (TLD) *vs* K_2O	146
5.6.3	Beta Dose Rates (α+K) *vs* K_2O, data taken from Zimmerman	148
6.2	Illustration of Beta Attenuation through Quartz Grains	161
6.5a,b	Distribution of Radioisotopes inside an Air and Clay Spaced Volume	161
7.5.2	Gamma Ray Soil Distribution to a Scintillation Detector	175
7,6a,b	Gamma Counting Arrangement for one of the Boxes and Detailed Setting of the Quartz Grains and Phosphors inside the Liquid Nitrogen Dewar	180
7.6.1	Automatic Liquid Nitrogen Filler	181
7.6.2	Calibration Curves Obtained by NaI(Tl) Scintillometer	184
7.7.1a,b	Glow Curves of Lif, SiO_2 and $CaSO_4$:Mn,Dy	189
7.8	Variations of Mass Energy Absorption Coefficient of Mixtures and Compounds with Gamma Energy	191
8.1A,B	Lay-out of four Boxes in the Terrain and Counting Geometry for the Scintillometer	202
8.2	Counts/Sec *vs* Mrads/Yr for the Lif Phosphor	204
8.2.1	Typical Gamma Soil Spectrum	206
8.3.1	Average Monthly Gamma Variation over a Period of 8 Months	208-209
8.5.2	Gamma Variation for the Last Fortnight of January due to snow cover	208
8.5..	Gamma Variation *vs* Temperature and Rainfall	211-212
8.5.1	Gamma Variations *vs* Temperature and Rainfall	214-215
9.3.1-5	Glow Curves of TL Dated Samples	220-221
9.4.2	Dose Plateau	226
9.4.3	First & Second Build-Up Curves of some TL Dated Samples	227-228
9.5	Sensitivity Change as Inferred from the Ratio NTL/Q+I *vs* Temperature	230
9.6	Testing of Parallel Slope Criterion by Plotting Ratio of 1st/2nd Build-Up Curves *vs* Temperature	231
9.7	Temperature Changes as Inferred from Oxygen Isotope Variations *vs* Time for the last 10,000 years	234
9.6.1	Distribution of Water Absorption Values for Potsherds and Clays	236
9.7	Variations of Accumulated Beta Dose with Grain Sizes	238
9.10	Plateau Tests for some TL Dated samples	245
9.11	C-14 Changes with Geomagnetic Moment	248

		PAGE
9.13.2-4	Phallus Object. Glow Curve, Plateau Test and Annealings	255
9.14.1	Typical Kiln	257
9.14	Kiln Sample AT7	260
9.15	Comparisons between TL and C-14 Dates	264
10.4	Gamma Counting Arrangement in NAA	278
10.4.1	Clustering Diagram for NAA for Dimini Material	280
10.4.4	Probability Evaluation for Dimini Pottery compared to Sesklo Pottery	283
10.4.2	Probability Evaluation for Sesklo Pottery Compared to Dimini Pottery	283
10.4.3	Clustering Diagram for NAA for Sesklo Material	284
10.4.5	Geological Sketch Map of Sesklo/Dimini	285
10.5	Comparative Columns concerning similarities of Sesklo/Dimini Materials Analysed by XRF	287
10.6.1	Photomicrographs of Thin Section of Potsherds from Sesklo and Dimini	290-292
10.8	Typical Dimini Vase	294
11.1	Schematic Diagram of Deposition of Speleothems in Caves	298
11.3.1	Isochrons of Th-230/U-234 vs(U-234/U-238)$_0$	304
11.6	Alpha Spectrometer for U/Th Dating Method	308
11.6.1	Alpha Particle Energies for U and Th Decay Series	309
11.6.2a,b	Typical Th and U Spectra	311
11.8	Spike Activity Ratio Growing Towards its Equilibrium Value Monitored for one Year	314
11.12	Calibration Curve for Measuring U Concentrations from Counting Rates	319
11.7.1	"Tailing Effect" of the Low Energy Part of an Alpha Particle Peak	319
11.17	Extraction/Purification and Alpha Counting of U and Th from Speleothems	328
12.1	Petralona Cave	330
12.2	Mausoleum Alcove	334
12.3	Excavated Section $A_1 - A_2$	336
12.4	Hypothetical Relation between Age and Position in a Slice of a Typical Stalagmite taken Normal to Growth Axis	338
12.4.2a	KZ2/5 Original Clay XRD Pattern	345
12.4.2b,c	XRD Patterns for KZ2/5 detrital Residue and 5th Layer Clay Sample	346
12.6	Variations of Initial U Ratios with U contents	356
12.7	XRD Patterns for P-12 Detrital Residue and P-13 Detrital Residue	364
12.7.1	Plotting of the Isotope Ratios for the Mausoleum Samples	367
12.7.2	P-13 Travertine Covering a Bone	370
12.7.3	XRD Patterns of P-1A and P6	371

		PAGE
12.7.4	Travertine P-4	373
12.7.5	XRD Patterns for P-3 -2 Detrital Residue and P-7 Carbonate	378
12.7.6	Corrected Ages for Different Initial Th-230/ Th-232 Detrital Ratios for P-ARST and PC-1	379
12.9a,b	Fission Track Photos for P-13 and P-7-3	389
12.10	Oxygen Isotope vs Time, from Ocean Cores for all Pleistocene Epoch	392
12.11	Characteristic Human Tools from Petralona Cave	399
12.11.1	Comparisons between Petralona Skull and Other Skulls	401
B,B1	Glow Curve and Build-Up Curve for the Quartz Used in Calibration of the Source	410
B2	Plotting of TL Signal vs Beta Mins of Radiation	411
C	Family of Curves Illustrating % Scatter of Various TL Readings per Dose against % Final TL Dose Accuracy for several Distributions of the Readings	414

PART I

CHAPTER I

INTRODUCTION TO THERMOLUMINESCENCE

1.1 Dating Techniques in Archaeology

Scientific Studies in contemporary archaeology encompass a wide spectrum of techniques which determine a chronological framework. The development of these techniques and their application contributes to our more precise understanding of the human evolutionary process. Archaeology's primary objectives are to construct and explain the past by interpreting excavational finds and artifacts, for example, pottery, metalwork, tools, architectural relics and human remains.

Apart from describing the history of mankind before literate civilisation occurred, archaeology must explain also the nature, the cause and the timing of historical and prehistorical events.

Science here enters the "scene" with its own unique contribution, towards the decipherment of the mysteries of the past through the application of various scientific dating methods, thus pinpointing in time the profound physical and biological changes on earth.

Whatever material an "archaic artifact" is made of, one senses that a structural feature will "age" either through an intrinsic mechanism or one environmentally controlled. The dating "clocks" commonly used in chronological studies, each one having its own accuracy and application limits on time and material, are summarized in Table (1)

1.2 Thesis Objective

Thermoluminescence (TL), (1.2.1,1.2.2) and Th-230/U-234, (1.2.3) radiometric dating investigations on ancient Hellenic material have been undertaken with the aim of resolving important chronological problems in archaeology.

1.2.1 The sites studied by the TL dating technique were: Crete, in the Bronze Age - c3,000 - c1,000 years BC - (Faistos, Kato Zakros, Agia

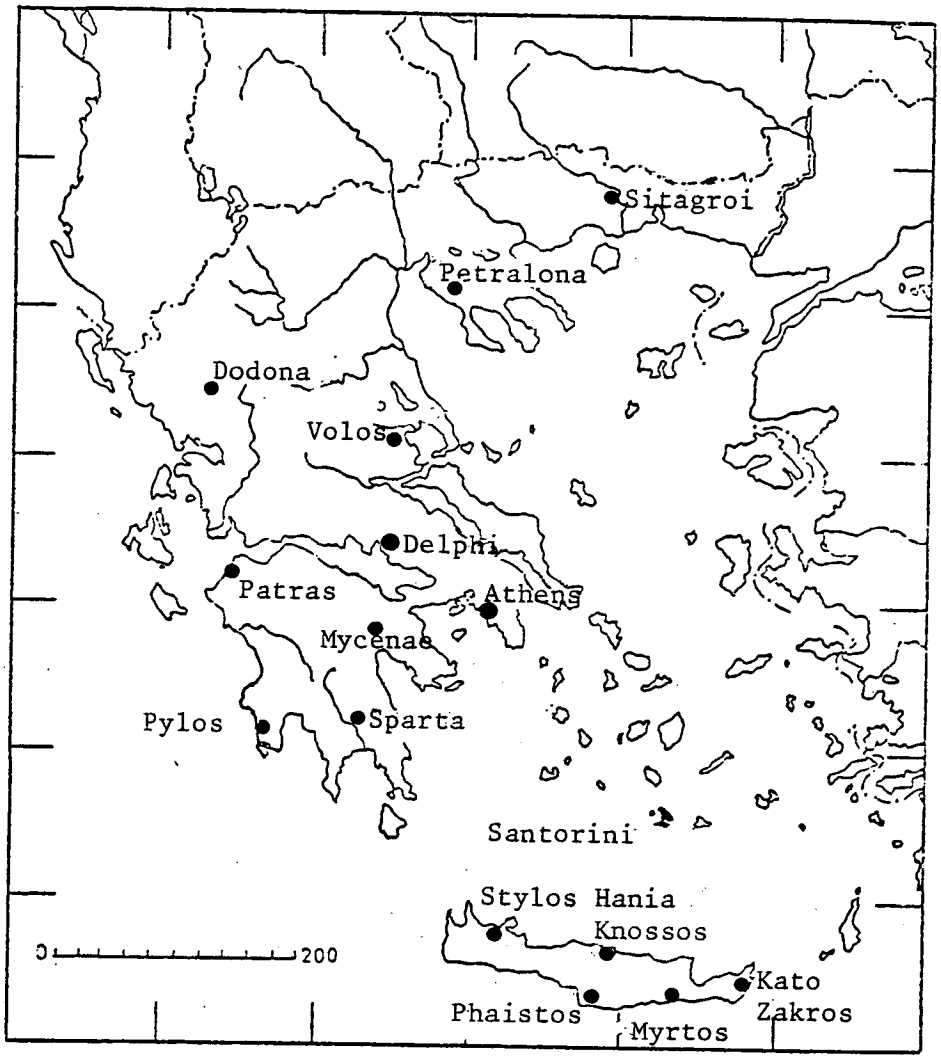


Fig. 1.1 Hellenic Archaeological Sites

TABLE 1

Dating Methods	Material	Time Scale (yrs BP)
Dendrochronology	Trees	0 - app. 6×10^3
Radiocarbon	Wood, crops, trees, calcites.	0 - app. 5×10^4
K-Ar and Ar-40—Ar-39	Pumice, lava, tuff, rocks.	5×10^5-onwards
Th-230 and Pa-231 decay	Calcites, sediments	0 - app. 5×10^5
Thermoluminescence	Pottery, burnt clays and rocks, calcite, flint, sediments	0 - app. 10^6
Fission Track	Glasses, fired materials, obsidian, pumice, zircon, apatite, volcanic materials	app. 10^3-onwards
Obsidian Hydration	Obsidian	0 - app. 2.5×10^4
Archaeomagnetism	Pottery, burnt clays	0 - app. 6×10^3
Paleomagnetism	Lake and oceanic sediments, rocks	0 - onwards
Bone analysis (U,F,N)	Bone	0 - app. 2×10^6
Amino-acid Analysis	Bones, skeletons	0 - app. 5×10^5

Chronological Scale and Material of Application of the Principal Scientific Dating Techniques used in Archaeology

Triada, Stylos Hania, Kalo Horio), and in Thessaly, mainland Greece, in the Neolithic period - c6,500 - c3,500 years BC - (Sesklo, Dimini.) The material from Crete consisted of kilns. The sites in which the kilns were situated had already been extensively studied by archaeologists and a relative chronology had been established, from cross-dating references,with neighbouring cultures,dominant over wide spheres of influence,in the culminating years of the Bronze Age, as for example Egypt, Mycenae and Anatolia, which had a stable chronology. This method involves relating characteristic archaeological "finds" (primarily pottery) from a known source with the place in which they were found. This highlights the cultural and economic relations. Egyptian finds were discovered in the palaces of Faistos, Mallia, Kato Zakros and Akrotiri (on Santorini). For example, pictures of Keftiu (ancient Crete) processions are found in the tombs of the Eighteenth Dynasty (1580 - 1350 BC). Thutmosis III, whose name is recorded on an alabaster vase from a tomb in the port of Knossos, reigned between 1500 and 1450 yrs BC. But the decisive factor for the archaeological interpretation is the presence of Minoan post-palacial vases (c1450 - c1100 yrs BC), in Tell Amarna, that is, in a site associated with Ikhaton, whose reign begun in 1364 BC. Thus the end of the Minoan palaces (post-palacial period), must be dated before 1364 BC. Likewise, the Linear B script in use in Knossos 1450 - 1400 BC is recorded in the Mycenean palaces of Greece, for example Pylos, between 1400 and 1200 BC. The tablets on which the script is inscribed are flat slabs of clay.

Another important fact related to the Minoan (for Minos was the king of Crete) chronology is the volcanic eruption of Santorini island c1500 BC. Pieces of lava and pumice found at Kato Zakros and other later palaces of Crete strengthens the view (of archaeology's and of

science) that these sites were destroyed by the same volcanic eruption that buried the Minoan site of Akrotiri under ashes. Others believe that they were destroyed by the earthquakes that accompanied the eruption c1450 BC. Apart from the other relative historical chronologies, radiocarbon dating has been applied as well. The results are not precise due to the indecisive correction factors for this period which have to calibrate conventional C-14 dates. For example, the method applied to Minoan sites puts the destruction of the palace of Knossos as closer to 1200 BC than to the 1450 BC date accepted by Minoan archaeologists. Similar problems are demonstrated in the series of C-14 dates from Pylos (Palace of Nestor), the palace destruction dating to late LH IIIB with a conventional C-14 date average of 1105 BC (see Fig.1.2). This could adjust to about 1280 BC using the historical curve correction which is just about acceptable for late LH IIIB. However, the palace construction timbers for mid-LH IIIB, with conventional C-14 dates as old as 1500 BC, are impossible to reconcile with Aegean chronology. This situation is, however, understandable when one appreciates that these massive timbers are in fact square beams which could well derive from the heart wood of trees centuries older than theperiod in which they were actually used. In general, C-14 dates give lower ages than for the historical dates, for example, for Egypt by about 600 yrs for C-14 dates ranged from c2500 to 2100 BC and 300 - 400 yrs from c1600 to c1100 yrs BC. Especially in Myrtos palace (Crete), several of the C-14 dates have been made which refer to the destruction levels of the palace site and date archaeologically to the end of the Early Minoan II B. A date range of 2400 - 2170 yrs BC is accepted for the Myrtos dates after tree-ring correction which agrees well with the relevant sherd dates. Considering the above situation the TL method offers a useful alternative

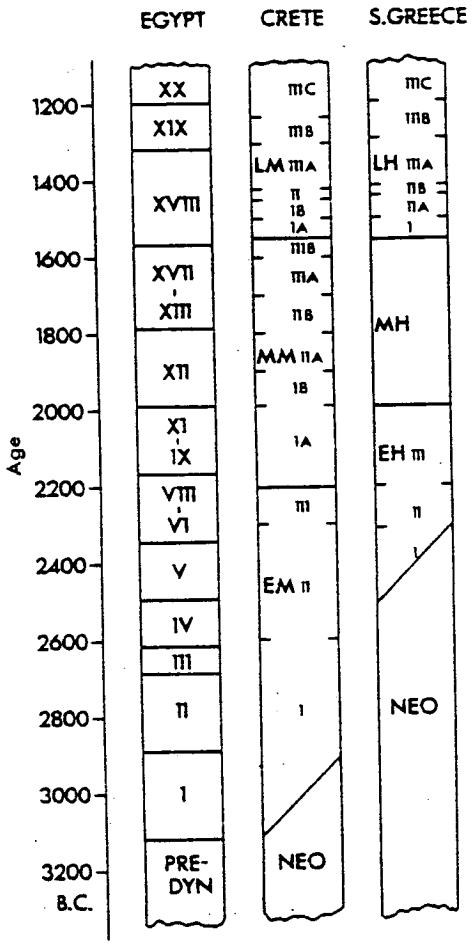


Fig. 1.2 Stylistic and Chronological Links between Egypt, Crete and Southern Greece, during Second and Third Millenium BC, Hayes (1970)

way of establishing a more certain basis for any attempt at Minoan chronology. These dates were also used in the archaeo-magnetic studies on the same materials in order to establish the ancient geomagnetic field variation curve for this period in the eastern Mediterranean region. The TL dates and their archaeological signifance are discussed in Chapter 10.

1.2.2 The materials for Thessaly were potsherds and well-fired clays for different excavational levels of the two Neolithic settlements, namely, Sesklo and Dimini. Sesklo's Acropolis-like structure is situated on the top of two hills with surrounding houses and settlements. A number of trenches have revealed depositional layers of different cultural phases covering the period from the 6th - 3rd millenia BC, Theoharis (1973), Renfrew (1973), Pigott (1965). Figurines and other sophisticated wares are the most important findings. The C-14 dates on some wooden samples from the site give ages of c5000 BC. When correction - based on the tree rings - is applied, these ages increase by about 900 yrs. This great correction factor is due to the high fluctuations of the earth's magnetic field at that time. Sesklo covers all the Neolithic phases (Early, Middle, Late), in Greece and is therefore the most important site to be studied extensively.

Dimini is a settlement situated nearby where occupation began c4700 BC. C-14 dates, of which only two are available so far, give a date for two wooden samples from Sesklo (though of the Dimini period) at c4300 yrs BC (corrected), Theoharis (1973) and one date for Dimini gives c3600 yrs BC (uncorrected), Renfrew (1970). Dimini was essentially inhabited continuously from the Late Neolithic to the Chalcolithic period and this is revealed from the many fortifications around a central point of the settlement (megaron). The pottery from Dimini is of characteristic

design and was produced and developed at this site, (though some scholars consider its origin enigmatic). Interaction between these two settlements as well as with other Neolithic settlements, for example, Hacilar VI in Anatolia,Nea Nikomedia, North Greece, have been assumed.

The present studies were undertaken with the aim of determining the chronological span of the different cultural phases of these sites (which means assessing the Neolithic period in Greece), and to find any possible cultural interaction by Neutron Activation Analysis (NAA) and TL dating, and also to compare TL and C-14 dates, since for that period the C-14 technique shows great discrepancies compared to other methods. Results and discussions are presented in Chapter 10. In parallel with the above applications of TL dating methods, experiments and theoretical investigations were undertaken concerning:

i) the validity of basic assumptions of TL procedures, for example, supralinearity, additive procedure (see Chapter 1, Section 1.10.2).

ii) beta dosimetry evaluation (see Part II). Some presently accepted assumptions of measuring beta radiation for ceramics (see Chapter 4) and the effect of beta stopping powers on different clays was extensively studied (see Chapter 6). The combined techniques ofthermoluminescence dosimetry (TLD) and alpha counting plus potassium analysis determination (α+K) were compared when applied to certain clay materials (see Chapter 5), and emphasis was given to the selected grain size used for alpha counting (see Chapter 4).

iii) gamma dosimetry experiments (see Part III) were conducted to calibrate a portable scintillometer NaI(Tl) 2" x 2" (NE PSR6) relative to quartz grains in the form of a simulated potsherd, (grains were inside a capsule and this capsule was inside a table tennis ball) for four different gamma spectral media. Comparisons were made with other

TLD phosphors and investigations were carried out concerning the different gamma spectral responses from different soils and their significance to the determination of the emitted gamma radiation by means of phosphors or a portable instrument (see Chapter 7).
In Chapter 8 seasonal gamma soil fluctuations as recorded by the above scintillometer and TLD phosphors are discussed and their significance to archaeological dating is emphasized.
Finally, the above calibration data curves are further tested with gamma dose values taken with phosphors which were left in situ for a year (see Chapter 9)

1.2.3 The site studied by Uranium disequilibrium dating was that of Petralona Cave, Chalkidiki Peninsula, Greece, and involved stalagmites and travertines (depositional calcitic layers.) Petralona Cave, the discovery site of an important early hominid, is partly filled with the detrital cave sediments containing skeletal remains of large Pleistocene vertebrates and stone artifacts. These strata include and are covered by layers of relatively impure travertine which have been dated by the Th-230/U-234 method, although large uncertainties are associated with these dates due to the low uranium concentrations.
The skull has since then been studied by several anthropologists and has been described as Neaderthal (35,000 - 130,000 yrs BC), Kanelis, Savas (1964); although Stringer (1974), Poulianos (1972, 1977, 1978, 1979), argue that it is morphologically most closely related to the homo erectus. Poulianos, the excavator, stresses that the Petralonian Archanthropus in general, presents a mosaic of primitive and progressive characteristics and places it in the transition from homo erectus to neaderthal types. This dispute continues and controversy has been the main feature of this important finding.
Dates have been provided by paleontological means , (Kurten, Poulianos 1977)

of around 400,000 yrs BP, by electron spin resonance (Ikeya, 1979), with a time span of 10,000 - 1,000,000 and by Schwarcz and the author (1979), between 65,000 - 650,000 yrs BP. The present studies were undertaken with the aim of resolving this controversial problem and to set a final age for the skull. Samples were taken by the author and, therefore, confidence in the sample location increases the value and reliability of the dating results found. Results and discussions of the dates, other aspects of the method concerned, Fission Track analyses and Thin Sections are presented in Part V and in Chapters 11,12

1.3 Theory of Thermoluminescence

Thermoluminescence is basically the electron-hole recombination process occuring in a crystal, due to the presence of impurities and structural defects (which modify the band model) and the emission-absorption processes.

Fig. 1.3 shows a model proposed by Halperin and Braner (1960). Depending upon the mechanisims involved, two theories have been developed; the monomolecular theory (with first order kinetics), Randall-Wilkins (1948) and the biomolecular theory (of second order kinetics), Garlick-Gibson (1949). Certain aspects of the TL theory is also reviewed and developed by Curie (1960).

1.4 Electron Traps and Mineral Inclusions of Pottery

The kiln firing of the mineral constituents of pottery in ancient times resulted in the removal of geologically caused thermoluminescence due to electrons trapped in levels of energy with a mean lifetime (τ) at the firing temperature short compared to the time of heating. Immediately after the pottery has cooled down, the radiation environment (which arises from trace impurities of uranium, thorium and potassium within the clay and the surrounding soil) will begin to induce thermoluminescence in the fired minerals.

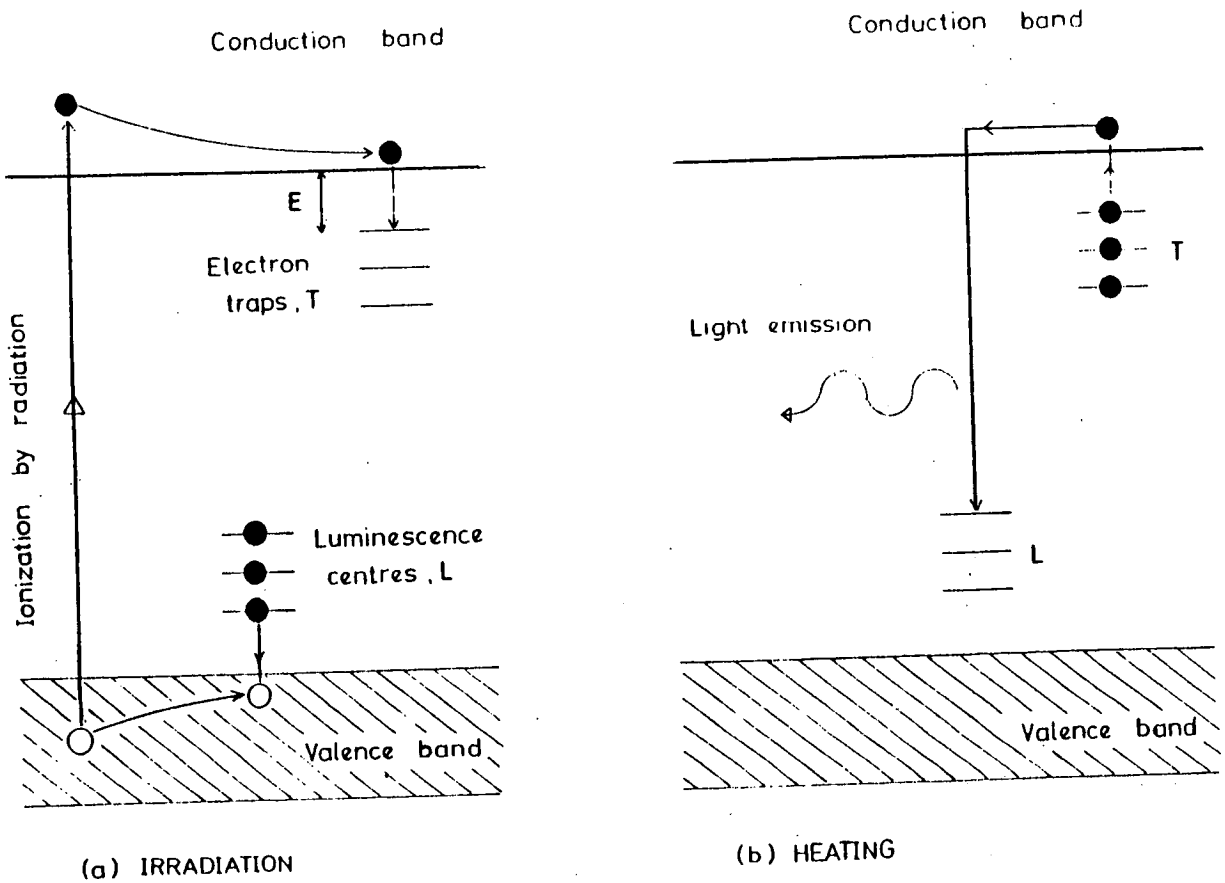


Fig. 1.3. The Thermoluminescent Process, (Halperin and Branner, 1960)

The rate of accumulation of TL will be directly related to the concentration of trapping sites in the minerals in the pottery fabric. Then the light levels observed at the present time may be expected to vary by at least an order of magnitude over a range ofpottery types. The light output observed in such a heating is termed the Natural Thermoluminescence. The concentration of trapping sites may be comparatively measured, however, by the addition of further TL by application of a known radiation dose from a calibrated, artificial source. This will obtain a value of A light units for a radiation dose D, where N andA would be made of comparable magnitude. Then the total radiation dose which thepot has received during archaeological burial is given directly by : N/A x D dose units (rads).

The rate of dosage of the material in units of rads per year may be obtained from analysis of the uranium, thorium and potassium contents of the surrounding environment, R rads/yr, and involves alpha, beta and gamma radiations emitted from them. Thus on the assumption of linear acquisition of TL with time (see sections 1.13-14 for further discussions on such non-linear acquisitions) for the stable temperature region of the glow curves taken, we obtain an estimate of the age of the pottery from the relationship:

$$\text{Age} = \frac{\text{Total Radiation Dose (in rads)}}{\text{Dose Rate (rads/yr)}} \cong \frac{N/A \times D}{R} \text{ years, where}$$

$$R = D_\alpha + D_\beta + D_\gamma + D_c$$

D_α, D_β, D_γ, D_c, are the radiation dose rates for alpha , beta gamma and cosmic radiation components.

It will be the fundamental criterion of linear acquisition of TL and the measurement of the annual dose rate R, which will be critically reviewed in this thesis.

For trapping sites within such minerals, the accumulation of electrons during archaeological times will now, however, be a dynamic process for such weak excitation rate, since electrons trapped at levels of mean lifetime comparable to this archaeological period will be substantially re-excited.

Thermoluminescence observed at the present time will thus be a function not only of the radiation dose suffered, but also the ambient temperatures of burial.

If the amount of TL observed is to be quantitively related to the radiation dose it has experienced during burial, the region of temperature in any glow curves obtained must be restricted to where the electron traps have suffered insignificant decay over the archaeological time. The restriction upon the working region of the glow curve analysis to temperatures greater than 300°C is consistent with earlier dating work, Fleming (1969).

1.5 Principles of TL Dating of Ceramics

Firing of pottery by ancient man was usually carried out at temperatures between 600°C and 1000°C, so that the electron traps which are of principal interest in the region of 300°C to 500°C will have been completely drained so that the defect centres responsible for the TL observed at the present time will have been completely emptied at the time of making of thepottery. The mineral constituents of the pot will then have been subjected to a constant radiation environment arising from the trace impurities of uranium, thorium and radiogenic potassium (K-40)within the pottery itself and from the surrounding soil and cosmic radiation.

The filling of the electron traps in the pottery minerals is then assumed to occur at a steady rate, resulting in linear growth of the thermoluminescence accrued to present time.

1.6 Review of the Development of TL Dating Techniques

The dating of ancient pottery by thermoluminescence measurements was suggested by Prof. F Daniels, Daniels et al (1953).

Encouraging initial trials of the technique were reported about twenty years ago , Houtermans (1960), Kennedy et al (1960), Grogler et al (1960), and wide-spread interest was aroused among archaeologists; not only would it provide a check of radiocarbon results but it would have the strong advantage of being applicable to a material which was more plentiful than carbon and which is the fabric of ceramic typology studies. Initially, the powdered pottery clay was used to measure the archaeological dose, and consideration was given to using the growth of a number of traps (as evidenced by an increase in TL sensitivity), as the basis of dating. Tite and Waine (1962) showed that the number of new traps created through crystal damage processes by the doses of the magnitude likely to be experienced in archaeological times was negligible compared to the number of existing traps. Using the concept of trap filling rather than the trap creation the technique was found to be viable, because the precision obtained was not usually better than $\pm$ 20% and the dating was relative, it was necessary to calibrate with pottery of known age, Aitken et al (1964). At this time - the most vital stage in the development of TL - Fremlin and Srirath (1964), pointed out some of the consequences of the inhomogeneities referred to the non-uniformity of luminescence in the clay matrix and quartz inclusions respectively, and following work by Ichikawa (1965), it was found possible to achieve correct absolute ages by restricting the TL measurements to quartz grains - instead of powdered clay - of about 0.1mm diameter extracted from the pottery. Fleming (1966), Mazess and Zimmerman (1966).

An attempt to calculate results on an absolute basis from laboratory

data, that is, to obtain the age directly in years by expressing the TL sensitivity (to beta radiation) in units of TL/rad and the radioactivity in units of rads/yr, yielded ages that were too low by a factor of five, Tite (1966). Part of this error was found to lie in theheterogeneity of the fabric of pottery. However, the previously introduced TL measurement on quartz grains started to be widely used, since for such grains the dosimetry is fairly straight forward and quantitively feasible. This "inclusion dating technique" was subsequently applied to pottery with an accuracy of around 10%, Aitken et al (1968), Fleming (1968).

Subsequently Zimmerman developed another technique based on the fine crystalline extracts of pottery in the size range of 1 - 8 μm, the "fine-grain"technique, Zimmerman (1967). In its initial test (Aitken et al, 1968), a dating accuracy of between ±15% and ±10% was obtained.

Further improvements have been made in both techniques, Mejdahl (1969), Zimmerman and Huxtable (1969), Ralph et al (1969), Fleming (1970), Mejdahl (1972 a,b).

Three other techniques were later developed. The "Subtraction" dating (in which the contribution from the environmental radiation is eliminated), based on the above two methods. In this technique the difference between archaeological doses obtained from the "inclusion" and "fine-grain" techniques can be attributed almost entirely to the TL energy build-up by alphas alone, which is the only dose rate parameter which needs to be evaluated. This technique has not a better accuracy than approximately ±15%, Fleming and Stoneham (1973).

The other technique was the "pre-dose" based on the usefulness of the pre-dose effect in quartz and its 110°C peak. The sensitivity of this peak is associated with its pre-irradiation is measured under laboratory conditions by applying test-doses and measuring the

the subsequent signal enhancement wich is linked to the archaeological dose, Fleming (1969, 1971, 1973). The age limits are around 1560 years and are applied to both dating and authenticity.

The third technique is the radioactive inclusions or "zircon technique", based on zircon grains which are self-radioactive containing high concentrations of uranium. By determining the dose rate and the total TL dose from those grains the age can be established, Zimmerman et al (1974). The attraction of this method is that it is independent of environmental factors. The method is mostly useful for authenticity and its dating application is restricted by its high, at present, error of approximately 20%.

Further improvements have been made in both the "inclusion" and "fine-grain" TL techniques and the present accuracy lies between ±5% to ±10%. Applications include authenticity tests, for example : on the vessels and figurines in the Haçlar style, using pre-dose and "fine-grain" techniques, with an accuracy of ±10% to ±15%, Aitken et al (1971); on Etruscan wall-paintings of terra-cotta, Fleming et al (1971); on core material from the bronze horse of the New York Metrolopitan Museum of Art, Zimmerman et al (1974); on the disputed Glozel findings, François et al (1977), McKerrell et al (1974), Aitken et al (1975); on some "Sixth Dynasty" figures from China, Fleming et al (1970) and on Nigerian terra-cotta, Fagg et al (1970).

Application of TL dating on pottery and other materials includes the baked clay balls of the povetry point culture by Huxtable et al (1972); fired clay from Dolni Vestonice of the upper Paleolithic, Zimmerman et al (1971); on some Greek pottery, Fleming (1971), Zimmerman (1970); on Megalithic sites of Neolithic period from Portugal, Whittle and Arnaud (1975); on the cemetery at Bellan Bandi palassa, Sri Lanka, Wintle et al (1972); on the Baderian cultures at the Hemamieh, Egypt, Whittle (1975); on ancient Danish pottery, Mejdahl (1972, 1969) and on Greek

Neolithic pottery, Liritzis et al (1978).

Other applications on pottery have been reported in the literature which however are not as extensively centred on Neolithic and older times. Most of themare tabulated in Table 1.6

Finally, in spite of some minor details of the dosimetry now being questioned (Bell, 1979 and Zimmerman, 1978; Sutton and Zimmerman, 1978), the quartz inclusion method has withstood the test of time satisfactorily and is gaining increasing popularity as the "fine-grain" method has become increasingly complicated, for example, in complexities such as anomalous fading, Wintle (1973), Whittle et al (1975).

The TL dating has also been applied to geological materials, for example, calcite, Wintle, (1975 , 1978), Bungert et al (1979), Flint, Bowman et al (1979), Wintle (1977), Goksu et al (1974) on lava, Aitken et al (1968), Sutton (1978), Valladas et al (1978), on bone Christodoulides et al (1971), Jasiska et al (1970), on sediments, Wintle et al (1978). More detailed accounts of other geological materials are to be found in TL of geological materials, edited by McDougall, (1968).

1.7 Errors Associated With The Inclusion Technique

There are several errors and basic assumptions associated with the principles of TL dating by the "inclusion technique". Each error factor having its own limits and varying degrees of effect on the final accuracy of the method. Most of the errors are fully discussed in the relevant chapter as detailed below:

i) Radon emanation problems - see Chapter 3 section 3.5 , Chapter 5 section 5.2.iii

ii) Fading and anomolous fading - ejection of electrons from deep traps through quantum mechanical effects "tunneling" or other complex mechanisms in a constant (fading) or irregular manner

TABLE 1.6

TL Applications	Materials & Origins		Techniques & Accuracy	Author	Publication & Date
Dating	Pottery	Various places Iran, Greece	powdered potsherd	Aitken et al	Nature vol 202, 1964
"	"	Egypt, Italy USA	powdered potsherd ±5-15%	Ralph & Han	TL of Geological Material, Academic Press, 1968
"	"	"	q.inclus. ≃ 8-14%	Fleming	" "
"	"	Peru	powdered potsherd ≃ 25%	Mazess et al	" "
"	Terracota	Nigeria	" "	Fagg et al	Archaeometry 12(1) 1970
"	Pottery	Turkey, Italy England, Jordan	powdered pottery 10%	Tite et al	Archaeometry 5 1961
"	"	Various sites	fine grains ≃ 5-10%	Zimmerman	Archaeometry 13 (1) 1971
"	Fired clay	Hungary	fine grains ≃ 10%	Zimmerman et al	Archaeometry 13 (1) 1971
"	Pottery	France, England	fine grains 10%	Aitken et al	Nature 219, 1968
"	Pottery	Various	q. inclus. 12%	Fleming	Ph.D Thesis, Oxford 1969
"	"	"	fine grains 5-10%	Zimmerman	Ph.D THesis, Oxford 1970
"	"	India	fine grains ≃ 8%	Huxtable et al	Antiquity XLVI (181) 1972
"	"	Columbia	q.inclus. 10%	Sampson et al	Archaeometry 14 (1) 1972
"	"		q.inclus 5-10%	Mejdahl	Risø Report 1969, 1972
Dating	Burnt Clay		q.inclus, & fine grains 6%	Huxtable et al	Archaeometry 18 (1) 1976
"	Pottery	Egypt	" "	Whittle	Archaeometry 17 (1) 1975
"	Ceramics	Portugal	fine grains & q.inclus. 6%	Whittle et al	Archaeometry 17 (3) 1975
Authenticity	Ceramics	China	" "	Fleming	Archaeometry 15 (1) 1973
"	Figurines	China	" "	"	Archaeometry 12 (1) 1970

(anomalous fading) render the method unsuitable for dating purposes unless the degree of TL loss by time can be found but this is unlikely to occur - see Chapter 9

iii) Water uptake - see Chapter 3

iv) Spurious TL - see Chapter 9

v) Th/U Disequilibrium - see Chapters 3 and 5

vi) Gamma soil fluctuations - see Chapter 7

vii) Beta dose rate evaluation - see chapter 2, 3 and 5

1.8 Why Choose the Inclusion Technique?

The "inclusion" method adopted in the present dating programme was chosen (in preference to the "fine-grain" technique) for the following reasons:

i) The existence of a large amount of mineral inclusions in the materials employed, due to the pottery technology during Neolithic times and kiln structures, for example, crude clay products and raw burnt clay; all materials being devoid of adequate refinement and thus of any significant proportions of fine grains.

ii) The removal of the inclusions' surfaces by etching carries away diffused impurities from the clay matrix which makes the glow-curve shapes more standardised in the high temperature region. Fleming (1969)

iii) For an emanation level of 40% and typical uranium, thorium and potassium contents, the error limit for fine grain is about 8% and about 2% for the inclusion technique (see Chapter 3)

iv) The "fine-grains" by their nature are more easily subjected to non-radiation-induced TL or spurious TL, Zimmerman,(1970).

v) As the most important parameter for "inclusion dating" is the determination of the external gamma radiation and the beta

radiation originating in the pottery rather than a precise measurement of alphas, it is less affected by possible inhomogeneities in the uranium and thorium distributions inside thepot, Zimmerman (1970). Thus, if the alpha radioactivity was present predominantly as inclusions, then the alpha dosage to the fine grains would again be heterogeneous depending on how close a particular fine grain happened to be to an inclusion. The size of the radioactive inclusions would affect the amount of self-absorption of alpha dose as well as the mean alpha energy seen by the fine-grains. The determination of the radioactivity by alpha counting would be ambigious depending on how finely the sample was ground. (See also Chapter 4 Section 4.3)

vi) Since the burial conditions of the materials and the general radioactivity of the sites involved were fairly well-known and accurately measured with cross-checking techniques, inclusion dating gained an important point in being conveniently more easily and reliably applicable.

vii) The vunerability of "fine-grains" to the creation of defects induced during vice crushing or the increased possibility of breaking down large grains to small (fine) ones, complicates matters, thereby resulting in low TL ages.

viii) The 2nd Build-up curves of quartz or feldspar grains with dose though thought to be a problem, seems to be well established. (See also sections 1.12 and 1.13)

ix) "Inclusion technique" also is usually devoid of the anomalous fading which is one of the greater problems in "fine-grains" technique.

1.9 Experimental TL Apparatus

Fig.1.9 shows a general layout of the apparatus. Spurious signals produced in the vacuum glow oven are adequately quenched by the absence of oxygen and water vapour impurity from the oven and a vacuum system enables the pressure to be rapidly taken down to 0.01 torr, before oxygen-free nitrogen is flushed through the oven at a rate of 5l /min. The nitrogen is the purest form available commercially, containing less than 1 ppm oxygen; the presence of the gas in the oven is essential to provide thermal conduction between the sample and the heating strip. A pirani gauge measures the pressure in the system and a water-cooling system was used to cool down quickly the heating strip. Also, the connection from the thermocouple in the oven to the input of the heating strip unit was as short as possible by a screened cable to minimise pick-up. A photomultiplier (PM), powered by the EHT supply on the multi-channel analyser detects the light emitted. Effectively, each photon detected at the photocathode by the emission of a photoelectron gives rise to a pulse of about 10^7 electrons which arrive at the anode within about 20nsec time spread. The signal then goes through a pre-amplifier to the 100 channel analyser used in a multiscaler mode. The counting time per channel is adjusted in relation to the cycle time of the linear circuit, so that the glow curve up to 500^{o}C occupies the 100 channels.

1.9.1. Vacuum glow oven

The sample is heated on a nichrome strip connected to the high current transformer; the heatingrate being $\sim$ 21 ^{o}C/sec. A chromel-alumel thermocouple spot welded to the underside of the heating strip enables the temperature to be measured. The oven has a tightly fitting lid; an O ring smeared with vacuum grease completes the seal. The lid contains a circular groove which takes the photomultiplies housing.

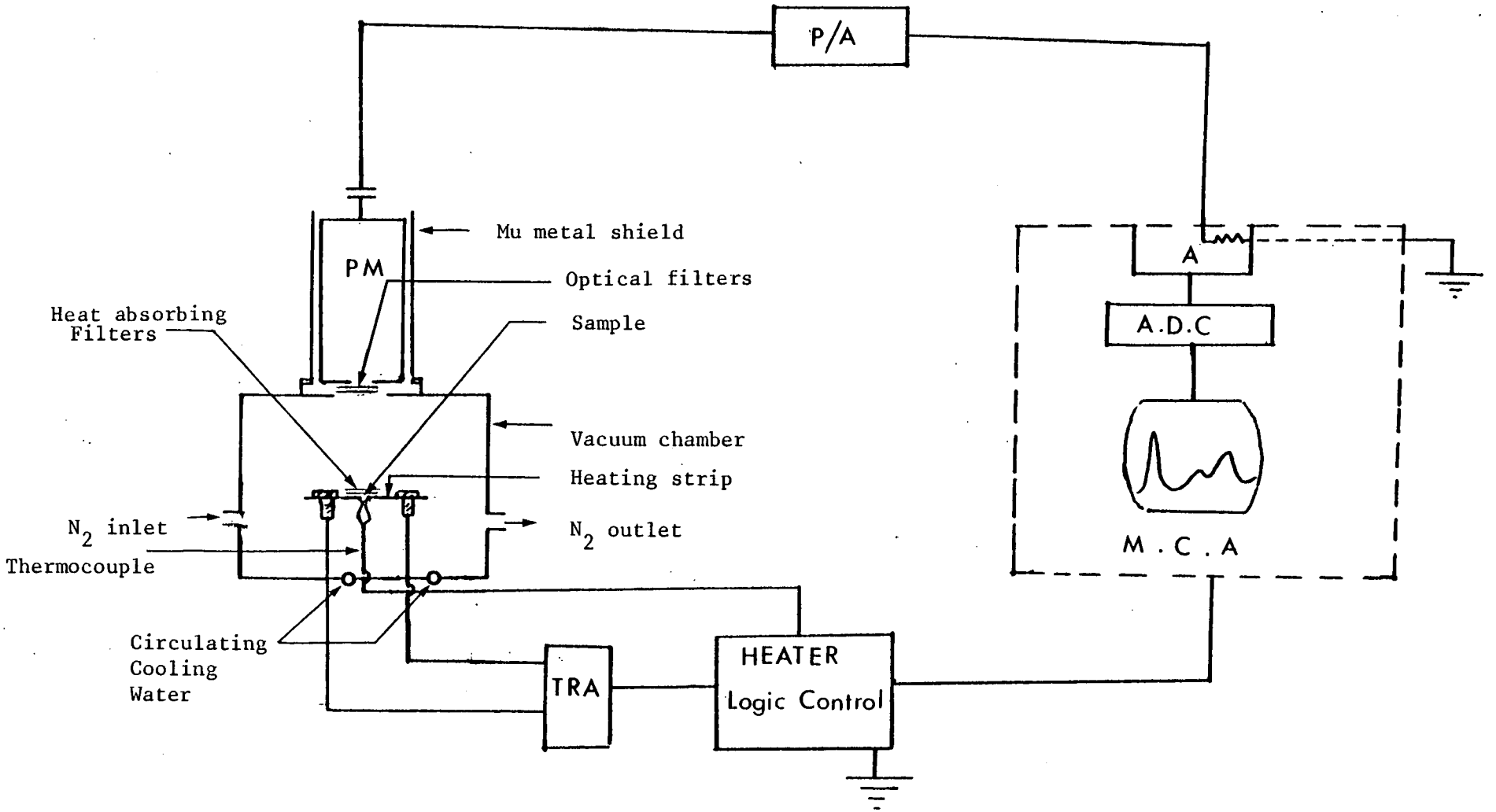


Fig. 1.9 Lay-out of the TL Apparatus

1.9.2 Thermal radiation

When the temperature reaches about 400°C, the thermal radiation detected by the photomultiplier begins to show and may interfere with the glow curve. This background may be reduced in several ways:

A) The central part of the heating strip ispainted silver

B) A "Black-body" shield is placed over the silvered heating strip. This consists of a strip of polished brass, of high specific heat, of the same width as the heating strip, and containing a hole to take the aluminium disc on which the sample is placed. The shield is held in place a few millimetres above the heating strip and insulated from it, by means of two bands of insulator. These are pieces of mica fastened to the brass with an inorganic insulating cement capable of withstanding the high temperatures reached.

Since the brass shield is insulated from the hot strip, its temperature will lag behind that of the heating strip as this is rapidly heated. The hot strip is now hidden from the view of the photomultiplier and the latter sees only the shield which is at a lower temperature. Thus the "black-body" contribution to the glow curve will be reduced.

C) Various filters may be placed between the glow oven and photomultiplier. The photomultiplier is sensitive to a wavelength range from 3000 A to about 5600 A, and it is this long wavelength part that becomes predominant at the higher temperatures and is to be filtered out. The thermoluminescent light is generally in the blue region. The filter used is a Chance-Pilkington OB 14 blue filter, having maximum transmission at about 3700 Å. A heat-absorbing filter HA 3 is also used.

These devices reduce the thermal radiation detected by photomultiplier to a very low level.

The heating circuit has
a reproducible heating rate which is linear to better than 1%.
A block diagram of the circuit is shown in Fig. 1.9.3. The output of the thermocouple spot-welded to the heating strip is compared with the linearly increasing voltage from a precision potentiometer driven by a precisely linear stepping motor. The comparator drives a thyristor trigger unit which controls two thyristors. These feed a.c. mains to a step-down transformer which provides high current to the heating strip. If the output from the thermocouple is lower than the reference voltage, the thyristors are triggered on to provide more power to the heating strip; if it is higher than the reference voltage, they do not fire until the reference voltage has "caught up". The counting time per channel in the multi-channel analyser is set to 0.2seconds, and the waiting time may be adjusted to provide exact coincidence between the two cycles. However, the motor and logic control get progressively more out of phase as measurements proceed; and this would lead to unreproducible glow curves. This problem was solved by introducing a microswitch operated by the stepping motor, so that the circuit is broken after precisely one revolution of the motor.

1.10 Non-Linear TL Response of Quartz and Feldspar Grains: Some Annealing Experiments

1.10.1 Introduction

Since the scope of this thesis was to apply the "additive procedure" to TL dating, it was a necessary task to investigate to some extent such effects and their implications on possible dating errors. Therefore, experiments were performed with particular emphasis on the crystal sensitivity change due to heating at various temperatures which also reflect the different degrees of linearity of the TL response curves. Also, some possible mechanisms causing such dramatic changes

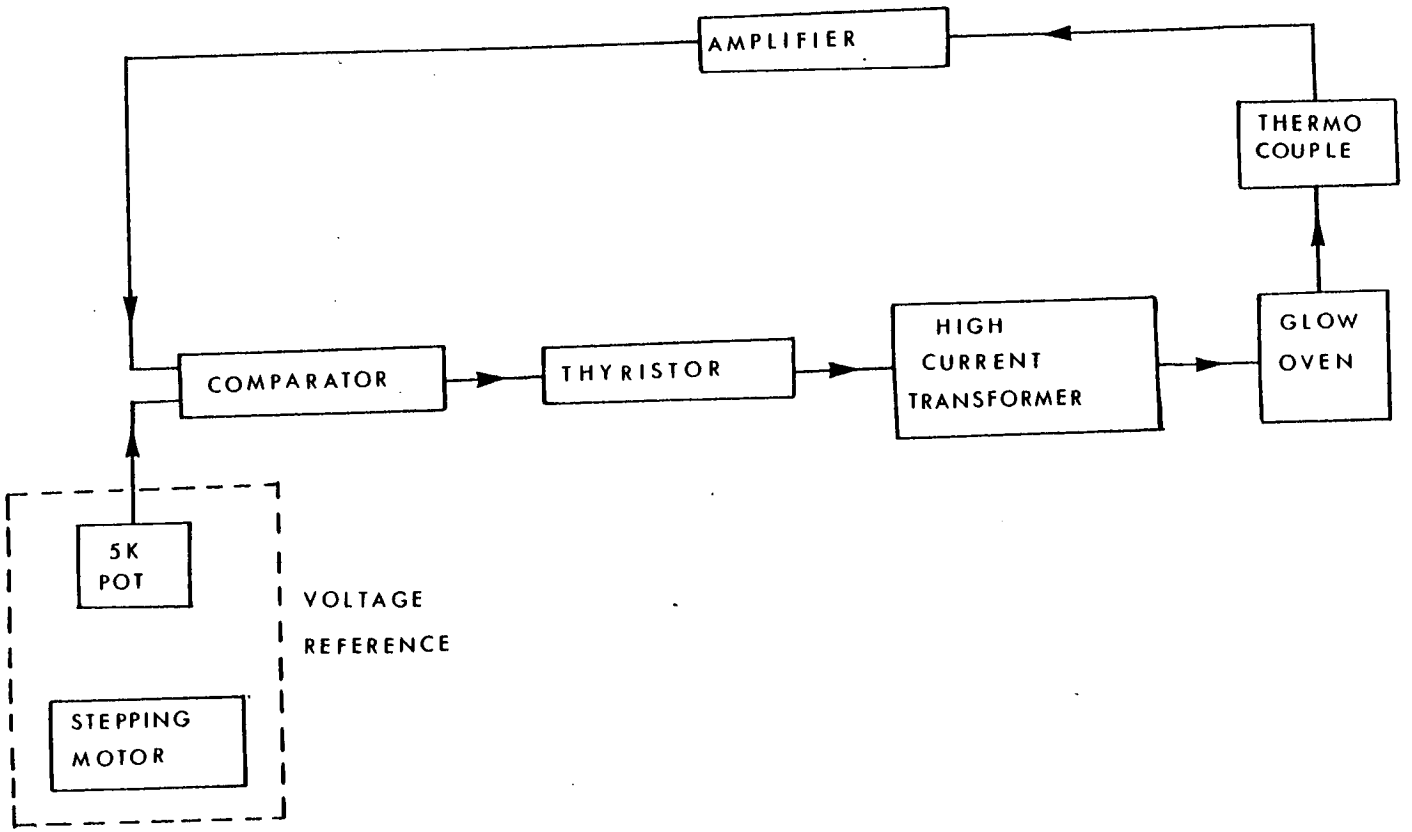


Fig.. 1.9.3 Block Diagram of the Linear Heating Circuit

1.10.2 Natural and Artificial TL acquisition

The TL observed for the quartz and feldspar from pottery samples increases linearly with beta (or gamma) radiation dose except for small initial doses of approx. 300 rads, for which the TL usually increases more slowly as shown in Fig. 1.10.2a.

This phenomenon is defined as supralinearity and is measured by the intercept I_N. Occasionally the TL response increases more rapidly initially to become linear subsequently. This phenomenon is called superlinearity. (Fig 1.10.2.b).

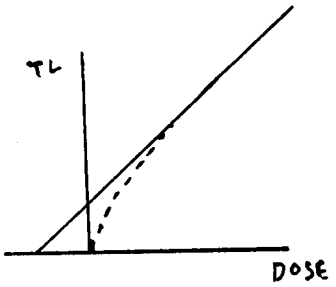
This initial ancient carvature which defines the intercept I_N is lost once the archaeological dose has carried the TL curve into the linear region.

We estimate I_N by making a second growth curve that simulates the ancient one. Thus we determine I_A.

We then ask whether the intercept I_A is equal to the ancient intercept I_N. (Fig. 1.10.2a)

Tite (1966), suggested that the drainage of a sample often caused a significant change of TL sensitivity due either to a transparency change associated with mineralogical alterations brought about by heating of the sample or to more subtle effects arising from the radiation dose recieved before drainage (pre-dose) (also Fleming 1975) .

In our attempt to measure the total archaeological dose a pottery sample has recieved since its last firing we follow the "additive procedure" which simulates the natural TL acquisition. The construction of the 1st build-up curve (Fig.1.10.2) is made by adding beta doses b_1, b_2, b_3, etc., to quartz samples, heated to 500°C with subsequent normalisation with the same monitor beta dose. The second build-up curve is made by draining out a sample by heating from 0°C to 500°C with a constant heating rate and subsequently adding different beta



b.

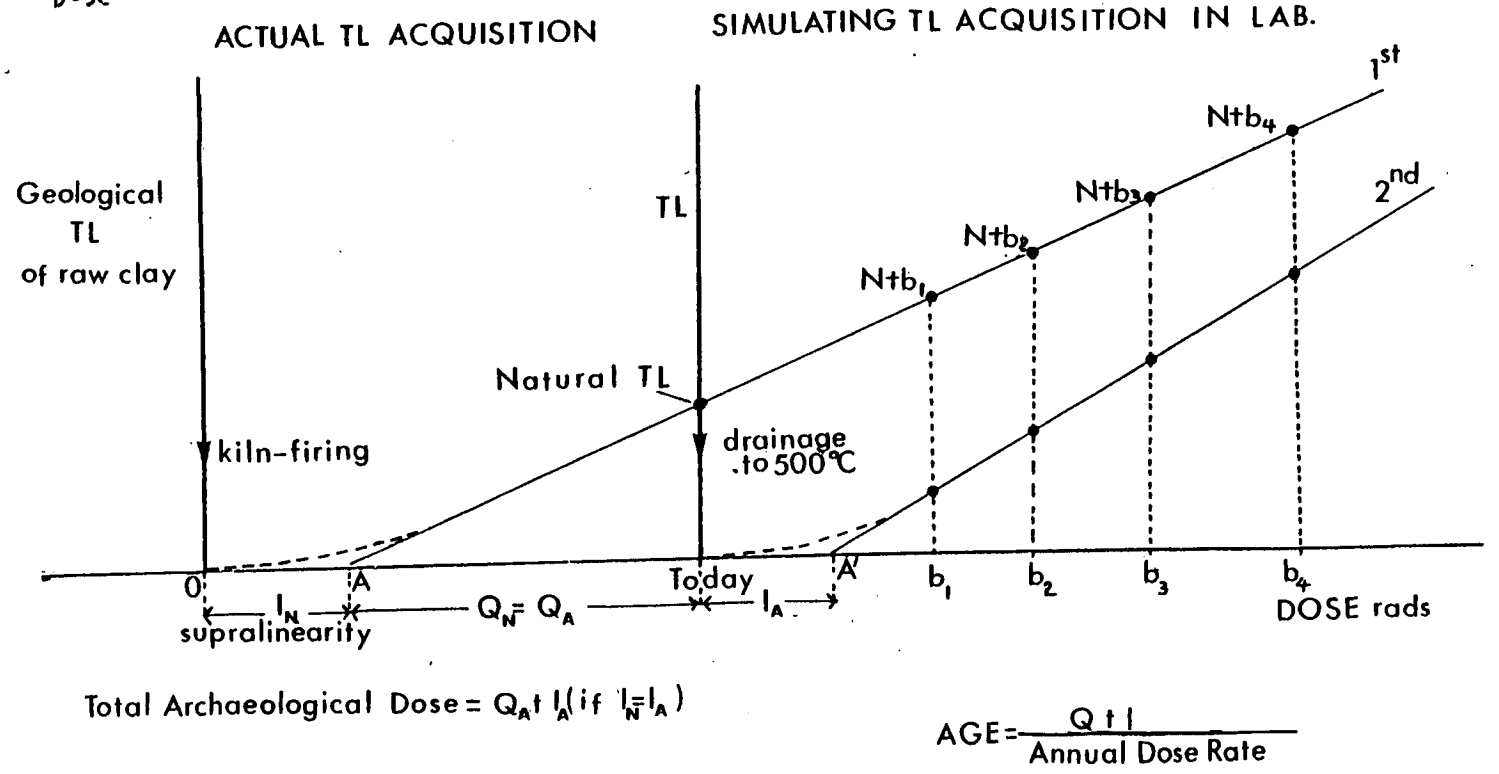


Fig 1.10.2a Calculation of Total Actual Dose with the "Additive Procedure" (supralinearity)
b. Superlinearity.

doses. The usual criterion of acceptance has been that the 1st and 2nd response curves should be parallel. Fleming (1970) has established that the 375°C peak in quartz satisfies this criterion so that $I_N = I_A$, but violent sensitivity changes often occur for the 325°C peak.

Bowman (1975) and Fleming (1975), tried to correlate the supra-linearity effect with predose for quartz and feldspars, and concluded that for some archaeological samples, there is no obviously simple variation of the intercept with pre-dose.

1.11 Experiment (1): Annealing of Quartz at Different Temperatures

To study the effect of sensitivity changes on different quartz temperature peaks due to different heating treatments, a situation quite often encountered in the analysis and study of glow-curves, the following annealing treatments were performed.

The quartz was extracted from a well-fired Neolithic-age sherd. Without any previous annealing, the samples were submitted to the following annealing procedures which drained the natural TL:

i) reading of NTL only

ii) 500°C for five minutes

iii) 500°C for thirty minutes

iv) 600°C for thirty minutes

v) 750°C for th irty minutes

They were treated with HF, for about 30 mins and HCL acid in order to dissolve any fluorides formed by the HF treatment. For read-out, a 10mgr sample was placed directly on the heating strip.

The two high temperature quartz peaks occurred at 300°C (peak 1), and 350°C (peak 2), respectively in our reader.

For read-out, the light was integrated over a temperature interval of 50°C. The radiation was done in the reader with a Sr-90 beta source giving a dose rate of 303 rads/min. A series of irradiations and readings were carried out for each sample. The results are shown in Fig.1.11 It also shows the sensitivity (slope) of the sample for the different annealing conditions and after some cycles of dosings of 280 rads and readings.

This study is linked with the observed sensitivity changes for different peaks in samples which were dated (see also Table 9.5 and Fig.9.5 Chapter 9)

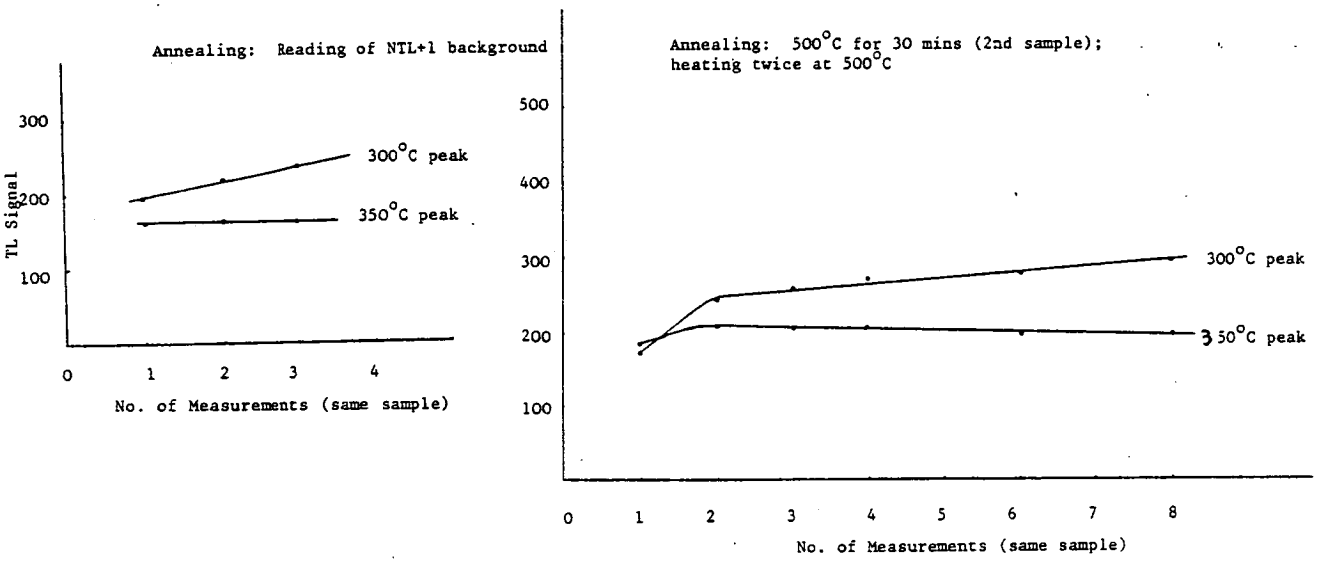


Fig. 1.11 Sensitivity Variations Under Different Annealing Conditions

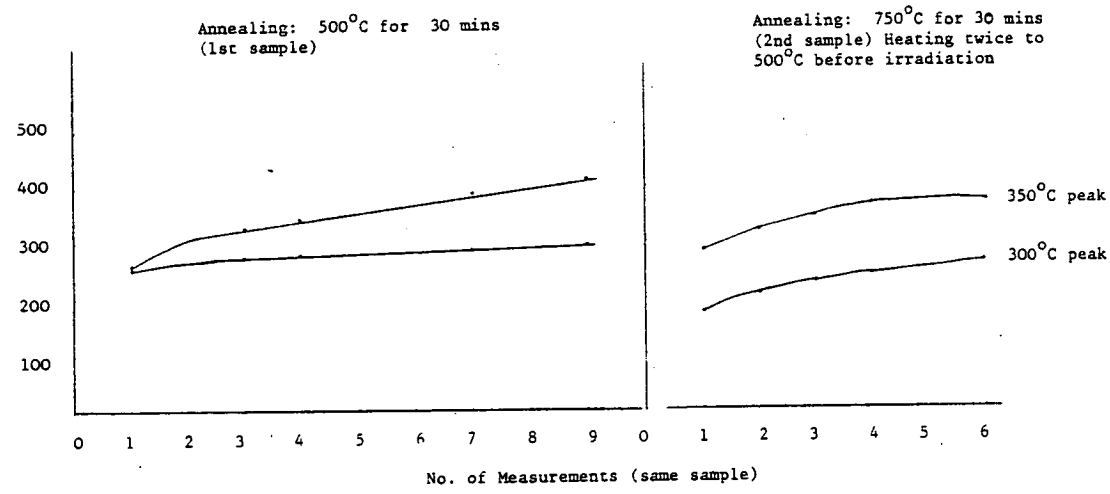


Fig. 1.11 (contd)

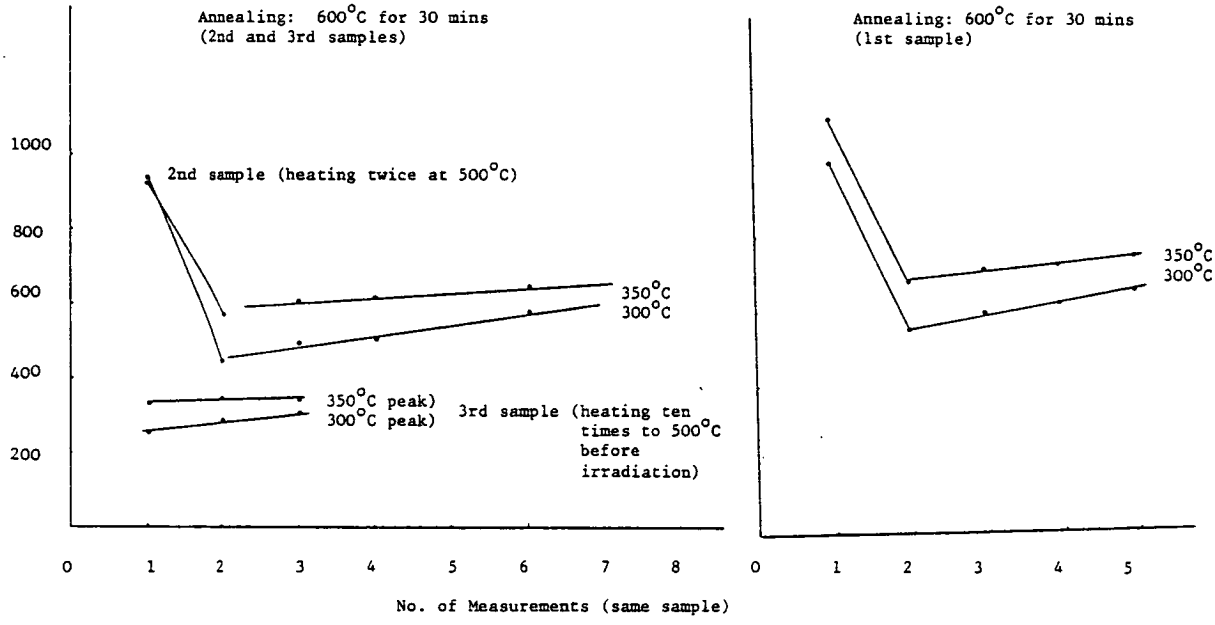


Fig. 1.11 (contd)

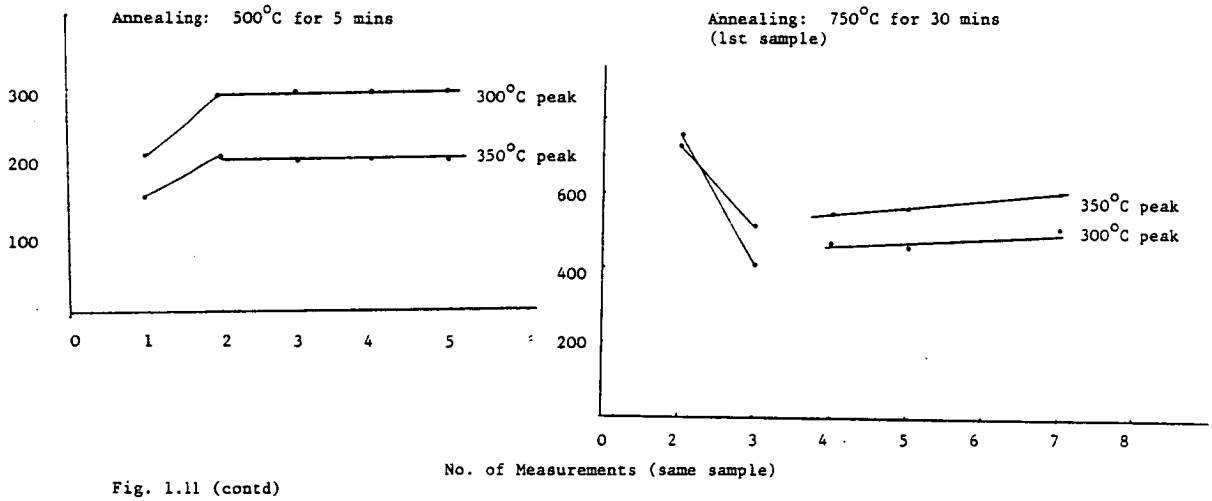


Fig. 1.11 (contd)

1.11.1 Results of Experiment (1)

The results are listed in Table 1.11.1. A summary of these results is as follows:

i) large change in sensitivity from first to second measurement of the same sample: increasing for annealing to 500°C, but this increase decreases with increasing annealing time. There is a large decrease for higher annealing temperatures.

ii) from the second to subsequent readings of the same sample (those of 280 rads): the increase in sensitivity is almost negligible for annealing at 500°C at least for the 350°C peak; but an increase of 5 - 6% per cycle occurs for annealing at higher temperatures for the 300°C peak, and 3 - 4% for the 350°C peak.

iii) increase in response to a dose of 280 rads by around a factor of 3 from 500°C - 750°C annealing temperature.

iv) for annealing at 500°C, peak 1 is more sensitive than peak 2, but in general, for 600°C and 750°C, peak 2 is higher than peak 1.

v) as a general observation, a single heating to 500°C could change the sensitivity of a previously annealed sample considerably.

1.11.2 Discussion and conclusion

The complex character of the TL glow peaks as noted above, imply that the sensitivity change is strongly dependent on the temperature treatment and there is not any reason to believe that such results obtained from archaeological quartz samples are of suspicious origin. In order to proceed further in dating such samples, we must establish the fact that these great alterations do not affect the determination of the total archaeological dose. This has been checked in the following sections.

TABLE 1.11.1

Annealing	Drain out NTL only+ 1 Bg.		500°C for 5 mins		500°C for 30 mins		500°C for 30 mins + Heat (x2) to 500°C		600°C for 30 mins		600°C for 30 mins + Heat (x2) to 500°C		600°C for 30 mins + Heat (x10) to 500°C		750°C for 30 min		750°C for 30 mins + Heat (x2) to 500°C	
Peak	300	350	300	350	300	350	300	350	300	350	300	350	300	350	300	350	300	350
Sensitivity increase 1st →2nd point%	-*	-	37	32	17.8	4.3	41	13.7	-45	-39	-52	-38	-	2.4	-46	-30	6	11
Sensitivity increase other pts%	-	-	0.3	-1	5	1.6	3.3	-1.5	6.2	3	7	3	-	-	5.6	4.9	6.6	3.5
Sensitivity increase over all pts %	10.3	0.3	-	-	-	-	-	-	-	-	-	-	9.4	2.4	-	-	9.6	5.7
Response to 1st 280 rads	197	162	210	155	266	250	170	180	995	120	940	920	250	345	469	549	865	740

* The missing figures from the columns comply with the form of response curves.

1.12 Experiment (2): Testing the "Additive Procedure"

One of the TL dated samples KZ2/5; with a glow curve as shown in Fig.1.12 gave the following results. The determination of the total archaeological dose was performed following the "additive procedure"; with the normalising factor in the second build-up curve being the natural TL.

Both peaks, 325°C and 375°C, gave the same total archaeological dose: $Q_{325} + I_{325} = Q_{375} + I_{375} = 909 \pm 60$ rads, Fig. 1.12.1

Another way of normalisation without changing the TL sensitivity of the crystal is to use the 110°C peak of quartz. By giving a small beta test dose to the sample, for example, 2 rads, and subsequently heating to 500°C, we normalise natural TL or the high temperature peaks on the 110°C peak. Similarly, before adding any beta dose to the natural TL, the response of the 110°C peak is measured by heating to 120°C and subsequently administering beta doses and heating to 500°C. In this case we do not alter the TL sensitivity of the crystal and the first build-up curve must indeed follow the extrapolated natural TL acquisition, Fig. 1.12.1

However, the total dose again is 909 rads ($\pm$ 30)

Another normalisation factor used was the TL/weight in mg. The slope of the first and second build-up curves are similar to 325°C curves and again, with total dose of 894 $\pm$ 30 rads. The above treatment for the determination of the TL dose reassures us that the final result is correct and also that there is no pre-dose effect on these two high temperature peaks, since any pre-dose would result in different Q intercepts as the normalisation factor (monitor beta dose being the same throughout the "additive procedure") will respond proportionately to the added beta doses, therefore giving erroneous results for each added dose. In general, the TL/110°C and TL/mg (if no xenocrysts

Fig. 1.12

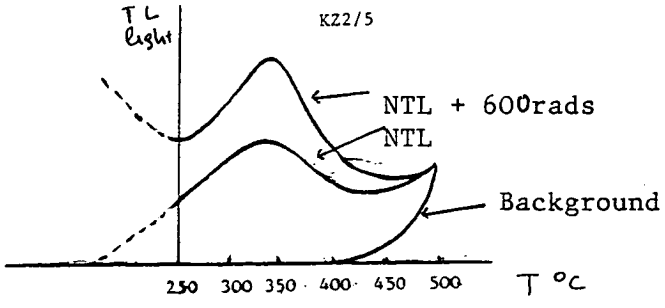


Fig. 1.12.1

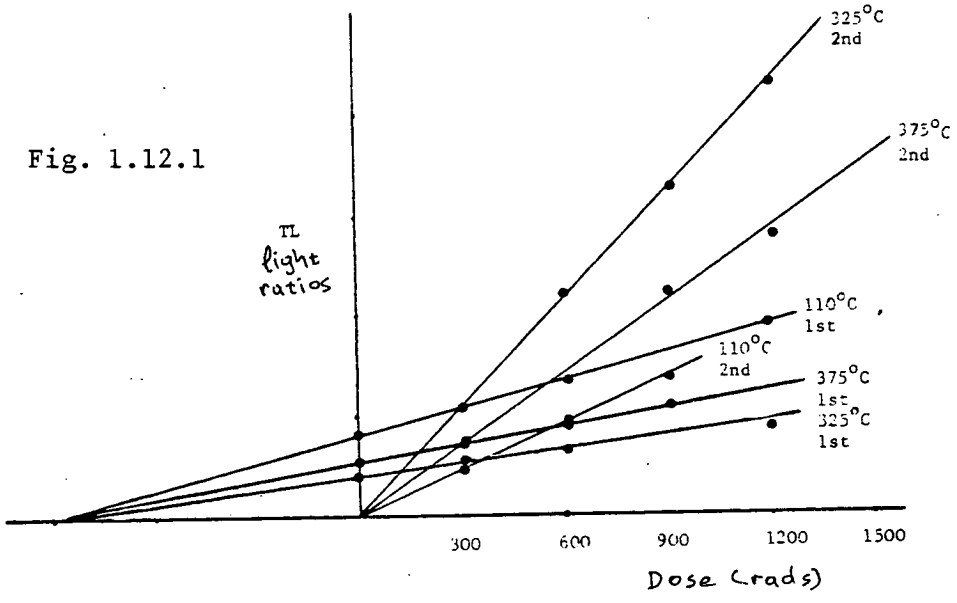


Fig. 1.12 Glow curve of KZ 2/5
Fig. 1.12.1 1st and 2nd Build-up Curves for Different Temperatures

are present which would give scattered points), guarantee the correct way of determining at least the first build-up intercept, that is, $Q_A = Q_N$.

1.13 Experiment (3): Annealing Effects on Intercepts

This experiment is sub-divided into four parts.

1.13.1 By draining out the NTL to 500°C from the above KZ2/5 sample and simulating a new NTL equal to 300 rads, the 1st and 2nd build-up curves shown in Fig. 1.13.1 The final (Q + I)intercept is the simulated dose of 300 rads, but with a negative 2nd intercept (superlinearity). Also, the slopes of the linear part of the curves are nearly parallel. It seems that a simple drainage to 500°C resulted in a considerable change in the slope of the 2nd build-up curve. However, it must be noted that the normalisation factor, TL/rads, for both growth-curves was the same, (see section 1.11.1 above).

1.13.2 By heating the sample to 1000°C for 3.5 hours and simulating an NTL dose of 300 rads and 600 rads, respectively, the results are shown in Fig. 1.13.2. Firing to 1000°C, the intercept, I, is zero. On the other hand, the slopes of the 1st and 2nd build-up curves are considerably different for two different TL simulations (that is, different pre-doses), and both give the expected total dose. The normalisation on the 2nd build-up curve was done upon the natural TL. It is obvious that, by choosing another normalisation factor for the 1st build-up curve, its slope will change,but not the intercept, Q. This means that the "parallel slope" criterion might not be satisfied here, without however altering the total TL dose.

1.13.3 Glozel clay was fired at two different temperatures; 830°C for 3 hours and 500°C for 5 hours. The grains extracted (75 - 106 μm), are feldspar and were given a dose of 909 rads. The sample fired at 500°C gave $Q + I = 990 \pm 50$ rads. The sample fired at 830°C gave $Q + I = 1015 \pm 60$ rads,

Fig. 1.13.1

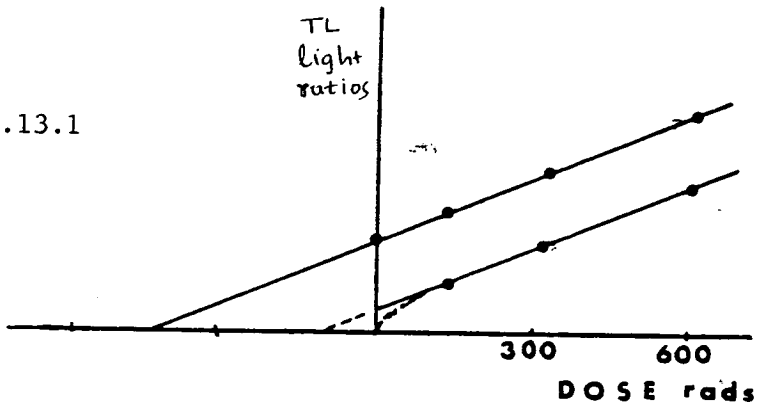


Fig. 1.13.2

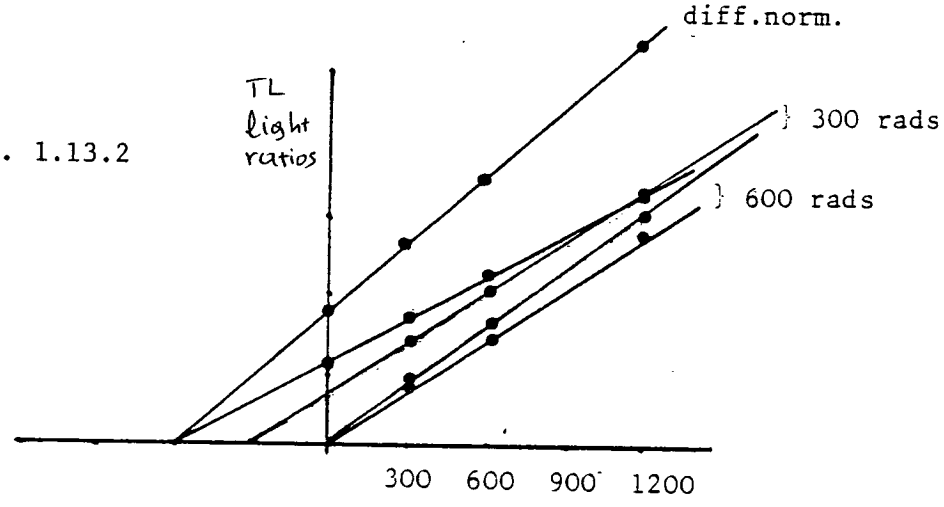


Fig. 1.13.1 1st and 2nd Build-up Curves of KZ2/5 Sample Simulation of Dose of 300 rads after Draining-out the NTL at 500°C

Fig. 1.13.2 1st and 2nd Build-up Curves of KZ2/5 Sample. Simulation of Dose of 300 and 600 rads after Heating the Sample at 1000°C for 3.5 hours.

The glow curves of both samples were of the same pattern, distinguished only by a "broader shoulder" at around 380 - 400°C region for the 830°C sample.

The 830°C sample gave slightly steeper 2nd slope than the 500°C sample. (This increase in slope was also obtained for the quartz annealing experiments, see section 1.11.1). There is a small but distinct difference in their intercepts because of their annealing conditions. All the temperature regions used for each sample, exhibited the same TL response. However, both treatments would give the same simulation dose of 909 rads only within $\pm 2\sigma$. Otherwise the obtained total dose values (Q + I) above, were around 10% higher than the simulated values. Unfortunately they were not checked for pre-dose effect, which could have explained such a difference.

1.13.4 One further experiment for testing the "additive procedure" was carried out. In this, BDH std. purified fine grain sand was annealed at three different temperatures, namely 600°C, 900°C and 1250°C for three hours each. A simulation beta dose of 909 rads was given and, following the "additive procedure", the 1st and 2nd build-up curves were obtained. Fig. 1.13.5 shows ~~their~~ representative glow curves.

i) glow curves The glow curves for the above quartz samples are quite different fromeach other. The annealing temperature have produced different peaks in shapes and intensities, (especially in the low temperature region). Further, the normalisation gave additional re-arrangement in the existing traps, resulting in different glow curves. It seems also, that the higher the temperatures the more stable are the glow curves, that is, no sensitivity change occurs on heating to 500°C, the 1250°C sample. (see also section 1.11.1 above)

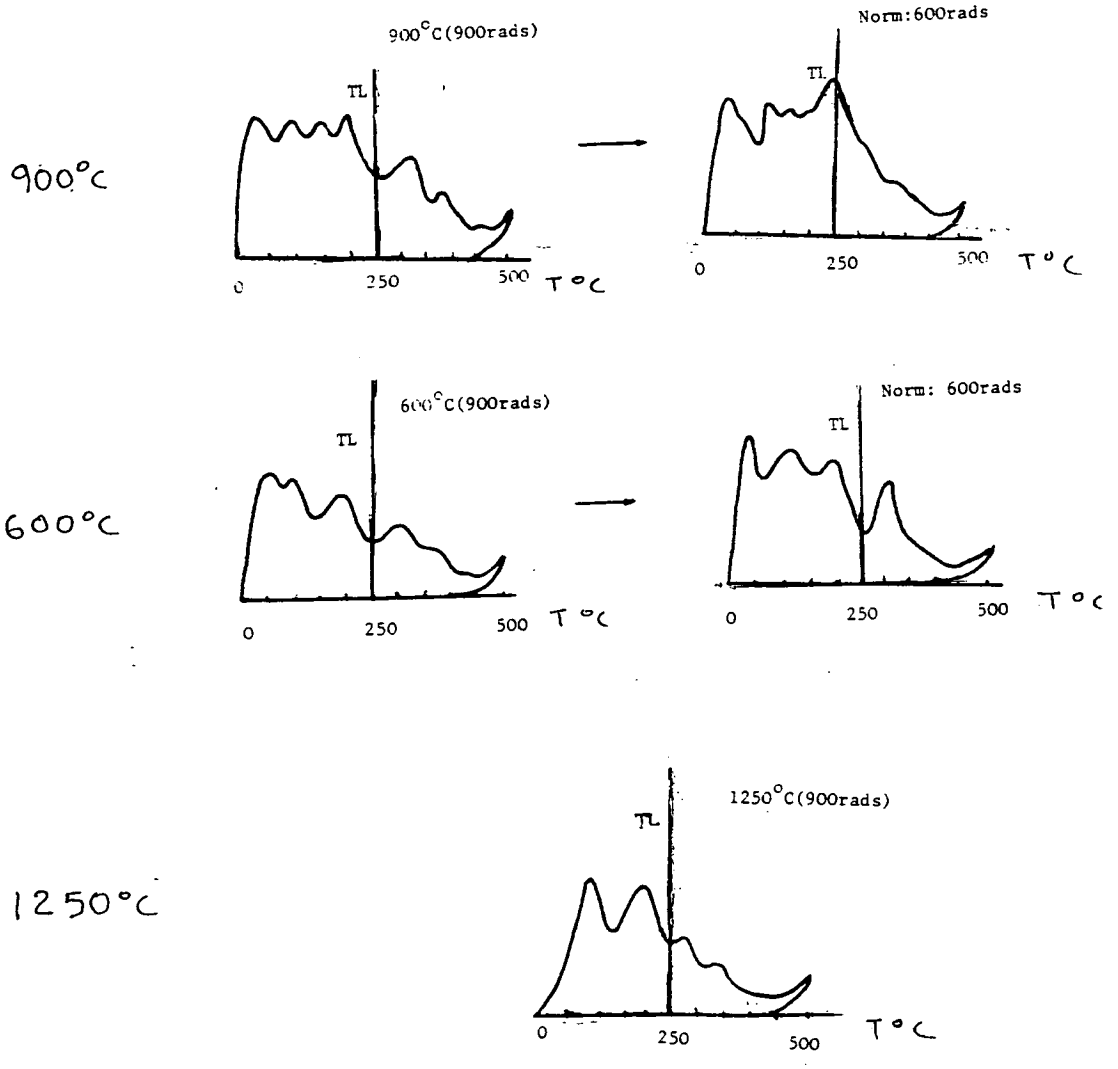


Fig. 1.13.5 Glow Curve for Annealed Quartz fired at of 900°C (Normalised dose of 600 rads) 600°C and 1250°C

ii) build-up-curves. As acticipated, these annealing treatments produced the three forms of build-up curve, i.e. linear, supra and superlinear discribed in section 1.10:

a) the 1250°C sample gave a straight line for the 265°C peak and supralinearityfor the 350°C peak. Both peaks gave the simulated dose of 909 rads. It was observed that the 265°C peak was not so sensitive or well-defined for doses less than 1000 rads, though it gave a higher TL response/rad than the 350°C peak.

b) the 900°C sample gave supralinearity for the 375°C peak, with a smaller intercept than the 350°C peak of 1250°C sample; and the 325°C peak a superlinear response. Though both finally gave the same simulated dose, the 375°C peak was more sensitive (x 1.5) than the 325°C peak. In addition, the 375°C peak satisfied the parallel slope criterion which, as noted in section 1.13.2, above, depends on the normalisation factor and the sensitivity change and it is not an austere criterion that renders the reliability of the "additive procedure" valid.

c) the 600°C sample gave supra- and superlinearity for the 375°C and 325°C peaks respectively. Thus the 375°C peak has the same form of response as that of the 1250°C sample. Also the 375°C peak gave higher TL response/rad (x 1.5) than the 325°C and both responses were lower than those are to 900°C (x 1.3)

1.13.5 Discussion of Experiment (3)

The α-β quartz transformation of relatively minor atomic movements involving no breakage of Si-O bonds or interchange of atoms,(Deer, Home and Zussman, 1977). occurs at 575°C.

The 600°C sample thus consists of β-quartz. At 870°C quartz is transformed to $\beta_2$quartz - (Tridymite) which on cooling reverts to α-quartz. This is the case for the 900°C and 1250C samples also. This is illustrated in Fig.1.13.6 which shows 3 X-ray Guinier (Powder) photographs. They demonstrate α-quartz to be the stable form at room temperature. There is no evidence here of other quartz forms, although the annealing process causes major atomic rearrangements (eg. α-quartz to β_2-tridymite, Fig. 1.13.6), it reverts to α-quartz again in cooling.
Some distinct TL characteristics may thus be attributed purely to impurity ion (centres or traps), rearrangements, during cooling.

1.14 Correlations Between Annealing Experiments and TL Dated Samples

The above results concerning the determination of the simulated dose received by quartz or feldspar grains and the resultant geometry of the 1st and 2nd build-up curves substantiate the results from some characteristic archaeological samples as follows:

i) for the SKB(I)2 sample, (feldspar grains), the build-up curves are shown in Fig. 1.14a Three different temperature regions, that is, the main peak and subsequent higher temperatures gave also the same total dose as TL/mg . Fig 1.14b shows the 1st and 2nd build up curves for the 350°C peak.

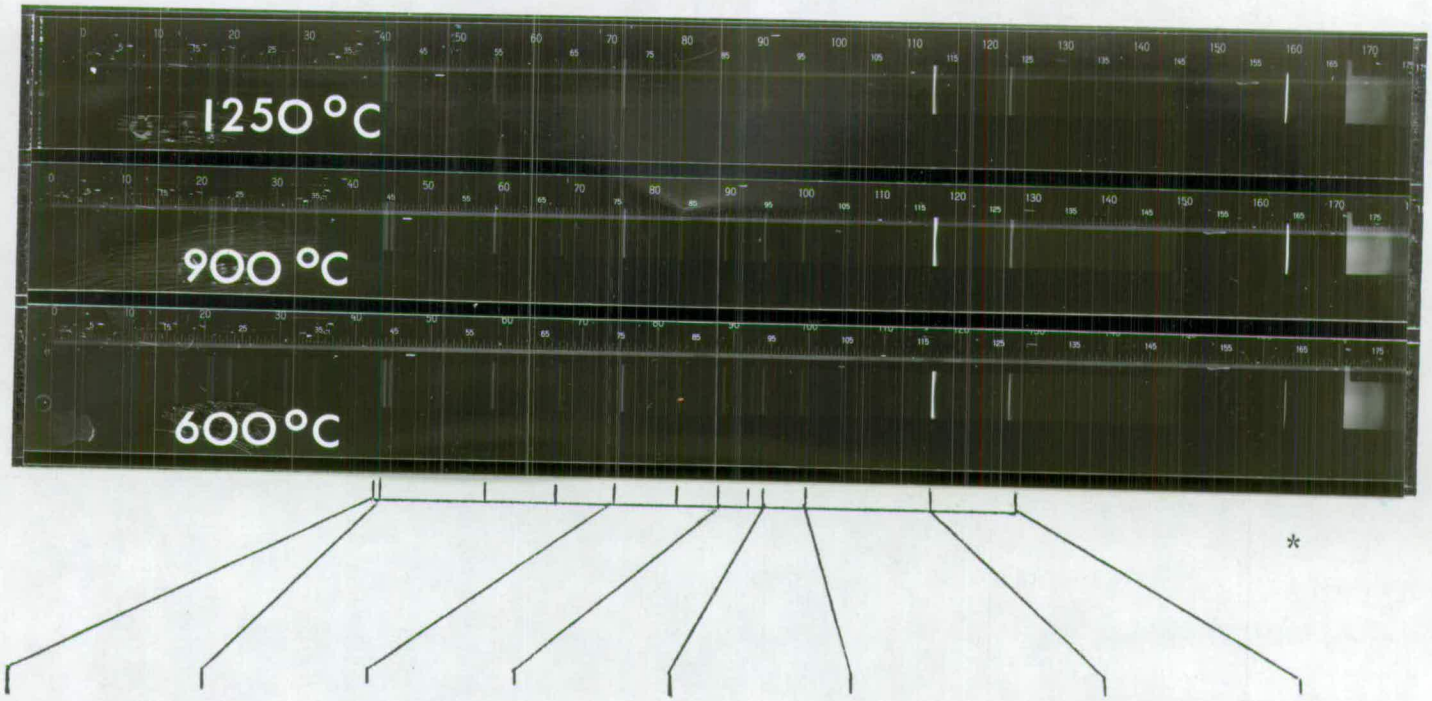
ii) Sample SKB(I)1, (feldspar grains), gave the same total dose with normalisation procedures of both TL/rad and TL/mg. (Fig. 1.14.1) The TL/mg normalisation procedure gave parallel 1st and 2nd curves which implies that no sensitivity change or colouration effect is caused by heating to 500°C. However, normalizing in TL/rad,

Fig. 1.13.6 X-Ray Powder photograph of Quartz annealed at three different temperatures.

The scaling on the opposite page gives the α-quartz powder indices and these are compared to the estimated values of 2Θ for the 900°C sample. By inspection, the 600°C and 1250°C photos are identical within the estimated error (in reading out the 2Θ values), with the 900°C.

Furthermore, the β-quartz and β-tridymite have quite different cell parameters from α-quartz, i.e.

	Crystal Class	aA^{o}	bA^{o}	cA^{o}	$T^{o}C$	Remarks
α-quartz	Trigonal	4.913	-	5.405	∿20	
β-quartz	Hexagonal	5.010	-	5.470	>573	Minor atom rearr.
β-tridy-mite	Hexagonal	5.030	-	8.220	>867	Major atom rearr.



α-Quartz Powder Indices

d-spacing (A^o)	1.371	1.374	1.815	2.126	2.280	2.456	3.341	4.257
Rel. Intensity	9	11	17	9	12	12	100	35
2θ, from standard Tables	68.37	68.20	50.21	42.48	39.49	36.56	26.66	20.85
2θ, Estimated for 900°C	68.24	68.12	50.11	42.38	39.41	36.49	26.65	20.93

* The reference line is indicated by the first sharp line (top). The 2θ values are read by subtracting each subsequent line from the origin multiplied by the camera's scale factor of 0.572.

the first and second build-up curves are not parellel but the same total dose value is obtained. It is worth noting that the 2nd build-up curve is of supralinear form.

iii) DM32 sample, (feldspar grains), gave 1st and 2nd build-up curves satisfying the "parallel slope" criterion, as shown in Fig.1.14.2.

iv) AT7 kiln sample, (quartz grains), gave the same total dose within the statistical error for both the 325°C and 375°C peaks, (Fig. 1.14.3).

v) SH2 siln sample, (quartz grains), gave, for both 350°C and 375°C peaks the same total dose ($\pm 1\ \sigma$). (Fig. 1.14.4).
Additionally the build-up curves had the same slope. Thus the points in Fig 1.14.4 for both peaks coincided.

vi) SKB(I)28 sample, (quartz grains), gave for both TL/mg and TL/rad on the same peak (365°C), the same total dose, (Fig. 1.14.5).

vii) DM33 sample, (quartz grains), gave for all peaks (300°C, 350°C, and 400°C), the same total dose, ($\pm 1\ \sigma$), which is similar to that obtained by TL/mgr for the same peaks, Fig.1.14.6.

viii) 744204, Glozel sample, (feldspar grains), gave the same intercepts, I, in the second build-up curve for two modes of normalisation, namely by natural TL and by the monitor dose of 900 rads which was used for all the points, Fig.1.14.7

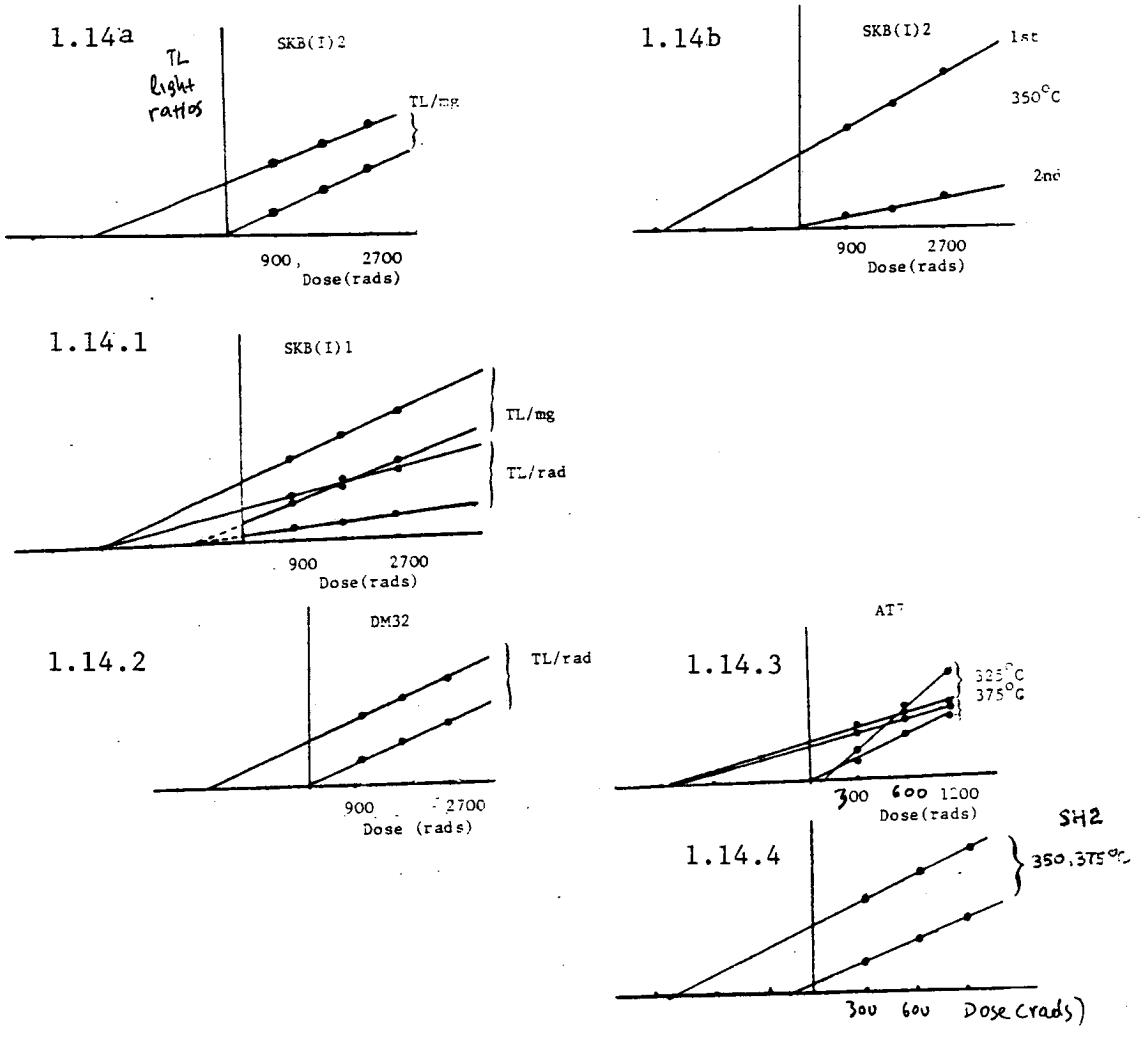
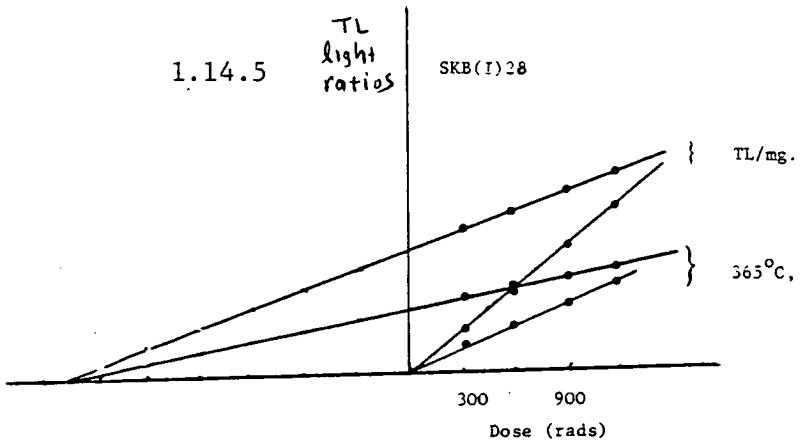
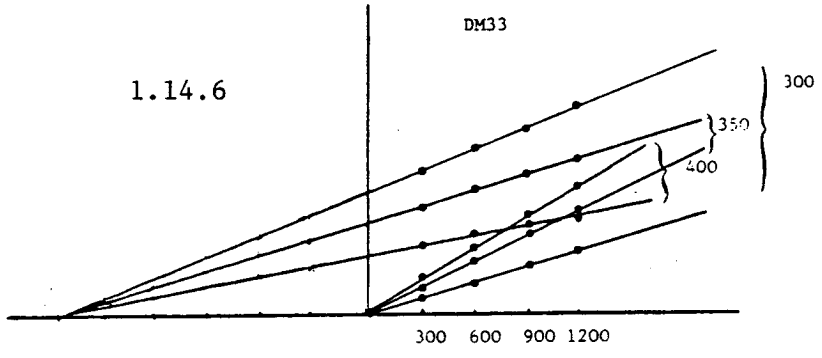


Fig.1.14 a, b, -1, -2, -3, -4. 1st and 2nd Build-up Curves of some TL Dated Samples





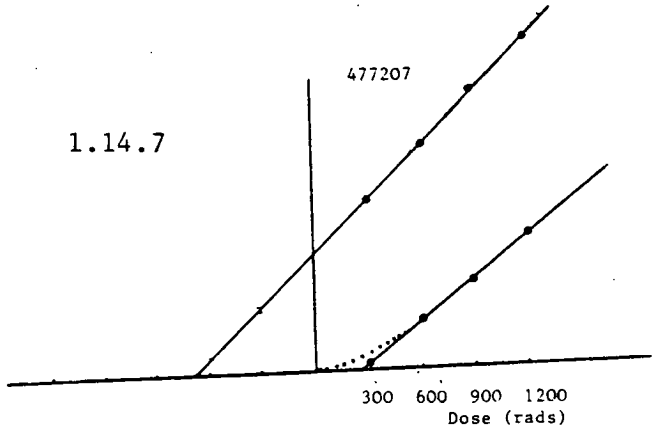


Fig. 1.14.5, -6, -7. 1st and 2nd Build-up Curves of some TL Dated Samples

1.15 General Conclusions on the Above Three Experiments

From the above results it is evident that:

i) the different annealing temperatures give different intercepts, I, of linear or supra or superlinear form.

ii) The different simulation beta doses for the same temperature peak does not alter the intercept I at least for small added doses.

iii) If there is no crystal sensitivity change by heating to 500°C, and the normalisation of the 1st and 2nd build-up curves is done on NTL, then the "parallel slope" criterion is satisfied.

iv) If the normalisation factor is different, we obtain different slopes for the 1st and 2nd build-up curves: The 2nd build-up curves remain the same when we normalise with NTL and the 1st build-up curves change slope according to the normalising factor.

1.16 Review of Mechanisms on Supralinearity

As shown above, the non-linear TL response for the initial doses is an important factor in dating. Some generally accepted important mechanisms are as follows:

i) Trap creation - Cameron et al (1967)

ii) Competition during irradiation between deep and low traps - Tite (1966), Suntharalingam and Cameron (1969)

iii) Enhanced availability of luminescent centres. This is associated with the trapping process during radiation and the enhancement of the probability of luminescence to occur, Zimmerman (1971b), Claffy et al (1968)

iv) Increased number of activated luminescent centres. This holds especially for the 110°C peak, Zimmerman (1971c). (extension of iii)

v) Strong dependence on ionisation density at low X-ray energy, Suntharalingam and Cameron (1969), Zimmerman (1972)

vi) Dependence on dose rate, Aitken et al (1968d).

vii) Luminescent F-centres, produced along the tracks of beta particles where holes are trapped at centres nearby the tracks. Claffy, (1968).

1.16.1 Some possible mechanisms responsible for the non-linear TL response

In general, any alteration to the distribution and electron trapping capacity of lattice defects in the quartz/feldspar grains responsible for the TL signals observed, will introduce TL sensitivity changes. Because these changes (supra/superlinearity) occur only for the initial 300 rads, approximately, with subsequent linear response We suggest possible mechanisms occuring for the initial and linear parts of the second build-up curve. We shall try to describe mechanisms based exclusively on temperature which was the only parameter which varied in the present investigations. Another consideration is some type of crystal lattice with its associated impurities. Therefore, it is reasonable to try to give an account of what happens in the crystal's dynamic equilibrium before and after any heat or radiation treatment:

i) At first, the excitation of electrons into existing traps, such as, lattice defects and impurity atoms, is caused by irradiation. The main requirement for emission of light (photons), is that the system should not be in equilibrium. This deviation from equilibrium requires some form of excitation which, in our case, was heat. This emission of light, or radiative transition, is expressed as the rate of photon generation per unit volume. Otherwise, from the TL point of view, in the excitation by electrons or γ-photons the crystal must emit secondary electrons for each primary electron captured and dispose the residual excitation

energy as photon or heat conduction in order to restore the status quo. Therefore, since TL involves thermally released electrons, the luminescent site may be a vacant electron trap or a thermally stable hole centre. If an excess of primary electrons is retained by the crystal, the excess electrons act as a chemical reducing agent and give the crystal a net negative charge which tends to repel further primary electrons. This could happen for the initial absorbed radiation dose which might produce a negative space charge in the outer surface of the grain, due to crystal edge deformation and thus easy accommodation of lattice defects, where the surface cations and anions might function, respectively, as donors and acceptors and may act as compensated pairs.

ii) Heating to 500°C may produce phase change in the quartz as already said in earlier pages.

iii) Another alteration during the different annealing procedures could be the interaction between impurities (Li, Al,Fe for SiO_2) or competing traps with a large cross-section and the surrounding crystal - the deformation potential.

These will re-arrange the distribution of TL traps and thus the emission of TL peaks will shift. Such dislocations usually occur at the edge of an extra plane of atoms, which could be the enhanced availability of luminescent centres, (supralinearity). It may also be that the low energy secondary particles (photons or electrons from the ionisation of crystal) are more susceptible to losses rather than the high energy particles, caused by: a) certain surface impurities, and b) temporary or permenant crystal imperfections. This, of course, depends upon the total number of electrons per unit volume. The distribution could be that which produces an enhanced availability of traps, hence an

increased TL sensitivity (TL/rad), for the initial doses til there will be a completion of these extra traps (supralinearity.) This creation of a permenant or temporary effect or a state of impurity distribution is, of course, a function of annealing temperature as the annealing experiments above have shown.

iv) Another reason for increased sensitivity could be the removal of competing non-radiative centres, which become occupied during the first 300 rads, approximately. These non-active traps may be self-trapping electrons in thelattice (localised excitations), during the radiation dose. This is due to the interaction of the existing electrons from the valent band or from the centres in the crystal lattice via its electrical charge, with the ions of the lattice creating a local deformation field. (The electron and the associated strain field is called a polaron.)

These"localised excitations" are a function of absorbed dose in the crystal, the impurities present and the lattice situation since the last firing temperature. Therefore, they could produce a strong "interaction" or otherwise some of the electrons coming from the first 300 rads, approximately, are not attributable to filling traps, but are inactive and do not re-combine with centres during the read-out process. These centres may be of a particular kind and position in the arrangement of the lattice.

v) Some of these "killers", say, of TL light for the first rads could be excitants or mutual interaction and inter-transferrance of emitted and absorbed energy between R, M, F, etc.

vi) Quantum statistical process is another mechanism, where possible "tunneling" transition depends on the thermal probability of occupancy of the initial vibrational state, for example, multi-



phonon radiationless transition, photon absorption, following phonon absorption.

vii) Stochastically, the process for "superlinearity" starts with the absorption of the first rads by the non-irradiated processes. Later on, with increased radiation doses, the TL emission is linear because of the linear filling and re-combination of the rest of the traps. The "free-carriers" are not involved in the first non-active transitional processes, but follow the law of absorption-emission, between the main meta-stable energy levels. These initial processes, depend on the kind of non-radiative processes which follow an exponential curve.

viii) For the "superlinearity", also, the decrease in TL/rad for the initial few rads of radiation could be due to thermally unstable hole centres. Anion vacancies probably trap free electrons and, as a result, could provide sites for important radiationless processes. The new creation of centres, sometimes being annealed with the second heating to 500°C. Therefore, on heating, the released electrons go via the conduction band to radiationless sites resulting in sensitivity decrease by dose, until these sites will cease to exist by being filled thus the curve becomes linear.

P A R T II

II.1 INTRODUCTION TO THE CONTENTS

Part two deals with the determination of beta dose rates in ceramics. Chapter 2 investigates the possibility of using the quartz grains themselves as a build up dosimeter as well as the correct procedure for measuring the betas in ceramics of different thicknesses. The results presented extend the discussion on different aspects concerning the significance of correct beta measurement in the quartz inclusion technique, which was used to date the materials studied here.

Chapters 3 and 4 examine the alpha counting method - one of the methods used in the present TL dating programme - stating its advantages and its disadvantages on aspects concerning radioisotope secular equilibrium radon emanation problems and the induced, possible systematic or random errors in the final calculation of beta dose rates. The way of grinding down the potsherd and counting is examined with an assessment being made of the significance of grain sizes against the number of alpha particles recorded by the alpha counter.

Chapter 5 describes the TLD (by $CaSO_4$:Mn) method used in most of the samples in order to determine their beta dose rates. In particular, the possible systematic or random errors induced throughout the procedure which would upset the final dose rate results are discussed. This part terminates with a brief account of the two above mentioned methods by comparing them and choosing the most appropriate method for dating purposes.

II.2 A Brief Outline on Dose Rates: Their Meaning and Significance to TL Dating

It is a necessary task to outline briefly the meaning andsignificance of the dose rate evaluation to the thermoluminescence dating of our samples, since Part II and Part III discuss these a great deal,

before using them to date the archaeological samples.

There are two steps in evaluating the dose rate that have been responsible for the latent TL which has been carried by the mineral grains in the fragment of pottery that is being dated. The first step is the calculation of therate at which radioactive energy is released, per unit weight of material, subdivided into the components carried by radiation of different penetrating powers - alphas, betas and gammas; additional to these there is a small cosmic ray contribution. On the infinite matrix assumption, the dose rate is obtained by equating energy absorbed to energy released. The second step is concerned with making allowance for deviation of the actual dose rate in the TL grain from the average obtained on the infinite matrix assumption.

The division of the dose rates into alpha, beta, gamma and cosmic components is necessary for three reasons:

i) because the TL/rad of deposited energy is substantially lower for alpha particles than for the other types of radiation;

ii) because of large and small scale inhomogeneities in the radioactive content - of which soil versus pottery and the clay matrix with quartz grains are the most obvious examples.

iii) because inhomogeneities in the mass absorption coefficient mean that one material may absorb more dose than another, for example, water, clay composition. This aspect can be conveniently termed rads/röentgen and the most important effect here is in respect of the water content of the pottery and soil; the rads/roëntgen for water are higher than for pottery and soil by: 50% for alpha particles; 25% for beta particles and 14% for gamma radiation. In order to evaluate such figures (which are taken from Zimmerman, 1971), one needs

to know the energy spectrum of each component, though the spectrum dependent effects are not so strong as to make it unrealistic to carry out discussion and to use the energy spectrum in terms of the four radiation components. Basic values for the rate of energy release per unit weight of parent radioisotopes are discussed by Bell, (1976, 1977) and Carriveau, (1978).

CHAPTER 2

BETA DOSIMETRY OF CERAMICS

2.1 Review of Beta Dose Rate Evaluation

Application of thermoluminescence (TL) phosphors for determination of the radioactivity of ceramics and other materials used for TL dating was first proposed by Aitken, (1968).

The principal advantage of thermoluminescence dosimetry (TLD) over those methods based on the determination of radionuclide concentrations (alpha counting, neutron activation analysis, fission track), is that it involves no assumption of equilibrium of long-lived radionuclides for the archaeological periods considered. Because of the mobility of uranium and the long half-lives of U-234 and Th-230, equilibrium cannot be assumed for clay sediments younger than one million years. However, though there is a slight dependence of the TLD standard materials on such secular equilibrium, the effect is not pronounced (see Section 2.15 below). Furthermore, TLD gets around the problems of calculating the absorbed dose (which is needed, for example, in alpha counting.)

2.2 Review of Previous TLD Systems

Several TLD methods for the determination of beta radiation in ceramics have been proposed. A quick resumé of those techniques now follows:

2.2.1 In the first TLD system for pottery dosimetry considered by Aitken, (1968), a pellet of $CaSO_4$:Mn was sandwiched between two fragments of pottery; this allowed a convenient determination of the beta dose rate at the surface of the sherds. Aitken further attempted to measure both alpha and beta radiation by mixing finely powdered clay with $CaSO_4$:Mn powders However, the alpha dose rate could not be measured with sufficient accuracy by this technique, because of the attenuation of the alpha particles by the phosphor grains.

2.2.2 The principle of mixing the clay with a TL phosphor was continued and further elaborated by Fleming, (1968, 1970) and by Aitken and Fleming, (1972), for determination of the beta dose rate in conjunction with the quartz inclusion technique. The TL phosphor was natural calcium fluoride (fluorite of a grain size similar to that of the quartz inclusion - about 100μ.) Prior to mixing, the outer layer of the grains were desensitized by heating the grains in humid air, which allowed elimination of the alpha contribution. The mixture of clay and fluorite was contained in a nylon capsule that was sealed in order to prevent escape of radon. After a few months exposure, the fluorite grains were recovered by sieving. Calibration was effected by exposure to Sr-90 beta radiation. Fleming's method is somewhat inconvenient, but it has the great advantage that attenuation of the beta radiation by the grains is automatically taken into account.

2.2.3 In the system described by Mejdahl, (1972), the pottery clay was contained in thepolyethylene bag, and the beta dose rate at the surface was measured by means of $CaSO_4$:Mn dosimeters attached to the bag. The dosimeter was a metal planchet with a depression in which the phosphor was fixed with a heat-resistant silicone resine (Dow Corning ms. 805.) The planchet also served as a heating element in the TL measurements. This technique allowed very precise measurements, doses as low as 1 mrad could be measured with a standard duration of less than 1%. This method had the drawback that the calibration of the dosimeter response was not absolute. Calibration was accomplished by comparison with the response of the dosimeter to Co-60 gamma radiation; but one parameter, the thickness of the layer of polyethylene foil between the dosimeter and the surface of the bag ($30mg/cm^2$) had been fixed by dating sherds of known age.

The technique was tested in an extensive programme in which the determination of the archaeological dose was based on feldspar inclusions, Mejdahl, (1972). Generally, the deviation of the TL dates from the known dates was less than 10%, but occasionally larger deviations (both positive and negative) occurred.

2.2.4 For the quartz inclusion and fine grain techniques, a TLD system that gives the beta dose rate has been developed by Bailiff et al, (1974). In this system, the clay is held in a non-sealed perspex container (volume 10cm^3), equipped with a thin window(125μ) of melinex foil. The dosimeter is a thin copper fluorite encapsulated in silicone resin (Dow Corning ms. 805). The system is calibrated by means of standard matrices (KCl and Thorium,Uranium minerals), with known concentrations of radionuclides and a quartz matrix is used for determination of gamma background radiation andphosphor of self dose. The dose rate at the position of the tray was related to the dose rate at the centre of each matrix by mixing the centre portion of the matrix with desensitized grains of calcium fluoride. The absorbed fraction of the gamma radiation emitted by the radionuclides in the clay was evaluated by means of a matrix of Zn-65, which is essentially a gamma emitter of energy 1.14 MeV.

The percentage error involved was variable between 5 - 16%.

2.2.5 McKerrell and Mejdahl, (1976) described a somewhat similar approach that was utilised for measurement of beta radiation from Glozel ceramics,Françoiset al, (1977). It is extensively described in Chapter 7.

2.2.6 In a revised beta TLD system, Mejdahl, (1978) modified his previous system of calibration now using a radioactive standard containing known amounts of Thorium, Uranium and Potassium mixed with a non-radioactive material. The method thus allows a reliable estimation of attenuation of the beta dose rate in pottery.

Assuming uncertainties of 10% for the thorium and uranium dose rates and 2% for thepotassium dose rate, the resulting uncertainty of the dose rate of the primary standard is less than 3%. The inter-comparison of the archaeological samples with the standard samples can be made with an uncertainty of about 3%. The abundance of radio-nuclides in the archaeological samples may differ somewhat from those in the standard clay, but unless the relative dose contribution from the potassium is very low, the effect of this variation will be negligible.

Uncertainties of the order of 2% will be associated with the correction of the measured dose rate for the effect of water and for attenuation by the quartz grains.

The final resulting uncertainty in the beta dose rate experienced by quartz grains embedded in pottery, estimated from the uncertainties considered is about 5%.

It must also be kept in mind that only the present day dose rate can be determined and this would not be representative if there has been a significant exchange of radionuclides between the sherds and the surrounding soil and water during the archaeological period. (This applies for all the above methods). In fact

Hedges and McLelan, (1976) have shown that the cation exchange capacity of fired clay is not negligible.

Summarising, all the above systems show uncertainties in the determination of standards, differences in the stopping powers of quartz in pottery and the phosphors used, differences in counting geometry with regard to potsherd thicknesses and the beta ranges, variations of relative abundance of radioisotopes as compared to that of the calibrating sample, radon problems, and its diffusion through the powdered pottery sample and solid pottery, natural water content of the pottery. The deviations of TL ages of samples which could be well dated archaeologically could well be attributed to errors in measuring the internal beta dose rates in the samples.

The following section describes a new version of beta dosimetry of pottery by measuring betas directly with quartz and the errors involved in the beta dosimetry procedure for ceramics.

2.3 Microdosimetry of Quartz: A New Practical Approach

Presented here is a practical approach to the "quartz microdosimetry technique", based on the 110°C low temperature peak of quartz, kept at liquid nitrogen temperature to prevent fading. As proposed by McKerrell & Mejdahl (1976), this work was done anticipating many advantages for the technique and with various objectives in mind, related to the absolute determination of beta dose rates for quartz grains inside a given pottery. The results pertaining to the above are discussed in section 2.6 and 2.10. (Liritzis & Galloway, 1979). Further studies related to the above objective were carried out concerning the simulation of potsherds and clay powders ~~which consisted~~ of different thicknesses, being in dry and wet states and having been fired at different temperature, Section 2.11 to 2.14.

2.4 Experimental Arrangements

Complementary notes with reference to the procedure of firing the clay to background readings and to the read-out manner of the phosphors are given here as they apply to each of the following experiments.

2.4.1 Procedure of firing the clay Cylindrical holes of diameter 3cm and depths 0.8, 1.3 and 2.3 cm were made on wooden tray. These holes were filled with powdered clay sieved to under 75μ and moisturised with water for the clay to acquire its plasticity. These samples were heated to 100°C when they contracted due to the loss of absorbed water. Afterwards, the samples were fired at 500°C, 750°C and 1000°C, for two hours at each temperature. This resulted in the loss of

water (lattice or structural water), as the dehydration product of the chemical reaction:

Kaolinite $Al_2O_3.2SiO_2.2H_2O \xrightarrow{T^oC} Al_2O_3.2SiO_2+2H_2O\uparrow$, Salamang, (1961).

It has been found by thermo-differential analysis(TDA)on the Glozel clay that this happens between 500°C - 600°C, McKerrell et al, (1974). This slow loss of water, however, is accompanied by contraction, that is, a continuance of shrinkage. The above pre-heating at 100°C also reassures uniform heating of the samples, since too rapid firing may open up the texture caused by shaping and create cracks at the subsequent high temperatures. The shrinkage then of the clays on the wooden cylindrical holes for the above temperatures was obvious, and the shape after removing them from the surface and cooling them down was as in Fig. 2.4.1a

These, then, were made in the desired size of 2.8cm diameter, and thicknesses of 0.5, 1.0 and 2.0 cm, (fig. 2.4.1b)

2. 5 Background Reading. The background dose on quartz and $CaSO_4$:Mn readings was evaluated by using a cylindrical ring filled with under 75μ quartz and 20% by weight fine sifted sand of a size between 75 - 106μ, specially annealed at 500°C for 1 hour. In the centre of the ring, a pair of the phosphors in discs were placed.

It must be emphasised that the teflon discs placed in themiddle of the cylindrical rings were exposed to a radiation field of 4π geometry, while the quartz grains near the edges do not gain the same exposure as those from the centre section, Fig. 2. 5.

2.5.1 Read-Out Manner of the Phosphors. Comparisons are made taking the averages of the two discs in the same cylindrical ring between the centre facing sides of the discs and the outer facing sides of the

Fig. 2.4.1 a

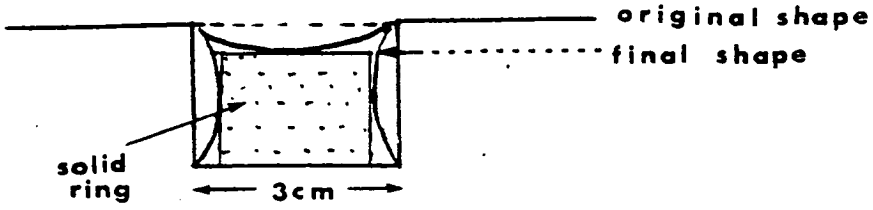


Fig. 2.4.1 a Shrinkage of clay frame after firing

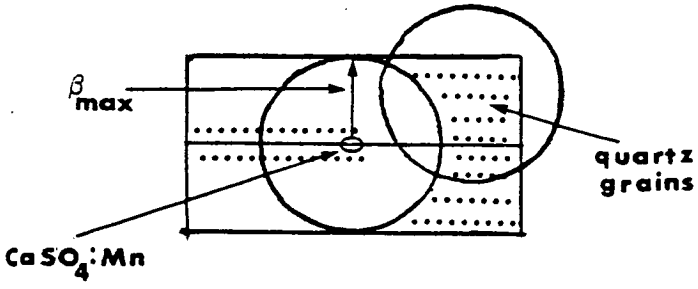


Fig. 2.5. Geometrical situation of the β-irradiated quartz and phosphor inside the ring.

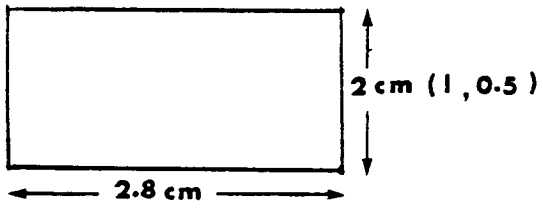


Fig. 2.4.1 b Final size of Solid Ring made by the fired clay

discs and the outer facing sides of the corresponding disc from the pair. The centre facing sides gave 18.1 mrads on average and the outer facing sides gave 19.4 mrads on average, that is app.7% higher dose from the centre facing sides. The reading from the centre facing disc corresponds to the centre facing disc of the mixed pair readings and the reading from the outer facing disc corresponds to the outer facing disc of the mixed pair readings. A single disc gave a higher reading than either combination of the above discs. This was of the order of app. 10%. In my experiments, the outer faces were taken as giving the "real" dose without attenuation effects.

2.6 Measurement of Beta Dose With Quartz Grains and $CaSO_4$:Mn Phosphor

Experiment (1)

Quartz, as is well known, has a low temperature peak with a sensitivity sufficient to measure doses in the mrad region, Fleming, (1973). In quartz, the 110°C peak can be activated to a high sensitivity by irradiation of the sample with a large dose (of some 20 Krads) and subsequent heating to 500°C or by annealing to 500°C for some hours. Since the peak is not stable at room temperature, the pottery samples must be stored at a low temperature during the irradiation period, and the subsequent preparation for measurement, (cleaning, etching, etc.,) must be timed accurately. Results of calculations of the stability of the 110°C quartz peak at various temperatures are summarized by McKerrell & Hejdahl (1976). The sensitivity of the low temperature peak in quartz grains used in the present experiment was as follows:

mg	mrads	counts	SD
50	21	15000	0.8%

The quartz was taken from a fine sifted geological sand, purified by acids, sieved between 75 - 106μm grain size and washed with HF and HCl

for 20 mins and annealed to 500°C for 2 hours.

This showed an enhanced sensitivity and stabilisation of the response of the 110°C to the subsequent 500°C read-out with a heating rate of 21 °C/sec. Such treatment upsets totally the pre-dose.

Therefore, the determination of the beta dose rate is carried out on identical grains and grain sizes as for the measurement of the total archaeological dose. Three cylindrical rings weremade from aluminium with a diameter of 2.8cm and thicknesses of 2cm, 1cm and 0.5cm, respectively, Fig 2.4.1b above.

Clay powder from Glozel area (section 2.4.1 above) was prepared by grinding down and sieving to 75μ and under. This clay powder was annealed to 500°C for 2 hours. The cylindrical rings of Fig. 2.4.1 were then filled with this powder. (2 pages above)

A pair of $CaSO_4$:Mn in teflon disc phosphors were placed in the centre of the rings, previously having been annealed to 300°C for 2 hours. This pair of phosphors was sealed with a double layer of sellotape, (that is, cellulose acetate-tri, $\rho = 1.267$ gr/cm^3 and A = 288.25). 20% of the powder weight of each respective ring was replaced by quartz grain. All the prepared rings were then sealed in a glass tube which was then kept at liquid nitrogen temperature for 25 days. The quartz grains were then separated from the powdered clay by sieving and while still cold, washing on watch glass in air. This procedure was timed accurately to last for 3 minutes, so as to reduce the possibility of fading which is less than 2% per minute.

A sample of the quartz grains of around 20 mg was then placed onto the heating strip and read out. The rest were kept in a black polypropylene container and placed in a glass tube, inserted in a liquid nirtogen container. It was observed that after repeated reading of the quartz samples, to 110°C signal increased by time. This enhancement was of irregular increase, but inclined towards higher values and varied from 8 - 75% after the first 3 - 5 readings had been taken. This was probably due to the condensation of water from the air on to the surface of the cold grains. It was also observed that the wet grains give an enhanced 110°C signal due probably to the creation of surface centres by the disociation of H_2O molecules to HO^- and O^{2-} on heating to 130°C, the read-out temperature. The heating to 130°C produces thermal vibrations to the cold grains, which may cause diffusion of the OH^- ions and increased reactivity at surfaces whose equilibrium has been disturbed. Such diffusion is possible, however, in the case of quartz with its imperfect structure, including anionic and cationic defects at the surface. Hence, caution was taken not to allow condensation on grains when taking them out of the tube from the liquid nitrogen dewar, by immediately sealing the tube with a rubber bung to prevent air producing moisture on the grains surfaces.

2.7 Results and Discussion of Experiment (1)

A comparison is attempted between the TL signal in mrads of the 110°C quartz peak with the $CaSO_4$:Mn for the different thicknesses of the clay powder in the cylindrical rings. The results are expressed as ratios of these two readings, Table 2.7 A.

TABLE 2.7A

Thickness(cm)	110°C*	TLD(mrads)	Ratios
0.5	13.4±0.65	13.3±0.79	1.007±0.09
1.0	15.4±0.67	14.7±0.82	1.04 ±0.06
2.0	17.4±0.70	15.8±0.87	1.10 ±0.05

Beta doses for the 110°C peak of quartz and $CaSO_4$:Mn phosphor in the powder cylindrical rings of 0.5, 1 and 2cm thicknesses

TABLE 2.7B

Thicknesses (cm)	Solid (T=500°C,2^h)	Powder	Powder + 20% grains
0.5	17.9±0.1	15.5±1.3	Lost
1.0	23.5±0.5	21.1±0.8	18.2±0.2
2.0	24.6±0.7	24.0±1.5	20.5±0.2

Beta doses for the $CaSO_4$:Mn phosphors in the solid and powder cylindrical rings

* The potassium content of the powdered clay was 3.62% K_2O (3.00% K), as measured by XRF. The alpha counting of this clay <75μ, was 103 alphas per 10^4secs. These gave an infinite beta dose equal to 454 mrads/yr.

TABLE 2.7C

Temperature 0°C		Dry Dose(mrads)	Wet Dose(mrads)	Density	D/W dose	Wet/Dry by Weight
	1,000	24.8±0.3	21.7±1.1	1.66	1.142	1.187
1cm	750	25.2±0.2	15.8±0.1	1.55	1.895	1.414
	500	23.5±0.5	17.5±1.5	1.64	1.342	1.193

Beta dose for dry and wel solid cylindrical rings.

TABLE 2.7D

Temperature 0°C		β_{wet} measured	Estimated
	1,000	21.7±1.1	20.1±0.1
1cm	750	15.8±0.1	16.6±0.1
	500	17.5±1.5	19.0±0.1

Beta doses as measured experimentally from the wet solid cylindrical rings and estimated theoretically based on the formula (4)

Also the $CaSO_4$:Mn readings and the 110°C peak of the quartz grains (20% by weight diluted in the powder ring) are not comparable as had been expected. This is due to:

i) the fact that the quartz grains and the phosphor are exposed in a beta radiation field under different geometries. The teflon discs placed in the middle of the cylindrical rings are exposed to a radiation field of 4π geometry, while the quartz grains near the edges do not gain the same exposure as those from the central section. If a clay layer was surrounding this clay powder with the grains distributed in it, then the quartz grains would have had a full 4π geometry and would be comparable with the TLD phosphor. Therefore, theratios of the table imply a comparison of the grains with thephosphor in the particular case where a potsherd is found in a site with a blank radioactive medium surrounding it, say, in a calcium carbonate medium.

ii) the way of calibration of the TLD phosphors which was done by normalising the discs with a monitor dose from a Co-60 source.

iii) the number of delicate considerations as regards the build-up and attenuation of gamma radiation in the discs and grains. Further, $CaSO_4$:Mn has a high γ-energy dependence due to its high effective atomic number ($\overline{Z}$ = 23). (our Co-60 gamma source was calibrated on quartz grains through a Sr-90 beta source at the Risø irradiation facilities).

This gave a dose rate of 3.62 mrads/min, while it was 3.42 mrads/min for the quartz. Additionally, the calibration of $CaSO_4$:Mn discs on a Co-60 gamma source underestimates the beta dose received by the phosphor, (due to its high response to gammas.) This has been obtained in the TLD results of Chapter 7 when the TLD readings were converted

to actual beta doses based on a standard sample. Further, the difference in stopping powers between quartz and $CaSO_4$:Mn for 0.5MeV electrons is approximately 3%, (calculations were based on formula of Chapter 6), despite the great difference in their effective atomic numbers, (Z_{SiO_2} = 10.8 and Z_{CaSO_4} = 23). Although the high betas from the clay pass through the 0.8mm thickness of the teflon disc, the thickness could have a small additional effect on the absorbed dose (or energy deposited per unit volume), by the phosphor as compared to that of the quartz grains of 90μ average diameter. This would increase slightly the stopping power of the $CaSO_4$:Mn.

iv) Also, the double layered sellotape (of 0.12 mm thickness), covering the teflon disc cuts off alphas (of average energy 3.7 MeV) and stops betas under, approximately, 0.1 MeV, as well. This energy region of 0 - 0.1 MeV is approximately 2% of the total beta energies.
However, a compensation for TL production would well be assumed, though an uncertain error is involved.
Table 2.11 gives the ranges for alphas and betas in the sellotape, and their role in TL contribution, therefore, can be seen.
It should be pointed out that this experiment was done with the objective of making comparisons, rather than to get results for dating. Therefore, the calibration was not so important here.
From the above, preliminary results, the use of the 110°C quartz peak seems to be applicable to routine internal dose measurements. However, for future use of this peak, in the determination of beta dose rates in ceramics, the calibration must be done not with the use of a Co-60 source, but with standards (as was done for TLD dosimetry, see Chapter 5 Section 5.2 .)

TABLE 2.7.1

	Energy(MeV)		Range R_{air}(cm)	Range $R_{cellul.}$(mm)
*	alphas	3.7	2.2	0.094
		5.0	3.2	0.137
**	betas	0.5	-	1.36
		0.2	-	0.30
		0.1	-	0.09
		0.05	-	0.02

* Alpha ranges were calculated from the formula $R = 3.2 \times 10^{-4} \sqrt{\frac{As}{\rho}} R_{air}$

** Beta ranges were calculated from the formula $R = 0.11 (\sqrt{1+2.24E_o^2}-1)$ for $0<E<3$MeV by Flammersfield (Seighbahn, 1955)

2.8 Fading of 110°C Peak at 0°C

To remove the surface alpha dose received by the quartz grains from the clay matrix, the grains must be etched in HF after sieving. As this cannot be done at liquid nitrogen temperatures, experiments have been carried out to see how much loss of TL signal occurs during handling prior to the TL measurements.

A part of the quartz grains in one of the powdered clay discs which gave a beta dose of 16.6 mrads, was divided into four equal parts and kept in black polypropylene bottles with HF pre-cooled at 0°C in a freezer. These four bottles were placed in a dewar filled with ice to produce the 0°C temperature which was kept constant throughout the experiment, and checked by a low temperature thermometer. Each time one bottle was taken out of the dewar and the quartz grains transferred ontoo a watch glass, by rinsing the bottle with pre-cooled (at 0°C) acetone. Within ≈3 minutes, the sample had dried and was then quickly measured in order to minimize fading at room temperature. Table 2.8.1 lists these results. The second column of the table lists the reduction in the radius due to the etching, calculated on average diameter of grains before and after weighing them and assuming the grains to be spherical. The fourth column of this table shows the remaining percentage of TL from the initial signal of 16.6 mrads. This is due mainly to the fading of the signal at 0°C, as is explained below. It has been calculated (Nickerell & Mejdahl, 1976), that the fading of the quartz 110°C peak at 0°C is less than 2% within 20mins.

A beta radiation reduction produced by the effect of HF acid etch accounts for a further 1%.

TABLE 2.8.1

initial TL signal = 16.6 mrads ±0.065				
Time at 0°C in hours	Radius reduction Δr(μm)	Dose (mrads)	% TL Loss	% Fading
0.5	2.5	15.4±0.12	7.2±0.80	7±0.28
1.0	3.4	14.9±0.12	10.2±0.09	10±0.40
1.5	4.3	14.6±0.11	12.0±0.11	13±0.52
2.0	5.5	13.7±0.10	17.5±0.16	16±0.60

TABLE 2.8.2

initial TL signal = 18 mrads	
Time at 0°C in hours	Ratios of Initial and Subsequent Signals
0.5	0.923
1.0	0.882
1.5	0.880
2.0	0.854
2.5	0.823
3.0	0.750

TABLE 2.10.1

Stability of the 110°C peak in quartz at different temperatures. Assumptions:
first order kinetics;
trap depth = 0.99eV;
frequency factor s = $1.7 \times 10^{15} sec^{-1}$ (for 0°C)
and $8 \times 10^{12} sec^{-1}$ for 20°C
life time at room temperature = 1 min
K = Boltzman's constant, $8.6 \times 10^{5} eV/°K$

Temperature (°)	Life time (fading less than 2%)		*Time in hours of 100% fading
20	1.0	min	3.99
18	1.47	min	5.20
0	20.0	min	16.00
-25	22.0	hours	-
-50	174.0	days	-
-70	80.0	years	-
-197	1.1×10^{43}	years	-

*These theoretically found results substantiate the respective experimental results for temperatures of0°C and 18°C (see Figs 2.10a,b). (5 pages on)

This observed signal reduction within the statistical error of measurement is then explained as thermal fading rather than TL from alpha contribution of the surrounding clay. A certain alpha contribution is very small to be confused with the statistical error of the measurements. Otherwise, the intrinsic inefficiency to the alpha radiation of this peak has been determined by Fleming(1969) using the quartz annealed at 500°C for 15 minutes, following the disc deposition technique of Zimmerman, (1968). This "K-value" was evaluated as $K = 0.010 \pm 0.001$. To appreciate qualitatively this low value, the model of the nature of dosages proposed by Aitken et al (1967), is recalled whereby the track of the alpha particles is treated as a region of localised ionisation causing saturation of the TL traps in the region of such a track.

The less than 2% fading of the 110°C peak within 20 mins at 0°C tested by irradiated quartz with 18mrads, (normalised by a monitor dose), and subsequently stored at 0°C for various times. Table 2.8.2.(1 page above) The first 3 mins of fast chemical reaction must occur which raises the temperature of the grains and so reduces the TL signal faster than is predicted, theoretically. Afterwards, the observed signal is similar to the predicted one (with $\leqslant$ 2% within 20 mins), within 2σ, see also section 2.9, below. (2σ systematic error, according to operators estimations The subsequent read-outs of the same quartz sample gave the same reading within 1σ, so we exclude any pre-dose effect which could confuse the normalisation of the signals by the monitor dose. Table 2.8.2 accounts for 25% fading for 3 hours or $\simeq$2%/20mins, within 2σ,

2.9 Quartz Etching at 0°C and at Room Temperature

By storing quartz grains 75 - 106μ diameter at 0°C and at room temperature,

respectively, inside a polythene bottle containing HF acid, the weight loss and subsequent radius reduction, (calculated on average radius of 45μ), because of HF etching, is shown in Fig 2.9 and Table 2.9.

It is well seen that there is a fast reaction in the first 30 mins and a slower rate later on. The rate of reaction at room temperature is higher than at 0°C. Also, in order to remove the outer 25μ layer of quartz grains (average range of α-energies for Uranium and thorium decay series, Fleming, 1969), we must etch the quartz with HF for 3 hours at room temperature.

2.10 Fading of 110°C Quartz Peak at Room Temperature

observations of the fading of quartz grains at room temperature previously irradiated with 18 m rads are shown in table 2.10. The errors involved are of the order of 5%.

Tables 2.8.2and 2.10 are partially supported by Table 2.10.1 (2 pages above)& Figs 2.10. (a + b).

The calculations were based on first order kinetics and the "life time" at room temperature was taken to be one minute. The fading in this period is less than 2%. The fading over the life times, calculated for lower temperatures, will then also be less than 2%. A trap depth of 0.99eV was assumed, Aitken and Fleming, (1972).

It is evident that storage at liquid Nitrogen temperature ensures the stability of the 110°C peak and at 0°C it has sufficient life time for cleaning and etching of grain samples at that temperature after storage.

However, the etching of the grains is not necessary, since (as shown above, section 2.8), for big grains, the alpha contribution is non-existant; while the cleaning with pre-cooled acetone at 0°C of the cold grains (just extracted from the liquid nitrogen temperature

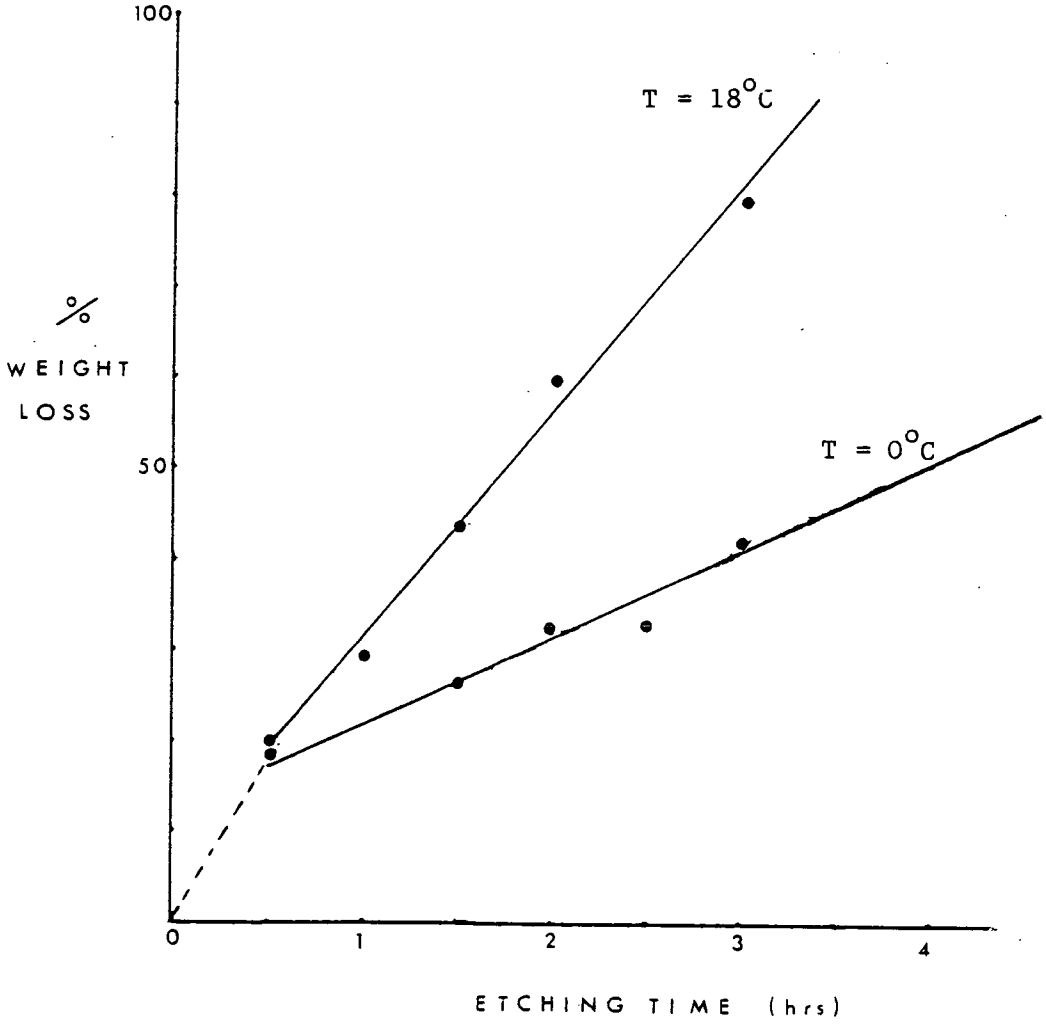


Fig. 2.9 Sand Etched at Two Temperatures

TABLE 2.9

Etching time in hours	% Weight loss at 0°C	Δr at 0°C in μm	% Weight loss at room temp.	Δr at room temp. in μm
0.5	16	2.5	20	3.25
1.0	21	3.4	32	5.5
1.5	26	4.3	45	8.1
2.0	32	5.5	59	11.5
2.5	37	6.4	69	14.5
3.0	42	7.5	83	20.0

TABLE 2.10

Time in minutes	0	47	69
Dose in rads	18	13.9	11
% TL left	100	77	61

Fig. 2.10.a

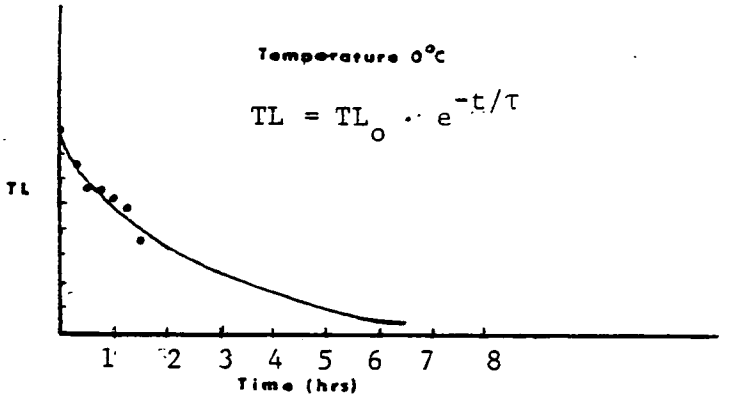


Fig. 2.10.b

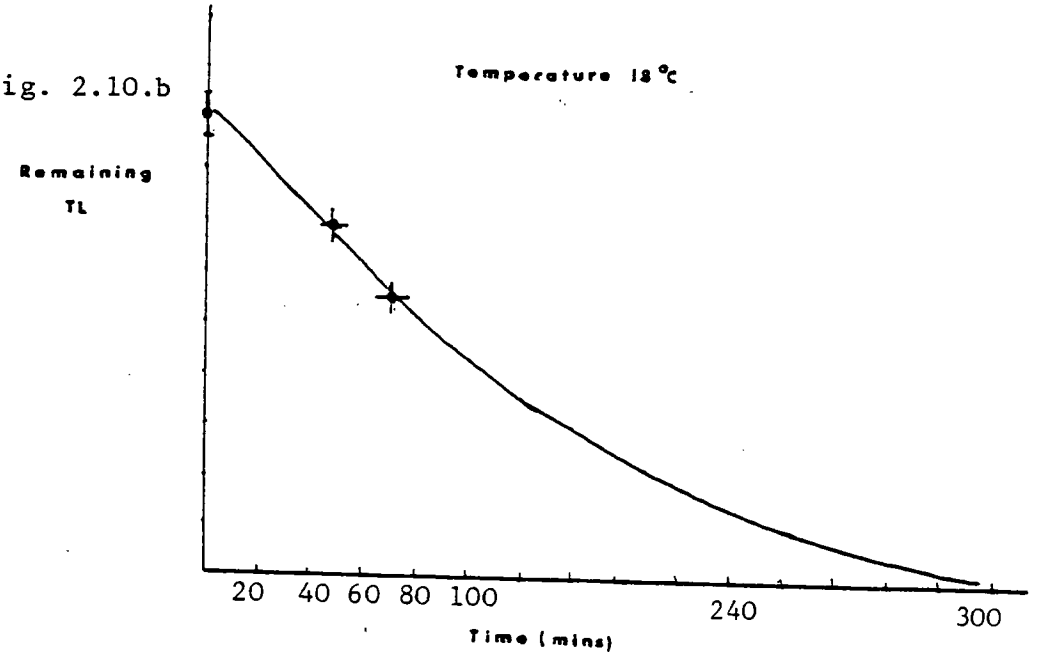


Fig. 2.10.a TL signal decay as a function of time at 0°C. It is obvious that, within 17 hours the signal has completely faded.
Fig. 2.10.b TL signal decay as a function of time at 18°C It is obvious that, within appr. 5.2 hours the signal has completely faded

dewar) excludes any possibility of fading during the grains' preparation time (3 mins, see section 2.5).

2.11 Measurement of Beta Dose on Simulated Potsherds

Experiment (2)

Solid sherds in the form of cylindrical disc of the same size as the powder discs above, but of 1cm thickness and made from the same clay, were fired at different temperatures, namely 500°C, 750°C and 1000°C for two hours in each temperature. Another solid cylindrical disc of 2cm thickness was fired at 500°C.

These solid discs were horizontally divided into two slices, (sandwiched.) A pair of teflon discs were placed in each small depression made at the centre of each slice, the depression being equal in size to the teflon discs and so firmly accommodating them, Fig. 2.11 (5 pages on) One set of those solid discs were saturated with water for 24 hours. All these solid rings were spaced one on top of the other at a distance of 1 cm., interspaced by quartz grains and then they were placed in a glass tube and sealed.

This tube was then kept in a liquid nitrogen dewar for 35 days.

2.12 Results and Discussion of Experiment (2)

The results are as detailed in Table 2.7. (11 pages above) when we compare solid discs of the same thickness of 1cm, but fired at different temperatures, we find that the 750°C solid disc gives a higher dose than the 500°C disc and this correlates with its low density, $\rho = 1.55$ gr/cm^3 (as measured).

At 750°C there occurs a loss of lattice water which lowers the density. In general, the density of the clays undergoes striking changes in the course of heating, (depending on the clay constituent, materials present and the heating rate.) At first, it usually

increases up to 300°C or more, which may be regarded as a corollary of the shrinkage that practically all clays differ above 100°C. Then it falls sharply up to about 700°C, which is due to the expulsion of thelattice water from the clay substance and from 700 - 1000°C, it again increases markedly due to the formation of an α-Al_2O_3 from γ-Al_2O_3 or of aluminium silicate, Salamang, (1961).

This happens because the resistance of the bonds to break down due to thermal vibrations of the atoms is the deciding factor in stability. So, in measuring beta doses of sherds we do not measure infinite beta doses, but doses delivered by the actual sherd, and so we must use the whole sherd with all inclusions rather than powder under a certain grain size.

An indication of increased dose with sherd thickness is shown in Fig. 2.12. Especially the solid discs gave higher doses than the powder discs of the same geometry. This is due to the densification of the clay in the solid form (see section 2.13).

Further, this densification effect is illustrated in Fig. 2.12.1, where the deviation of β-doses from the solid discs (in dry & wet states) that have been fired at different temperatures, that is, 500°C, 750°C and 1000°C, from the β-doses of 1cm and 2cm powder discs.

are plotted against the fired temperatures. The effect could be of the order of 20%. Also, from Table 2.7B, the 0.5cm solid ring gives around 20% less beta dose than thepowder of above 1cm thickness.

The increase of beta dose between 0.5 and 1cm thickness is not exclusively due to the betas, but to the fact that an appreciable self-originating gamma dose isproduced from the solid or powder rings themselves. This gamma self dose depends on two factors:

i) the sherd's radioactivity, and

ii) the sherd's dimensions.

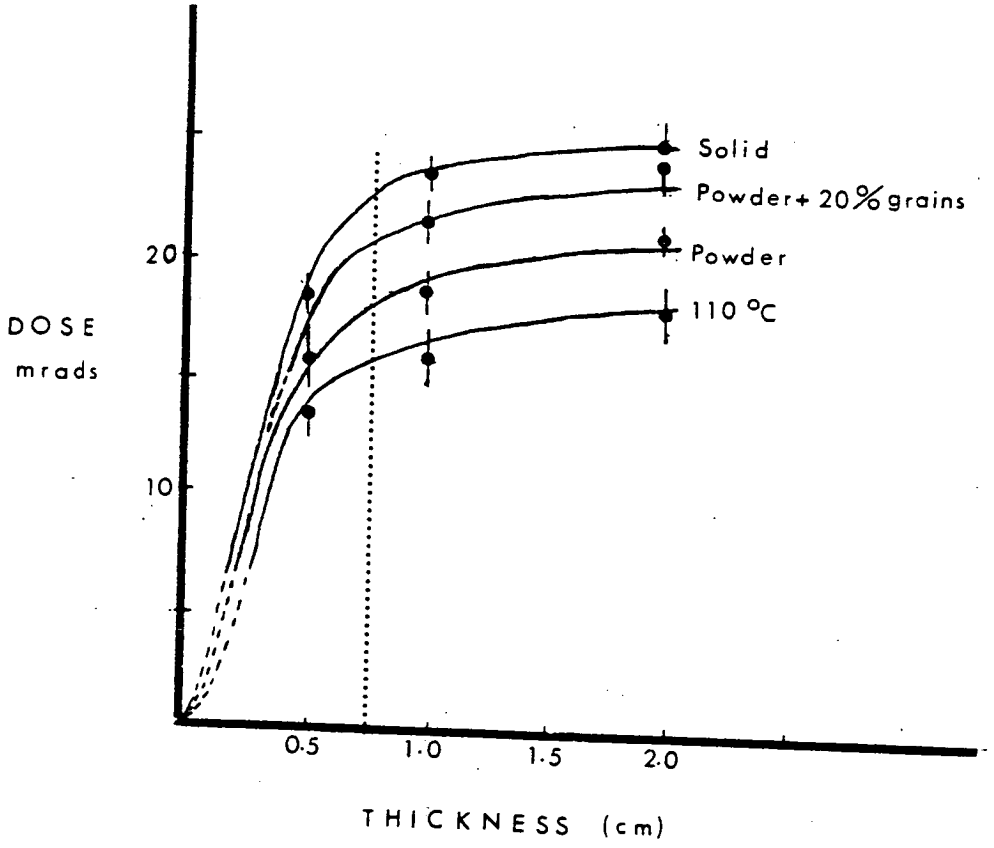


Fig. 2.12 Beta Dose is Plotted against the Thickness of the Powder or Solid disc. Above 0.7 cm, saturation occurs in the Beta ranges (Table 2.12), and an appreciable Gamma Dose (Self-Dose) starts to contribute significantly. The "initial rise" of the curves is expected from the Theory of Distribution of beta ranges and mean path lengths for electrons traversing an absorber.

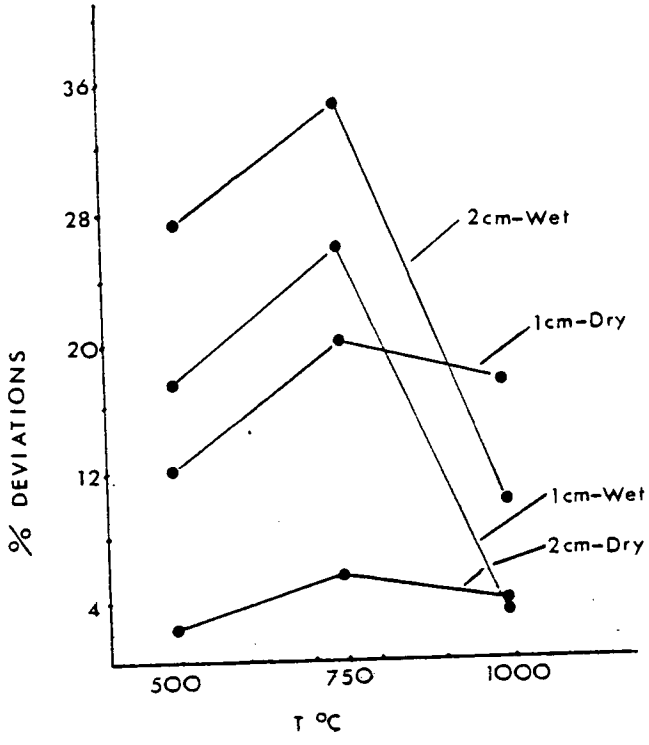


Fig. 2.12.1 The beta doses of the respective firing temperatures are plotted against their % deviation from the 1cm and 2cm powder disc doses. Results obtained are shown in the table below.

	(on Dry Solid Disc)	(on Wet Solid Disc)
	% Deviations from 1 cm powder	% Deviations from 1 cm powder
Temperature		
1000°C	17.5	2.76
750°C	19.4	25.00
500°C	15.4	17.00
	2 cm powder	2 cm powder
1000°C	3.3	9.60
750°C	5.0	34.00
500°C	2.0	27.00

Theoretically, the maximum beta ranges to the clay depends upon its composition and density, (though the variation is small), which however, is smaller than the quartz (ρ_{SiO_2} = 2.65 g/cm^3). Table 2.12 shows the beta ranges for different beta energies to quartz. For average beta energy of 0.35MeV; this range is 0.47mm(Note: More than 90% of the TL induced in quartz comes from beta energies above 100KeV). The maximum beta energy of ≃0.55MeV has a range of 0.89mm.

For clays with a typical composition and density of 1.3g/cm^3 the 0.35MeV betas have a range of 0.822mm and the 0.55MeV betas have a range of 1.55 mm, Table 2.12.1

Therefore, it is unsafe to remove less than ≃ 1.5mm from the outer part of a potsherd, since the betas originating in the soil will contribute to thegrains inside the sherd and this produces further problems in the evaluation of the annual dose rate. Also, Mejdahl (1972).

In reality, when at least 1.5mm of the outer pottery is removed, in the dating programmes, this procedure has a two-fold effect:

i) we do not account for the external betas and hence limit the infinite beta dose to the internal beta dose of the sherd itself

ii) we do not include grains which have not had a full 4π geometry.

So what is measured in theinternal beta dose is that dose which contributes to the grains to be dated. In this case, a phosphor (teflon disc) reading will give the actual dose as it is inside the belt of the Fig. 2.12.2.

2.12.1 Table 2.12.2 also shows the significance of gamma self dose at 1 MeV and 1.5 MeV gamma energies for 0.5, 1 and 2cm thickness of the rings used in the present experiment. For the one month's period, concerned here, this gamma dose can be of the order of 2mrads in the 2cm thickness rings. (Also, Carriveau,pers. comm., reaches similar results working out a theoretical formula.)

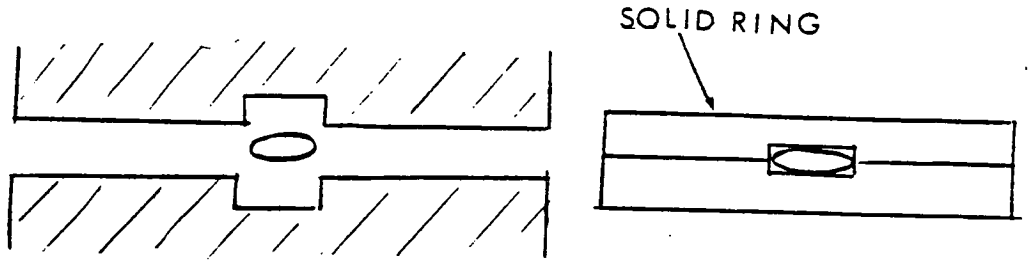
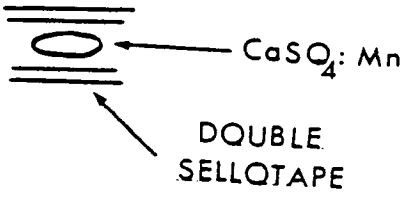


Fig. 2.11



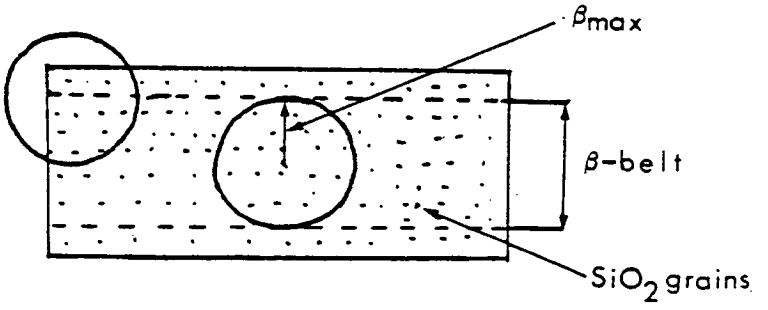


Fig. 2.12.2

Fig. 2.11 Schematic Representation of the Solid Cylindrical Rings with a pair of $CaSO_4$:Mn Phosphors at the centre.

Fig. 2.12.2 Geometrical Arrangement of the Phosphor inside the clay ring spanning the maximum β range.

TABLE 2.12

β-ranges to SiO_2*

Energy MeV**	O = 0.533***	Si = 0.466	gr/cm^3 SiO_2	Ranges μm
0.010	1.544×10^{-4}	1.609×10^{-4}	3.150×10^{-4}	1.2
0.015	3.150×10^{-4}	3.230×10^{-3}	6.386×10^{-3}	2.4
0.020	5.234×10^{-3}	0.531×10^{-3}	1.055×10^{-3}	4.0
0.025	0.777×10^{-3}	0.782×10^{-3}	1.559×10^{-3}	5.9
0.030	1.072×10^{-3}	1.070×10^{-3}	2.142×10^{-3}	8.1
0.035	1.406×10^{-3}	1.403×10^{-3}	2.809×10^{-3}	10.6
0.040	1.779×10^{-3}	1.768×10^{-3}	3.547×10^{-3}	13.4
0.045	2.185×10^{-3}	2.166×10^{-3}	4.351×10^{-3}	16.4
0.050	2.627×10^{-3}	2.600×10^{-3}	5.227×10^{-3}	19.7
0.055	3.106×10^{-3}	3.060×10^{-3}	6.160×10^{-3}	23.2
0.060	3.613×10^{-3}	3.559×10^{-3}	7.172×10^{-3}	27.0
0.065	4.150×10^{-3}	4.080×10^{-3}	8.230×10^{-3}	31.0
0.070	4.718×10^{-3}	4.630×10^{-3}	9.350×10^{-3}	35.3
0.075	5.310×10^{-3}	0.520×10^{-2}	10.510×10^{-2}	39.7
0.080	0.593×10^{-2}	0.581×10^{-2}	1.174×10^{-2}	44.3
0.085	0.658×10^{-2}	0.644×10^{-2}	1.302×10^{-2}	49.0
0.090	0.725×10^{-2}	0.709×10^{-2}	1.434×10^{-2}	54.0
0.095	0.796×10^{-2}	0.777×10^{-2}	1.573×10^{-2}	59.4
0.100	0.868×10^{-2}	0.847×10^{-2}	1.715×10^{-2}	64.7
0.150	1.705×10^{-2}	1.650×10^{-2}	3.350×10^{-2}	126.0
0.200	2.716×10^{-2}	2.620×10^{-2}	5.340×10^{-2}	201.5
0.250	3.854×10^{-2}	3.707×10^{-1}	7.581×10^{-1}	285.3
0.300	5.090×10^{-1}	0.488×10^{-1}	0.997×10^{-1}	376.0
0.350	0.640×10^{-1}	0.613×10^{-1}	1.253×10^{-1}	473.0
0.400	0.679×10^{-1}	0.770×10^{-1}	1.513×10^{-1}	571.0
0.450	0.919×10^{-1}	0.878×10^{-1}	1.797×10^{-1}	678.0
0.500	1.064×10^{-1}	1.016×10^{-1}	2.080×10^{-1}	785.0
0.550	1.214×10^{-1}	1.157×10^{-1}	$2.371-10^{-1}$	894.0

* density of quartz was taken as $\rho_{SiO_2} = 2.65$ gr/cm^3

** data for electron ranges in Silicon are taken from Berger &Seltzer (1966) and in Oxygen from Berger &Seltzer (1964)

*** fraction by weight

TABLE 2.12.1

Energy (MeV)	β-ranges in Soil* Si = 0.29	O = 0.43	Al = 0.077	Fe = 0.045	Total (gr/cm^2)	Range in mm for ρ=1.3 gr/cm3	ρ=1.8
0.100	0.00527	0.00700	0.001435	0.000949	0.01465	0.113	0.0814
0.150	0.01029	0.01377	0.002800	0.001840	0.02870	0.220	0.159
0.200	0.01630	0.02190	0.004440	0.002900	0.04550	0.350	0.253
0.250	0.02307	0.03109	0.006287	0.004099	0.06450	0.496	0.358
0.300	0.03039	0.04100	0.008290	0.005380	0.08500	0.654	0.472
0.350	0.03816	0.05160	0.010418	0.006750	0.10690	0.822	0.594
0.400	0.04628	0.06270	0.012628	0.008170	0.12978	0.998	0.721
0.450	0.05466	0.07417	0.014920	0.009640	0.15339	1.180	0.852
0.500	0.06320	0.08590	0.017270	0.011137	0.17750	1.365	0.986
0.550	0.07200	0.09790	0.019660	0.012660	0.20220	1.555	1.123

* Based on the main constituents

TABLE 2.12.2

	Radius(cm)	Absorbed Dose Fraction (F)	Self γ-dose (mrads/mth)
For γ = 1MeV and ρ = 1.8 gr/cm^3			
$\mu_{lin.coeff}$ = 0.09702 $\mu_{abs.coeff}$ = 0.04230	0.5 1.0 2.0	0.0388 0.0788 0.0998	1.005 2.040 2.590
ρ = 1.25 gr/cm^3			
$\mu_{lin.coeff}$ = 0.06740 $\mu_{abs.coeff}$ = 0.02940	0.5 1.0 2.0	0.0268 0.0545 0.0687	0.696 1.417 1.785
For γ = 1.5MeV and ρ = 1.8 gr/cm^3			
$\mu_{lin.coeff}$ = 0.07848 $\mu_{abs.coeff}$ = 0.03850	0.5 1.0 2.0	0.0344 0.0700 0.0889	0.894 1.820 2.313
ρ = 1.25 gr/cm^3			
$\mu_{lin.coeff}$ = 0.05450 $\mu_{abs.coeff}$ = 0.02675	0.5 1.0 2.0	0.0237 0.0490 0.0617	0.616 1.270 1.600

The linear attenuation coefficent ($\mu_{lin.coeff}$) and mass energy absorption coefficient ($\mu_{abs.coeff}$) were calculated from data by Evans, (1968) and Storm & Israel, (1970), respectively.
The self gamma dose was calculated based on a Glozel clay's gamma dose which was 312 mrads/yr.

The μ values were evaluated from:

$$\mu = \rho_{mater.} \sum \frac{\mu_i}{\rho_i} \omega_i \text{ , where}$$

$\rho_{mater.}$ is the measured density of the matrice and the summation is taken over the i constitutes of the matrix, according to their fraction by weight, ω_i. (air spaces and water were ignored.)

(F) is the absorbed dose fraction in the centre of a sphere of radius, r.

$$F = 1 - e^{-\mu_o r}\left[1 + (\mu_o - \mu_a)r\right], \text{ where} \qquad \text{(Evans, 1955)}$$

$\mu_o = \mu_{lin.coeff}$ and $\mu_a = \mu_{abs.coeff}$.

This could mean that between 0.5 to 0.7 cm thickness, the beta dose is obviously increased (with background-subtracted) to level off at above 0.7cm and towards 1cm and 2cm, (saturation.) That was found to be within ($\pm$ 1σ) error in the measurements, Fig. 2.12. above.

In conclusion, it must be emphasized (from Fig. 2.12.1) that the beta dose as measured from the powdered samples does not always represent the true betas inside the sherd.

Because the solids have more clay (by weight) than the powders (depending upon the temperature at which they were fired), of the same geometry or disc size, they will give greater beta dose. This is not compensated by increasing thepowder thickness in the counting ring, because ~~this~~ is limited by the maximum beta ranges and the appreciable increase of the gamma self dose.*

2.13 Increased Beta Dose Due To Clay Densification

Presented here are two explanations for the observed high doses in solids rather than in powder discs.

i) Several authors have proposed empirical models to explain the electron passage through matter in order to derive geometrical or influence functions. Each of them assume that the electron track is straight and that the stopping power is continuous and equal to the electron LET. Charlton, (1970), introduced a model of electron stopping powers based on Spencer's calculations of the average energy dissipated near point isotropic sources of mono-energetic electrons. This treatment by Spencer has been extensively tested by Cross, (1968). The model is based on the following principle:

The electron stopping power is dependent on energy over the entire track and slightly on the medium, (Z, clay composition),

* The ideal would be to break down the sherd with all its inclusions and follow the 110°c peak technique or use whole sherd sandwiched and using a pair of $CaSO_4$:Mn in the centre with subsequent conversion of the reading to quartz readings, (the conversion factor having been found from powder disc experiments).

and for different geometrical cases. Hence, between media of different mean atomic numbers, for example, spherical quartz grains with the clay matrix, where the sources are isotropically distributed, the absorbed dose in each point inside the grain (or in terms of energy dissipated per unit volume) is given by :

(1) $$D(Y) = \frac{N_o \cdot E_o}{K(Z_i)} \cdot \frac{1}{n_m} \cdot S(Y)$$, Charlton (1970)

where,

N_o is the number of electrons originating per unit volume, with initial energy E_o outside the grain.

$K(Z_i)$ is the density of medium with Z_i,

n_m is the mass range ratio,

$S(Y)$ is the influence function for the point in the medium and it is a function of dE/dx, θ and other geometrical parameters.

The dose, then, absorbed by the quartz grains is dependent upon:

a) the number of electrons (secondary) originating outside the grain,

b) the density of the grain,

c) the initial energy of the electron for the respective radionuclidic source, and

d) the mass range ratio $n_m = \frac{r_o(Z_2).K(Z_2)}{r_o(Z_1).K(Z_1)}$, where

$r_o(Z_1)$ and $r_o(Z_2)$ are the ranges in Z_1 and Z_2 media, respectively, travelled by an electron originating in a medium Z_1 and depositing part of its energy in another medium, Z_2, which in turn is clearly dependent upon the respective densities, that is, that of quartz and that of clay.

Further, considering the influence of different clay densities (even of the same composition), on beta ray attenuation and rate of secondary particles production, the following concept has been derived:.

According to Fano's theorem, in a medium exposed to a uniform flux of primary radiation, the flux of secondary radiation is also uniform and independent of the density of the medium as well as the density variation from point to point, Fano, (1954). Hence, in our case, for a powdered disc clay of uniform density and with radioisotopes distributed (not necessary isotropically) throughout the clay matrix, there will be a certain uniform flux of all the secondaries of the radiation.

Suppose now that the density of the clay is increased by a factor, f, by say, pressing the previously unpacked powder disc so that all free electron paths become fX smaller and the source density is also increased f - fold. The resulting flux of any secondary radiation will be equal to that when the powder was unpacked.

Nevertheless, once we change the clay composition by firing it or by adding water to the clay (dampened) and making another solid disc of the same thickness, the source density of the radionuclides as implied by the above theorem, must be increased more than the decrease of the secondary radiation (or beta attenuation). Thus, the phosphor records a higher dose which is what was found to be the case. Otherwise, the density does not affect the attenuation of the betas except if water is present or if its composition is altered markedly. Therefore, the beta stoppingpower and attenuations are both a

function of electron energy and atomic number or composition of the medium.

ii) It can be seen from the Mott and Bethe's formula which gives the mean energy loss per centimetre path for small energy that this energy loss is dependent upon the density of the radionuclides present in a potsherd (see equation 2, Chapter 6, Section 6.3). For the clay, this energy loss will be according to Bragg's additivity rule:

(2) $$dE/dx = \Sigma_i E_i (dE/dx)_i$$, Zimmerman, (1970),

where,

E_i is the fraction by weight of the i^{th} element in the compound. The deviation in the stopping power predominates at low energies which is the case for betas in clays (under 0.5 MeV).

In Table 2.6 the density of powder in sherds is shown. This would mean that stopping power of electrons will not be the same to these materials. Also, the mean excitation energy I in solid is higher than in powder as is explained below. It is:

(3) $$z \ln I = \Sigma_i f_i \ln E_i$$, where

f_i is the oscillatory strength of the i^{th} transition with excitation energy E_i. In the solid packed state where the density ρ is higher than in the powder, the oscillating atoms (atoms/unit volume) are more numerous, hence the stopping power dE/dx or S/ρ, in solid is higher than in powder, or the betas shall be more attenuated. This depends on the beta energy. However, variations of a few % in I give variations of a few tenths of % in the stoppingpower, which implies that the beta attenuation will be negligible with respect to the increase of the radioisotopes in the solid disc.

The density effect or polarisation begins to be important at very high velocities of betas ($\beta > 0.9$), when a fundamental correction has to be made, Sternheimer, (1952, [illegible], 1956 and 1966).

The effect on the beta dose will be an increase which is due to the densification and water expulsion of the fired clays, plus a negligible decrease due to the attenuation of betas for the respective densities. This increase predominates as the attenuation is very small and this is observed in the results of Table 2.7.

Finally, the fact of the relative attenuation to different clay compounds has been investigated further for many Hellenic potsherds and is presented in Chapter 6.

2.14 Discussion of Water Uptake Corrections of Solid Discs

The dose rates determined in the above experiments are functions of the thickness of the potsherds in dry and wet states. What is normally required in inclusion dating is the average dose rate experienced by quartz imbedded in pottery that is saturated with water or has its natural wetness from a fresh archaeological excavation. The measured dose rate must therefore be corrected for the effect of the water and for beta attenuation by the grains. Saturation of the clay by water has two effects:

i) dilution of the radionuclides and ii) increase of the average stopping power, because of the relatively large stopping power of water. Both effects are taken into account in the expression derived by Zimmerman, (1971):

$$\beta_{wet} = \frac{\beta_{dry}}{1 + \left(\frac{\text{sherd wet}}{\text{sherd dry}} - 1\right) \cdot \frac{S(\text{water})}{S(\text{sherd})}} \quad , \text{ where} \tag{4}$$

β_{dry} and β_{wet} are the β-dose rates in wet and dry sherds, respectively,

S_{water} and S_{sherd} are the stopping powers for water and clay,

sherd wet, by weight, is the sherd saturated with water and

sherd dry is the weight of the dry sherd.

Zimmerman obtained the stopping power ratio of the water to that for the sherd of 1.25 by assuming that the stopping power of the clay is equal to that of aluminium. This assumption has been further investigated in Chapter 6 and seems to be valid.

The technique for beta dosimetry offered an interesting opportunity to test expression (4) by measuring the beta dose rate of sherds in the dry condition and when saturated with water. Results are presented in Table 2.7D. The somewhat higher values of the estimated wet doses, could be due to the fact that the ratio of $(S/\rho)_{water}$ to $(S/\rho)_{Glozel\ powder}$ is less than 1.25. In this case, because the dose is relatively small, the error introduced will not be negligible as found in Chapter 6, but appreciable. This error could well result in the observed higher values.

2.15 Conclusions and Suggestions

The above experimental results have a number of advantages which can be summarized as follows:

i) Absolute calibration of dose rate values is not required provided that the same source, or two accurately intercalibrated sources, are used for calibration of beta and gamma dose rate measurements and the measurement of the archaeological dose (in my work a Sr-90 source with 303 mrads/min on quartz and a Co-60 source with

3.62 mrads/min on quartz.) The resulting dose will then be derived from a consistent dosimetry system, independent of any tabulated figures and of absolute calibration of radiation sources. However, the energy spectrum plays an important role in the source calibration and a more sophisticated way of calibrating the source should be sought. This is by preparing standard samples in the following manner. Many standards of different U/Th ratios and K content must be prepared and the quartz 110°C peak must be measured, normalised by a beta or gamma source.

In the unknown sample, the 110°C quartz peak reading will be normalised with the same monitor dose and subsequently converted to the 'standard samples' ratio (backgrounds being subtracted). Nevertheless, the effect, as mentioned previously, on this isotopic variation will produce an error in the source calibration of about 10% only for extreme values of potassium content. However, this can be overcome by chosing a standard with low potassium content. Thus a variety of standards has to be available.

ii) Since both the beta dose rate measurement and the measurement of archaeological dose are carried out on identical samples, no correction is needed for attenuation of the beta radiation by the grains. In fact, all grain sizes present in the material can be utilized. A large grain size of, say around 150μ, would further eliminate any remaining doubt about the alpha contribution, which for smaller grain sizes is obscured from the measuring errors.

iii) Whole sherds saturated with water can be used for the dose rate measurement. The attenuation of theradiation by the water

can be then included directly in the measurement so that no knowledge of the stopping power of water relative to that of clay is required. Such measurements will avoid the possible erroneous estimation of beta dose measurements on powder discs.

Addition of water equal to the water which would have been present when the sherd was buried and the presence of grains (as % by weight, equal to those present in the sherd), as well as surrounded by clay from the vicinity of the found sherd and using the above mentioned calibration with many standards would:

a) dilute the radioactivity,

b) account for radon emanation,

c) cause a true beta attenuation due to water content, and

d) avoid complications concerning the beta energy response and the gamma self dose energy response.

iv) In addition to the beta dose rate, the measured value will include a small contribution from gamma rays, the so-called gamma self dose, originating from the radioactivity in the pottery. The latter is particularly difficult to evaluate with the dosimeters for gamma radiation described in Chapter 9, the calculations of the gamma dose values will be facilitated considerable.

Therefore, problems associated with water uptake, radon escape, beta attenuation through grains, gamma self dose, energy response of the grains to the clay and source calibration are likely to be reliably assessed with the above new techniques. Though, at present, it has an error of around 5% due to measuring procedure of the grains only, this could be reduced by measuring a larger number of quartz samples.

CHAPTER 3

MEASUREMENT OF BETA DOSE RATE BY MEANS OF ALPHA COUNTING AND POTASSIUM DETERMINATION ((α+K) METHOD)

3.1 INTRODUCTION

This chapter concerns an enquiry into the determination of β-dose rates in ceramics by the α-counting method. Former studies by Tite et al (1962), Zimmerman (1970), Aitken et al (1972), Desai and Aitken (1974) Desai (1975), Aitken (1975), Huxtable et al (1976) and Aitken (1978), have demonstrated the advantages and disadvantages of this method for the determination of beta dose rate in inclusion dating.

The most remarkable characteristics of alpha counting are the high count-to-background ratio (100/1 for typical pottery) and the ease with which counts due to beta particles (and gamma radiation), are excluded because ZnS is not sensitive to these radiations. The most serious disadvantages are: first, that unless precautions are taken there is a risk of "overcounting" for a sample from which the escape of radon is substantial and, secondly, that because of the short range of alpha particles, only a small part (about 0.1g of the sample), is analysed and when the sample grains are internally hetrogeneous there is liable to be some dependence on the degree to which the sample is powdered, (see Chapter 4 Section 4.3). Where numerical quantities are given, they refer to a system in which the diameter of the Zns screen is 42mm and the electronic threshold is set so that for a sample containing Th-232 in equilibrium, 85% of the pulses are recorded. The finite threshold avoids any recording of beta particles, of photo-multiplier noise, etc., but it does give some dependence on the reflectivity of the sample (Huntley and Wintle, 1978), though unless exceptionally white or black samples are being counted, this reflectivity effect is not substantial.

Further, the conversion of instrumental readings to dose rates depends upon the extent to which the Uranium and Thorium series are in radioactive equilibrium. However, secular equilibrium of soils has been accepted universally (Adams et al, 1959), provided that these are older than half a million years. Variations in the Th/U ratio have been reported in Meakins et al (1978), Carrireau (1978).

3.2 Radioisotopes Embedded in Ceramics

As has been described in Chapter 1 Section 1.4, the technique of thermoluminescence (TL) dating relies upon the ability to measure accurately both the archaeologically acquired radiation dose and the rate at which this dose has been delivered to the material under study. The origin of the radiation lies with three main groups of naturally occuring radioactive elements: a) the Uranium series; b) the Thorium series, Fig. 3.2.1 a,b, and c) the Potassium-40, Fig. 3.2.2. The method employed here to determine the annual dose rate from the Uranium and Thorium series is to measure the alpha activity of the sample by conventional counting methods, Turner et al (1958) and Tite et al (1962), and then to calculate the radiation dose rate. After measurement of the α-activity, the calculation of the annual dose rate requires an exact knowledge of the decay characteristics of all the contributing radioisotopes. This is taken from recently revised tabulated conversion data, Bell (1977).

It is necessary, in evaluating the dose rate data, to assume that the decay series have reached radioactive equilibrium. This implies that the activity (rate of decay) of each member of the series is precisely the same as that of any other member. Tables 5.2 and 3.2.1 For the natural abundance of its unstable isotope, K-40 (with a half-life of 1.28×10^9), is 0.0118% of the total potassium content.

TABLE 3.2.1a

URANIUM-238 SERIES*

Element	Symbol	$t_{\frac{1}{2}}$	Energy (MeV) α	Energy (MeV) β	Energy (MeV) γ	Percentage γ Occurrence	Remarks
92 Uranium	U-238	4.5×10^9 y	4.20	-	0.048	23	
90 Thorium	Th-234	24.1d	-	0.19	0.090	4	
91 Protoactinium	Pa-234	1.17m	-	2.29	1.000	0.6	
92 Uranium	U-234	2.5×10^5 y	4.80	-	0.050	28	
90 Thorium	Th-230	8.0×10^4 y	4.80	-	0.068	24	
88 Radium	Ra-226	1602y	4.80	-	0.186	4	
86 Radon	Rn-222	3.82d	5.49	-	0.500	0.07	
84 Polonium	Po-218	3.05m	6.00	-	-	-	Branched decay:
82 Lead	Pb-214	26.9m	-	0.65	0.240(.35)	4(36)	α to Pb-214 (99.9%);
83 Bismuth	Bi-214	19.7m	5.50	1.50	0.610(1.76)	47(17)	β^- to At-218
84 Polonium	Po-214	164μs	7.70	-	0.800	0.014	(0.02%)
82 Lead	Pb-210	22.0y	-	0.016	0.046	4.1	
83 Bismuth	Bi-210	5.0d	-	1.160	-	-	Branched decay:
84 Polonium	Po-210	138d	5.30	-	0.800	0.001	α to Tl-210 (0.04%);
82 Lead	Pb-206		(stable)				β^- to Po-214 (99.96%)

* After Adams & Gasparini (1970) and Lapp & Andrews, (1972).

TABLE 3.2.1b

THORIUM-232 SERIES *

Element	Symbol	$t_{\frac{1}{2}}$	Energy (MeV)			Percentage γ Occurrence	Remarks
			α	β	γ		
90 Thorium	Th-232	1.40×10^{10} y	4.00	-	0.06	23	
88 Radium	Ra-228	6.7y	-	0.054	-	-	
89 Actinium	Ac-228	6.13h	-	1.110	0.90	30	
90 Thorium	Th-228	1.91y	5.43	-	0.08	28	
88 Radium	Ra-224	3.64d	5.68	-	0.24	5	
86 Radon	Rn-220	55s	6.29	-	-	-	
84 Polonium	Po-216	0.16s	6.78	-	-	-	
82 Lead	Pb-212	10.6h	-	0.360	0.238	81	
83 Bismuth	Bi-212	60.6m	6.05	2.200	0.04	17	Branched decay:
84 Polonium	Po-212	300ns	8.87	-	-	-	β^- (66.3%) to
81 Thalium	Tl-208	3.1m	-	1.79	2.62	100	Po-212 α (33.7%)
82 Lead	Pb-208		(stable)				to Tl-208

*After Adams & Gasparini, (1970) and Lapp & Andrews, (1972)

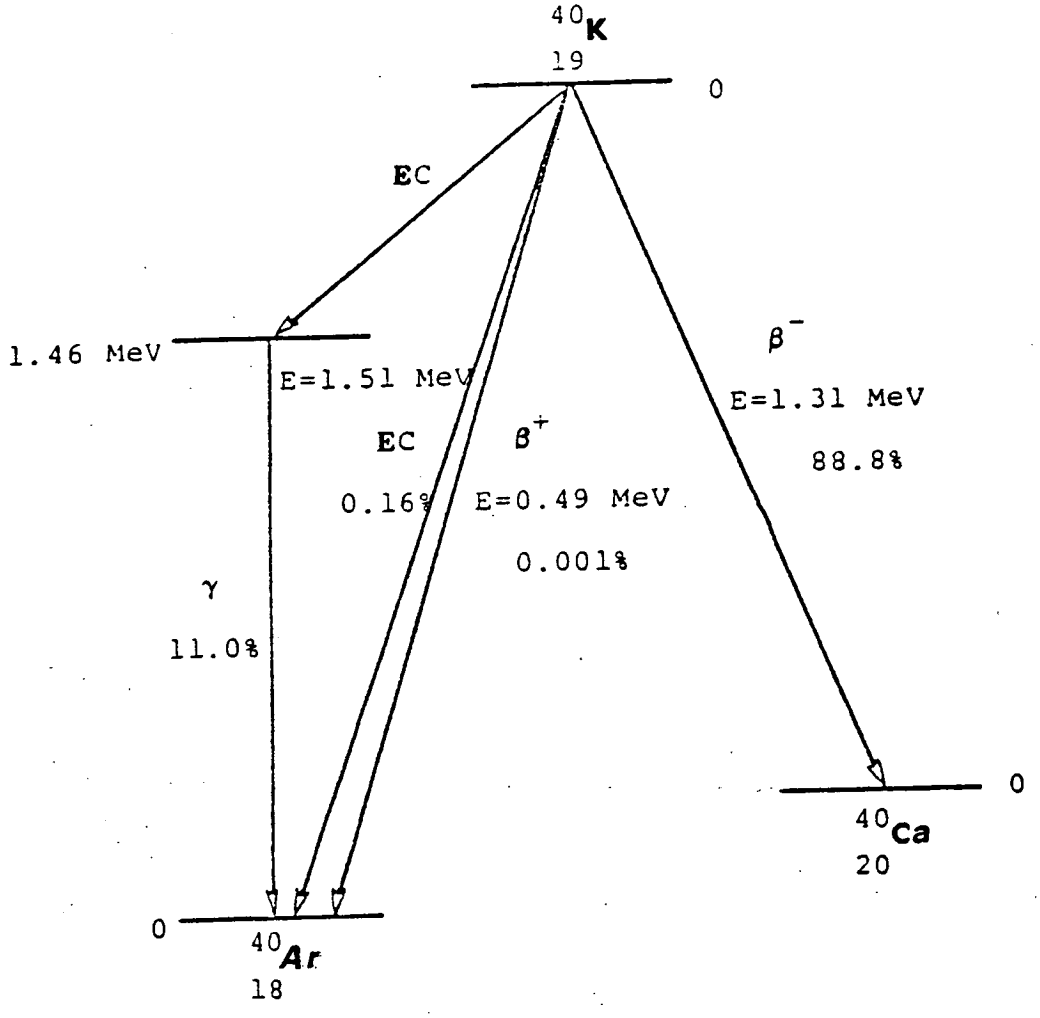


Fig.3.2.2 Decay scheme of potassium-40

The total potassium content has been determined in the present studies by flame photometry or by X-ray fluorescence and expressed as the percentage of K_2O (MW=94.2), in the sample. K-40 decays in 89.3% of cases by emission of a beta particle with an average energy of 0.583 MeV Fig. 3.2.2 and in the other 10.7% of cases, by electron capture and then by gamma ray emission with an energy of 1.4608 MeV. Summing the contributions for beta particles and auger electrons and also gamma rays and X-rays give the resultant K-40 dose rate. K-40 dose rate contributions are given in Table 3.2.3 Bell (six pages on) The U-235 natural isotopic ratio is 0.7114 (± 0.0007%), Hyde et al (1964), and has not been found to vary in nature. The activity of the U-235 series is greatly overshadowed by that of the U-238 series. According to Waine (1964), the error introduced by ignoring the U-235 dose rate in pottery is less that 0.5%. The activity of the U-235 series can then be neglected for all TL and gamma measurements.

3.3 Description of the Alpha Counting Method

The method of determining the Uranium and Thorium contents of the sherd and soil consists of counting the alpha particles emerging from a thick sample using a zinc sulphide scintillometer.

The sherd and soil samples were dried and broken into fragments of less than 75μ in size. The sample was then placed in a perspex ring, prepared as follows. This ring (12.8mm radius or 513mm^2), was covered with a layer of sellotape which was trimmed to the correct size of the ring and sprinkled with zinc sulphide,(Levy, West, Harlow and Essex). The excess zinc sulphide was shaken off and the sidewalls of the ring cleaned. The ground sample was then spread evenly on top of the zinc sulphide, in the ring. This assemblage was then placed in a perspex container and a lid screwed down onto an O-ring, Fig. 3.3 The sample occupied the total volume of the

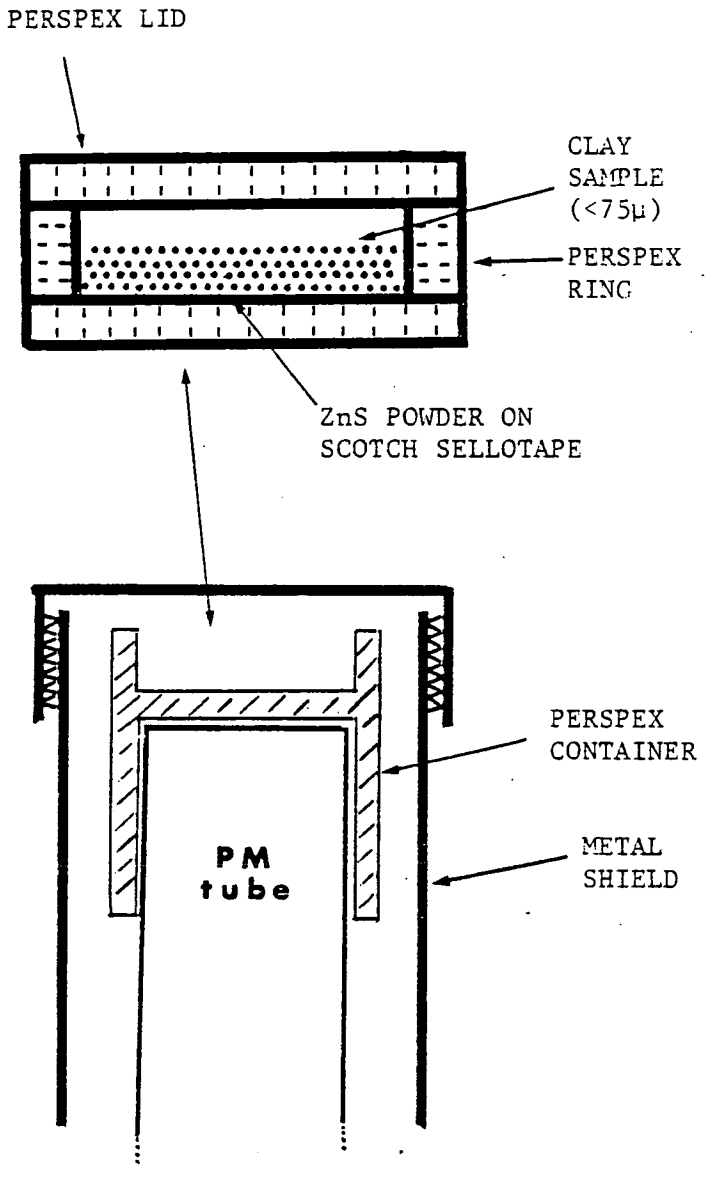


Fig. 3.3. Assemblege of the α-cell and Photomultiplier in the α-counting

container, thus counting the radon gas and the sample with equal efficiency. This is not achieved entirely as there are some gaps where the gas can escape, (hence it will not be counted), as well as some gaps between the ZnS grains (where it will be counted, with closer to 4π than to 2π efficiency). However, the error associated with this should be small as about 2/3 of the gas occupies the space between the solid sample grains. It should be noted that the lid of the perspex container above the ring does not stop radon escaping completely. Other possible sources of radon leak are the O-ring, diffusion through the perspex and through adjacent compartments. Also, no vacuum grease was used. It has been shown that the rate of build-up of the alpha counts measured as a function of time is exponential approaching saturation with the radon half-life of 91 hours, Zimmerman (1970). The ring container was counted within 24 hours and after 15 days again. Under these conditions, radon and thoron would not escape from the detector in the first 24 hours, so the degree of emanation is assessed be recounting the ring after 15 days (time allowance for radon to build-up in equilibrium with its daughters, T = 3.8 days). The effect of radon emanation on temperature is not well known. This is mentioned in order to relate any radon escape from buried pottery in soil with that of powdered pottery in a counting mode under lab conditions.

3.4 Comparison of "Sealed" Alpha Counts within 24 Hours and After 15 Days

Sherds from the test programme have been alpha-counted both within 24 hours and after 15 days. Table 3.4 shows the percentage differences between these two counts. From the table we note that 72% of the samples show a difference of less than 10%. These two readings were then averaged as the best estimated approach to the real situation which occurs in the buried sherd. In most cases, the two total counts, one

TABLE 3.4

Sample Number	%Difference of $24^H/15^D$ Counts*
DM13	2
DM1/2	10
DM41	9
SK2	4
SK4	12
DM11	3
SK6	9
KZ2/5	5
KZ1/9	12
AT7	2
AT8	3
FS3/8	4
KH5	20
KH7	20
SH2	10
KZ3/2	2
FS1/5	2
SH6	1
DM35	1
FS3/9	1
DL1/1	1
SKB(1)27	2
SH11	5
KZ3/1	3
DM6/6	3
SKB(1)1	13
SKB(1)98	2
SK15	17
SKB(1)18	38
DM10	2
DM33	2
DM39	19
SK6	4
SKE3	3
SKB(1)28	2
D6	3
D5	2
SK8	8
SK17	20
DM16	11
SKE5	2
STGZA2	4
STGZA43	12
STGZA68	6
EX INS 2	33
EX INS 1	5
SKE	17
SKE1	2
SKE6	1
SKB(1)1	9

Samples = 50
28% of samples differ by more than 10%.
72% of samples differ by less than 10%

* % difference under 5% is taken as statistical error

taken within 24 hours and the other after 15 days agreed to within the statistical error (±5%) of each measurement.

3.5 Radon Emanation in Ceramics

About half-way through the decay chains of the Uranium and Thorium series are gases: Radon-222 ($t_{1/2}$=3.8 days) and Radon-220 ($t_{1/2}$=52 sec). These gases are able to emanate from the fired ceramic (Gabrysh et al, 1963), and from soil (Tanner, 1964). Waine (1964) has shown that the percentage of radon emanating from various dried sherds ranges from less than one percent to at least 40%. Zimmerman (1970), investigated the radon emanation as measured in sealed and unsealed alpha count models for a variety of sherds and soils and found that from 87 sherds, 31% of them did not increase within the experimental error (±5%), while 10% showed a difference of 30% (Compare with section 3.4).

The emanation is important in two circumstances:

i) the first is during burial, when emanation from the soil would affect the archaeological dose

ii) the second is during the laboratory radioactivity measurements when emanation would affect the number of alpha particles detected.

The first is approached by recording the amount of radon emanation with the alpha counter, considering the radioactivity of the soils surrounding the buried sample and comparing the final dose rates with TLD ($CaSO_4$:Dy) dosimetry measurements in situ (see Chapter 9)

Very little is known about the movement of radon in pottery, but some facts are known about its movement in soil. The isotopes of radon move through soil (and other porous media), by diffusion and transportation by water, Tanner, (1964). The distance moved by each isotope is approximately proportional to $\sqrt{T_{\frac{1}{2}}}$. The distance moved is also a function of the porosity of the medium, the rate of flow of the ground water and the ambient temperature and wind. Tanner presents the

experimental data are shown in Table 3.5 These data are supported by the observation of the dependence of the concentration of radon in the air on rainfall, (Gold et al, 1964), and the observation of a decrease in the radon concentration within two meters of the surface in a dry allumium soil, Kraner et al (1964), (Also see Chapter 8)

In considering the relevance of those facts to our problem one figure to bear in mind is that 95% of the gamma dose comes from a volume of soil surrounding the sherd of radius 30cm (Aitken, 1968). Therefore, as far as the gamma dose goes, movement of radon of less than 30cm will have only a small effect. This could be the case for Rn-222, (see Table 3.5), for soils which are wet-to-saturated and for which the flow of ground water is fairly small. The movement of Rn-220 should be negligible in all cases. In the cases where there is a greater than 30cm movement, if the soil is uniform for a sufficient distance, then the flow of radon outward will be compensated by a similar inward flow. The most obvious exception to this will be near the ground surface.

Let us now consider the situation in the sherd. No data are available on the flow of radon in fired ceramic materials. However, as the pore sizes in sherds are generally much smaller than those in soils, it is reasonable to suppose that the rate of both diffusion and transportation will be lower. Furthermore, a sherd in soil will probably be nearer its saturation water content than the soil, because the smaller pores will exert a greater attractive force on the water. The greater degree of wetness of the sherd will further reduce the movement of radon in the sherd. On the other hand, the critical distance in the case of the sherd is about $\frac{1}{2}$ to 1cm. Until more information is available it is impossible to draw a definite conclusion, but it is possible that for wet-to-saturated sherds, the radon and thoron will not be

TABLE 3.2.3

	Dose-Rate (mrad/yr) for 1ppm by weight of parent *		
	α	β	γ
Thorium series			
no thoron loss	74.0	2.90	5.00
100% thoron loss	31.0	1.05	1.83
Uranium series			
no radon loss	278.3	14.64	12.68
100% radon loss	126.2	5.93	0.69
Potassium-40			
for 1% K_2O	-	68.2	20.5

* after Bell, (1977)

TABLE 3.5

Approximate Migration Distances of Radon Isotopes in Soil*

		Mean Migration Distance (cm)	
		Rn-222 (radon)	Rn-220 (thoron)
	Water Content of Soil		
diffusion	dry	200	2
	moist	50	0.5
	wet	4	0.04
	saturated	2	0.02
transportation	max (∿1.5m/day)	200	2
	min (∿1.5m/day)	10	0.1

* from Tanner, (1964)

able to diffuse appreciably out of the sherd. For dry sherds, the radon will possibly diffuse out, in which case the radon from the surrounding soil can diffuse in as well. The net effect will then depend on the relative radioactivities and emanating powers of the soil and sherd (see Chapter 8).

The magnitude of this effect can be illustrated by the following calculations based on different percentages of radon loss, from 5% to 100%. The concentration of Thorium was 12ppm and of Uranium 3.8ppm. Four different values for potassium were chosen - 0.5%, 1%, 2% and 3%, and three gamma doses, namely 80 mrads/yr, 120 mrads/yr and 150 mrads/yr Table 3.5.1 (.2.3.4 and .5). In another computational example, lower values of Thorium and Uranium were used, Th=9ppm and U=2.84ppm, with different percentages of radon loss and two external gamma doses, Table 3.5.6. The effects were presented as ratios of D_T to D_R where D_T is the total dose for the respective potassium and U, Th concentrations with no radon loss, and D_R is the dose of the respective percentages of radon loss.

For the fixed values of Th=12ppm and U=3.8ppm, the following conclusions can be drawn:

i) the higher the external gamma dose and the potassium content, the lower the errors involved with radon losses. In concrete terms, a 5% deviation from the actual total dose (beta plus gamma), would occur for 30-35% radon loss if the gamma dose rate is above 120 mrads/yr and the potassium content above 0.5%.

ii) a deviation of up to 3% is observed for radon losses up to 15% and for potassium contents above 0.5% - which occurs in most cases - and for gamma doses higher than 80 mrads/yr.

iii) in the extreme case of complete radon loss (100%), the involved error depends upon the potassium contents and the external gamma dose varies from 26% down to 12%, which is quite substantial.

TABLE 3.5.1

Th = 12ppm U = 3.8ppm % Radon Loss	β-dose rate from (U,Th)	Total Doses for Respective % of K-40 0.5%	1.0%	2.0%	3.0%
0	90.4	131.5	1.72.6	254.8	337
5	87.66	128.76	169.86	252.1	334.26
10	84.7	125.8	166.9	249.1	331.3
15	82.1	123.2	164.3	246.5	328.7
20	79.34	120.44	161.54	243.74	325.94
25	76.63	117.73	158.83	241	323.23
30	73.84	114.94	156	238.2	320.44
35	71	112.1	153.2	235.4	317.6
40	68.29	107.39	150.5	232.7	314.89
45	65.53	106.6	147.7	229.93	312.13
50	62.7	103.8	144.9	227.1	309.3
60	57.18	98.28	139.38	221.58	303.78
70	51.65	92.75	133.85	216	298.25
80	46.18	87.28	128.38	210.58	292.78
90	40.6	81.7	122.8	205	287.2
100	35.1	76.2	117.3	199.5	281.7

TABLE 3.5.6

Th = 9ppm U = 2.84ppm β-dose rates for (U,Th)	% Radon Loss	Total Doses for Respective % of K-40 0.5%	1.0%	2.0%	3.0%
67.67	0	108.8	147.9	232.0	314.3
61.43	15	102.5	143.6	225.8	308.0
46.96	50	88.1	129.2	211.4	293.6
26.29	100	67.4	108.9	190.7	272.9
Total (β+γ) doses if γ=80mrads/yr					
	0	188.8(1)	229.9(1)	312.0(1)	394.3(1)*
	15	182.5(.96)	223.6(.97)	305.8(.98)	388.0(.98)
	50	168.0(.89)	209.2(.90)	291.4(.93)	373.6(.95)
	100	147.4(.78)	189.0(.82)	270.7(.87)	353.0(.89)
Total (β+γ) doses if γ=150mrads/yr					
	0	258.5(1)	300.0(1)	382.0(1)	464.3(1)
	15	252.5(.97)	293.6(.89)	375.8(.98)	458.0(.99)
	50	238.0(.92)	279.0(.93)	361.4(.95)	443.6(.95)
	100	217.4(.84)	259.0(.86)	340.7(.89)	423.0(.91)

* the numbers in brackets represent the ratios of the total dose (with respective potassium, and U, Th fixed values) with no radon loss (0%) to the dose of the respective percentages of radon loss.

TABLE 3.5.2

Effect of %Radon Loss (D_L) for K=0.5% and γ=80,120,150 mrads/yr. (D_T=total dose from U, Th and K)

% Radon Loss	β-dose rate from (U,Th,K)	Ratios D_L/D_T	γ=80	D_L/D_T	γ=120	D_L/D_T	γ=150	D_L/D_T
0%	131	1.0	211	1.0	251.0	1.0	281	1.0
100%	76	0.58	156	0.74	196	0.78	226	0.80
90%	81	0.62	161	0.76	201	0.80	231	0.82
80%	87	0.66	167	0.79	207	0.82	237	0.84
70%	92	0.70	172	0.82	212	0.84	242	0.86
60%	88	0.75	178	0.84	218	0.87	248	0.88
50%	103	0.79	183	0.87	220	0.88	250	0.90
45%	106	0.81	186	0.88	226	0.90	256	0.91
40%	109	0.83	189	0.89	229	0.91	259	0.92
35%	112	0.85	192	0.91	232	0.92	262	0.93
30%	114	0.87	194	0.92	234	0.93	264	0.94
25%	117	0.89	197	0.93	237	0.94	267	0.95
20%	120	0.91	200	0.95	240	0.95	270	0.96
15%	123	0.94	203	0.96	243	0.97	273	0.97
10%	125	0.95	205	0.97	245	0.98	275	0.98
5%	128	0.98	208	0.99	248	0.99	278	0.99

TABLE 3.5.3

Effect of % Radon Loss (D_L) for K=1% and γ=80, 120, 150 mrads/yr

% Radon Loss	β-dose rate for (U,Th,K)	Ratios D_L/D_T	γ=80	D_L/D_T	γ=120	D_L/D_T	γ=150	D_L/D_T
0%	172.6	1.00	252.6	1.00	292.6	1.00	322.6	1.00
100%	117.3	0.68	197.3	0.78	237.3	0.81	267.3	0.83
90%	122.8	0.71	202.8	0.80	242.8	0.83	272.8	0.84
80%	128.4	0.74	208.4	0.82	248.4	0.85	278.4	0.86
70%	133.8	0.77	213.8	0.84	253.8	0.87	283.8	0.88
60%	139.4	0.80	219.4	0.87	259.4	0.88	289.4	0.89
50%	144.9	0.84	224.9	0.89	264.9	0.90	294.9	0.91
45%	147.9	0.86	227.9	0.90	267.9	0.91	297.9	0.92
40%	150.5	0.87	230.5	0.91	270.5	0.92	300.5	0.93
35%	153.2	0.88	233.2	0.92	273.2	0.93	303.2	0.96
30%	156.0	0.90	236.0	0.93	276.0	0.94	306.0	0.95
25%	158.8	0.92	238.8	0.94	278.8	0.95	308.8	0.96
20%	161.5	0.93	241.5	0.95	281.5	0.95	311.5	0.96
15%	164.3	0.95	244.3	0.96	284.3	0.97	314.3	0.97
10%	166.3	0.96	246.9	0.98	286.9	0.98	316.9	0.98
5%	169.8	0.98	249.8	0.99	289.8	0.99	319.8	0.99

TABLE 3.5.4

Effect of %Radon Loss (D_L) for K=2% and γ=80, 120, 150 mrads/yr

% Radon Loss	β-dose rate for (U,Th,K)	Ratios D_L/D_T	γ=80	D_L/D_T	γ=120	D_L/D_T	γ=150	D_L/D_T
0%	254.8	1.00	334.8	1.00	374.8	1.00	404.8	1.00
100%	199.5	0.78	279.5	0.83	319.5	0.85	349.5	0.86
90%	205.1	0.80	285.0	0.85	325.0	0.86	355.0	0.87
80%	210.6	0.83	290.6	0.87	330.6	0.88	360.6	0.89
70%	216.0	0.85	296.0	0.88	336.0	0.89	366.0	0.90
60%	221.6	0.87	301.6	0.90	341.6	0.91	371.6	0.92
50%	227.0	0.89	307.0	0.92	347.0	0.92	377.0	0.93
45%	229.9	0.90	309.9	0.92	350.0	0.93	380.0	0.94
40%	232.7	0.91	312.7	0.93	352.7	0.94	382.7	0.94
35%	235.4	0.92	315.4	0.94	355.4	0.95	385.7	0.95
30%	238.2	0.93	318.2	0.95	358.2	0.95	388.2	0.96
25%	241.0	0.94	321.0	0.96	361.0	0.96	391.0	0.96
20%	243.7	0.95	323.7	0.97	363.7	0.97	393.7	0.97
15%	246.5	0.96	326.5	0.97	366.5	0.98	396.5	0.98
10%	249.1	0.98	329.1	0.98	369.0	0.98	399.0	0.98
5%	252.1	0.99	332.0	0.99	372.0	0.99	402.0	0.99

TABLE 3.5.5

Effect of %Radon Loss (D_L) for K=3% and γ=80, 120, 150 mrads/yr

% Radon Loss	β-dose rate for (U,Th,K)	Ratios D_L/D_T	γ=80	D_L/D_T	γ=120	D_L/D_T	γ=150	D_L/D_T
0%	337.0	1.00	417.0	1.00	457.0	1.00	487.0	
100%	281.0	0.83	361.0	0.86	401.0	0.87	431.0	0.88
90%	287.2	0.85	367.0	0.88	407.0	0.89	437.0	0.89
80%	292.8	0.87	372.0	0.89	412.8	0.90	442.8	0.90
70%	298.2	0.88	378.0	0.90	418.0	0.91	448.0	0.92
60%	303.8	0.90	383.8	0.92	424.0	0.93	454.0	0.93
50%	309.3	0.92	389.3	0.93	429.0	0.94	459.0	0.94
45%	312.1	0.92	392.0	0.94	432.0	0.94	462.0	0.95
40%	314.9	0.93	395.0	0.95	435.0	0.95	465.0	0.95
35%	317.6	0.94	397.6	0.95	437.6	0.96	467.6	0.96
30%	320.4	0.95	400.4	0.96	440.0	0.96	470.0	0.96
25%	323.2	0.96	403.2	0.97	443.0	0.97	473.0	0.97
20%	325.9	0.96	405.9	0.97	446.0	0.97	476.0	0.98
15%	328.7	0.97	408.7	0.98	449.0	0.98	479.0	0.98
10%	331.3	0.98	411.3	0.98	451.0	0.98	481.0	0.99
5%	334.3	0.99	414.3	0.99	454.0	0.99	484.0	0.99

For lower radionuclide concentrations, of say Th=9ppm and U=2.84ppm, the general conclusion is that the error involved is lower. Radon losses up to 50% give rise to deviations in the total dose rate of between 5-10% depending again on the potassium contents and gamma dose contributions.

The higher these parameters, the lower the error. For a fairly average case of 15% radon loss, errors of the order of 2-3% are encountered. The above computational investigations applied to our samples produced a negligible error due to the relatively high potassium contents and gamma dose parameters. In general, under normal circumstances, the "radon emanation" is not a serious problem as has been considered up till now by some TL workers, Aitken, (1978).

Attempts to calculate such radon emanation have been demonstrated by Desai and Aitken, (1974). However, the escape must take place predominately through the pores and as the pore volume is generally 10-20% of the total volume, it would probably be reasonable to assume that the escape of radon would not exceed 20% (see Table 3.5), taking into account the inwards movement of radon for the surrounding soil as well. Most of our sherds from Dimini were found within 30cm of the ground surface and those from Sesklo were found in an excavated section of 5m depth. Since they were covered by soil and additionally did not result in great radon emanation problems, we trust that the average of the alpha counts within 24 hours and after 15 days is representative of the actual value for evaluation and radon escape.

The Cretan kiln samples were taken from various parts of the kiln. The slope of the kiln walls and their fused state, indicate that the samples were not saturated and radon emanation is difficult to assess. The average is considered as the best value again.

3.6 Alpha Counter Calibration

Theoretically, the activity of the sample is given from the basic equation :

$$S = \frac{4N_o}{R\rho\Phi} \text{ , where}$$

S is the activity of the material;

N_o is the number of alpha counts per second;

$R\rho$ is the range of an average alpha particle in the sample, and is measured in units of g/cm^2.

Φ is the area over which the alpha counts were taken and is measured in units of cm^2.

This activity (S) is analogous to the activity λN (λ disintegration constant of the particular radionuclides with N number of atoms), except that S refers to the series as a whole. If S is divided by the number of alpha particles released by each of the series (8 for Uranium and 6 for Thorium), then making the following assumptions the dose rates can be calculated. These assumptions are:

i) Uranium and Thorium series are in radioactive equilibrium;

ii) screen-to-screen variations of the perspex container are small;

iii) the ratio Th-232/U-238 is 3.16.

The dose rates per alpha particle, counted per Ksec., for each of the two series were obtained using a screen of 12.8mm diameter and taking the values of $R\rho$ to be 6.94 mg/cm^3 for the Thorium series and 5.84 me/cm^3 for the Uranium series. In addition, threshold fraction and conversion functions were taken from Bell, (1977), and adjusted to our counter.

The standard material used was Uranium ore NBL analysed sample No.74-A with 0.1%U and Thorium ore NBL analysed sample No. 80-A, with 0.1%Th, and 0.001%U. ($\pm$1%)

From these concentrations the threshold for the Thorium standard material was favourable at 86%, 89% and 87%, respectively, for the three photomultipliers in our alpha counting system.

As our screen area is 2.73 times smaller than Bell's screen, and taking into account the respective thresholds our conversion table for U and Th radionuclides is as in Table 3.6.

TABLE 3.6

Dose rates (mrads/yr) per alpha particle/10^4sec		
Alpha	Beta	Gamma
42.2	1.96	2.35
40.8	1.90	2.28
41.6	1.94	2.32
41.7±0.006	1.93±0.04	2.31±0.05
For 1%K	82.2	24.7

Notes
Each of the above three numbers corresponds to the respective threshold for each of the three photmultipliers.

3.7 Alpha Counter Description

Three alpha counting systems, each as shown in Fig. 3.7, were used. The three photomultipliers were EMI type 9824B with linear dynode chains. The photomultiplier (PM) was shielded by mu-metal. A pre-selected counting time of $8x10^4$sec(approximately 24hours), was used. The photocathode of the PM was negatively earthed to avoid electrostatic effects in the perspex screen which might produce a radon retention or increased alphas as has been reported, Wintle, (1978)

3.8 Alpha Counting Results

Table 3.8 gives the results of total alpha counts and potassium determination and the respective beta dose for thesamples which were dated in our TL programme. A systematic error in the α-counting was taken as ±5%(±1σ)

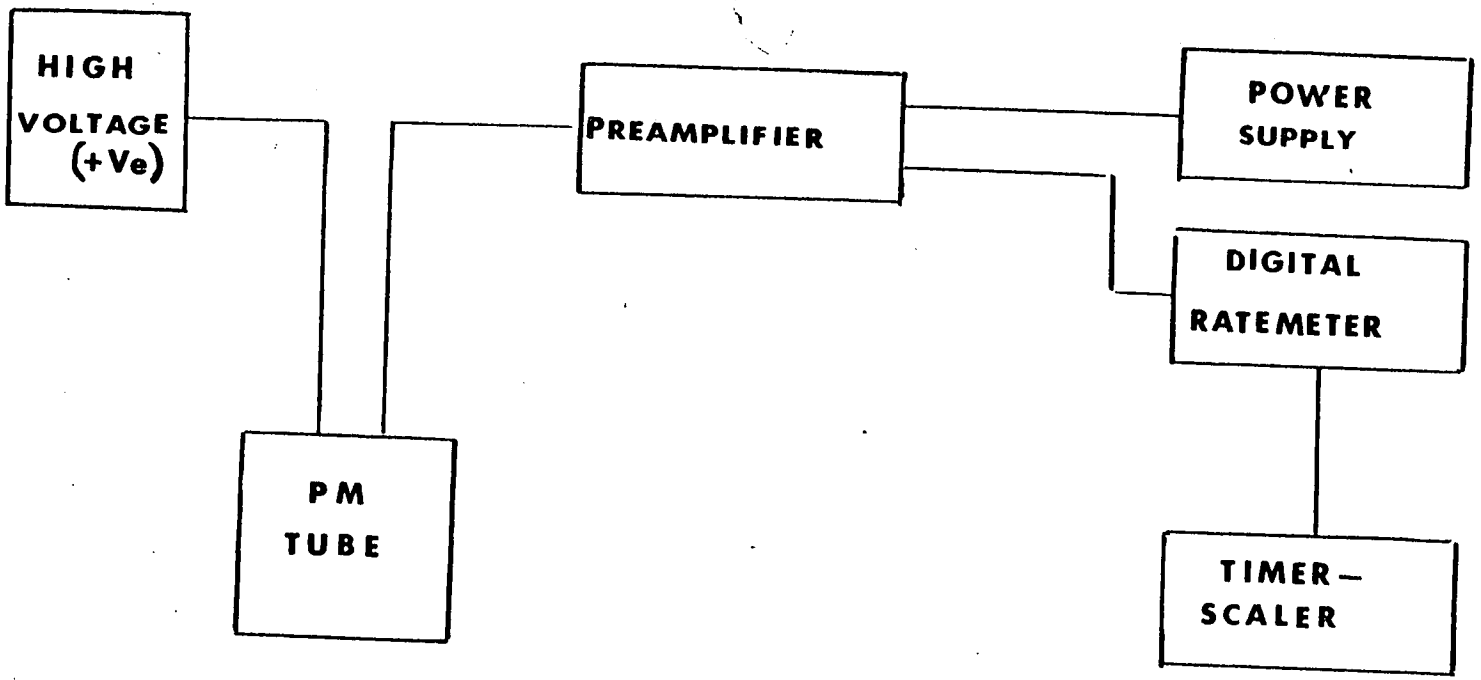


Fig. 3.7. Block diagram of α-counting system

TABLE 3.8

Sample	α-Particles/10^4	β(mrads/yr)U/Th	%K		β(mrads/yr)K	Total β (mrads/yr) on dry sample
SK1	48.4	93.4	2.50	*	205.5	268± 9
SK2	45.8	88.4	2.40	*	197.3	283±11
SK3	63.8	123.1	2.70	*	221.9	343±12
SK4	46.4	89.5	3.08	*	253.2	341±13
SK6	80.3	115.0	0.96	*	78.9	232± 8
SK8	51.9	100.0	3.00	*	246.6	345±13
SK12	84.0	162.0	-		-	-
SK13	41.0	79.0	-		-	-
SK14	66.6	128.5	2.50		205.0	330±10
SKE1	59.4	114.6	2.26		185.7	297±10
SKE3	45,0	86.8	2.20		180.7	265± 9
SKE4	36.8	71.0	3.92		322.0	390±13
SKE5	57.8	112.0	2.69		221.0	330±10
SKE6	53.9	104.0	2.10		172.6	274± 9
SKB(I)1	53.2	102.7	4.20		345.0	444±14
SKB(I)2	47.0	90.7	3.30		271.3	359±11
SKB(I)18	77.7	150.0	2.92		240.0	386±12
SKB(I)27	42.0	81.0	3.59		295.0	374±12
SKB(I)28	38.1	73.5	4.03		331.0	400±13
SKB(I)98	38.6	74.5	3.34		274.5	346±11
SKB(I)1972	115.0	221.9	2.00		164.4	385±13
SKE	60.8	117.0	3.78		311.0	427±15
SK15	53.8	103.8	2.68		220.3	324±10
SH2	48.7	94.0	0.87		71.5	163± 6
SH6	45.5	87.8	0.79		65.0	150± 6
SH11	43.1	83.0	0.94		77.3	158± 6
DM1/2	39.4	76.0	2.60	*	213.7	288±11
DM6/6	36.6	70.6	2.14		176.0	244± 9
DM8/12	34.0	65.6	2.10	*	172.6	238± 9
DM10	32.5	62.7	2.40	*	197.3	260±10
DM10/20	43.0	83.0	-		-	-
DM11	28.1	54.2	1.30		106.8	161± 6
DM11/22	31.4	60.6	1.60	*	131.0	189± 8
DM14	39.0	75.3	1.82		149.6	233± 8
DM15	43.8	84.5	-		-	-
DM16	49.7	96.0	1.70		139.7	236± 8
DM32	45.0	86.8	2.26		185.7	271± 9
DM33	40.6	78.4	2.26		185.7	261± 9
DM35	53.3	103.0	2.62	*	215.0	318±18
DM39	39.3	75.8	3.27		268.8	341±11
DM41	25.0	48.0	1.64	*	134.0	181±10
KZ1/7	31.6	61.0	1.54	*	126.6	186± 8
KZ1/9	32.1	62.0	1.88	*	154.5	217± 8
KZ2/5	36.9	71.2	1.22	*	100.0	169± 7
KZ3/1	54.2	104.6	1.59		130.7	232± 8
KZ3/2	39.2	75.6	2.30		189.0	263± 9
744105	80.6	155.6	3.47		285.2	438±14
744106	85.5	165.0	3.28		269.8	431±14
744107	96.4	186.0	3.30		271.0	453±14
744401	78.7	151.9	3.42		279.5	430±14
FS1/5	33.4	64.5	1.48		121.6	184± 6
FS3/8	31.3	60.4	1.73	*	142.0	202± 8
FS3/9	28.6	55.2	1.418		116.6	170± 6
KH5	27.6	53.3	1.52		125.0	176± 6
KH7	27.2	52.5	1.57		129.0	179± 6

TABLE 3.8 (cont)

AT7	21.8	42.0	2.30	*	189.0	231± 9
AT8	45.0	86.8	1.79	*	147.0	232± 9
AT9	28.9	55.8	1.49	*	122.4	176± 7
STG ZA2	66.65	128.0	3.25	**	267.0	394±13
STG ZA43	48.2	93.0	3.85	**	317.0	409±14
STG ZA68	54.9	106.0	2.71	**	223.0	328±11
D6	33.4	64.0	2.69	**	211.0	409±14
D13	40.4	78.0	2.69	**	221.0	298±11
DL1/1	41.0	79.0	2.30		189.0	268± 9

Group	Average of All
SK	number of samples, n = 21 mean value μ = 3 40 standard deviation σ = 55 mean error = 12 coefficient of variation = 16%
DM	number of samples, n = 13 mean value, μ = 252 standard deviation σ = 54 mean error = 15 coefficient of variation = 21%
SH	157±5(3%)
KZ	215±10(5%) Site 3: 250±12(5%) Site 1: 204±12(6%)

Group	Average of All
AT	214±11(15%)
FS	188±32(17%) Site 3: 189±39(21%)
KH	179±5(3%)

Most of the potassium determinations were done by XRF (in Geology Department, Edinburgh University), with an accuracy of ±1%.
* Flame photometry (in the National Museum of Antiquities, Edinburgh), with an accuracy of ±3%
** Flame photometry (in the Geology Department, Edinburgh University), with an accuracy of ±2%
***The background in the alpha counting system (in the order of 1%) was subtracted

In the final error, a provision has been made to allow for an additional 4% error (sampling variance) which might be due to the potassium microvariations within the same sample. This has been found to be the case for a particular analysed powdered sample. Also, it must be noticed that without mixing the ground-down potsherd, two different parts of this potsherd could differ in potassium by as much as 30% (see Table 5.11)

which accounts for:

i) the small deviations of the U/Th ratio from the assumed value of 3.16

ii) the screen-to-screen variations of ZnS screen

iii) the conversion of betas and gammas (mrads/yr) from the adopted and tabulated conversion tables by Bell, (1977)

iv) the radon emanation uncertainty.

3.9 Potassium Determination

The potassium analyses were done by flame photometry (National Museum of Antiquities), two to three times for each sample of which the average was taken; by X-ray fluorescence (Geology Department, Edinburgh University). The results were given as K_2O percentages.

Table 3.9 shows the variations of K_2O for samples from Dimini, and Sesklo Neolithic settlements. Table 3.9.1 shows the variations of K_2O in samples from Cretan kiln sites.

The variations are very pronounced within one sample or within the same kiln area, Table 3.9.1 This is important in the determination of the beta radiations in ceramics. As part of the powdered sherd to be measured for its internal beta radioactivity must by the same powdered sample that is to be dated. Taking into consideration the fact that most of the beta contribution in ceramics comes from potassium, an error in this determination would result in serious errors in the final calcuated age.

The beta rate ratios derived from potassium are very important to the total dose of the potsherd and its accuracy must be carefully checked.

The final calculated error in the beta dose was that for alpha counting (±5%) and for potassium determination by flame photometry (±3%), or X-ray fluorescence (±1%), and an additional 4% due to the possible micro variation of potassium determination within the same sample.

TABLE 3.9

Dimini K_2O%		Sesklo K_2O%	
DM1/2	2.980	SK1	2.925
DM6/6	2.577	SK2	2.808
DM8/12	2.480	SK3	3.159
DM10	3.396	SK4	2.370
DM10/20	2.942	SK6	1.160
DM11	1.560	SK8	3.510
DM14	2.198	SK9	1.890
DM16	2.012	SK15	3.216
DM32	2.731	SK16	3.773
DM33	2.730	SK17	1.372
DM35	3.161	SK18	0.700
DM39	3.937	SK19	0.982
DM41	1.918	SKE1	2.725
DM11/22	1.866	SKE4	4.430
		SKE5	3.241
		SKE6	2.536
		SKB(I)1	5.074
		SKB(I)2	3.976
		SKB(I)18	3.522
		SKB(I)27	4.325
		SKB(I)28	4.860
		SKB(I)98	4.024
		SKB(I)1972	2.423
		SKE	4.560
		SKE3	2.650
n = 14		n = 25	
μ = 2.606		μ 3.048	
SD = 0.65 ($\pm$25%)		SD = 1.03 ($\pm$34%)	

TABLE 3.9.1

Stylos Hania K_2O%		
SH1	0.996	
SH2	1.048	
SH3	0.939	
SH4	1.979	Average of all:
SH5	1.136	1.14±0.35(±31%)
SH6	0.962	
SH7	0.919	
SH11	1.132	
Kato Zakros K_2O%		
KZ1/1	1.717	Variations within the
KZ1/2	2.732	same sample but from
KZ1/3a	1.405	different parts
KZ1/3b	1.687	KZ1/7: 33%
KZ1/4	1.600	KZ1/9: 22%
KZ1/7a	1.830	KZ2/1: 30%
KZ1/7b	1.343	
KZ1/9a	1.800	Average of all:
KZ1/9b	2.200	1.9±0.52(±27%)
KZ2/1a	2.863	Site 1=1.8±0.38(21%)
KZ2/1b	2.108	Site 2=1.8±0.66(35.7%)
KZ2/1c	1.116	Site 3=2.788
KZ2/1d	1.861	
KZ2/5	1.420	
KZ3/2	2.788	
Faistos K_2O%		
FS1/1	1.788	
FS1/4a	1.436	
FS1/4b	1.418	
FS1/5	1.776	Average of all:
FS3/1	2.707	2.07±0.50(±24%)
FS3/3	1.666	Site 1=1.555±0.17(±11%)
FS3/4	2.792	Site 3=2.40 ±0. 5(±21%)
FS3/5	2.801	
FS3/8	2.020	
FS3/9	1.708	
Agia Triada K_2O%		
AT1a	1.827	
AT1b	0.863	
AT2	1.616	
AT3	2.259	Average of all:
AT4	1.785	1.86±0.50(±26.7%)
AT7	2.700	Variation within the
AT8	2.100	same sample but from
AT9	1.740	different parts:
		1.345±0.34 (±0.5%)
Kalo Horia K_2O%		
KH1	1.976	
KH2	2.204	
KH3	2.699	
KH4	2.644	Average of all:
KH5a	1.832	2.26±0.35(±15.7%)
KH5b	2.766	Variation within the
KH6	2.064	sample but from different
KH7	1.895	parts: KH5: 33%
Others K_2O%		
Pressos 1	1.324	Variation within the
Pressos 2	1.264	same part of the sample,
		Average: 1.29±0.045(±3.5%)
		(35%)
Delphi1/2	2.774	
Sitagroi ZA2	3.920	
Sitagroi ZA43	4.640	or 3.943±0.3(±8%)
Sitagroi ZA68	3.270	
Dimitra 5	3.490	
Dimitra 6	3.10	or 3.28±0.09(2.3%)
Dimitra 13	3.490	
Exohi	3.00	

CHAPTER 4

ALPHA COUNTING AND GRAIN SIZE DISTRIBUTION

4.1 Experimental Procedure and Results

In order to demonstrate that the alphas emerging from a clay powdered sample (515mm^2 in area) are a function of the non-radioactive grains present in the clay, the following investigations were pursued on seven pottery fragments. By grinding down, gently, a piece of potsherd, and selecting different fragment sizes (by sieving them in a mesh), the resulting powdered clays were alpha counted. Plotting the number of alphas/10^4sec against the respective powdered clay sizes produces the diagrams of Figs 4.1. Table 4.1 also lists some radon emanation levels on different clay inclusion sizes and solid rings. Such emanation levels reflect the samples' porosity and radioactivity. The two photographs taken by scanning electron microscope explain the former by comparing the pore sizes with the grain sizes. (Note that the gaseous radon or thoron escapes much more easily through such air spaces than through clay matrix), Fig 4.11.

4.2 Interpretation of the results

Though not of similar shape, the graphs of Fig 4.1 can provide some interesting conclusions which are summarized below.

i) the number of alphas recorded by the ZnS screen in our alpha counter is a function of the size of grains in the space between the surface area of the clay which is in contact with the screen, down to a depth of around 40μm, which is, the alpha clay band (maximum alpha range in clays.) This is the factor of dilution of radioactivity in a pottery which is an important parameter in the evaluation of its internal radioactivity.

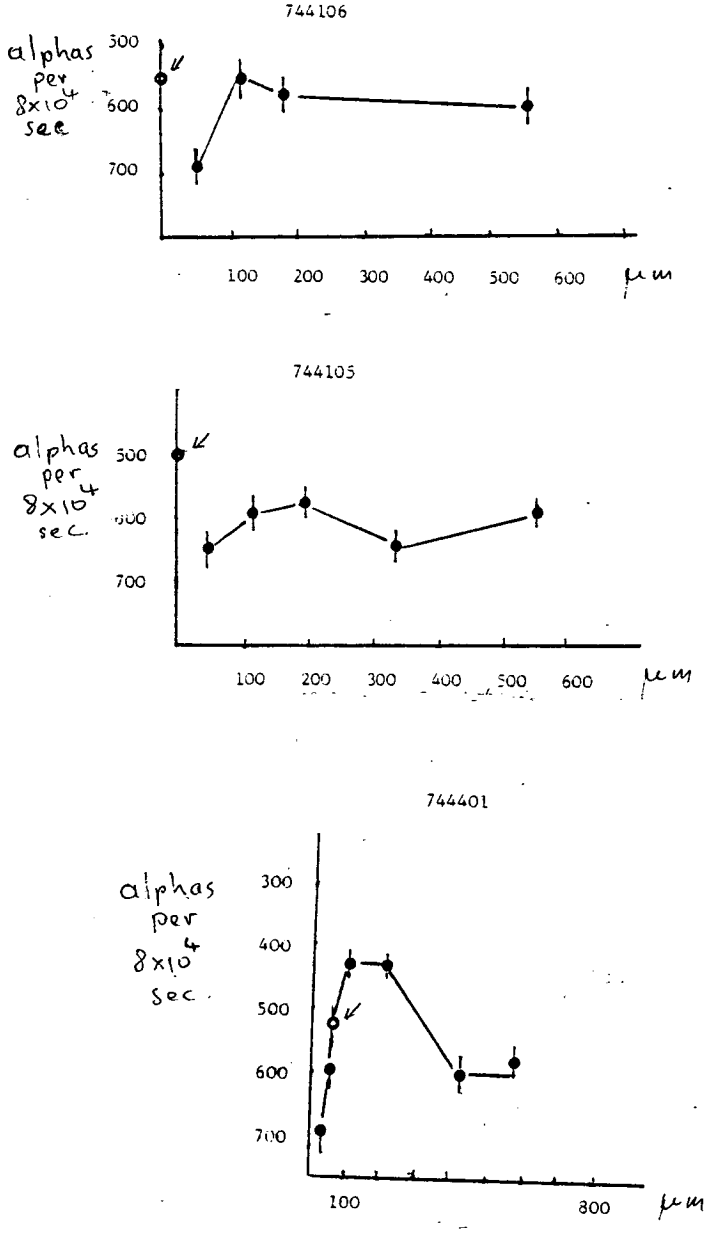


Fig. 4.1 Number of alphas as a function of grain size of the respective ground-down potsherd. The error bars reflect an error of ± 5% of the average value of two readings taken within 24 hours each. Open circle (-O-) repesents the solid disc value.

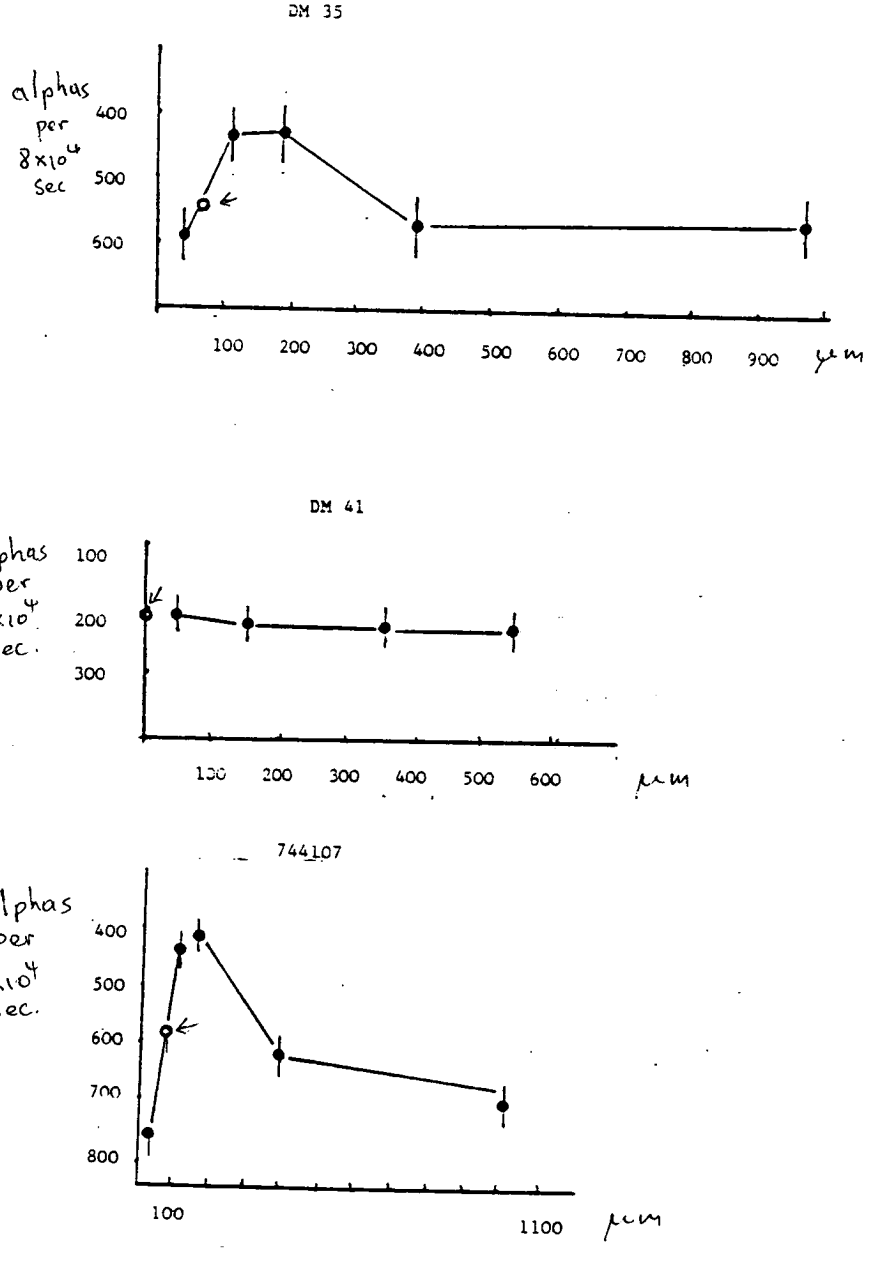

DM 35
alphas per 8x10⁴ Sec
400
500
600
100
200
300
400
500
600
700
800
900
μm
DM 41
alphas per 8x10⁴ sec.
100
200
300
100
200
300
400
500
600
μm
744107
alphas per 8x10⁴ sec.
400
500
600
700
800
100
1100
μm

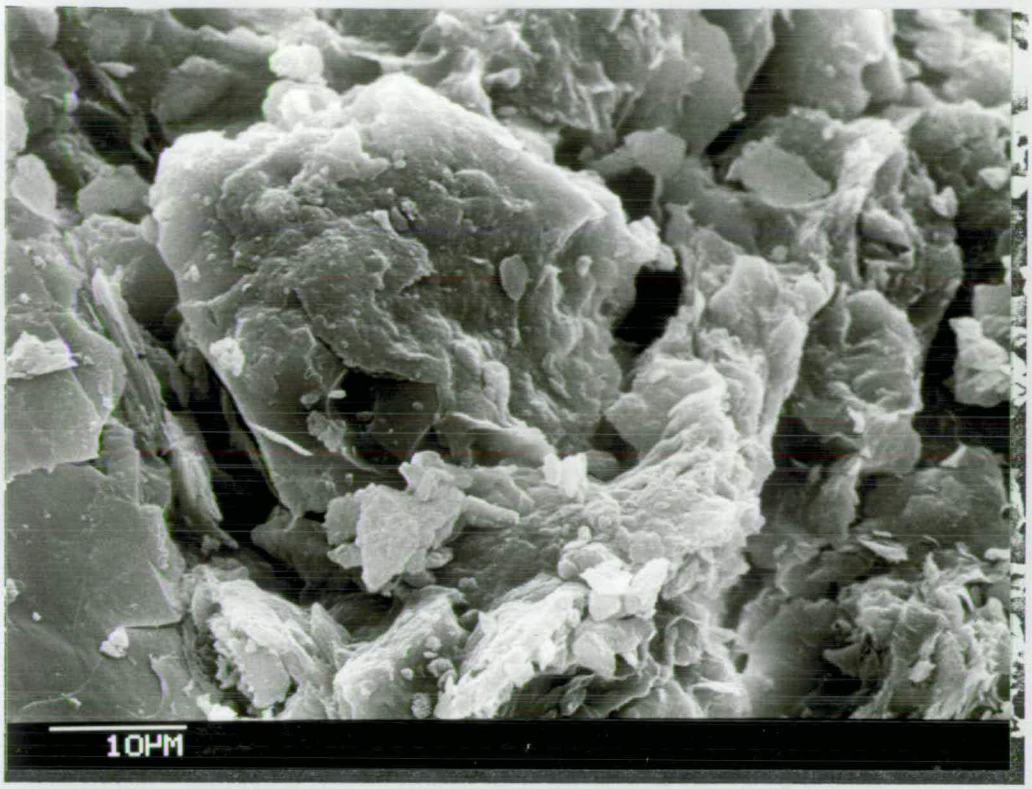
Fig. 4.1. (cont)

TABLE 4.1

% Radon emanation for different powdered clay sizes and solid rings

Sample No	Clay Size (μm)	% Radon Emanation
744107	125 - 250	4
744107	solid ring	6
744106	<75	2
744106	500 - 600	14
744106	150 - 212	8
744105	500 - 600	2
744105	150 - 212	8
DM35	<75	6
DM35	solid ring	6
DM41	<75	9
DM41	solid ring	12
DM41	500 - 600	14
DM41	75 - 212	8
744401	<75	3
744401	solid ring	7
744401	500 - 600	2

DM35



744106

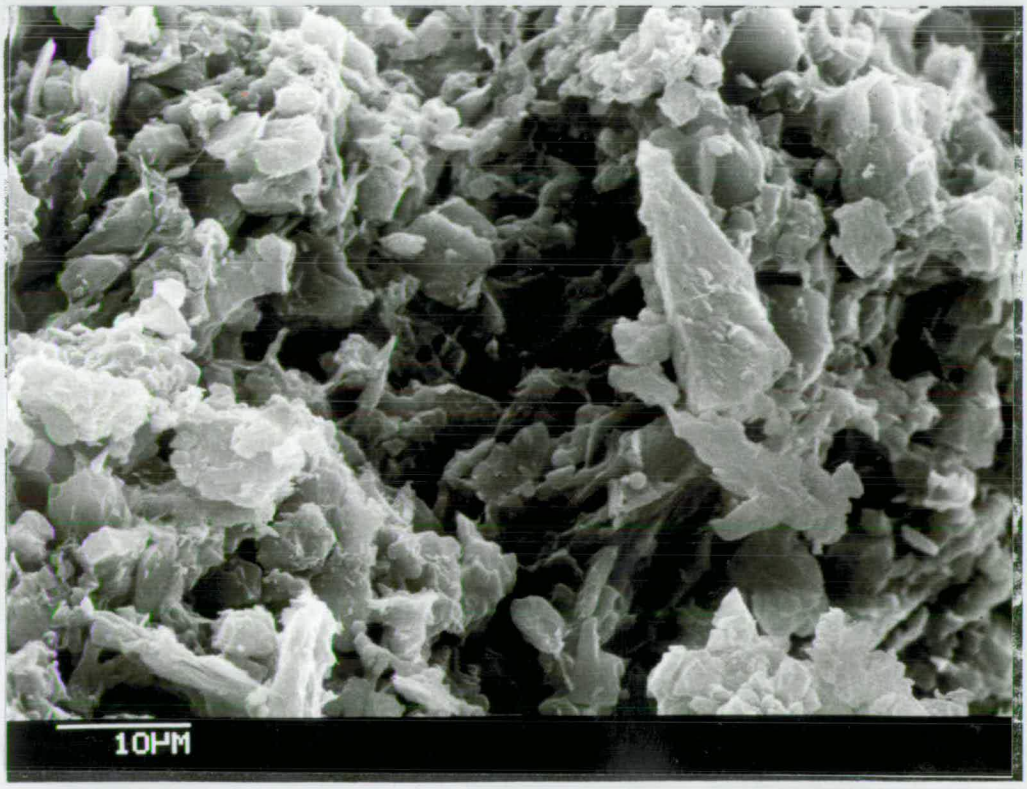


Fig. 4.1.1 Electron Scanning Microscope pictures on two samples. The size of grains and cavities is a measure of the porosity and uniform distribution of radioisotopes in the potsherd.

ii) the < 75μm powdered clay gave considerably higher alpha values. This is due to the fact that there are no grains present to dilute the alpha radioactivity.

iii) the solid rings (cylindrical pieces of potsherd made so as to fit the alpha cell), gave alpha values which fall between the values appropriate to <75μm and around 150μ sizes of alpha counted powdered clay and inclines to the average, of all the above 150μ grain size, number of alphas.

iv) well ground-down and alpha counted potsherd(<75μ) with all its inclusions produce the same number of alphas as other selected powdered clay sizes, for example, in DM41.

This would imply that the amount of grains in all cases occupy the same volume of space in the alpha clay band. This can be seen from thin section photographs in Fig 4.2 for the DM41 sample. As a result, the beta dose rate, calculated from this value of alpha counting plus potassium determination (α+K), that is 182 mrads/yr, was similar to that made by TLD ($CaSO_4$:Mn phosphor) of 181 mrads /yr.

Similar results were obtained for the Glozel clay sample, where the (α+K) gave 454mrads/yr, while the TLD gave 440 mrads/yr. In contrast, a characteristic example is that of DM35, where the TLD gave 278 ±10 mrads/yr and the (α+K) was calculated purely on <75μ powder, that is, without having included its inclusions, then the result of (α+K) was 362 ± 10 mrads/yr, or an erroneous higher estimation is obtained.

v) for large powdered clay grains sizes, the number of alphas approach the highest value given by the <75μm one. That could mean that the number of grains in this region is small, therefore the clay inclusions are of pure clay as the <75μ samples.

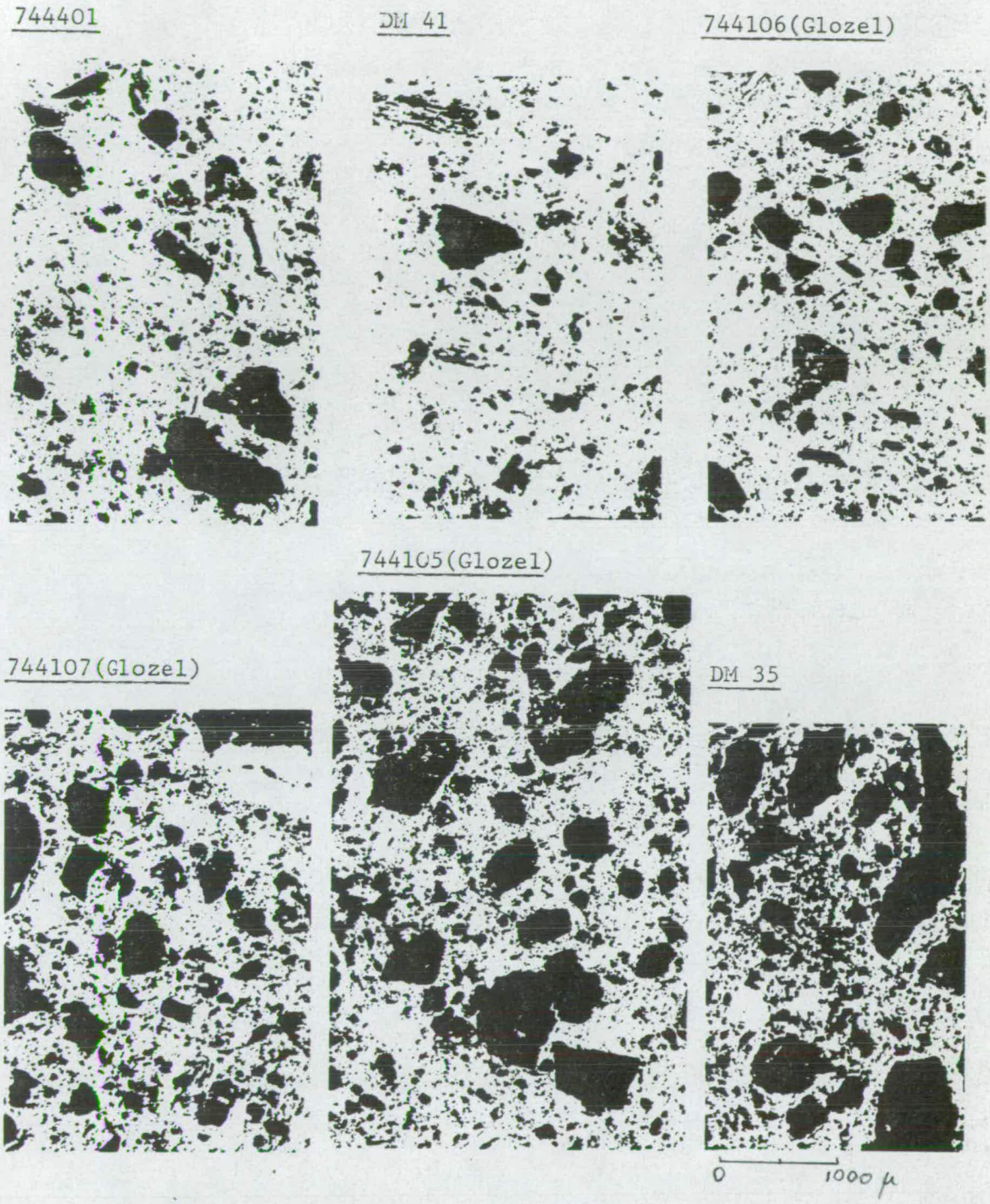


Fig. 4.2. Photomicrographs of Thin Sections of potsherds. Each photograph covers a representative area of the potsherd. The different percentages of different grain sizes present in each sample are shown.

The black grains are quartz, feldspars; the heterogeneous grey are mica, rock fragments and the white (difficult to be distinguished from the white background) are others, eg., magnetite. The rest of the white is the clay matrix.

This can be supported at a first glance, from thin section photographs taken on polished sections of the pottery sample. It should be mentioned here, that this does not show the actual (but a smaller) number of large grains, but is only an indication since the sectioned surface of the pottery might produce grain surfaces which are parts of larger grains (intersection problem.) Further, the slightly smaller alpha values of this high grain size from that of <75μ could also be attributed to air-spaces between the grains and the ZnS screen.

vi) the soft or fragile grains during grinding break down to smaller grains and, therefore, are included in the small grain size distribution.

vi) some grains are radioactive, for example, zircon, apatite, which give rise to alphas - in spite of the fact that they are counted as non-radioactive grains.

4.3 Discussion

It was not possible to attempt an estimation of such grain size distribution to the total clay matrix and to compare it with thin section grain size distribution, because in thin section measurements, the distribution of observed random grain diameters is not a reflection of sieve-size distribution, Friedman, (1957).

However, as a general conclusion, the number of grains of <75μ was of the order of (x20) higher than the other higher sizes.

This, of course, is balanced by the fact that the volume occupied by the high grain size is comparable with that occupied by many grains of small size.

The above results have an obvious effect on the determination of alpha-dose delivered to quartz fine-grains, and to the subsequent calculation of beta dose from observed number of alpha particles, in

the "inclusion technique". Nonetheless both the techniques (α+K and TLD) will be subjected, also, to the following effects:

i) large radioactive inclusion will not show up the alphas for powdered clay of grain size greater than the alpha range, while it will be shown in fine powdered clay.

ii) For a very coarse-grained sherd, e.g. DM41, containing a large fraction of low radioactive inclusions, the alpha count rate will decrease when it is ground down because the interiors of these inclusions will now dilute the average radioactivity as seen by the ZnS.

4.4 Conclusions

From the above, the way of grinding down and alpha counting of a sample is of great significance in the determination of the beta dose (for the TL dating) experienced by the quartz inclusions in it. The resulting powdered clay of <75μ in size must include all those inclusions which will "dilute" the radioactivity, as actually occurs inside the sherd.

Finally, it was found that most of the grain sizes occur in the 100-200μm region and that the amount of grains and the porosity of a sherd reflects different radon emanation and observed radioactivity.

CHAPTER 5

MEASUREMENT OF BETA DOSE RATE BY TLD

5.1 INTRODUCTION

In this chapter the TLD method is examined and comparisons are made with the alpha counting method as described in Chapter 3 An outline of their respective features is undertaken in order to determine the most reliable beta dose rates for the samples which are to be dated by thermoluminescence.

5.2 Measurement of Beta Radiation by $CaSO_4$:Mn

Application of sensitive phosphors for determination of the radioactivity of ceramics used for TL dating, has been reviewed in Chapter 2 . A version of the technique for measuring betas in ceramics suitable for practical application has been designed at Edinburgh, (McKerrell & Mejdahl, 1976) and adopted in the present programme. This technique involves a small polypropylene wafer, with diameter of 12mm and thickness of 0.8mm, with a depression which can accommodate a pair of $CaSO_4$:Mn teflon discs, each 5mm in diameter and 0.4mm thick. (Fig 5.2).

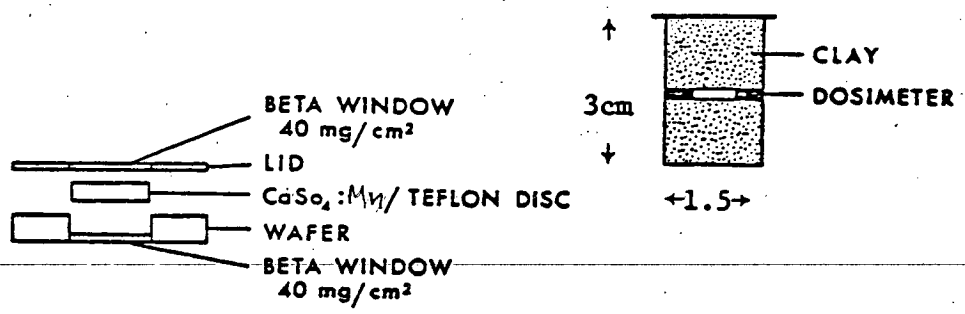


Fig. 5.2. TLD β-Counting Configuration

About 2gr of sample is required to fill the capsule with 1gr on either side of the phosphor. The sample was powdered by breaking down a part of the sherd with all its inclusions inside, since they account for the radioactivity dilution effects.

The capsule, which was sealed with a lid in order to prevent the escape of radon and thoron, was then stored in a freezer at -28°C for one month.

Calibration of the readings of thedosimeters after storage is done by comparison with dosimeters stored in capsules containing standard material with a known concentration of potash feldspar with an equivalent potassium oxide content of 11.2%, hence the potassium was 9.3% by weight. (Note that 2/3 of the beta radiation in a sherd originates from the potassium). Background readings were taken from dosimeters stored in capsules containing sodium chloride powder. The calibration is thus based on calculations of beta-ray intensities for known amounts of the potassium radio-isotope and the resulting dose rate value is referred to a point in an infinite medium of the material. The calculations are based on the conversion values given by Bell, (1977). The dose was calculated by the formula:

$$D = \frac{764(R-R_{Bg})}{(R_s-R_{Bg})}$$

where,

764 mrads/yr comes from 9.3%K,

R is the ratio of the TL reading taken immediately after taking a phosphor out of the freezer to the reading obtained from the normalisation dose by a CO-60 source,

R_{Bg} is the background reading ratio obtained as formerly,

R_s is the standard's reading ratio obatined as formerly.

The method outlined above is very convenient and for homogeneous material it can be reliable. There are, however, a number of perturbing factors which will affect the overall accuracy of the beta dose rate value. Some of these are discussed briefly, below:

i) Variation in relative abundance of radioisotopes

The relative abundance of the three radiation sources, potassium and the uranium and thorium series, can vary markedly from sample to sample.

The consequences of isotopic variation was investigated in some detail by Mejdahl, (1978), by preparing anumber of radioactive standards where the Th/U ratio and the total beta dose rate was kept the same, but the potassium content was decreased in steps down to zero. A certain effect of isotopic variation amounting to 10% for small potassium concentrations was observed.

ii) Attenuation of beta radiation by quartz and feldspar inclusions

As mentioned above, the dose rate value obtained from the measurements refers to a point in an infinite matrix of homogeneous material. However, the value of interest in inclusion dating is the average dose to quartz and feldspar grains of a finite size varying from 0.05 to 2mm. Therefore, correction must be made for attenuation of the beta radiation by the grains.

Since the individual attenuation for the three beta contributors (uranium, thorium and potassium) as well as for the different components as IC auger electrons, internal conversion electrons, included in the beta dose contributions differ somewhat, then, the resulting attenuation curve will depend on their relative abundance. The variation in abundance normally encountered will not cause any significant deviation from the attenuation curve, but in extreme cases, it might be substantial.

The attenuation factor calculated for the present case accounts for:

a) the chosen average diameter value of the sifted powdered pottery in the respective grain sizes, and

b) the soft beta particles being stopped and discarded in the outer 20μ of the grains (when they are etched to exclude any alpha contribution in the total dose)

iii) The radon problem

This problem has been described previously (Chapter 3 and section 3.5). The first consideration concerns the build-up of radon to equilibrium in a sample which has been sealed off in the capsule for measurements of beta dose rates. Assuming that all radon was lost from the sample at the moment of sealing, the activity will grow to about 80% of its equilibrium in a period of two weeks.

Calculations (McKerrell, Mejdahl, 1976) show that the difference in doses accumulated during four weeks in the two extreme cases of build-up from total disequilibrium (if no radon is present initially) and of full equilibrium during the whole period is about 3%.

In practice, total initial loss of radon would be unlikely, and, in any case, the problem could be eliminated by extending the storage period. Assuming that the measurement period has been of a sufficient length for build-up effects to be negligible, the beta rate values obtained will refer to complete retention of radon. However, since the pottery could have been losing radon (and possibly thoron) during burial in the ground, the true dose rate during burial might have been lower than that derived from the laboratory measurement. In our cases, a loss of less than 10% occurs in the major part of our samples which would mean

that the final error involved in the TLD is negligible.

iv) Water content of pottery

At northern latitudes, sherds buried in soil will normally be almost saturated with water perenially. Since the water causes attenuation of the beta radiation, the true dose rates, as calculated by means of alpha counting or TLD, will be lower than the values derived from laboratory measurement on dry pottery clay. When the dose rate is measured by means of TL phosphors, the correction can be incorporated in the measurement by adding the calculated amount of water to the dry clay in the capsules and thereby, water and radon are contained and estimated simultaneously. Further studies on checks of this kind of measurement, but on solid fragments, were done (see Chapter 2). Finally, the principal drawback of the technique is the necessity to base the calibration on dose rate values, calculated from given concentrations in the standard samples, and their accuracy.

We have investigated the possibility of avoiding some of the above problems, for example beta attenuation, the differences in stopping powers, dilution of the radioactivity of the sherd by the grains present, by using the quartz (110°C peak), inclusions themselves, as built-in dosimeters for measurement of the beta dose rate (see Chapter 2)

5.3 TLD Results

Tables 5.3,- 1 show the beta dose rate results from the $CaSO_4$:Mn phosphors from a variety of Hellenic archaeological samples. The respective beta

TABLE 5.3

Beta Dose Rates of Cretan Materials

Sample No	Beta Dose Rates by TLD(mrads/yr)	
KZ1/7	140 ± 12	
KZ2/5	141 ± 5	Average of all: 150±16(11%)
KZ1/9	148 ± 15	Site 1: 144±4 (3%)
KZ3/2	223 ± 19	Site 2: 114±26(22%)
KZ3/1	226 ± 31	Site 3: 224±2 (1%)
KZ2/2	113 ± 17	
KZ2/3	136 ± 5	
KZ2/4	74 ± 5	
AT7	173 ± 6	
AT8	204 ± 30	Average of all: 154±41(27%)
AT9	91 ± 8	
AT6	149 ± 10	
FS3/8	231 ± 20	
FS1/5	184 ± 5	
FS3/9	143 ± 17	Average of all: 195±47(24%)
FS1/6	158 ± 10	Site 1: 182±18(10%)
FS1/7	175 ± 2	Site 3: 209±61(29%)
FS1/9	210 ± 26	
FS3/12	162 ± 5	
FS3/10	299 ± 26	
SH6	100 ± 5	
SH11	168 ± 18	Average of all: 116±29(25%)
SH10	83 ± 7	
SH12	105 ± 5	
SH9	127 ± 10	
KH14	114 ± 8	Average of all: 115±48(42%)
KH13	175 ± 4	
KH12	56 ± 2	
Presos	80 ± 10	
Delphi 2	122 ± 36	
Delphi 13	96 ± 3	
Delphi 1/1	218 ± 5	

TABLE 5.3.1

Beta Dose Rates on Dimini, Sesklo Materials

Sample No	Beta Dose Rates by TLD(mrads/yr)	
DM8/12	260 ± 23	
DM11	110 ± 5	
DM32	265 ± 15	
DM11/22	133 ± 8	
DM1/2	205 ± 11	
DM35	278 ± 41	
DM10	255 ± 35	
DM41	182 ± 14	
DM7/8	206 ± 10	
DM2/4	114 ± 5	Number of sherds, n = 18
DM5	193 ± 10	Mean Value, μ = 183
DM10/21	214 ± 10	Standard Deviation, σ = 26
DM12/25	140 ± 7	Mean Error = 6.2
DM1/1	162 ± 10	Coefficient of Variation = 14.2
DM19	114 ± 4	
DM15	185 ± 12	
DM13/28	197 ± 17	
DM12/26	144 ± 15	
SKB(I)27	305 ± 36	
SKB(I)2	364 ± 17	
SK1	292 ± 11	
SK8	285 ± 18	
SKE6	207 ± 12	Number of sherds, n = 16
SKE4	279 ± 15	Mean Value, μ = 279
SKB(I)72	380 ± 23	Standard Deviation, σ = 27
SKE3	205 ± 9	Mean Error = 6.7
SKB(I)1	464 ± 19	Coefficient of Variation = 9.6%
SK3	340 ± 12	
SK4	249 ± 19	
SK15	264 ± 38	
SK2	200 ± 34	
SK9	237 ± 14	
SK13	193 ± 12	
SK11	202 ± 7	

dose rates quoted in this chapter are without the necessary correction, for water uptake and attenuation through the grains. These are correctly presented in the appropriate chapter (chapter 10) with the other dating results. These uncorrected values are then compared, since they represent the same powdered clay in the dry state.

In order to emphasize the degree of variations in beta dose within the same kiln or sites, the results were grouped and the average from samples taken from different parts of the same site were taken and their standard deviation was calculated. Certainly, such variations were expected, because of the widely different values found for the potassium contents, potassium being the major contribution to the beta dose rates. (Chapter 3, table 3.1). Tables 5.3 and 5.3.1 show the set of results from Crete and Thessaly, respectively.

5.4 Comparisons of Alpha Counting and TLD Techniques

Some of these samples were measured by both (α+K) and TLD techniques. The comparison between β-dose rate evaluation using the two techniques for 35 pottery samples, (Tables 3.8 and 5.3 & 5.3.1) shows that 22 samples (62%) agree within one standard deviation (±1σ); 5 (15.1%) of these samples agreed within two standard deviations (±2σ) and 8 samples (23%) did not match well. In general, the alpha counting results are higher than the $CaSO_4$:Mn ones.

5.5 Discussion on Alpha Counting and $CaSO_4$:Mn Methods

It has been mentioned earlier that for evaluation of alpha dose rate by alpha counting, the sample should be in ground form with the errors (Zimmerman 1970) caused in extreme cases of having many large radioactive inclusions or radioactivity attached to the surface of the individual grains. In either case, the way of grinding down is very important. For the determination of beta dose rates the sample should be finely-powdered. This was done by selecting fine powder of under 75μ in size.

5.5.1 Discussion of the problems associated with the $CaSO_4$:Mn method

i) If feldspar grains are present with a high potassium content, the breaking down of these grains will destroy the attenuation effects which would be present in the unbroken grains before reaching the $CaSO_4$:Mn phsophor. This, of course, will give an increased dose to the phosphor equal to the self-absorbed dose by the feldspar grains, due to the beta attenuation in passing through them. In the present instance, that does not occur, because of the negligible potassium content in the grains.

ii) the use of TL dosimetry for beta dose rate eliminates not only the potassium analysis, but also extra alpha counting. Nevertheless, it has been noted (Chapter 2) that the potassium analysis is necessary for calibration reasons.

iii) the most serious problem that interferes with beta TLD is that of achieving a response that is isotope-dependent, that is, that evaluates the beta dose rate correctly whether Th, U or K is dominant.

Particular attention must be given to the strong variations in relative potassium concentrations which have been found (see section 3.9, Table 3.9,-1). There are two causes of isotope-dependence in beta TLD. First, the need to shield off betas from alpha particles introduces attenuation of the beta dose rates which however, is the same for samples and for standard samples, and this is dependent upon the beta spectrum. Secondly, although the absorption coefficients for gamma radiation are much lower than for betas there is nevertheless a gamma contribution whose significance is dependent upon the

differences in the radioactivity between sherd and soil , and the ratio of gamma to beta dose rates is strongly isotope-dependent: 1.8/1 for the thorium series, 0.8/1 for the uranium series and 0.3/1 for the potassium,

iv) the calibration for TLD dosimeters is another problem which, together with isotope dependence problems, could upset the calculated results. In our situation, the variations of U, Th and potassium and the preparation on only one standard material, such as potash feldspar, have to be considered, as introducing probable errors in the measured samples, (depending on the sherd's potassium content).

v) fading of some samples during transfer between freezers or because they were stored near the door of the freezer can not be taken into account but it could explain why some TLD results tend to be lower than the respective alpha counting ones.

vi) further, the energy response of the $CaSO_4$:Mn to beta particles after being attenuated through the clay matrix might not give the real response as compared withthat of quartz or feldspar grains, depending on the relative concentration of the radioisotopes at the standard calibration samples. However, except for samples of abnormally weak radioactivity, beta TLD will not introduce gross errors and its advantages in being independent from Th/U ratio helps to avoid some uncertain errors.

vii) the characteristics of the set up dosimeter unit such as: sample weight, dosimeter thickness, geometrical configuration andmaterials of

tray, because of back scattering effects has also to be taken into account. The "infinite medium" assumption in measuring beta doses with the geometrical arrangement mentioned in section 5.2, might not be valid for some sherds, because their thicknesses are smaller than, say, 0.7cm. (As it was found to be in Chapter 2)

It is now necessary to outline the alpha counting method's features.

5.5.2 Discussion on the Problems Associated with (α+K) Method

The Th/U ratio is assumed to be constant for all samples. Thus dose rates have been calculated on the assumption of the decay chains being in equilibrium and on a Th/U ratio of 3.16 by weight, which corresponds to the activity of Th-232 being equal to the combined activities of U-238 and U-235. If the decay chains of U and Th are in equilibrium, the alpha counting is straightforward. If this is not so, some degree of inaccuracy is introduced. For beta dose rates, derived from (α+K), the inaccuracy arises only with respect to the Th/U ratio. Any error arising from the uncertainty in the Th-232/U-238 ratio is considered as a systematic error, because it is possible that all samples from the same context are likely to have about the same ratio. Although the Th/U ratio can be evaluated from each sample by means of the "pairs" technique (based on the 0.15 sec half-life of Po-216 in the Th chain, Aitken, 1978), it is not practical to do this on a routine basis, because of the long counting time required. For example, a week or more is required to get the statistical error below 10%, (Aitken 1978 and Huntley and Wintle, 1978), though an indication of a gross deviation from average can be obtained in about two days.

The Th in the present samples varies from 5 - 20ppm, (see Table 10.4.1, from NAA) for which a characteristic value of 12ppm has been chosen, with U being around 4ppm. Deviation from the above value will alter

the Th/U ratios. Deviations, for example, of ±2ppm from the respective concentrations, produce an error in the final beta dose evaluations, which with four different potassium contents, are displayed in Tables 5.5.1 and 5.5.2.

As can be seen from the complete loss of Th or U an extreme situation, which is very improbable , the errors are as high as 60%. In such cases, where there is an absence of Th and where U concentrations are higher than, about 6ppm, the error involved is negligible. In cases where the potassium content is even higher than 2%, the respective error in the above extreme cases is lower than 25%. From ratios varying between 1.6 to 7, the respective errors are relatively low; particularly when the potassium content is higher than 2%, the involved error is < ±8%. The last error could have been introduced in our calculation if the assumed Th/U ratio 3.16 is no longer valid. Nevertheless this error, in such cases, would be much less in the age calculation due to dilution of these percentages by other components of the total dose rates.

Another cause of inacurracy could result from:

a) determination of the nominal value of the standard material,

b) counting statistics (quoted accuracy),

c) calculations based on conversions of radioisotope activities to dose rates,

d) sizeable radioactive inclusions present in the sherd and their effect on thealpha counting during grinding down and

e) screen-to-screen variations (perspex container for measuring alphas see Chapter 3).

TABLE 5.5.1

Deviations of ±2ppm from Initial Th = 12ppm and U = 4ppm Concentrations, Produce different Th/U Ratios (in brackets)

Uppm / Thppm	0	2	4	6
10	29	(5)58.3	(2.5)87.6	(1.6)116.8
12	34.8	(6)64.0	(3.0)93.4	(2.0)122.6
14	40.6	(7)69.9	(3.5)99.2	(2.3)128.4
0	0	29.3	58.6	87.8

The above results are compared with those calculated on initial concentration of Th = 12ppm and U = 3.8ppm (ratio = 3.16). These values give a beta dose of 90.4 mrads/yr.

TABLE 5.5.2

Th/U Ratios	1.6	2	2.3	2.5	3	3.5	5	6	7	Th = 10,12, 14ppm U = Oppm 10	12	14	Th = Oppm U = 2,4,6ppm 0	0	0
% Deviation from 90.4mrads/yr	+26.0	+32	+38.0	-3.0	+3	+9.0	-32	-26	-20	-61	-56	-50	-61	-32	-3
% Deviation from total dose of 255 mrads/yr K = 2%	+10.0	+12	+15.0	-1.0	+1	+3.5	-12	-10	-8	-24	-22	-19	-24	-12	-1
% Deviation from total dose of 173 mrads /yr K = 1%	+15.0	+18	+22.0	-2.0	+2	+5.0	-18	-15	-11	-35	-32	-29	-35	-18	-2
% Deviation from total d ose of 337 mrads/yr K = 3%	+7.0	+10	+11.0	-1.0	+1	+3.0	-9	+7	-6	-18	-16	-15	-18	-9	-1
% Deviation from total dose of 131 mards/yr K = 0.5%	+20.0	-24	+29.0	-2.0	+2	+7.0	-24	-20	-15	-46	-43	-38	-43	-24	-2

The plus and minus signs refer to the greater or lesser (%) deviations of the beta dose for the respective Th/U ratio values from the total beta doses (mrads/yr) for Th = 12ppm, U = 3.8ppm plus the respective K%

5.6 Tests on Choice of the Most Appropriate Technique

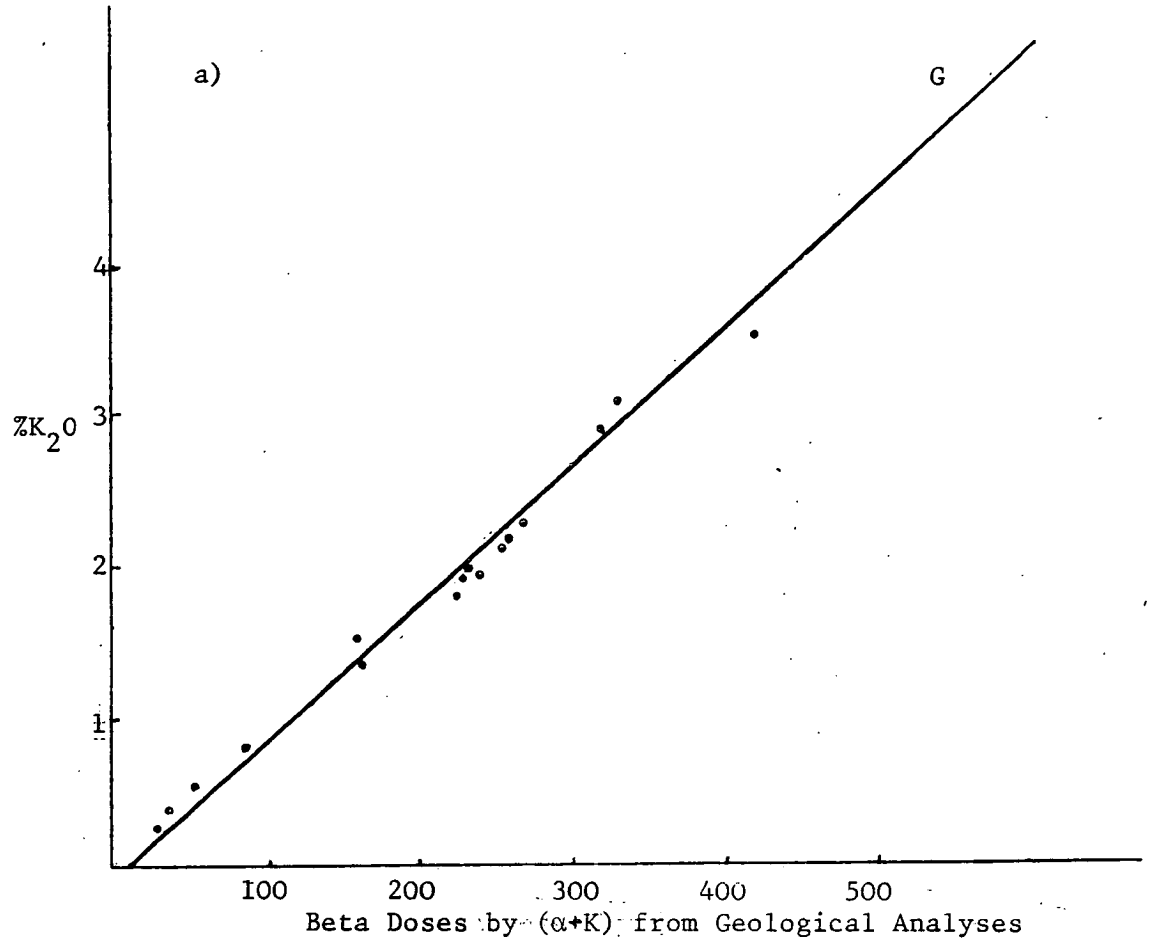
From the above discussion and presentation of the "Achilles Heels" of both methods, it appears that the calculated beta dose rates for 62% of the samples are correct since both methods agree within $\pm 1\sigma$ of the errors involved; for 15% of the samples the methods agree to within 2σ. However, there remains 23% of the samples for which alpha counting and TLD do not agree.

In order to decide which results to use for dating purposes, the following facts were considered:

i) approximately two thirds of the beta dose radiation in ceramics comes from the potassium content. Correct determination of this parameter would avoid random errors introduced for the assumptions made to evaluate beta radiation from U and Th contents. Especially for our samples with their high potassium content of above 1.5%, the alpha counting method would be unlikely to produce large errors in the final evaluation of beta dose rates despite the other uncertainties involved and extensively examined and discussed in Chapter 3 and briefly above.

ii) whilst the TLD method produces uncertainties due to fading or misreading of the phosphors thus would affect some of the results which would well amount to approximately 20%. However, the above predicament in choice was tested by other means.

Geologically, the almost universal tendency for the concentration of U and Th to increase towards thelater members of an igneous differentiation series has been documented repeatedly, Peterman,(1963), Hamilton,(1959), Gottfried,(1959), Heier and Rogers,(1963) in "Handbook of Geochemistry" Vol II-5, 1978. Fig. 5.6.a shows such a linear tendency(line (G)) when Th and U



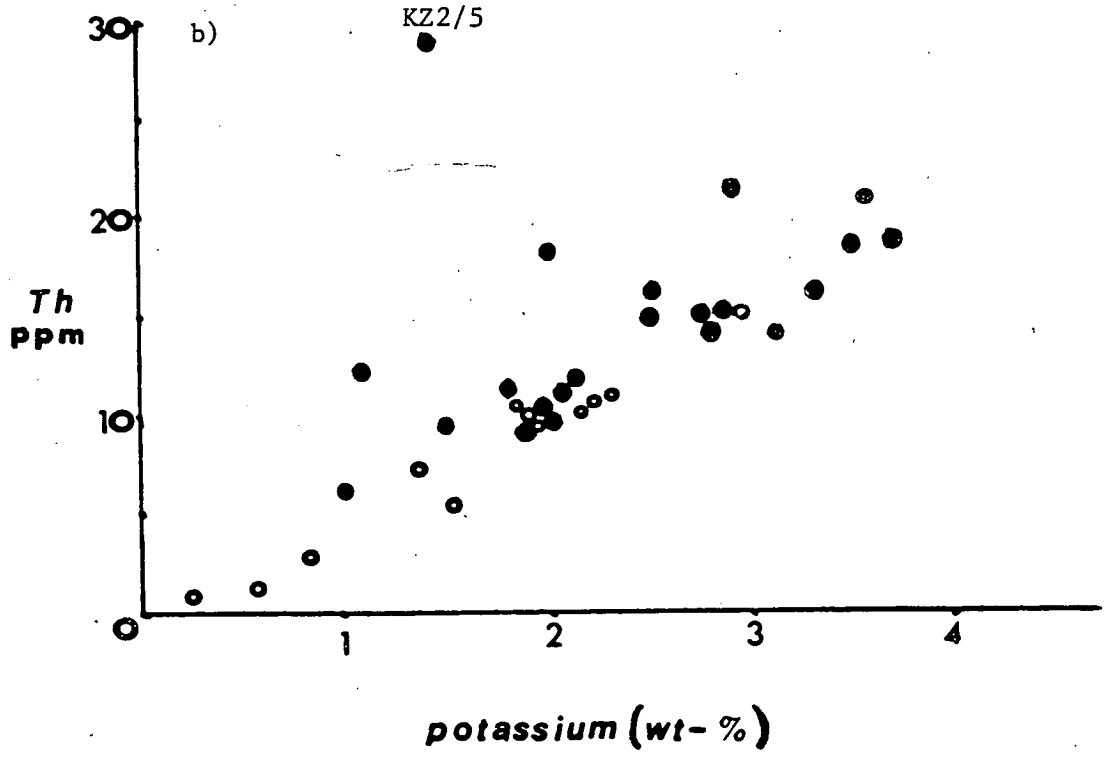


Fig. 5.6a) Linear Distribution of β-dose rate →K_2O for Geological Materials. b) Thorium(ppm) →K for Geological Materials (open circles, after Peterman, 1963), and from present studies (black dots).

ppm values converted to mrads/yr are plotted against their counterpart potassium from data taken from Peterman (1963).

Therefore, it was decided to plot the potassium content of each sample against its respective beta dose rate (mrads/yr) as measured by (α+K) and TLD.

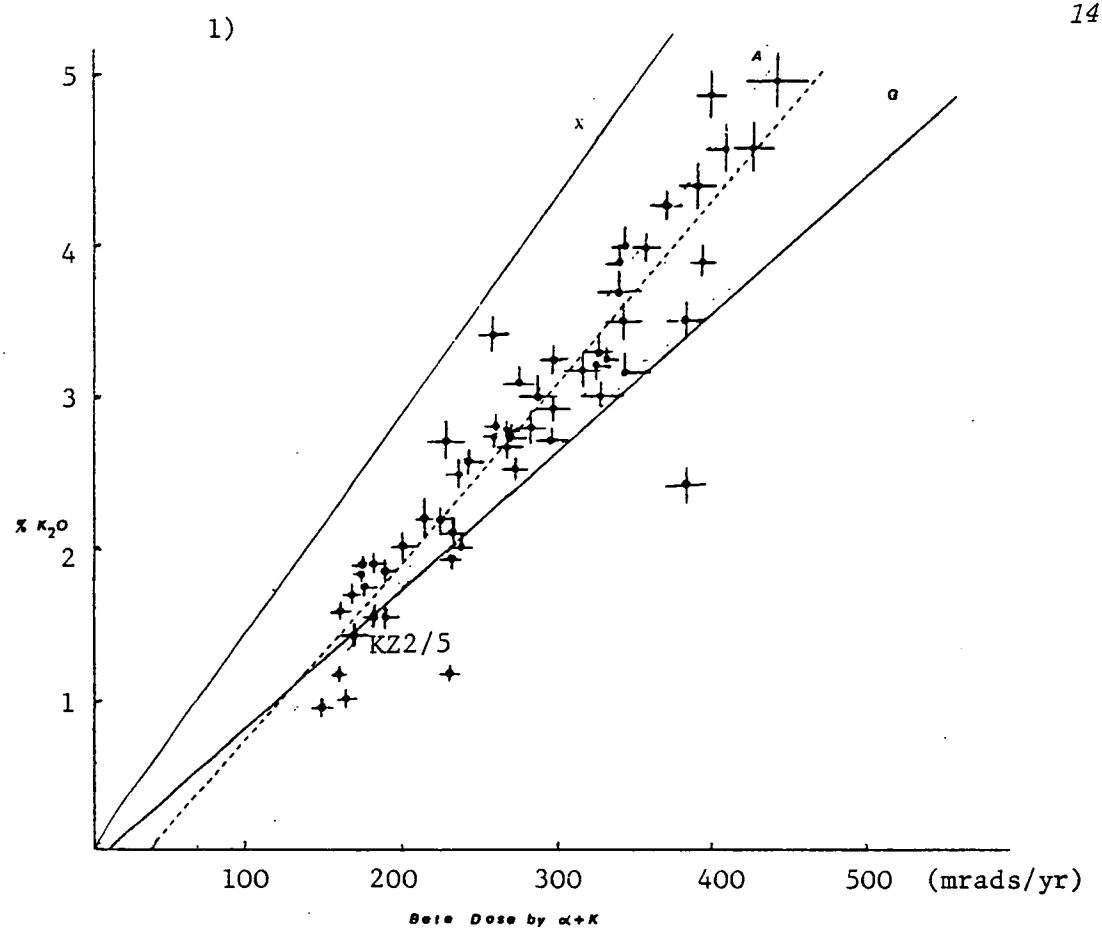
It seems that the beta doses by (α+K) → K_2O% have linear distribution and most of the points with their standard errors lie along line (A). (see Fig.5.6.1). Some scattered points could imply systematic error derived from some assumptions .

There appears to be a higher scatter in the case of beta dose as measured by TLD (line (T), Fig.5.6.2).

In particular, if there were no Th and U present in a sherd, the X-Curve of Figs.5.6 and 5.7 would indicate the lower linear boundary of the expected uniform distribution.

In the presence of Th, U the corresponding distribution would incline towards higher beta dose values. Generally, the Th and U correlates with the K such that a curve with a slightly reduced slope compared to the X-Curve would result.

As there is no indication of this, and so there is no reason to suppose that typical clay minerals have depleted U and Th contents (as NAA has shown for clays over all the world, McKerrell, pers. comm); there should be no scattering points to the left, i.e. the lower part of the distribution curves, but only towards the right or upper part of the distribution curves.



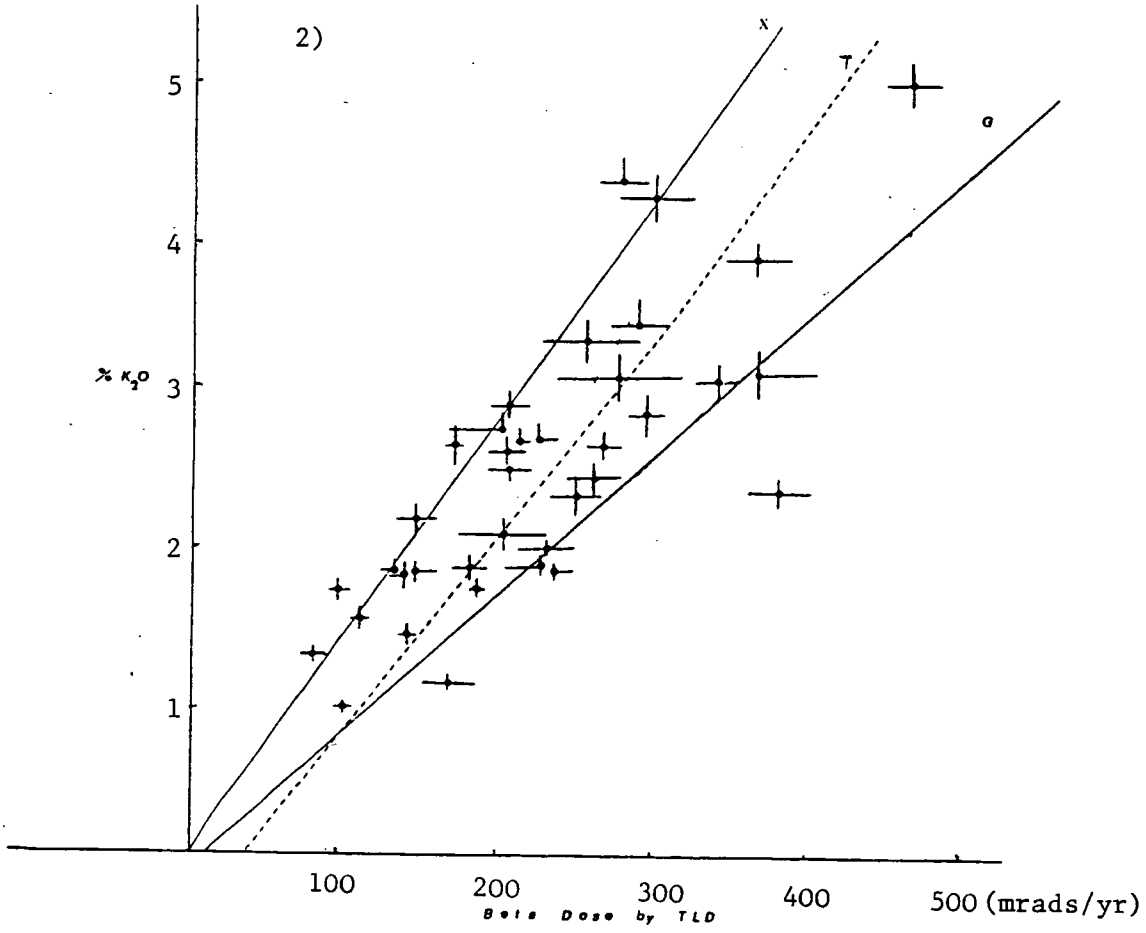


Fig. 5.6.1) Plotting of β-dose rate (α+K) → K_2O
2) Plotting of β-dose rate (TLD)→ K_2O

hus for excessive Th and U, or an excessive Th/U ratio, then the points would be expected to lie even further from the line of the band. However, deviations of ±2ppm from initial Th = 12ppm and U = 4ppm concentrations produce different Th/U ratios, which do not adjust proportionately with their respective increased β-doses, (Tables 5.6), and this depends upon the U content of the ratios.

Additionally, this was also substantiated by plotting 62 Potassium contents of sherds against their respective total beta doses (by α+K) taken from Zimmerman's thesis, (1970), linear curve (Z), Fig 5.6.3*

In conclusion, considering the above inconsistencies, we prefer to take an average for these two methods when they are comparable within 1σ, and favour alpha counting for deviations larger than 1σ.

A further attempt to test the above proportionality was to plot Th (as deduced from NAA), against potassium contents for each sample. However, a more realistic approach would be to plot Th/U against potassium, but due to lack of U results, the Th was considered as a plausible solution, Fig. 5.6b (three pages above)

Otherwise, this proportionality has been observed in other analysis (McKerrell pers comm) and Peterman (1963).

In the exceptional case of sample KZ 2/5, (which falls approximately into the linear distribution belt of potassium against (α+K) beta dose), it does not come within the linear distribution belt when plotting K→Th.

---

* It is noticeable that the geological curve (G) has a slightly lower slope than the curves (A), (T) and (Z). This can be explained as:

i) due to the small number of geological samples analysed and

ii) that these geological analyses are variations of U, Th and K_{40} concentrations in three gabbro-granophyre sequences, which could obey to different distributory mechanisms than those in clays.

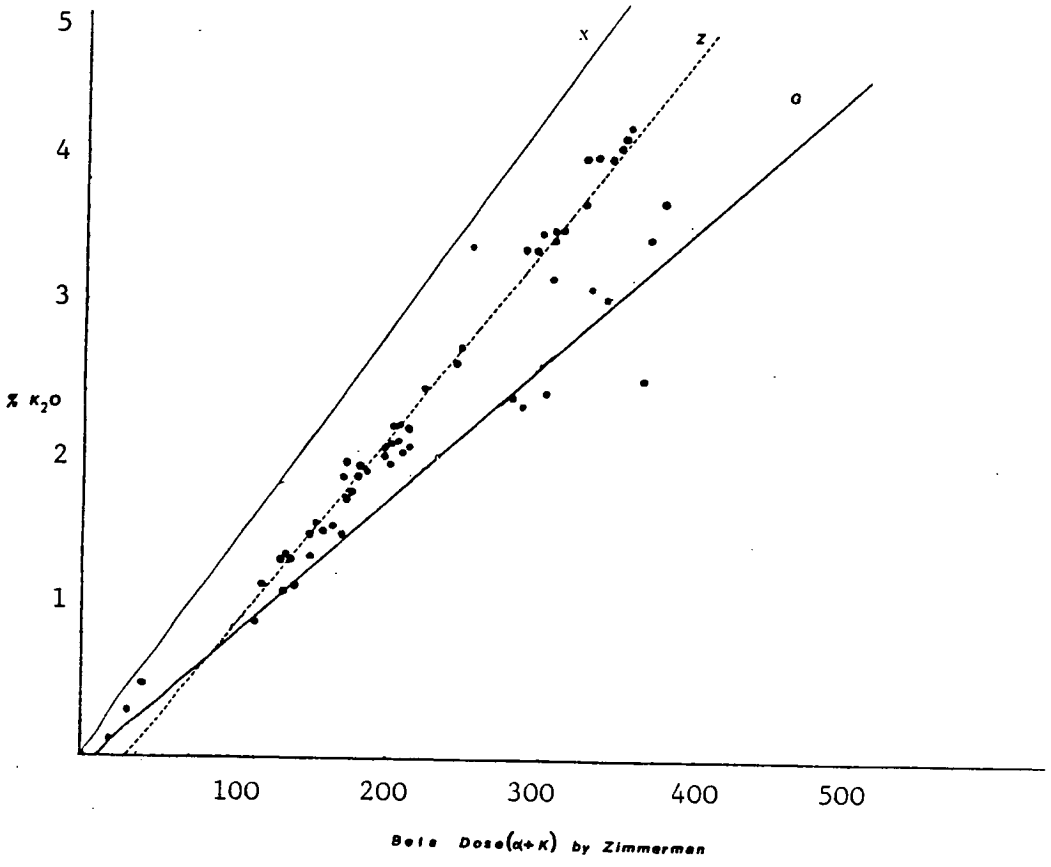


Fig. 5.6.3. Plotting of β-dose rates (α+K) →K_2O
Data taken from Zimmerman Ph.D Thesis, (1970)

This means that it has either a high Th or a low potassium, respectively. This could be explained as follows: Radiochemical analysis of this sample gave a Th content of 28.39ppm and a U content of 8.81ppm, i.e., a ratio of Th/U of 3.2.(see Chapter 12, section 12.4.1.) Since the K-40 contributes more than the U,Th to the beta dose, any major deviation of a sample to be included in the distribution belt of $K \rightarrow (\alpha+K)$, (Fig. 5.6a), would be likely to reflect an inconsistency to the K-40 value rather than to the U,Th values. Thus for the KZ 2/5, the K-40 value shouldbe higher and the Th value somehow lower. The former will place the KZ 2/5 sample into the linear distribution belt of $K \rightarrow Th$ plotting and both will keep the sample within the linear distribution belt of $K \rightarrow (\alpha+K)$ plotting.

Finally, such a distribution (curve (A)) of beta dose against K, can be used as a reference curve, that approximated beta dose rate values can be readily obtained, by knowing only the K content of the sample.

5.7 Conclusion

It is concluded that the "alpha counting method" of beta dose rate is to be preferred (in the present work), although in those cases in which the alpha counting and TLD method give consistent results, an average value is appropriate.

CHAPTER 6

VARIATIONS OF BETA DOSE ATTENUATION IN DIFFERENT CLAYS

6.1 INTRODUCTION

An investigation has been carried out concerning problems on the relative attenuation and stopping powers of beta particles in varied composition pottery clays. The aim of this study was:

i) to study the effect of different clays on the calculated values of beta doses through the quartz grains;

ii) to study the variation of stopping powers in these clays as compared to that of quartz;

iii) to check the validity of the expression derived by Zimmerman, (1970)

$$\text{(I)} \qquad \beta_{wet} = \frac{\beta_{dry}}{1+(\frac{w}{d} - 1)\,\frac{(S/\rho)_{water}}{(S/\rho)_{sherd}}}, \text{ where}$$

β_{wet}, β_{dry}, are the beta dose rates in wet and dry clay, respectively; $(S/\rho)_{water}$, $(S/\rho)_{sherd}$ are the stopping powers for water and clay. Zimmerman obtained the stopping power ratio 1.25, by assuming that the stopping power of clay is equal to that of aluminium.

What is normally required in inclusion dating is the average dose rate experienced by quartz embedded in pottery that is saturated with water. This wet sherd dose rate must, therefore, be corrected for the effect of the water and for the attenuation by the grains. Saturation of the clay by water has two effects "dilution" of the radioactivity (decrease ...) and an increase of the average stopping power, because of the relatively large stopping power of the water, relative to clay.

6.2 Distance Scaling Factor and Its Theory (Some Aspects on β-Interaction With Low Z Materials)

A simple way of deriving the dose distribution for a given emitter in any medium from that measured or calculated in one "standard" medium such as air is described by Cross, (1968). Fundamental to this method is the observation that beta dose distribution in different low-Z media have almost the same shapes, differing only by a distance scaling factor (sf) and a closely related normalisation factor. For example, the dose in water at a distance R (measured in gr/cm^2), is proportional to the dose in air at distance 1.12 R, where 1.12 is the sf. of water, relative to air. The distance scaling factor between two media gives their relative rate of dose attenuation per gr/cm^2, which will be referred to as their relative attenuations.

The similarity in the shapes of beta ray attenuation curves in different media has often been observed in measurements of beta flux,* although the shapes are different for some geometrical arrangements of absorbers and detectors, (Chapter 5 Section5.9.2 , where this effect is encountered in measuring beta doses by the phosphor $CaSO_4$:Mn, encapsuled in a polypropylene wafer which acts as an absorber of $40mgr/cm^2$, and thus the beta spectrum shape derived from the radionuclides in the clay matrix is different to that which is reached and recorded by the phosphor.)

---

* The commonest assumption, which is made about the relative attenuation (in the β-distribution in low Z media), is that the attenuation is proportional to the number of electrons/unit area, Loevinger, (1956). In conclusion, for such β-distribution, two mechanisms appeared to be involved, both comfirmed experimentally; a) The shape of the energy spectrum remains nearly constant throughout the absorption and b) The angular distribution pattern of β-rays remains substantially constant during absorption.

The interaction of any incidence of electron with the atomic elements of an absorber with low-Z is characterised by the fact that the energy transferred to the atom per collision is very small, even for the very high primary energies, (in general terms, for a beta spectrum of many beta energies), excitation is more probably than ionisation, and the resulting secondary electrons have a mean kinetic energy of only a few eV. The total energy loss after passage through an absorber, for example, quartz or clay, is, therefore, the result of a great number of small energy losses, or the mean energy loss per cm path is nearly independent of incident energies . (Also, see Fano's theorem in Chapter 2 Section 2.13).

Scaling factors between a small number of low-Z media and air were obtained by comparing the dose distribution from point beta sources, calculated from Spencer's theory, for the medium and air. These scaling factors divided by the appropriate relative stopping powers are shown to lie on a smooth curve when plotted against $\overline{Z}$, an effective Z for the medium, (for higher Z, that is above Z = 40, rapid changes occur.) This curve, along with values of stopping powers and Z used then to obtain scaling factors for our low-Z clays.

Attenuation of electrons depends on both their energy loss and elastic scattering.

Therefore, in the case of two media (1 & 2), which have the same probability of scattering (through angle θ) per unit energy loss, $S(\theta,E)$, then their relative attenuation will be in proportion to their stopping powers. For example, if dE/dx in medium 1 is twice that in medium 2, and the values of $S(\theta,E)$ are the same, then a layer of thickness dx of medium 1 will change both energies and directions by the same amount as a layer of 2dx of medium 2. Attenuation is then

proportional to stopping powers and some function of $S(\theta, E)$

For a single element the scattering probability per unit energy loss is approximately proportional to Z^2/Z. For a medium, such as clay, containing several light elements, the scattering probabilities from all nuclei may be added, because the angular distributions are nearly independent of Z. Stopping powers are also additive. Hence, $S(\theta,E)$ is proportional to $\overline{Z}$ as given by the equation:

(3) $$\overline{Z} = \frac{\Sigma\, Z_i^2\, N_i}{\Sigma\, Z_i\, N_i}, \text{ where}$$

N_i is the number of nuclei of charge Z_i.

The distance scaling factor of a medium relative to air is, therefore, proportional to S/S_{air}, the relative stopping power, multiplied by some function of Z for the medium.

6.3 Procedure for Calculating Stopping Powers and Relative Attenuation In Clays

An average Z-value for SiO_2 and other clays was calculated from the expression, Cross, (1968) (3) above. Table 6.3 The relative stopping powers for the clays was obtained from an empirical expression derived by Roesch, Cross, (1968):

$$S_{Z\text{-air}} = 2.39\left[f_i Z_i (1 - \ln Z_i/11.5)/A_i\right], \text{ where}$$

f_i is the fraction by weight of the element with charge Z_i and mass A_i.

Since the relative stopping power depends to some extent on energy, the ratio of the ranges of 500KeV electrons (r_{air}/r_{media}) was chosen as a convenient measure of average relative stopping powers (S_q/S_{air}.)

The above formula fits Berger and Seltzer's relative ranges to about 1%, Berger and Seltzer, (1964).

This chosen value of 500KeV electrons is a good approximation to the average beta energy occuring in clays. However, using the range values (gr/cm^2) given by Berger and Seltzer (1964, 1965), a ratio r_0 (water)/r_0 (SiO_2) of 0.833 was calculated for 0.5MeV electrons. Over the energy interval 0.01 to 3 MeV the ratio varies from 0.771 to 0.864, which, over the major part of the interval, the ratio differs by less than 4% from the value of 0.5 MeV.

The relative attenuation factors were obtained by linear regression using the values given by Cross, (1968), Table 6.3.1

TABLE 6.3.1

Attenuation, relative to air, for low-Z media. Values of relative attenuation in the table below were calculated from Spencer's tables and used to obtain the linear curve (of Fig. I) quoted from Cross, (1968)

Medium	Relative Stopping Power	$\bar{Z}$	Relative Attenuation
Beryllium	0.927	4.00	0.83
Ethane	1.288	4.33	1.18
Polyethylene	1.205	4.75	1.12
Polystyrene	1.118	5.29	1.04
Carbon	1.007	6.00	0.96
Water	1.150	6.60	1.12
Air	1.000	7.36	1.00
"Bone"	1.063	8.74	1.09
Aluminium	0.890	13.00	1.00
Argon	0.808	18.00	1.00

Table 6.3.2 shows the analytical XRF results of 12 out of 31 samples studied; and their relative percentage contribution of each element to the total of each sample. Table 6.3 gives the results of stopping powers (S), relative attenuation (a) and average atomic number $\bar{Z}$. Table 6.3.3 shows some analytical calculated stopping power values for each element (additive rule of stopping powers.) Table 6.3 also shows the actual calculated ratios of stopping powers of water to those of the respective sherd which appear in the formula (1) for water uptake corrections.

Further, the differences in values between beta dose rates on dry state and on wet (saturated by water) are presented. The ratios β/β', imply the observed differences between the corrected beta doses (for their water content) based on their actual stopping power coefficient as found and those using the assumed value:

$$\frac{(S/\rho)_{water}}{(S/\rho)_{sherd}} = 1.25$$

6.4 Actual Correction of Beta Dose Rates Due to Water Uptake

The beta dose rate values upon which actual corrections were applied were those derived by (α+K) or TLD methods in the TL dating programme of the present study.

The error involved in calculating beta dose rates - due to the presence of water in the sherd which acts as an absorber of beta radiation - based on actual stopping powers ratio of water to that of the sherd from that calculated on the assumed ratio of 1.25 or the ratio of β/β' in Table 6.3 , is negligible.

The deviation is of the order of $\pm$1-2% (with only one sample deviating by -5%) This error is overmasked by the final error taken as $\pm 1\sigma$, of the measurements. Therefore, the approach proposed by Zimmerman, (1970) stands by itself as correct.

6.5 Discussion of the Results on Relative Attenuation and Stopping Powers of Beta Particles in Clays

When we study beta attenuation problems in ceramics of variations of

TABLE 6.3

Sample	W/D	a	S_{sherd}	a/S	$\bar{z}$	β_{dry}	β_{wet}	$\frac{S_{H_2O}}{S_{sherd}}$	β'_{wet}	$\frac{\beta_{wet}}{\beta'_{wet}}$
DM39	1.135	1.02	0.940	1.086	11.47	345±17	295±14	1.223	296±14	0.99
DM14	0.140	0.96	0.870	1.107	12.36	225±11	191± 9	1.322	200±10	1.00
DM6/6	1.070	0.93	0.843	1.106	12.33	246±12	226±11	1.364	224±11	1.01
DM35	1.090	1.05	0.965	1.086	11.46	318±18	286±16	1.191	287±16	0.99
DM32	1.060	0.95	0.872	1.096	11.87	359±18	334±16	1.318	322±16	1.00
DM33	1.072	0.92	0.838	1.095	11.95	264±14	242±13	1.372	240±12	1.00
SKB(I)27	1.010	1.00	0.919	1.089	11.62	374±19	332±17	1.251	332±17	1.00
SKE3	1.105	1.06	0.975	1.088	11.58	268±14	237±12	1.179	238±12	0.99
SKB(I)1972	1.170	1.00	0.920	1.089	11.60	385±19	318±15	1.250	318±15	1.00
SKB(I)1	1.077	1.05	0.966	1.089	11.61	448±23	408±21	1.190	410±21	0.99
SKE4	1.120	1.02	0.932	1.099	12.01	394±20	342±17	1.233	343±17	0.99
SKE6	1.105	1.08	0.994	1.086	11.47	277±14	245±12	1.157	247±12	0.99
SKE6	1.123	1.03	0.948	1.086	11.47	333±17	289±15	1.213	290±15	0.99
SKE1	1.120	1.08	0.997	1.087	11.53	301±15	261±13	1.153	264± 1	0.99
SKB(I)28	1.680	1.07	0.988	1.090	11.65	404±21	367±19	1.163	374±19	0.98
SKB(I)2	1.100	0.96	0.881	1.092	11.73	359±18	319±16	1.305	317±15	1.00
SKB(I)18	1.100	1.00	0.924	1.083	11.35	390±20	346±17	1.244	347±17	0.99
SKB(I)98	1.120	1.00	0.923	1.092	11.72	349±18	303±15	1.246	303±15	1.00
KZ(2)1	1.060*	0.98	0.906	1.091	11.68	114±26**	106±24	1.269	106±24	1.00
KZ(1)2	1.060*	0.96	0.886	1.083	11.37	204±12*	189±11	1.298	189±11	1.00
KZ1/1	1.060*	0.97	0.867	1.126	13.14	204±12*	189±11	1.326	188±11	1.00
KZ2/1	1.060*	1.02	0.943	1.086	11.49	114±26**	106±24	1.219	106±24	1.00
SH2	1.220*	0.87	0.777	1.127	13.19	165± 9	129± 7	1.480	124± 6	1.04
SH7	1.220*	0.91	0.811	1.120	12.80	159± 5*	124± 4	1.418	121± 4	1.02
SH3	1.220*	0.86	0.773	1.117	12.77	159± 5*	124± 4	1.487	121± 4	1.02
SH6	1.220*	0.85	0.752	1.130	13.33	152± 8	119± 6	1.529	113± 6	1.05
FS1/4	1.340*	0.91	0.808	1.127	13.19	182±18	127±12	1.423	122±12	1.04
FS3/1	1.150*	0.81	0.728	1.121	12.95	189±39*	159±33	1.579	153±31	1.04
DL1/1	1.070	0.99	0.914	1.091	11.71	268±14	246±13	1.258	246±13	1.00
AT1	1.200*	0.97	0.869	1.123	13.00	214±11*	171± 9	1.323	169± 8	1.01
KH1	1.130	0.99	0.902	1.107	12.35	179± 9*	154± 7	1.295	153± 7	1.00
SiO_2		1.03	0.958		10.80					

* The marked samples are the average of the respective location, due to the lack of available beta dose rates. The respective errors reflect the deviation of the various results from the average for the same location of a site

** Due to the lack of many results from the alpha counting, the TLD results were used instead on average from the respective locations

TABLE 6.3.2

A characteristic selection of samples used to illustrate the

Sample	SiO_2	Al_2O_3	FeO	MgO	CaO
KZ2/1	S 30.82*	A 9.02	F 4.49	Mg 1.14	Ca 0.482
	O 35.22*	O 8.03	O 1.93	O 0.75	O 0.192
KZ1/2	S 32.58	A 7.66	F 3.70	Mg 0.77	Ca 0.90
	O 37.23	O 6.82	O 1.59	O 0.50	O 0.36
FS1/4	S 17.95	A 4.66	F 3.35	Mg 2.41	Ca 18.56
	O 20.32	O 4.15	O 1.44	O 1.58	O 7.41
SH2	S 19.83	A 4.66	F 2.73	Mg 0.65	Ca 16.78
	O 22.66	O 9.14	O 1.18	O 0.43	O 6.69
AT1	S 20.87	A 5.39	F 3.68	Mg 3.17	Ca 16.94
	O 13.86	O 4.79	O 1.58	O 2.09	O 6.76
SH7	S 21.85	A 5.46	F 3.36	Mg 0.70	Ca 14.19
	O 24.97	O 4.85	O 1.44	O 0.46	O 5.66
SH3	S 20.39	A 4.56	F 2.74	Mg 0.59	Ca 15.84
	O 23.31	O 4.05	O 1.18	O 0.39	O 6.32
KZ1	S 20.57	A 5.63	F 3.92	Mg 2.50	Ca 16.47
	O 23.51	O 5.00	O 1.69	O 1.65	O 6.57
SH6	S 17.01	A 4.37	F 2.53	Mg 0.57	Ca 19.72
	O 19.54	O 3.89	O 1.09	O 0.38	O 7.87
KH1	S 24.14	A 6.63	F 4.75	Mg 3.26	Ca 9.69
	O 28.16	O 5.89	O 2.04	O 2.15	O 3.87
KZ 2(1)3	S 36.01	A 4.88	F 2.65	Mg 1.49	Ca 0.94
	O 40.16	O 4.34	O 1.14	O 0.98	O 0.37
FS 3(1)	S 15.92	A 2.61	F 1.69	Mg 4.60	Ca 14.52
	O 18.20	O 2.34	O 0.73	O 3.03	O 5.79

* The two numbers added together give the relative percentage contributions of each element to the total of the respective sample

calculation of their average atomic number ($\bar{Z}$)

Na_2O	K_2O	TiO_2	MnO	P_2O_5	Total Oxygen	Total Average $\bar{Z}$
Na 0.54 O 0.19	K 2.37 O 0.49	Ti 0.49 O 0.35	Mn 0.022 O 0.006	P 0.034 O 0.004	47.20	11.68
Na 0.79 O 0.27	K 1.48 O 0.30	Ti 0.27 O 0.18	Mn 0.030 O 0.009	P 0.019 O 0.024	45.86	11.37
Na 0.95 O 0.32	K 1.19 O 0.24	Ti 0.33 O 0.22	Mn 0.053 O 0.015	P 0.073 O 0.947	35.80	13.19
Na 0.14 O 0.05	K 0.87 O 0.18	Ti 0.33 O 0.23	Mn 0.054 O 0.016	P 0.608 O 0.790	36.35	13.00
Na 0.99 O 0.34	K 0.71 O 0.15	Ti 0.33 O 0.22	Mn 0.089 O 0.026	P 0.063 O 0.082	39.90	12.89
Na 0.10 O 0.03	K 0.73 O 0.16	Ti 0.40 O 0.26	Mn 0.052 O 0.015	P 0.651 O 0.841	38.69	12.77
Na 0.16 O 0.05	K 0.78 O 0.16	Ti 0.32 O 0.22	Mn 0.059 O 0.017	P 0.530 O 0.680	36.37	12.09
Na 0.82 O 0.29	K 0.15 O 0.32	Ti 0.36 O 0.24	Mn 0.604 O 0.018	P 0.080 O 0.100	39.39	13.14
Na 0.04 O 0.03	K 0.78 O 0.16	Ti 0.29 O 0.19	Mn 0.044 O 0.013	P 0.640 O 0.830	22.97	13.33
Na 0.59 O 0.20	K 1.64 O 0.34	Ti 0.06 O 0.04	Mn 0.077 O 0.023	P 0.490 O 0.630	43.35	12.35
Na 1.74 O 0.60	K 1.17 O 0.24	Ti 0.31 O 0.21	Mn 0.046 O 0.013	P 0.860 O 0.110	49.60	11.49
Na 2.86 O 0.10	K 2.25 O 0.46	Ti 0.16 O 0.11	Mn 0.031 O 0.009	P 0.200 O 0.260	31.91	12.95

TABLE 6.3.3

A characteristic selection of samples used to illustrate the calculation of stopping powers (S)

Sample	Si	Al	Fe	Mg	Ca	Na	K	Ti	Mn	P	O	S
KZ(2)1	.2838	.0807	.0360	.0132	.0044	.0049	.0205	.0039	.0001	.0003	.4620	.906
KZ(1)2	.3000	.0685	.0295	.0088	.0082	.0714	.0128	.0027	.0002	.0002	.4490	.886
FS(1)4	.1653	.0417	.0267	.0278	.1680	.0084	.0168	.0025	.0004	.0006	.3502	.808
SH2	.1826	.0417	.0218	.0075	.1519	.0013	.0075	.0025	.0004	.0054	.3560	.777
AT1	.1922	.0482	.0294	.0366	.1534	.0090	.0062	.0026	.0007	.0006	.3900	.869
SH7	.2014	.0489	.0292	.0081	.1285	.0009	.0066	.0031	.0004	.0058	.3780	.811
SK3	.1877	.0408	.2190	.0067	.1434	.0014	.0067	.0025	.0005	.0050	.3560	.773
KZ(1)1	.1894	.0504	.0313	.0289	.1491	.0023	.0133	.0028	.0047	.0007	.3850	.867
SH6	.1574	.0391	.0202	.0066	.1785	.0033	.0069	.0023	.0003	.0057	.3380	.752
KH1	.2269	.0593	.0376	.0376	.0877	.0053	.0142	.0047	.0006	.0044	.4240	.902
KZ2(1)3	.3316	.0437	.0211	.0172	.0085	.0157	.0101	.0025	.0003	.0076	.4850	.943
FS3(1)	.1466	.0233	.0135	.0531	.1315	.0259	.0194	.0013	.0002	.0018	.3120	.728

$\frac{(S/\rho)_{water}}{(S/\rho)_{sherd}}$ has to be taken into account. This ratio in the present study was found to vary from 1.179 to 1.579. This depends on the concentration of elements with atomic number Z_i in each sherd. The average, though, of the actual stopping powers, is 1.289 $\pm$ 0.2($\pm$ 1.5%), which differs by 3.7% from the assumed ratio of 1.25. On the extreme values of water uptake, such as 1.01 and 1.4 and the beta dose (on dry powder) of 100 mrads, the errors involved are shown as follows, with 8% being appreciable in the case of S' = 1.579:

W/D ratios	%Error $S_{1.179-1.25}$	%Error $S_{1.579-1.25}$
1.01	0.07	0.32
1.40	1.90	8.00

However, for higher beta doses this error is much less. Especially the beta dose rate values in the present studies which were of the order of 200 mrads/yr, rendering the effect negligible.

The effect of the atomic number on the beta dose measured by the TLD or the alpha counting methods is pronounced when we consider the scaling factor (sf) or relative attenuation of betas (relative to air). The sf's in Table 6.3 vary between 0.81 to 1.08 with an average of 0.891. This average is approximately 16% less than that of quartz.

Deviations of -27% for the lowest value and +4% for the highest value are recorded. These are important differences, which are due to the inhomogeneity of quartz inclusions and the clay matrix. Otherwise, the density of quartz, approximately 2.65 gr/cm^{3}m is different as compared to that of the pottery, which is around 1.6 - 2 gr/cm^2. This density difference seems to affect the assumption of inhomogeneity in the system of pottery assembly, (clay matrix plus non-radioactive grains.) Therefore, the beta dose received by the quartz or feldspar grains in a potsherd originating from the radioactive inclusions in the matrix will show attenuation effects, which will alter the beta spectrum and hence the beta dose reached or absorbed by the grains. Even though,

the secondary radiations will be uniform throughout the clay medium and so to every quartz grain interface,(Fano (1954)), this uniformity will be of different density flux and intensity; (depending on the interaction process, i.e., the rate of production and attenuation), which occur in the medium outside the grains. This, in turn, is obviously a function of clay composition or $\bar{Z}$.

The calculations of the beta attenuation in these grains will probably be subjected to an uncertain factor or relative attenuation by altering the assumption of a homogeneous system in pottery.

The effect of such variations in relative attenuation on the beta attenuation studies should be examined to see the error introduced in the final beta dose rates due to beta attenuation through the respective grains. An example for understanding the effects of sf. on the calculated beta doses is as follows:

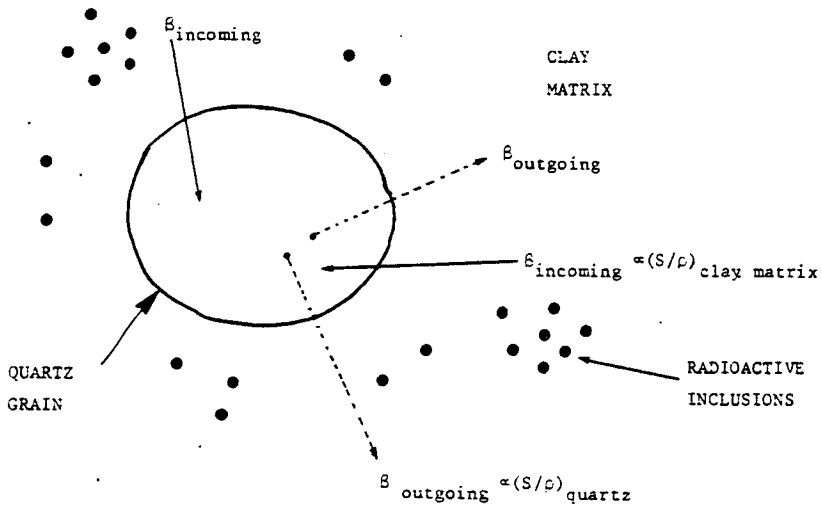
Assume a beta dose rate of 100mrads/yr originating from the same concentration of radionuclides in pottery samples of different clay composition.

An illustration of the position of these radioisotopes inside the volume of the sherd, but in air as medium is as in Fig 6.5a.

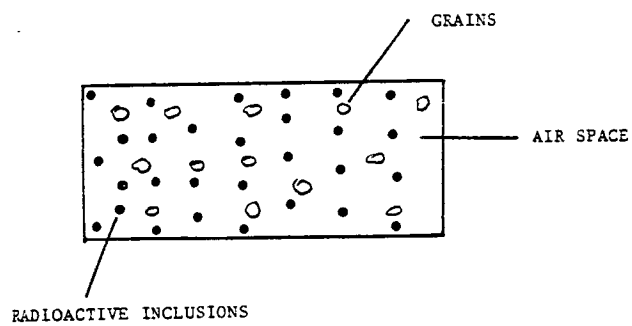
An analogue picture for the same sherd size, but with the air space occupied by the respective clay matrix, is as in Fig. 6.5b.

The beta dose rates received by the quartz inclusions in each of the sherds will be as in Table 6.5. These doses will vary proportionately to those in air. This conversion is obtained by using the sf's for each sherd. Therefore, the converted beta doses in air are comparable. This also follows from the explanation below. The dose D_p in each pottery, at distance R (in gr/cm^3) equals the dose in air D_{air} at distance R multiplied by $n_{air} \times (\rho/\rho_{air})^2$ or D_{pot} is proportional to $D_{air} \times n_{air}^3$ where D_{pot} is the dose in the potsherd and D_{air} the equivalent dose in air, n_{air} is the attenuation relative

6.6



6.5 a



6.5 b

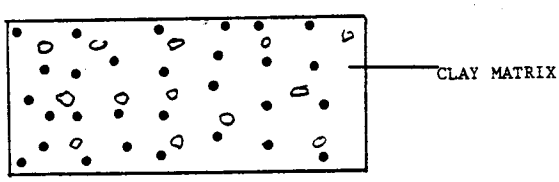


Fig. 6.6 Illustrative effect of β - attenuation through the quartz grains and its dependents on stopping power of the clay matrix.

Fig 6.5 a Distribution of radioisotopes inside an air spaced volume similar to a sherd size.

Fig 6.5 b Distribution of radioisotopes inside the same volume occupied by clay.

TABLE 6.5

Sample Number	D_{pot}
DM39	102
SKB(1)27	100
DM14	96
DM6/6	93
SKE3	106
SKB(1)1972	100
SKB(1)1	105
SKE4	102
SKE6	108
DM35	105
SKE5	103
DL1/1	99
SKE1	108
DM32	95
SKN9I)28	107
DM33	92
SKB(I)2	96
SKB(I)18	100
SKB(I)98	100
KZ2/1	98
KZ1/2	96
FS1/4	91
SH2	87
AT1	97
SH7	91
SH3	86
KZ1/1	97
SH6	85
KH1	99
KZ2/1/3	106
FS3	81
AVERAGE	89 mrads/yr

$D_{pot} \propto D_{air} \cdot n^3_{air}$

$D_{pot,\ dry} = 100 mr/yr$

For comparison reasons : $D_{pot,\ dry} \times a \propto D_q$, where

D_q = proportional dose absorbed by the quartz grains.

to air.

As the stopping power values for the quartz grains and the clay matrix are not identical, the attenuation factor for a grain size will not exactly equal ; 1- the absorbed dose function or self-dose, that would result if the grain had a content of radionuclides equal to that of the matrix, Mejdahl, (1978). (Eight pages above). An illustration of such effects also is shown in Fig 6.6. Since the absorbed dose for the incoming betas depends on stopping powers of the clay matrix, the attenuation of such betas through the grain, considering the above assumption is not equal in both directions (income and outcome of betas).

The stopping powers finally of the sherds vary between 0.728 to 0.997 with an average of 0.891, Table 6.3. This average is 7% different from the quartz respective value. Deviations of 24% for the lowest value and 4% for the highest recorded (similar percentages as for relative attenuations). Our results concerning stopping powers of clays thus are not in agreement with those of three clays by Mejdahl, (1978). This is probably due to the wider distribution of samples being investigated in this study as well as the higher number of elements detected by the XRF analysis, and included in such calculations.

Also, the above variation of stopping powers for different sherds apply only to dry clays. As sherds buried in soil are almost saturated with water (Section 9.6 . Chapter 9), the respective stopping powers of these wet clays will be higher. The above will have an additional though small effect on the relative attenuation factors which as found depends upon the atomic number and stopping power of the material, Cross, (1968). This effect is negligible when considering its importance on beta dose rate corrections which account for the water uptake as proved. This effect of wet clays, however, does not even change the attenuation factor of betas through different grain

sizes since this effect is included in the water uptake correction. Finally, the variations of relative attenuation due to the clay composition will have an effect on beta attenuation estimations through the grains. Depending upon the radioisotopic concentration in a ceramic, the beta energies involved (beta particles, IC, auger electrons), will be subjected to different attenuation effects on penetrating quartz grains.

6. 6 Conclusions

Overall, the stopping powers of clays are not similar to the quartz, and the variation of relative attenuation due to the clay composition will have an effect on beta attenuation estimation through the grains, and the water uptake corrrection in some cases of relatively low beta doses and extreme S's values.

In general terms, in the formula (1) for water uptake corrections, the value S = 1.25 is valid, and any errors involved for extreme cases of S's are insignificant to the TL age calculation.

P A R T III

ENVIRONMENTAL DOSIMETRY

CHAPTER 7

EVALUATION OF GAMMA DOSE RATES IN ARCHAEOLOGICAL SITES

7.1 INTRODUCTION - CONTENTS

Part III deals with the evaluation of gamma dose rate in the environment of ceramics. Chapter 7 initially outlines certain aspects on terrestial gamma radiation and subsequently describes the calibration of a portable gamma scintillometer NaI(Tl) 2" x 2", as counting rate against dose, for four different gamma spectral media, namely Potassium mixed with sand, Uranium doped sand, Thorium doped sand and Uranium doped peat.

The calibration is made on quartz grains, by using this quartz as a build-up dosimeter for its 110°C peak to develop for a short period of time and under liquid nitrogen temperature.

Dose rates from the above four radioactive matrices are recorded also with LiF and $CaSO_4$:Dy phosphors. A comparison is made between the phosphors and subsequent discussion is carried on concerning their gamma responses. Emphasis also is given to the significance of such a calibration for applications in archaeological sites.

Chapter 8 presents results of gamma fluctuations from four different soil types as recorded by the NaI(Tl) device and LiF and $CaSO_4$:Dy phosphors, for a period of around a year. Meteorological parameters influencing these fluctuations are discussed and their importance on the determination of gamma radiation in situ is emphasised.

7.2 Aim of These Investigations

In the determination of the age of pottery by thermoluminescence, it is necessary to know the radiation dose rate that the pottery fragment

has received during its centuries of burial.

A substantial contribution of this dosage is due to gamma rays from radioelements in the surrounding soil and in the "inclusions dating technique", this soil dose is typically 30% and can approach 50% of the effective total, Table 7.2.

TABLE 7.2

Dose Rates Incurred by Quartz and Feldspar Grains Imbedded in a Sherd Buried in Soil

Type of Radiation	Typical Dose Rate (mrads/yr)	Relative Contribution %
Beta and gamma* from radioisotopes imbedded in sherd	200	62.5
Environmental gamma radiation from the soil	100	31.2
Cosmic	20**	6.2
TOTAL	320	100.0

* in the inclusion technique, the grains selected for measurement are so large that alpha particles will be stopped in the outermost layers and, therefore, not contribute significantly to the radiation dose.
** at a depth of 30cm (Aitken, 1969). At the surface of the earth the dose rate for cosmic rate for cosmic radiation is approximately 30 mrads/yr.

Although there are some well-established techniques for estimation of this gamma soil radiation, the present, newly employed, technique is to determine the absolute gamma dose experienced by quartz and feldspar grains rather than on other dosimetric phosphors.

It should be emphasised, otherwise, that it is necessary to match the effective atomic number of any dosimeter system as closely as possible

to the atomic number of the irradiated material of interest; if the dose absorbed in the dosimeter is to be related meaningfully to the dose absorbed in the material. Consequently, the ideal dosimeter, here, would be to use quartz which inevitably is used to measure the total TL absorbed dose. Although it is not relevant to compare the number of photons interacting in scintillation cystals with those interacting in individual grains of quartz or feldspar, however, the following considerations are taken into account:

i) the grains are not irradiated in isolation, but included in a sherd (here a table tennis ball), which is buried in the soil ,

ii) the dose to the grains will be delivered mainly from photons interacting in the grains. The situation is not drastically different from that of scintillation crystal irradiated in a narrow hole in the ground.

7.3 Review of the Techniques

i) use of phosphors Aitken (1968, 1969) recognised the advantages of TL dosimetry for measurement of environmental radiation at archaeological excavation sites and introduced a technique based on natural calcium fluoride.

Following the development of $CaSO_4$:Dy (Yamashita et al, 1968 and Mejdahl, 1970, 1972), developed a technique based on this phosphor.

Other phosphors in some respects superior to CaF_2 and $CaSO_4$:Dy are available and discussed by Mejdahl, (1978) and Murray, et al, (1978) Amongst the desirable properties of a TL phosphor for environmental measurements are the low levels of detectable dose (1 - 5 mrads), high sensitivity , negligible self dose, small fading over a period of 1 - 2 years, and the most important characteristic is that they

record the gamma soil fluctuations and gave a true representative gamma dose for the respective site and include the small cosmic contributions.

A number of the phosphors (including quartz, feldspar and calcite), that have been used or suggested for environmental measurements are compared in Table 7.3

A disadvantage is that they have quite different gamma responses with respect to that of quartz and attempts to shield these phosphors with other materials in order to equalize their responses with that of quartz induced errors have been made. The energy response values (at 50KeV) are relative to air and were calculated from the $(\mu/\rho)_{tot,en}$ values given by Strom and Israel, (1970).

The phosphors CaF_2:Mn and CaF_2:Dy also have sufficient sensitivity but are not included because of their rather complex fading characteristics.

The dependence of the response of the phosphors on energy, the main drawback, is considered in more detail in Section 7.8 , Fig. 7.8

ii) by alpha counting andpotassium determination (α+K)

the principle of this method is similar to that described in Chapter 3 .

A representative soil sample from the vicinity of the buried pottery is alpha counted and analysed for potassium. Then from conversion tables the gamma dose rates are evaluated. The drawback with this technique is the assumed Th/U ratio as 3.16 and the assumption of "representative soil sample".

Another serious problem is the effect of radon emanation.

TABLE 7.3

Number	Phosphors	$\mu/\rho_{tot.en}$ Relative** to air at 50 KeV
1	Air	1.000
2	Lif:Mg,Ti*	1.080
3	$NaAlSiO_2O_8$	2.203
4	Al_2O_3:Si,Na	2.853
5	Mg_2SiO_2:Tb	3.019
6	SiO_2	3.330
7	$KAlSi_3O_8$	4.150
8	Na_2SO_4:Dy	4.440
9	$CaCO_3$	8.23
10	$CaSO_4$:Dy	8.27
11	CaF_2	10.48

* Activators not included

** Computed from Strom and Israel, (1970)

As it is known, approximately, 90% of the gamma radiation comes from a radius of 30cm (see also Section 7.11 V) then if the surrounding soil is unhomogeneous then the gamma dose measured on a single soil sample would give an erroneous gamma dose. This inhomogeneity has been found in Chapter 3, where potassium and thorium values vary very much within a few centimetres. This has also been found to be the case when this technique was applied to Neolithic samples from Greece, as compared with dosimetry and NaI(Tl) readings, Liritzis, McKerrell, (1978).

Nevertheless, by collecting a number of soil samples from the vicinity of the pottery, provided that this is a nearly homogeneous material, the gamma dose can easily be evaluated.

When stones surround the pottery, then this technique does not give

correct results. In such cases, phosphors placed in that site wouldbe ideal or scintillation techniques as will be described in the next section.

In particular, when a burnt clay layer is to be dated, the (α+K) technique is the easiest one, since it gives both the internal beta and external gamma dose rates with the same measurements of alpha's and potassium.

Other errors involved for this technique are those of soil moisture, and the somewhat uncertain value for cosmic radiation.

iii) scintillation techniques In this technique, a portable scintillometer is employed, well calibrated with radioactive sources of well known energies and the count rates are converted to dose rates. Many workers have used it for field measurements. Adams, (1964) Løvborg et al, (1974), Huxtable et al (1976) and Murray et al, (1978).

For a 2" x 2" NaI(Tl) crystal, adopted in the present studies, Løvborg and Kirkegaard (1974) showed that the integrated count rate above a fixed energy threshold of 0.37 MeV is proportional to the exposure rate irrespective of variation in the abundances of Uranium, Thorium and Potassium. The same relation can be expected to apply to a 4π geometry obtained by placing the detector in a narrow hole drilled into the ground. The main advantage of this technique would be that the excavation itself would not be disturbed by TL probes and that all measurements on a site could be completed in a single day.

The drawback of this technique is the absolute calibration on quartz inside a sherd and the estimation of a correction factor to account for the seasonal fluctuations. The last seems to

be somehow solved by the TLD technique, but over the past thousands of years, both are subjected to the same uncertainty.

7.4 Physical Aspects of Terrestrial Radiation

The terrestrial component of the external gamma radiation environment results from the natural occurence of the primeval radionuclides, K-40, Th-232, U-238 and U-235 in rocks and soils. Other, generally less intensive, components are introduced by the slowing-down of cesmic secondaries in the earth's atmosphere and by the presence of airborne or precipitated radiodaughters. In describing the interaction of gamma radiation with matter, the processes of incoherent and coherent scattering, photoelectric absorption and pair production are considered.

At low photon energies , the most important process is the photo-electric ejection in which an atom absorbs the photon and emits an electron. The atom, which isleft in an excited state, returns to the ground state by the emission of auger electrons or X-rays. Also important at low energies is coherent (Rayleigh) scattering, a process in which the photon is deflected by the atomic electrons with no loss of energy.

In the middle energy range (0.5 to 1.5 MeV), themain process is incoherent (Compton) scattering, in which a photon is scattered by an atomic electron, with transfer of momentum and energy to the struck electron sufficient enough to put it into an unbound state. The deflected gamma photon goes on with diminished energy, depending on the angle of the emerging electron. The electrons are continuously disturbed between zero and a maximum value, given by:

$$E_{max} = \frac{E}{1 + \frac{m_o c^2}{2E_\gamma}}$$ where,

$m_o c^2$ is the rest energy of the electron (0.511 MeV).

At high energies ($E\gamma \geq 1.02$ MeV), an important process is pair production, the creation in thefield of a charged particle of an electron-positron pair.

The high energy electron of this pair produce Bremsstrahlung radiation (which happens to be negigible for media of low atomic number), as well as ionisation along its path while the positron is eventually annihilated with the production of new 0.51 MeV photons.

After a photoelectric incoherent scattering, or pair production interaction, a portion of the incident photon energy is resident in the photons produced (scattered, fluorescence, annihilation, Bremsstrahlung photons), and the remainder is transferred to particles, (electrons, positrons.)

As gamma radiation passes through matter, it is attenuated exponentially by the three effects above with increasing thickness of absorber. The decrease in theintensity can be expressed by Lambert's law: $I = I_o \exp(-\mu x)$, where I_o is the intensity of the incident beam of photons, I is the intensity after passing through thickness x of material and μ is the linear absorption coefficient. Here it should be noted that the attenuation of a given gamma spectrum is not linear, but depends on the relative contribution of the respective energies which subsequently have different absorption coefficients and thus show different attenuations.

7.5 Fluctuation and Distribution of Soil Gamma Rays

7.5.1 Fluctuation

The most characteristic gamma rays from soils are emitted by the isotopes Bi-214 (1.76 MeV) Th-208 (2.62 MeV) and K-40 (1.46 MeV). The K-40 is a direct gamma emitter, while the other two isotopes occur almost at the end of the U-238 and Th-232 series, respectively. Possible fluctuations in the soil gamma field may be due to loss of the secondary products Radon-224 and Thoron-222. They belong

to the middle of the Uranium and Thorium chain, respectively, and carry 96% and 63% of the gamma and X-ray energy as post-products, so that their loss would lower the gamma dose rates, Table 7.5

TABLE 7.5

	% Contribution	
Th-232	Post Thoron	Pre Thoron
β+IC+Auger (Total=4.768MeV)	(3.090MeV) 64.8	(1.678MeV) 35.2
γ+X-ray (Total=2.427MeV)	(1.538MeV) 63.4	(0.887MeV) 36.6
alphas (Total=35.937MeV)	(20.870MeV) 38.1	(15.062MeV) 41.9
U-238	Post Radon	Pre Radon
β+IC+Auger (Total=8.29)	(4.980MeV) 60.0	(3.310MeV) 39.9
γ+X-ray (Total=2.014MeV)	(1.930MeV) 95.8	((0.804MeV) 4.16
alphas (Total=42.866MeV)	(24.489MeV) 57.1	(18.377MeV) 42.9

Ra-226 (1.6×10^3 yr)

For 100% leaching of Ra-226 68.2% of the α-dose is lost

59.3% of the β-dose is lost

96.3% of the γ-dose is lost

This loss would occur because of emanation of Radon through soil by diffusion and transportation by water, Tanner, (1964).

The gamma dose from the wet soil is given by the formula:

$$D_{\gamma wet} = \frac{D_{\gamma dry}}{1 + \left(\frac{W}{D} - 1\right) \frac{(\mu_\alpha/\rho)water}{(\mu_\alpha/\rho)soil}}$$, where

W,D are the weights of the soil in wet and dry state;

$$\frac{\mu_\alpha/\rho \text{ water}}{\mu_\alpha/\rho \text{ soil}} = 1.14,$$

is the ratio of the mass absorption coefficients for 1 MeV gamma rays in water and Aluminium (assumed to be similar to soil, Evans, 1955, Zimmerman, 1971).

7.5.2 Distribution

Much of the gamma flux (more than 60%), coming from the soil *in situ* is in the form of low energy photons resulting from severe degradation of the relatively energetic primaries, Gustafson et al, (1954), Løvborg et al (1976).

The significance of the low energy spectrum to the responses of different materials is considerable, (also in Fig. 7.8)

The medium II (in Fig 7.5.2) represents soil containing distributed natural gamma ray emitters, while medium I represents the air in which radiation from the soil and background is detected. In describing the interaction of gamma radiation with the scintillometer the contribution of annihilation photons to the radiation field in medium I is not significant. It is furthermore supposed that the gamma ray detector does not perturb the radiation field at the surface of the scintillation crystal. However, this will be the same for all applications and so does not induce any errors. Each emission line from the radionuclides in medium II gives rise to an uncolided flux component with the same energy as the line and a scattered flux component showing a range of energies between zero and the line energy.

However, the number of interactions which do occur are dependent upon the energy of the photon and the density of the soil (or $\overline{Z}$).

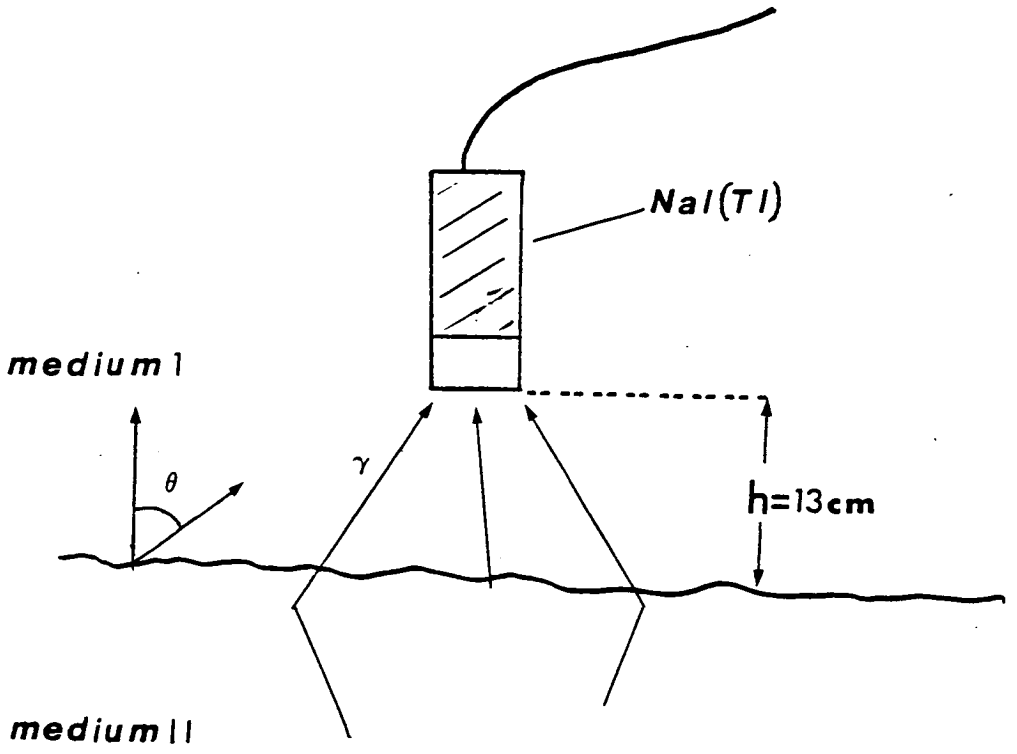


Fig. 7.5.2 γ-ray soil distribution to a scintillation detector. Medium I represents soil countaining distributed natural γ-ray emitters. Medium II represents the air in which the radiation from the soil and background is detected.

There is a preferential absorption of photons in materials composed of elements with high atomic number (Z), compared with that in materials with low Z, so that for the same exposure to a photon-flux the radiation dose absorbed by photo-electric interaction will be greater in the high atomic number materials. Also, the energy distribution of gamma photons could vary with the depth under the ground surface for unhomogeneous soils and with the composition of the soils (since they will have different absorption coefficients). In peat, for example, a material of organic matter (carbon, etc), the flux density contains a larger fraction of low energy photons than in a sandy soil.

This is due to the relatively low atomic number (Z) of peat compared with that of, say, sand, of higher Z. Therefore, in the peat, there is a preferential absorption of photons, than for the exposure to a photon flux the radiation dose absorbed by photoelectrical interaction will be greater (than, say, the Compton effect). For the sand and soils, the Compton effect predominates over a wide domain of photon energies.

The integral angular flux distribution is obtained for 0^{o} to θ^{o}, taking into account that in the upward direction a box would produce approximately 12% less scattered flux than an infinite source of the same radio-element concentration (Løvborg, et al, 1976) and that more than 20% - 30% of the signal registered by a scintillometer counter over an infinite source is due to "skyshine". This contribution is virtually absent in a calibration experiment, because a negligible fraction of the air-scattered gamma rays from a small source returns to the source.

The low energy photons would give an erroneous estimation of the

true gamma radiation in situ, when measured by a scintillometer without preselected threshold, since there is not a linear response in the low energy region for the instrument in use. This non-linearity of the response at low gamma- and X-ray energies of thallium activated sodium iodide NaI(Tl), has been reported by Engelkemeir, (1956) and Kaiser et al (1962). The integration for above 370 KeV does not introduce errors into absorbed dose rates estimated, as shown by Løvborg and Kirkegaard, (1974).

From the above, the position of the recorded gamma spectra in an infinite soil area depends on the actual geometry of counting and the soil type in general. Therefore, in any calibration of a scintillometer, these factors have to be considered in order to avoid systematic errors. The above theoretical background is very essential to gamma dosimetry studies as they further support the experimental arrangements constructed for the calibration of the NaI(Tl) 2" x 2" scintillometer

7.6 NaI Calibration: Experimental Arrangements

In measuring "absolute" gamma dose rates, as part of the TL programme on ancient Hellenic materials, the NaI(Tl) 2" x 2" (PSR6 NE) is used which was calibrated on quartz grains based on the 110°C peak of quartz. The calibration was done on four different gamma spectral media - namely potassium mixed with sand, uranium doped sand, thorium doped sand and uranium doped peat.

The dimensions of the 4 boxes were 58x40x50 cm^3, a volume equivalent to a sphere with a radius of approximately 30.3cm. During the mixing of the constituents of the four boxes with radioactive ore, a different radioactive dopant was added. These are given in Table 7.6. The boxes were kept 10cm apart during the experiment.

TABLE 7.6

Principal Dopent	U-238 Series	Th-232 Series	K-40
Half life	4.49×10^9 yr	1.40×10^{10} yr	1.28×10^9 yr
Source	New Brunswick USA Pitchblade ore 6A 67.91±0.051 U_3O_8	New Brunswick USA Monazite sand 7A 9.7%ThO_2 0.35%U_3O_8	Potassium Carbonate (BDH) Anydrous
Weight added to the total sand*	11gr(6.33gr U)	120gr (10.22 grTh + 0.36 gr U)	20.5kg (14.8% K_2CO_3or 8.4%K)
To the principal peat	5.7gr (3.28 gr U)	—	—
Primary gamma energy (MeV)	up to 2.45	up to 2.61	1.46

* the weight of sand was 150Kg, of the peat 67.5Kg and of the K_2CO_3, 20.5Kg

The experiment started three weeks after the mixing and construction of the four boxes.

Because of the small amounts of radioactive materials used per weight of sand andpeat, thorough distribution of the respective dopant cannot be assumed, and therefore, the nominal activity is higher than the experimental data - particularly for peat and sand doped with uranium - and so cannot be used in comparisons. Apart from

the quartz dosimeter, the gamma dose of these matrices was also measured by TLD dosimetry, that is Lif/teflon disc on polythene and $CaSO_4$:Dy in brass and polypropylene tubes.

The assemblage of phosphors and quartz grains were arranged in a dewar which was subsequently placed in the centre of each of the above boxes. These dewars were filled with liquid nitrogen, using an automatic liquid nitrogen filler for a period, of approximately 20 days for the quartz 110° peak to develop and 2 months for the phosphors, Figs 7.6 and 7.6.1

The quartz grains 75 – 106μ were placed in each of the three capsules. Each capsule could accommodate up to 550mgr of grains. These grains were specially annealled beforehand and etched (as in the beta experiment, Chapter 2), to avoid pre-dose. A table-tennis ball (tt ball) was filled with sand and the capsules placed as in Fig 7.6, with the objective of :

i) simulating potsherds of different thicknesses measuring 3.5 10.5 and 17cm from the circumference of the tt ball to the centre of the 1st, 2nd and 3rd capsule, respectively, and

ii) studying the attenuation of gammas through these thicknesses. The tt ball was surrounded by an extract (sand/peat) from the boxes and mixed with a proportional amount of radioactive ore.

The experiment was conducted indoors, so that there was not any subsequent meteorological effects.

Readings were taken with the scintillometer, both before and after the experiment. The counter was calibrated before and after the measurements by a Cs-137 gamma source, in order to choose the appropriate threshold and check for the stability. (It was observed

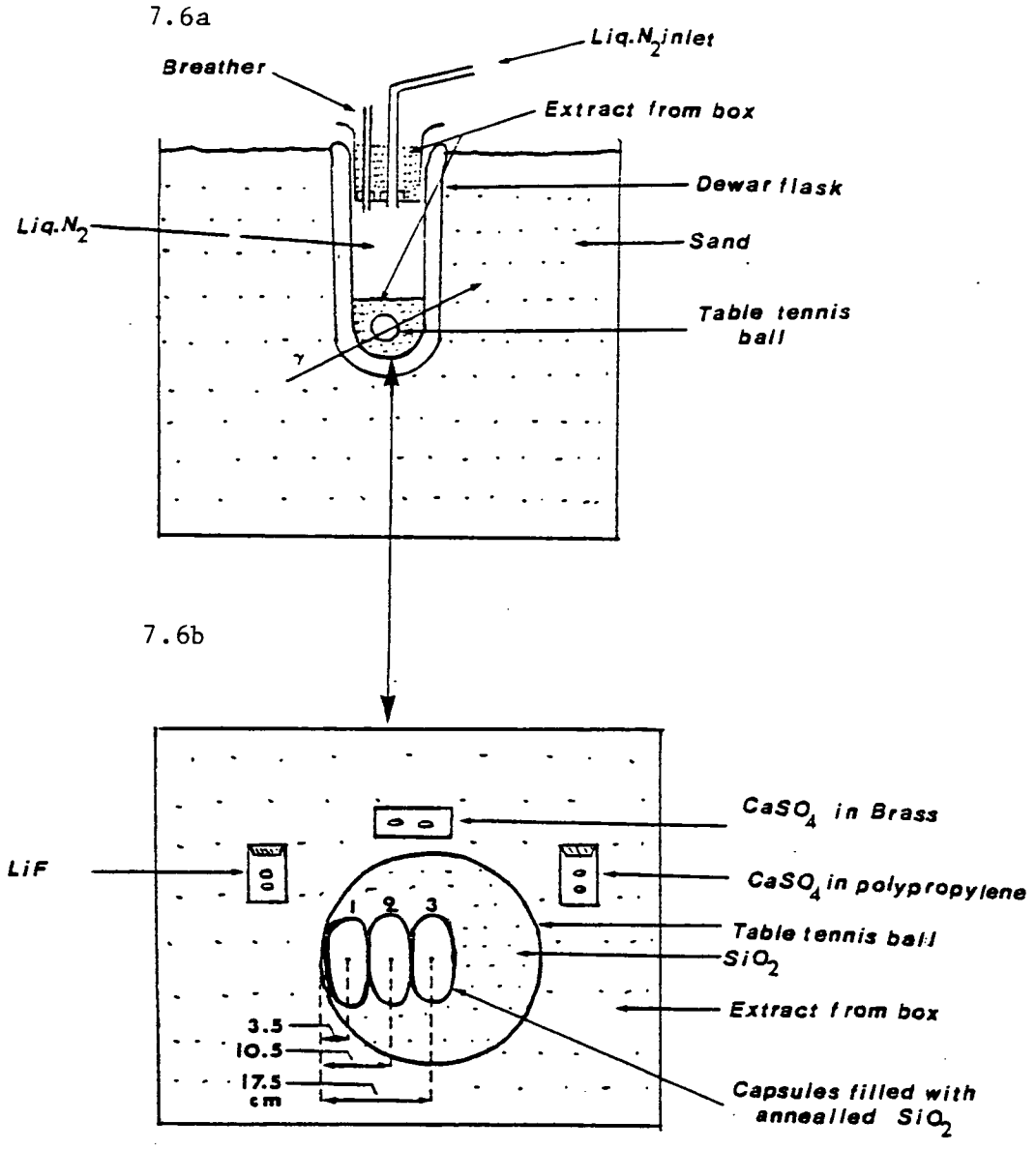


Fig. 7.6a Cross section of one of the boxes with the counting arrangement.

Fig. 7.6b Detailed setting of the quartz grains and the phosphors inside the liquid nitrogen dewer.

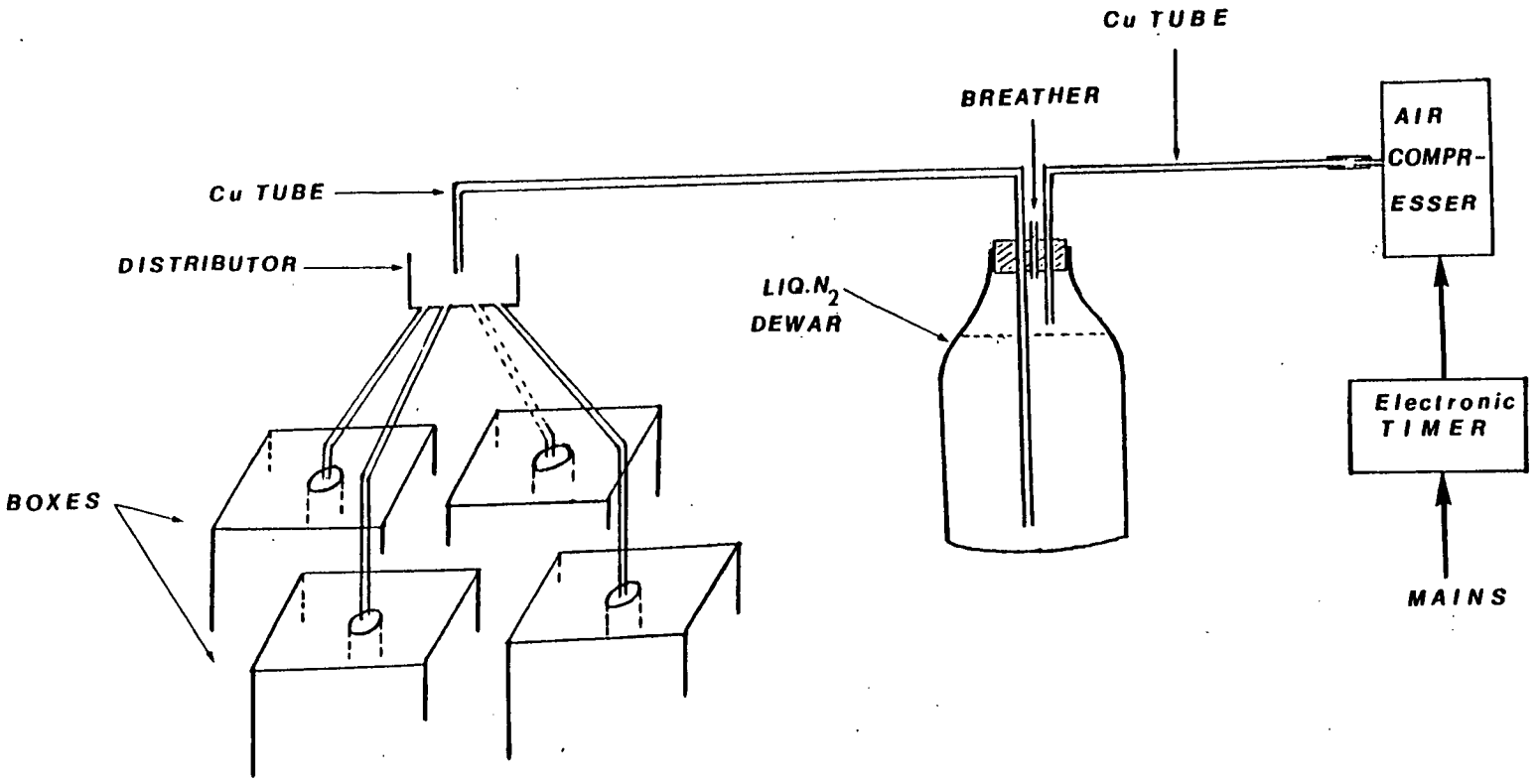


Fig. 7.6.1 Lay-out of the automatic liquid Nitrogen Filler.

that there was a shift in the threshold with temperature changes, therefore, it was necessary before starting to switch on for sometime beforehand in order to adapt to the environmental temperature. This was most obvious in situ measurements (see Chapter 9)

A small difference in readings were observed for each box after the first 20 days, which kept constant for the next 2 months. This was attributed to the settling of the sand andpeat during the first weeks and subsequent displacement of the dewar so that samples would not exactly be in the centre of the boxes.

Nevertheless, this was not considered serious, provided that the recorded doses followed this settling, thus the average of the readings taken initially and afterwards could have corresponded to the true gamma dose reading from the phosphor.

Radon emanation levels were measured by alpha counting and were found to be of the order of 5 - 10% (see 7.11 ii)

The above readings, as counts/sec, were used in averages and corresponded directly to the dose (mrads/yr) of the phosphors and quartz, Table 7.6.1.

The calibration curves are shown in Fig. 7.6.2. (For discussion of these curves see section 7.9, below).

TABLE 7.6.1

	γ-dose (mrads/yr)	Poly/Brass	Brass/LiF	c/s
Potassium Box				
Polythene	364± 4	1.08	1.41	81.7
Brass) $CaSO_4$:Dy	336±11			
LiF	238± 8			
Thorium Box				
Polythene	536± 3	1.14	1.44	124.5
Brass	468±12			
LiF	325± 3			
Peat Box				
Polythene	518±24	1.29	1.53	107.3
Brass	410±20			
LiF	261±13			
Uranium Box				
Polythene	585± 9	1.2	1.33	131.2
Brass	487±27			
LiF	366± 3			

SiO_2

Boxes	Capsule1	Ratios Caps1:2	Capsule2	Ratios Caps2:3	Capsule3	Ratios Caps1:3
Potassium	255±18	1.094	233±15	1.0*	254±16	1.0*
Thorium	396±19	1.042	380±27	1.021	372±26	1.164
Peat	338±19	-	-		318±10	1.062
Uranium	410±22	-	-		384±24	1.063

* within 1σ

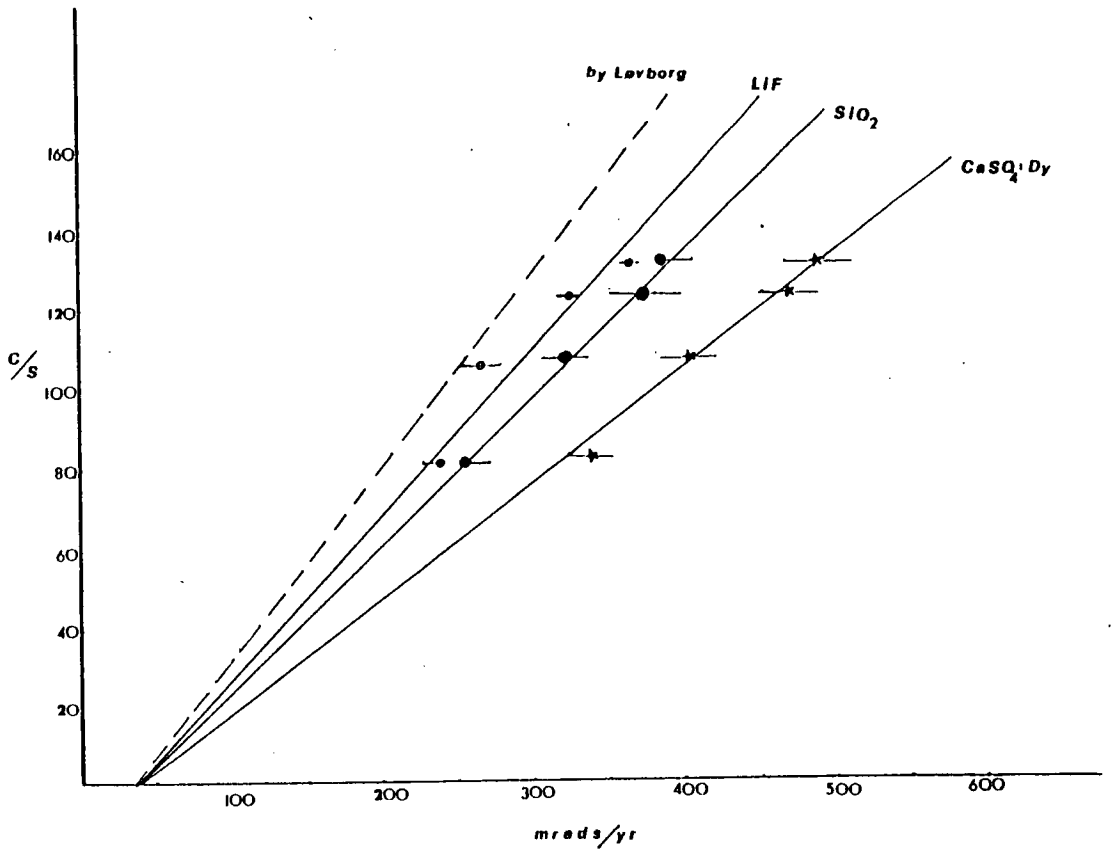


Fig. 7.6.2 Calibration curves obtained by the NaI (Tl) scintillometer, for the respective phosphor (compare . with that made by Løvborg using a different counting geometry).

7.7 About $CaSO_4$:Dy and LiF Phosphors

Lif

Lithium fluoride was studied by Daniels as early as 1957 (Daniels, 1957), and is, today, one of the widely used phosphors for radiation dosimetry The properties and behaviour of Lif have been discussed in detail by Cameron et al, ((1968), Becker (1973), Cameron (1970), Corbics et al, (1967), Zimmerman et al,(1966). The phosphors for the present studies were purchased from Pitmans Limited in the form of teflon discs. The annealing procedure was that recommended by Cameron, (1970) and Robertson, (TLD Notes, Pitman). The LiF was annealed at 320°C for 5 hours, followed by 24 hours at 80°C. The last heating has a prodounced effect by reducing the magnitude of the low temperature peak, Fig 7. 7.1 a (3 pages on)

Since teflon has a transition point at 327°C, the recommended high temperature annealing for LiF teflon dosimeters is 300°C. The annealing treatment is of great importance in the calibration of LiF discs exposed to an unknown gamma field. The discs were calibrated in Co-60 gamma radiation as follows:

A dosen discs were specially annealed, as above, and half of them were sent to Risø, Denmark, where a precise gamma dose of 4 rads was administered. The signal was than read in the TL reader. The same discs were annealed similarly to above and a beta dose (equivalent in minutes of irradiation) from the Sr-90 source in a collar position (12cm above the heating strip where the discs were placed) was administered to them. This signal was then converted into the original gamma irradiated dose for the same phsophor. The above exercise calibrated our Sr-90 source from a Co-60 source on LiF. The dose rate was 1.63 mrads/min.

To check if the second annealing process changes the sensitivity properties of the LiF which would result in a miscalculation of the calibration, another set of teflon discs, initially annealed (together with those which were gamma irradiated afterwards), were irradiated with the beta source. The numbers again gave a dose rate of 1.63 mrads/min, however.

The main peak appeared at 270°C. The super sensitive properties of the LiF induces greater caution with regards to its operational considerations. This is shown in Table 7.7.1, where different annealing temperature cycles produce quite different TL light. Therefore, it was calculated that annealing stands are required to ensure that all dosimeters go through the same temperature cycle. The stand should be of fairly large thermal capacity and of high raised above the oven floor to minimise temperature gradients. The oven itself should have low temperature gradients throughout its heated volume. For LiF, the use of oxygen is recommended. After the high temperature annealing, thephosphor is transferred to an oven, pre-stabaiised at 80°C, By this means, a faster, more stable and reproducible cooling rate is achieved. The possibility of contamination of the phosphor by the annealing stand should be considered. A clear porcelain crucible was used as a suitable stand.

Also, taking into account that different batches of dosimeters have different sensitivities, in our TLD dating study, LiF (similarly $CaSO_4$:Dy) were from the same batch.

Re-Use of the same phosphors does not produce an error. This is also seen in Table 7.7.1 where the 1st and 6th readings (at

TABLE 7.7.1

Different Annealing Procedures for the same Lif Discs

Heat Treatment	No. of Integrated Channels	Counts
1. 320°C for $\frac{1}{2}^h$, increased to 380°C for $\frac{1}{2}^h$	20	2367
2. 320°C for 1^h, increased to 380°C for 20 mins	20	7438
3. 350°C for $1\frac{1}{2}^h$, increased to 380°C for 2^h	20	1920
4. 330°C gradually to 350°C for $1\frac{1}{2}^h$	20	2800
5. 330°C to 360°C for 45 mins, increased to 380°C for 15 mins	20	2200
6. 320°C for $1\frac{1}{2}^h$, increased to 380°C for $\frac{1}{2}$h	20	2350

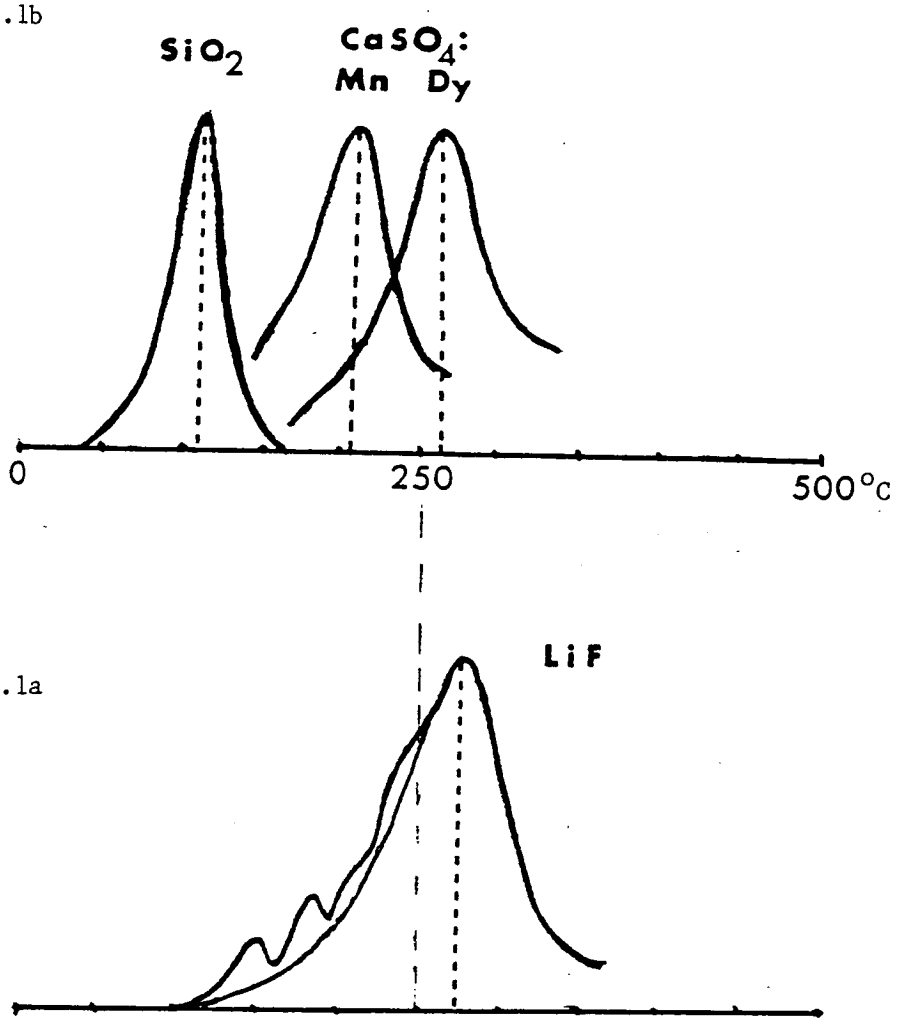
different times) for the same phosphors gave the same light output. Finally, the LiF discs were of 13mm x 0.4mm and contained 30mg of phosphor. The readout was performed with a PM overall voltage at 950 volts, and without the use of the blue filter. For the dose range involved here, the LiF has a linear response per absorbed dose. Also, no fading has been noticed. This has been checked from field measurements (see Chapter 8). The energy response is low to low energy photons, lower than that of the quartz.

$CaSO_4$:Dy

Calcium sulphate activated by Dysprossium or Thalium was introduced by Yamashita et at (1968) and further discussed by Yamashita et al, (1971). Depending on the concentration of the activation and different manufacturing in general $CaSO_4$:Dy produces a glow peak at around 230°C, Fig 7.7.1.b. This phosphor can measure gamma exposures of less than 1 mrad. Properties of the phosphor including the effect of radiation on activator concentration have been studied by Schmidt et al, (1974). Kinetic studies have been reported by Nambi (1975), Fiorella et al (1976) and Mangia et al (1977).

It has been extensively used in the TL dating by Mejdahl, (1970, 1972, 1978). $CaSO_4$:Dy in teflon was purchased from Pitmans Ltd. No fading was found for a period of onemonth (from field measurement, see Chapter 8.) In the present experimental arrangements, where phosphors were kept in liquid nitrogen, the fading was non-existent. It has an attraction with respect to LiF, from its simple annealing procedure(300°C for 2^h). The responses of CaSO:Dy are very high to low energy photons higher than quartz, Fig. 7.8 below. For the last reason, thephosphors were contained in brass tubes with a wall thickness of 1.5 mm, Mejdahl, (1978). The effect of

7.7.1b



7.7.1a

Fig. 7.7.1b Glow curve of the phosphors used in the experiments.

Fig. 7.7.1a Glow curve for LiF. the annealing procedure eliminates the low temperature peaks (annealing of traps), thus the peak becomes somehow symmetrical (Peak 270°C).

the brass tube is to compensate for the large response of $CaSO_4$:Dy at low photon energies by cutting off the low energy part of the spectrum. The relative response of the brass probe is nearly that of quartz, Mejdahl, (1970). However, variation in the low energy gamma spectrum relative to the total gamma spectrum would undoubtedly change even these small differences in the responses of quartz and $CaSO_4$:Dy. The gamma reading was calibrated on a Sr-90 beta source (which was subsequently calibrated on a Co-60 gamma source) in the same manner as LiF. The dose rate calculated for the Sr-90 source was 1.84 mrads. in the collar position. (The calibration values found to be 1.63 mrads/yr. 1.84 mrads/yr and 1.74 mrads/yr for Lif, $CaSO_4$:Dy and SiO_2, respectively, are in agreement with their respective gamma responses).

7.8 The Mass-Energy Absorption Coefficient of Mixtures and Compounds

In order to demonstrate the response of gamma radiation to mixtures, compounds and phosphors; materials frequently encountered in the gamma dosimetry of TL dating, the following illustrative investigation was undertaken.

Fig. 7.8 shows the variation of the absorption coefficient relative to air for a typical clay, clay + 25% H_2O, clay + 50% H_2O, clay + 100% H_2O, sand, 86% sand + 14% K_2CO_3, quartz, peat, $CaSO_4$, LiF, concrete and NaI. It is common to all, except clay + 100% H_2O, clay + 50% H_2O and NaI, the similar response or absorbed dose for photon energies above 200 KeV.

In the low energy region, the absorption coefficient varies markedly for the same medium and between different media.

The absorption coefficient has the following physical meanings: for the phosphors it means the response per roëntgen, which subsequently implies different Thermoluminescent efficiency in light

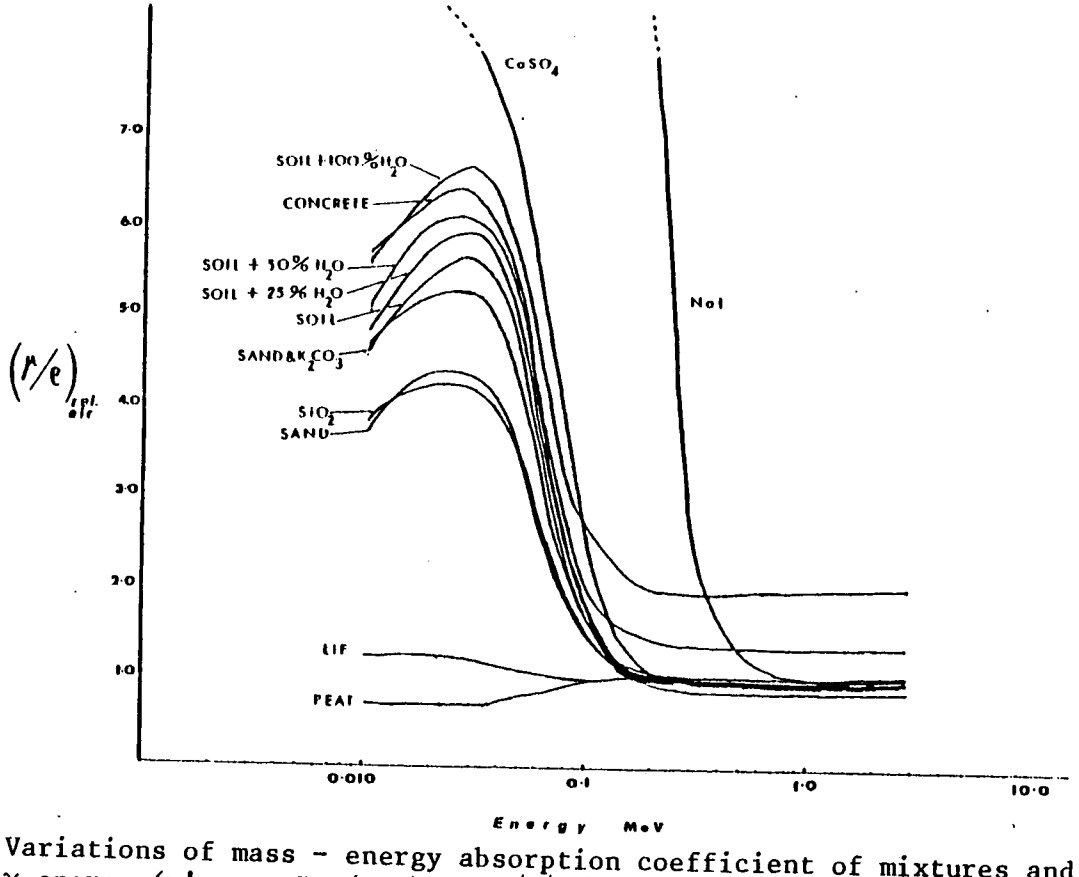


Fig. 7.8 Variations of mass - energy absorption coefficient of mixtures and compounds with γ-energy. (μ's vs. E (MeV) were calculated from Storm and Israel (1970)). By multiplying $(\mu/\rho)_{rel.air}$ with the energy absorption per Roëntgen in one gram of air (0.869 erg/gR), one can determine a factor for converting exposure to absorbed dose.

units, and for the other media, it means energy absorption (for example, in rads), which subsequently implies gamma attenuation through the respective medium, for example when clay is compared to clay + 100% H_2O. This depends on the density and composition of the compound.

The NaI has a higher response than quartz, therefore, its calibration on a particular phosphor and on a wide spectrum of known radioactive media is necessary for γ-field measurements. The obtained curves of Fig. 7.6.2 thus reassures that, in spite of the different isotopic composition of the boxes, the NaI(Tl) scintillometer gives correct results, as deduced by the linearity of the curves. Moreover the selection (choice) of a proper medium to carry out the calibration is very important and this can be seen for clay, sand and concrete media.

It is worth noting from Fig.7.8 that the best way to calibrate the NaI(Tl) is to choose a relatively wide selection of soils, as usually occurs in archaeological sites, rather than mixing different isotopes on the same medium, for example, clay or concrete only.

Finally, the peat has similar behaviour to LiF. The former agrees with its very low density.

7.9 Discussion of the Calibration Curves Obtained

Firstly, we will consider the different slopes of the curves corresponding to LiF, $CaSO_4$:Dy and SiO_2(Quartz), of Fig. 7.6.2. The difference in the mass-energy absorption coefficient of these phosphors accounts for their different response per absorbed dose. (Since the stopping power is proportional to the absorption coefficient, comparisons between absorption coefficients (μ/ρ) of a particular

energy between two phosphors provide a meaningful comparative estimation of their respective thermoluminescent sensitivities.

The dependence of the response of a wide range of phosphors on low energy is considered to 50KeV energy, Table 7.3

The response curves for quartz at low photon energies is higher than those of LiF andlower than that of $CaSO_4$:Dy. As more than 60%* of the gamma spectra in the soil (Løvborg, et al, 1976), consists of low energy photons lower than, say, 500 KeV, the differences in response of the above phosphors considered will be very pronounced as seen from an inspection of the curves in Fig 7. 8. As the critical lower part of the soil spectrum cannot be obtained with sufficient accuracy, it is not possible to accurately calculate the response to calcium sulphate or LiF phosphors. Dosimeters based on these phosphors must, therefore, be compared in a soil spectrum with a quartz (or quartz equivalent) phosphor, Mejdahl, (1978), which otherwise was the main purpose of the present work's investigations. The curve for quartz was used to convert NaI (Tl) readings taken in situ to dose rate. This obtained curve was of the following form, $y = 3.2x + 31$, with an overall standard error ($\pm$ 1σ) of $\pm$14 mrads.

The upper curve(Fig. 7.6.2)was by Løvborg et al, (1976), obtained by a NaI(Tl) scintillometer placed 12cm above radioactive concrete boxes, and also by using a Ra-226 source at a distance from the detector, as follows:

i) four concrete cement pads doped with Uranium, Thorium and Potassium and a pad containing no naturally radioactive constituents.

The dose rates from each of the above pads were calculated at a

---

* In a preliminary exercise we found that ∿76% of γ-soil spectrum consists of low energy photons, lower than 350KeV.

distance of 12.5cm above the pads, in the air, by using TLD phosphors, (LiF). Readings were taken also with a NaI(Tl) 2" x 2" detector before and after the dose integration period, (similar to Fig. 7.5.2). The normal concentrations of potassium and equilibrium uranium and thorium were calculated by extensive computational studies and the results compared with spectrometric studies. Although a straight line was obtained for potassium, thorium and the neutral pad, the uranium value deviated by around 23% due to the radon emanation. The pads were subjected to meteorological factors, in particular, the moisture.

ii) comparative calculations were made of an integral spectrum of a broad parallel beam of photon indicating perpendicular to the end face of the detector.

It was verified that the calculated rates are mutually consistent but the values were not confirmed experimentally.

Finally, the calibration of the present scintillometer based on the above geometrical positions of counting gave the straight line of Fig. 7.6.2, as $y = 0.531x - 22.807 (\sigma = \pm 5\%)$.

This calibration was performed in air and in a nearly 2π ($\lesssim 2\pi$) geometry, where the derived gamma spectrum is not ultimately equal to that inside the pads, Fig. 7.5.2. There are two main points in the calibration by Løvborg:

a) the NaI response to gammas is different depending on the relative contribution of the respective energy part of the spectrum and

b) the absorbed dose was measured in LiF whose energy response underestimates the actual dose. This subsequently depends upon the relative low energy photons present.

Additionally, the pads used were cemented concretes, which are somehow of different energy absorption coefficient to the typical soil or sand ones, (Fig.7.8) which implies that the derived gamma spectra would be different. This could have an effect on the detected dose in phosphors.

Also, it has been noted that differences in density between two or more media does not mean only an effect on the attenuation of gammas, but a degree of distortion of the gamma spectrum as well.

7.10 Results: Comparison of Dose Rates with PPM Values

Table 7.10 gives the radioactivity content of each cox. For U-238, Th-232 and K-40, this was assessed from the known weight of material added. The size of the box was considered nearly infinite. Additionally, the radiation from U, Th and K content of the sand and peat was measured and included in the total dose. The density for the peat was 0.4 gr/cm^3 while that of the sand was 1.3 gr/cm^3 because of dilution from shells which is lower than its equivalent quartz.

7.11 Discussion

From the data given in Table 7.10, and 7.6.1, it would appear that the theoretical

and experimental data agree reasonably well for K-40 and Th-232, but not for U-238, in peat and sand. A number of possible reasons for this discrepance have been considered and discussion is carried out on these results.

i) inhomogenities. About 50% of the gamma dose is contributed by approximately the first 12cm surrounding the capsule. (This however depends on how high the gamma dose is.) For the sand/peat part surrounding the tt ball, of approximately 350gr, mixed with a proportional amount of ores by weight, related to the total amount in the boxes, a homogeneity can be assumed. It was found otherwise to be the case when samples from different parts of the boxes were alpha counted. The variations due to mixing are obvious, Table 7.11. The small amounts of radioactive ores used were 11gr for U, 120gr for Th and 5.7 gr for peat and did not mix well with the sand (130Kg) and the peat (67.5Kg) in the boxes. This difficulty was initially anticipated, but the principal idea was to keep the ppm levels as low as possible in order to:

   a) simulate actual gamma spectra of soils in situ and
   b) be able to measure the subsequent signal of the phosphors involving only a small statistical error due to the number of counts.

ii) disequilibrium. There are two possible forms of disequilibrium. The first could be due to the recent formation of the sample or preferential leaching of a chain member; the second is due to possible emanation. Although by use of alpha counting measurements it is possible to detect escape of radon and thoron. (For the sand doped with thorium, such escape was found to be

TABLE 7.10

Radioactive Dopants	Theoretical γ-dose (mrads/yr)	Sand/Peat Self γ-dose	Total Theoretical* γ-dose of the boxes (mrads/yr)
Uranium	554	26.3	580
Thorium	384	26.3	410
Peat	616	27.4	643
Potassium-40	207	26.3	233

Density (gr/cm^3)	
Peat	0.4
Sand	1.3
K_2CO_3	2.43

* The contribution from the radioactivity of the sand measured by alpha counting was 26.3 mrads/yr and the potassium content of 0.068% giving 0.169 mrads/yr which is negligible. Similarly, for the peat, the potassium was megligible and the alpha counting gave 27.2 mrads/yr. The water content of the sand was 3% and that of the peat negligible.

TABLE 7.11

Sample		Alphas*/10^4sec	Estimated(ppm)**		Theoretically Calculated (ppm)
Sand	Th extract	96.8	52.4	66.8±7%	78.7
	Th top, box	140.0	76.5		
	Th middle, box	131.0	71.6		
Sand	U top	833.0	134.0	49.0±51%	43.7
	U middle, box	270.0	43.0		
	U middle, edge				
	bottom	63,0	10.0		
	U extract	61.0	9.8		
Peat	U top	33.0	5.3	63.0±35%	48.6
	U middle, box	625.0	100.0		
	U middle, edge	426.0	68.7		
	U extract	486.0	78.4		

* For our alpha counting system 1ppm Th - 1.8288 alphas/10^4sec
1ppm U - 6.2116 alphas/10^4sec

** To the estimated ppm values a small contribution from the U and Th of the sand and peat themselves have been subtracted. The sand itself gave 11.4 alphas/10^4 and the peat 12.9 alphas/10^4sec.

v) box size. The density of the sand (1.3) is surprisingly low. The typical value is 2.6gr/m^3. That of peat was 0.4 gr/m^3. These low density values could be problematic (as was found to be the case theoretically, Tables 7.11.1), since they raise the question of whether the boxes are infinite (or nearly infinite) matrices for the gamma energies involved.

However, though the "infinite" assumption is not satisfied, (despite the box sizes, equal in volume to a sphere of 30.25 cm radius), the position of the four boxes nearby to each other could compensate for this discrepancy. This (and the gamma spectra produced thus in any box) does not induce any error in the calibration since the counting rate recorded by the NaI would be, in either case, proportional to the gamma intensities; otherwise the results obtained exclude such a possible error, that is, the obtained linearity of counts/second against gamma dose.

Finally, it should be emphasised that the radioactivities involved for the sand/peat extracts (from the boxes) surrounding the tt ball would give a high γ-dose in the capsules, in spite of the calculations in Table 7.11.1, because the high percentage of low energy γ-spectrum to the total contributes significantly to the total gamma absorbed dose in the centre of a sphere which have a radius of approximately 7cm, bearing in mind that the extract surrounding the tt ball is a sphere of approximately 3.5cm radius, Table 7.11.2

TABLE 7.11.1

% Fraction of Absolute Dose at the Centre of the Sphere of radius R=30.25 cm *

Energy MeV	Soil	Peat	Sand
0.02	1.000	0.997	1.000
0.05	0.999	0.738	1.000
0.100	0.972	0.618	0.992
0.200	0.903	0.530	0.967
0.300	0.852	0.487	0.942
0.500	0.783	0.429	0.898
0.600	0.756	0.409	0.875
0.800	0.707	0.375	0.843
1.000	0.673	0.313	0.814
2.000	0.554	0.279	0.685
3.000	0.490	0.224	0.614

TABLE 7.11.2

Radium(cm)	Energy(MeV)	% Fraction of Absorbed Dose ** at centre of the Sphere
3	1.00	11.0
3	0.30	14.2
3	0.20	15.5
3	0.05	21.2
7	1.00	25.6
7	0.30	35.8
7	0.20	40.0
7	0.05	85.7

* Calculations for both tables were made using the formula of Table 2.12.2
** On sand

CHAPTER 8

GAMMA SOIL FLUCTUATIONS DUE TO METEOROLOGICAL FACTORS

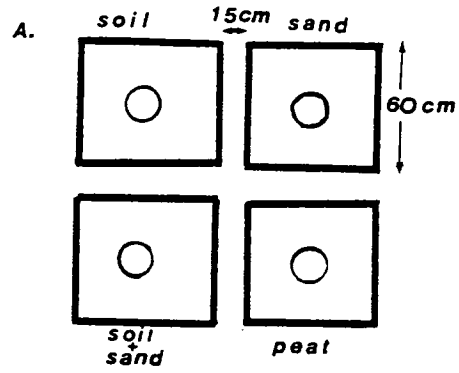
8.1 INTRODUCTION

The following study was undertaken with the objective of measuring the degree of seasonal variation of gamma dose in soil and of investigating the question which frequently arises: does the one-day reading in an archaeological site by a portable scintillometer represent the true annual gamma dose rate and subsequently the average dose rate over the past archaeological years? For this, four boxes were made, (60 x 60 x 60cm), being loosely constructed in order to allow the water to escape as naturally as it would through the ground. The boxes contained soil, sand, soil and sand, and peat, respectively, buried in a soily terrain outdoors, and placed at intervals of 15cm apart. Fig 8. 1

At frequent intervals readings were taken with the NaI(Tl) 2" x 2" scintillometer, by inserting the probe to a depth of 30cm into the centre of each box. At the centre of each box Lif and $CaSO_4$:Dy dosimeters in brass and polythene containers were placed.

8.2 Results

For eight months measurements were taken with the scintillometer and the phosphors were measured by the TL apparatus. The results, expressed as mrads against counts/sec are shown in Table 8.2 and in Fig.8.2 for Lif. Also, in Table 8.2, the annual average counts/sec for the respective boxes is shown with the corresponding average deviation from the average. It is worth noting that the annual average (counts/sec) on top soil, that is, 2π counting geometry, is approximately 71% of the annual average inside the soil, (30cm under the surface), that is 4π counting geometry. This has to be taken into account when counting



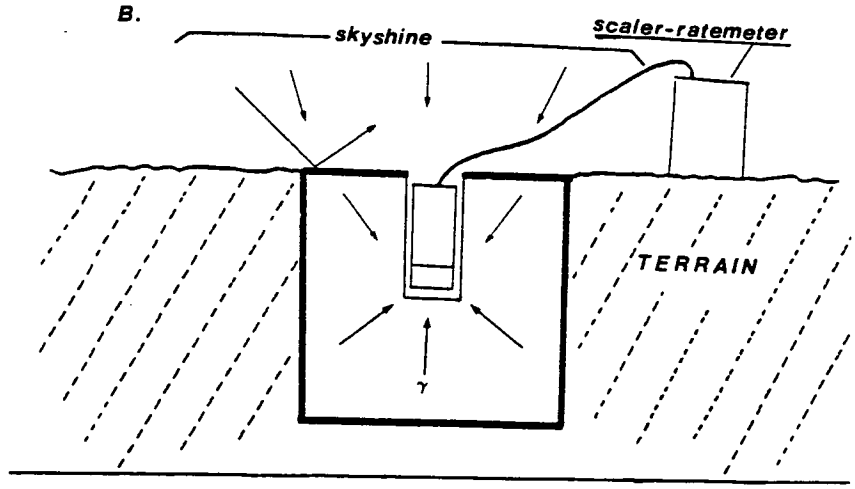


Fig. 8.1 A Lay-out of the Four Boxes in the terrain (top view)

Fig. 8.1.B Counting Geometry of each Box

TABLE 8.2

	c/s	Lif mrads/yr	Poly/Brass $CaSO_4$:Dy)	Yearly Average c/s	%Deviation from average of min yearly value	%Deviation from average of max yearly value	% Water uptake for full saturation	%Water uptake for natural state	Density (gr/cm^3)
Sand	11.6±0.6	56.9±4	1.019	11.6	-10.2	+10.9	50	5	1.62
Peat	17.5±0.9	76.9±7	1.22	17.5	-17.2	+25.9	73	55	0.36
Soil	37.1±1.8	149.0±13	1.09	37.10	- 7.6	+ 9.4	71	18	1.12
Soil & Sand	23.4±1.1	90.9±11	1.14	23.4	- 8.2	+12.7	94	16	1.55
Top Soil				26.3	- 9.4	+ 8.5			

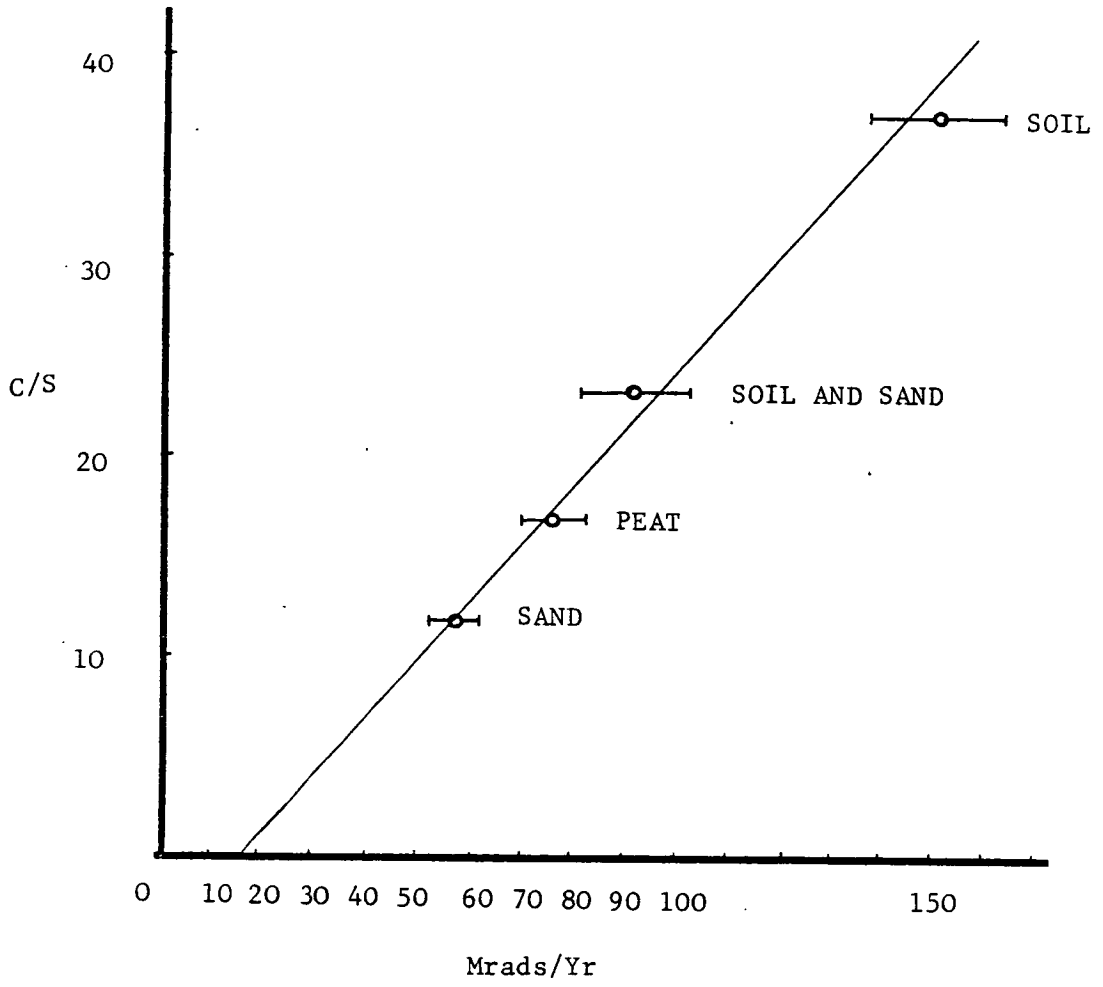


Fig. 8.2 Counts/Sec vs mrads/Yr for the LiF phosphor discs
The phosphors were calibrated in Risø with a Co-60 γ-source

geometries (2π) are encountered.

The extent of variation depends on soil type, that is composition, porosity and density as illustrated in Table 8.2, where each soil type retains differing amounts of water in saturated and natural conditions. The ratios of doses measured by $CaSO_4$:Dy phosphors in polyethelene and brass containers are also shown in Table 8.2. This was tried in order to emphasise the effect of low energy photons of different soils in the determination of gamma radiation. The high ratio obtained in the peat box is probably due to the high number of low energy photons in the peat and thus, a high response for the phosphor in polyethelene resulted (Chapter 7 Section 7.5.2) Apart from the peat, in general, the gamma spectra from the other media do not vary considerably. This has also been found in Chapter 7. This data also indicates that the calibration of the NaI(Tl) is reliable, and for typical archaeological soils, this instrument can be used with trusted accuracy. Fig. 8.2.1shows characteristic gamma soil spectrum as recorded by the crystal scintillometer probe and the multi-channel analyser. Previously, the counting system was calibrated with a Cs-137 (0.662 MeV), Co-60 (1.17 MeV, 1.33 MeV) and potassium nitrate (1.46 MeV). The resolution obtained was 7.2%.

8.3 Annual and Monthly Gamma Variations

The variations of gamma radiation in the aforementioned soils have been recorded by taking measurements periodically with the NaI(Tl) detector. The NaI was calibrated with CO-60 and CS-137 gamma sources. Prior to any measurement, the instrument was left outdoors to equalise its temperature with the air temperature, in order to avoid voltage shift. selection (see 8.4 below). Fig 8.3 illustrates some readings as a function of time,and,correlation with meteorological factors, that is, rainfall, snow and temperature is made.

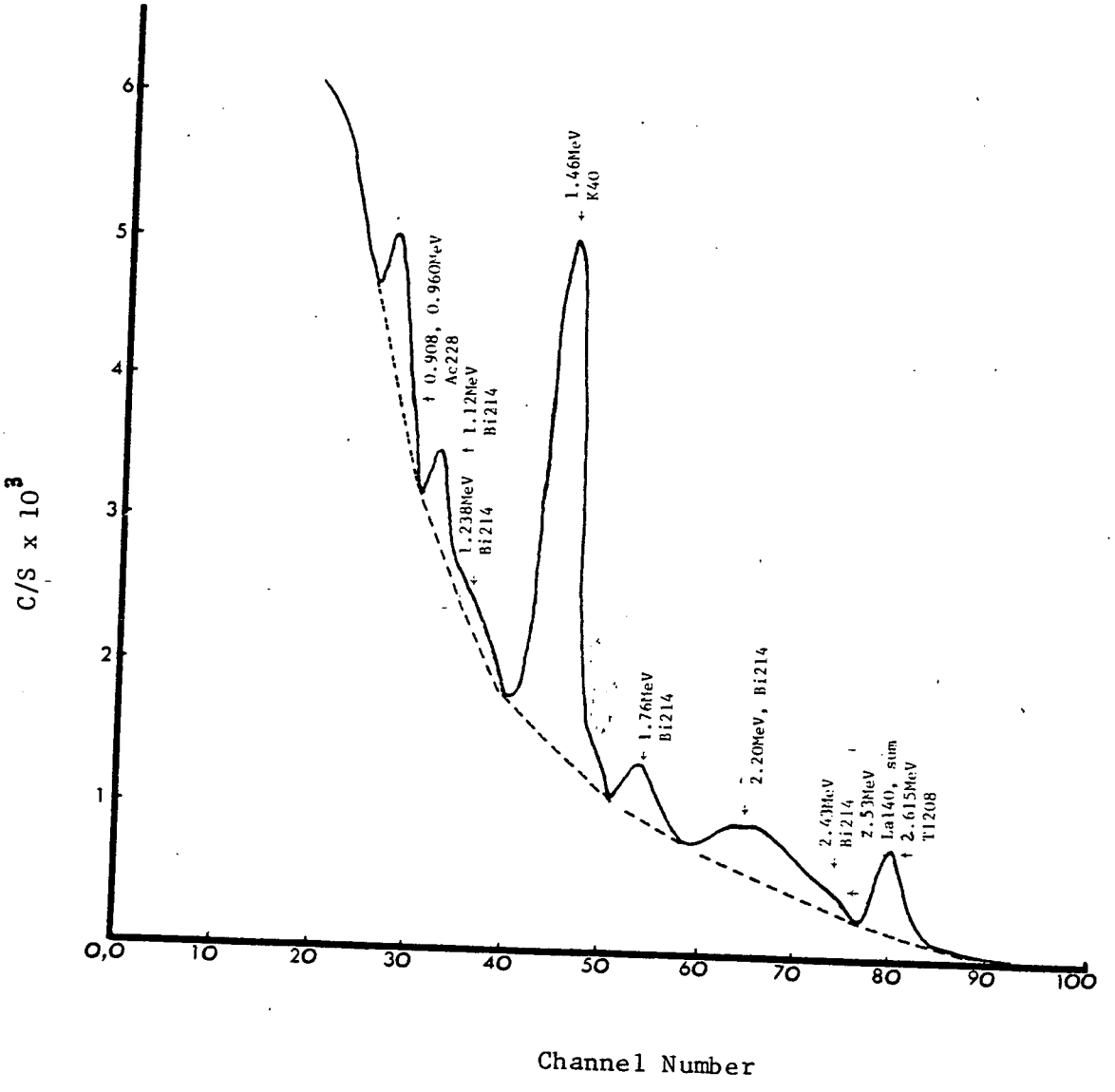


Fig. 8.2.1 Typical γ-soil spectrum as recorded by the Scintillation Probe (PM tube 9635 Q/A type) and a (Labentype) Multichannel Analyser The dashed line represents the Background. (mainly the compton scattering components of the primary γ-rays).

The data provided by these readings help us to evaluate the environmental gamma radiation. Depending upon when a reading is taken, a correction needs to be made to convert this reading into an annual average. This correction factor depends on soil type and climatological conditions. Fig. 8.3.1shows such a variation over a period of eight months, and Table 8.2 presents the maximum and minimum deviations from the total average. It is obvious that for gamma, the winter values are lower than the summer values. Therefore, if a reading is taken in winter, a correction factor for a typical soil would be +10%, while for the peat, for example, it would be +21%. This must not be confused with the water uptake correction. For example, for a measurement in winter, the correction for water uptake would produce a lower value than the actual. This is because the gamma measurement on dry conditions is not represented during winter. Conversely, during summer, the dry soil will not give a higher dose than that which holds over the year. Here such a correction is not necessary since the water correction (for the present or former years) taken this into account.

8.4 Threshold Drift

It has been observed that drift in the instrument arises from temperature changes and decline in the voltage of the nine batteries, (battery life is 120 hours). The lattter is quite systematic with regards to direction and rate and is however checked by turn function control to BATT position, so that if the meter reading is in the red section the batteries are replaced. Although the temperature range for the instrument is 0^{o}-50^{o}C, with stability in voltage of 0.01% per ^{o}C, the threshold position changes by about 10.2% for temperature changes of 11.5^{o}C (or 0.0174 volts.grad-1). The drift, as observed, is probably due to a combination of effects in the photo-multiplier, the amplifier and the discriminator.

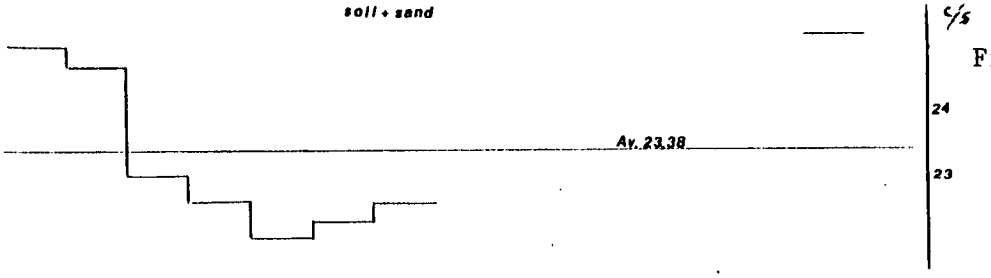


Fig. 8.3.1

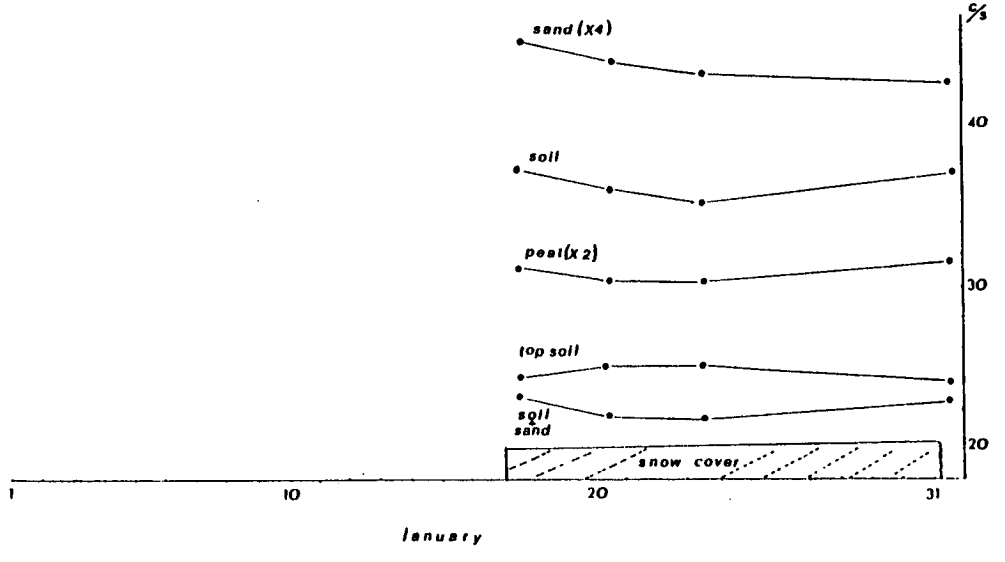


Fig. 8.5.2

Fig. 8.3.1 Average monthly gamma variation over the period of 8 months.

Fig. 8.5.2 Gamma variation over the last fortnight of January due to snow cover

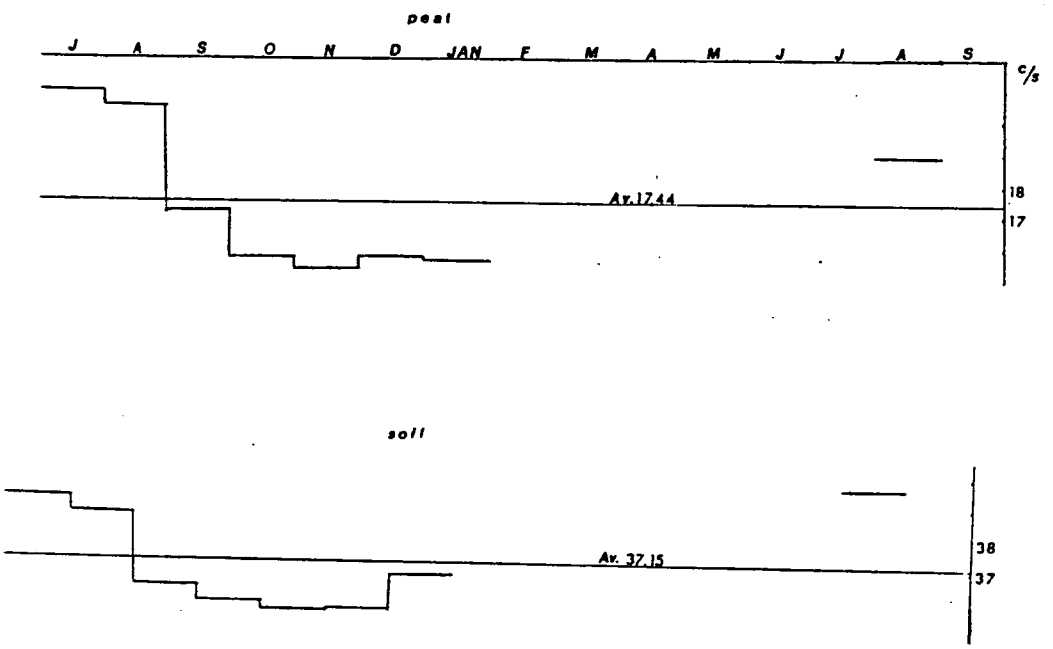


Fig. 8.3.1 (cont.)

Measurements were made only of the overall "system-gain" which includes such factors as bias suitability. Only large temperature changes produce noticable drift, which are not likely to occur during normal counting intervals, provided that the instrument switch on the left is in situ for around 15 mins before taking a reading. Furthermore, the standard procedure for pulse height calibration before and after each measurement was followed and thus any drift that might occur was noticed and corrected.

8.5 Interpretation of Seasonal Gamma Soil Fluctuations

Some characteristic features on monthly gamma variations for July, August, September of 1977 are described and studied in some detail, Fig8.5 Subsequent periods are based on the same interpretation. Considering the Fig.8.5. which applies for the month of July, the 8mm of precipitation which occured on the 15-16 July increases temporarily, the gamma reading due to the fact that radon isotopes (sealed by the rain) are depleted in the uppermost layer of the 30cm of the soil. This occurs in all the boxes. The subsequent fortnightly readings flucuate around this monthly average and at the end, tend to decrease following the temperature drop. A variation of approximately 3% from average during this month for soil and and approximately 5% for peat was observed. This corresponds to a 7% temperature variation. A continuous rainfall, even of small amounts, initially tends to increase the gamma and subsequently stabalizes it, being lowered in longer periods, because of the attenuation of gammas from the surrounding terrain due to the increased absorption coefficient from the water. This stabalisation might also be due to the downward modulation of K-40, Lanthanum-140 and Zr-95 - Nb-95, build-up by the rainfall, Adams, (1964).

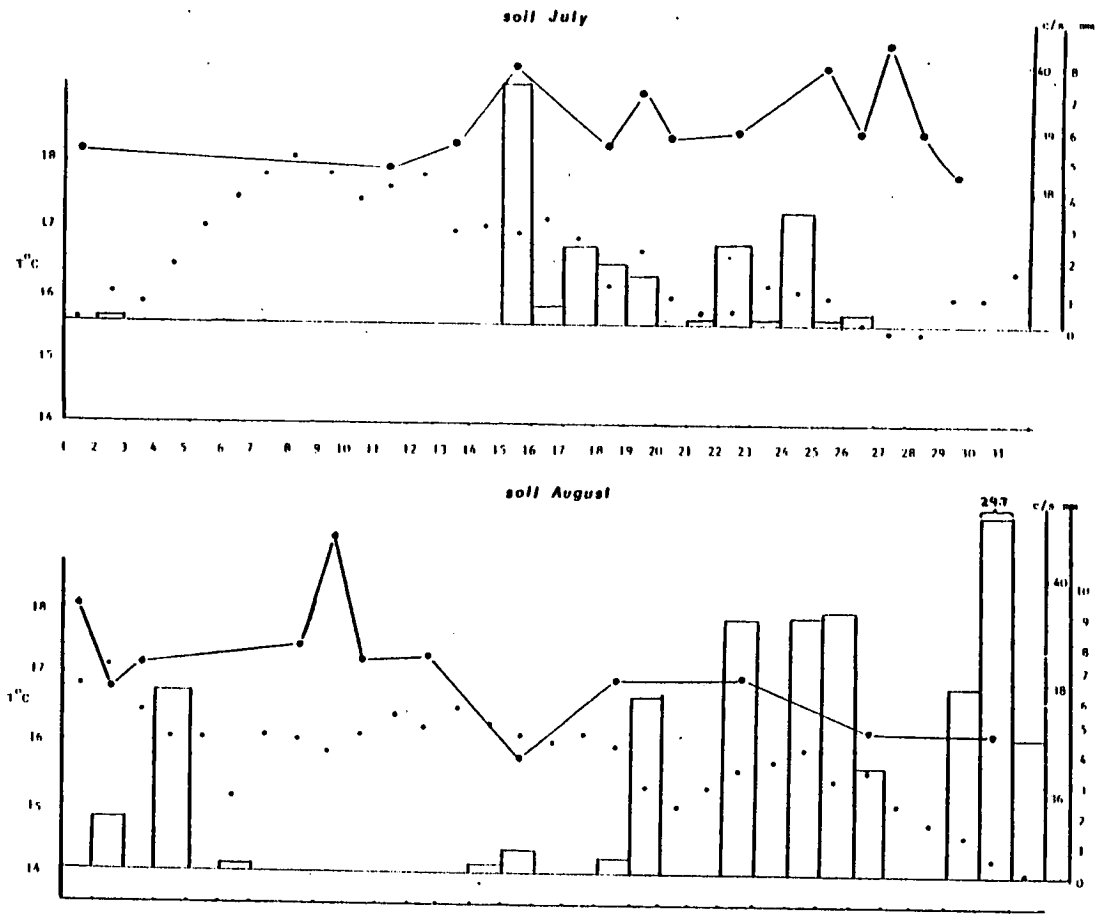


Fig. 8.5 Monthly gamma variation as a function of meteorological factors (i.e. temperature, rainfall)

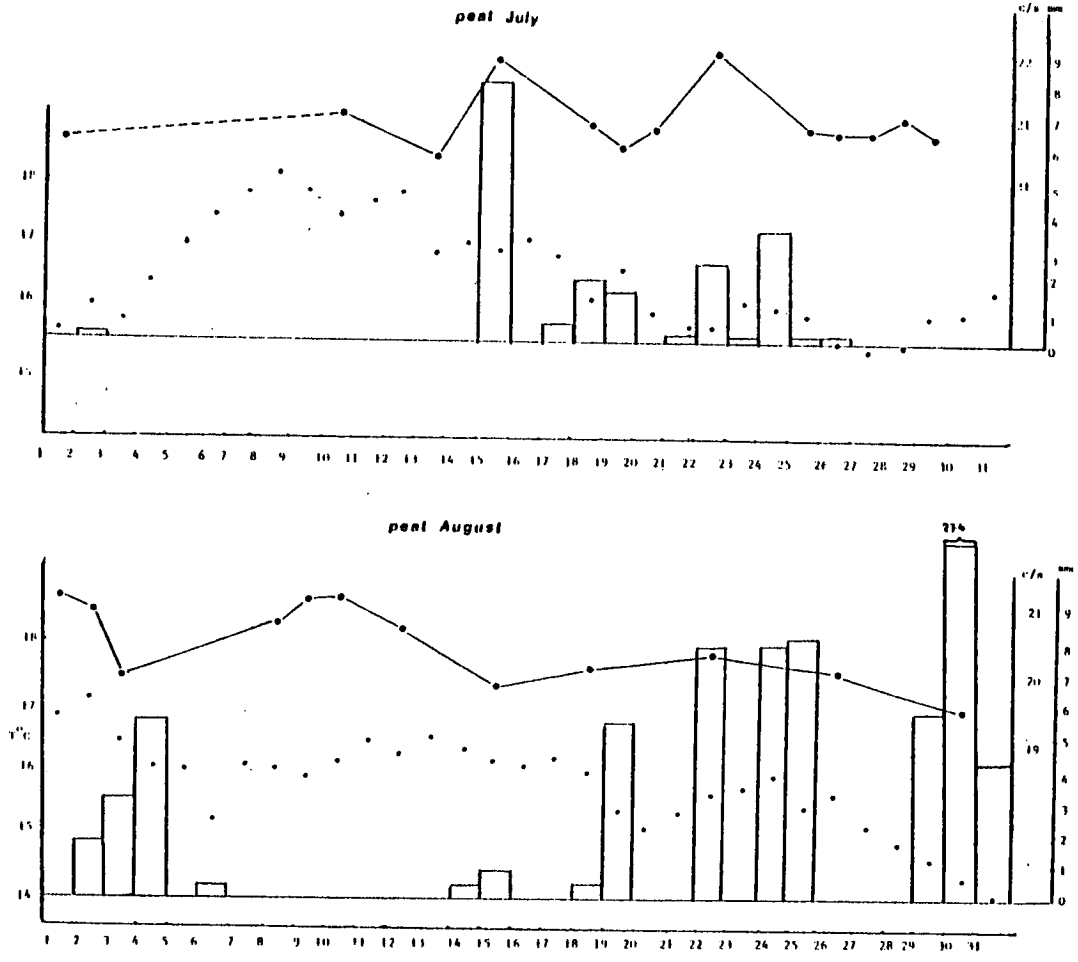


Fig. 8.5 (cont)

In August, the temperature continued to drop as did the readings. The heavy rainfall during the last two weeks of this month washes down the gaseous radioisotopes or radon and thoron. After the fifth day of this month, a recovery seemed to occur with subsequent drop due to radon exhalation in the atmosphere, Fig. 8.5
For all cases, in water-saturated media, the diffusion coefficients of Ra-222, Ra-220 and Ra-219 depends on their porosity. On the 22nd day, a low reading for the soil in 30cm depth corresponds to high reading on the top soil, that is, on the surface, because the radon has been trapped in the uppermost layer of the soil box. In September, Fig. 8.5.1, the temperature still goes down and the readings follow the extent of rainfall. Thus, the low readings at the beginning of this month (a week with daily rain), follows a high reading due to recovery of radon after two weeks (radon reaches its maximum activity with a half life of 3.7 days), to drop again on the 27th day of the month due to the 21.2mm rainfall. The other months also support the above remarks. However, by the end of January, snow covered all the ground. Measurements gave a relatively high reading inside the boxes, and a lower reading on the top soil. Fig. 8.5.2 Subsequent readings gave a lower value inside the boxes and a higher one for top soils. This is due to the fact that freezing or snow cover - like an appreciable precipitation - will tend to seal the ground, to cause build-up of the radon concentrations in the important uppermost layer and to increase gamma ray source strength in the broud and deplete this gamma source in the atmosphere subsequently. (Fig.8.5.2, 5 pages above). From the above, the general conclusion is that for moderate rainfall, say of 8mm, or snow covering the ground, followed by a dry spell of two weeks, we find a recovery of radon by the end of this period. Though continuous rain, of the above rate, washes down the radio-siotipes and thus reduces the gamma radiation. Finally, for rainfall higher than, say 10mm, the gamma drops considerably. Also,

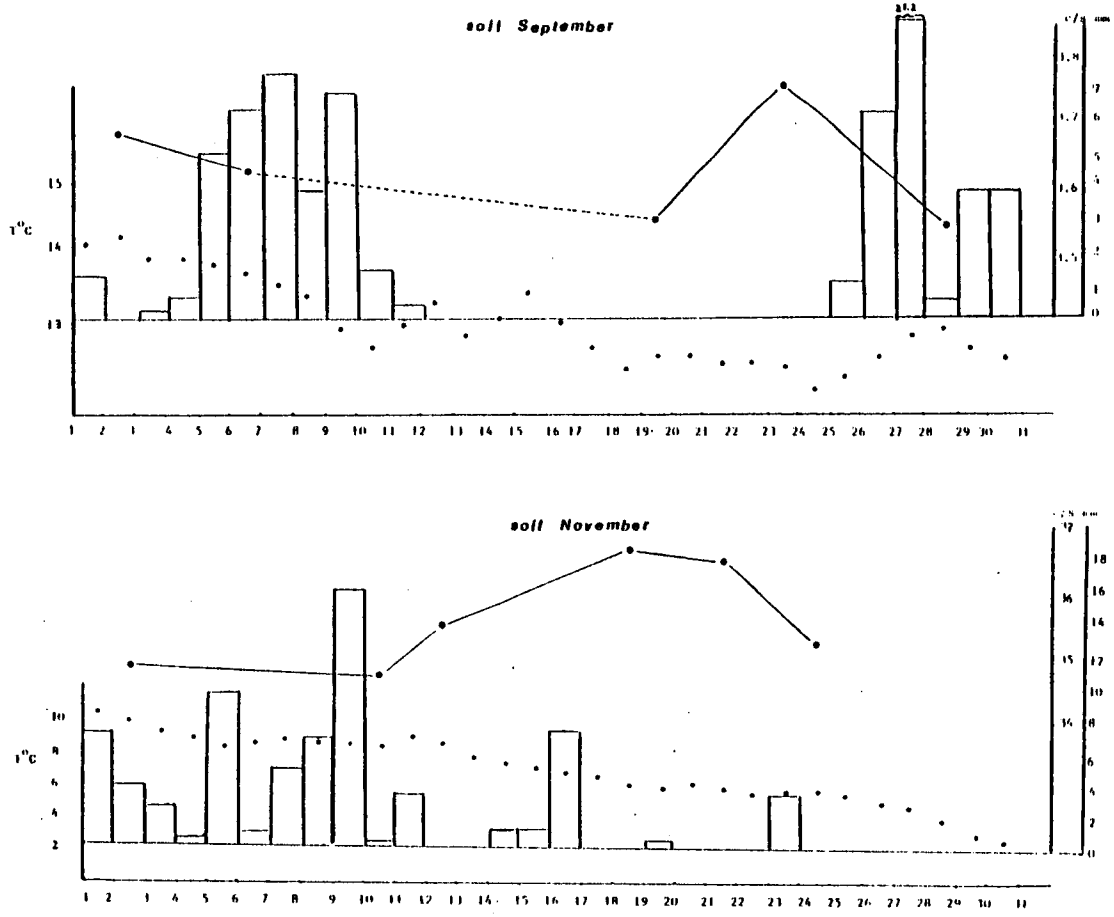


Fig. 8.5.1 Monthly gamma variation as a function of meteorological factors (i.e. temperature, rainfall).

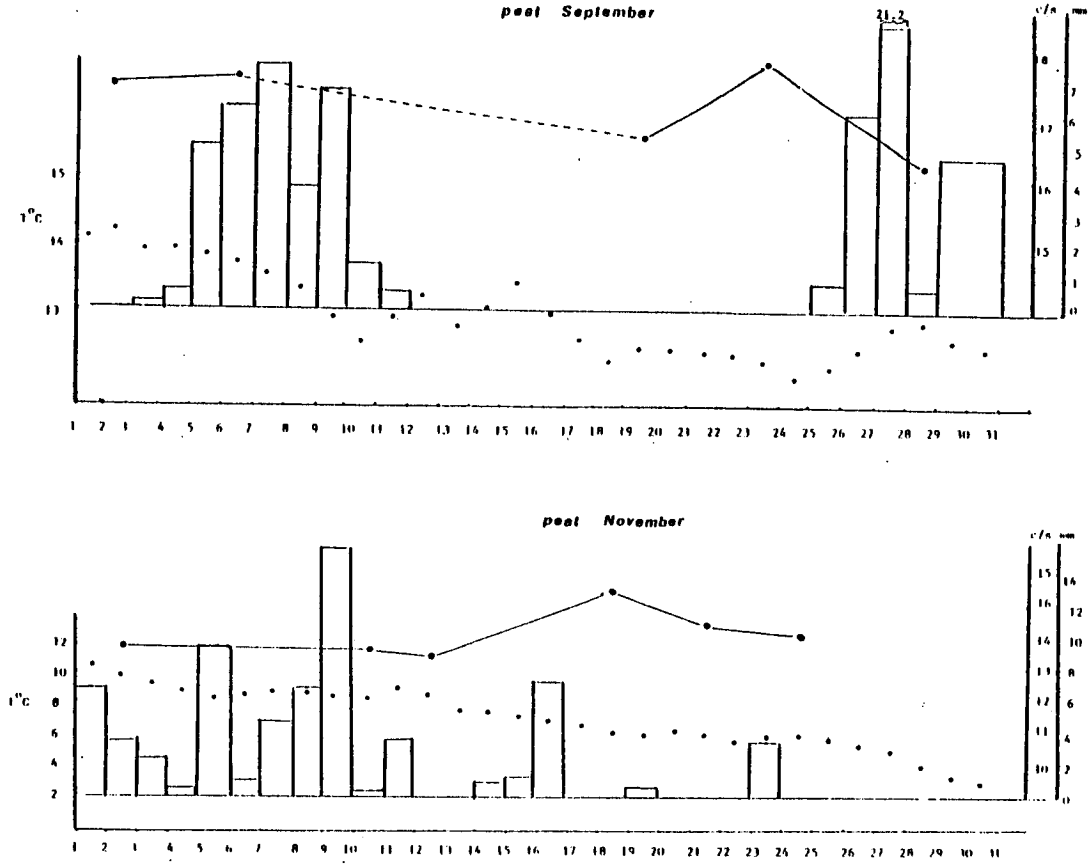


Fig. 8.5.1. (cont)

as a rule, temperature changes follow changes in gamma readings.

8.6 Conclusions

In conclusion, different soil types produce different extents of seasonal gamma fluctuations and this depends on:

i) the ability of the clays to retain water or the ease of evaporation;

ii) the climate of the site and the geomorphological position;

iii) the diffusion and transportation for leaching or enrichment of radioactivity.

In particular, the peat has the greatest seasonal deviation from the average. The above gamma variations are of great importance when environmental radiation of a site has to be measured for the purpose of dating archaeological samples by thermoluminescence. The difficulty of assessing the water uptake over the archaeological period in connection with such great variation make the problem of evaluation of the environmental gamma radiation very difficult. However, knowing the type of soil involved, that is, soily, stoney, peaty, etc., the geomorphology of the site the burial conditions of the archaeological artefact and temperatures and rainfall averages and extremes, we can approach a reasonable average value for the hydraulic condition of the soil and thus further limiting the uncertain deviation of gammas from the annual or ancient gamma average. This could reduce the final error in the estimation of the environmental gamma radiation, which subsequently will be further reduced from other parameters of the age equation. Nevertheless, in such cases, the higher the gamma radiation, the lower the involved error is likely to be.

PART IV

CHAPTER 9

THERMOLUMINESCENCE DATING RESULTS AND DISCUSSION

9.1 INTRODUCTION

This chapter presents results from two dating programmes. In terms of the techniques used, the present application represents a further extension of the TL method by using the feldspar and quartz inclusion techniques. The aim of these chronological studies was:

i) to date Minoan kilns (well-fired clays), from Crete, in order to determine the last firing events which are related to the destruction of the Minoan palaces. This dating programme is linked with archaeomagnetic work on the same material in order to establish the secular magnetic variation curve for this Mediterranean area, Liritzis and Thomas (1979).

ii) to define the Neolithic period of Greece by dating pottery and fired clays from two Neolithic settlements, Sesklo and Dimini, in Thessaly, Central Greece. Also to test the TL technique by comparing TL dates with some corrected C-14 results from these settlements as well as from Sitagroi settlements, North Greece, which fall chronologically between the two above Minoan and Thessalian dates.

Some work was also carried out on Glozelian materials from France, in order to substantiate the age of this controversial Glozel material. Discussion is presented of the sample preparation, (section 9.3), glow curves and normalisation procedures (section 9.4 and 9.5). The beta radioactivity measurements (section 9.7) were presented in detail in Chapter 5 , based on TLD and α+K methods, while the gamma radiation measurements were done by the well-calibrated NaI(Tl) scintillometer,

Chapter 7, and comparisons are made with those made by α+K values, (section 9.8). Water uptake values are presented in section 9.6. The results and the comparisons with C-14 corrected dates are presented in sections 9.14 to 9.18.

9.2 Sample Preparation

Several sherds were found to be sensitive to incandescent bulb light, white fluorescent tube light and day light. Therefore, operations in the preparation and use of the TL samples were carried out under red light to reduce the possibility of optical bleaching effects. Most of the samples were unaffected for the first three hours, but some were affected by at least 5% in this time. The sherds were of average thickness, 0.7cm or more, and the procedure of separating the grains from them was as follows:

i) wash to remove soil adhering to the outer surfaces,

ii) removal of most of the clay by gentle wet grinding in a mortar and washing with cold water,

iii) wet sieving, the grain size being 75 - 106μ, 106 - 125μ or 125 - 150μ depending on the available grain size present in the particular sherd,

iv) treatment with diluted mixed acids Hℓ, HF and $HClO_4$ with the use of an ultrasonic bath for about 15 - 30 mins, initially, depending upon the hardness of the mineral constituents of the clay, with a further 30 mins treatment (this treatment discards around 20μm of the outer layer of a grain thus removing the major alpha contribution and a part of the soft beta contribution. An estimation for the latter is given in section 9.7. When the ultrasonic bath was not used, HF was used instead for three hours,

v) wash with diluted HCl (3 aliquots), for removal of fluorides.

vi) rinsing with water and acetone and drying in the oven (approximately 50°C).

The grains involved were identified simply by staining part of them with cobaltinitrate solution (Gabriel and Cox, 1929), yielding a distinctive yellow colour for the potash feldspar grains. Carbon grains were removed simply by gently blowing on them. The organic material was most distinctive in Dimini, possibly because of the presence of radiolaria (see Chapter 10, Fig. 10.4) The provenance of the samples are detailed in Appendix A

9.3 Glow Curves from Pottery

9.3.1 Glow Curve Shapes. The glow curves of the materials studied varied widely in shape. Single peaks or multi-peaks were found in the temperature region between 275 - 450°C, as well as in the low temperature region, that is 110 - 250°C. This may be because the TL is coming from a wide distribution of trap depths within a single material. Quite different TL glow curve shapes and mineral behaviour concerning crystal sensitivity was noticed from samples from Crete and Thessaly due to the different geological origin of the clays in the respective areas. Representative glow curves for Minoan kilns are shown in Fig. 9.3.1. For Neolithic Dimini, in Fig. 9.3.2 for Neolithic Sesklo. Fig. 9.3.3 for Glozel in Fig .9. 3.4 and for Neolithic Sitagroi, Fig. 9.3.5 . The higher the temperature of the region of the glow curves being considered, the greater will be the thermal stability of the associated electrons at ambient temperature. The very broad glow peaks or multi-peaks or bands offer an advantage as it is easy to find the region of thermo-stability by the plateau test, section 9.10 . If the TL has appeared in a sharp peak, resulting from traps of a single energy depth,

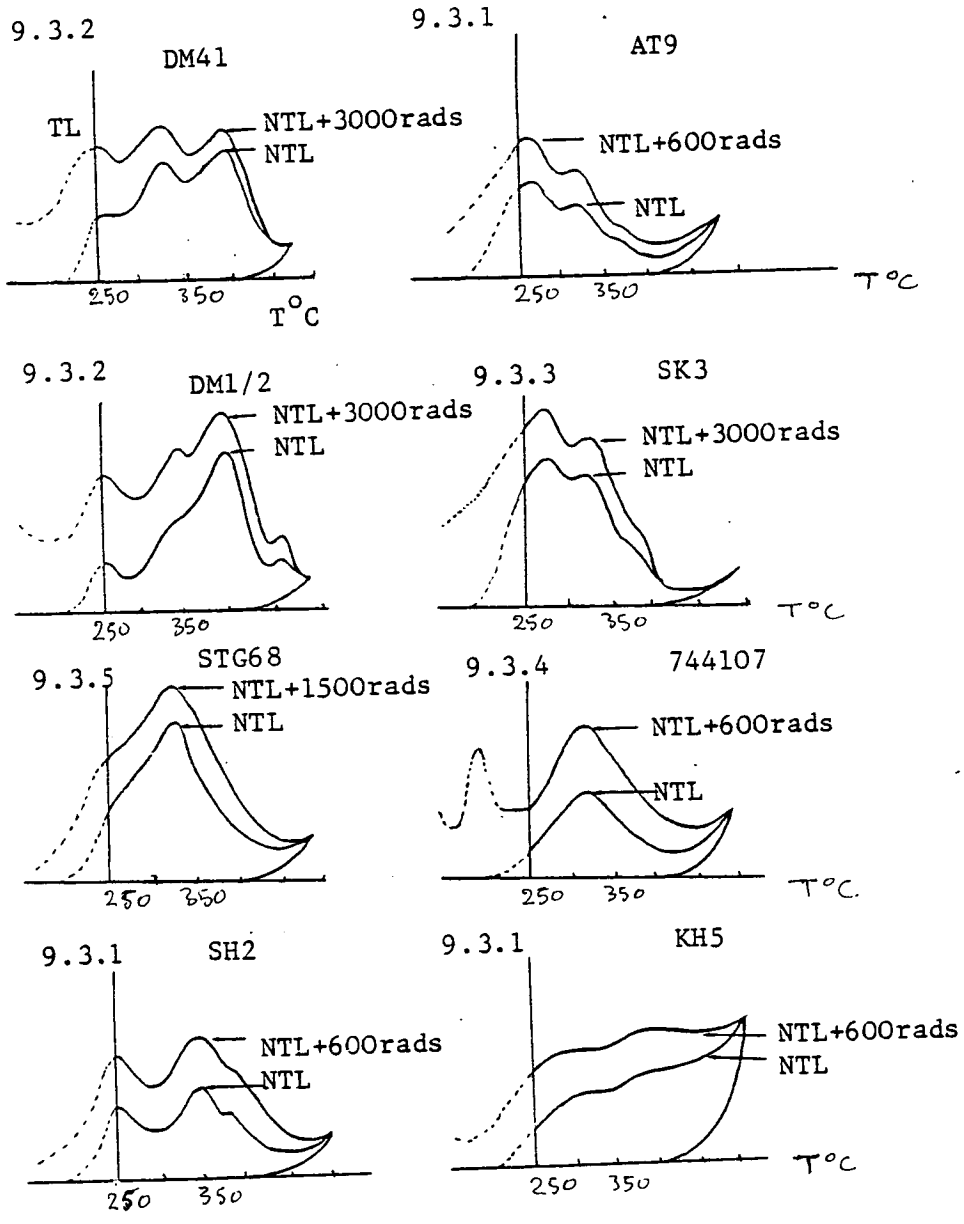


Fig. 9.3.1, -2, -3, -4, -5. Representative Glow Curves for some TL Dated Samples.

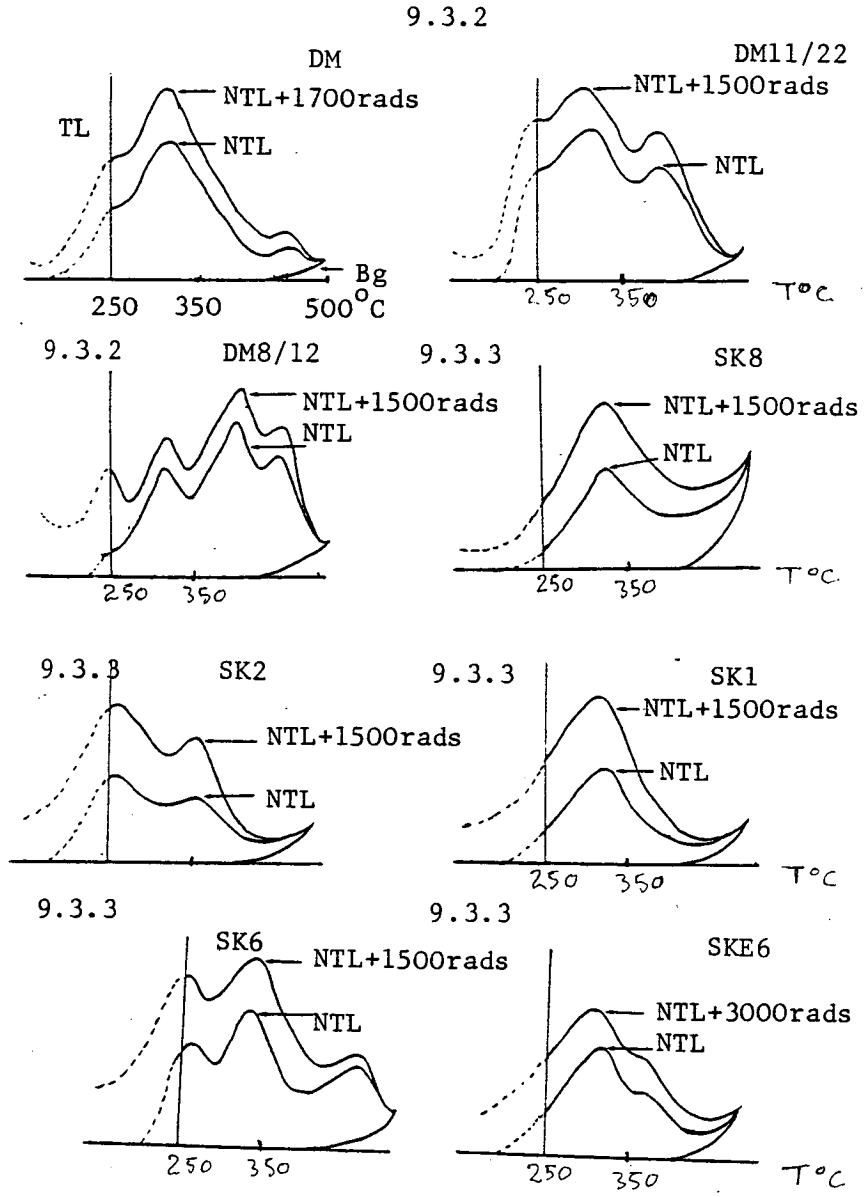


Fig. 9.3.1, -2, -3, -4, -5 (cont.)

with first order kinetics, it would be impossible to tell if the peak had decayed during archaeologic time, by simply looking at its shape, as this would be unchanged. However, a second monitor dose would reveal such a decay since the peak position would shift towards lower temperatures. The above-described glow curve shapes are those produced by beta radiation. The irradiation was carried out with the Sr^{-90} source, mounted 1.5 cm from the sample surface on the heating strip of the glow oven to improve irradiation uniformity. This geometry yields a radiation dose of 303 rads/min, (calibration of the source is described in Appendix B).

9.3.2 Classification of Glow Curves. The minerals responsible for the TL were quartz and feldspar. They were identified by the staining technique (see section 9.3 above), and by thin section analysis, Fig.10.6.1. Several of the commonly occurring shapes are shown in Fig.9.3.1-5. The different mineral types are characterised by glow curve shapes, number and temperature position of peaks and sensitivity. However, materials from the same context present the same pattern of peaks though for different periods, differences are striking especially concerning sensitivity effects. In the low temperature region, the 110 and 120°C peaks are characteristic, while others at 60°, 80°, 165°, 200° and 250°C, were observed. Apparently, the 120°C peak in some samples was split into two, 60°C and 80°C peaks, after normalisation with a beta dose. Therefore, heating to 500°C re-arranges this trap depth. This occurred only in feldspars. Further investigations could use this peak as a "thermometer" to find the firing temperatures in ancient times. In the high temperature region, the peaks observed occurred at 275°, 325°, 335°, 350°, 365°, 370°., 400° ; 425° and 450°C temperatures.

9.4 Thermoluminescence Measurements

9.4.1 Measurement of First Radiation Sensitivity

The archaeological dose was determined by the additive procedure, Aitken and Fleming, (1972), Zimmerman, (1970), Mejdahl, (1977 and 1978), though a new normalisation procedure based on the 110°C peak was used when appropriate, Chapter 1, section 1.12. The natural TL was measured on 3 - 5 samples, with subsequent normalisation with a monitor beta dose (the normalisation by weight or by 110°C peak was also used with some advantages, see Table 9.15.1). The natural build-up curve was obtained by adding beta doses to the archaeological dose. The dose range to normalise the first glow curve or to induce artificially TL were dependent upon the sample's sensitivity. Different sized beta doses were used to check that the TL growth is linear and that no saturation effect occurs. The re-irradiation of the sample for normalisation purposes has been quite often found to give changes in the sensitivity of the sample by as much as a factor of three. Provided that this change alone is involved with no other complication such as pre-dose effects of peak irreproducibility, no errors are involved since this change is proportionally the same for all the samples, (see section 9.5). Peaks which were not stable after the first heating were not used in the final TL measurements. Shifting of the peak position was caused either by simple heating (attributable to second order kinetics) or because of fading of its lower temperature part. Sometimes, but rarely, a natural well-defined peak after the first heating shifted to a low temperature, that is, from 325 → 275°C, or from 400 → 365°C, though when it was used as a normaliser, it gave satisfactory results, when compared with a well-behaved peak of higher temperature. For each point in the

natural build-up curve, the background was subtracted. Sensitivity, as given by the slope of the first response curve in light units/rads of peaks are listed below for the samples with many peaks, Table.9.5. See also below Fig. 9.5 and Fig. 9.6

Some of the samples had reached saturation and so were further excluded from dating, some others reached saturation at NTL + 300 rads. In general, the samples were extrapolated at NTL + 2500 rads, which makes their total received dose equal to around 5000 rads and saturation was not reached.

9.4.2 Measurement of Second Radiation Sensitivity. The characteristic non-linearity of the TL glow curves at low doses below the natural dose was found for most of the samples, Fleming, (1969) and Mejdahl, (1979). Especially all three forms of the second build-up curves, namely supralinearity, superlinearity and straight line through the origin, were observed. To correct for this, a construction of a second build-up curve was required to simulate TL acquisition of the sample in its early times after thelast heating in thekiln. For this, the technique of monitoring was reversed, that is, the natural TL of each sample was taken and used as a control of mass and transparency for a second irradiation then applied to the sample in the position of the heating plate The dose levels employed for this second irradiation varied between 150 rads and 2400 rads. The intercept,I, obtained by this was added algebraically to the first intercept, Q, this correction has been accepted with satisfactory results,(see also Chapter 1 section 1. 12). Reproducability of this, as well as the first monitoring technique, was estimated as better than 3%. Further, the error involved in the two intercepts was calculated as the standard error of the respective straight lines, (using a least squares programme), and was kept to around 5%. Samples with a big scatter, for example,

higher than 20% were discarded, while for those falling between 5 - 20% increased numbers of points were taken in order to reduce the statistical errors. A further investigation of this error is carried out in Appendix C. The final calculated total dose error was that which derived from the dose plateau illustrations, when average total doses from two to three peaks was taken only when these doses were within two standard deviations, see Fig. 9.4.2. Representative first and second build-up curves are presented in Fig. 9.4.3 It must be emphasised that because of the normalisation change in sensitivity or of the different normalisation factor used, the slopes of thenatural and the second build-up curves are not necessarily comparable.

9.5 Aspects of Pre-Dose and Sensitivity Effects

The normalisation procedure will be valid only if the pre-dose effect for the peaks used can be regarded as negligible. A test for pre-dose effect was made for quartz and feldspar grains (75 - 106μ) for all the samples in the following way:

i) initially, the sample with its natural TL is annealed at 500°C and given a beta dose of 1000 rads in the reader, and the resulting TL signal was measured,

ii) then other samples were given beta doses (pre-dose) of 500, 1000 and 2000 rads, respectively, (additional to their natural TL), and all samples were heated to 500°C (normal read-out cycle),

iii) then, for comparison with the first set of measurements, all samples were again irradiated with 1000 rads of beta radiation and measured.

The ratios of the results obtained in the third measurement to those obtained in the first measurement is close to 1. This indicates that there is no pre-dose effect. Though some samples show a pre-dose

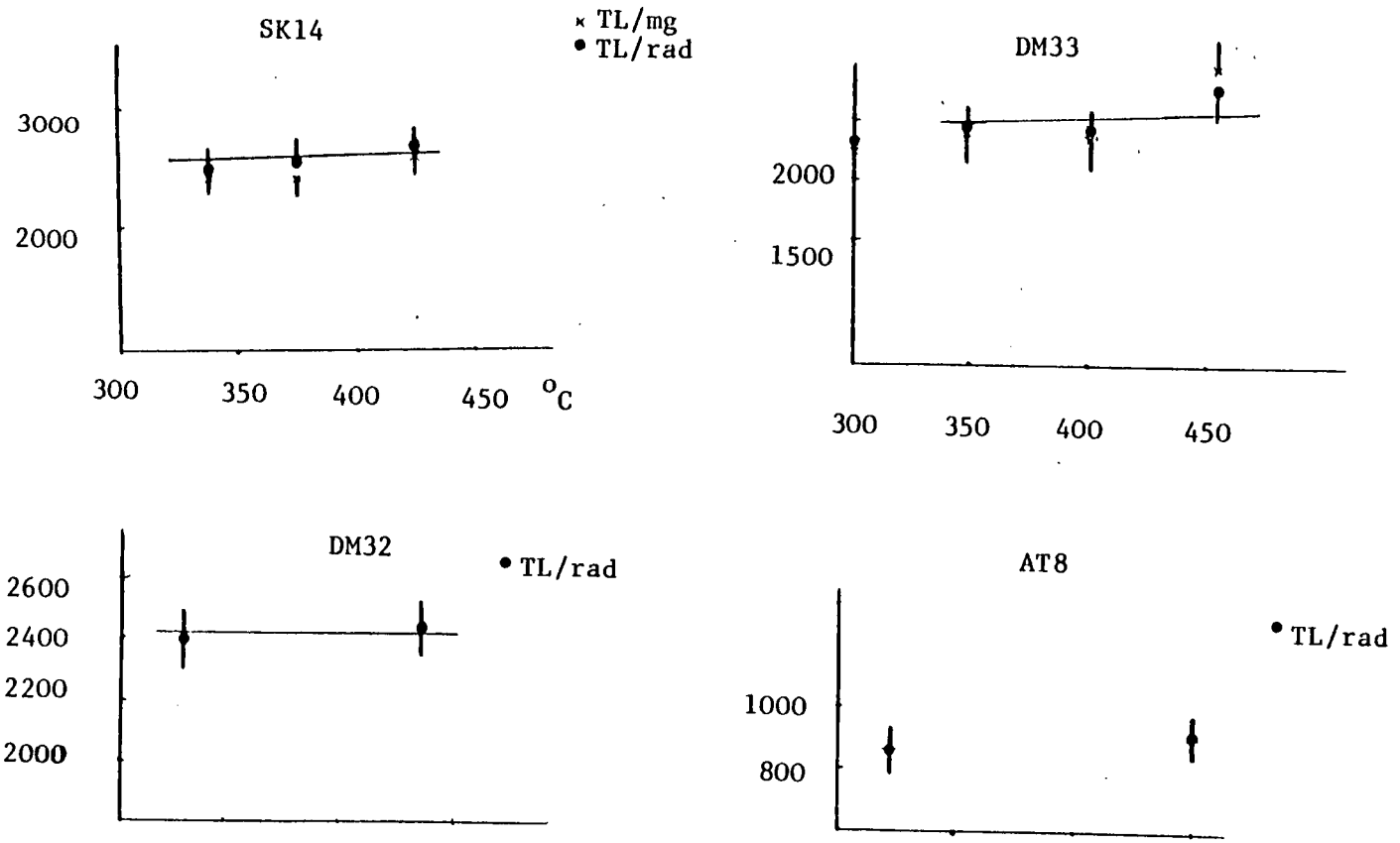


Fig. 9.4.2 Total Dose Error derived from the Dose Plateau. The average Total Doses from two or three peaks was taken only when these doses were within 2 standard deviations.

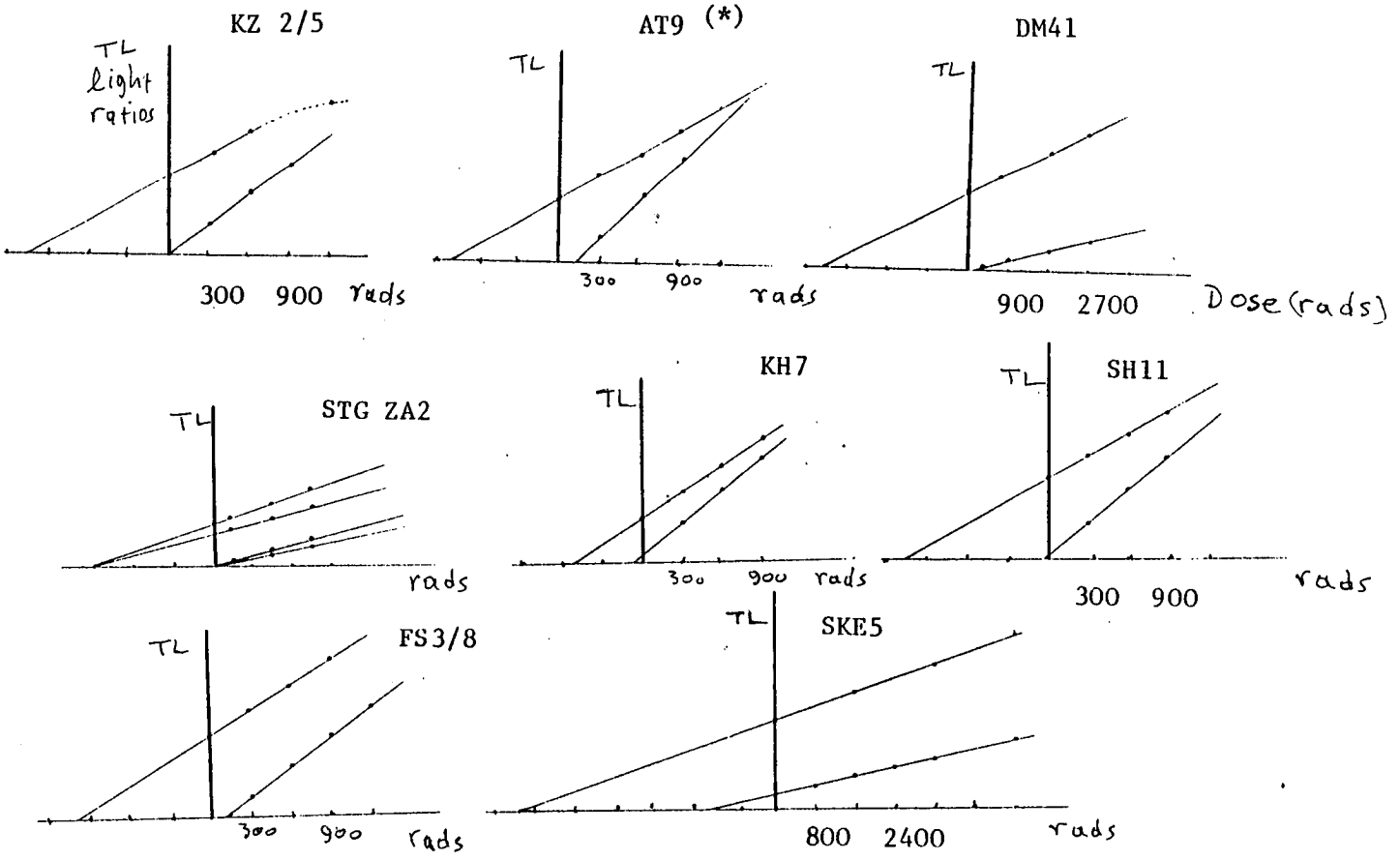


Fig. 9.4.3 Representative First and Second Build-up curves of some of the TL dated samples.(*) It was noticed that almost all the Cretan Kiln Samples gave "malign" form in their build-up curves. Probably the number of heatings which a kiln had in the past caused the high sensitivity of the quartz grains in the subsequent TL readings (irradiation, read-out)

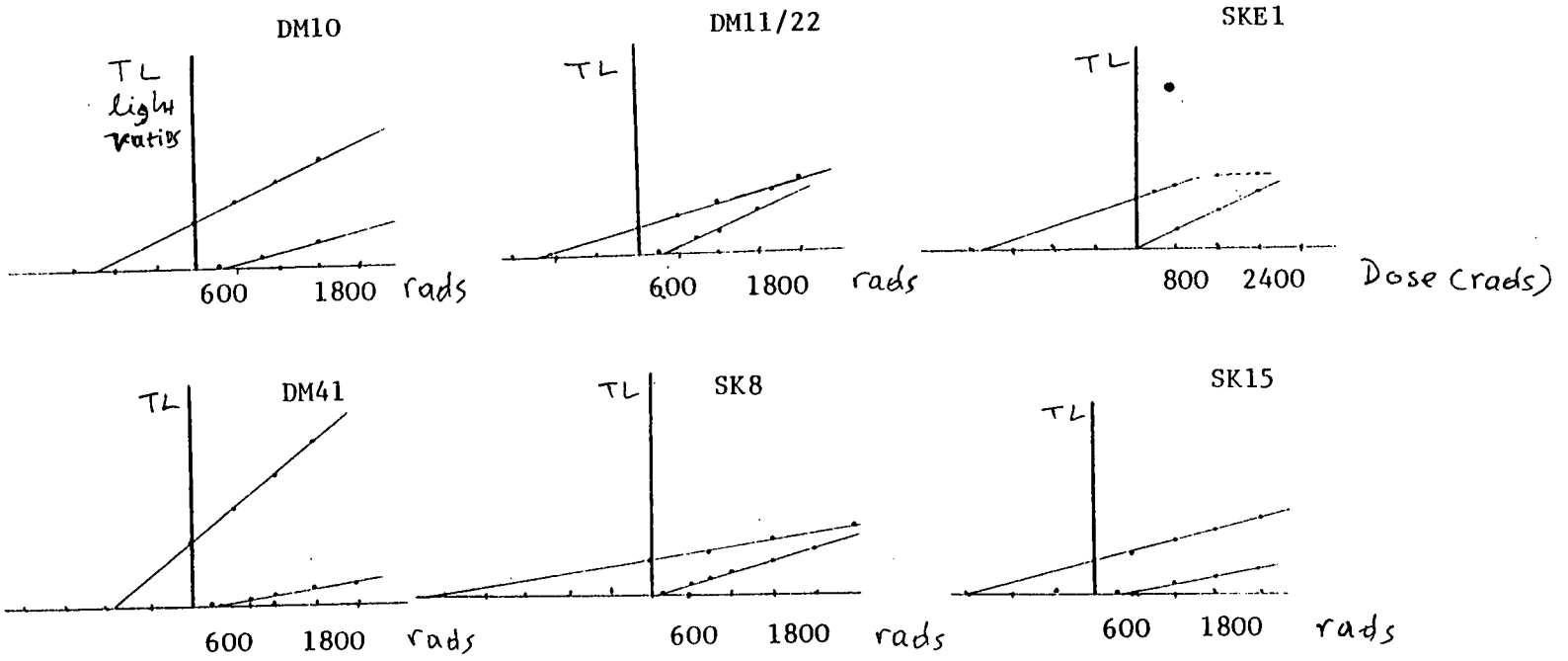

DM10
TL
light
ratio
600
1800
rads
DM11/22
TL
600
1800
rads
SKE1
TL
800
2400
Dose (rads)
DM41
TL
600
1800
rads
SK8
TL
600
1800
rads
SK15
TL
600
1800
rads

Fig. 9.4.3 (cont.)

and were not included in the dating programme.

Also, for the samples that did not receive pre-doses, the ratio was sometimes less than 1, which implies that heating to 500°C has caused a change of sensitivity (see also Chapter 1 Section 1.11). An illustration of such an effect is shown in Table 9.5 from the ratios of NTL to normalisation dose of 3min of beta source, that is, 909 rads, with regard to the total archaeological dose, as determined with the additive procedure. Fig 9.5

Also, in Fig 9.6 the ratios of the slopes of the two curves - 1st and 2nd build-up curves - are plotted against the respective temperature. In general, in spite of some exceptional high points (decrease of sensitivity), the 325°C peak is more sensitive than the higher peaks, and inclines towards diverted build-up curves, (see also Chapter 1, Section 1.11).

The higher temperatures give an average slope ratio different than 1, within the scattered error of the points, which implies that the "parallel slope" criterion is not necessarily satisfied due to the normalisation procedure.

Though at 325°C, 400°C and 450°C, temperature regions show the smallest fluctuations around 1, it is not possible - at present - to draw conclusions due to the small number of points and the unknown TL trapping mechanisms for different crystals.

9.6 Water Uptake Values

The water uptake is very difficult problem to be assessed, and this produces a high error in the beta and gamma dose rates. However, the following points have to be taken into acount in any attempt to evaluate such a correction:

i) the water acts as an absorber of beta and gamma radiation, because

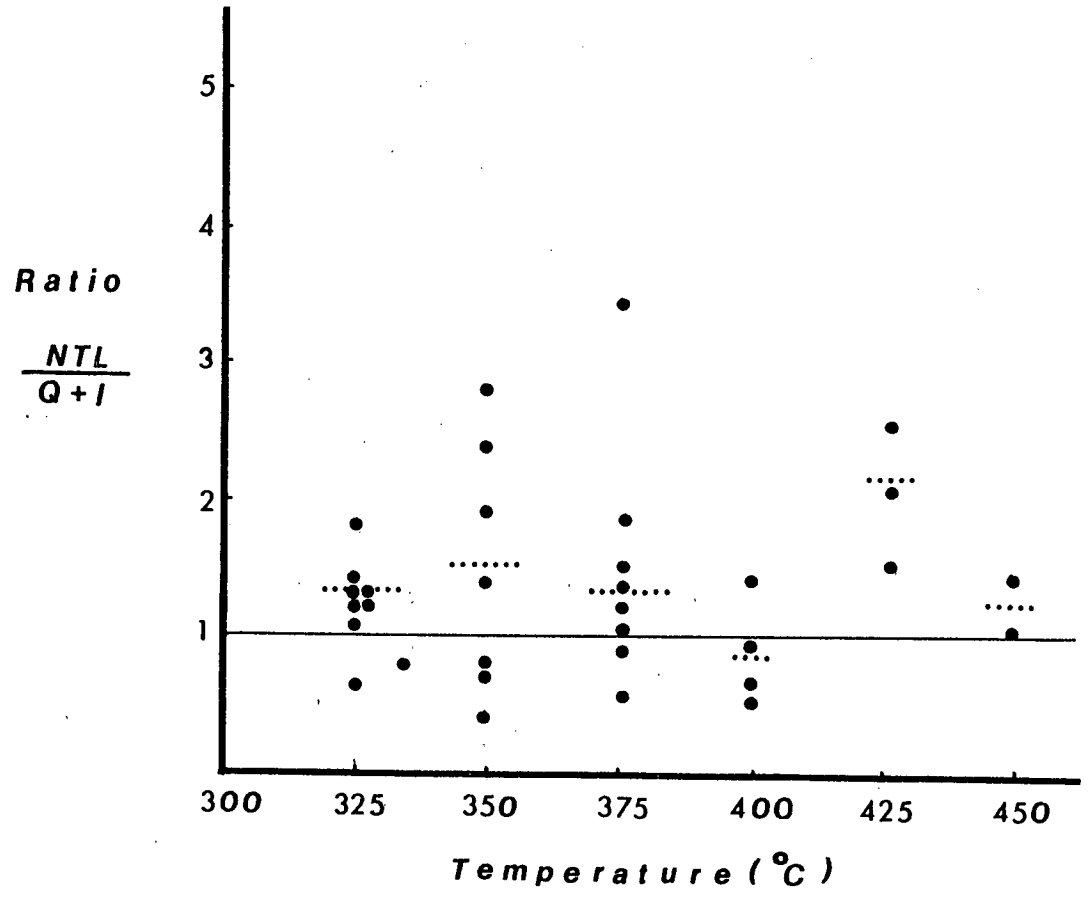


Fig. 9.5 Illustration of Sensitivity Change by simply heating to 500°C as inferred from the ratios of the Natural TL to Normalisation of 3 mins of Beta source, i.e., 909 rads, to that of the total archaeological dose (Q+I), normalised with 3 mins of Beta source.

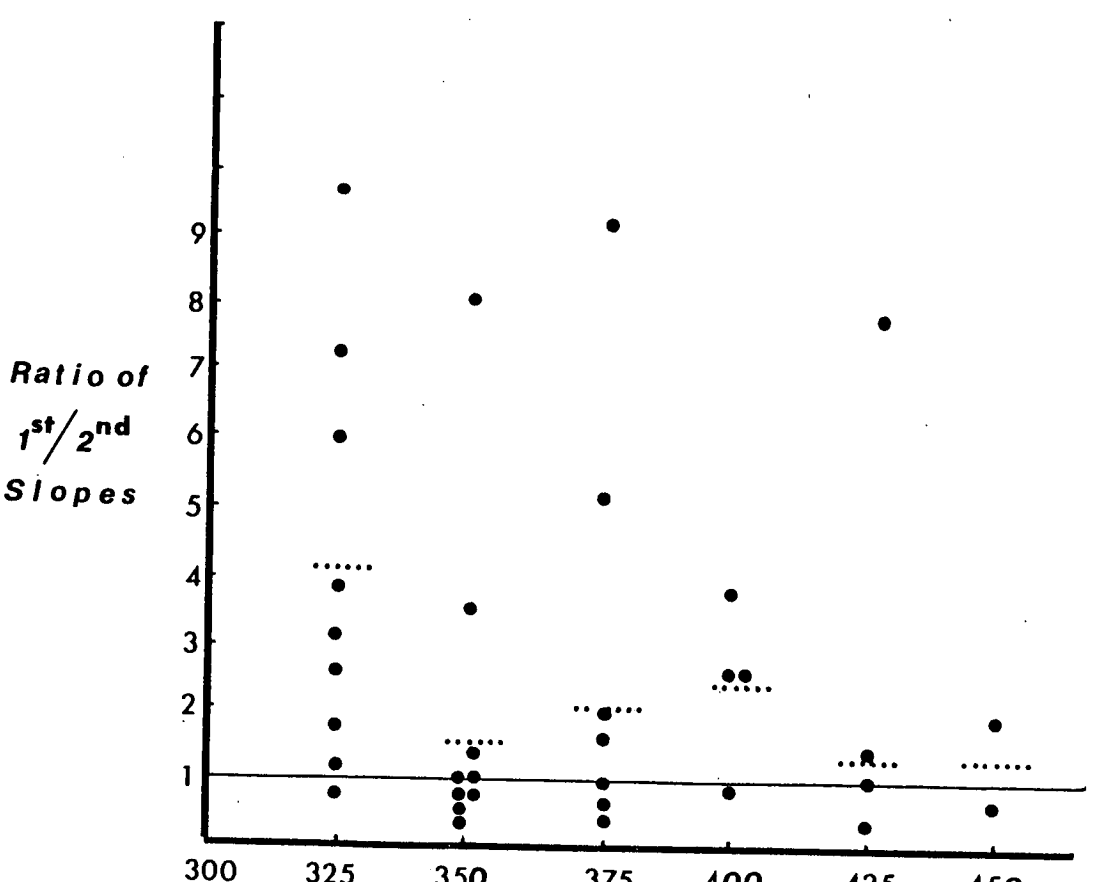


Fig. 9.6. Testing the "Parallel Slope" criterion of many peaks by plotting the Ratios of 1st to 2nd Build-up curves against their respective temperature.

TABLE 9.5

Sample No	T°C	Ratios of norm NTL	Total dose Q+I rads	Slope of 1st build-up curves	Ratios of* norm(Q+I)	Ratios of** 1st/2nd build-up curves
SKB(I)2	325	3.80	2340	0.47	(0.67)2.57	4.70
"	400	2.65	2340	0.33	(0.97)2.57	3.00
SKE1	350	1.42	2969	0.13	(2.30)3.27	0.76
SKB(I)98	350	1.21	3161	0.10	(2.80)3.47	0.40
"	425	1.96	3161	0.15	(2.80)3.47	1.25
SKB(I)'72	375	1.62	2891	0.19	(1.96)3.18	0.70
"	350	1.36	2891	0.13	(2.33)3.18	0.56
SKB(I)27	350	2.08	2674	0.35	(1.40)2.94	2.69
SKE6	375	1.01	2000	0.09	(3.30)3.30	0.41
SKE4	325	3.20	3636	0.23	(1.25)4.00	7.60
SKE3	350	2.14	2557	0.30	(1.30)2.80	1.15
"	325	2.90	2557	0.33	(0.96)2.80	3.00
SK14	325	2.74	2660	0.28	(1.06)2.92	4.00
"	375	2.74	2600	0.42	(1.06)2.92	1.18
DM11/22	400	1.31	1781	0.28	(1.50)1.97	0.64
"	325	1.60	1781	0.39	(1.50)1.97	0.90
DM10	450	1.29	1758	0.28	(1.49)1.93	0.62
"	325	2.09	1758	0.48	(0.92)1.93	2.00
DM32	325	2.04	2392	0.22	(1.29)2.63	2.40
"	425	1.00	2433	0.10	(2.67)2.67	0.40
DM6/6	375 (mg)	-	1769	1.18	1.95	0.14
"	375	3.48	1666	0.65	(0.52)1.83	7.30
DM33	350	1.15	1969	0.20	(2.20)1.90	0.77
DM39	375	1.81	2088	0.28	(1.27)2.30	1.47
"	425	1.48	2196	0.20	(1.62)2.40	0.91
"	325	1.82	2115	0.27	(1.26)2.30	1.35
DM8/12	450	1.93	1912	0.32	(1.09)2.10	1.60
DM1/2	400	3.28	2121	0.61	(0.70)2.33	2.18
"	335	2.49	1888	0.56	(0.83)2.07	1.51
DM41	400	2.49	1466	0.78	(0.54)1.60	3.00
DM14	325	1.50	2482	0.18	(1.80)2.70	0.86
"	425	1.40	2625	0.14	(2.06)2.88	0.93
"	425 (mg)	-	2341	1.07	2.57	0.05
"	375 (mg)	-	2514	1.58	2.76	0.07
"	325 (mg)	-	2573	1.11	2.83	0.12
STG ZA43	325	4.05	2877	0.40	(1.27)3.15	4.44
"	375	3.10	2550	0.36	(1.12)2.75	4.00
"	400	2.30	2450	0.25	(0.87)2.64	1.66
STG ZA68	325	2.98	3342		(0.80)3.70	1.80
STG ZA2	325	1.98	2061	0.34	(0.96)2.06	1.62
"	375	1.52		0.27	(0.73)2.06	1.17
FS3/8	325	1.25	1199	0.88	(1.05)1.32	
AT7	325	0.81	1042	0.24	(1.40)1.14	
"	375	0.96	1042	0.23		
KH7	375	0.64	530	0.33	(0.90)0.58	0.51
"	350	0.66	530	0.38	(0.90)0.58	0.59
SH5	350	1.41	885	0.70	(0.69)0.97	1.09
KZ1/7	325	0.83	970	0.28	(1.29)1.07	0.59
KZ3/2	350	3.50	1200	0.66	(0.37)1.32	6.30
DL1/1	325	3.06	1625	0.57	(0.58)1.78	0.62

* Numbers in parenthesis are the ratios of norm (Q+I)/norm(NTL), which indicate changein sensitivity by simply heating to 500°C.

** When the ratio of slopes between the 1st and 2nd build-up curves is equalto one the curves are parallel, for greater than one, (benign form), the sensitivity decreases and the curves are diverted, for less than one (malign form) the sinsitivity increases and the curves interesect

mg: TL/mg

it increases the absorption coefficient of the clays (see also Chapter 6). The stopping power of water to betas is 1.25 times higher than for clay and the stopping power for gammas is 1.14 times higher than clays.

ii) the radon and thoron gaseous radioproducts emanate in dry soil with a high diffusion coefficient, while they are trapped in wet soil. From first glance, that means that in a wet soil, the gamma/beta radiation is attenuated, but at the same time, is increased because of the radon contribution.

The net effect will depend upon :

a) the soil/pottery porosity and diffusion coefficients (see also Chapter 3, Section 3.5), and

b) the geomorphology of the drained site. For example, some sites are well drained, therefore washing down the radon and thoron and thus having increased radioactivity in the deeper layers of the soil(as in a soily hill).

Some other sites are not well drained and water is trapped there for a considerable length of time.

iii) climate - When we consider the past archaeological periods, the best way to resolve the water uptake problem is to know the past climatological conditions, in the area concerned, in particular the temperatures & rainfall as compared to the present weather. This can be derived from oxygen analysis or palynological (pollen) studies. A paleotemperatures diagram for the past 10000 years for Europe has been made by Dansgaard et al (1971), Fig. 9.7 Additional pollen analysis for Greece shows the kind of trees grown for thelast 10,000 years, which is a direct indication of

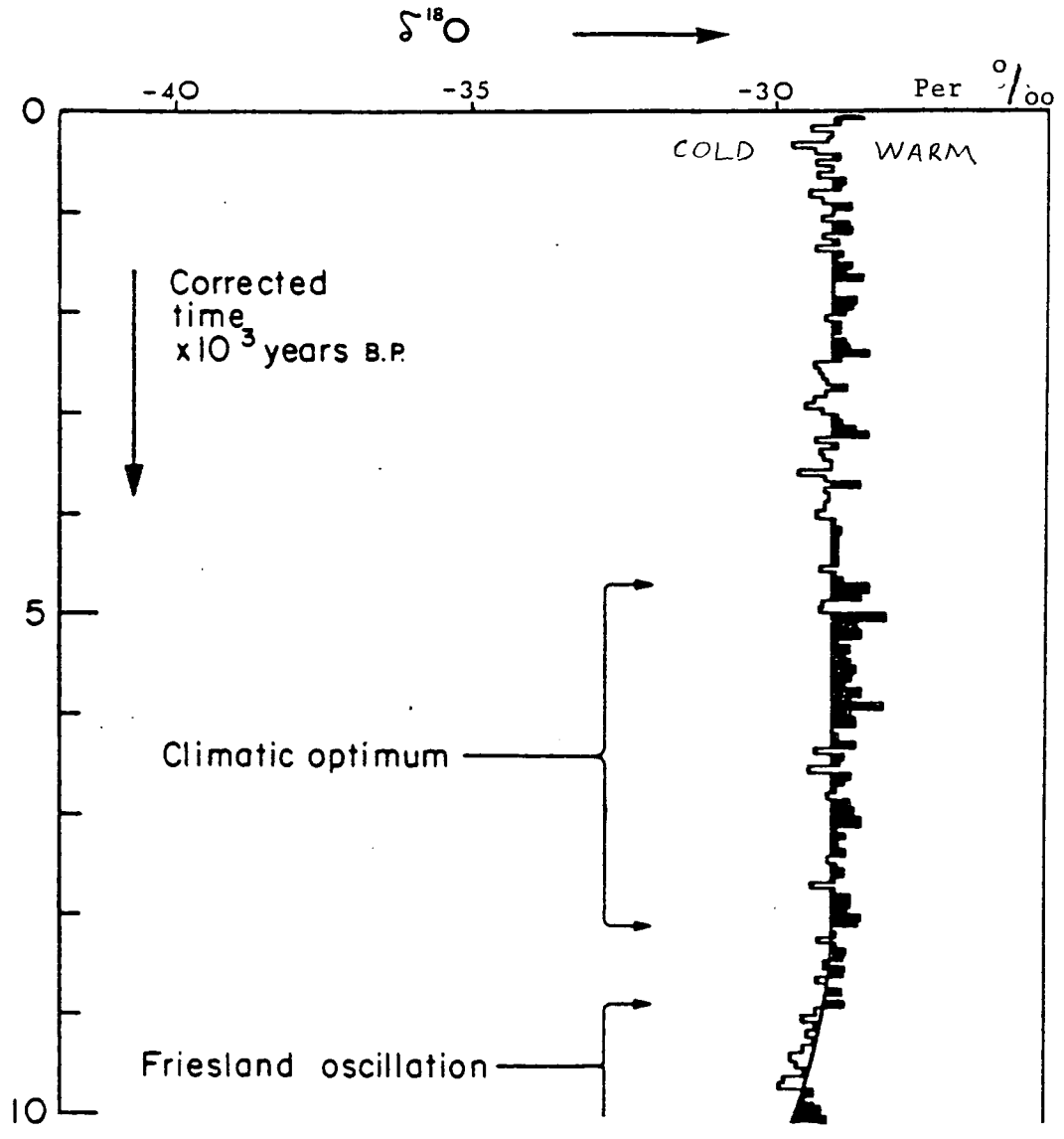


Fig. 9.7. Temperature changes as inferred from $\delta^{18}O$ variations plotted on a corrected time sacle, for the last 10,000 years. All δ's exceeding a smooth curve are set off in black (from Greenland ice core , Camp Century 77°N 56°W, dated by the flow model method; after Dansgaard et al, 1971).

the climate, Wijmstra, (1969), and Van der Hammen et al, (1971), (Dates were obtained with the C-14 method)

As a conclusion, the average weather over thepast 10,000 years could well be identified with present climatological conditions in Greece.

Taking into account the above three points, the following water uptake values for the samples studied were:

i) for Cretan kilns of well-fired clay,some of which were well fused, 25% of the saturation value was taken as a correction factor (1/4± 1/4)

ii) for Neolithic Dimini, 50% of the saturation value (½±1/4) and for Sesklo - where all the samples were found in an excavated section of 5m depth - a full saturation value is taken for beta dose rates and (3/4±½) of the saturation vlaue for gamma dose rates was assumed. For the respective kilns, a value of (1/4±1/4) was taken.

iii) for Neolithic Sitagroi, (1/4±1/4) was assumed.

In general, the water uptake for clays was, on average, 1.7 for Dimini, 1.66 for Sesklo and 1.5 for Sitagroi. These values were used where appropriately for the respective sherds.

Finally, a distribution of percentage water absorption values against number of samples for potsherds and fired clays from different archaeological periods in Greece is shown in Fig. 9.6.1

It is obviously seen that the major number of samples studied had such porosity that could accommodate a maximum water value of 10-14% by weight in dry condition.

9.7 Beta Dose Values

The beta dose measurements were obtained by the TLD and α+K techniques

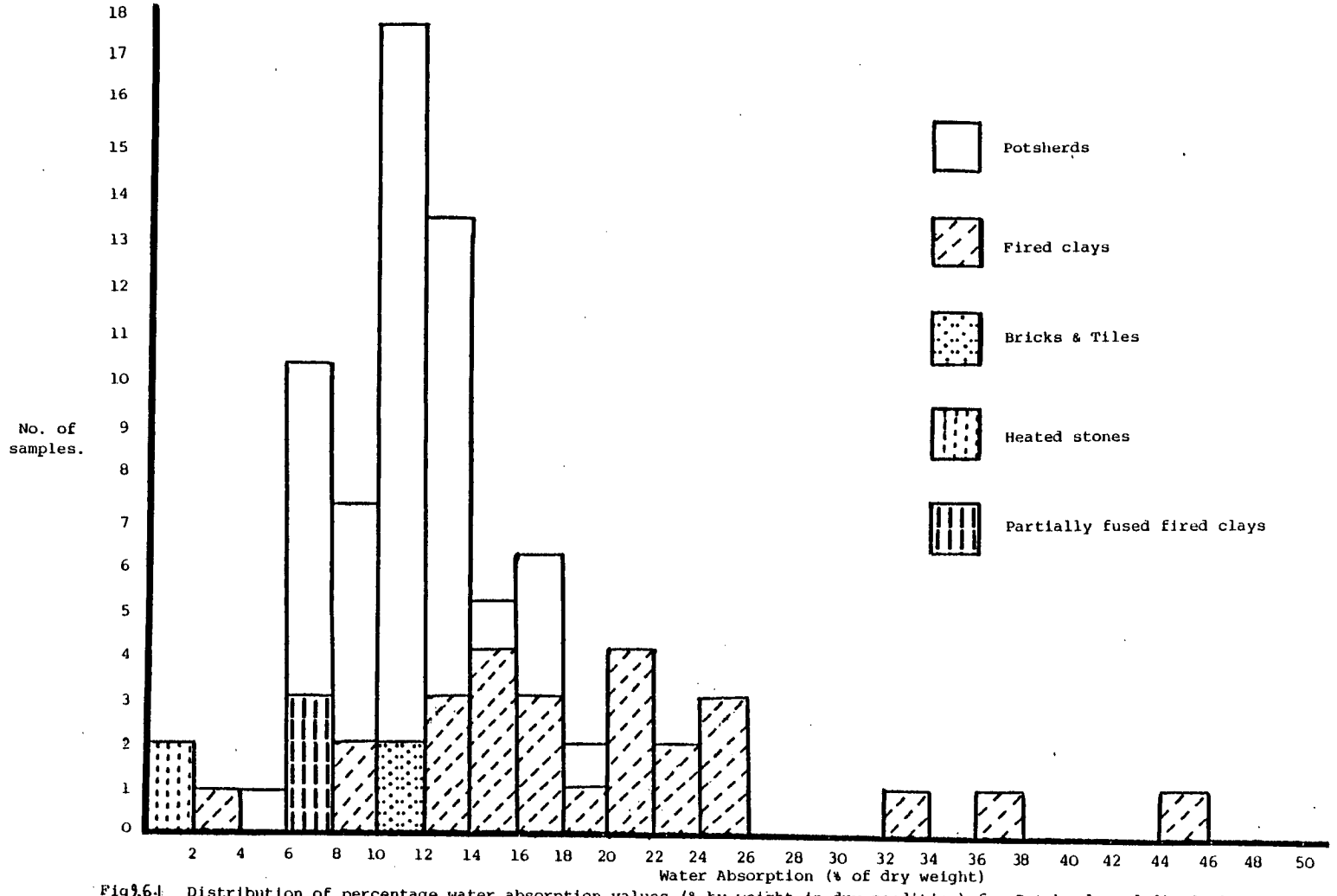


Fig 9.6.1 Distribution of percentage water absorption values (% by weight in dry condition) for Potsherds and fired clays from Neolithic, Minoan and Roman sites in Greece.

as described in Chapter 5. Due to the observed discrepancies and the advantages of the α+K over the TLD in the foregoing procedures, an average of the two values was taken when the techniques agreed within one standard deviation, as the best value and the α+K technique was preferred for deviations higher than 1σ, for reasons explained in section.5.6 The associated errors were accounted for in the final beta dose rate value. The beta attenuation* through the grain sizes used, that is, those of average diameter 90μ, 140μ and 160μ, respectively, was calculated based on a theoretical calculation by Mejdahl, (1978). Because the etching in the sample preparation removes a part of the soft beta radiation, stopped in the outer part of the grains, an estimation of this lost TL part was based on the idea that the beta particles most likely to be stopped are those of internal conversion and auger electrons of less than 0.06MeV, which contribute to the TL dose of the grains. (From Table 2.1 the $\beta<50$KeV are stopped in the first 20μ of the quartz grains.) Table 9.7 shows the relative dose contributions of beta particles and conversion electrons derived from the total values of beta av and IC given by Bell, (1976, 1977) and Mejdahl, (1978).

TABLE 9.7

Series	Beta Particles	Conversion Electrons
Th-232	0.868	0.132 (15%)
U -238	0.933	0.067 (7%)

* Since the beta radiation will be attenuated when traversing a large grain, its intensity at the centre of a grain will be less than the average intensity in a sherd. One might expect, therefore, that the value obtained for the accumulated exposure would depend on the size of the grains used for the determination. However, results of a preliminary investigation of this effect, Fig9.7 indicated that the variation of accumulated exposure with grainsize was not significant. Similar results were found by Mejdahl, (1972)

Also the relative beta dose rates corresponding to 12ppm Th, 3ppm U with 1%, 2% and 3% K-40 are as in table 9.7.1.

TABLE 9.7.1

	Th	U	K
1%	0.217	0.272	0.511
2%	0.143	0.181	0.676
3%	0.107	0.135	07 58

Table 9.7.2 also gives the absorbed bate dose fractions $\phi(D)$ (taken from Mejdahl, 1978)

TABLE 9.7.2

Diameter (mm)	K-40 β	Th-232 β	Th-232 IC	U-238 β	U-238 IC
90	0.0297	0.077	0.512	0.064	0.453
100	0.0463	0.104	0.608	0.089	0.513
160	0.0529	0.114	0.637	0.098	0.534

From these tables, an estimation of the beta attenuation factors were derived which include the etching effect. It has to be noticed, otherwise, that the stopping powers or absorption characteristics of beta particles is a function of their beta energies and relative abundances. Therefore, for the respective potassium concentrations, (major beta contributor) and the corresponding average grain diameters, the following correction factors were found:

	d=90μm	d=140μm	d=160μm
K=1%	0.925	0.900	0.891
K=2%	0.940	0.918	0.909
K=3%	0.952	0.931	0.924

A further correction to the beta dose rates was for the water uptake The formula given by Zimmerman (section 7.5.1), was applied to all the materials.

In general, the corrected final beta dose rate values varied as follows:

i) for Cretan kilns, between 126 - 222 mrads /yr, with an average of 172.3 mrads/yr .

ii) for Neolithic Dimini, the dose rates were higher and varied from 145 - 297 mrads/yr with an average of 218.8mrads/yr. In Sesklo the variation was between 190 - 382 mrads/yr, with an average of 370 mrads/yr.

iii) for Glozel samples, the radioactivity in general was the highest of all the sites and the beta dose rates varied from 313 - 430 mrads/yr, with an average of 351 mrads/yr.

9.8 Evaluation of Gamma Dose Rates

The gamma dose measurements were obtained by the portable NaI(Tl) scintillometer which was calibrated on quartz grains as described in Chapter 7.

Because (in most samples) the internal dose of the sherd itself is higher than the external gamma a self-originating gamma dose which had to be taken into account, otherwise, it is considered to cancel out with the attenuation of gammas through the pottery and the fact that the potsherd occupies a space in the soil environment where there is a lack of gamma soil.

A water correction was included (see section 9.6), since the readings were taken in summer time (on dry season), and following the results of the investigation of season gamma soil fluctuations in Chapter 8 In particular, instances comparisons were made between TLD phosphors

($CaSO_4$:Dy teflon discs) and the NaI(Tl) scintillometer readings

Therefore, for the Sesklo kiln area, the phosphor gave a value of 300 mrads/yr, which corresponds to approximately 237 mrads/yr on quartz. (see fig 7.6.2), which value agrees within the statistical error with that evaluated by the NaI(Tl) of 2.29 mr/yr

Phosphors in polythene tubes gave a gamma value differing by 4.6% from that inside a brass tube.

Similarly for Dimini (excavated section K), the phosphor gave a value of 170 mrads/yr. The position of the phosphor was at the base of a stoney wall and, therefore, as expected, gave a high value. This high value as compared with the value in the kiln area of Dimini, of 136 mrads/yr, is reasonably good.

In conclusion, the above tests reassure that the way of measuring gamma doses with the portable NaI scintillometer is reliable.

The gamma dose rates subsequently were compared with values deduced from the α+K method on clay samples of the respective sites. These results as compared with the relative ranges of gamma values for the respective sites are as follows:

i) the ranges of gammas of Cretan kilns were from 103 - 156 mrads/yr, with an average of 130 mrads/yr. This value agrees within 1σ to 2σ with the γ-dose rates estimated by (α+K) on the same kiln.

ii) the Dimini gamma ranges were from 90 to 136 mrads/yr with an average of 108 mrads/yr. In Sesklo, the gamma dose rates varied from 130 - 230 mrads/yr with an average of 151 mrads/yr. Table 9.8 shows a comparison between these values and those derived from (α+K)$_\sigma$

iii) for Glozel, the gamma dose (by $CaSO_4$:Dy) gave an average of 274 mrads/yr ($\pm$2%). This value is in reasonable agreement with that of (α+K) of the Glozel soil corrected for water uptake which was 259 mrads/yr.

TABLE 9.8

Dimini Sample No	γ-dose Rate by NaI mr/yr	γ-dose Rate by (α+K) mr/yr	
DM10	113	119	
DM32	116	118	
DM6/6	99	105	
DM33	88	109	
DM39	116	136	
DM8/12	109	103	
DM1/2	114	124	
DM kiln	136	97	
Sesklo Sample No			
SK15	140	130	
SK14	140	128	
SKE5	134	123	
SKI	134	121	
SKE3	134	158	
SKE4	134	128	
SKE6	138	175	
SKB(I)28	129	131	
SK6	130	146	
SK3	173	150	
SKB(I)27	128	130	
SKB(I)1972	146	314?	abnormally
SK4	229	183	high U or
SKB(I)98	157	121	low K-40
Cretan Sample No			
KZ1/7	147	110	
KZ3/2	143	160	
KH7	157	109	
AT8	113	103	
FS3/9	103	119	
FS1/5	126	109	
FS3/8	103	119	
SH11	125	128	
Glozel Sample No			
744204	274	259	
744111	"	"	
744107	"	"	
744004	"	"	

All the above comparisons helped to test the extent of confidence in the determination of gamma dose rates. However, since the radioactivity changes from location to location in the same site an exact agreement for the different methods employed was not anticipated. Nevertheless, when possible, the average gamma dose rate derived from (α+K) of many soil samples of the same area gave concordant results with gamma dose rates as measured by the NaI(Tl) scintillometer.

9.9 Fading and Spurious TL Checks

A correct interpretation of TL glow curves is imperilled by one more problem: anomalous fading. Fortunately, there is no such effect in the present samples and the temperature regions used. This was checked as follows. After a period of one year, the natural TL point of the first response curve was repeated. Any fading would show a reduced ratio of NTL/normalisation as compared to the original value. However, no such decrease was observed. It is worth mentioning that in parallel with fading, tests on non-radiation induced TL of chemical or mechanical origin were made. The first was eliminated by keeping the sample with the heating chamber under nitrogen atmosphere, oxygen free and with rubber tubes through which the nitrogen passes free of water vapour impurities. Any residual spurious TL is suppressed by the optical system (Chapter 1, Section 1.9.2), as its emission is predominately at 3700A^{o}. For the second, care was taken not to induce TL by gently crushing down the sherd.

9.10 Plateau Tests

It has been estimated (Fleming, 1969), that the TL glow peaks of around 400^{o}C originate from traps having sufficiently long lifetimes for archaeological dating. Also, experimental studies by Tite and Waine (1962) on two pottery fragments showing well-defined peaks indicate that the high temperature TL has adequate stability. However,

because of the variety of minerals, for example, quartz, feldspar, it would be dangerous to assume that this is true for all pottery fragments and it is thus desirable to check each sample for stability. This is done by two methods:

i) temperature plateau: This is obtained by comparing the glow curve shape of the natural TL with that of the TL from a second undrained portion that has been artificially radiated. Fig 9.10 shows the ratio of thelight output as a function of temperature for some typical pottery samples. This ratio is effectively zero below 250°C, but at high temperatures, the ratio rises and quickly reaches a constant level. The onset of the plateau usually occurs in the range 325 - 450°C. Since the life time varies very sharply with temperature of TL emission (Aitken and Fleming, 1972), the occurrence of the plateau indicates the absence of fading for TL emitted from the plateau. This same plateau test also checks against the possibility of leakage from traps by way of "mechanical tunneling", that is, leakage that is independent of temperature. It is extremely unlikely that such leakage could be to the same degree for all traps concerned and consequently, if such a process had in fact occurred, there would be no plateau. However, this normal fading has to be distinguished from the previously anomalous fading that is not detectable by the plateau test, Wintle et al (1971). In the present samples, this plateau test was repeated after some months to receive again the plateau of Fig9.10

Some samples failed to show a plateau. The reason may be either the presence of a non-radiation induced TL possibly to be attributed to the differing degrees of sensitivity in different parts of the glow curve, or to the fact that the sample was poorly fired.

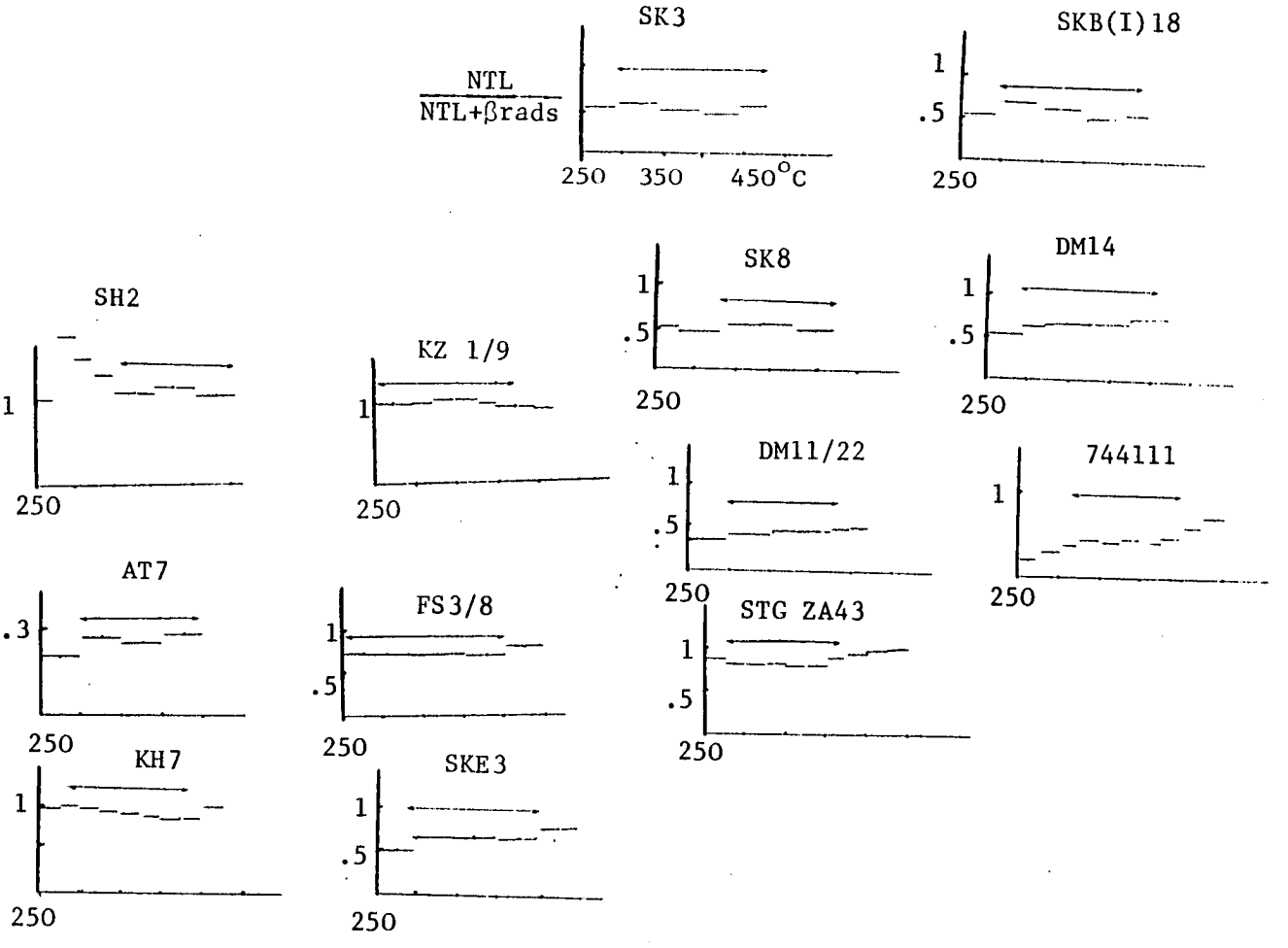


Fig. 9.10 Typical Plateau Tests for some TL Dated Samples.

Also, sometimes, a worse plateau was obtained, when the natural glow curve is compared with the artificial TL of a portion from which natural TL has been drained instead of with the natural plus the artificial TL for a second undrained portion of the sample. This is because the drainage (by heating) causes changes in sensitivity which differ in magnitude and different glow curve temperatures (see Table 9.5 and Fig 9.5-6).. In particular, SH2 showed a peak for NTL+600 rads at 250°C, which shifted to 200 - 225°C with a second heating to 500°C.

ii) age plateau. This was obtained by plotting the temperature peak used to determine the total archaeological dose (Q+I) - which was obtained with different normalising methods, for example, as TL/rad, TL/mgr, TL/110°C peak - against this total dose, Fig.9.4.2. Again this test reassures that there is not any fading to the total dose of the respective peak used for dating, However, scattering of points in the onset of the plateau region were observed due to the reasons mentioned above, though they were lying on the onset of theplateau within their respective error bars. In general, the dose plateau test followed the temperature test and this was a good criterion in choosing themost appropriate total dose value.

9.11 C-14 Dating and Calibration

It is now nearly 20 years since the first radiocarbon dates for the late Neolithic cultures of Europe astonished and perplexed archaeologists by falling a millenium earlier than the existing chronologies had suggested.

While initially C-14 was accepted as a conventional dating method now a second radiocarbon revolution is taking place now. This is due to the face that the changesin the earth's magnetic field causes fluctuations in theproduction of C-14 atoms. It was found by Elsasser, Ney and

Winckler (1956) that the decrease of magnetic moment is followed by an increase in the production rate of carbon-14 atoms. Higher values of the field have an opposite effect. These new radiocarbon measurements carried out on dendrochronologically and historically dated samples, have made it possible to find deviations from the radiocarbon content as calculated with a half life of 5568 and 5730 years (5568 years value as recommended by the 6th International C-14 and H-3 Dating Conference, (196), and 5370 years ±40 years value as found to be physically more correct.), Suess, (1969), Ralph and Michael, (1969), Berger and Libby, (1967).

An interesting comparison can be made when the time variations of radiocarbon deviations is compared with the time variation of the earth's magnetic moment. A close correlation of both phenomena is apparent (Fig. 9.11) in that high value of the earths field in turn causes a low rate of C-14 production. (Abrahamsen 1976). In particular, for the Neolithic period or around 3000 - 6000 years BC, the geomagnetic moment has a minimum value forming a trough and, so, the C-14 ages appear to be much smaller than the present values, Bucha, (1970). This causes an error in the conventional C-14 dates of around 1000 years.

C-14 dates can now be corrected by using a dendrochronological calibration curve.

The availability of these calibration curves has been widely heralded and they have already been used, perhaps somewhat prematurely, to derive important and far reaching archaeological conclusions. It is however essential to point out that the fine form of the curve has not yet been established, and that slight (but important) differences do exist between different workers, Demon et al (1973).

The curve generally used is derived from the work of Suess, (1970)

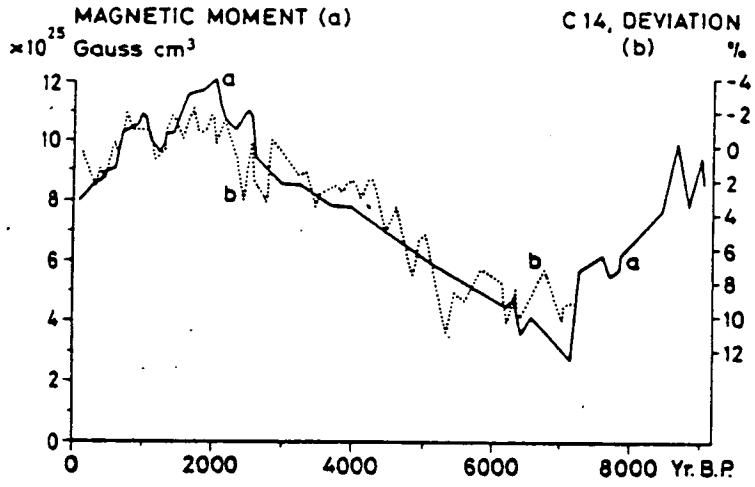


Fig. 9.11. Comparison of C-14 deviations (b). with changes in the geomagnetic moment (a). (Redrawn from Bucha, 1970).

In general, there has not been much critical discussion of the use of such curves for archaeological purposes. The fact that good agreement exists between early Dynastic Egyptian historical dates (first half of the Third Millenium BC) and dendrochronologically corrected dates [illegible], but a more rigorous comparison with historically determined Egyptian dates is made with material from the early Second Millenium BC or around the Twelfth Dyansty.

Here, with the recorded heliacal rising of Sirius in 1872 BC during the seventh year of the reignof Sesotris III, historical dating can be of extreme accuracy, Parker (1960-7)

In the present studies, the conversion of the available C-14 dates for comparison with TL dates was based on tables by McKerrell (1975) which correct conventional C-14 dates to dates in calendar years based on tree ring and historical documents.

for example, Egyptian, Aegean, Sumerian, written evidence; represents at present the best information available. Further, this new system of chronology to calibrate the C-14 dates has been successful in many archaeologically important sites in South East Europe, Neustupny, (1968, 1969), such as Sitagroi in Greece, Vinca, Gumelnitsa in Yugoslavia, and in Egypt and Mesopotamia, Renfrew, (1970).

Further, the availability of absolute dates and comparison with corrected C-14 ones is still an essential need. Thermoluminescence dating offers such a basis of absolute technique and was used to test such C-14 corrections.

Table 9.11 gives the C-14 dates of some well-known Neolithic sites in Greece, and the corrected ones by adding an appropriate correction factor. A comparison with TL dates from the respective sites is also made.

TABLE 9.11

Some C-14 Dates from Hellenic Neolithic & Bronze Age Sites.				Some TL Dates from Hellenic Neolithic & Bronze Age Sites.		
Site	Sample No	C-14 yrs BC	Corrected C-14 yrs BC	Sample No & Type	Museum Ref.	TL Dates yrs BC
PRE-CERAMIC						
Seskło	P-1680	5350±93	6300	SK2(FC) d)	Aceramic, 1962 N.1	6850±660
" "	P-1081	5805±97	6700			
" "	P-1682	5533±72	6500			
EARLY NEOLITHIC						
Seskło	P-1678	5477±78	6400	SK3(P)	Section, layer 0.40 - 0.65 under P, No.16	6394±590
" "	P-1679	5661±83	6600	SKE6(P)	Potsherds from early levels.	6225±590
Argissa	GrN-3502	5550±90	6500	SKE4(P)		5961±570
" "	GrN-2454	(4420±80)?	(5300)?	SKE3(P)		5245±606
Elatia	GrN-3037	5410±90	6300	SKE5(P)		6263±600
" "	GrN-2972	5530±70	6430	SKE1(P)		5318±570
" "	GrN-3041	5240±100	6140	SKE(P)		6200±590
Achilleion 1_a	UCLA 1882B b)	5485±175	6450			
" "	P-2118 b)	5491±77	6450			
" " 1_{b+c}	UCLA b)	5284±155	6200			
" " 11_{a2}	La Jolla 3328 b)	5331±50	6200			
" " 111_{a1}	La Jolla 3182 b)	4946±52	5850			
" " 111_{a1}	P-2120 b)	5366±68	6200			
N.Nikomedia	P-1203A	5331±74	6231			
" "	P-1202	5607±91	6500			
Asfaka	-	5430±240	6330			
Frachthi	P-1525	5754±81	6650			
" "	P-1394	5844±40	6750			
MIDDLE NEOLITHIC						
Seskło	P-1672	4554±85	5500	SKB(I)27(P)	Of mixed early & middle level sherds	4512±480
" "	P-1674	5014±92	(5900 same	SKB(I)'72(P)		4563±370
" "	P-1675	4744±87	5600 wood?)	SKB(I)18(P)		4440±590
" "	P-1676	4367±84	5300	SKB(I)98(P)		5207±519
" "	P-1677	4791±103	5700	SK4(P)	Keramameos	
Sitagroi 1	Bln-779	4315±75	5100	SK6(P)	House 68 Trench A, Sq.3	4537±340
" " 111	Bln-776	3770±100	4570	SK1(P)	Layer 68, No.80 1963, T.2, Layer 20	5880±580
Achilleion 111_c	La Jolla 2941 b)	4274±51	5100			5673±460
				SK14(FC)	Trench 3, Lev 5, 90-100	4639±410
				SK15(FC)	Trench 3, Lev 16, 100-105	4550±530
				SK8(K)	Keramameos kiln	4143±330
				STG (P)	ZA68, Phase 1	4912±350
LATE NEOLITHIC						
Seskło	P-1671 a)	3672±80	4600	DM33(P)	DM'75 House M.inside	3795±380
Dimini	H	3680±150	4600	DM11(K)	DM1976, kiln	3314±339
Saliaggos	P-1311	4222±74	5020	DMA/12(P)	DM1976 House A	3833±388
" "	P-1396	4124±79	4920	DM1/2(P)	DM1976, MegaronB, $\delta_{\epsilon\iota}$.	3955±350
ArgissaIII/IV	H	3680±150	4480	DM39(P)	-	3187±310
Sitagroi IV	BM 6502 a)	2413±56	3200	DM6/6(P)	DM1976, areaB.A, Megaron B	3567±270
" " III	Bln-774 a)	3150±120	3800	DM32(P)	-	4722±419
				DM10(P)	DM1975, House N, δ5	4240±420
				DM35(P)	-	3571±330
				DM11/22(P)	DM1975, Nδ9	4615±450
				DM14(FC)	DM/76, 1/X.8.54 -Ψ.7.86	4787±400
				DM41(P)	Inside kiln	3794±420
				STG	ZA43, Phase III	3290±295
				DL1/1(P)	Korycian Cave	3247±350
				D13(P)		3166±320
				SKB(I)1(P)	Late levels,	3359±380
				SKB(I)2(P)	mixed potsherds	3773±490
				SKB(I)28(P)	with Mid. Neol. ones	3404±390
MIDDLE BRONZE AGE						
Myrtos	Q-950 e)	1855±85	2265	SH1/11(K)	Kiln	1932±247
Sitagroi	e)	c.1800	2180	SH1/2 (K)	" "	1890±218
Palaikastro	St-1263 e)	1585±70	2015	SH1/6 (K)	" "	1813±278
Pylos	P-326 e)	1500±58	1910	FS3/8 (K)	" "	1865±206
Thera	P-1401 e)	1456±43	1790	FS3/9 (K)	" "	1812±211
LATE BRONZE AGE						
Thera	L-362 e)	1410±100	1675	AT1/9 (K)	" "	1595±198
Pylos	P-329 e)	1306±55	1600	AT1/7 (K)	" "	1522±181
A. Irini	P-1282 e)	1176±48	1460	FS1/5 (K)	" "	1516±223
Mycenae	P-1456 e)	1085±65	1365	KZ3/1 (K)	" "	1420±184
" "	P-1457 e)	998±49	1170	KZ1/9 (K)	" "	1339±170
				KZ1/7 (K)	" "	1569±190
				KZ2/2 Brick		1249±160
				KZ2/5 Brick		1189±180
ROMAN						
				KH5 (K)	" "	10±5% AD
				KH7 (K)	" "	

Most of the quoted C-14 Dates were taken from Theoharis, (1973).
a) from Renfrew, (1971); b) from Fergusson et al, (1976); c) corrections for C-14 were based on the 50-year averaging by McKerrell, (1975). Extrapolation to 6th-7th millinea are unlikely to be more than 100 years in error. C-14 corrected numbers are the averages of the respective ranges proposed by McKerrell, (1975); d) abbreviations: DM, Dimini; SK, Seskło; SGT, Sitagroi; FS, Paistos; KZ, Kato Zakros; SH, Stylos Hania; KH, Kalo Horio; DL, Delphi; and (P), pottery; (FC), fired clay; (K), kiln; e) from Snodgrass, (1975).

In spite of lack of tree-ring results further back than the Fifth Millenium BC, our extrapolation of the correction is unlikely to be more than 100 years in error (McKerrell, pers. comm.). These corrected C-14 dates will then be compared with the TL dates, (see Sections 9.16-17 below and also Fig 9.15

9.12 Thermoluminescence and C-14

The great attraction and performance of the TL work, however, is not only that it is applied to the most usefully dated archaeologic material, but also that it is the absolute method quite independent of half-life accuracy and the earth's past magnetic history, though other difficulties are assocciated with the method. As discussed in previous chapters the errors amount at best up to 5%.

The TL dates obtained are related directly to the context of interest; for example, a wooden sample does not necessarily represent the exact time of early human activities, since it could have been cut from the tree some centuries earlier. Furthermore, the apparent drastic "short-term fluctuations of C-14 (wiggles), might sometimes confuse the correction factor added to the conventional C-14 dates. In particular such chronological complexities appear when these changes occur within the time span of adjacent strata, which represent important cultural phases, Pilcher, (1979).

9.13 Results and Discussions

TL Dating Programmes and Their Archaeological Interpretation

9.13.1 Glozel For three out of four objects, the dates fall in the range of 578 AD to 1474 AD; the fourth gave an age of 482 BC and was considered high, because the material was poorly fired, as checked with a plateau test and other treatments (see below). The peak used was c350°C which was part of the geological region of the glow curve, Fig. 9.13.2. Results are presented in Table 9.13.

TABLE 9.13

Sample No	Water Uptake	β dose rate* mrads/yr	γ dose rate mrads/yr	Dose Intercepts(rads) Q	I	Ratio of 1st/2nd curve	TL Age, years
1. Lamp 744204	1.18	334	274***	611	137	1.67(1.59)**	AD 757±56
2. Vitrified 744111	1.05	430	274	355	0	1.55(0.79)	AD 1474±51
3. Face Urn 744107	1.18	328	274	638	206	1.14	AD 578±143
4. Phallus 744004	1.22	313	274	1341	103	0.79	482±245BC

* the beta dose rate values of 1, 2 and 4 were taken from François et al (1977), and corrected (for water and beta attenuation, appropriately. Particularly, because the average grain size of 160μm diameter, the value 0.909 was used for beta attenuation (including beta soft), see Section 9.8

** the numbers in brackets refer to the normalization by NTL of the 2nd build-up curve (see also Chapter 1) Section 1.13) despite the different slopes, the values of the 2nd intercept (I) are similar in both normalizing ways

*** gamma dose rates were measured by $CaSO_4$:Dy in situ by V Mejdahl. François et al (1977). See also, section 9.8. From their average value of 288 mrads/yr a 5% fraction has been subtracted, in order to convert the $CaSO_4$:Dy in steel tube and which has a similar response to quartz grains

These ranges are in agreement with some dated samples by François et al (1977), Aitken and Huxtable, (1975) ; though most of their dates fall between 350 BC to 250 AD, François et al (1977), McKerrell et al, (1974) and a C-14 date was 50 AD, which imply that an occupation time around the birth of Christ would be the most likely period. The present dates must not be explained as later dates since the uncertainty of the measurements indicate at least the extent of a possible habitation of theplace during the obtained ages. However, the possibility of a second heating, in connection with latter activities at the site, has been investigated in an inscribed tablet with TL dates 1093 AD, François et al (1977), Aitken et al, (1975), and Barbetti, (1976), have found that the tablet has had at least two heating histories.

Also, there is plenty of evidence of glass manufacture at Glozel. From archaeological estimations for comparison with other glass furnaces in the region is that the glass-working activities took place at a fairly recent date, perhaps as late as the 18th century, AD.

Especially, for the vitrified fragment No.744111 and the phallus object No. 744004 measurements were made by Zimmerman on zircon grains for the purpose of determining whether if the samples had been given an artificial irradiation by a clever hoaxer to produce an incorrectly "ancient" result in the TL measurement. The results rule out any possibility of that sample being modern.

In general, archaeologically, Glozel still presents an intricate problem, because of the incredible mixture of objects and the complete lack of parallels. Further, combined archaeological and scientific efforts have to be made to clear up this mystery.

9.13.2 Phallus object. From the first glance, it does not seem to have been adequately fired. Fig. 9.13.2 shows characteristic glow curves of this tablet from feldspar grains. It is obvious that the addition of a beta dose, above the natural level, does not increase its TL for the temperature region of above approximately 350°C. That means that the traps which correspond to temperatures above 350°C are filled with electrons. This implies that the TL above ≃ 350°C does not represent the natural TL but the geological TL instead, Fig. 9.13.2 Comparisons between these glow curves and those from geological clay of the Glozel region results in the following conclusions. Above ≃ 350°C there is a similarity between NTL, geological TL and NTL+1000 rads. It reassures that the feldspar grains of the geological raw clay are saturated given, thus, a very high age (≃250,000 years!). The above are supported by the plateau test, Fig 9.13.3, also. This test determines the temperature region, suitable for dating as the 310 - 350°C.

Further, when the clay is fired at different temperatures (for one hour at each temperature), such as to erase the TL of the respective temperature, the glow curves of Fig. 9.13.4 are obtained.

At 350°C temperature, the geological TL is that which has remained in the tablet. Fig. 9.13.3 explains such observations. (Note that the firing time does not alter the obtained glow curves. This is because for a given ambient temperature, the residence time of the electrons in a particular set of traps is a very sharply rising function of the temperature at which the trap energy in the course of the glow curve, Aitken, (1971).

9.14 Crete in Bronze Age

The TL dates were obtained for well-fired clays from Cretan kilns. The number of dates produced was limited by weathering or vitrification

Fig. 9.13.2. Phallus Object No. 7441004, Glozel.
(a) NTL + 1000 rads
(b) NTL
(c) Black Body radiation
(d) Glow Curve of Geological Clay fired at 300°C.
The increased ratio (a/a+b) in Fig. 9.13.3 of the "Plateau Test" between 350 to 380°C is explained as the enhanced TL of the geological clay in the case (d).
Beyond 380°C all the glow curves overlap, or the ratio (a/a+b) in the "Plateau Test" becomes one.

Fig. 9.13.3. Plateau test for Phallus object.
(a) NTL
(b) NTL+1000 rads
The ratio (a/a+b) becomes one when the natural TL signal coincides with the geological TL. That becomes gradually, which implies that in that point the TL is purely the geological TL; (d) of Fig. 9.13.2.

Fig. 9.13.4. Geological Glozel clay, fired at:
(a) 0°C
(b) 230°C
(c) 250°C
(d) 275°C
(e) 300°C
(f) 350°C

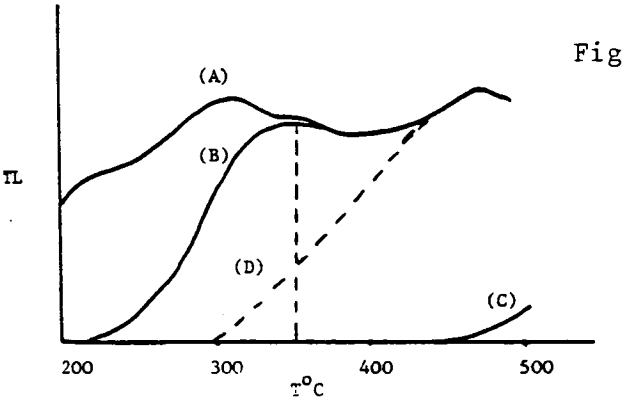


Fig. 9.13.2

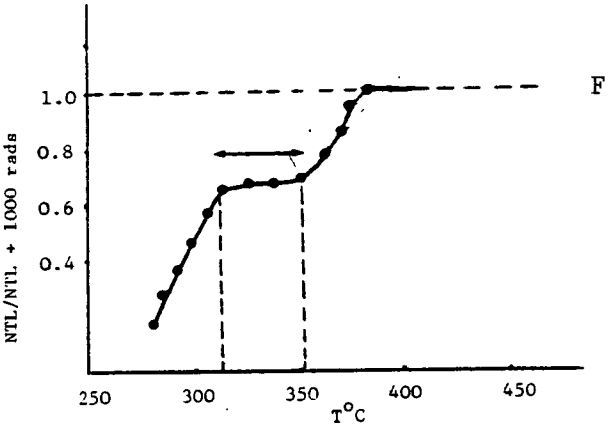


Fig. 9.13.3

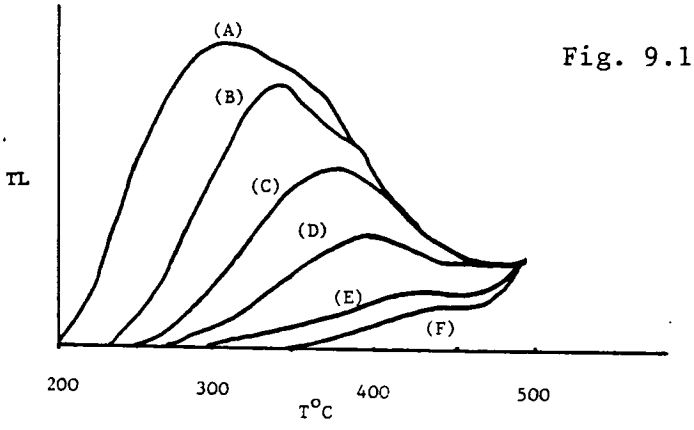


Fig. 9.13.4

of most of the samples and by lack of available well-fired material. However, the results seem to be in good agreement with the archaeological evidence, though one, Stylos Hania, seems to be much older than was thought. It is essential to discuss briefly the construction of a typical kiln site and the sampling method adopted.

9.14.1 Description of a Typical Kiln

Fig. 9.14.1 shows a typical kiln design. Kilns were usually of circular shape of 2 - 5 m in diameter and 1 - 2m in height. The pottery samples were placed on the perforated or firing floor (sol à orifices), thereby being in the middle of the flames. Heat channels led the heat from the fuel to the pottery. All this was encased beneath the kiln chamber, thus creating a uniformity of firing temperature. Depending upon the firing temperature and firing time, the warm air draft (which is released through the chimney), could easily circulate, thus producing an oxidised atmosphere. By controlling the oxidisation by air inside the chamber, the ancient pottery could regulate the resultant colouring of the pottery. The temperature was normally raised to around 900 - 950°C (Belche et al, 1963), though there are indications that this temperature range was sometimes exceeded, up to 1300°C as deduced from the green fused clay surface of the firing floors. This was found in nearly all cases, that is, in Kato Zakros, Phaistos, Agia Triada and Kalo Horio, but not at Stylos Hania. The black conflagration found in various kiln floors also, suggests over-heating in reduced atmosphere or cooling of the sample inside the kiln without breaking the kiln chamber. Pumice deposits were found in the vicinity and fabric of the kiln. It is not known whether the pumice was natural to the island or imported from neighbouring islands of Santorini, Milos or Nisiros.

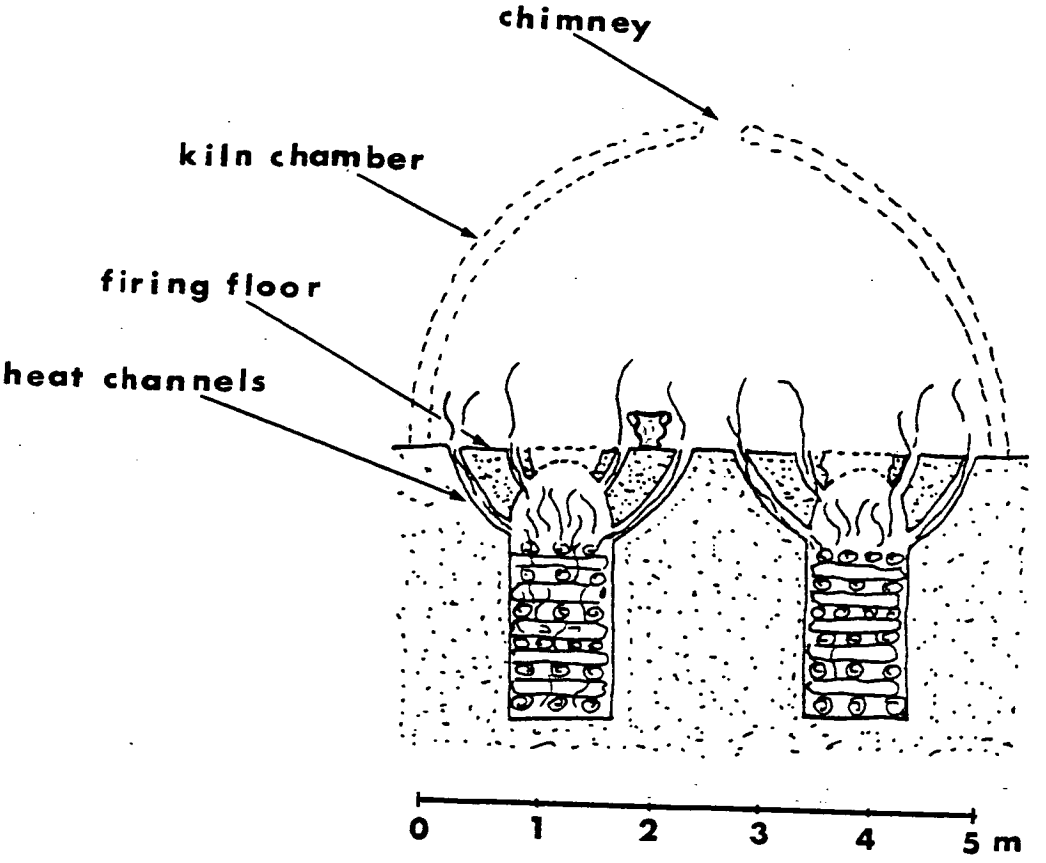


Fig. 9.141 Schematic representation of a typical kiln (after Orlandos, 1955)

9.14.2 Up-to-date Archaeological Evidence of Minoan Chronology and Their Correlation with Thermoluminescence Dates. From the pottery style found in thepalaces and kilns the following divisions of the Minoan periods are presented together with their respective TL dates.

Phaistos. This palace was built around 1900 - 2000 years BC. The kiln FS3 belongs to this palacial period. It was destroyed at around 1730 BC by earthquakes. On the ruins of the early palace, a more magnificent building was constructed. The kiln FS1 belongs to this new palace. The later palace was apparently largely destroyed by the great earthquakes, following possibe influences of the Santorini volcano at around 1500 BC, Pichler, et al (1977). The palace was not re-built; instead the Phaistians built a new palace at the site of Agia Triada. Samples of well-fired clay were taken from the firing floor of FS3 and from the surface walls of the heat channels of FS1, for thermoluminescence dating. The TL dates obtained were 1834 (±4%) years BC and 1516(±6.5%)years BC, respectively and they relate to the last firing event in the kilns. The dates are generally acceptable, in the order of the expected time span, even though the error is high in comparison with the accuracy of archaeological age.

Agia Triada. This palace was occupied c. 1400 - 1500 years BC. During this time the kiln was built and used. The absence of late Minoan II pottery on this site implies that the palace could not have been used later than this. Three samples, AT7, AT8 and AT9 were dated by thermoluminescence. AT7 was from beneath the surface of the green-fused clay, where the material was well-fired sample; AT8 was of black fused material and sample AT9 came from the vertical firing floor nearby to the air vent entrance. AT8 gave scattered points in the first and second build-up curves for the determination

of the total archaeological dose, possibly because the TL properties of the quartz were altered, so the results were discarded. Samples AT7 and AT9 together gave a TL date of 1558(±4%) years BC, consistent with the archaeological evidence. see Fig. 9.14

Kato Zakros (1700 - 1400 years BC). This palace, according to Prof. Platon, the excavator, was not re-built or inhabited after the last catastrophic earthquake between 1450 - 1400 years, BC. Sampling was done on the existing kiln and from the burn area of the western part of the palace with fired tiles. Assuming that thekiln ceased functioning simultaneously with the destruction of the palaces, as exemplified in the burnt tiles (site 2 and site 3), it would be reasonable to expect the age of the kiln and the age of the tiles to agree. The average of these three sites assuming the synchronisation of the firing events is 1353(±2%) years BC. The date of the kiln samples done is 1454(± 4%)years BC. Both TL dates agree with the archaeological and C-14 evidence (Platon, pers.comm), Warren, (1975), Hutchison,(1962), Wunderlich , (1977) and Pichler, (1977).

Stylos Hania The kiln was found empty of pottery. The excavator believes that it is of late Minoan age, about 1300 years BC, because the nearby village, Stylos, is of late Minoan period. Sampling was done on burnt clay. The wall structure was not well-fired and the surrounding and kiln fabric soil contained a high amount of calcite, (Table 6.4.3,XRF results), which made the burnt clay even softer. However, the TL results for this kiln were self-consistent and gave an average date of 1795(±4%) years BC, which corresponds to the first palacial development in Crete, about 400 years older than estimated by the excavator.

Archaeomagnetic studies yielded a geomagnetic field intensity quite

AT7



Fig. 9.14. Kiln Sample AT7. The outer (surface) part is black (extending to a green-fused material in situ), whilst the inner part is a well-fired red clay. The quartz inclusions (white grains) are well seen in the black layer.

TABLE 9.14.2

CRETAN TL DATES

Sample No	Beta Dose Rate (mr/yr)	Gamma Dose Rate (mr/yr)	Peak °C	Dose Intercepts (rads) I	Dose Intercepts (rads) Q a)	Age (yrs BC)	Average kiln Age **** (yrs BC)
SH1/11	143	125	375	-12	1060	1932 ± 247	
SH1/2	148	125	350	-48	1160	1890 ± 218	1878 ± 4%
" "			375	-199	1200		
SH1/6	134	125	350	0	982	1813 ± 278	
SH1/5 **	126	125	350	272	612	1548 ± 220	
FS3/8	209	103	325	112	1087	1856 ± 206	
FS3/9	150	103	325	66	840	1812 ± 211	
" "			350	0	1012		1834 ± 4%
AT1/9	164	113	325	115	873	1595 ± 198	
AT1/7	215	113	325	112	1036	1522 ± 181	1558 ± 4%
AT1/8 ***	195	113	325	0	1092	1739 ± 276	
" "			450	0	1199	" "	
FS1/5	170	126	350	-139	1199	1516 ± 223	1516 ± 6%
KZ3/1 *	210	143	350	114	1199	1420 ± 184	
KZ3/2 *	222	143	350	190	987	1249 ± 160	1286 ± 3%
KZ2/5 *	144	143	350	0	909	1189 ± 180	av. 1353 ± 2%
KZ1/9	200	147	350	84	1069	1339 ± 170	
KZ1/7	169	147	350	0	1123	1569 ± 190	1454 ± 3.7%
" "			325	0	970		
KH5	163	157	325	64	618	175 ± 154	
"			375	70	627		10 ± 5% AD
KH7	164	157	375	0	585	155 ± 120 AD	

a) from pages 227, 228.
* tile: other samples are from kiln
** semi-fired, worse "plateau test"
*** black - fused material
**** average estimated percentage error

different from that of c1300 yrs BC, which was obtained from Kato Zakros material, whilst it is similar to Sitagroi material of c1800 BC.*

Kalo Horio This is a well-preserved Roman kiln, situated beside the bank of a river. In many parts of the kiln, the clay was vitrified. Sampling was done from the inner part of these fused surfaces. The result of 97(±5%) AD is in agreement with its Roman origin. In particular, a vitrified sample KH6, which was taken from the kiln roof, gave non-reproducable glow curves. The sensitivity of the quartz sample changed remarkably from portion to portion. Also, this sample was already saturated. These effects are attributed to the fact that the sample was vitrified and the quartz properties were destroyed. Results of the above measurements are presented in Table 9.14.2.

9.14.3 Conclusions Thermoluminescence dating is potentially an effective dating tool for materials such as fired kiln clays and burnt tiles, which are of direct relation to human activities. Although the method does not yield the precision sought by archaeologists for this somewhat well explored Minoan period, it helps to reassure their chronological estimations. The presently quoted errors are of the order of 5% and the confidence limits can be improved by taking many TL dates from the same site.

9.15 Aegean Neolithic Settlements

9.15.1 Sesklo and Dimini The Dimini settlement represents the late Neolithic period in Greece and the transition to the Chalkolithic, Theoharis, (1973). Recent excavations have revealed many fortifications around the "megaron"-like structure of the settlement. Sesklo shows a continuum of occupation from the aceramic to the late Neolithic times. There are not, so far, enough C-14 dates for the Dimini sites, but from the nearby counterpart of Sesklo (acropolis), a C-14 date gave

* Liritzis, Thomas, (1979).

a date of 3672yrBC (Radiocarbon, 1973), which with a MASCA correction becomes 4372 years BC and this corresponds to the respective Dimini period. Though this dating involves uncertainties, (see also section 9.12.1.), and because no other dates are available for Dimini, the TL dating technique was applied on various potsherds which were found in the first 30cm depth in different locations of the site. Because sufficient stratigraphic information was not supplied with the samples, we cannot present our TL dates as a function of depth. However, according to the estimated errors no dates fall outside its appropriate period by more than approximately one standard deviation. These error bars then, imply a continuous model for this site, Fig. 9.15

Statistically, these dates may be regarded as maximum confidence time spans and we may be reasonably sure that the culture in question was in occupation of this settlement during its maximum confidence span. In the former case, the duration for Dimini culture seems to span from c3000 - 4800 years BC. This span includes the earlier mentioned corrected C-14 date and no date falls outside the period appropriate to this phase.

The earlier part of this period (late Neolithic 4150 - 4800 BC), overlaps with the late part of the Middle Neolithic from Sesklo. This implies that at the same time with Dimini, there was still an active Sesklo, but from pottery abundance and style, not so productive and and artistic as Dimini. The later part of this period thereof being

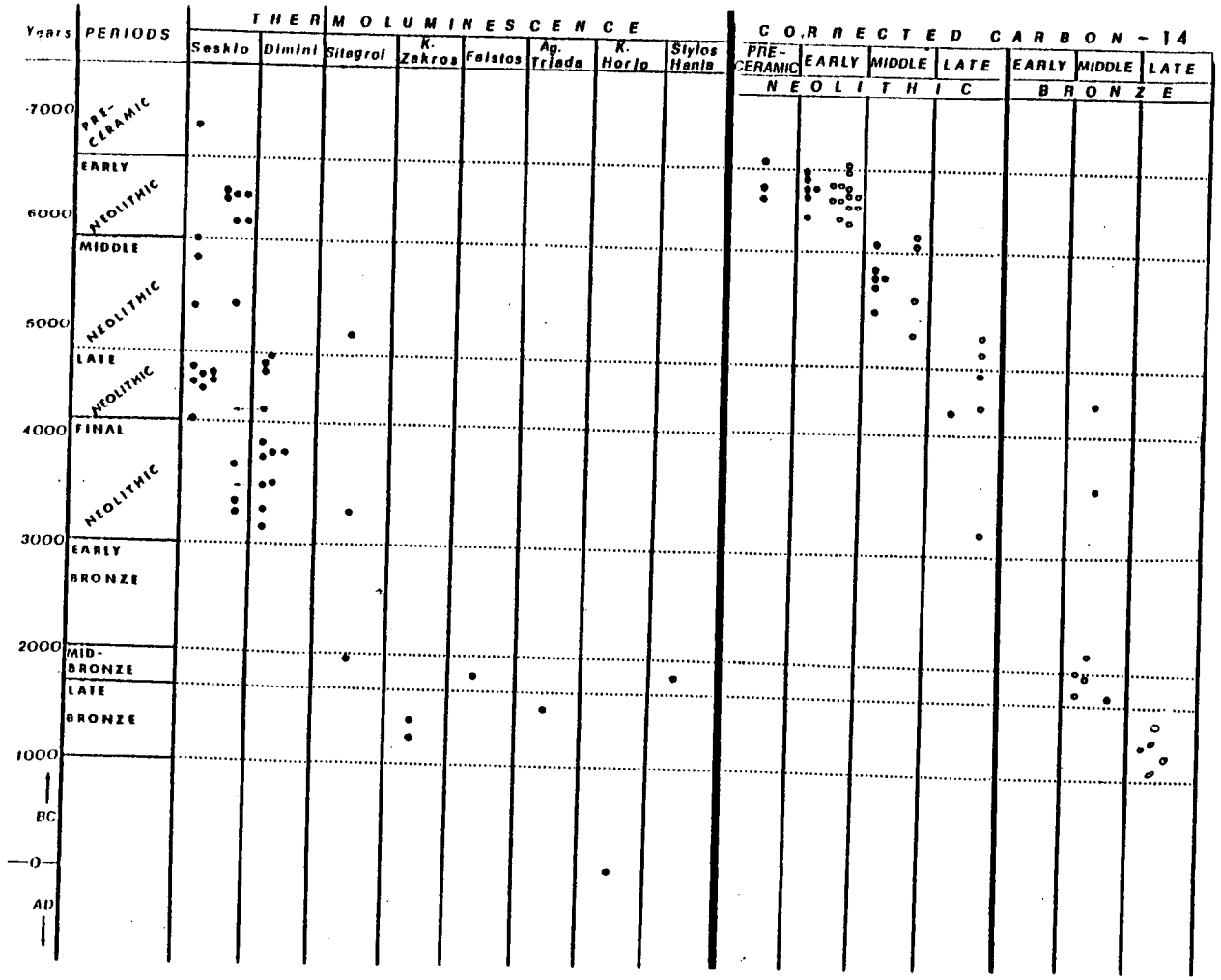


Fig. 9.15 Comparisons between TL and C-14 dates for Hellenic Neolithic and Bronze ages. Samples dated by TL are pottery and Kiln materials and do not correspond exactly to the C-14 samples. The circles represent C-14 dates from other than the quoted sites, but, of the same period. Arrows indicate potsherds found in the one site but originated in the other (as NAA proved).

the final stage of the Late Neolithic 3000 - 4180 years BC . The Middle Neolithic period of Sesklo has a duration, for the reasons explained above, which spans from c.4150 - 5450 years BC. with a high confidence level. The fact that two dates, those of SK6 of 5860 and SK1 of 5673 years BC seems to be significantly different from the average of the other dates, could mean a spread towards higher ages, but within the 1σ error of dates. Therefore, the probable duration for this middle period would be 4150 to approximately 5750 years BC.

For theLate and Middle Neolithic periods, it appears then that a possible cultural interaction between these two settlements is most likely to have had occurred between 4150 to 4800 years BC.

This last hypothetical "fact" is further supported by the following:

i) the neutron activation analysis for sherds and clays from Sesklo and Dimini revealed that potsherds found in Dimini seem to have originated in Sesklo and vice versa, (Chapter 10). In spite of the closely situated sites, the geomorphology of the area is a fairly complex matter (Chapter 10, Fig 10.4.5)

ii) from the technological point of view, on pottery composition, and manufacturing, the late and middle periods appear to be similar and distinctly different from the early ones. This has been shown with thin section analysis on representativepotsherds and clays from both the settlements, (Chapter 10).

The above investigations strengthen the views of the excavator (Prof. Chourmouziadespers. comm.), who extends this interaction in a further statement that the people of Sesklo were those who migrated and inhabited (colonised?) Dimini, therefore, it is logical to keep

relations with their previous land and people especially of an exchange character . The reasons, according to Prof. Chourmouziades were economical and due to the lack of sources of working material. Furthermore, Dimini is closer to the sea than Sesklo, Chourmouziades, (1979). For the Early Neolithic period, the group of materials dated gave an average of 6000 (±223, ±85) yrs B.
A probable occupational duration of this period could be from c5800 to 6600 years BC approximately.

The later part is in good agreement with the beginning of themiddle Neolithic period, and the earlier part is in reasonable chronological relation with the aceramic burnt layer which dated was found to be 6849±660 years BC.

In spite of the fact that only one dating result was obtained for this early burnt layer , and considering the 68% confidence level for which this date is correct, this number stands as correct when compared to the commencement of the ceramic or early Neolithic period.

Finally, some potsherds from Sesklo gave very low results with an average of 3512 (±247 ±142; surface potsherds) yrs BC. Nevertheless a late Sesklo period could well have existed and overlapped with the final Dimini period.

All the dates, above, indeed give a coherent sequence and allow the time span in question to be divided into a number of periods seen in Fig. 9.15. Results are listed in Table 9.15

9.16 Comparison of TL and C-14 Dates for the Sesklo and Dimini Neolithic Settlements

In Fig. 9.15 the arrows indicate pottery found in one site which appears to have originated in the other (after NAA analysis.) For the late Aegean Neolithic there is an obvious spread of dates and the higher ones agree well with the only one C-14 result. The Middle

TABLE 9.15

Sample No		Neolithic Period	0°C Peak	Water uptake (W/D) ratio	β-dose rate	γ-dose rate (mrads/yr)	Intercept I	Intercept Q	Total Arch dose Q+I	TL Age Yrs BC
DM33	(Q)*	Late Neolithic		1.090	233	88	230	1623	1853	3795±380*
DM11	(Q)	"		1.666	145	136	150	1337	1487	3314±339
DM8/12	(F)	"		1.111	220	109	94	1818	1912	3833±388
DM1/2	(F)	"		1.164	247	114	515	1627	2142	3955±370
DM39	(F)	"		1.135	297	116	100	2033	2133	3187±310
DM6/6	(F)	"	-***	1.090	220	99	84	1685	1769	3567±270
"			425				57	1954	2011	
"			325				121	1509	1630	
"			375				48	1618	1666	
"			325 (TL/mg)				242	1487	1730	
DM32	(Q)		-	1.075	241	116			2392	4722±419
"		"	300				-736	2818	2082	
"		"	325				-869	3220	2351	
"		"	425				-670	3103	2433	
DM10	(F)	"	-	1.104	231	113	-	-	2139	4240±420
DM10	(F)	"	325	-	-	-	405	1658	2063	
"		"	450	-	-	-	496	1719	2217	
DM35	(Q)	"	375	1.087	269	99	-200	2242	2042	3571±330
DM11/22	(F)	"	400	1.138	155	118	364	1436	1800	4615±450
DM14	(F)	"	400 (TL/mg)	1.175	204	142	35	2308	2342	4787±400
"		"	325				-12	2494	2482	
"		"	375 (TL/mg)				110	2405	2514	
"		"	375				-369	2887	2518	
DM41	(F)	"	400	1.060	164	90	327	1139	1466	3794±420
		"								
SKB(I)27	(F)	Middle Neolithic	350	1.125	238	128	0	2674	2674	4512±480
SKB(I)98	(F)	"		1.120	283	157	-	-	3161	5207±519
"		"	350 (TL/mg)				-33	3393	3360	
"		"	350 (TL/110°)				-106	3069	2963	

TABLE 9.15 (cont)

SKB(I)98	(F)	"	450				-27	3427	3400	
SK4	(F)	"	375	1.122	310	229	294	3218	3512	4537±340
SKB(I)'72	(Q)	"	-	1.170	296	146	-	-	2891	4563±370
"		"	375				0	2706	2706	
"		"	350				-60	3136	3076	
SK6	(F)	"	325	1.127	193	130	-	-	2546	5880±580
"		"	400				-634	3320	2686	
SK1	(F)	"	325		241	134	194	2675	2869	5673±460
SK14	(Q)	"	-	1.155	262	140	-	-	2600	4639±410
"		"	425				-430	3090	2660	
"		"	335				-72	2573	2501	
"		"	375 (TL/110°C)				-342	2939	2597	
"		"	375 (TL/mg)				-275	2654	2380	
"		"	425 (TL/mg)				-497	3154	2657	
"		"	335 (TL/mg)				-45	2452	2410	
SK15	(F)	"	325	1.364	190	140	321	1833	2154	4550±530
SK8	(F)	"	325	1.207	307	229	118	3163	3281	4143±330
SKB(I)18	(F)	"		1.100	315	128	-	-	2843	4440±590
"		"	375				21	2778	2799	
"		"	325				51	2836	2887	
"		"	250				0	1187	1587	
"		"	375 (TL/mg)				20	2730	2750	
SK3	(F)	Early Neolithic	325	1.113	281	173	1001	3614	3714	6194±590
SKE6	(Q)	"	375	1.105	227	138	-497	3497	3000	6225±590
SKE4	(F)	"	325	1.105	324	134	0	3636	3636	5961±570
SKE3	(Q)	"	335	1.105	220	134	-33	2627	2557	5245±606
"		"	365				394	2127	2521	

TABLE9.15 (cont)

SKE5	(Q)	"	325	1.123	276	134	-1954	5333	3379	6263±60
SKE1	(F)	"	350	1.120	242	134	-273	3242	2969	5918±570
SKE		"		1.070	374	173	-	-	4474	6200±590
"		"	350				-121	4566	4445	
"		"	400				-197	4648	4451	
SK2	(Q)	Preceramic	350	1.286	196	192	87	3338	3425	6849±660
SKB(I) 1	(F)	Late Neolithic Sesklo		1.116	383	125	-	-	2709	3359±380
"		"	350				-78	2484	2406	
"		"	400				-890	3605	2715	
"		"	450				-542	3245	2703	
"		"	400 (TL/mg)				-781	3105	2324	
"		"	450 (TL/mg)				-	2702	2702	
SKB(I)2	(F)	"		1.125	302	125	-	-	2450	3773±490
SKB(I)2	(F)	"	350				109	2451	2560	
"		"	400				-90	2430	2340	
SKB(I)28	(Q)	"		1.08	342	128	-	-	2530	3405±390
"		"	365 (TL/mg)				75	2269	2344	
"		"	325 (TL/mg)				224	1805	2030	
"		"	325 (TL/110°C)				238	2266	2499	
"		"	365				100	2460	2560	
										AVERAGE:3512(±247,±142)
Delphi 1/1	(Q)	Late Neolithic	325	1.050	229	82	0	1625	1625	3247±350
Dimitra 6	(Q)	"	325		256	150	157	1069	1226	1884±580
"		"	360				351	945	1296	
Dimitra13	(Q)	"	350		277	147	-	-	2181	3166±320
"		"	325				12	1821	1833	

* Q = Quartz, F = Feldspar
** Depending on the relative errors of parameters of the age equation, the overall error in the TL dates was between ± 5% to ±8%
***The dash indicates that the total dose was calculated from the average of many peaks

Neolithic period is somewhat confused. There seems to be an overlapping betwee the late and middle periods. Also the C-14 dates for this period almost agrees with the TL dates. It seems though that most of the given sample, for that period come from a higher occupational level, (or C-14 tend to be higher, probably due to the reasons mentioned above in section 9.12). In the early Neolithic period, the agreement between TL and C-14 dates is remarkable.

In conclusion, the TL dates support the corrected C-14 dates. However, the lack of adequate information about the corresponding stratigraphic order of the samples, dated by these two methods, (due to the confusion which occurred in the Museum concerning listing of samples after the unexpected loss of Prof Theoharis, the excavator of the site), do not allow us to make a more direct comparison between samples of the same layers.

9.17 Sitagroi Neolithic Site

The importance of chronological "cross-checking" between C-14 and TL dating techniques has further been tested for the Neolithic settlement of Sitagroi, Northern Greece.

The stratigraphic sequence from this site on the excavated finds, for example pottery, permitted a division of the strata into five separate phases, Renfrew, (1970, 1971).

Attempts to date these stratigraphic layers were made by C-14 and many samples, such as charcoal, vetch, acorns come mainly from the trench namely Z A. The dates indeed give a coherent sequence and allow the time span in question to be divided into a number of periods The three potsherds dated by TL come from the archaeological phases (levels) I,II and Vb. Results on the above samples are listed in Table 9.17.

TABLE 9.17

Sample No	Arch Phase	Period	K_2O%	Peak ^oC	β-dose rate (mrads/yr)	γ-dose rate (mrads/yr)	W/D	Total* Arch. dose rads	TL dates yr/BC (±1σ)	C-14 Uncorr yr/BC dates	Corr C-14 dates yr/BC
STG ZA2	Vb	Middle Bronze	3.25%	325,375	367±12	156±20	1.080	2061±60	1962±186	c1800	2210-2150
STG ZA43	III	Final Neolithic	3.85	325,375 400	380±14	168±22	1.077	2887±86	3290±295	c3100	3850-3800
STG ZA68	I	Middle/ Late Neolithic	2.71	300,325	303± 7	182±22	1.080	3342±100	4912±350	c4400	5340-5250

No fading effect, or predose effect was found. The radon emanation was found to be negligible, at 12% and 6%. respectively, for all three sherds. Due to the high potassium content, the high gamma dose rates, and the fact that the major beta contribution comes from thepotassium, though even the highest radon loss of 12% would produce an error of less than 2%, which becomes negligible in the calculation of the statistical error of the age (see also Chapter 3 Section 3.7.2)

* An average of the respective peaks, only within ±2σ.

From first glance, it appears that the uncorrected C-14 dates are lower than the TL dates. Apart from phase III the other phases as defined by TL dating are higher and within the range of correction of C-14 dates. Due to the "short-term wiggles" of C-14, during those times an exact deviation of corrected C-14 dates from the uncorrected cannot be assessed. However, considering these C-14 changes, we believe that unless TL dates are in agreement with corrected C-14 dates, based on an average correction factor, disagreements must be dealt with caution and if the dating materials come from the same strata, this would help to reinforce a more reliable C-14 correction curve, Liritzis, (1979).

9.1 8 Conclusions

In conclusion, the TL dates support corrected C-14 dates for the time span from the Seventh to the First Millenium BC, where severe changes in the production of C-14 atoms in the atmosphere had occurred. At the same time, the general harmony between the TL dates and the calibrated radiocarbon dates likewise lends support to the general reliability and precision of the TL method.

As a result, the present classification of the Neolithic and Bronze periods in Greece to different cultural phases seems to be correct and the two dating techniques seem to provide a very useful cross-check for such chronologies.

The applied C-14 calibration seems to support the idea of correction of the conventional C-14 dates and a precise calibration curve must be therefore sought in the direction of a new chronology. Nevertheless, TL dating method would always play the role of absolute technique, with which comparisons with C-14 must be made.

However, in such comparisons, we have to be extremely cautious when dealing with some chronological complexities caused by:

i) disturbed strata,

ii) sample contamination,

iii) different chemical preparatory methods,

iv) stratigraphically relative to the respective pottery phases ;

v) errors in the tree-ring calibration curve as related to the "added factor" in the C-14 correction, due to the sample size and the geographical origin of the material concerned. ("Principle of simultaneity" in the earth-atmosphere mixing reservoir of C-14), Berger, (1978).

Anyhow, for such comparisons, the overall statistical error ($\pm 1\sigma$) of the two methods have to be duly considered and the present degree of accuracy not be exaggerated for either. With this caution, the present agreement between them appears encouraging.

Finally, combining these two methods, the chronological scale of the remote past cultures will be more precisely established.

INTENDED FUTURE WORK

The importance of the above-mentioned Neolithic settlements to our understanding of the evolutionary process during the Hellenic Neolithic period, prompts us to pursue a more extensive TL dating programme in the near future.

This programme shall be comprised of the dating of many potsherds belonging to the same depositional layer or archaeological phase, with the objective of reducing the overall dating error and of producing more accurate stratigraphic information for those respective cultural phases in question. The statistical emphasis shall stress the "normal" distribution of the dates from each layer, as opposed to the "scattered" distribution presently employed.

This prospective shall be linked synchronously with TL dating work on sedimentary and calcitic materials (Chapter 12)

CHAPTER 10

APPLICATION OF ANALYTICAL TECHNIQUES TO SESKLO AND DIMINI

10.1 Neutron Activation Analysis, X-Ray Fluorescence and Thin Section Analysis on Artefacts from Sesklo-Dimini Neolithic Settlements

This chapter concerns an investigation on materials (pottery, kilns, clays) from the two Neolithic settlements of Sesklo and Dimini, by Neutron Activation Analysis Technique (NAA) and X-Ray Fluoresence Analysis (XRF), anticipating the finding of some cultural interaction between them at certain times in the past. Thin Section Analysis (TSA) also illustrates the differences or changes in pottery composition and technique that occurred during the different Neolithic periods of the two sites.

10.2 Some Introductory Aspects Concerning NAA

The NAA can be defined as the revelation of chemical composition through the modification of nuclear behaviour. This analytical technique requires a group of samples and chemical standards of known composition to be placed in a nuclear reactor and so to be irradiated with a flux of thermal neutrons, which, upon interaction, converts the elements in the sample to various radionuclides, Perlman & Asaro, (1969) and also in Advances in Activation Analysis, (1972).

The factors that determine the detection sensitivity of the nuclei, nuclear in origin, are: the probability (cross-section) that a given type of nucleus will absorb neutrons and the half life for radioactive decay.

Following the irradiation of a set of samples and standards, it is only necessary to determine the energies of gamma rays emitted by the samples.

Since each radioisotope emits gamma rays having energies characteristic only of that isotope, unambiguous identification of the type of elements

present in the sample is possible. Also, from the intensities of the emitted gamma rays and from comparison with the intensities of the same gamma rays emitted from the standards, it is possible to determine the percentage composition of the samples.

Therefore, by comparing the characteristics of an object of an unknown origin with the characteristics of a reference object or raw materials from known origin, the unknown object may be assigned to a specific origin, Oates et al (1977), Davidson & McKerrell, (1976).

It is the elements present in small amounts at the ppm levels that are often the most imformative. Of necessity, therefore, certain precautions must be taken so that the samples and standards are irradiated and analysed under reproducable conditions and fairly complex electronic equipment is needed, in order to obtain highly accurate data.

Methods ofhandling such data are readily feasible using computer procedures (Here with mini-computer of the Wang type.)

Deciding which analysis is most similar to another is generally performed by clustering procedures (Sneath, Sokal, 1973), so that one readily derives groups of analyses or clusters which are analytically very similar. The results of cluster analysis are commonly presented in the form of dendrograms which are "trees" showing the order and levels of specimen clusterings.

Any cluster thus generated needs careful examination as to its real meaning. An acceptable method is by using Mahalonobis' distance statistics, which have provided a powerful procedure yeilding a percentage probability for inclusion within a cluster of each mumber of the cluster or indeed for any desired comparative analysis. (Basically, Mahalanobis' distance is a measure of the conformity of a given sample

to a particular group. Thus by calculating a particular Mahalanobis distance between a particular point and a given group, one can calculate the probability that the group will include that point). Finally, the analytical precision which needs to be sought to establish significant groupings in an archaeological context is expressed as the observed overall variance (parameter measuring the total error) of one group of samples, for example, made from a given clay source. This depends on:

i) the variance in the "natural" distribution of the concentrations of the various elements present in the pottery type,

ii) the sampling variance introduced by the degree to which the sampling technique has failed to average out unhomogeneity within a given sherd,

iii) the analytical precision that is the total variance introduced by counting statistics; weighing errors, computing errors in spectrum processing; neutron flux variations in the reactor, decay correction (due to possibly incorrect values for half-lives): background corrections; random contamination and counting geometry errors. A most usual state of analytical precision of the order of ± 5 - 10%, is quite sufficient, Bieber et al (1976)

10.3 Archaeology of the Context

Sesklo and Dimini are two Neolithic settlements in central Thessaly, Greece. Dimini is located on a soily hillock with more than one phase of fortification. Sesklo's Acropolis-like structure is on the top of a hill with surrounding houses and sub-settlements. A number of trenches have revealed despsitional layers of different cultural phases, Theoharis, (1973), Piggott, (1965), Chourmouziades pers.comm, (1979), Liritzis et al, (1978). The importance of these sites stimulated us

to attempt some analytical studies in order to find any similarity based on their pottery composition, which would imply cultural interaction. Because the two settlements are separated by a distance of only 5Km, the pottery exported from one of these sites could possibly be identified by NAA to have come from the other site and then the degree of overlap between the prehistoric occupations of the settlements could be better assessed.

10.4 NAA Procedure

Small samples, of abour 0.1gr, were removed from pottery by diamond grinding, made into pellets and fired to 1000^{o}C to yield a robust pellet of accurate dimensions, containing little residual water, organic material or carbonate. Batches of 61 pellets from Sesklo and Dimini were irradiated at the thermal neutron irradiation facility of the Radiochemical Centre, Harwell, each batch of pellets containing dispersed standards prepared from a substantial supply of a commercial terra cotta clay, accurately intercalibrated against the pottery standard of the Berkley Laboratory, (Perlman & Asaro, 1969). Although the induced radioactivity is initially intense after some two or three weeks it is sufficiently reduced to present no handling problems.

The pellets were then automatically counted for their long-lived induced radioactivities using standard procedures and data reduction. The block diagram of the associated electronics in the gamma counting arrangement is shown in Fig. 10.4.

So far we have relied solely on the cluster analysis to break down the analytical groupings, but more complex statistical procedures are necessarily involved in further refinements of such analysis, Oates et al, (1977).

Although immensely valuable in handling large quantities of data,

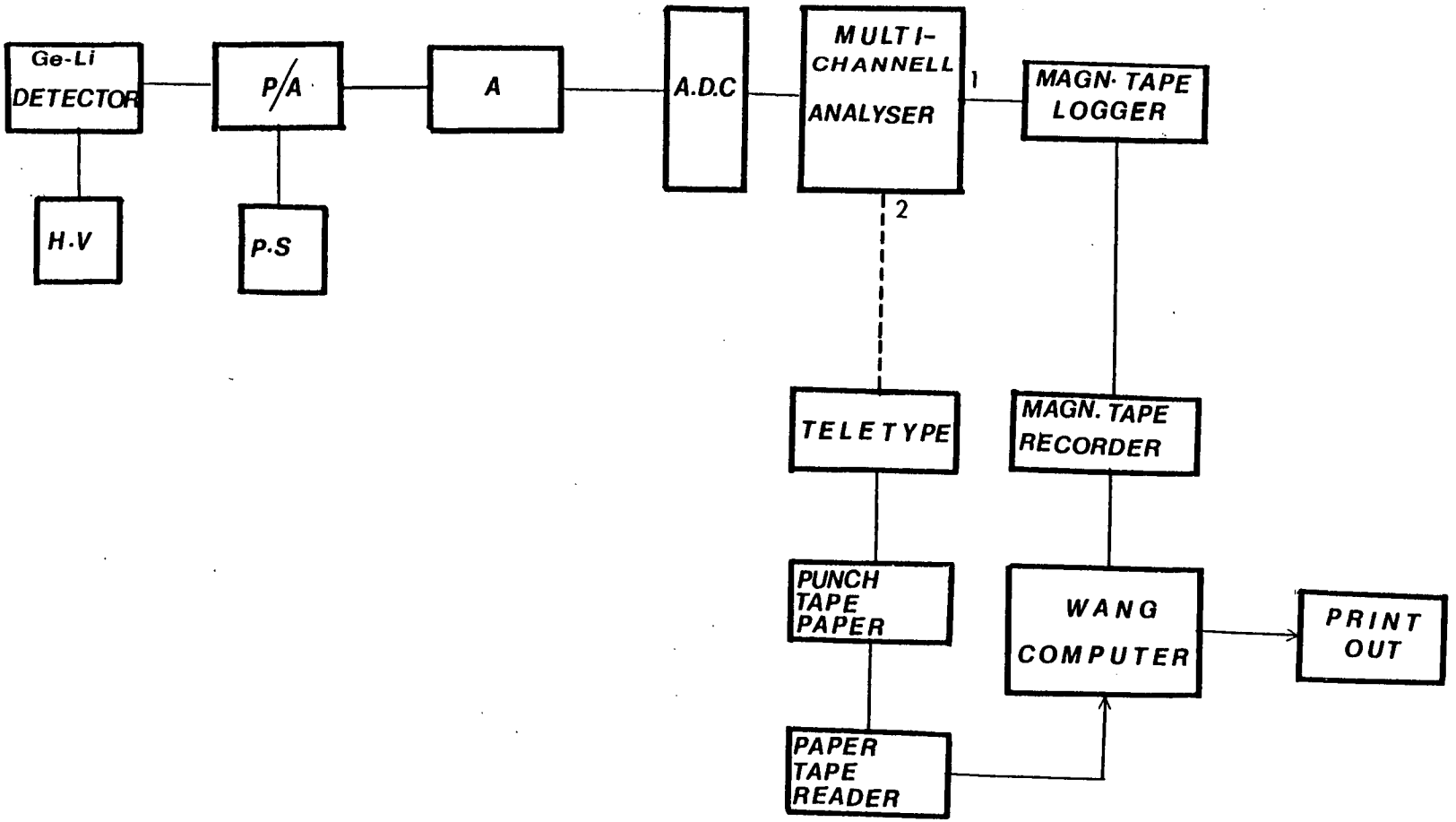


Fig. 10.4 Block Diagram of the Associated Electronics in the Gamma Counting Arrangement

dendrograms must be interpreted with great caution, especially when they illustrate material of a highly complex nature, for example the pottery origin of Sesklo and Dimini and their clay source, in this particularly complex geological region of Volos. The most certain procedure, however, is such situations is first to isolate one or more sizeable clusters from a reasonable number of analyses of pottery based on Mahalanobis distance. It is thein possible to test such an isolated main group, first for internal consistency and then, sherd-by-sherd for comparability with other analyses.

Such a grouping has a high probability, not merely of an analytical compactness, but also on entirely likely manufacturing reality, involving only one clay or sediment source.

Such procedures provide for each sherd a value representing the percentage probability for analytical compatibility with (or within) the main groupings; thus, for example, pottery coming from the same source would typically produce a probability of at least 50% while material entirely foreign to such a source could fall below 0.1% probability.

10.4.1 Results and Discussion Applying such procedures to the material of interest we have derived our main grouping for Dimini and Sesklo. Fig. 10.4.1 shows the cluster analysis of Dimini samples which are analytically presented in Table 10.4.1 This reveals that there was undoubtedly a group (D01 - D41) characterised as a local Dimini group of clays, sherds and kiln materials with a high probability of matching each other. (see also Appendix A, Provinance of samples) Another group (D24 - D42) does not cluster within the local Dimini group, except for one sherd (D25), with a probability of 51%. When this non-local Dimini group is compared to the Sesklo group, then two Sesklo potsherds (SK05, SK06), with probability of 51% and 69.9%, seem

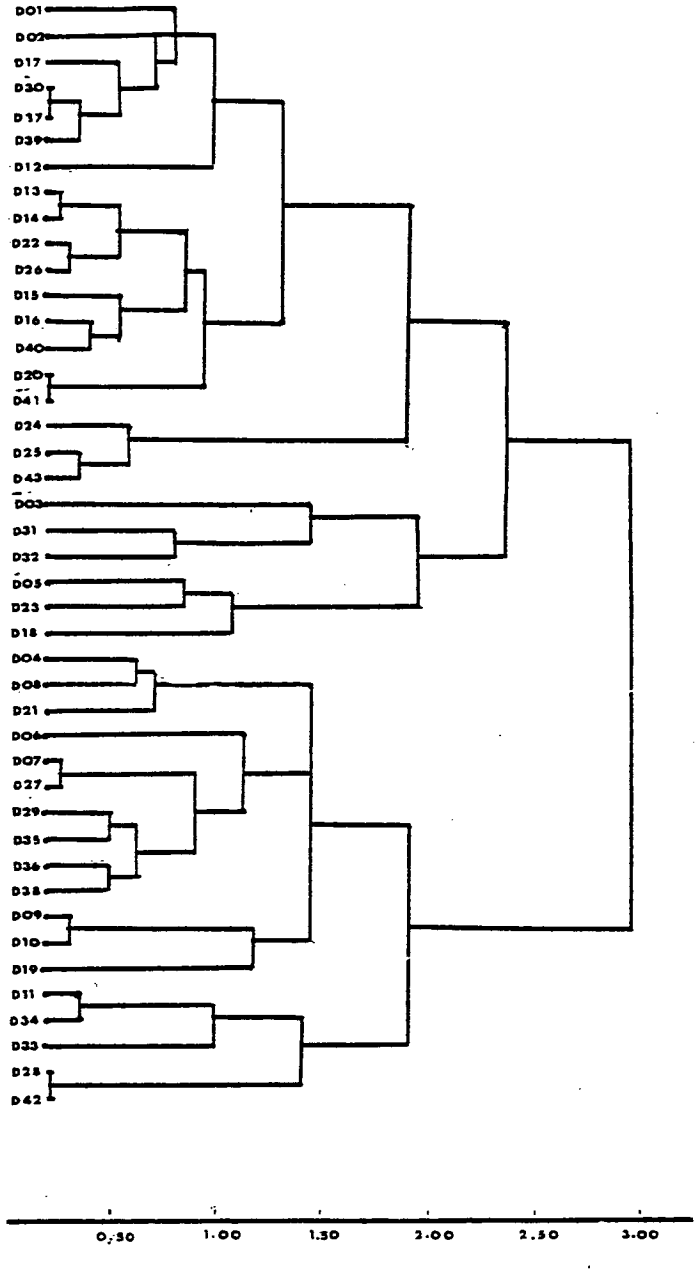


Fig. 10.4.1 Maximum distance Clustering diagram, with 8 elements, for NAA analyses of pottery and clays from Dimini.
D01-D41 is Dimini's main local group of potsherds and clays.
D24-D42 is Dimini's non-local group.
The lower axis scale represents the dissimilarity level.

TABLE 10.4.1

NAA No	Sample No	Th	Cr	Hf	Cs	Sc	Fe	Co	Eu
1	DM1/1	13.19	630.06	4.96	2.81	22.85	45074.72	27.45	1.23
2	DM1/2	13.37	317.79	5.06	9.24	22.00	46524.99	23.33	1.17
3	DM2/4	4.95	149.75	2.97	12.10	30.26	77262.41	36.18	1.06
4	DM5	14.96	89.81	6.20	3.15	19.27	46241.51	16.86	1.43
5	DM6/6	15.14	228.76	4.50	3.36	29.07	65957.16	31.85	1.91
6	DM6/7	22.01	164.31	6.45	6.17	15.90	26991.03	22.49	1.62
7	DM7/8	20.45	253.49	4.52	7.34	17.54	42590.64	19.93	1.36
8	DM7/9	17.90	109.38	5.85	2.20	14.05	37550.04	13.16	1.42
9	DM8/12	16.40	90.29	4.56	5.90	11.59	30980.51	10.25	1.03
10	DM8/13	16.16	122.63	4.52	5.81	12.74	33257.62	12.42	1.09
11	DM10	16.26	118.10	7.37	3.29	19.68	50207.42	18.26	1.77
12	DM11	9.85	209.20	4.65	4.16	16.91	37955.26	19.28	1.30
13	DM15	15.44	246.57	4.98	3.86	19.79	45366.20	22.96	1.44
14	DM16	18.10	263.52	4.97	5.21	21.44	44784.26	24.17	1.45
15	DM9/17	18.57	525.22	5.80	5.54	24.51	60683.38	28.28	1.34
16	DM9/18	16.40	352.44	5.81	7.94	27.19	60801.41	32.49	1.43
17	DM14	11.62	326.90	4.29	3.42	23.21	50693.93	26.25	1.31
18	DM19	15.12	775.00	3.53	4.55	34.82	76136.81	54.78	1.68
19	DM10/21	20.68	57.50	5.36	22.14	16.66	39800.08	8.99	1.43
20	DM11/22	11.18	231.90	4.79	2.78	29.04	61898.64	31.80	1.28
21	DM13/28	10.44	64.59	5.23	2.21	14.96	40241.12	12.01	1.45
22	DM12/25	13.04	259.63	5.31	4.87	22.11	56672.97	24.60	1.56
23	DM34	9.05	348.35	4.26	3.06	39.39	81193.22	43.89	2.05
24	DM39	9.44	196.72	3.06	3.54	16.34	40144.32	18.67	0.87
25	DM41	9.37	220.69	4.02	3.66	17.35	44079.21	20.28	0.97
26	DM2/3	12.34	226.93	5.63	5.13	21.28	51604.76	21.76	1.40
27	DM10/20	20.85	202.34	4.54	7.82	17.99	38585.49	21.08	1.44
28	DM11/23	10.73	189.41	6.30	26.90	21.86	52586.53	22.55	1.26
29	DM12/24	20.28	150.23	5.11	4.52	15.86	38010.07	15.74	1.49
30	DM12/26	10.97	243.53	4.72	4.05	20.34	51450.62	21.87	1.12
31	DM13/37	6.17	247.49	4.48	22.15	29.16	68261.92	37.94	1.60
32	DM130	9.24	403.91	3.44	27.40	36.60	65302.53	35.60	1.79
33	DM31	24.21	103.88	7.18	15.17	19.22	48133.35	17.57	2.04
34	DM32	13.90	119.83	8.20	4.05	17.30	46412.89	18.65	1.83
35	DM33	16.17	132.43	4.02	4.67	14.39	38860.75	14.72	1.41
36	DM35	22.23	144.42	4.80	6.91	13.04	31357.68	14.76	1.33
37	DM36	11.14	262.34	4.78	4.35	20.62	52397.73	24.11	1.15
38	DM37	15.43	129.84	5.47	6.10	13.06	32863.20	13.22	1.33
39	DM38	10.20	260.58	5.23	3.22	22.36	53373.19	26.68	1.10
40	DM40	13.95	294.17	5.85	4.29	26.16	61578.01	29.08	1.41
41	DM41	10.16	263.94	4.91	3.77	27.83	59557.36	32.82	1.28
42	DM42	11.13	183.26	5.76	26.62	21.93	53067.60	22.62	1.37
43	DM43	11.10	231.15	3.60	4.16	19.20	47171.70	21.94	1.03

Table 10.4.3

1	SK1	21.85	359.74	5.97	6.88	15.21	38381.80	20.31	1.65
2	SK2	14.23	108.62	4.09	3.99	10.24	25053.02	10.52	1.02
3	SK3	28.97	274.70	3.69	7.35	19.10	40662.17	19.95	1.51
4	SK4	18.79	126.76	4.50	5.82	12.61	35806.95	15.91	1.03
5	SK5	10.68	322.47	4.92	2.01	22.61	53677.83	30.71	1.26
6	SK6	12.34	158.13	4.96	7.38	20.53	47546.18	24.18	1.29
7	SK7	15.16	40.33	5.28	6.76	8.68	24135.63	8.55	1.03
8	SK8	18.67	46.56	7.90	7.50	10.19	27762.64	6.82	1.21
9	SK9	19.69	62.36	5.43	2.65	13.92	34762.96	9.11	1.44
10	SK10	2.47	130.05	0.47	102.64	51.22	76695.64	75.49	0.89
11	SK11	20.02	44.92	6.70	4.28	11.49	31223.09	8.15	1.48
12	SK12	20.36	64.41	6.75	3.46	11.52	39777.21	7.29	0.91
13	SK14	16.30	51.72	4.32	6.30	9.90	26300.85	7.97	1.04
14	SK15	11.91	115.77	7.98	9.32	26.08	48370.03	18.17	1.84
15	SK16	22.33	37.65	5.81	7.40	11.05	32298.49	6.80	0.85
16	SK17	19.36	43.03	5.81	8.12	9.11	23191.40	5.19	0.94
17	SK18	14.34	40.66	6.74	1.70	33.53	67725.13	3.04	0.59
18	SK19	20.99	64.28	6.18	1.65	26.75	66456.14	5.60	0.66

to have originated from the local Dimini group. (Another sample, SK1 has a probability of 25%), Fig. 10.4.2. Fig. 10.4.3 shows the Sesklo cluster analysis and Table 10.4.3 shows the analytical results. The cluster SO2 - S15 is characterised as the local Sesklo group. This local group, when compared with the Dimini non-local group reveals that there is a high probability for 5 sherds from this non-local Dimini group to have originated in Sesklo, (namely, DO8 - 45%; DO9 - 87.6%; D10 - 62.9%; D19 - 84.4% and D35 - 52.5%), Fig. 10.4.4. However, it must be noted that although the clays which were sampled were of "local" origin, there could probably be other clay sources from either site forming cluster groups such as: DO1 - D18; DO4 - D38; D11 - D42; for Dimini and SO1 - SO5 for Sesklo, which were not sampled, and which could have been used in the making of pottery. In particular, from the non-local Dimini pottery samples, D10 gave a TL age of 4240±420 BC and DM35 a TL date of 3571±331 BC. (The others were not dated). The above TL dates correlate with an existing Sesklo during the Middle Neolithic period as indicated by the date of the Sesklo kiln which was 4143±330 BC and the corresponding date of Late Sesklo pottery of 3582±247 BC. This suggests that there was an apparent overlapping of these two Neolithic cultures and this implies possible intercommunication (social mobility or economic relations). Nevertheless, the NAA interpretation, as it concerns the derivation of clays does not alter the conclusion that there was cultural interaction between the two settlements, which is partially supported by the geomorphology of the area (Fig 10.4.5) (See also Fig. 10.8 end of Chapter, showing characteristic clay jar from this Late Dimini period).

Further tests were attempted by XRF and TSA on some pottery from both sites.

Fig 10.4.4

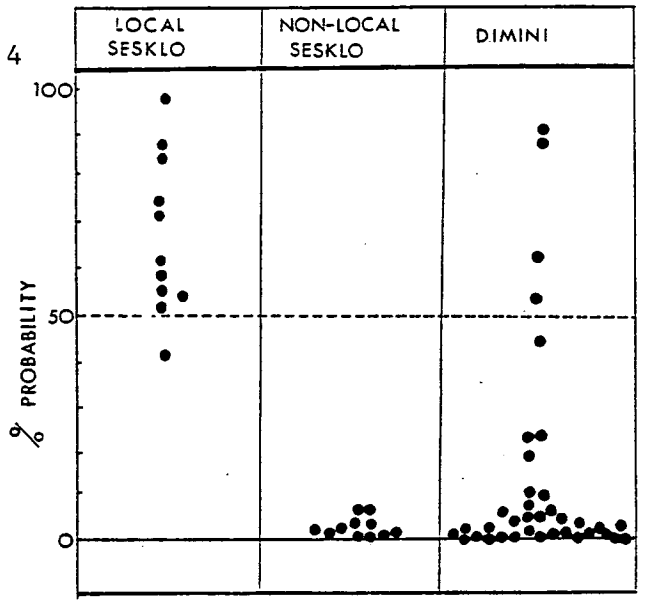


Fig 10.4.2

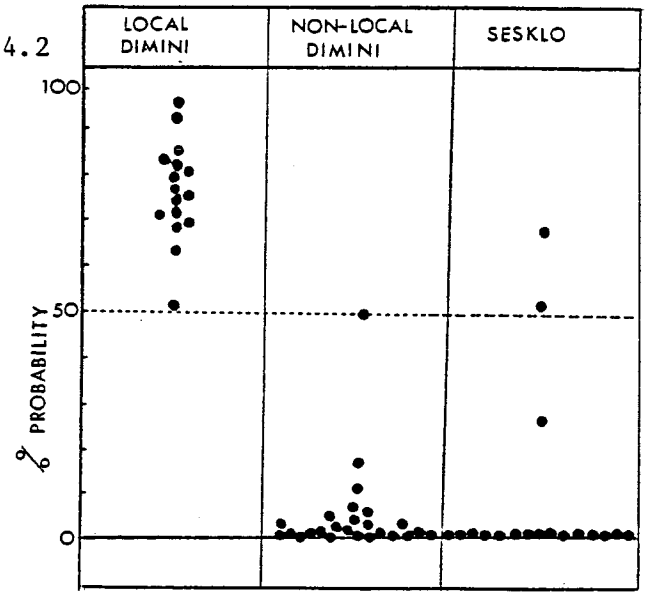


Fig. 10.4.4 Dimini pottery as compared to Sesklo pottery. Probability Evaluation based on Mahalanobis D^2 Statistical Analysis for Th, Cr, Hf and Co.
Fig. 10.4.2 Sesklo pottery as compared to Dimini pottery. Probability Evaluation based on Mahalanobis D^2 Statistical Analysis for Th, Cr, Hf, Cs, Fl, Fe, Co and Eu.

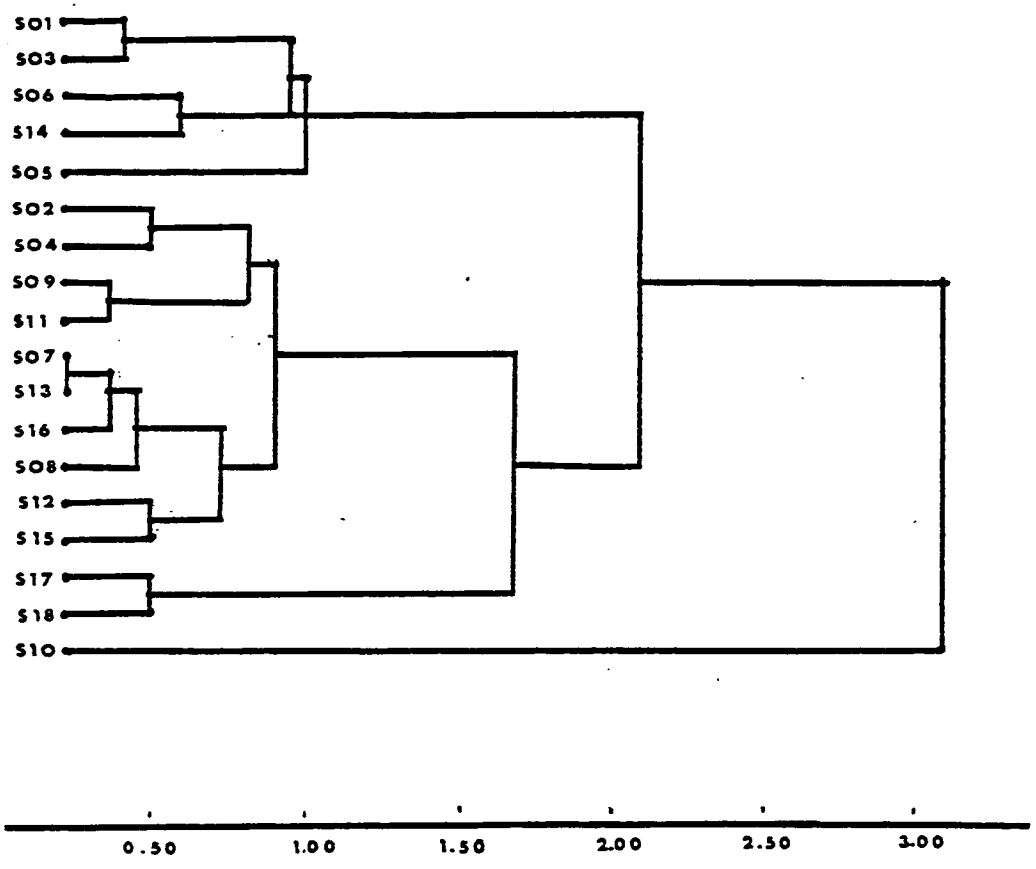


Fig. 10.4.3 Maximum distance Clustering diagram, with 8 elements, for NAA analyses of pottery and clays from Sesklo.
SO2 - S15 is Sesklo's main local group of potsherds and clays.
The lower axis scale represents the dissimilarity level.

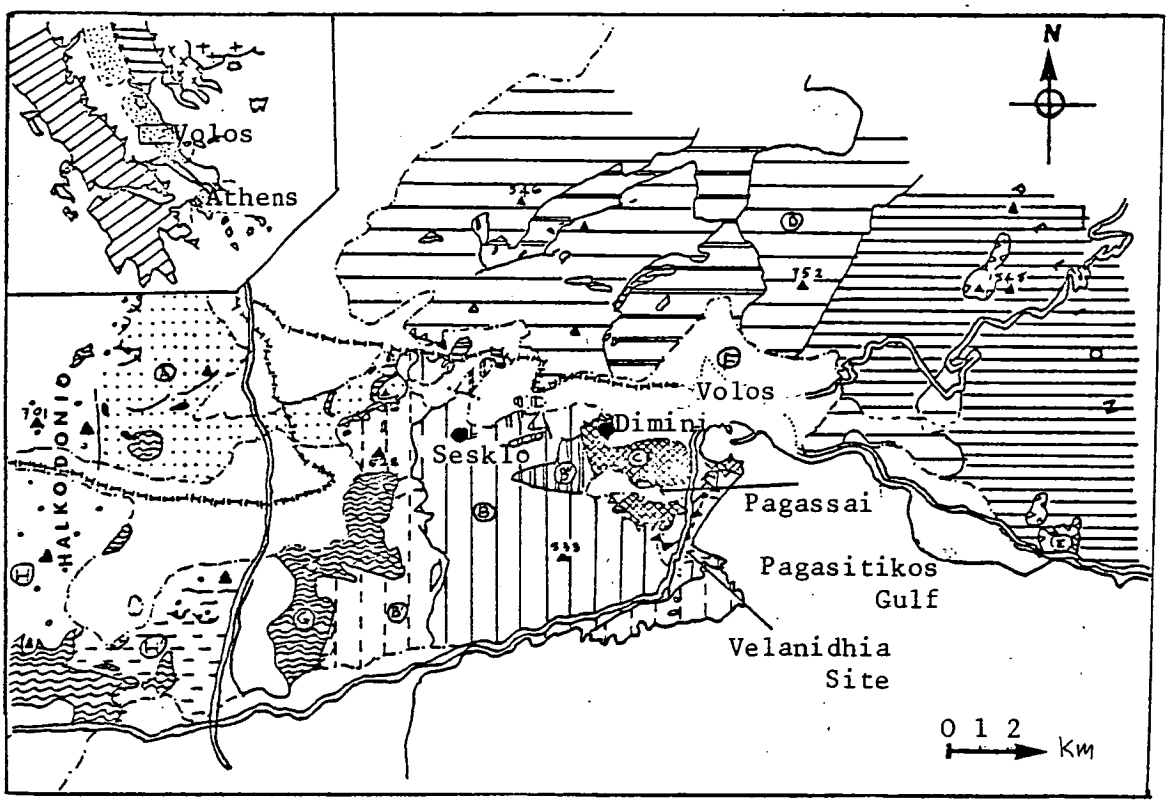


Fig. 10.4.5 Geological sketch-map of the Volos Region after Ferriere (1976). Sesklo and Dimini lie near the "boundary" between the Pelagonian and Sub-Pelagonian Tectonic zones of Mainland Greece.

A - Rudist marbles, upper Cretaceous conglomerates with igneous detritus. Sandstones and shales; B - Feldspathic schists (meta-arkoses); B' - Marbles and schists; B'' - Marbles; C - White marbles; yellow schists with Radiolaria; cherts and volcaniclastic sediments; D - Schists and marbles with overlying probable upper Cretaceous Flysch; E - Tectonic contact; F - Alluvium sediments; G - Serpentinized ultramafic rock; H - Schists; H' - Crystalline limestones. H and H' - western sector.

10.5 X-Ray Fluorescence Analysis

18 samples were analysed for ten major elements. By plotting each element (as percentage amount), we derive comparative columns concerning their similarities, Fig. 10.5. The mean average of each group is taken to indicate their degree of spread. Though differences in these groupings are abvious within the statistical error of the spread of values which is supported by the complex geomorphology of the area, the elements constituent for XRF does not seem to discriminate well between pottery from Sesklo and Dimini; in contrast with analyses made by others such as F. Schweizer (1971).

However, there are some samples from either site which are more than 1σ out from their respective mean value and which correlate with groups from the opposite site. These samples could well have derived from clay sources of their opposite site. Moreover, despite some indications of such a distinction, the results are not conclusive. In particular, with the DM35 potsherd, NAA has shown that it most probably derived from the "local Sesklo group", XRF appears to substantiate this assumption, though it is itself not an objective determinant.

10.6 Thin Section Analysis

Thin Section Analyses were made on characteristic samples (based on the NAA results and TL dates), such as clays and pottery, belonging to different periods, with the aim of studying the technology of the making of the pottery or the pinpointing of the different clay sources. Table 10.6, lists the samples analysed and their location.

All samples have a broadly similar, and quite restricted range of rock fragments in them.

The original sediments (according to Dr. J Dixon, Geology Department, Edinburgh University), were coarse grained and contained fragments of

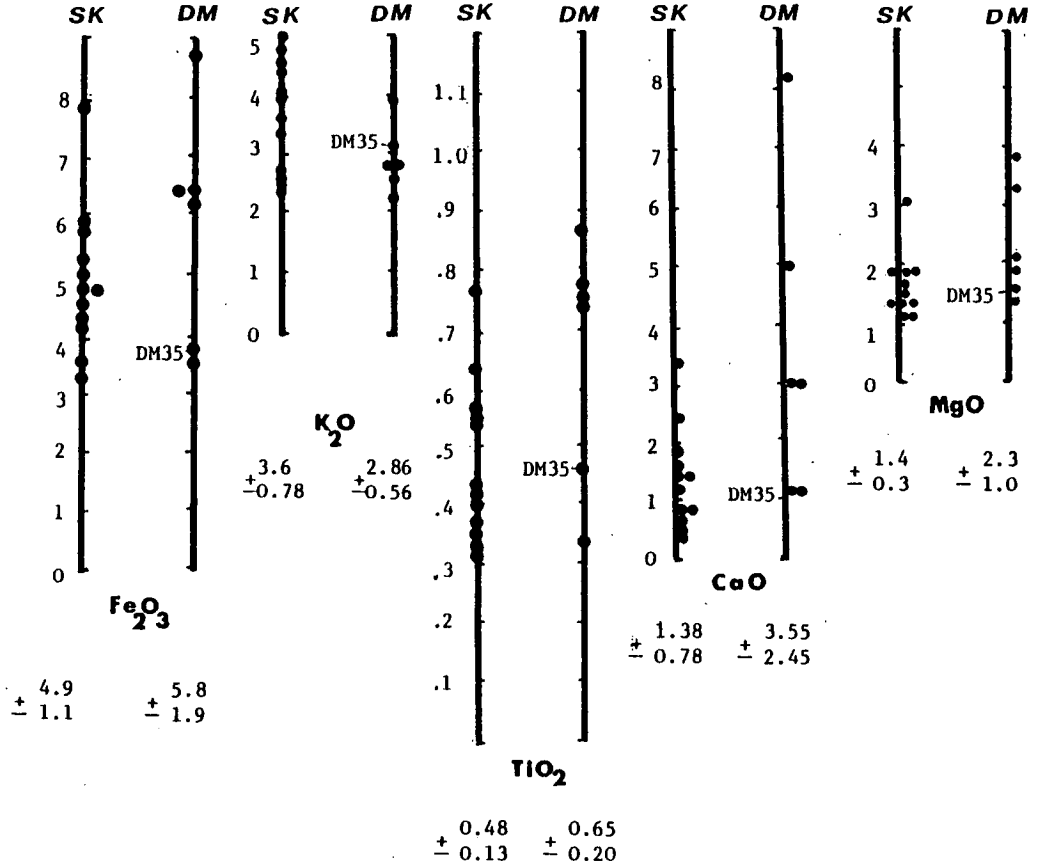


Fig. 10.5 Comparative Comumns concerning similarities between the Sesklo and Dimini pottery samples, analysed for their major elements by XRF.

quartz, plagioclase feldspar, potassium feldspar (orthoclase); so that some of the present rock fragments are either all quartz (common) or quartz with larger angular feldspar fragments and individual feldspar grains, (main grain constituents that the "inclusion dating" was based upon, Chapter 9).

10.6.1 Differences and Similarities

i) All samples with the exception of SKE6 contain some grains with a distinctive "fine grained quartz" texture, shattered at the boundaries of larger quartz grains. These grains are present in all the clay samples and in DM11 (kiln), Fig. 10.6.1 illustration DM35 and SK3.

ii) SK3, SK4, SK18, SK19 and DM 11 have a virtually identical rock fragment content where "fine grained quartz", feldspar and mica also occur, Fig. 10.6.1, illustration SK3.

iii) DM35 and SK6 are very similar to the first group and differ only in having generally larger and uniform fragments. However, such difference is certainly not significant in terms of provenance, Fig. 10.6.1, illustration DM35.

iv) DM41 and DM9/17. Although similar to the other groups, they contain a somewhat distinct range of rock types. They contain coarse and fine grained sediments, showing little trace of deformation and also some very fine grained tightly folded micaceous sediments, Fig. 10.6.1, illustration DM9/23. DM41 has also calcitic fragments of unknown origin.

v) DM11/23. It is transitional in "character" between all the preceeding samples and SKE6. It's rock fragments are coarser and much less stained. Grains are flattened, but generally have clearly defined boundaries. This sample was found in the same

house N of the settlement, with the DM11/22. The latter gave a TL date of c.4700 BC, or, at the transitional period from the Middle to the Late Neolithic periods, Fig.9.15

vi) SKE6. This differs in that it shows an even greater degree of textural equilibrium than DM kiln, with sharp grain boundaries. The fragments are even more tabular than DM samples, with rectangular quartz grains and prominent micas, Fig. 10.6.1, illustration SKE6.

From the above, the greatest "extreme" is between the early Sesklo pottery fragment SKE6 and the local Dimini ones.

There is a distinction between the filler in local Dimini and local Sesklo and this probably reflects a general convergence of sand composition in an area of such a geological complex, Fig. 10.4.5.

In the making of pottery it is more difficult to find suitable clays rather than sands for use as a filler; bearing in mind that the NAA groupings relate to the clay matrix and also the sands are similar, (and quite variable in the same way), in both Sesklo and Dimini.

Though the differences between the textural "groupings" identified should not be overemphasised, due to the complex geomorphology of this area, the variety of features at different periods implies different technological stages.

However, the above are conclusions supported to some extent by archaeological evidence concerning the style and technology of pottery making during these Neolithic times. The difference there appears to be only in some kinds of design due probably to the casting structures, Chourmouziades, (1979).

Fig. 10.6.1

Photomicrographs of Thin Sections of potsherds from Sesklo and Dimini. Each photograph covers an area of approximately 2 x 1½mm.

The five examples are approximately in order or increasing degree of metamorphic recrystallisation and annealing of cataclastic (Mylonitic) fabrics.

DM9/17 (Left) Large grain of fresh feldspathic arkose showing a weak fabric with very little undulose extinction or grain boundary granulation. (Right) A quartz grain showing irregular suturing of grain boundaries due to deformation.

DM35 Two typical quartz-rich rock fragments. The left hand larger one shows no clear grain boundaries and irregular areas of undulose extinction due to massive concentrations of dislocations. Fine grained micas lie to each side of the central quartz area. The right hand grain shows the same irregular extinction pattern cahracteristic of strongly deformed quartz grains.

SK 3 Large grey fractured fragment of orthoclase feldspar with attached quartz grains (left centre) and a curved quartzose fragment (upper right) showing the distinctive fine undulose texture of poorly annealed mylonites.

DM11 - 23 Quartz-mica-'schist' fragment showing generally tabular quartzes, thin micas parallel to the flattening plane, but generally uniform extinction in individual quartz grains in contrast to the quartz in SK 3 and DM 35.

SK E6 Quartz-mica-'schist' fragment showing very pronounced tabular shape overall, as well as of the quartz grains themselves. Large mica flakes (speckled appearance) lie along the bottom edge and to the left of the centre and are much coarser than any in the other samples.

ILLUSTRATION DM9/17

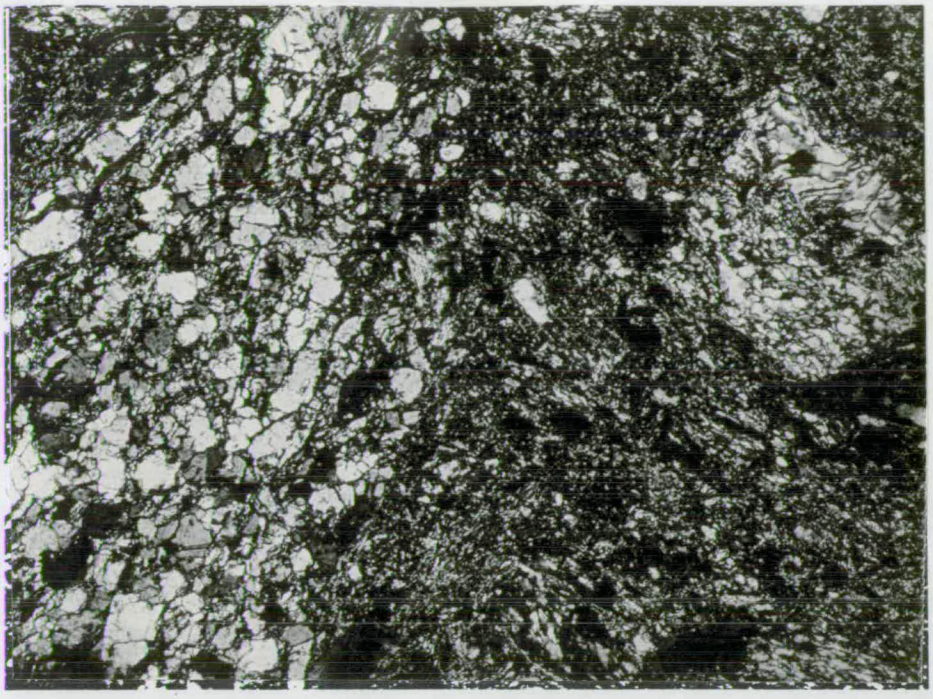


ILLUSTRATION DM 35

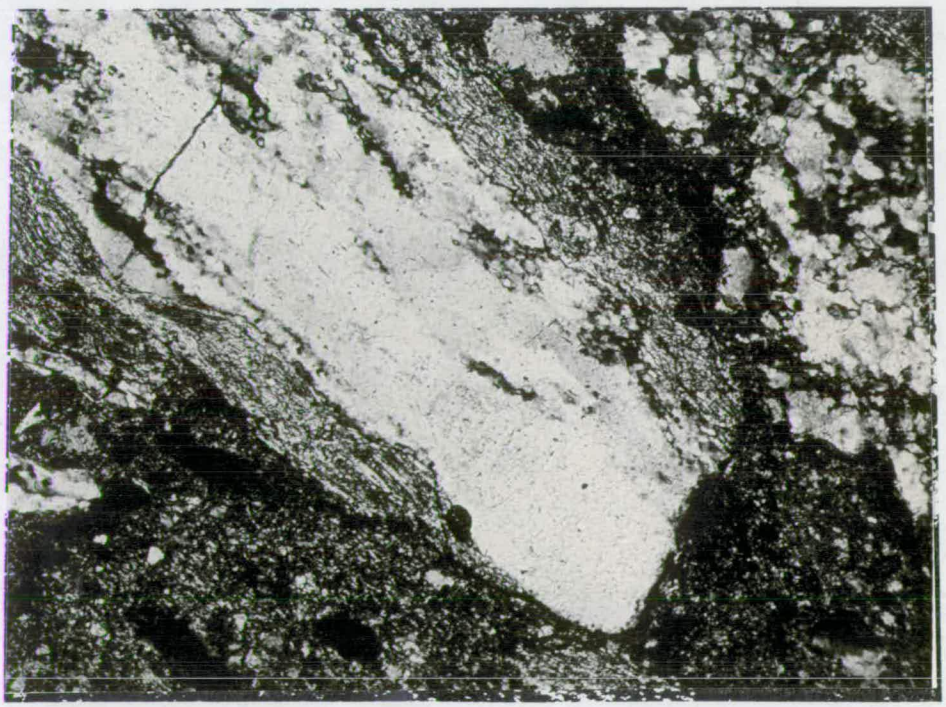


Fig.10.6.1

ILLUSTRATION SK3

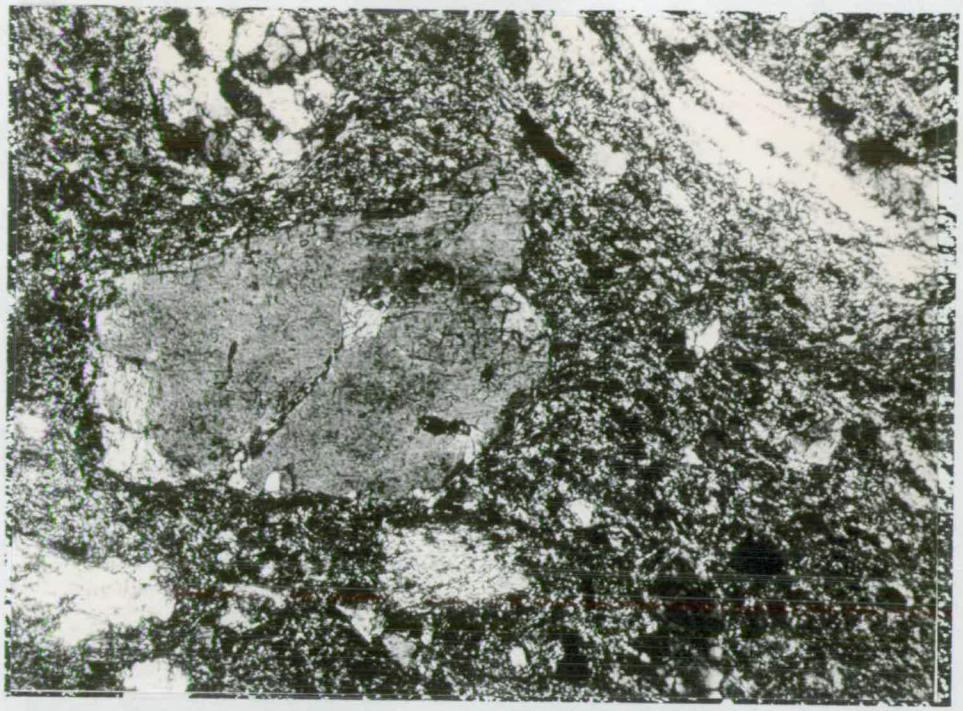


ILLUSTRATION DM11/33

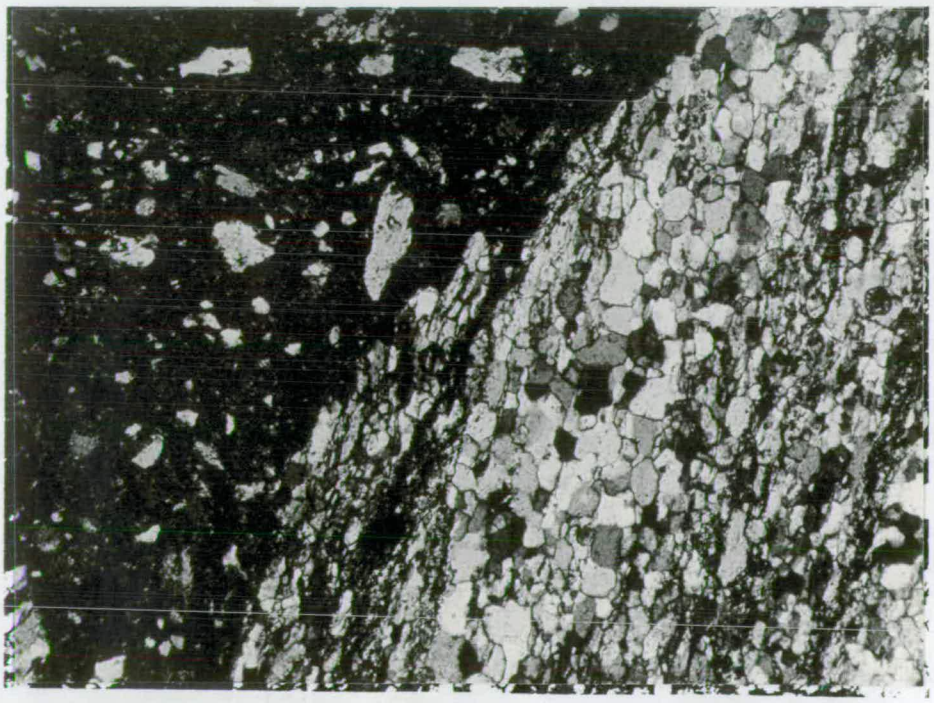


Fig. 10.6.1

ILLUSTRATION SKE6

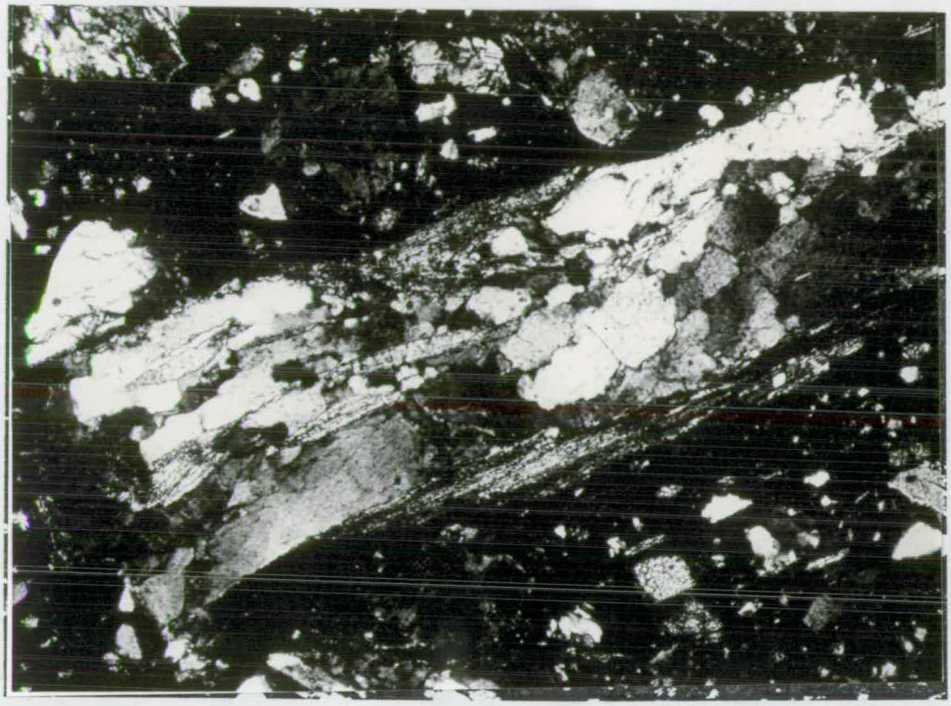


Fig. 10.6.1

Taking into account the cultural overlapping between these two settlements as found by TL dating, and NAA, (Liritzis, McKerrell, 1978), one more point which can be put forward from the above analysis, concerning the technology in the making of pottery is that in Middle to Later Neolithic was somewhat similar (with one exception, DM11/23, at the transitional stage) while it contrasts with the raw materials and rock fragments used in earlier times.

10.7 Conclusions

As c.4100 to c.4700 BC is the period when the last part of Middle Sesklo and the beginning of Late Dimini overlapped; which was clarified chronologically by TL (Chapter 9); a possible intercommunication between these two settlements could be most credible during this time. This assumption has been tested and given some support by NAA, XRF and TSA.



10.8. A Clay vase from Dimini, of the Late Neolithic period, c. 4150 - 3000 BC. Vases of this period belong to the "Dimini Style" and display characteristic zigzags, meanders and spiral designs.

PART V

URANIUM/THORIUM SPELEOCHRONOLOGY

(Nuclear Instrumentation, Chemical Procedures and Dating Method)

The work which has been undertaken in the following two chapters concerns dating investigations on a controversial early human fossil found in Petralona Cave Greece. Till now there have been no serious attempts to study this speleoenvironment, by radiometric dating and analyses, and to relate the existance of many calcitic depositions (all over the cave) to different geological epochs and archaeological phases.

The present study has three advantages over previous work on this cave:

i) the samples were collected by the author and, therefore, are directly related to the problems in question,

ii) the samples come from important places in the cave in relation to the skull,

iii) though the principles of the U/Th dating method for pure calcitic materials have been well established, the detrital state of the samples used for such an important site, creates serious difficulties in the determination of the age. Therefore, the present application is an extension of the method for contaminant material with particular emphasis being given to possible correction modes of the uncorrected ages obtained.

CHAPTER 11

NUCLEAR INSTRUMENTATION AND CHEMICAL PROCEDURES OF U/TH DATING METHOD

11.1 Speleothem Deposits - Description and Mechanisms

The most common speleothem forms - stalagmite, stalactite, flowstones and travertines - are developed by precipitation of calcium carbonates. Such deposits tend to be macrocrystalline, compact and not subject to post-depositional leaching, Hill (1976). Pure calcite speleothems with well-preserved internal stratigraphy can be reliably dated by the ratio of Th-230 to U-23 4 (the Uranium content may range from 10ppb to 10ppm.)

The precipitation of calcium carbonate is brought about:

i) by diminution in the amount of atmospheric carbon dioxide present

ii) by evaporation of water

iii) by bacterial or organic action and presence of certain ions.

In (i), if the partial pressure of the carbon dioxide dissolved in water is lower than the partial pressure of the free atmospheric carbon dioxide, the solution is not in equilibrium and calcium carbonate is precipitated. If the partial pressure of the dissolved carbon dioxide is greater than that of the free carbon dioxide, the water will attack and dissolve calcium or limestone. Dissolution of calcium carbonate is shown by the general equation

(1) $CaCO_3 + CO_2 + H_2O \rightleftharpoons Ca(HCO_3)_2$ (calcium bicarbonate)

Condition (ii) (that is, evaporation of water), is fairly signficant in the precipitation of calcium carbonate. However, in most caves where the cave atmosphere is already

saturated with a relative humidity near 100%, little evaporation can occur and thus little calcite can be deposited through this process. (for condition (iii) see (e) below). Some speleothems are described as follows:

A) Dripping and Running Water Forms of Calcite Deposits

These are best known speleothems and include stalactites and stalagmites as in Fig. 11.1. Stalactites also occur in the form of curtains, long, continuous sheets which hang from cave roofs. These are flowing, not dripping water deposits.

Stalagmites are more varied than stalactites because they are built up from the floor. In most cases water falling from the roof contains a high level of calcium bicarbonate. As the water falls evaporation takes place and the drop reaches the floor again super-saturated. When the drop reached the ground it spreads out radially. Many successive fallen drops form the candle-like shape dictated by gravitational forces.

Generally, the growth of stalactites and stalagmites depends upon a great variety of conditions some of which reflect changes in climate or changes in the rate of water seepage and flow within the cave.

B) Flowstone and Rimstone Deposits

Water flowing down the walls of caves or over the floor gives rise to flowstones in which the crystals are orientated perpendicular to the surface of deposition. The surface is usually smooth (irregularities form rimstones). Calcite is deposited where water runs over a ledge or a projection where carbon dioxide is lost. Flowstone formed in caves is normally crystalline **usually layered** or bedded. When it occurs in substantial deposits it is known as travertine, frequently

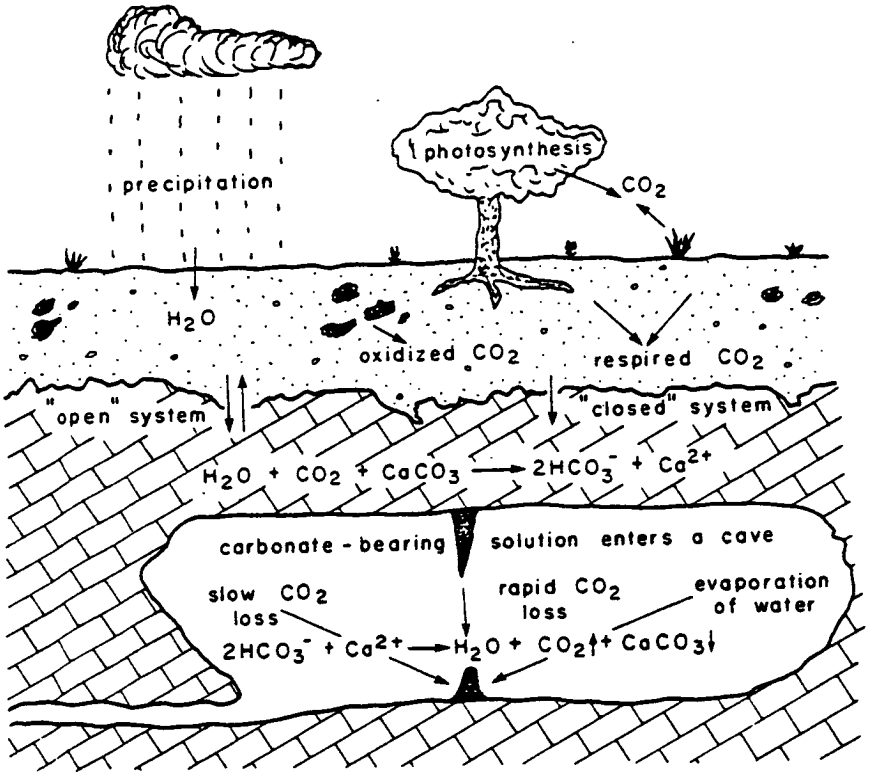


Fig. 11.1 Schematic diagram of the process leading to the deposition of carbonate speleothems in caves (after Hendy, 1971).

related to inter-glacial periods. Under these flowstones a plethora of human implements are frequently found.

C) Seepage Deposits

These are irregular stalactites

D) Deposits Formed in or Under Water

Some speleothems form under water, growing from the walls and floors. When the pools drain away these remain as witness to the former occupation of static water in the cave. At present submerged stalagmites could provide us with useful information about sea-level fluctuations in the past through dating by the Uranium/Thorium method. In some very dry caves rafts of calcite crystals form on the surface of standingppools of cave water. These are very thin layers supported by surface tension and easily disturbed.

E) Micro-Organism Factor Contribution

Rock-milk or moon-milk occurs either as white paste or as a soft crumbly powder or chalky substance on cave floors, walls and fissures. Moon-milk is thought to form through the disintegration of limestone by micro-organisms. It is possible also that freezing of limestone may produce a milky rock fluid due to the expulsion of carbon dioxide as the rock is frozen.

11.2 Geochemistry of Uranium/Thorium

Although chemically similar, certain elements of the actinide series exhibit important differences. Uranium has many oxidation states U(3+, 4+, 5+, 6+). Thorium and protactimium do not have the 3+ valence. Uranium and Thorium are present in the 4+ valence state in primary igneous materials. The unique chemical properties of U relative to Th can be related in a fundamental way to the two extra electrons that U has in the inner, unfilled (sf) electron shell. However,

during weathering in oxidising environments U is readily oxidised to U+6 and combines with oxygen to form the Uranyl ion UO_2^{2+} which forms several soluble complexes which is markedly different (chemically) from teravalent Th^{+4} , Thurber, (1964). Because of its high ionic potential Th+4 ions are quickly absorbed or precipitated as insoluble hydrolysates when brought into solution, Adams et al, (1959). Thus, there is a strong depletion of Th with respect to U in ground waters as a result of differential mobilization during weathering of terrestial rocks. This results in the wide variations of the Th/U ratios shown by surficial material and this is readily obvious when comparing the crustal (U/Th = 1/4) and oceanic (U/Th = 200/1) ratios, Koczy, (1954). Once present in the marine environment, U in aqueous solution is subsequently co-precipitated with carbonate sediments, whereas Th is incorporated into detrital oceanic sediments, Piciotto and Wilgain, (1954), Sackett, (1958). Thus, the average marine limestone contains about 2ppm U and less than 0.1ppm Th, Adams et al, (1959). Following lithification, diagenesis, uplift and subsequent exposure U and Th may be remobilized. As before, U tends to form soluble aqueous complexes and is transported in solution, whereas Th, with its strong affinity for clay minerals (hydrolysates) is quickly removed from solution. During weathering process U isotopes may be fractionated (see also Section 12.4.3), U-234 being enriched in ground waters with respect to its parent U-238. This is attributed to two factors:

i) the change in oxidation state from U-238 to U-234, Koide and Goldberg, (1963)

ii) the increased mobility of the radiogenic daughter products Th-234 and U-234 which occupy radiation-damaged lattice sites as a result

ofalpha recoil-induced displacement within the crystal lattice, Ku, (1965), Kaufman et al (1969) and Kigoshi (1971).

This enrichment of U-234 in natural systems during weathering was first recognised by Cherdyntsev et al (1965). Later, Thurber, (1962, 1964) demonstrated that the U-234/238 ratio of the oceans is constant at 1.15± 0.02, but Isabaev et al, (1960), Thurber, (1964) Kronfeld, (1971) and Thompson et al (1975) have shown that the ratio for fresh water is highly variable going up to 12.2, although most measured values fall within the range 1.3 - 3.0. Once U is in solution, in ground waters, within a carbonate terrain, it is transported as the very soluble anionic complex $(UO_2(CO_3)_3)^{4-}$. (in small concentrations usually 1µg/1t).

In a cave, U-bearing seepage waters may become supersaturated with respect to calcite due to the dissolution of carbon dioxide, ultimately resulting in the precipitation of a calcite speleothem containing a finite amount of U. The exact mechanism of U incorporation in the speleothem calcite is not well understood. The removal of carbon dioxide may cause dissociation of the Uranyl carbonate in to UO_2^{2+} and carbon dioxide with the Uranyl ion subsequently incorporated into the calcite lattice; or the whole Uranyl complex may be directly co-precipitated into the calcite. In addition, U^{4+} ($r=0.99A^{o}$) and Ca^{2+} ($r=0.95A^{o}$) have similar ionic radii and U^{4+} will therefore be fairly easily accommodated in the calcium carbonate lattice. The UO_2^{2+} (U^{4+} after being released from the host igneous rock and oxidised to U^{6+} forms UO_2^{2+} which is very soluble), with its awkward shape is presumably less easily accommodated. This conclusion is supported by the study of Kolodny and Kaplan (1970) who showed that U^{4+} is preferentially incorporated into phosphorites and is presumably substituting for the Ca^{2+} ion.

In either case the secondary calcite speleothem forms a U-bearing, Th-free

system with a U-234/U-238 ratio similar to that of the parent waters, Thompson et al, (1975). The concentration of U, incorporated into a calcite speleothem depends on many factors including the U content of the parent solution, the extent and rate of carbon dioxide exsolution during deposition and the geomorphological properties of the depositional environment. U concentrations in speleothems have been found to range from approximately 10ppb to 100ppm, Harmon et al, (1975), Harmon (1975).

11.3 Th-230/U-234 Dating Method

All the nuclides involved in this method are members of the U-238 series, Fig. 3.2.1b. This method is valid if we consider the following hypothetical case: the Th is not present in the carbonate speleothem at the time of deposition, and thus the Th-230, subsequently found to be present in the speleothem, is precisely equal to that which has grown into equilibrium with the U isotopes, U-238 and U-234, initially present.

Th-230 isproduced from the decay of U-234 and its parent nuclides Th-234 and U-238. (U-234 has two origins, i.e. U-234 authigenic from U-238 as previously stated, and U-234 which is non-supported or in excess, commonly plentiful in natural waters), Let us assume that at an instant in time, t=0, the radionuclide U-238, isolated from its daughter products, and U-234 which is in excess, start to decay. Specifically speaking, this is the time when a speleothem starts to form and the above two incorporated U isotopes are co-precipitated with the calcite deposition, whereas Th is rapidly incorporated into detrital clays , Piciotto and Wilgain, (1954), Sackett, (1958). Then the "radioactive decay clock" is set to zero from the time when Th-230 is produced, with a decay rate, from U-238 and

U-234 in excess. The rate of Th-230 production in this deposit, in which Th was initially absent, is then given by the expression:

$$(1)\quad \left[\frac{\text{Th-230}}{\text{U-234}}\right]_t = \frac{1-e^{-\lambda 230 t}}{\left[\frac{\text{U-234}}{\text{U-238}}\right]_t} + \left(\frac{\lambda_{230}}{\lambda_{230}-\lambda_{234}}\right)\left(1-\frac{1}{\left[\frac{\text{U-234}}{\text{U-238}}\right]_t}\right)\left(1-e^{-(\lambda_{230}-\lambda_{234})t}\right)$$

where $\left[\frac{\text{Th-230}}{\text{U-234}}\right]_t$ and $\left[\frac{\text{U-234}}{\text{U-238}}\right]_t$ are the measured activity ratios at time t and $\lambda 230$ and $\lambda 234$ are the respective decay constants of Th-230 and U-234.

A graphical solution of equation (1) for various values of (t) and $\left(\frac{\text{U-234}}{\text{U-238}}\right)_0$ has been constructed, Schwarcz et al, (1979), Fig. 11.3.1.

Any Th-bearing detritus minerals inside the carbonate host, or present as surface coatings, will result in a h igh obtained age, because of the presence of non-radiogenic Th-230.

Because this detrital Th-230 is always accompanied by Th-232, a rough correction for the detrital component has to be made. This is fully explained in Section 12.5

The Th-230 half-life of 75000 yrs (Atree et al, 1962), gives the Th-230/234 method a range of about 350000 - 450000 years, depending onthe type of material analysed..

11.4 Suitability of a Speleothem of Archaeological Significance for Dating Purposes

The suitability of a speleothem for dating purposes, depends on many factors. Providing that it is associated with archaeological material, the following considerations must be taken into account and checked:

i) the "degree of purity" of the speleothem. Impure substances, commonly called detrital, for example, organics, biological activity, soils, etc., incorporated during the creation and growth of the speleothem, cause discrepancies: in particular, large traces of contamination with apatite $Ca_5(Cl,F)(PO_4)_3$.

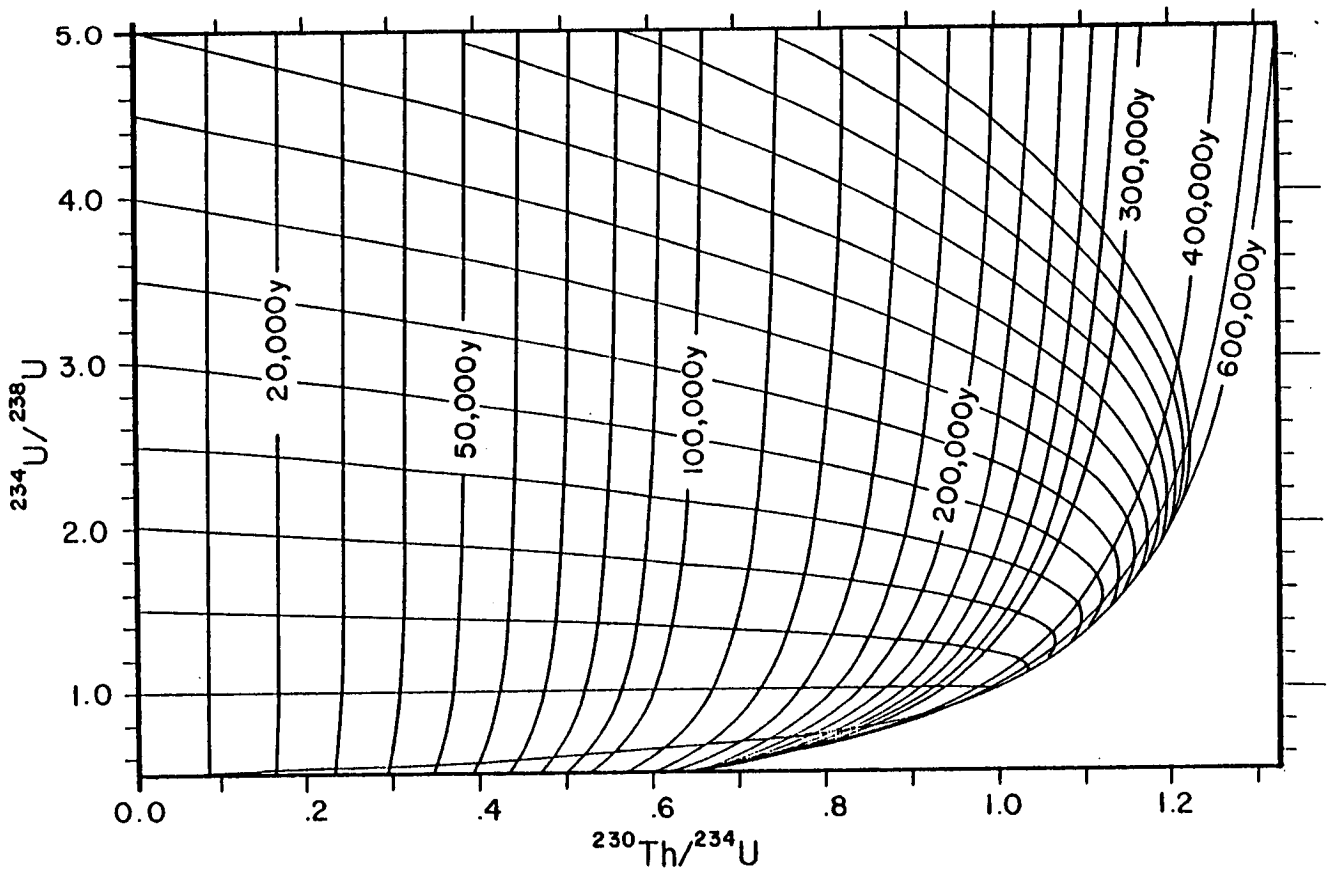


Fig.11.3.1 Relation between Th-230/U-234 and U-234/U-238 Ratios for samples of constant age: Isochrones are steep curves labelled "20,000y" etc. Horizontal curves are loci of evolution of closed systems with initial U-234/U-238 ratios given by Th-230/U-234=0 intercepts of curves.

from the bones.

ii) "soil zones" could be indicators of palaeoclimatic changes and calcitic growth. This soil contamination contributes U and Th to the already existing radionuclides in the calcite, thus giving an erroneous dating result.

iii) any sign of post-deposition, submersion or resolution

iv) The condition that speleothems start to form with U isotopes (Th free), that is, assumption of the "closed system", or, at the time of formation the ratios Th-230 and Ra-226 to U-234 are negligible. This can be checked by the presence of Th-232.

v) No nuclide from U-238 to Ra-226 in the U series entered or left the sample since the time of formation (or within a negligibly short time thereafter). Here, since Ra-226 is an alkaline earth, as is calcium, it might be expected that it would be incorporated into the $CaCO_3$ crystal in substantial amounts, whenever carbonates are formed. Seepage waters would leach Ra-226 appreciably. Deficiency or excess of Ra-226 has been observed in shells, Kaufman, (1964), due (i) in the case of deficiency: to rainfall seepage waters, since the alpha recoil energy phenomenon of the type of bond holding uranium to the surface, might not be the right one for holding daughter products and (ii) if in excess: to secondary U addition or secondary Th-230. Secondary precipitation of $CaCO_3$ would be apparent under the microscope and would probably be in the form of calcite. In this case, the different ions co-precipitated will give different colour in the "growth zones" of a stalagmite or in the subsequent deposited layers of a flowstone or travertine (see also Fig 12.7.4).

However, sulphate ions, if present in high enough concentrations could precipitate radium and barium in greater preference to calcium.

Studying a sample, eg., a travertine, which is exposed for some time to percolating waters in the phreatic zone would mean nuclides from these aqueous solutions might have precipitated on the exposed surfaces. Leaching could also occur.

Since alpha recoil energy is expended every time a Th-230 or Ra-226 atom is generated, the bonds which hold them are weakened and leaching of these nuclides would be enhanced.

Solid state diffusion would be too slow to affect deeper layers in a crystal lattice unless recrystallization occurred, (see (9) below).

Any secondary migration of U inwards or outwards within a speleothem causes problems to arise. These are more serious in marine molluscs than in speleothems, Broecker, (1963).

vi) How the archaeological material in the context is related to the history of the speleothems, for example, bones, tools, etc., embedded in stalagmites.

vii) Sufficient U must be present in the sample to allow for accurate determination of activity ratios in reasonable counting times

viii) The isotopic disequilibrium ratios must exhibit a progression towards secular equilibrium with time and be consistent with stratigraphic relationships.

ix) The sample should show no evidence of re-crystallisation, which might cause loss or enrichment with either U or Th radionuclides. However, this can be checked to some extent by microscopic or X-ray diffraction analyses (see Section 12).

x) The resultant age determinations should agree with ages determined by other methods (if possible) or by intercomparisons with

other laboratories, or at least by following a stratigraphic order.

11.5 Epilogue

The rhythmic changes of successive phases in a speleo-environment, towards the creation of a speleothem, are evidently caused by changes in the external environmental forces. Consequently, studies of cave deposits reflect palaeoclimatic history, the earth's magnetic field variations, chronological classifications of epochs, and archaeological and anthropological interpretations towards man's evolution.

11.6 α - Spectrometer

Alpha-counting spectrometry was used to measure the radioactivity of the chemically purified U and Th from each speleothem sample. The configuration of the equipment used to detect, measure and resolve the U and Th isotopes of interest is shown schematically in Fig. 11.6. The elements of the detector theory pertaining to the present study has been discussed by Thurber, (1964).

For prolonged life the silicon surface-barrier detector (Ortec, 350mm^2) was used with a small applied voltage. The proximity of thesource to the detector (especially during calibration with a mixed source), resulted in contamination of the detector by alpha-particles recoil nuclei thus necessitating periodic monitoring of the detector background.

The configuration of the spectrometer system is typical of that commonly used for high resolution alpha particle spectrometry. Under vacuum, the decay of the isotopes of interest, Th-232, Th-230, U-238, Th-228 U-234 and U-232 produce alpha particles which strike the biased surface barrier semiconductor, with a characteristic energy, Fig. 11.6.1. This signal is analysed to produce a composite energy spectrum. A typical

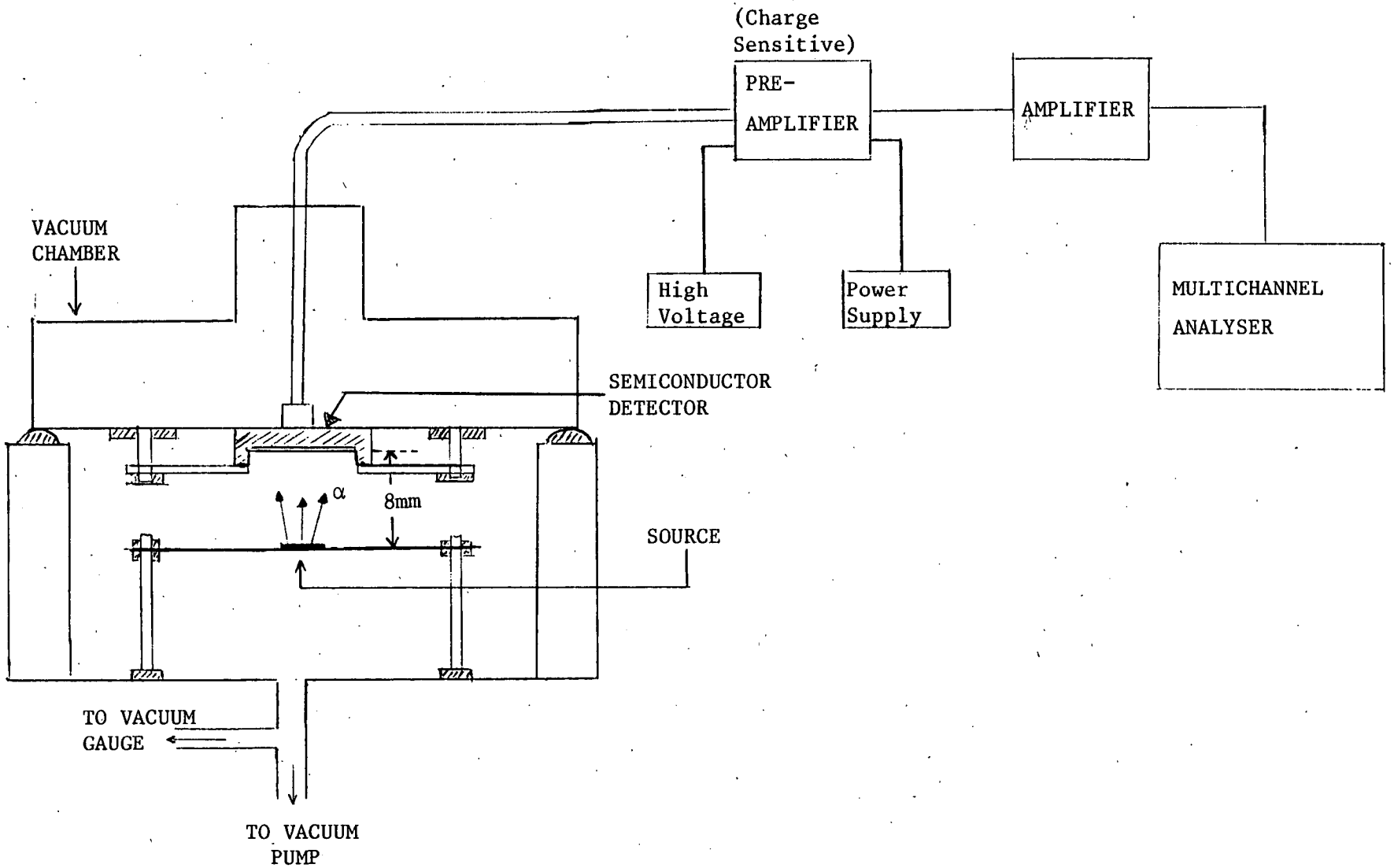
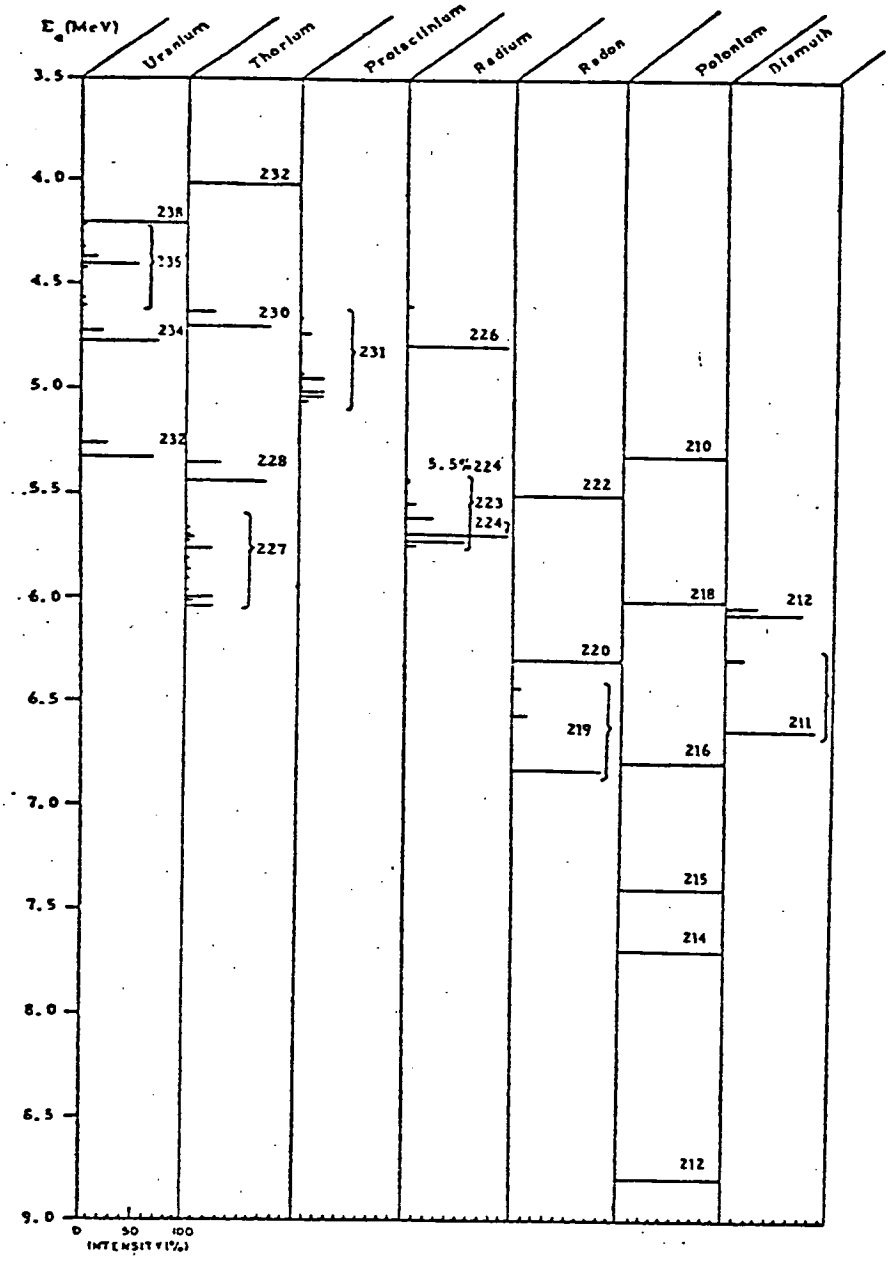


Fig. 11.6 Diagram of Alpha Spectrometer employed in the U/Th Dating Method



Data from: Table of Isotopes, 6th Ed., Lederer et al editors, 1967

Fig 11.6.1 Alpha particle energies of isotopes in the uranium & thorium decay series. (The length of each horizontal bar indicates the percent of monoenergetic α-particles emitted from each isotope) Redrawn from Harmon, (1975)

Th spectrum is illustrated in Fig. 11.6.2. a. The peaks shown from left to right are Th-232, Th-230, the artificial tracer Th-228 and its daughter products Ra-224, Bi-212, and Ra-220. Similarly, Fig. 11.6.2b illustrates a typical U spectrum. The peaks shown from right to left are U-238, U-235, U-234, the artificial tracer U-232 and daughter nuclides Ra-224, Bi-212, Rn-220.

Peak amplitudes are related to the concentration of each isotope present, and these corrected (for background) peak ratios are a direct measure of activity ratios.

The construction of the vacuum chamber and the place of the detector and pre-amplifier is such that the stray capacitance, the microphony and the sensitivity to electric noise is kept at a minimum at the input stage of the amplifier.

After pre-amplification and appropriate shaping the pulses are fed into the multi-channel analyser, operated at the higher conversion range of 512 - 1023 channels, with window width of 4mv/channel. The threshold was set at 0.020 volts to cut off background signals. The pressure was kept as low as 0.02 Torr.

11.7 Counter Calibration and Spectral Resolution

The source used for calibration was a mixed source of three isotopes. which contained the following accurately known nuclides:

Nuclide	Energy (MeV)
Pu-239($t_{\frac{1}{2}}$=24400yrs)	5.16
Am-241($t_{\frac{1}{2}}$=458yrs)	5.49
Cm-244($t_{\frac{1}{2}}$= 18yrs)	5.81

and with nominal activity of 3×10^5 dpm (0.2μCi).

The source to detector distance was 8mm and the resolution was

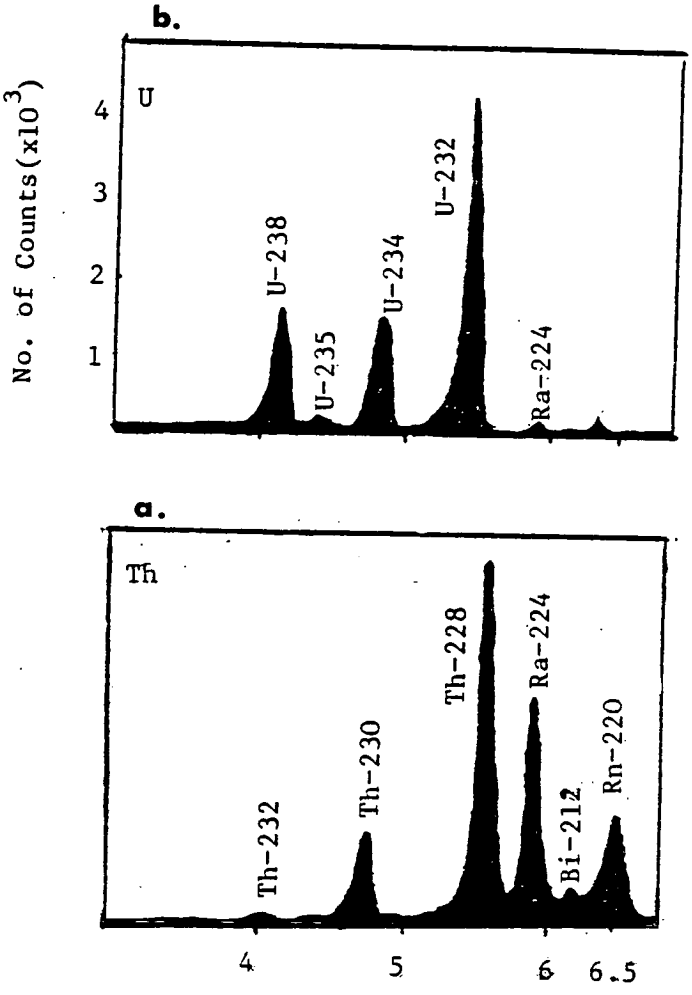


Fig. 11.6.2a.Typical Th Spectrum
b.Typical U Spectrum

0.860% or 47KeV FWHM with counting efficiency of around 10%.

11.7.1 Alpha Spectra

The alpha peaks as in general, were of gaussian shape, but in the low energy part the geometry differs from that of the highest energy part.

The low energy part is a tail (Fig. 11.7.1 8 pages on), which may result from several different contributions, as:

i) deficient collection of the charge carriers at the edge of the detector surface, due to the large source area

ii) self-absorption in the source due to thesource thickness

iii) size of the active surface area of the source. This effect could be of significant importance if a peak is "sitting" on the low energy part of another region, thus being overcounted. Fortunately, this was not a problem in the present study. Also, "shift" in the peaks could occur due to the instability of the measuring equipment.

11.8 Spike Activity Ratio

An aliquot of 50 μG of U-232 in 3N HCl ($t_{\frac{1}{2}}$=72 yrs) was purchased from Amersham, England.

The spike was sold in disequilibrium with its daughters. Therefore, frequent efforts to monitor the ratio U-232/Th-228 were necessary. Otherwise it takes some 12-15 years for the spike ratio to reach its transient equilibrium ($t_{\frac{1}{2}}$ of Th-228 is 1.91 yrs), see Fig. 11.8. A spike solution was made as 10^{-5} μCi/ml. Growth into equilibrium was monitored by the use of a known activity of U-238 solution as follows:

0.0477 gr of pitchblende ore (67.91±0.05%U_3O_8) was dissolved via HF/AR using a hot sand-bath into 2 lt of 3M HCl. The solution

made had an activity of 16±0.0117 μg U-238/ml (or 14.16ppm of U-238). The pitchblade has a Th-230/U-234 activity equal to one.

Also we assume that:

i) no Th-232 (and hence Th-228) are present. This was also checked.

ii) the system was remained closed for over 1million years, that is, there is not U-234 in excess. A volume of pitchblende solution was mixed with a known volume of spike and put through the extraction procedure, see section 11.17. Activities obtained from counting were used, then, in the following equation, where Th-230/U-234 =1.

$$(1) \qquad \frac{\text{Th-230}}{\text{U -234}} = \left(\frac{\text{Th-230}}{\text{U -234}}\right)_{meas} \times \left(\frac{\text{Th-228}}{\text{Th-232}}\right)_{spike} \times \left(\frac{\text{U-232}}{\text{Th228}}\right)_{meas} = 1$$

Thus the spike ratio $\left(\frac{\text{Th-228}}{\text{U -232}}\right)$ is obtained. This equation assumes that for any loss of Th or U of pitchblende, a proportional loss of Th and U of the spike occurs (same chemical affinities).

The original spike ratio was 0.643±0.016(2.5%) which within 6 months became 0.716±0.013 (1.8%), within ten months became 0.740 ±0.02 (2.6%) and within one year became 0.781±0.018 (2.3%).

Depending on the dates a sample was analysed, an appropriate spike ratio was used, Fig. 11.8.

An error, in the spike ratio, becomes more pronounced in determining high ages, Table 11.8.

It is also worth noticing that errors as high as ±3σ of the spike ratio, give results which otherwise fall within the time span of ±1σ error bar of the calculated age (for the errors quoted).

11.9 Measurement of Uranium Concentration

For a dated speleothem with an observed $(\text{U-232/U-232})_{obs}$ ratio and weight w, the U concentration is:

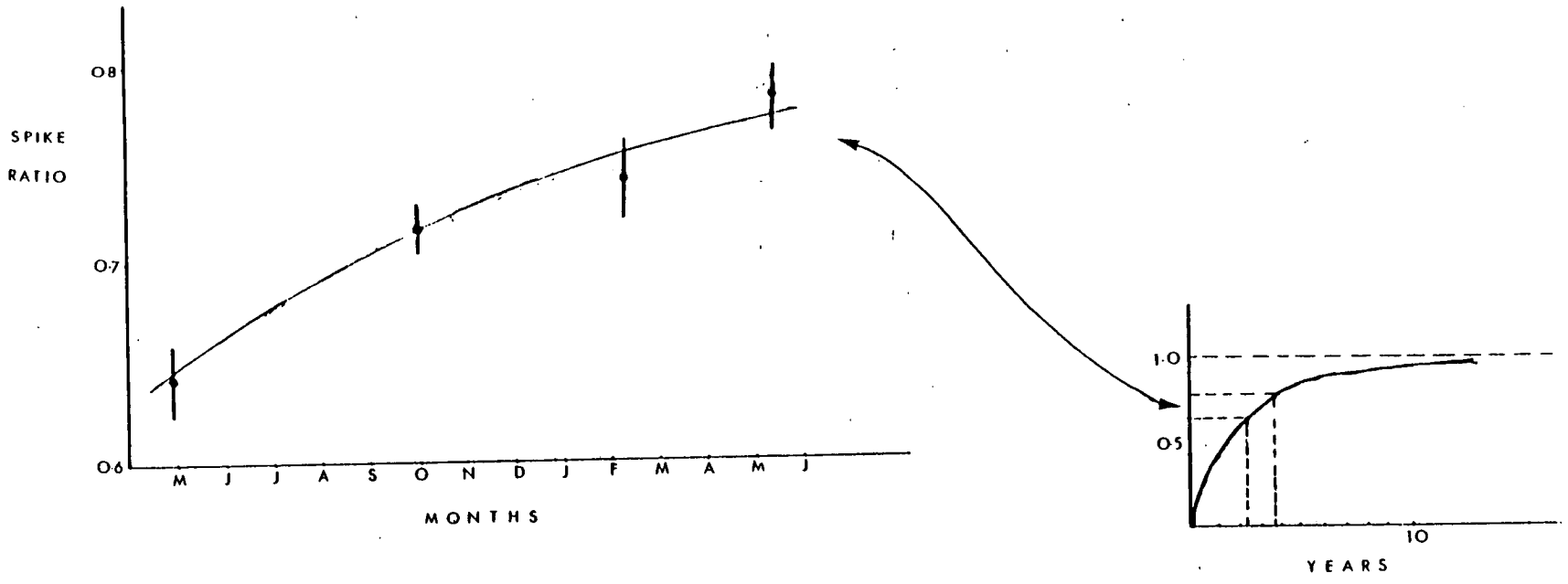


Fig. 11.8 Spike activity ratio growing towards its equilibrium value (right); and the time interval of one year of the monitored spike ratio (left).

TABLE 11.8

The Effect of Variations in Spike Ratios on Three Different Ages, A_1, A_2 and A_3

		+1σ	+2σ	+3σ	−1σ	−2σ	−3σ
Spike Ratio	0.716*	0.729	0.742	0.755	0.703	0.690	0.677
AGES x 10^3 yrs	A_1 = 89.0± 9.30	92.2± 9.70	95.5±10	99.0±10.4	86.0± 9.0	83.0± 8.70	80.2± 8.4
	A_2 = 173.7±48.30	182.2±53.00	191.5±59	201.5±66.4	165.8±50.5	158.5±40.70	151.6±37.6
	A_3 = 203.1±45.40	218.7±52.90	236.9±63	258.4±78.0	189.4±40.0	177.3±35.4	166.4±31.8
		% Difference from 0.716 Value					
A_1	0	±3.5	±6.8	±10			
A_2	0	±4.7	±9.3	±13.8			
A_3	0	±7.1	±14.3	±21.4			

* The spike ratio is 0.716 ± 0.013 (±1.8%)

(2) $\left[\frac{U\text{-}238}{U\text{-}232}\right]_{obs} \times \frac{As}{A\text{-}238} \times \frac{Vs}{W}$, where Vs is the volume of spike used, A-238 is the activity of 1µg of U-238 (=0.73965 dpm) and As the U-232 activity in dpm/ml. $\frac{As}{A\text{-}238} = B$ is the weight of µg of U-238 whose activity equals the activity of U-232 in 1 ml of spike, W is the weight of the sample. The only assumption here is that U-232 and U-238 are extracted with equal yield andthat there is an equal probability of measurement of disintegration(S) by the counting equipment (no assumption about detector geometry need be made, though it must be the same throughout all the experiments).

11.10 Detector Calibration and Yield Determination

The yield of U-238 and Th-230 in the extractions is given by the observed U-232 and Th-228 activities. However, the "geometric" efficiency of the detector must be known in order to make this calibration.

This efficiency was determined by plating out (with assumed 100% yield by TTA - organic solvent for extracting U and Th) and counting one aliquot of a U or Th standards solution. In either case the efficiency E is given by, $E = \frac{A_{obs\ (cpm)}}{A_{theor(dpm)}} \times 100\%$ (3)

Yields are calculated as:

$$Y_U = \frac{U\text{-}232_{obs}}{(U\text{-}232)_{sp} \times E \times V_{sp}}, \text{ where} \quad (4)$$

$(U\text{-}232)_{sp}$ is U-232 activity (cpm) of 1ml of spike solution and V_s = volume of spike used.

Also, $$Y_{Th} = \frac{Th\text{-}228_{obs}}{(U\text{-}232)_{sp} \times E \times V_s \times R}, \text{ where} \quad (5)$$

R is the spike activity ratio (Th-228/U-232).

11.11 Determination of Constants

Two "constants" have to be introduced in the computer programme in order to determine certain aspects of the computerized sample, which are related to the accuracy and precision of the analysis. The determination of the B4 and B constants used in the programme, section 11.15, for Th-230/U-234 dating are described as follows:

B4 - is the activity in counts per min/ml (cpm/ml) of U-232 in spike solution using detector and geometry as used with given sample.

B - is the weight in micrograms of U-238 whose activity is equal to the activity of U-232 in 1ml of spike.

The steps for such determinations are:

i) prepare a solution of U of known activity of U-238 in disintegrations per minute/ml (dpm/ml). This is done with the pitchblade solution already described (section 11.8)

ii) mix a volume V_u of U solution with a volume V_s of spike

iii) prepare a U disc for counting from this mixture as usual, removing all Th; The counting activity measures the ratio U-232/U-238

iv) Take V'_u ml of the U-238 solution and plate out all the U from it on a disc, using TTA. This is done carefully so as to come as close as possible to 100% yield. Count and observe activity of U-238.

B4- The pitchblade has 16µg/ml of U-238 . 1 mol of U-238 = 2.923×10^{-16} = $6.0235\times10^{23} \equiv 1.7607\times10^{8}$ dpm. Activity of 16µg U-238 = $\frac{1.7607\times10^{8}}{238} \times \frac{16}{10^{6}}$ = 11.84 dpm/ml, let A_u = activity in dpm/ml of U-238 = 11.84 dpm/ml

Cu = cpm of U-238 on disc plated in step iv above. Then the counter efficiency is given by $E = \frac{Cu}{A_u V'_u} \times 100\%$. Let r = activity ratio of U-232/U-238 in step iii, above. Then $r = (U\text{-}232/U\text{-}238)_{obs} = \frac{V_s}{V_u} \cdot \frac{(\text{dpm of U-232})/\text{ml}}{A_u} = \frac{V_s}{V_u} \cdot \frac{B_4 E}{A_u}$, so, $B_4 = \frac{V_u}{V_s} \cdot r.A_u.E.$

The efficiency was around 10%. The constant B_4 was found to be 5.99cpm (±0.049).

B - The constant B is obtained from step iii. Let A_s = U-232 activity of spike in dpm/ml. Thus $r = \frac{V_s}{V_u} \cdot \frac{A_s}{A_u}$ or $A_s = A_u \left(\frac{V_u}{V_s}\right) r$. But from equation (2) it is apparent that B is given by: $\frac{A_s}{0.74}$ or $B = \frac{V_u}{V_s} \cdot \frac{A_u}{0.74} \cdot r.$ This was found to be 91.9µg. (This is the weight in µg of U-238 with activity equal to A_s).

11.12 Alternative Measurement of Uranium Concentrations

A calibration curve (Fig. 11.12) made to measure U concentrations directly from the count rates recorded by the detector and analyser. Aliquots ofthe standard pitchblade U solution (buffered at pH of 3.5) and containing 16µg/ml of U-238 were extracted with 0.25M TTA in Benzene and the organic phase evaporated onto stainless steel discs.

The straight line of Fig. 11.12 implies that the extraction efficiency was reproducable and of 100%; also its slop reflects the geometry of the counter which is constant.

11.13 Errors

Errors in the precision and accuracy of a Th-230/U-234 age determination can be the result of four factors:

i) analytical error in the chemical procedures

ii) statistical counting errors* (see overleaf)

iii) possible post-depositional migration of U and Th in or out of the speleothem sample, and

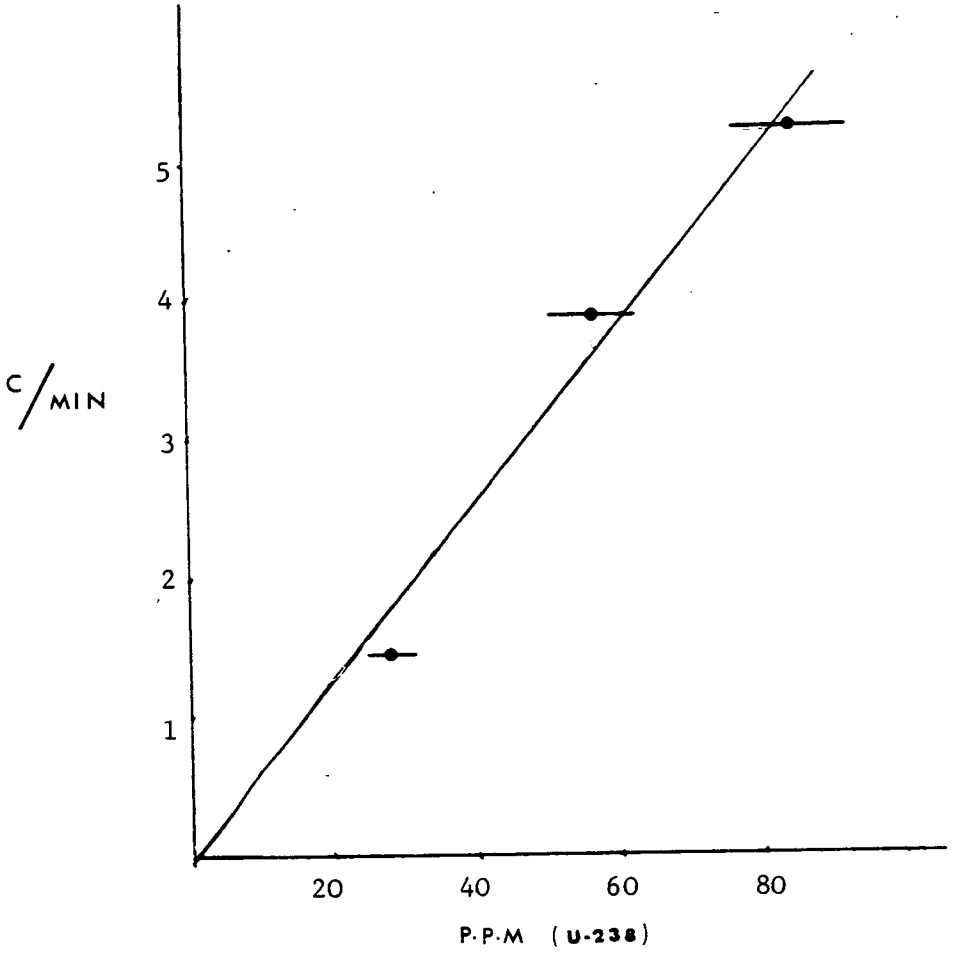


Fig. 11. 12. Calibration curve for measuring U concentrations from counting rates.

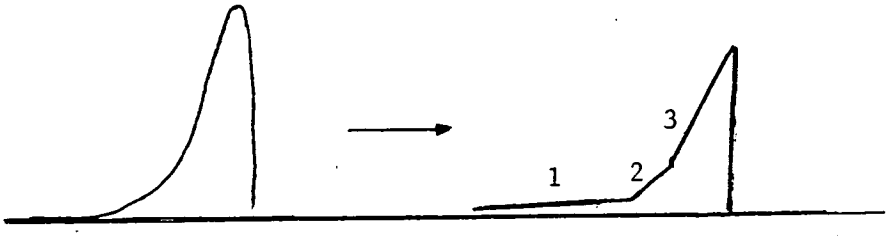


Fig. 11. 7.1 "Tailing effect" of the low energy part of an α- particle peak.

iv) an initial contamination of a speleothem with detrital Th., eg. from the clays.

11.14 Determination of Approximate Ages Greater than 350,000 Years

Interpretation of the spectra is an important, but somewhat subjective step in finally determining the age. Especially for ages greater than 350,000 years, an approximate age may be readily determined by using the isochron plot diagram, Fig. 11.3.1 together with the error of the associated isotope ratios, as calculated by the computer programme.

11.15 Th-230/U-234 Age Programme

The Th and U isotope spectra accumulated in the multi-channel analyser are fed into the computer for further processing. The programme used was kindly supplied by Prof H Schwarcz, McMaster University, Canada, and was written in Fortran IV. Data input and output formats and content have been arranged in such a way so that all variables used in the age calculations are printed out together with the data of running.

---

*When measuring the count rate of a source a separate measurement of the background rate (b) must be made. If in time Tb, a total background of b.Tb counts is recorded then the average background rate, B, and its error is $B = (bTb \pm \sqrt{bTb}) \frac{1}{Tb} = b \pm \sqrt{\frac{b}{Tb}}$. Note that the magnitude of the error is inversely proportional to the square root of the length of counting time. Therefore, for a source of activity, S, the best estimate of total count rate (S+B) is:

$$S+B = \left[(s+b)Ts \pm \sqrt{(s+b)Ts}\right]\frac{1}{Ts} = (s+b) \pm \sqrt{\frac{s}{Ts}+\frac{b}{Ts}}\ .$$

So, for the average count rate due to the source alone:

$$S = S \pm \sqrt{\frac{s}{Ts}+\frac{b}{Ts}+\frac{b}{Tb}}$$

Here background appears twice, once for variation in measuring (s+b) and once for variation in measuring b alone.

In brief, the programme routine is to:

i) determine corrected count rates for each nuclide, allowing where necessary for natural contamination, for example, Th-230 from Th-232.

ii) correct Th-228 activity for decay since separation from parent U-232

iii) use equation below to determine Th-230/U-234 ratios

(1) $$\left(\frac{\text{Th-230}}{\text{U -234}}\right)_{\text{true}} = \left(\frac{\text{Th-230}}{\text{U -234}}\right)_{\text{meas}} \times \left(\frac{\text{Th-228}}{\text{U -232}}\right)_{\text{spike}} \times \left(\frac{\text{U-232}}{\text{Th-228}}\right)_{\text{meas}}$$

iv) allow for the growth of Ra-224 into the Th-228 peak during the period of counting. This correction is generally small if the Th sample is counted immediately after plating out, that is separation from its daughters.

v) calculate sample age (t) using the ratio of example (1) above; and the measured U-234/U-238 ratio. This is done by interaction in a subroutine using the age equation as follows. An estimate of the age (t_o) is used to calculate t*, the true age of the sample by the Newton method of successive approximation. This method states that if F(t) = 0, then

$$t_{n+1} = t_n - \frac{F(t_n)}{F'(t_n)}\ ,\ \text{where } t_n = \text{the nth iterative step, and}$$

$$F(t) = \left[-\frac{\text{Th-230}}{\text{U-234}}\right] + (1-e^{-\lambda_{230}t_n}) \Big/ \frac{\text{U-234}}{\text{U-238}} + \left[\frac{\lambda_{230}}{\lambda_{230}-\lambda_{234}}\right]\left(1-\frac{\text{U-238}}{\text{U-234}}\right)^{-1}.$$

$$\cdot(1-e^{-(\lambda_{230}-\lambda_{234})t_n})$$

and $$F'(t) = \frac{U-238}{U-234}\lambda_{230}e^{-\lambda_{230}t_n} + \lambda_{230}(1 - \frac{U-238}{U-234})(1 - e^{-(\lambda_{230}-\lambda_{234})t_n})$$

$F'(t)$ is the derivative of $F(t)$.

When $\frac{t_{n+1}-t_n}{t_{n+1}} < 0.001$

$t_{n+1} \simeq t^*$

$(U\text{-}234/U\text{-}238)_o$ is calculated from the Th-230/U-234 age and the measured U-234/U-238 ratio.

This iterative procedure is repeated until two consecutive age determinations differ by less than 0.1%.

vi) count rate errors ($\pm 1\sigma$) are determined and then used as upper and lower limits in the subtraction to find the standard deviation of the calculated age.

Th-230/Th-232 ratio, U concentrations, U&Th chemical yields, are also determined and printed out along with the age data. (Table 11.14 illustrates such data input and the data output cards.)

11.16 Radiochemical Procedure

11.16.1 interiors of carbonates The extraction of U and Th from pure calcites presents few problems, Thompson (1973), Harmon, (1975). The elements that are precipitated when a sediment-free solution loses CO_2 (outgasses), are those which form stable carbonates from bicarbonate solution, for example, Ca, Sr, Fe and Mn.

Many elements that are picked up in solution as a result of acid leaching in soil zone, for example, Si, Al, Na, K will remain insolution when $CaCO_3$ is precipitated.

Transition elements impurities precipitated in the calcite include Mn

and Fe (giving a red colouration).

White, et al (1970) has reported the presence of Ni (up to 500 ppm) which imparts a green or yellow colouration. Mn, Ni and Fe cause no problems since Fe is largely extracted with iso-propyl ether and Mn, Ni are not absorbed on Cl^- anion exchange resin.

11.16.2 U/Th isotopic analysis Theobject of the chemical separation is to extract radiochemically pure U and Th from the $CaCO_3$ samples. Both U and Th are mounted on Stainless Steel discs for alpha counting and isotopic analysis.

The isotopic ratios of interest are Th-230/U-234, U-234/U-238 and Th-230/Th-232. These are two considerations of prime interest when preparing U and Th:

i) the final preparation should not be contaminated with chemical impurities because these would be deposited on the planchet and this constituted a "thick" source when counting. A sample thickness of more than approximately 100μg/sq.cm leads to attenuation of the alpha particles and a tailing of the low energy side of a peak into adjacent peaks of lower energy. It is possible but more troublesome to correct for this effect, (see section 11.8.1)

ii) the final preparations should also be radiochemically pure, that is free from radioisotope impurities with similar α-particle energies.

Naturally occuring isotopes which fall in this category can be classed in two groups, namely those that interfere with the U spectrum and those that interfere with the Th spectrum. Th-232, Th-230, Th-228 Ra-226, Po-210 and Bi-210 are isotopes of the first group U-234,

Ra-226, Po-210 and Bi-210 comprise the second group.

Good resolution of the alpha spectra will discriminate between those peaks though the Po-210 has a very similar alpha energy to U-232 and Th-228 and cannot be easily detected as an impurity. The extraction and purification of U and Th is accomplished via a series of steps that are designed to discriminate against both chemical and radiochemical contamination.

Fig. 11.17 shows a schematic flow diagram of the radiochemical procedure for the extraction of U and Th. However, it isworth mentioning some important features encountered during these analyses.

11.17 Chemical Procedure for Extraction of Uranium and Thorium

i) Check for detrital silicate material. Detrital speleothem indicates impure material. In dealing with stalagmites, stalactites, travertines and flowstones, these impurities inside or outside the body of the sample are due to clays, bacterial organisms or organic materials. Most clays are derived from outside the caves and from outside the limestone environment; some, however, are derived from the decalcification and ion exchange replacement of the limestones. Clays are indicative of past weather. So varved clays are related to alterations of weather, for example, more decalcified clay depositing during cold periods, Sweeting, (1972). Terra rossa, by contrast, is regarded as an indicator of former warmer conditions.

So a variety of clays will descend down into caves through cracks and passages, following streams, vadose and seepage waters, rainfall and any pheatic solutions. Organic matter, phosphates plants, etc., may participate in speleothem deposition causing different colours in the deposit. (It has been observed that

certain trace elements give certain colours in the speleothem, Harmon,(1975). Organisms are effective agents of dissolution and extraction of many elements. Because of the enormous multiplication rate of micro-organisms, their total effect can be considerable and probably significant in any transfer of minor and trace elements in these speleothems. Contamination upsets the purity of calcite producing subsequent difficulties in the extraction-purification procedures of U/Th from them.

ii) The spike was not sold in equilibrium with its daughter, and an accurate monitor determination of the activity ratio (Th-228/U-232) was available from isotope dilution analysis.

The effect in variations of spike ratios on speleothem age is pronounced (section 11.8 above).

Nevertheless, it is worth while noting that because of the $\pm$0.01 precision in the determination of the spike activity ratio by counting or isotope dilution technique, the age error should also reflect uncertainty in the spike activity ratio. Moreover any natural Th-228, which contributes to the total Th-238 spike peak intensity, could not be traced; therefore, adding another uncertain error in the final age equation. However, this is not considered serious since, even if present in an amount of the order of the respective Th-232 it is overmasked completely in the calculations, by the high spike Th-228 activity, which is around 20 times higher.

iii) Fe extraction ether phase. This stage of the procedure, although not likely to contribute significantly to U or Th loss can produce many problems such as imcomplete iron extraction (iron

is extracted between 9-10 pH), the generation of three or more phases, variable solubility of aqueous and etheral phases in one another, gelled organic layers and a critical dependence on acid strength. These difficulties are prevalent in the analysis of contaminated samples, (by clay, organic materials, etc.) Some observations are:

a) A ferric hydroxide precipitate is best dissolved in concentrated hydro-chloric acid (12N) and the filter paper washed with 9N hydro chloric acid, since the use of 9N only throughout may result in the lowering of acid strength, after reaction with the precipitate, to below 7N so that incomplete iron extraction with ether occurs.

b) In contrast, if too much concentrated hydrochloric acid is used the resulting solution becomes "non-polar" and acid solubility in the ether "disappears" during the extraction only to suddenly reappear as a separate layer during the boiling-off stage. The addition of more water usually overcomes this problem.

c) If the iron concentration in the aqueous layer is initially high the first ether extraction may yield three layers instead of two, the middle one being a deep green colour. This is the pure iron-chloride-ether compound.

d) Sometimes, no matter what is done, the iron will not extract completely into the ether. Two possibilities exist;

   (1) either the aqueous layer can be boiled down to dryness treated with concentrated aqua regia and re-extracted from 9N hydrochloric acid, or,

   (2) the iron can be extracted at a later stage after elution

(together with U from the U column).

e) On occassions, a white floccular precipitate appears slowly in the ether bottle, presumably due to the formulation of unstable peroxides by gradual absorption of oxygen. This often gives rise to charred residues in the subsequent evaporation stages but their effect can be removed by treatment with aqua regia as previously described. It is therefore best to use freshly-filtered ether in the iron extraction process. Experiment shows that essentially no U or Th is lost into the organic phases at this stage, Gasgoyne, (1977).

iv) Evaporate to dryness of Th eluate. This often caused Th loss. It has to be done in a very slow heat, otherwise the creation of Th oxide appears as a residue at the bottom of the beaker thus preventing further successful extraction of Th, which results in poor Th-yields.

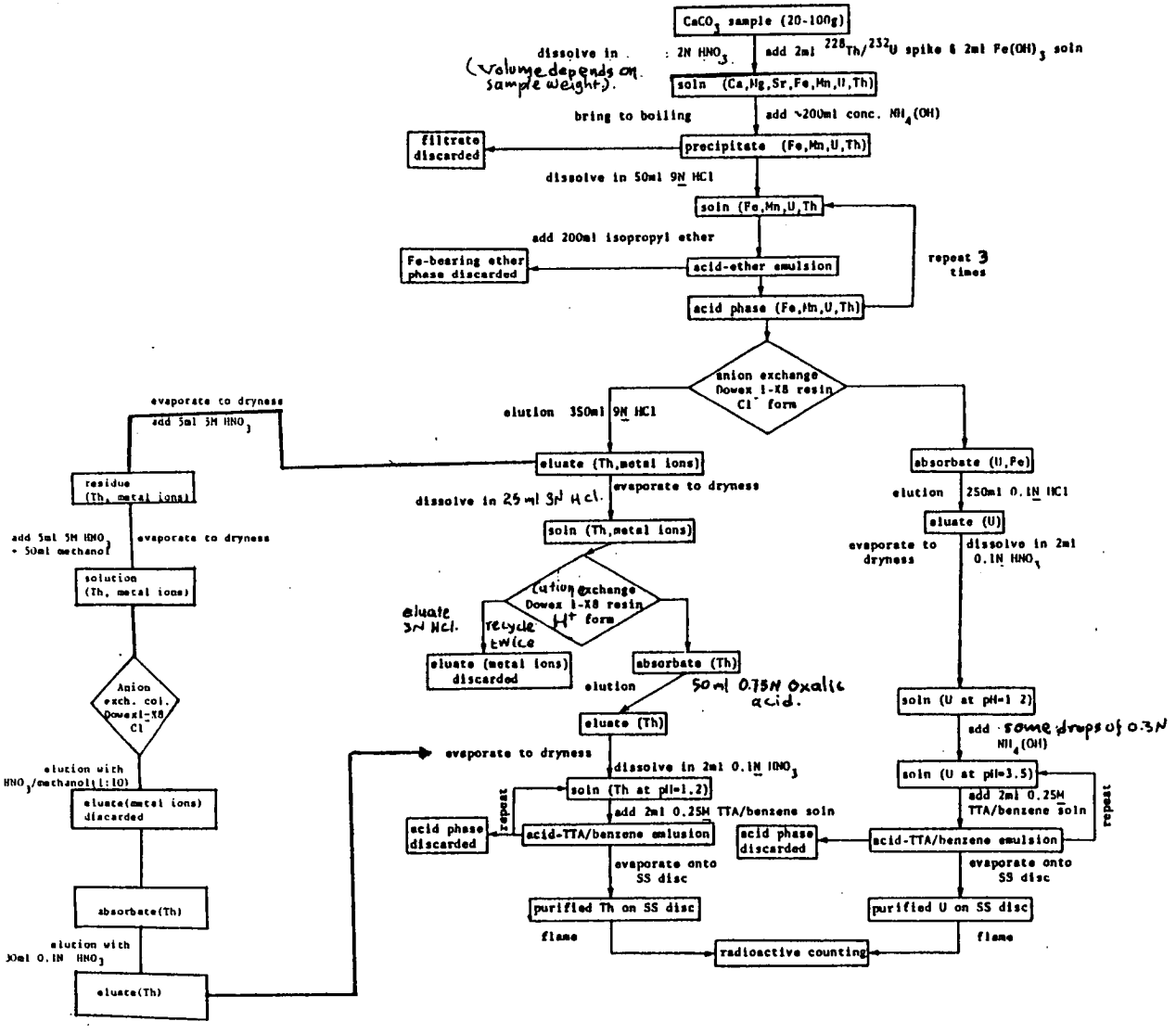


Fig. 11.17 Schematic Flow Diagram of the Extraction-Purification and Alpha-Counting of Uranium and Thorium from Speleothems.

CHAPTER 12

U/TH DATING OF PETRALONA CAVE

12.1 Archaeological Context of the Cave

Petralona cave, the discovery site of an important early hominid, is partially filled with detrital cave sediments containing skeletal remains of large Pleistocene vertebrates and a plethora of stone artefacts. This cave, on the Chalkidiki Peninsula, Northern Greece, has been described by Kannelis, (1962)

A skull of Homo Sapiens appearance was discovered in this site, Kokkoros and Kannelis, (1960), and excavations by Poulianos, (1978), have shown the existance of sequences of layers containing an abundance of human implements and animal remains. The skull has been studied by several anthropologists and has been described as Neanderthal, Kannelis and Savas, (1964). Although Stringer, (1974) argues that it is morphologically most closely related to the Homo Erectus, (Fig. 12.11.1) and Poulianos (the excavator) stresses that this Archanthropus Europeus Petraloniensis ("Elladopithecus "), skull forms a mosaic of primitive and progressive hominoid type, Poulianos, (1971, 1972, 1974, 1976, 1977).

Fauna of possible Mindelian aspect (app 350 Ka* BP) have been described by Kurten & Poulianos, (1977).

In Fig. 12.1, a sketch map is shown of the cave showing the location at which the skull was found. Also shown is the site of trench $A_1 - A_2$, from which the faunal remains studied by Kurten & Poulianos were recovered.

The site of the skull is an alcove about 1m x 1m (the "Mausoleum"), isolated from the main passageway by a fallen limestone block. The skull is thought to have been originally attached to the post-cranial

* 1Ka = 1000 yrs

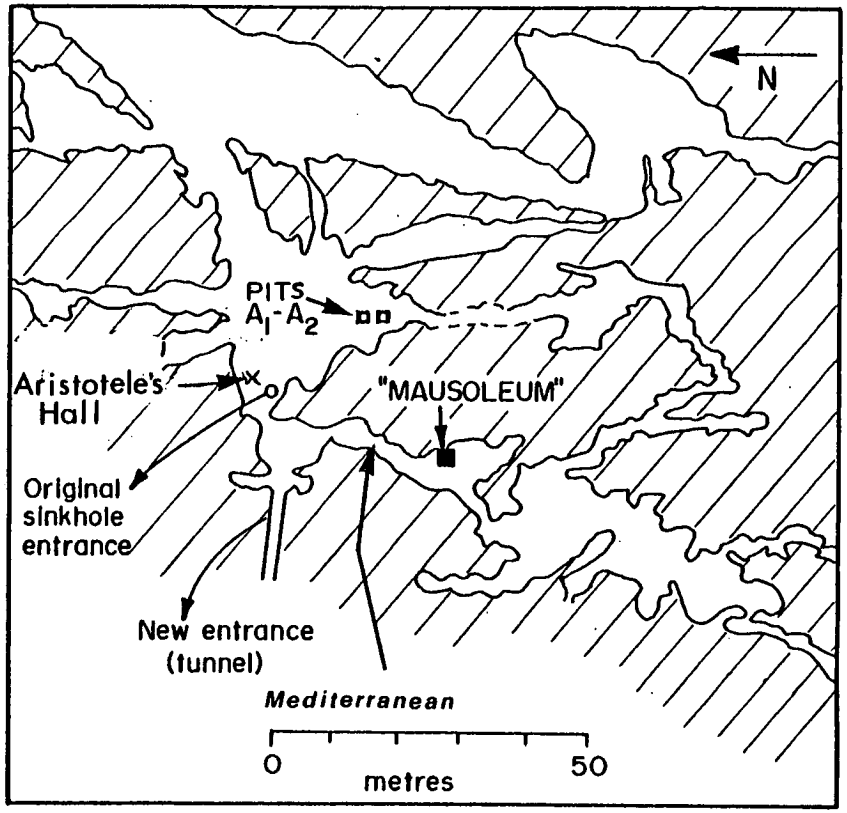


Fig.12.1Schematic representation of part of Petralona cave, showing sampling sites (after A. Poulianos)

skeletal bone, but the latter were accidentally destroyed during the removal of the skull, Poulianos, (1977). The skull was heavily encrusted with travertine and deposits of similar travertine are still present at the site of the former burial.

The samples studied were derived from sites which are in relation to the former position of the skull and the associated skeleton and were collected by the author or co-author (Prof. Schwarcz) in the paper Schwarcz, Liritzis, Dixon, (1979), directly from the site, with the assistance of A Poulianos. Because of the uncertainty of the exact place of the fossil with respect to the sampled locations and in order to prevent further confusion in the interpretation of our data it is worth relating the discovery of the Petralona skull.

The cave where the skull was found was discovered in a most unusual way :

"A man from the village of Petralona had been told by an old shepherd that he had heard "water running under-ground at the foot of Katsika, ("Goat") Mountain, which rises directly behind the town. Shown the spot in September, 1960, the man removed a few loose stones and literally fell into the cave. A quick search showed that the floor was littered with animal bones. On a subsequent visit, he found the human fossil represented by an entire skeleton lying on its right side, with legs drawn up. The skull and hips were "hanging in the air", almost a foot above the ground held by a stalagmite formation. He told other villagers that night, that he had found the remains of a "big monkey" in the mile long cave.....!"

Apparently around about the skeleton 6 - 7 bonal needles , 10 - 11mm in length, and other small stone tools which were presumed to have been used by the archanthropos, were found, Poulianos, (1977).

About 15cm from the Mausoleum is the "Mediterranean" site, a narrow passageway through limestone walls covered by large amounts of stalagmitic material (surface travertines). About 30m from the Mausoleum, separated by a complex,but sub-horizontal series of passage-ways, is the site of "Aristotle's Hall", where the original sinkhole entrance was situated, Fig.12.1. 20m further away is the site of trench $A_1 - A_2$. This trench has been dug into a series of sedimentary layers capped by a broad flowstone sheet which is locally surmounted by stalagmites up to 2m in height.

The trench, now dug to about 5m in depth, Kurten & Poulianos, (1977), intersects another flowstone layer about 5m thick, at a depth of 1.8m. The sediments above these layers are mixtures of reddish grey clay and sand ("terra-rossa" soil) and limestone fragments ("breccia"), encrusted with clear prism of calcite in layers up to 2mm thick. Vertebrate bones and crude stone tools have been recovered from these sedments.

It is of particular interest to point out that during the age of the 10th - 11th layer of the section, i.e., the 1.8m deep flowstone layer , most of the human activity in the cave seems to have been densely concentrated. Also, "traces of fire" is thought to have been found along the section, for example, in the 2nd - 3rd layers and in the 16th layer, as well as in other places inside the cave.

12.2 Sample Provenance

Samples were taken from many parts of the cave with the aim of indirectly dating the archanthropos shull and other human and animal remains.

i) Mausoleum site The importance of the site lies in the fact that this is the former burial place of the ancient man. One travertine layer sampled is approx.4 cm thick. This sample comprised of an upper series of lime (o.1 - 1mm) reddish grey layers about 1.5 cm

thick on a thick unlaminated sheet of prismatic calcite, colourless to pale brownish-grey. This layer was deposited on an irregular surface of silty red brown clay-rich detrital sediments containing abundant 0.5 to 10mm long fragments of bone.

The uppermost surface of the travertine sheet is smooth and pale reddish brown. Samples GR-4, GR-4-2, GR-4-3 for dating were taken from the clear prismatic layer; and sample P-12 from another brownish travertine layer around the presumed former burial spot. Sample P-6 was a thin trimmed crusty layer of stalagmite (0.5cm thick) presumably having covered the fallen skull, 1m away from the sampling of the above travertines, Fig. 12.2.

Around 2m away from these locations another sample was taken, P-13, which incorporated a bone (hipbone?), Fig. 12.3.

(ii) Excavated Trench $A_1 - A_2$ The stratigraphy of this section is thought (by the excavator) to represent certain periods of the early human activities in the cave. In particular, the 10th - 11th layer to represent the presently top layer of the Mausoleum site, where the skull was found. The travertine capping of the pit site is composed of alternating layers of white and reddish brown speleothem, composed of equant crystals of about $1cm^3$ interstratified with layers of finer crystals. The stalagmites were deposited on this layer. Samples P1Aex, P1A int, 75026-1, and 75026-2, come from the stalagmites above the travertine. Detritus rich layers are evident and the base of the travertine rests on reddish-brown ("terra rossa") cave sediment, containing bone fragments. Samples 75022-2, 75GR1-4. P-TR, P-7-2 and P-7-4, for dating from this travertine included both reddish-brown and white layers,(the former being dominant >75%).

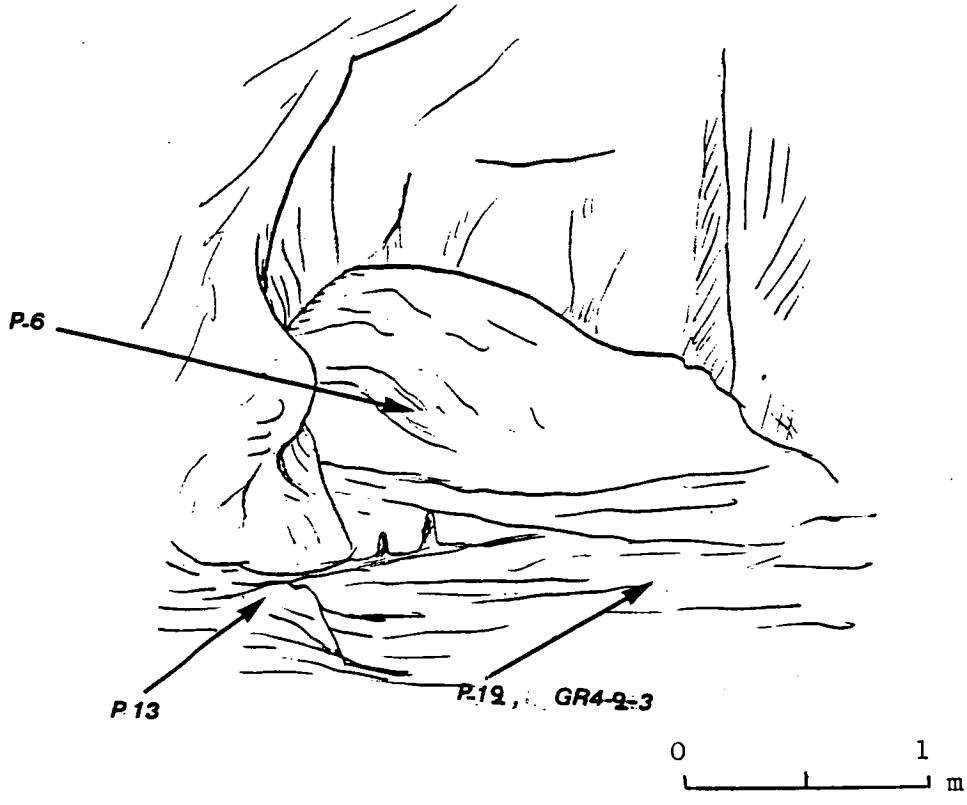


Fig. 12.2 Schematic representation of the mausoleum alcove and the sampling locations.

The travertine layer interrupting the pit sequence at 1.8m depth is thinly laminated, reddish-borwn to yellowish-pink. Samples P-C10,76GR3-1a and 76GR3-1b were collected.

Between this 1.8m deep travertine layer and the top of the section, the sediments consist of breccia, soil of different colours and hardnesses, though of predominant reddish clay. Numerous fossils and implements were found along this 1.8m deep trench encrusted with stalagmite and numerous pieces of rock with crystalline drops on them. Detailed description is given by Kurten & Poulianos, (1977), Fig. 12.3

(iii) Aristotle's Hall Two samples, PC-1 and P-ARST of surface travertines yellowish to brown in colour, were collected. They were collected in order to find the later depositional calcitic growth, which occurred in the cave and which is correlated chronologically with other parts of the cave.

(iv) Mediterranean Site Samples P-3-1, P-3-2, P-4-1 and P-4-2 are surface slightly brown, multilayered travertines of ∿1.5cm thick. They represent the upper stalagmitic level of a distructive event in the site, which brought down parts of this upper layer ("sunken level"). The importance of this site lies in the fact that such surface travertines which appear all over the cave covered a plethora of human and animal bones and presumably indirectly related to the presence of the early human activities in the cave and more probably to the presence of the Archanthropus Petraloniensis.

12.3 An Appraisal of Former Dating Results

Former dating results for this cave are summarized as follows:

(i) C-14 dating at Heidelberg University, gave an age of 44Ka BP, for surface organic material, Ikeya, (1977). Remembering that

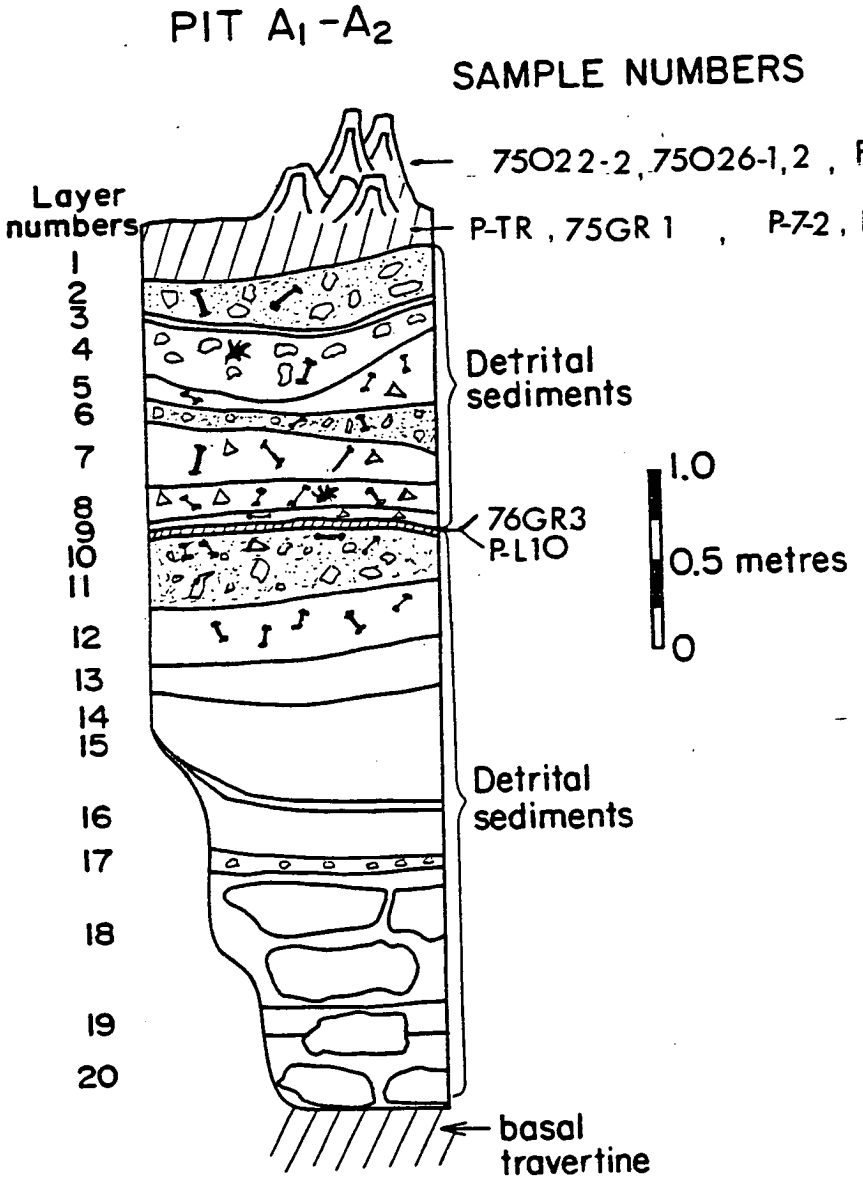


Fig.12.3. Excavated section A_1-A_2 and sampling positions.
(After A Poulianos 1973, 1977)

this is almost the maximum range of the C-14 method, this age represents a minimum for human activities in this cave.

(ii) Ikeya, (1977) using Electron Spin Resonance (ESR) measurements of unpaired electrons, produced by ionizing radiation and trapped at lattice defects in calcite crystals, dated the stalagmite upon the capping layer of the pit $A_1 - A_2$. The estimated age on the outer part of a stalagmite (10cm diameter) was ≃68Ka BP, (no errors are quoted for this age). Extrapolation to the centre, assuming a linear increase in age produced an age of at least 250Ka.

However, most stalagmites grow with flat tops (especially those above the trench $A_1 - A_2$) and at any given height their age profile will be essentially flat over some central region, Fig. 12.4 Therefore, it seems unlikely that the centre of this stalagmite is as old as inferred by Ikeya, even assuming that his age estimates for the outer portion are correct. His data are however lower than our estimate, in particular, the external part of this stalagmite was found to be approximately 100Ka BP, while the inner core of the stalagmite was found to be recrystallised, thus giving an erroneously "infinite age". However, Ikeya does not also appear to have taken into account the lack of equilibrium between U-238 and its daughter isotopes, which has been observed as a part of our dating procedure, or the presence of trace amounts of aragonite, which would imply a degree of uncertainty of the age of the stalagmite.

Additionally, uncertainty in other parameters including the relative efficiency of α-particles and γ-rays in depositing electrons in ESR traps (assumed to be 1:10 throughout) is probably as great as the error due to disequilibrium.

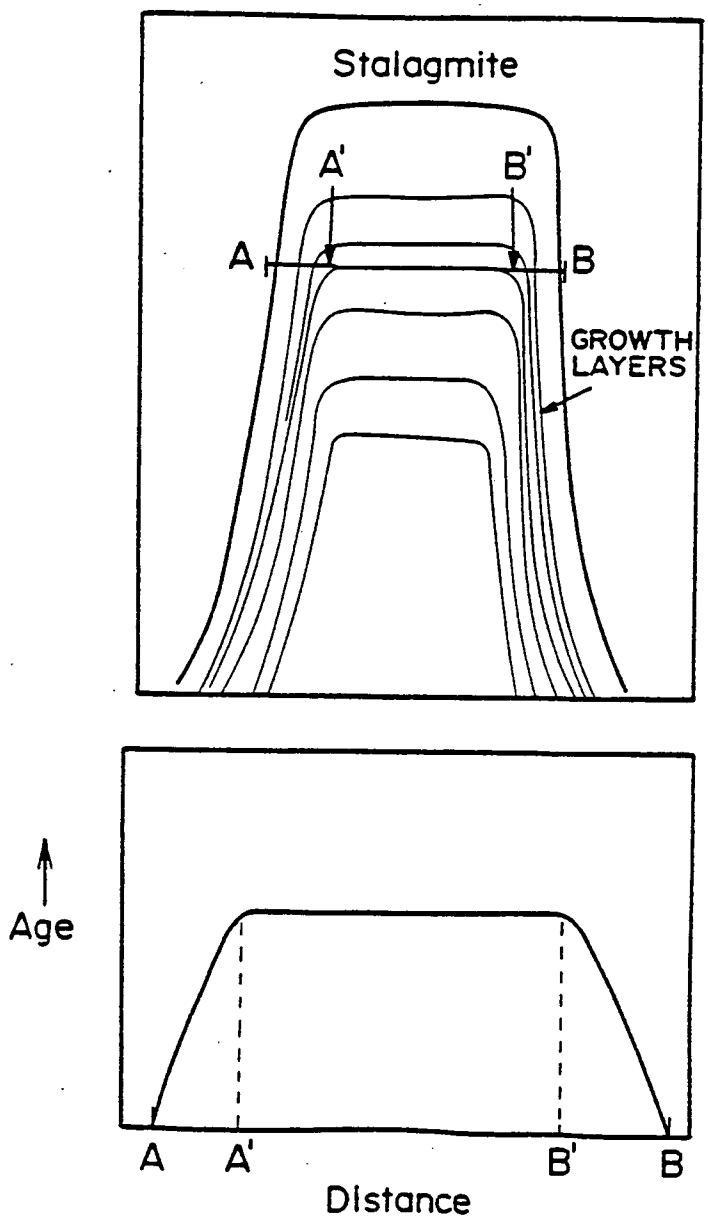


Fig12.4 Hypothetical relation between age and position in a slice of a typical stalagmite taken normal to growth axis. Note that age of material between points A and B is approximately constant (or somewhat less than the age of the points A' and B'), corresponding to the flat top of the stalagmite of some past growth episode.

Further attempts by Ikeya (1977) using Fission Track detection, Ikeya, (1977), was not successful, because of the young ages involved 200 - 300 Ka, and the low content of Uranium encountered, (around 0.2ppm).

Another date, by the same author, using ESR for the thin flow-stone layer from the 1.8m depth, in the section A_1 - A_2, gave an age of around 200Ka BP.

One more recent result using ESR on a fired stalagmitic cave floor gave an age of about a million years, Ikeya, (1979). This was obtained using an annual dose rate of 0.3r/yr. A potassium value was assumed and thus a corresponding beta dose rate, and an annual β-dose from the (U,Th) radioisotopes of 0.2r/yr as was found for the stalagmite above.

(iii) Schwarcz and the author obtained dates for the stalagmitic material from the section A_2 with ages ranging from 60 - 200Ka and for the Mausoleum, with ages between 280 - 600Ka, Schwarcz, Liritzis, Dixon, (1979).

(iv) Henning, Bangert, (1978), using Th-230/U-234 dating method, dated travertine samples from the floor of the section A_1 - A_2 and obtained ages ranging from about 60 - 150Ka. The latter age was obtained by TL with an error of ±50%, while a sample from the Mausoleum limestone bedrock gave a TL age of around 900Ka, Bangert, Hennig, (1979).

(v) Palaeomagnetic measurements on sediments of the section A_2 did not show up any geomagnetic reversal for at least the 1.8m deep accumulated sediments, which could imply that this part of the section is less than 700Ka , the well known Matuyama geomagnetic reversal, Papamarinopoulos, (1978). (The age of 90ka for the 1.8m deep section A_1, presented as pers. comm. to the above Ph.D Thesis is not correct due to the wrong sample ref. supplied by the excavator. In contrary this age represents the Aristotele's Hall.).

(vi) Palaeontologically. The stratigraphy based on the structure of of the sediments and their contained faunal and artefactual material indicated that Petralona cave was a site occupied by man during the whole of the middle Pleistocene, Poulianos, (1968, 1969, 1971). See also Fig. 12.10

In the last mentioned report, doubt was expressed on the alleged Würmian age (∿100Ka to 12000 BP) of the top layer of the section $A_1 - A_2$.

Later, Sickenberg, (1971) also revised his opinion on the fauna suggesting a mid-Pleistocene age. Newly found artefacts (pebble tools and hand axes) suggested a revised dating of the top layer, showing that it should also be regarded as middle Pleisetcene, Poulianos, (1976), and indicating a probable age between 300 - 400 Ka BP.

12.4 Corrections Applied in the Case of Detrital Speleothems: A Reappraisal of the Two-Component Mode

Pure calcium-carbonate precipitated from fresh water can be dated by Uranium Disequilibrium dating methods. Gascoyne et al, (1978), Ku et al, (1979), Schwarcz et al, (1979). However, in attempting to date speleothems , eg., travertines stalagmites and stalactites, from caves, we commonly observe the presence of a detrital contaminant.

Typically, dating procedures for such contaminated deposits begin by attacking the sample with concentrated or diluted nitric acid, Turekian et al, (1976), Liritzis et al, (1979).
Is is believed that during such an attack the detrital component may contribute some Th-230 andother radioisotopes to the solution.
If a Th-230/U-234 age is determined from this solution, an erroneous age estimate may result. Various schemes have been proposed to

correct for this detrital components, Ku et al ,(1979), Turekian and Nelson, (1976), Schwarcz ,(1979).

In the following sections we shall discuss the corrections used in this study for the presently obtained dates and we propose a possible now way of correcting the dates based on certain assumptions, which,so far, seem to be satisfied by experimental test.

Prior to this discussion, a description of the method for analysing cave sediments will be presented and discussed.

12.4.1 Determination of Thorium and Uranium in Petralona Cave Sediments

The clay samples analysed were derived from along the excavated section $A_1 - A_2$, from the Mausoleum site, others from the detrital residues of dated materials and one archaeological powdered potsherd.

The dissolution of these clays was done as follows: The well-ground, fine, powdered clay of 0.3 - 1gm was transferred to a polyethene beaker; ≃20ml HNO_3, ≃5 - 10ml $HClO_4$ and ≃20 - 50ml HF acids added and placed on a hot sand bath overnight with a polyethene lid on the beaker. This dissolves the clay entirely. A white to pale residue sometimes remainded and was discarded. After this the lid was removed to allow the solution to dry down. Then 30 - 50ml of HCl acid was added and the usual chemical procedure for the determination of U and Th as for the speleothems was followed, Chapter 11, section 11.7.

The results of these experiments are shown in Table 12.4.1

It can be seen from the three entries for the archaeological clay sample KZ 2/5, the ratios of Th/U, Th-230/U-234 and U-234/U-238 remained almost constant, in spite that dissolution of this clay with a weak HNO_3 acid (of similar strength and dissolution time as used for the carbonates, i.e. ∿ 2N). Also the amounts of U and Th leached (this solution is called filtrate) are small with respect to the remaining

TABLE 12.4.1

RADIOCHEMICAL DATA FOR PETRALONA CLAY SEDIMENTS

SAMPLE NO	TH/U	TH-230/ TH-232	U-234/ U-238	% YIELDS U	% YIELDS TH	PPM VALUES U	PPM VALUES TH	COMMENTS
P-5. 5th layer from Section A_2	1.44	1.835 ±.1	1.171 ±.083	59	63	11	15.84	XRD Analysis: main - fluorapatite/ apaptite, calcite, quartz, feldspar trace - illite, kaloinite
P-16 16th layer from Section A_2	3.93	0.997 ±.2	0.971 ±.326	87	17	6.97	27.41	-
P-8 3-4 layer of Section A_1	4.56	0.589 ±.1	1.094 ±.259	36	27	6.44	29.37	-
P-13 $_{cl}$ clay sample under P-13 travertine	2.39	8.855 ±1.3	7.689 ±1.013	5	5	7.07	16.91	-
KZ 2/5 original powdered tile from the archaeological site K Zakros, Crete	3.22	1.606 ±.3	1.174 ±.334	80	22	8.81	28.39	XRD Analysis: main - quartz, calcite, chlorite trace - feldspar kaolinite, illite/mica
KZ 2/5 filtrate solution due to dissolution of KZ2/5 original clay by weak HNO_3 acid	3.5	1.461 ±.2	0.757 ±.334	88	63	.31	1.09	-
KZ 2/5 residue residue of the above dissolution	3.05	1.618 ±.2	1.024 ±.327	88	63	8.09	24.5	XRD Analysis: main - quartz, feldspar, chlorite trace - calcite kaolinite, illite/ mica
P-4-1 detrital residue from sample P-4-1	1.076	2.086 ±.2	0.925 ±.146	33	47	10.93	11.76	-
P-13 detrital residue from sample P-13	4.63	1.634 ±.1	0.967 ±.077	63	27	9.24	42.81	-
P-18 detrital residue from sample P-18	2.38	0.956 ±.2	1.10 ±.144	33	10	2.9	6.91	-
P-12 detrital residue from sample P-12 (lower travertine)	4.22	0.960 ±.1	1.67 ±.472	12	43	1.93	8.15	-

KZ 2/5 residue. This is encouraging because in the actual dissolution process of the detrital carbonates, this leachable U and Th activities will not be greatly contributed to the "actual" U, Th activities of the calcite to be dated.

However, even small amounts can upset completely the assumption of the "close system", Chapter 11, section 11.3, and could produce erroneously higher (or lower) ages.

12.4.2 Some Aspects on Leaching Studies

Here it should be noted that, Pliler and Adams, (1962), performed 28 Uranium analyses of the leachable solutions for 17 shales(using 2N HCl acid).From the quoted data the ratio of dissolved leached U and Th varied from 1.3 to 4.4 or similar ratios found in our analyser. From these limited data it was interesting to note that the relative amount of Thorium removed by acids and was constantly high varying from 65 - 82% of that present.

The amount of leachable U varied widely from 22 - 74%.

These leaching studies provide clues as to the "sites" or Uranium and Thorium, in the weathering-transportation-deposition process of the water-limestone clay system in the formation of speleothems. If the U is mainly present in the common detrital minerals and the insoluble heavy minerals, it would be relatively unleachable (white-pale residue of the dissolved clays in our case?).

On the other hand, much of the adsorbed Uranium present in the acid-soluble heavy minerals, eg., apatite, and precipitates eg., hematite and calcite, could be removed by a strong acid leach; though using a weak acid some of it remains (The former is the U, associated with the detrital clay.).

In this case an attempt to use the obtained U and Th ratios from those clays as monitor values to correct the ages is not correct because the

apatite or presence of bones would contribute to the initial dissolution of the carbonate rock.

However, from the one analysis made here on sample KZ 2/5, it appears that ≈5% of the Uranium is leached. Furthermore, the exact minerals in trapping sites of U and Th in a detrital residue though difficult to determine on the basis of leaching studies alone, it is possible to identify them through X-Ray Diffraction (XRD) analysis, Fig. 12.4.2a,b on KZ 2/5. and Fig 12.4.2 c on 5th layer clay.

On the other hand, acid leaching in the laboratory is a more rigorous process than is found in nature. Consequently, materials which are insoluble in nature may be soluble in the laboratory. An example of this may be found in apatite, which frequently occurs as a resistate mineral in sedimentary rocks, but is easily dissolved by acid in the laboratory. Other minerals, such as allanite (U carrier) may react in the same manner.

Another important factor to consider is the grain size. Mineral grains in a shale may be extremely small, and as a result, may be effectively leached or attacked by acid, whereas larger grains of the same minerals would be slightly affected.

The effect of acid leaching on individual minerals containing U and Th is a subject which must be investigated further, before more exact interpretations of leaching studies can be made.

However, the grain size of the present detrital clays was very small (very fine-grained) mostly clay particles which would have distributed their U and Th contents uniformly throughout their body.

12.4.3 Discussion of the Radiochemical Analysis of Clays

From Table 12.4.1 one can see that the Th/U ratios varied between 1 - 4.6, with an average of 3.08±1.4 (45%), which approaches the

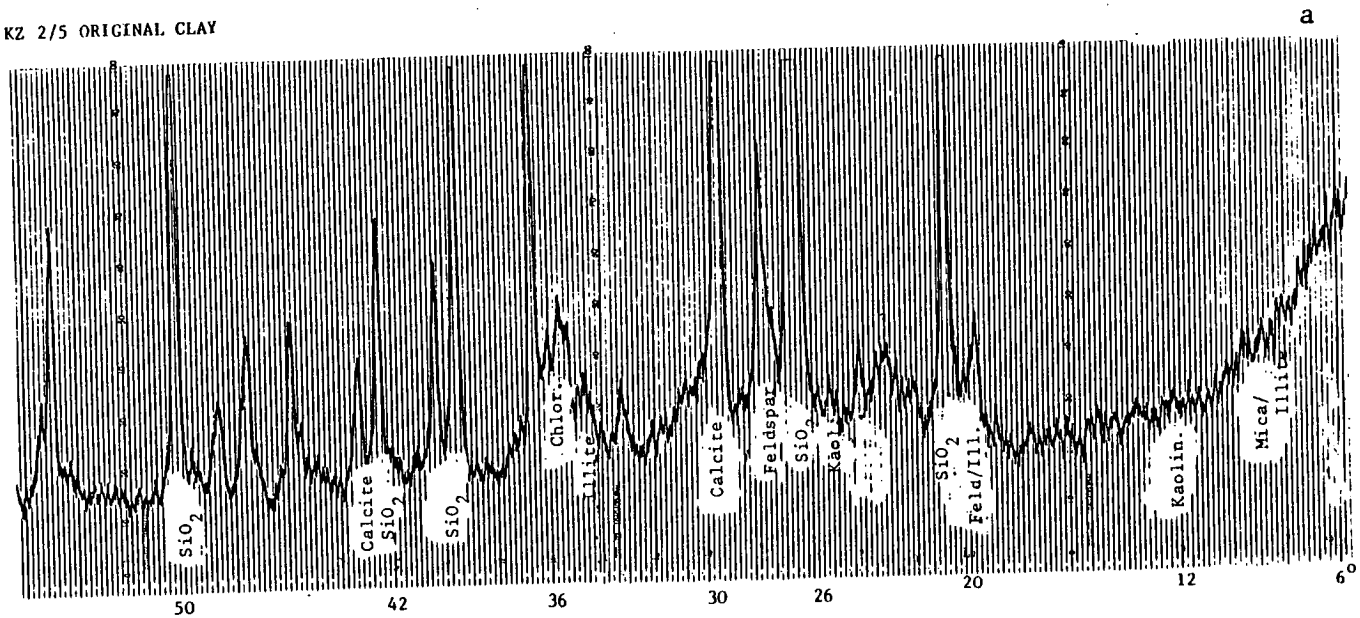

KZ 2/5 ORIGINAL CLAY
a
SiO2
Calcite
SiO2
SiO2
Chlor.
Illite
Calcite
Feldspar
SiO2
Kaol.
SiO2
Feld/Ill.
Kaolin.
Mica/
Illite
50
42
36
30
26
20
12
6°

Fig. 12.4.2a

KZ 2/5 DETRITAL RESIDUE

b

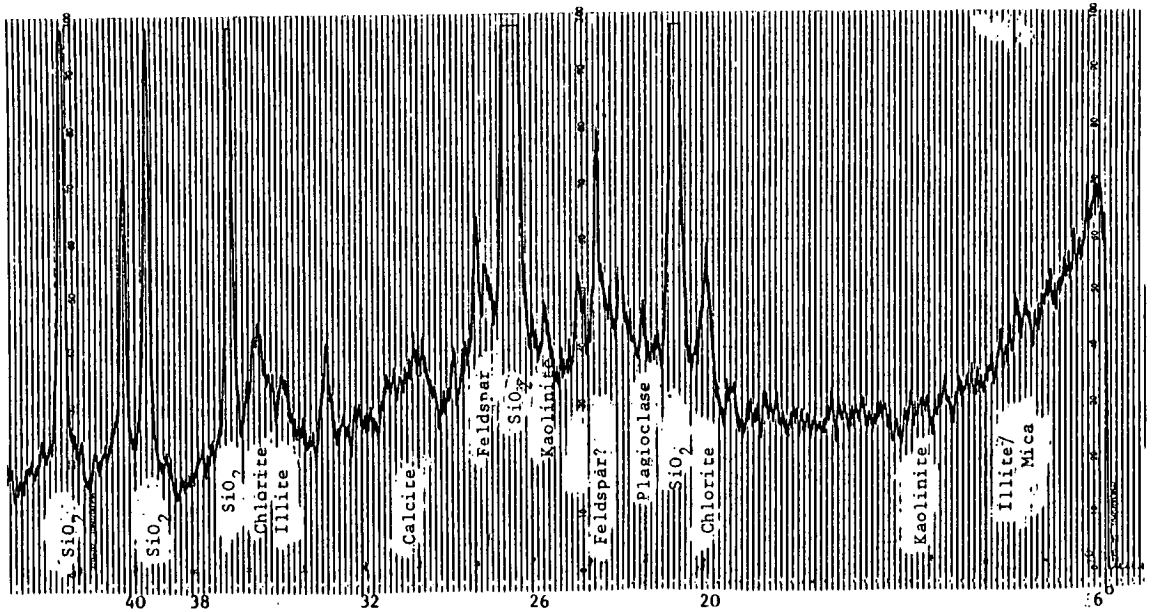
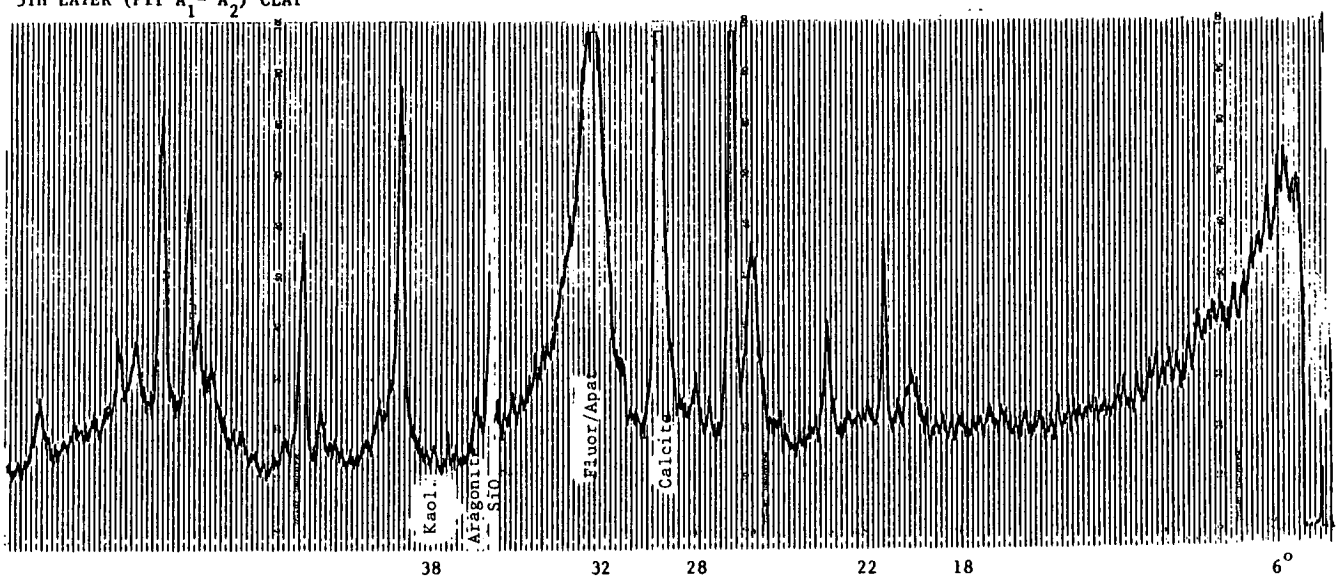


Fig.12.4.2

5TH LAYER (PIT A_1 - A_2) CLAY

c



usual ratio of various igneous rocks which is between 3 - 4.

The ratio U-234/U-238, with an average of 1.12±0.22(20%), are scattered around one within ± 1σ. (With one exception of P-13). The latter should be under "normal" conditions, which means that the U-238 is in secular equilibrium with its daughter U-234, due to the old age of these sediments.

The Th-230/Th-232 ratio varied from 0.9 - 2.0 with two exceptions of P-1B and $P\text{-}13_{cl}$ of 0.589 and 8.855, respectively.

The average of 1.44±0.18 (±12%) agrees with that found in terrestial rocks.

The U ppm values ranges from 2 - 11ppm and the Th ppm values from 7 - 40ppm.

Therefore, the great variations in the U and the Th within a cave system imply that it is not possible to assume a value from the above mentioned ratios in order to apply them in the correction of the ages. Also, it implies that for each calcitic deposition the water which carries U and Th from outside of thecave and through the limestone bedrock isa carrier of quite different U and Th contents. In such situations generally, drainage systems play a great role.

However, these different ratios could be due to many reasons some of which are explained below:

i) in ground waters the U-234/U-230 ratio varies considerably according to the chemical composition of the rock type being weathered. Isabaev et al, (1960) measured ratios as high as 7.8 with an average of 3.0 for waters draining off granitic rocks.

Surface waters varied over a relatively narrow range of 1.15 to 1.40.

ii) in general, the U-234/U-238 ratios for waters draining sedimentary rocks is low, ranging from 1.0 - 1.36, Cherdyntsev et al (1963). However, this ratio can be higher in the vicinity of carbonate rocks, Thompson, (1973), Thurber, (1964).

iii) when rocks which have previously lost a large proportion of their U are weathered, the U-234/U-238 isotopic composition of the water may be less than unity.

iv) post-depositional mobility of U, in sediments, shows evidence of oxidised and reduced zones. U is concentrated in reduced zones, whereas Th appears to be immobile.

v) the unique chemical properties of U relative to Th which can be related in a fundamental way to the two extra electrons that U has in the inner unfilled (sf) electron shell (more is described in section 11.2)

vi) in silicates Th and U may be in isomorphic substitution in important amounts, eg., in allanite, sphene, apatite. For the letter the tetravalent Th and U may be isomorphically substituting in the calcium position.

The presence of apatite has been revealed by XRD analyses, where abnormal results in age were obtained.

vii) the pronounced fractionation which would occur when the tetravalent Uranium (U^{4+}) is oxidised to uranyl ion UO_2^{++} (or U^{6+}) which is markedly different chemically from tetravalent Thorium (Th^{4+}).

viii) chemically, if oxidisation of U^{4+} to U^{6+} in solution is incomplete, then a wide range of U^{4+}/U^{6+} ratios might be expected. The U-234/U-238 ratio in the two valence states, should be different if account is taken of the fact that more U-234$^{(6+)}$ atoms will be

leached in preference to U-234$^{(4+)}$ atom . This is because Th-234 recoil atom is partially stripped of electrons during the decay process and U-234$^{(6+)}$ is produced. Kolodny and Kaplan, (1970) verified this in a study of sea floor phosphorites. The U-234/U-238 ratio of U^{4+} in the mineral was consistently less than unity, whilst this ratio in the U^{6+} was consistently greater then unity.

Therefore, as the U^{4+}/U^{6+} ratio in solution increases the U-234/U-238 ratio shall decrease.

From this rather simplified treatment it might be expected as the U content of the water increases, the U-234/U-238 ratio should decrease. Also, U^{4+} ion is more easily accommodated into the $CaCO_3$ lattice due to its radius site (0.99 A^{o}), than the UO_2 ion.

ix) the Thorium content is primarily a function of siliceous clastic content. The clastic insoluble residues of a limestone have Th and U ppm values like those found in common shale.

Adams and Weaver, (1958), concluded that all of the Thorium and only about 20% of the Uranium in the average carbonate rock is contained in the detrital essentially shale (i.e., average Th ≃ 13ppm, average Th/U ≃3.9)

x) U and Th are incorporated in different minerals. In shales, U and Th are to be found largely in fine-grained well mixed resistate mineral suites. These show different leaching effects on the Th and U due to acid treatment.

If most of the U and Th were held in or on secondary hydrolysate minerals, differences in sedimentary environments might be expected to cause much wider ranges in U, Th and Th/U ratios.

It should be noted that zircon is the only major resistate carrier of Uranium that also has a low Th/U ratio and this it must play a major role if the entire resistate heavy mineral suite in shales is to dominate the U and Th concentrations.

Finally, the U is retained primarily by resistate minerals eg. Zr, ground waters; while Th is incorporated in both resistates and clays (hydrolysates) and ground waters.

xi) the complex ions which participate to the U and Th transportation-absorption-deposition processes, also plays a role as to the preferential selection of either U or Th.

xii) Uranium is known to be absorbed from solution by organic material (Swanson, 1963) and also by clays Coldsztaub and Wey. (1955). The amount absorbed by clays is proportional to the normal base exchange capacity of the clay.

12.5 A Reappraisal of the Two Component Method

12.5.1 Some Theoretical and Experimental Considerations A correction scheme, which is believed to be reliable given certain assumptions about the sample, is based on the principle that together with the leached Th, a proportional amount of U is leached as well, Schwarcz (1979). The number of radiochemical analyses carried out necessary for the correction are two rather than a higher number of analyses of sub-samples using a linear regression method, as proposed by Schwarcz, (1979).

In most previous applied schemes it has been assumed that:

a) only Th-230 is leached from the detritus, in sufficient amounts to be of concern in the age determination, and,

b) that Th-232 is also leached and can been used as an index of the amount ofexcess Th-230 (leached) that has been added, that is, the detritus has a constant Th-230/Th232 ratio in its leachable thorium.

The first assumption is probably nearly correct in most young samples with a small detrital contamination. For the second assumption the following theoretical calculations will explain its effectiveness in the age determination.

If we assume that for the detritus, the Th/U actual ratio is about 4 and the Th-230/Th-232 activity ratios is between 1 and 2 (both typical values in terrestrial materials and experimentally confirmed as well or cave sediments, Table 12.4.3, above), then for a sample of 10^5 years of age, with an observed Th-230/Th-232 ratio of 10 (i.e., moderately contaminated), we expect the excess (leached) uranium and thorium to have been added as follows:

i) observed Th-230/Th-232 = 10, assuming that 5% and 20%, respectively, of the total Th-230 is detrital.

ii) expected detrital activity ratio U-234/Th-232 = U-238/Th-232 = 0.75 (since $\lambda_{238}/\lambda_{232} = 3.1$ and Th/U = 4 → U/Th = 0.25 → 0.25 x 3.1 = 0.75). Assuming the above Th detrital values, and assuming a ratio of U-234/U-238 = 1, i.e. secular equilibrium, (which is not always the case as it was found to be, Table 12.4.3), the U detrital value will be 0.75 x 0.05 and 0.75 x 0.2, respectively.

iii) observed Th-230/U-234 = 0.5

iv) corrected Th-230/U-234 = $\frac{0.5 - 0.05}{1 - 0.038} = 0.467$ and $\frac{0.5 - 0.2}{1 - 0.038} = 0.312$, respectively.

Therefore, the "corrected" Th-230/U-234 ratios are 0.467 and 0.312 or 4% higher and 31% lower, respectively, from the 0.45 ratio with only Thorium correction and 7% and 38% respectively lower from the uncorrected observed 0.5 ratio.

However, in all such cases, it is reasonable to take the elemental Th/U ratio of the detritus as an estimate of the Th/U ratio that will be leached by HNO_3 only under certain conditions concerning the mineralogy of the detritus; therefore the true U contribution could be more or less dependent upon it.
The last has been already described in Section 12.4.3 above. From the above assumption the second one, that the initial Th-230/Th-232 ratio is known is unsafe, bacuase of thepossibility of selective leaching of such sites which also leads to anomalously high U-234/ U-238 ratios in ground waters.
The Th-230 mobility for such sites may be similarly enhanced.
Another recognised problem also of detrital contaninants is that they may include particles of dolomite and calcite which are entirely soluble in HNO_3, which contains significant amounts of U in equilibrium with its daughters, but which contains relatively little Th-232 as the Th/U ratio of limestones and dolomites are typicallt less than non-carbonate clastic detritus, Rogers, Adams, (1969). Also, Adams, and Weaver, (1958) reported that an average of 80% of the U in a carbonate rock can be brought into solution by dissolving in weak acid.
An attempt is made to estimate the amount of this leached U by analysing the detrital clays which remain as insoluble residues after complete dissolution of the calcite has taken place.

12.5.2 Determination of U and Th Detrital Component ([U,Th] correction mode)

If a small sample of contaminated speleothem is analysed, it is safe to assume that different parts of that sample consist of mixtures of two uniform components i) detritus (D) and

ii) pure $CaCO_3$ (T).

Let us assume that the calcitic material representing an horizon (single depositional layer) is brought totally into solution with weak HNO_3 ($\sim$2N).

The dissolved sample is then filtered. The filtrate is spiked with a U/Th tracer and is analysed radiochemically for Th-230, Th-232, U-234 and U-238. The detrital insoluble residue in the filter is dissolved completely as described in Section 12.4.1, then spiked with a tracer and analysed radiochemically as the filtrate carbonate.

Then the observed radionuclides of the carbonate filtrate are those of the pure carbonate and the respective fractions coming from the detrital clay during the acid attack.

The assumptions introduced for the above dissolution procedure are the following:

i) all Th-232 activity is associated with component (D), and subsequently some is present in (T).

ii) the U-234, U-238 radioisotopes are leached in proportion and the U-234/U-238 ratio of the (D) is the same as in the original clay in the carbonate.

iii) the Th-230 and Th-232 also are leached in a proportion. The (ii) and (iii) above are supported by their chemical affinities.

iv) the obtained activities must satisfy the "additive rules" for the two component model, i.e., there is no preferential absorption effects of any radioisotopes from the respective

U and Th series to the glassware or ion exchange columns.

The procedure, then, for the calculation of different U and Th leachable radioisotopes is as follows:

From the Th-232 present in the carbonic filtrate and the (Th/U) ratio of the analysed detrital component (D) we can determine the leachable U-238 (in ppm values) which accompanies this leachable Th-232.

Then, from the detrital (U-234/U-238), ratio, the leachable U-234 can ne estimated.

From the detrital (Th-230/Th-232) ratio and the Th-232 activity value of the carbonic filtrate the true Th-230 also can be assessed.

These values are then subtracted from the respective total values of the carbonic filtrate.

This correction has been applied to the dated materials where appropriate.

12.5.3 Th-230/Th-232 Decay Scheme (initial Th only correction)

Any Thorium bearing detritus minerlas inside the host carbonates or present as surface coatings will result in a high age, because of the presence of non-authegenic Th-230.

Because this detrital Th-230 is always accompanied by Th-232, a rough correction for the detrital component can be made using the ratio $(Th\text{-}230/Th\text{-}232)_i$ observed in modern samples (since non-authegenic $Th\text{-}230_i$ is inevitably accompanied by Th-232 which can be considered as being of constant activity ($t_{\frac{1}{2}} = 1.4 \times 10^{10}$ yrs), over their life time of the deposit.

Thus, by subtracting the product of the assumed initial $(Th\text{-}230/Th\text{-}232)_i$ ratio with its decay parameter, from the measured $Th\text{-}230_{obs}$

activity the authegenic Th-230 can be determined, Kaufman, (1964), Kaufman & Broeker, (1965). That is,

$$Th\ 230_{obs} - Th\ 230_i\ e^{-\lambda 230\ t} = Th\ 230_{auth} \quad (1)$$

$$Th\ 230_i = (Th\ 230/Th\ 232)_i Th\ 232_{obs}\ e^{-\lambda 230 t} \quad (2)$$

from (1) and (2):

$$Th\ 230_{auth} = Th\ 230_{obs} - (Th\ 230/Th\ 232)_i\ Th\ 232_{obs}\ e^{-\lambda 230 t} \quad (3)$$

It should be noted that this Th-230 detrital component is the unsupported by any Uranium present in the detrial state.
This Th-230 decays with time; and for ages of ,say, higher than 200Ka this correction is negligible, if the contamination by Th-232 is not high. The above correction does not take into account the detrital Th-230 component which is supported throughout the years by the associated Uranium.
Therefore, there are three Th-230 components of different origin. The radiogenically produced by the Uranium of the pure (T) $Th\text{-}230_{auth}$, the supported Th-230 by detrital Uranium $(Th\text{-}230)_{detr,\ radiog.}$ and the unsupported detrital Th-230 $(Th\text{-}230)_{unsup.}$

12.5.4 Total Detrital Th-230 as Inferred from Detrital Th-232

(This forms part of 12.5.3 above)
Here the total detrital Th-230 activity is measured, i.e., supported and unsupported.
This is based on the Th-232 present in the carbonic filtrate and which is a purely contaminant component. The Th-230 corrected value is determined as described in section 12.5.2. (at the end)

12.6 Variations of the Initial Uranium Ratios

Fig. 12.6 shows initial $(U\text{-}234/U\text{-}238)_o$ ratios of dated carbonates as plotted against their respective U content.
It is a distinct fact that the range of the U content of the samples

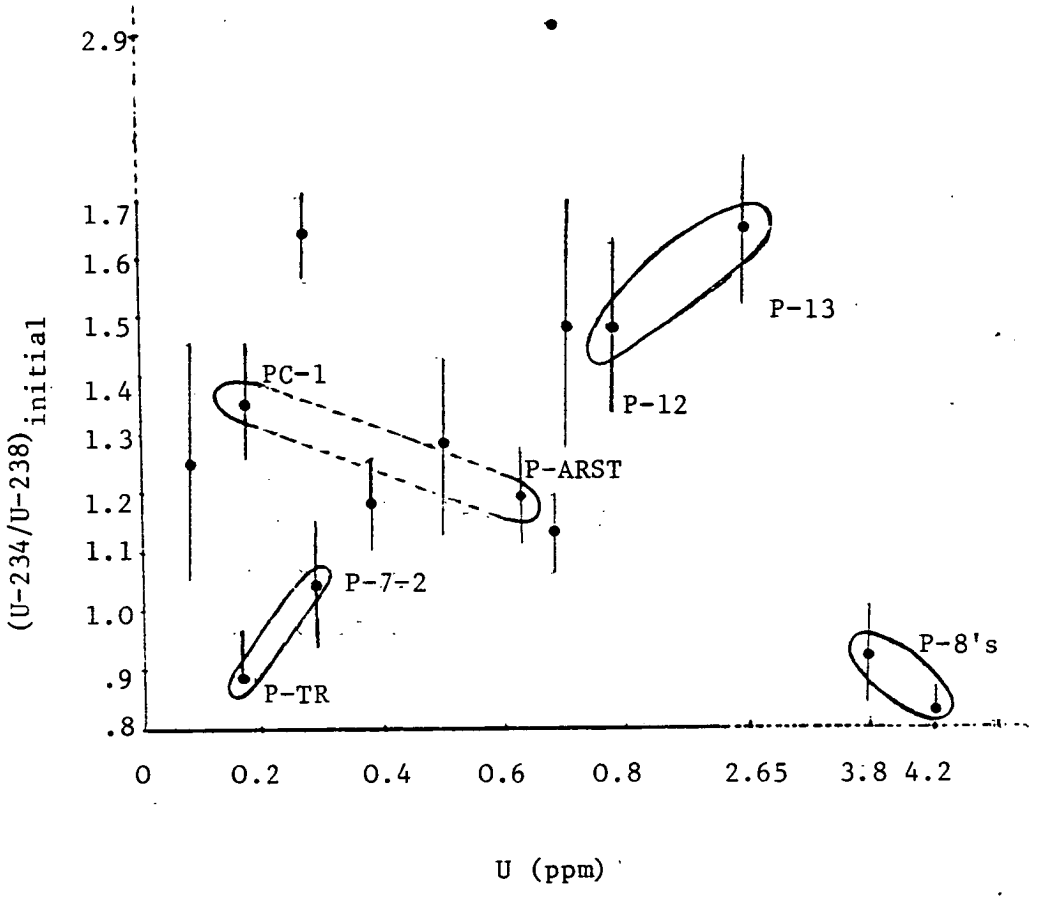


Fig. 12.6 Variations of initial uranium ratios with the respective U contents. Each loop includes samples from the same sample or location.

from Petralona cave, is less than ≈0.7ppm. Some high values presumes contamination by bones. Also, the initial U ratios vary considerably between 0.9 and 1.6.

Adjacent calcitic layers or nearby situated samples show consistent intiial U ratios within ± 1σ, (circled samples in the Fig. 12.6). The last statement was used, where appropriately, to obtain the age for samples with "infinite age", i.e. >350Ka, as inferred using the Th-230/U-234 dating method, by applying the U-234/U-238 dating method, see section. 12.7

12.7 Radiometric Data from Petralona Cave

The isotopic data obtained from the speleothem samples are given in Table 12.7 , together with ages based on these data. Because most of the samples had a Th-230/Th-232 ratio less than 10, the corrections already described above were made.

The variations in the resulting ages gives an estimate of the dependence of the age on this corrective parameter. Whereas yields of Th and U in analyses of speleothems from the deep interiors of caves are typically 30 - 60% we have sometimes obtained much smaller yields, especially for thorium during the analyses of these samples. This has contributed considerably to the uncertainty in age determinations at this site, since counting rates for planchets of Th and U have been correspondingly low.

Errors quoted below are in all cases estimated on the basis of α-particle counting, assuming poisson statistics. That necessitated

TABLE 12.7

RADIOMETRIC DATA ON PETRALONA SPELEOTHEMS

SAMPLE NO	LOCALITY	TH-230/ U-234	$(U\text{-}234/U\text{-}238)_{obs}$	$(U\text{-}234/U\text{-}238)_0$	Th-230/ Th-232	PPM Values U	PPM Values TH	AGE(x 10^3) years BP*
P-12top	Mausoleum	0.953 ±.045	1.272 ±.049	1.476 ±.156	3.00	0.75	0.91	250^{+49}_{-34}
(U,Th) corr.		0.780 ±.042	1.171 ±.053	1.264 ±.095	∞	0.59	0	$154.4^{+19}_{-16.4}$
							R = 1.44	199.2^{+56}_{-42}
							R = 2.0	164.4^{+62}_{-48}
							R = 1.10	214^{+54}_{-39}
							R = 0.6	232^{+51}_{-37}
							R = 0.25	243^{+50}_{-35}
							R = 0.10	247^{+49}_{-35}
P-12 lower	" "		1.993 ±.213	2.153 ±.391		0.10		
P-13	" "	0.980 ±.046	1.315 ±.031	1.656 ±.163	15.00	2.70	0.73	269^{+58}_{-39}
(U,Th) corr.								150^{+15}_{-13}
							R = 1.25	261^{+60}_{-41}
P-6	" "	0.540 ±.160	1.005 ±.051	1.006 ±.066	8.00	8.12	1.70	84^{+46}_{-32}
							R = 1.1	75.7^{+50}_{-37}
GR-4 top	" "	0.912 ±.068	0.974 ±.060		>1000	0.26		272.9^{+122}_{-68}
GR-4-2 lowest	" "	1.0414 ±.058	1.182 ±.073		17.2	0.16		$451^{+\infty}_{-150}$
U dating method				$U\left(\pm.113\right)_{0,av}$* & $U\left(\pm.043\right)_{obs,av}$**				≈468 (300_{min}-650_{max}).
(U,Th) corr.		1.05 ±.082		1.180min ±.098		0.15		≈500(340_{min}-660_{max})
GR-4-3 lower	" "	0.958 ±.057	1.131 ±.075		14.8	0.15		283^{+84}_{-57}
HU-38	" "	1.058 ±.0868	1.126 ±.046		>13.0	0.19		>450
75026-1	Sect. A_1-A_2 stalagmite inner part	8.363 ±.300	1.447 ±.604		20	0.34		>350
75026-2	ditto: outer layer	2.753 ±.933	1.104 ±.390		>1000	0.09		>350
75022-2	another stalagmite inner part	1.113 ±.072	1.043 ±.070		41.8	0.32		>350
P-1A	stalagmite inner part	2.683 ±.0247	1.151 ±.082		4.3	0.13	0.28	>350
P-1A ext	ditto: outer part	0.657 ±.027	1.486 ±.058	1.644 ±.092	11.6	0.24	0.06	$107.4^{+7.2}_{-6.8}$
							R = 2.00	$78.8^{+4.9}_{-4.7}$
							R = 1.25	$90.2^{+5.8}_{-5.5}$
P-TR	Sect A_1-A_2 top travertine	0.542 ±.085	0.919 ±.057	0.897 ±.067	7.7	0.16		$86^{+23.4}_{-19.1}$
							R = 2.0	64.4^{+35}_{-39}
							R = 1.5	$69.2^{+32}_{-27.7}$

SAMPLE NO	LOCALITY	Th-230/U-234	$(U\text{-}234/U\text{-}238)_{obs}$	$(U\text{-}234/U\text{-}238)_0$	Th-230/Th-232	PPM Values U	PPM Values Th	AGE (x 10^3) years BP*
P-7-2 second travertine layer	" "	0.913 ±.0262	1.017 ±.049	1.033 ±.109	5.5	0.26	0.14	$248.3^{+99.8}_{-51.4}$
(U,Th) corr							R = 1.25	=170 $223.6^{+104.3}_{-55.9}$
P-7-4 fourth travertine layer	" "	1.117 ±.113	1.075 ±.123		3.0	0.15	0.17	>350
(U, Th) corr								>250
			Th correction on slope: (for GR1-3 & P-7-4)		slope = 0.864			=220
GR1-4	" "	0.950 ±.09	1.115 ±.113		13.0	0.11		277^{+159}_{-70}
GR1-3	" "	1.135 ±.191	0.831 ±.160		8.1	0.08		>350
P-4-1 first layer	Mediter-ranian	0.788 ±.047	1.128 ±.0037	1.188 ±.068	49.0	0.35	0.19	$159.6^{+22.9}_{-19}$
(U,Th) corr							R = 2.08	$141.4^{+23.4}_{-19.6}$ ≈120
							R = 1.25	$137.2^{+26.6}_{-22.9}$
P-4-2 second layer	ditto	1.178 ±.040	0.995 ±.031		37.0	0.24	0.02	>350
(U,Th) corr		1.200 ±.042	0.996 ±.033					>600
U dating method			0.995 ±.031	1.188 ±.068				≈500 $^{+200}_{-150}$
P-3-1 first layer	" "	0.775 ±.061	1.208 ±.094	1.275 ±.152	2.4	0.48	0.57	$150.7^{+27.5}_{-22.2}$
							R = 1.25	$100^{+35.2}_{-30.6}$
P-3-2 second layer	ditto	1.278 ±.042	1.082 ±.030		4.6	0.44	0.41	>350
(U,Th) corr		2.587 ±.180	2.112 ±.184			0.06		>600
U dating method			1.082 ±.0830	1.275 ±.152				450±100
P-ARST	Aristotle's Hall	0.630 ±.044	1.186 ±.097	1.228 ±.129	3.0	0.24	0.18	$104^{+12.5}_{-11.2}$
(U,Th) corr								$75^{+11.6}_{-10.6}$
							R = 2.0	56^{+10}_{-9}
							R = 1.44	66^{+11}_{-10}
							R = 1.25	$72.8^{+16}_{-14.9}$
PC-1	" "	0.573 ±.035	1.281 ±.076	1.354 ±.104	9.7	0.17	0.04	$88.6^{+8.3}_{-7.8}$
							R = 1.0	$81.8^{+9.8}_{-9}$
			Th correction on slope: (for P-ARST & PC-1)		slope = 0.46			=73
P-110	1.8m flowstone	1.321 ±.280	2.924 ±.717		3.6	0.68	2.28	>350
(U, Th) corr.								$303.6^{+115.8}_{-142.5}$

SAMPLE NO	LOCALITY	TH-230/ U-234	$(U\text{-}234/U\text{-}238)_{obs}$	$(U\text{-}234/U\text{-}238)_0$	Th-230/ Th-232	PPM Values U	TH	AGE(x 10^3) years BP*
GR3-1a)	" "	0.900 ±.115	1.252 ±.194		13.0	0.06		211^{+118}_{-58}
GR3-1b)	" "	0.967 ±.113	1.618 ±.027		4.3			230^{+114}_{-60}
U dating method								
P-8-2	4m deep	0.675 ±.345	0.928 ±.008	0.910 ±.094	4.3	3.80	1.69	$550(360_{min}\ 730_{max})$ $124.9^{+365.7}_{-81.1}$
U dating mehtod			0.928 ±.008	0.808(on P-8-1) ±.012				>260approx (350±100)
P-15A	Precipe No 1	0.873 ±.078	1.067 ±.026	1.119 ±.074	13.8	0.68	0.14	$213^{+79.5}_{-46.1}$
P-15B	" "		1.105 ±.017			3.71	R = 1.25	204.4^{+85}_{-52}
U dating method								
P-1B	Sect. A_2 stone encrusted stalagmite	0.790 ±.092	1.339 ±.106	1.486 ±.218	4.4	0.72	0.53	≈215±90 $152.4^{+42.7***}_{-31.5}$
(U,Th) corr								$104.6^{+24.6}_{-21}$
							R = 1.25	$128.5^{+50.6}_{-40.3}$

* All the errors quoted are of ± 1σ.
** Initial uranium ratios are the average of all the samples from the same location.
***The age of this sample is considered low due to the possible selective leaching of Th-230 or enrichment by U-234 as is deduced from the respective Th-230/U-234 and U-234/U-238 isotope ratios. The former seems to be severe, thus explaining the obtained low ages. In such cases, the (U,Th) correction is not effective.

us to use the isochron curves of Fig. 11.3.1 , which, together with the quoted standard error of the ratios of interest could define possible ages with maximum confidence limits.

The corrections applied, where appropriate, are those described in Section 12.5.2,-3, -4, and their effect on the obtained ages is discussed. Due to the detritus state of the materials, discussion and interpretation is necessarily made for each sample separately.

i) Mausoleum Site Three of the samples, GR-4, GR-4-2 and GR-4-3, were analysed at McMaster University, Schwarcz, Liritzis, Dixon, (1979). It is apparent from Table 12.7, that there is considerable variation in the isotopic comparisons of these samples, i.e. between the GR's taken from the same 4cm thick layer and the P-12,-13 samples taken from other partsof the same Mausoleum floor. The U-234/U-238 ratio varies from 0.974 to 1.305, while the uranium concentration ranges from 0.10 to 0.75ppm.

The GR samples do not show any serious contamination as evidenced by their high Th-230/Th-232 ratio.

The lowest U-234/U-238 ratio in the Mausoleum samples, is within $\pm 1\sigma$, one, and the highest ratios could be explained as partial enrichment by U which may be due to ground waters which might exhibit a high U-234/U-238 ratios, and the presence of fluorapatite/apatite in the detrital residue of the P-12 and P-13 samples, (Fig. 12.7).

However, contamination by bones is not high since the values of the U concentrations obtained are typical of those found elsewhere in the cave. When applying the above-mentioned corrections (Section 12.5.2), the age of the upper travertine layer of sample P-12 drops from 250Ka down to 160 Ka BP.

Th only correction brings the age even lower, down to 90Ka.

The initial ratios of Th-230/Th-232 of R = 2 and R = 1.44 (average value of the analysed clays in the cave) gives ages of: 170Ka and 200Ka, respectively. It isnoticed that, for a considerable correction for initial Th ratio, (R = 2), the age coincides within $\pm 1\sigma$ with the (U, Th), corrected age.

It must be emphasised that the applied initial Th correction gives the minimum subtractable detrital Th-230 activity, that is, produces a higher age,higher than the actual corrected age; and sometimes is between the Th only correction and the uncorrected ages. This is because the accumulated total detrital Th-230 activity is not present in the observed Th-230 activity of the carbonate, but only a fraction which is the leached Th-230 from the dissolution of the sample. The rest remains in the detrital residue of the clay, (Section .2.5.2). This corrected Th value, together with a small detrital U contribution would give the most probable age. Thus the value of R = 2, coinciding with the applied (U, Th) corrected age would probably mean that:(a) the most probable minimum age could be an average of their overlapped error limits, or approximately 170Ka BP and with a probable maximum span of 200Ka BP. (b) the U and Th are present in fine grain clay particles and that the non-supported Th-230 detrital component predominates over the supported one, which would mean that it is not combined with resistates.

This minimum is furthermore reinforced (*i*) purely from the stratigraphy of this top layer, (*ii*) by the presence of bones which would contribute U so that the actual subtracted detrital U is likely to be considerable, thus producing a higher age. For the latter, it is believed that the U and Th from the bones

have been leached only in trace amounts since their major part remained in the detrital residue which was subsequently revealed by X-Ray diffraction analyses (Fig 12.7). The dated sample had an obvious multilayered appearance which presumably implies different times of deposition. The upper layer, having the lower age, could be as low as 80Ka and the lower part of this layer could be as old as 250Ka, as further explained in (ii) below. Although other R values, arbitrarily chosen, duly considered, would be likely to give ages which are within $\pm 1\sigma$ similar to the average found above (with its prabable maximum span). Finally, the fact that we work out only maximum error limits of 1σ is supported by the basic assumption upon which the applied corrections of the samples and their associated travertine systems, already described(Sect 12.4.2 and 11.1) are based. The range of uncorrected ages for the GR samples is from 250Ka to greater than 350Ka BP.

The oldest sample (Gr-4) reached the limit of the Th-230/U-234 dating method and has associated errors which allow a wide range of possible ages, Section 11.14. There samples with a clear calcitic appearançecame from another part of the Mausoleum. The sample GR-4 gave an age of approx. 270Ka BP. Sample Gr-4-2, one which had the highest U and Th yields, gave an age of ≃450Ka, which becomes around 600Ka if a (U, Th) correction is applied, (based on average isotope ratios of clays.)

An alternative technique for such high ages, is to use the U-234/U-238 dating method. That requires a knowledge of the initial U-234/U-238 ratio when the carbonate started to form. The formula applied is the following:

P-12 DETRITAL RESIDUE

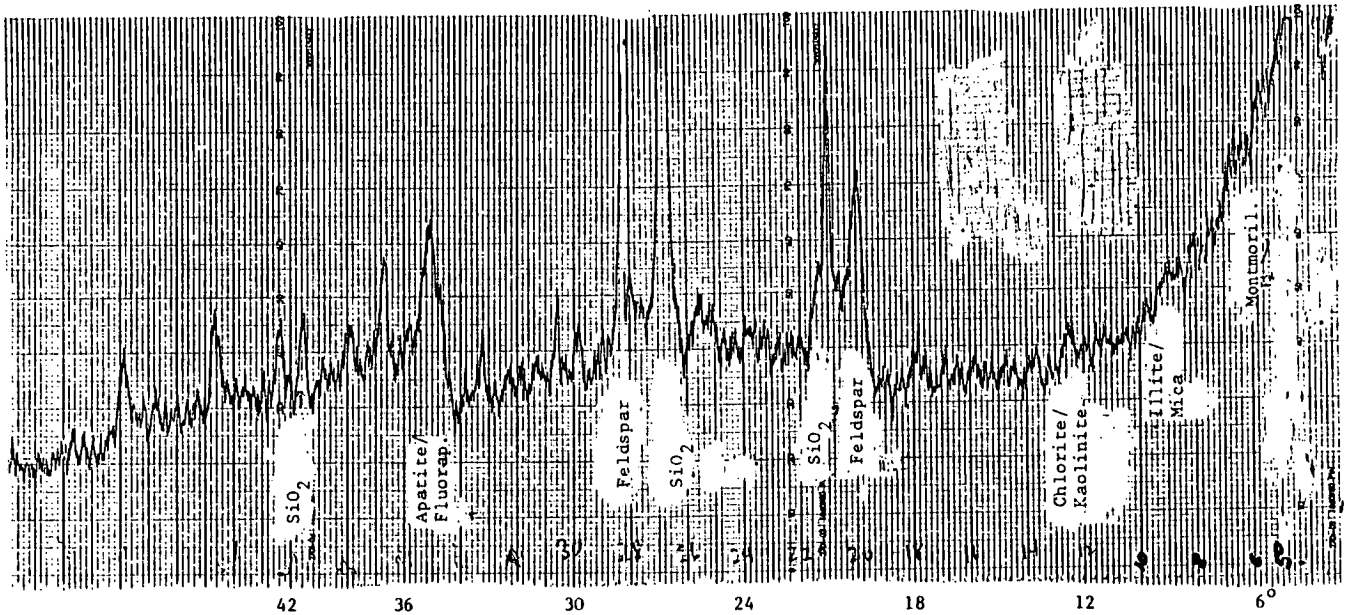
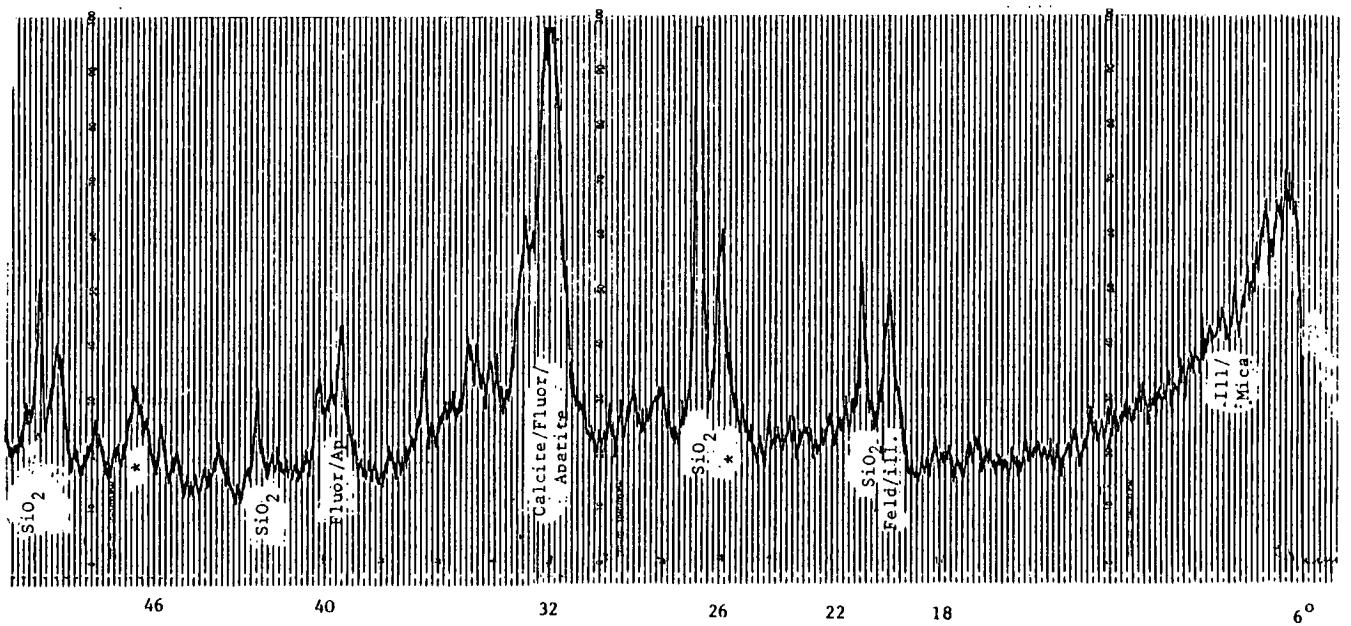


Fig. 12.7 X-Ray Diffraction pattern of detrital residues from P-12 and P-13 samples

P-13 DETRITAL RESIDUE



Fluorapatite/Apatite

$$\left[\left(\frac{U\text{-}234}{U\text{-}238}\right)_o - 1\right] = \left[\left(\frac{U\ 234}{U\ 238}\right)_{obs} - 1\right] . e^{-\lambda_{234} . t} \rightarrow$$

$$t(yrs) = \frac{\log\left[\left(\frac{U\ 234}{U\ 238}\right)_o - 1\right] / \left[\left(\frac{U\ 234}{U\ 238}\right)_{obs} - 1\right] \times t_{\frac{1}{2}\ 234}}{0.298} \qquad (1)$$

The initial U ratios of 1.566 ± 0.113 in the present cases is the average of the P-12 and P-13 top layers, and the observed U ratio of 1.154 ± 0.043 is the average of GR-4-2 and HU-38 samples with "infinite age" i.e. >350 ka. The obtained age of 468 (300min-650max) ka is in reasonable agreement with ages of the top layers and of the expected order of magnitude. With an U_{obs} of HU-38, the obtained age is 540 (350min-780max), see table 12.7, page 358.

For such high ages any attempt to correct for initial Th will not have any significant effect . From the above, we see that GR-4 was the youngest sample for the one of the travertine samples and with the lowest U-234/U-238 ratio. If the source of U was being progressively leached over a long period, a decrease in U-234/U-238 ratio over time would be expected but not an increase on U concentration.

The sample GR4-2 give a higher age when a (U, Th) correction is applied, in contrast to the P-12 which gave a lower age after a similar correction. This age is 500Ka BP (340 - 660Ka BP). Also, the GR-4-3 with an uncorrected age of ≃280Ka BP almost agrees with the uncorrected P-12, which means that it comes from top part of the travertine or it represents a little earlier aged calcitic stratum than the P-12.

Plotting those values on the isochronic graphs the corrected ages overlap within ±1σ in the range between 400 - 600Ka BP;

extending from 220Ka to higher than 600Ka BP

Thus we appear to have within a 4cm thick calcite deposited over a period of more than 200Ka, from at least 750 Ka to 280Ka BP.

However, each of the "age" estimates have a large uncertainty associated with it, and there is an actual overlap between the ranges of probable age. There is a 65% probability that the true age lies within $\pm 1\sigma$ of the estimate of each sample. Considering the $\pm 1\sigma$ error limits of each sample, we see from Fig 12.7.1 that the older samples have a common range of possible overlap with its uncorrected age in the time interval from 350Ka to greater than 600Ka BP, Fig12.7.1 In particular, this range is within -1σ of the U-234/U-234 dating method result. These time ranges overlap with the probable time spans of the corrected ages, Fig. 12.7.1.

While this is not convincing proof of the age of the layers, it indicates that the isotopic analyses are consistent with possible finite ages. (Another sample HU-38, made by Schwarcz in Israel, also gave a high result >450Ka, see Fig 12.7.1)

Overall, the calcitic deposition in the Mausoleum seems to have ceased growing at least 80Ka ago, while it existed since 750Ka BP.

Nevertheless, it should be mentioned here that due to unusually slow calcitic growth it is difficult to assume that the surface of the P12 (upper layer) was formed at the quoted age $\pm 1\sigma$.

The alternative possibility of being a intermitent age has to be taken into account.

As it has been shown (Section 12.8), by thin section analyses, this layer was developed under poor conditions and thus the very

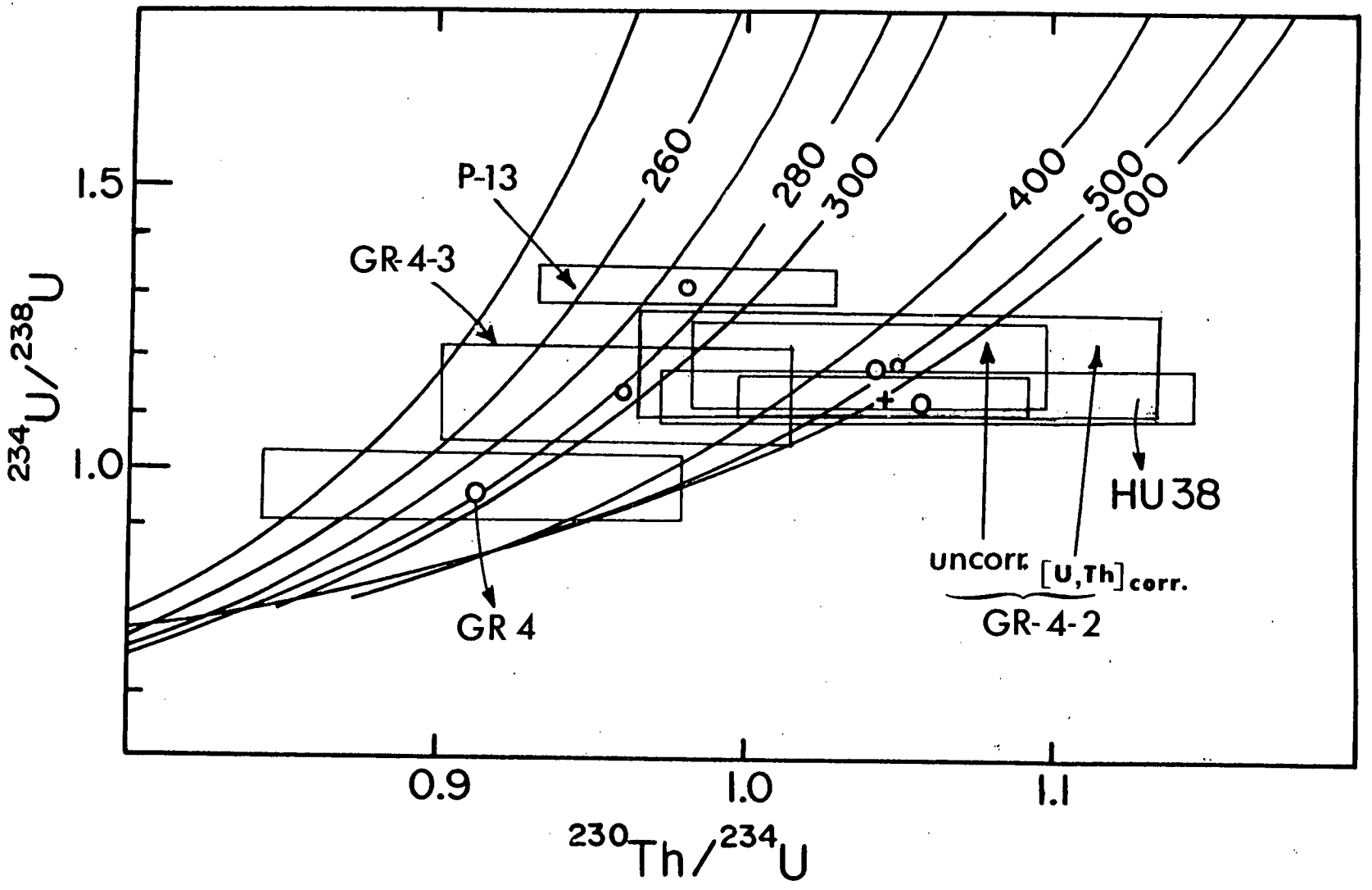


Fig. 12.7.1. Plotting of the Isotope Ratios (together with their ± 1σ) in the higher part of the isochrone graph, for the Mausoleum samples

slow deposition could well have continued till the last 80Ka BP In this case the lower part of this upper layer would be as old as 250Ka. The last suggests an average growth rate of $\simeq \frac{0.003}{1000}$ cm yrs

Typical growth rates for speleothems deposits such as these in temperate climates, are from 0.1 to 1.0cm/1000 yrs (Harmon et al 1975). Rates less than 0.02cm/1000 yrs as implied by the age date are unusual, and would be expected to be associated with finely laminated speleothem whose composition and texture had varied many times over such a long growth history.
The dated stratum of GR while being interstratified with such laminated desposits, is itself homogeneous and unlaminated, while the P-12 appeared also to be interstratified but not homogeneous being intermittently brown and white layered.
GR also appears to have been deposited in one single episode.

Arguing on the basis of the appearance of this travertine layer and from experience with rates of deposition of such strata (Schwarcz, pers. comm.), we would suggest that deposition at this site began not much before 750KaBP and continued intermittently until about 80Ka ago. In this case, the interval between 200 - 300Ka BP would be a very unsatisfactory (or very slow) calcitic growth period (see *ii* below, where the same situation was met in the Mediterranean site, as well).
The P-13 sample comes also from the Mausoleum, but from another part. This travertine of 1cm thick, is monocrystaline, (Fig. 12.7.2) and represents the upper part of the Mausoleum main travertine.
It gave an uncorrected age of $269\ ^{+58}_{-39}$ Ka BP, which when corrected for (U, Th) based on its detrital residue isotope ratios

became ≃ 150Ka.

An initial ratio of R = 4 does not make any difference to the uncorrected age (i.e., it is high, that is the detrital Th-230 has decayed away). Due to the existence of Fluorapatite in the detrital residue, Fig. 12.7, the sample seems to have been contaminated by bones; otherwise it was covering a bone Fig.12.7.2.

That could produce an uranium contribution to the carbonate isotopes, which would reduce the age. The uranium concentration of 2.70 ppm is an indication of such contamination (when compared with other samples in the cave), which in addition gives a high U-234/U-238 ratio of 1.315, whilst that of the detrital clay was only 0.967.

In conclusion, the quoted uncorrected age, with its associated error is taken as the probable age of this layer, that is 180 - 320 Ka BP.

This time span represents a part of the depositional period in the Mausoleum site which lasted until about 80Ka ago, as argued above. The growth rate in this sample, is also very small of the order of 0.004cm/1000 yrs.

The last sample from this site is P-6. This comes from a thin flowstone covering a limestone rock in the interior of the Mausoleum.

This calcitic deposition presumably had partially covered the skull, Fig. 12.2.(above). The obtained age of 84Ka is not meaningful due to the very low U, Th yields, though it sets a minimum age for the actual calcitic layer and for the skull as well.

It was severely contaminatedby bones as evidenced by X-Ray Diffraction, Fig. 12.7.3, and the U content was 8.12ppm. Though it has a detrital Th-232 component of 1.70ppm still the Th-230/Th-232



Fig. 12.7.2 P-13 Travertine which covered a bone (hipbone?) from the Mausoleum site.

P-1A STALAGMITE (SAMPLES A1 → A3, RADIALLY FROM EXTERNAL → CORE)

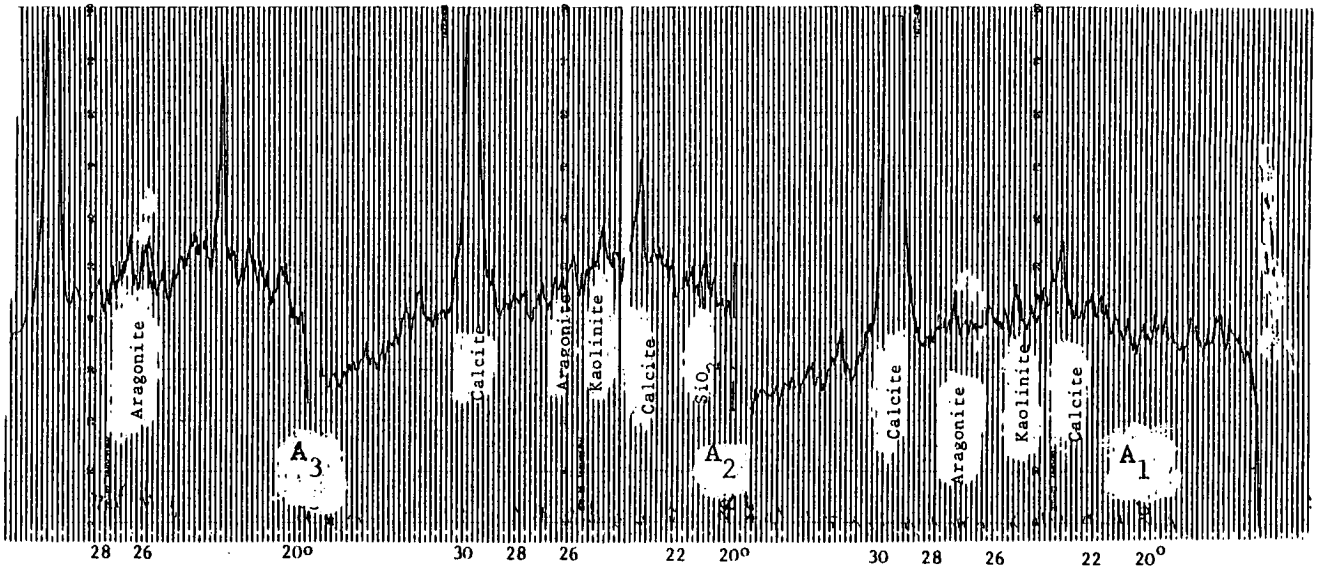
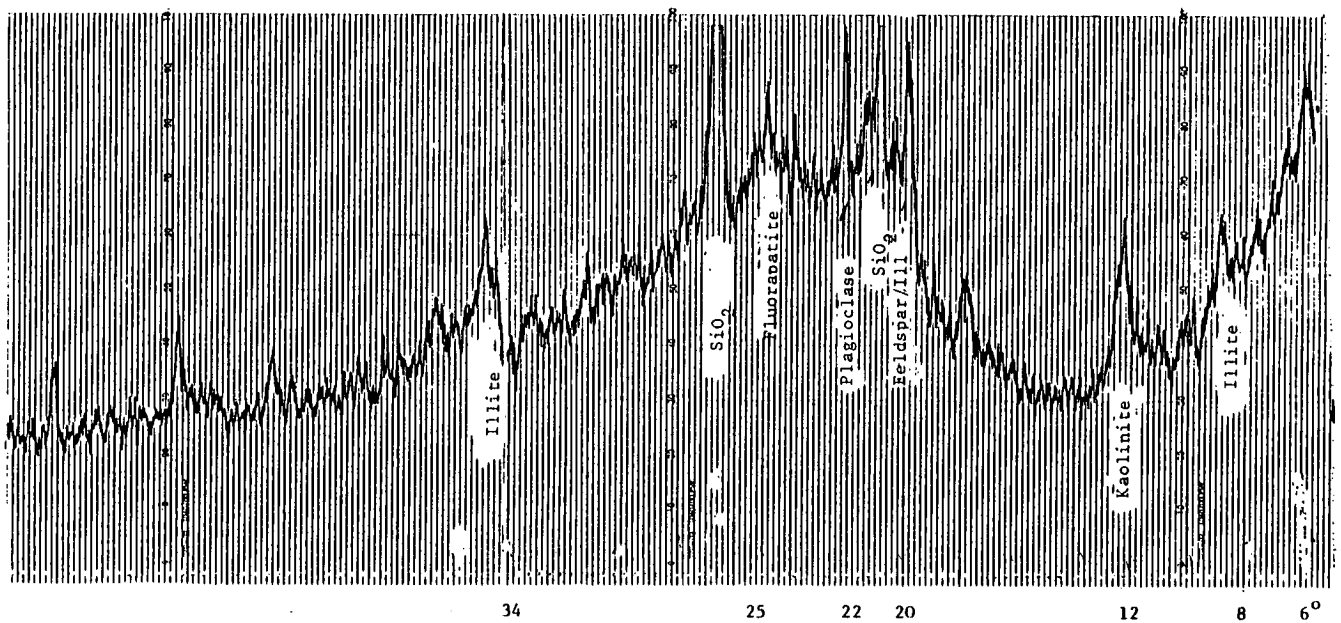


Fig. 12.7.3

P-6 DETRITAL RESIDUE



ratio of eight was not low enough to imply that the Th-230 from the sample had a higher value than that produced by the U of the pure calcite only, presumably being supported by the U-234 from these bones. (high $\frac{Th-230}{Th-232}$ ∿ low Th-230/U-234, i.e. here 0.540) Therefore, a considerable correction has to be made for the Th-230 and U-234. Though with caution we give this result, we are confident that it is not less than 80Ka BP. Since this upper (0.5cm) calcitic layer comes from the Mausoleum site, where thecalcitic growth ceased at least 80Ka ago, as proven above, the arguement that the P-6 should be at least or equal to ≃80Ka is in concordance with the last calcitic growth andis likely to represent this upper depositional event of the Mausoleum site. Otherwise, its textural appearance of being crusty, trimmed, with saw-like small crystals of calcite, justifies its later formation.

ii) Mediterranean Site Sample P-4-1of 0.8cm thickness was a light brownish with obvious interstratification (at least 8 layers counted), Fig. 12.7.4. The uncorrected age was 160±20Ka. Its detrital residue (<1%) gave a Th-230/Th-232 ratio of 2.08. Taking this value as the initial Thorium ratio the age becomes around 120Ka, which is still within ±1σ in the range of the uncorrected age.

A probable age after correction for (U, Th) is 140±20Ka. This compatibility is very encouraging considering the validity of the applied (U, Th) correction, and this is the average age for this upper part of the travertine.

Here, the two possible interpretations of this age result must be clarified.

a) if indeed there was a very slow deposition of calcite by, say, some kind of slow flow rate of water carrying clay, then the



Fig. 12.7.4. Travertine P-4. The upper part (interstratified) represents the P-4-1 sample. The second layer represents the P-4-2 sample. The lower parts end with encrusted stones and embedded bones.

age of 140±20Ka represents some intermittentpart of this 0.8cm layer.

That is, the upper surface could be as young as 70Ka and the deeper stratum as old as 210Ka. It has been calculated by trial and error that for an interstratified stratum the average obtained age corresponds to the middle layer within ±5% depending on the growthrate and the number of respective sub-strata. This suggests a growth rate of 0.004cm/1000 yrs.

b) if there was a very thin film of water being deposited over a short period of time, then the obtained age within its error represents the true age of this upper layer, This suggests a growth rate of 0.006/1000 yrs.

The first (a) agrees with the ages obtained for the top travertine layer from Aristotle's Hall and the section A_1 - A_2 and is considered as the more plausible solution.

In addition, such very slow growth rates, quite often occur in some cave systems. The white opaque calcitic layer terminating the last deposition, Fig. 12.7f, implies a dissication and subsequent drying out of the cave (last glacial around 80Ka ago). The alternative soily white layers along the travertine mean intermittent development of this flowstone, where very thin films of water carrying each time different ions and soils. In temperate regions it has been found that the alternation of weather conditions from summer to winter (a parallelism to interglacial-glacial periods) may give rise to varved clays.

At the end of the summer, percolating waters contain relatively little clay and only sand is deposited. At the end of the winter by contrast, the soil is more decalcified and the clay is free to be moved and is deposited.

The P-4-2 is the second part of the above travertine, of 0.5cm thick, Fig. 12.7.4. The uncorrected age is >350Ka and with a (U, Th) correction based on the detrital clay of the P-4-1 sample, gives an even higher age, higher than 600Ka. If we attempt to use the U-234/U-238 dating method, with caution as to how certain we can be of the constancy of the initial U-234/ $U\text{-}238_0$ ratio; a crude age is obtained which when calculated from the formula above and taking into account the respective errors of the U ratios, yields an age of 500^{+200}_{-150} Ka. The initial U-234/ U-238 ratio was that of the P-4-1 and the observed uranium ratios that of the P-4-2.

This in fact co-ordinates with the time span of the lower travertine of the Mausoleum site.

Also, it should be mentioned here that these two stalagmitic layers were the upper parts of this P-4 travertine, which additionally consisted of a further lower part (texturally implying a single event which was badly contaminated by clay and a plethora of small bones, thus being rendered unsuitable for dating. The clay was obviously diluted in to this lower stalagmitic material, implying a warm period with poor calcitic deposition.

Furthermore, the upper 0.8cm thick floor was easily separated from the lower (second) layer, displaying a smooth inner surface which broke clearly and followed the contours of the lower surface; which suggests a possible lapse of time before the growth of the upper layer upon the lower layer. This "Hiatus" could have delayed the calcitic deposition for the period from ≈200 - 350Ka BP.

P-3-1 is another borwhish interstratified thin upper layer of travertine of 0.5cm thickness. Though from another locationof

the Mediterranean site (4m away from P-4), it represents another stalagmitic deposition from the lower sunken floor on the way to the Mausoleum.

The age of this upper layer is 150±25Ka BP or similar, as anticipated, to that of the upper P-4 layer (growth rate 0.003cm/1000yrs). This age suggests an age of 75Ka for the top surface layer and an age of ≃220Ka for the lower part of this upper layer.

P-3-2 is the only lower part (1cm thick) of this travertine, which gave an age of >350Ka BP. Under the lower layer, small bones were found. Fig. 12.7.5.(2 pages on)

Due to the small amount of the detrital (<1% , by weight of the sample) the possible contamination by detrital U and Th is thought to be small. However, applying the U dating method, we get a substantiated age of 450±100Ka BP. This suggests an age of ≃350Ka for the upper part of this lower layer, and an age of ≃550Ka for its lowest part.

Therefore, the above two travertines P-4 and P-3 represent the same stalagmitic depositional events. Both travertines are a further extension and are given support by the implications concerning the Mausoleum site travertines; that there was indeed an old calcitic precipitation at the same time, but in different parts of the cave. Also, it seems that between ≃200Ka - 350Ka BP there was not any obvious calcitic growth, as it is also evidenced texturally from the clear separation of the upper and lower layers, as if these represent two different times.

This last statement has been given some support considering the glacial-interglacial climatic phases in the upper and middle Pleistocene epochs, section 12.10.

iii) Aristotle's Hall Sample PC-1 was a white yellowish calcite from the top travertine layer of the above hall. It gave an uncorrected age of ≃ 88Ka BP. An initial Th correction of R = 1.44 makes it 79Ka and for R = 2.0 becomes 75Ka BP, Fig. 12.7. 6 (2 pages on) Sample P-ARST was another yellowish top travertine from another part of this Hall. A slight residue remained on initial dissolution of dark brown colour. It gave an uncorrected age of 104±12 Ka BP Applying a (U, Th) correction assuming certain isotope ratios, (i.e. U-234/U-238 = 1.12; Th-230/Th-232 = 1.44; Th/U = 3), the age becames 75±11Ka BP, while for initial Th correction for R =1.25 the age becomes 73Ka, for R = 1.44 it becomes 66Ka and for R = 2, even lower, down to 56Ka BP. Though the error bars of ±2σ, satisfy the above different obtainedcorrected ages the significance of the correction becomes obvious for such low ages, Fig. 12.7.6.

Furthermore, the Th-232 content for the PC-1 sample,was 0.048ppm, with an U content of 0.17ppm; whilst the P-ARST had a Th-232 content of 0.18ppm, and a U content of 0.24ppm. Thus, it appears that the P-ARST was badly contaminated giving thus a higher (higher Th-232) while the PC-1 with its lower Th-232 gave a lower age and naturally most correct.

From these data, we favour a lower age rather than the P-ARST, though in order to justify the most probable age it was thought to approach the matter from two different angles.

a) first we plot the Th-230/Th-232 ratios against their respective U-234/U-238 ratios from the two samples, Turekian & Nelson, (1976). The obtained straight line would give the ratio Th-230/U-234 which reflects the age of this top travertine. This plotting is an indirect Th only correction (including

P-3-2 DETRITAL RESIDUE

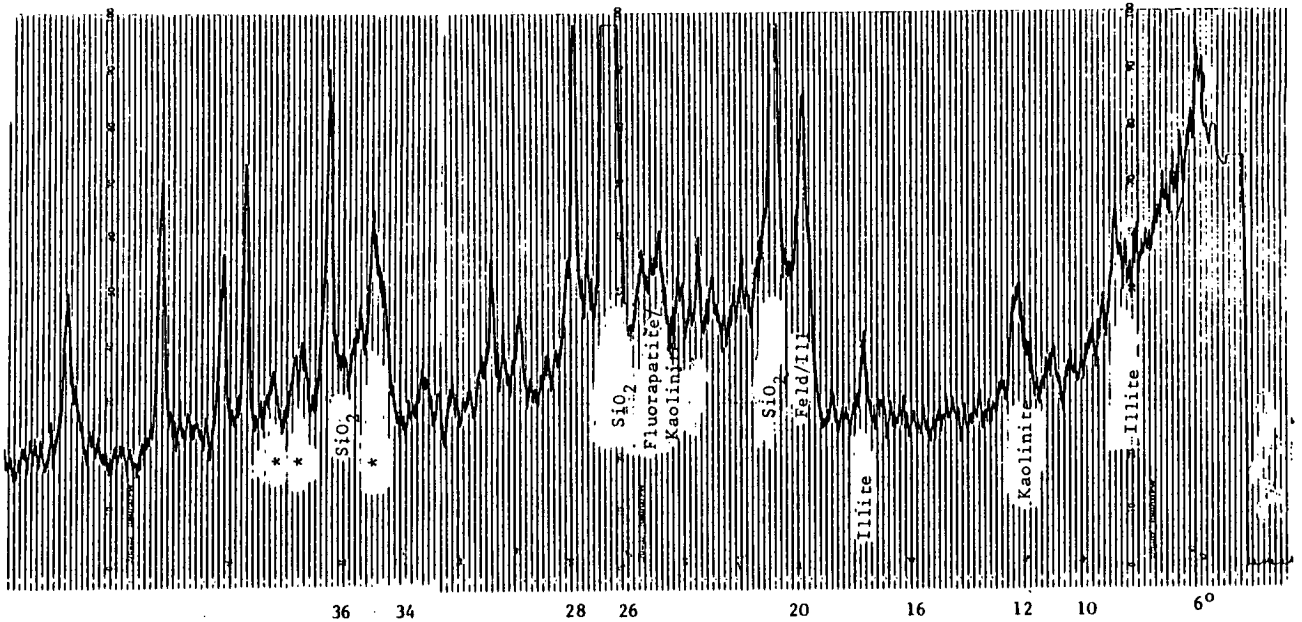
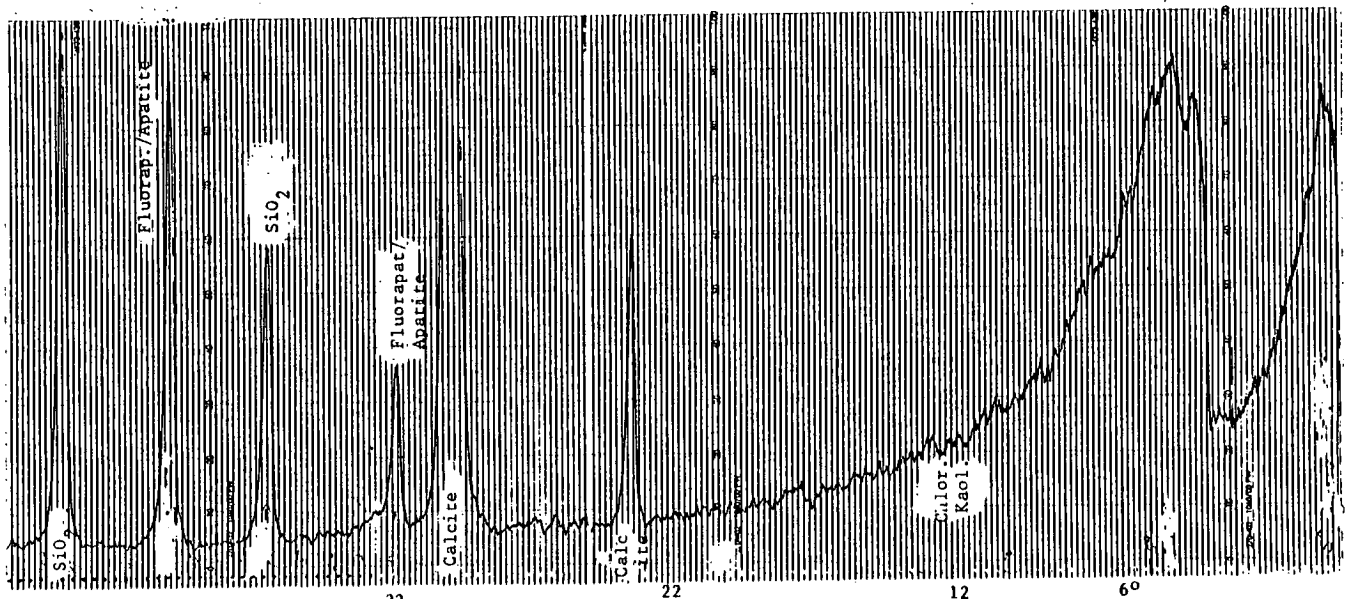
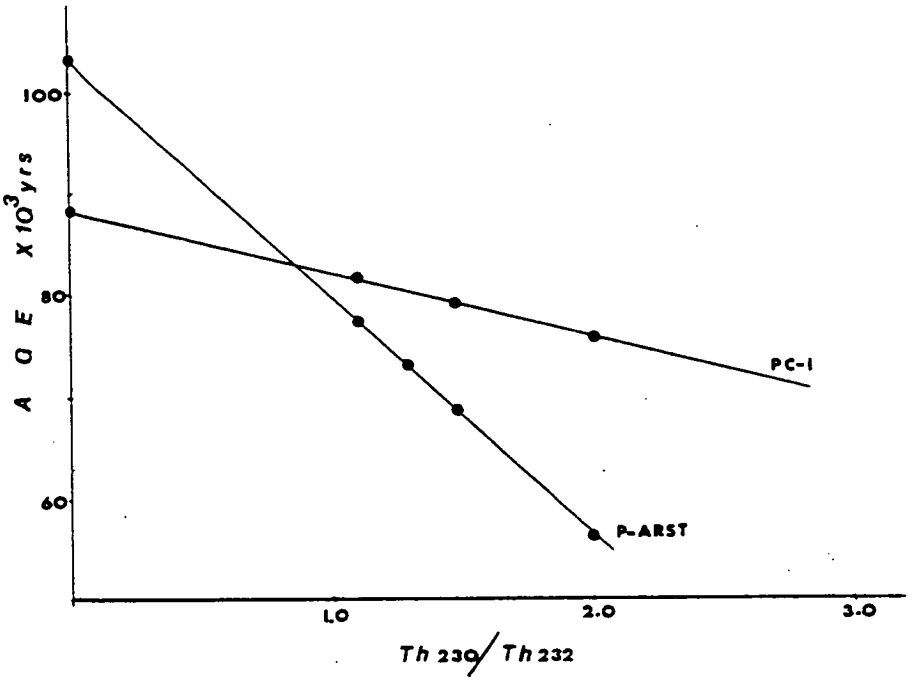


Fig. 12.7.5

*Fluorapatite/Apatite

P-7 (LOWER LAYER) CARBONATE





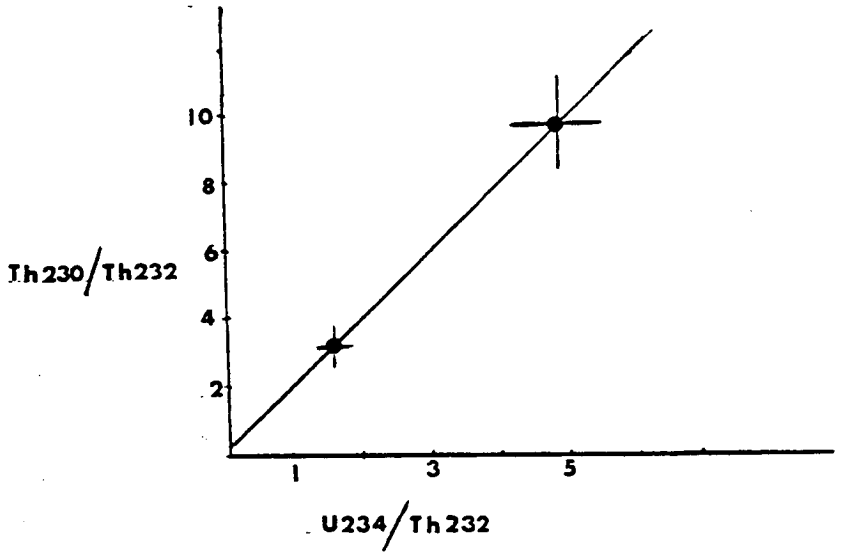


Fig. 12.7.6 Corrected Ages for different initial Th230/Th232 detrital ratios.

Assume: Ratio $(Th230/Th232)_0$ in the leachable detrital component was the same in both samples at the time of deposition.

Then Today : $\left[\frac{Th230}{Th232}\right]_t = \left[\frac{Th-230}{U-234}\right]_a \cdot \frac{U-234}{Th-232} + B_t$, $B_0 = B_t \exp(-\lambda_{230} t)$

Slope: 0.48

AGE : 73,000 yrs BP.

B_t = detrital leachable ratio today.

a = authegenic calcite ratio.

detrital Th-230 and background Th-230 initially present).

The slopes of 0.48 represents an age of 73Ka BP, Fig. 12.7.6.

b) from the initial U-234/U-348 ratio obtained in P-ARST and the observed U-234/U-238 ratio in PC-1 the U dating method yields an age of 75Ka BP.

In conclusion, the age of 70±10Ka BP the average of all the corrections with its associated error is taken as the best age representing this upper travertine.

iv) Stalagmites above the Top Travertine of the Section $A_1 - A_2$

Two stalagmites deposited on this travertine layer have been analysed.

They both show signs of chemical disturbance and their Th-230/U-234 ratios are all greater than possible equilibrium values. (See Fig. 12.7.3, nine pages above). In particular, the 75026-1 gave extraordinary ratios of 8.4 and 2.7 for its inner and outer layers, indicating extensive migration of radioisotopes in these samples. (curiously they do not display any textural indication of having been chemically disturbed).

The 75022-2 sample gave also an infinite age.

P-1A of the same stalagmite gave an age of >350Ka.

Fortunately, X-Ray diffraction analysis of this inner part of P-1A showed traces of aragonite,(Fig, 12.7.3,)which meant that the above stalagmites (especially their inner parts) were recrystallized sometime in the past, with subsequent migration of radioisotopes, and thus producing an erroneous age. The other part of P-1A, (1.25cm thick) gave an uncorrected age of 104±7 Ka. There was no detrital residue left, and the detrital Th-232 component was 0.06ppm. Though there were traces of clay spread in certain layers. A correction based on Initial Th correction, for R = 2,

yields an age of 79.8 Ka BP. However, in spite of the lack of any detrital residue or other textural information, except an XRD analysis which showed possible traces of aragonite, (see Fig. 12.7.3) and in view that the inner part was disturbed with selective leaching of U-234 atoms, the age of 104Ka is considered higher than it should have been.

Also, because these stalagmitic columns are growing with flat top formation, then at any given height, their age profile will be essentially flat over some central region (A' - B' of Fig. 12. 4, p.338). Thus it is unlikely that the centre of this stalagmite is older than the outer. However, the appearance of this material shows obvious distinction between outer and inner layers.

Overall, it is interesting to see that during recrystallisation the U radioisotopes are leached more than the Th ones, thus producing a higher age.

v) Capping Travertine Layer of Section A_2

It is an interstratified thick travertine which was divided into five parts. The lower being texturally similar to the fourth, but incorporating bones thus being unsuitable for dating.

The P-TR comes from the top-upper layer of this travertine. It yields an age of 86±20Ka, which becomes ~65±30Ka for Initial Th correction with R = 2. When it is compared to the external part of the above P-1A stalagmite, it agrees with it to within ±1σ. This piece consisted of some layers of different colour which further suggested that the surface of this upper layer could be slightly lower than the quoted age. However, we believe that these ages would oberlap to within ±1σ.

P-7-2 is the second layer of this flowstone (under P-TR) and

it yielded an age of 250^{+99}_{-51}Ka BP.

This was a light reddish-yellow sample, interstratified with some porous parts present. Unfortunately, its detrital residue was not kept. By assuming clay isotope ratios (the average values found for the clays, Table 12.4.1) a corrected age of ∿170Ka BP is obtained.

In order to interprete this uncorrected age, three more results from the lower layers are presented and discussed.

P-7-4 is the 4th layer, 1cm thick, interstratified with 22 layers counted, it gave an age of >350Ka though with obvious signs of contamination, from the presence of Th-232 being 0.17ppm. The contamination was mainly from bones, Fig. 12.7.5, above.

A (U, Th) correction based on average clay isotope ratios yields an age of 250Ka BP

The two other samples GR1-4 and GR1-3 are from the very base of another travertine.

GR1-4 yields an age of 277^{+160}_{-70} Ka and contains 0.11ppm of U. The other has a Th-230/U-234 = 1.135±0.191, that is, greater than the equilibrium value corresponding to "infinite age". The U content of the latter sample is similar (0.08ppm), but its U-234/U-238 is considerably lower than that of the first sample, (i.e.GR1-4)

In view of the large uncertainty in the Th-230/U-234 ratios (due to the low U content) it is impossible that both samples have the same finite great age. The two analyses' Th-230/Th-232 value agree within ±1σ, but a mean value for their isotope ratios (ie U-234/U-238 = 0.953, Th-230/U-232 = 1.040) yield an "infinite age".

The relatively low U-234/U-238 ratio of GR1-3 suggests it might

have suffered uranium loss, since the leaching of uranium from rocks is commonly associated with a decrease in this ratio. But, it would be unsafe under the circumstances to assume that one sample was leached and the other was completely unaffected. We thus appear to be dealing here, with material that has been geochemically disturbed and it is consequently difficult to establish a single, exact age for the base of this capping layer. In addition to this, a plethora of small bones embedded in the immediately lower layer was found also for many parts of the same travertine.

A possible correction for an initial Th-230/Th-232 ratio based on the supported Th and its associated U for these lower layers of GR 1-3 and P-7-4) yields an age of 220Ka BP.

Overall, it is impossible to establish a single exact age for the base of this capping layer. From the overlapped error limits of the ages it may be as old as 270Ka BP.

vi) 1.8m Deep Flowstone SampleGR3 was collected by A Poulianos. Two attempts to date this sample gave concordant results, namely 211^{+118}_{-58} and 230^{+114}_{-60} Ka BP. The average age is therefore about 220^{+100}_{-60} Ka BP.

Another one P-L10 (dark brownish) gave very low Th and U yields and an uncorrected age of >350Ka BP. This was severely contaminated giving a residue of 6% by weight of the sample. The detrital Th-232 content was 2.28ppm(!) and the U was 0.68ppm.

Applying a possible (U, Th) correction based on the isotope ratios of a clay sample from the nearby 16th layer of the trench see Table 12.4.1, the obtained corrected age becomes $\geq 304^{+115}_{-142}$Ka BP

This correction brings the U content down to 0.08ppm, similar to

the GR3-1a.

Due to the very low yields and the large contamination only a crude age can be given to this flowstone. Therefore, in addition to the above possible corrected age, once more we apply the (U-234/U-238 dating method based on the initial U ratio from the P-L10 sample and the observed U ratio from the GR3-1a.

The obtained minimum age is 360Ka BP and the maximum 730Ka BP.

By working out the overlapped age regions, within $+1\sigma$ a probable age of 300 - 420 Ka is obtained, while within -1σ an age span between 180 - 320 Ka BP is obtained.

Taking into account the time span of the top travertine of this section i.e. from 75 - 270Ka BP, we favour the $+1\sigma$ time span as the most likely time of deposition of that flowstone.

Here it should be mentioned the attempt to date another flowstone P-8 at ≃ 4in deep. P-8-1 (half part of p-8) was found to be contaminated by boyes (U content = 4.2ppm) and subjected to selective teaching of U-234 (U-234/U-238 = 0.928 on p-8-1). The Th yield, also, was very low due to the difficulty of dissolving the Th The other half part P-8-2 gave an age of $125\ ^{+365}_{-\ 81}$ ka which is considered the minimum age.

dating method based on initial U ratios from another piece of the same travertine, gave a minimum age of 260Ka BP

In summary, the cave sediments encountered below 1.8m, in the section A_2 appear to have been deposited approx. 270Ka BP (at least). The younger (upper) sediments exposed in this section are capped by a stalagmitic layer that has been altered radiochemically with the result that the apparent Th-230/U-234 ages range from approx80,000to greater than 350,000yrs BP. - The physical appearance of these stalagmitic layers does not suggest which,

if any, of these layers might give the "correct" date.

The samples Gr1-4 (277^{+160}_{-170}Ka) P-7-2 (250^{+89}_{-81}Ka BP) and P-7-4 (>350Ka) with their uncorrected ages are consistent with the dates observed deeper in the pit.

By contrast the U-234/U-238 ratio of sample GR1-3 is too low to be consistent with the proposed age of app 270Ka BP. Such an anomalously low U-234/U-238 ratio could be the product of leaching of an old speleothem.

Whilst the sample P-TR giving an age of about 70Ka is consistent with the external part of the stalagmite growing above this layer (which has a maximum age of 100Ka).

From the above results a possible history of the site of section A_2 would involve rapid accumulation of clastic sediments up to about 270Ka; followed by much slower growth of a capping travertine sheet extending across much of the floor of this part of the cave (including the site of Aristotle's Hall , the Mediterranean and the Mausoleum sites) and ceased at around 70±10Ka BP.

The second travertine layer with its (U, Th) correction yielded an age of 170Ka seems to have the same depositional time with the upper part of the Mediterranean floor travertine (140±20Ka) This justifies the already made interpretation that this age represents a middle part of this upper travertine, with an upper (top) layer age of ≃70Ka BP.

Finally, should be pointed out the relation between the observed "hiatus" in the Mediterranean and Mausoleum sites, between 200 to 350 Ka BP , and the accumulation of clastic sediments ("breccia") in the trench at >270Ka BP.

vii) Precipe No.1 The sample P-15A is the upper layer of a yellowish travertines (1-6cm thick) with some white lumps incorporated into the main calcitic body.

There was no residue left; and the detrital component was very small.

It yielded an uncorrected age of $\simeq 213^{+80}_{-46}$ Ka BP which with a small correction for initial Th becomes 204Ka. Its U content was 0.68ppm.

A second part of this travertine P-15B did not produce any Th yield due to incomplete Th extraction. Nevertheless the U of this sample (with a high U yield) is 3.71ppm or much higher than the first. Although the U-234/U-238 ratio is both cases was similar, which suggests that the sample was subjected to a selective enrichment by U radioisotopes. The age of P-15A is related to the results already mentioned above concerning the second and third calcitic layers of deposition in the flowstones. The deduced growth rate is around 0.008cm/1000 yrs.

It has to be mentioned that the U dating method yielded an age range between 130 - 300Ka BP when we consider the extreme values of the obtained ratios and their associated errors of $\pm 1\sigma$. The initial ratio is from P-15A sample and the observed ratio from the other half, i.e., P-15B. This time span does not disagree with the P-15 sample and could be given as 215±90Ka BP.

12.8 Thin Section Analyses

Some provisional comments from Thin Section Analysis (TSA) on three samples namely, P-6, P-12 and P-13 are as follows:

1. The textures are all typical of calcites from cave deposits, "speleothem calcites".

2. P-6 as sectioned is of fast formation, but the growth is more on an irregular radiating basis, rather than as parallel prisms. Prior to 1978 , such textures were conventionally interpreted as being due to replacement of acicular (needle-like) carbonate. This is now not thought to be the case. Kendal & Broughton, (1978), present convincing case for growth in situ of these columnar calcites by coalescence of small syntaxial overgrowths ("crystallizes") on the surface of the growing crystals. The principal evidence is the arrangement of inclusions which reveal incomplete coalescence andmap out the progress of the growing crystals. Our samples show several of the same inclusion patterns cited by Kendall & Broughton

3. P-13 It has a more complex trexture in which the earlier growth layers were very rich in impurities, preventing crystallizes from coalescing and leading to friable white or yellow calcite with a granular texture.

   The later growth layers of the calcite(presumed, from the direction of the growth of the crystals) were less inclusion-filled, so that local patches of larger crystals with a texture approaching that of the other samples could develop. The sample was obviously porous at some stage, as pyramidal growth stages, picked out by inclusions, can be seen in places indicating growth into voids. These were then filled with clearer calcite perhaps during a wetter period .

   At present there is no evidence of any definite recrystallization having occurred, if the arguements of Kendall et.al are employed.

4. P-12 is also of a complex texture probably because of its location

on the ground in an environment probably subject to very intermittent and often unsatisfactory calcite-growth promoting conditions i.e. flow of a thin film of water over the surface or immersion in $CaCO_3$ water during flooding. This particularly shows the characteristic fast length columnar growth of calcite known as "palisade" calcite. Of similar texture to P-12 were P-4-1, - 2 and P-3 -1,- 2 samples, while similar to P-13 was P-8.

The above comments give support to theobtained ages for the respective samples, section 12.7, and justify the already suggested "slow growth rate" and the "hiatus" observed in them.

12.9 Fission Track Analyses

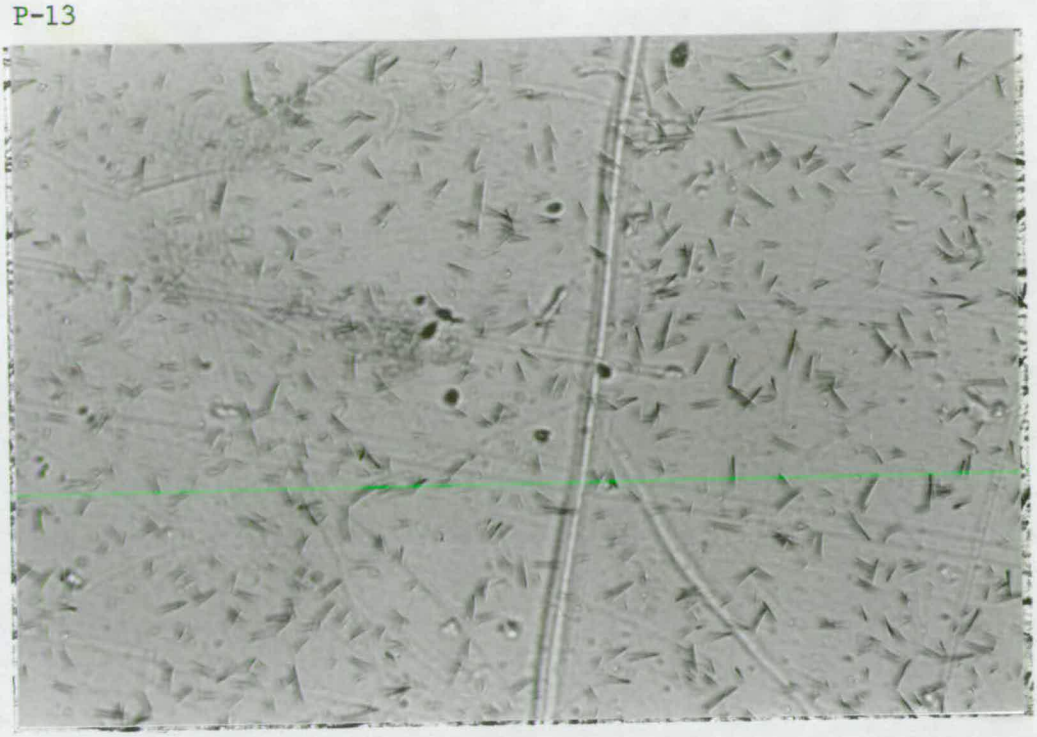
Fission track analyses* on these materials show differences which are illustrated by the great variation of microdistribution of U within the same sample.

It is therefore essential to note that the selection of a particular stalagmitic layer within any one stratum is of great importance to the obtained dates and to their interpretation (section 12.7). Fig. 12.9a shows a characteristic intesity distribution zone of sample P-13 and Fig. 12.9b characteristic zones of densified and non-densified tracks which reflect sampleP-7-3's stratification.

---

* These analyses were performed at East Kilbride Reactor Centre, by Dr A Mackenzie. The plastic plate used for track detection is a polycarbonate (Makrolon). The plates were held in close contact with a flat surface of the carbonate samples for 24 hours at a flux of 10^{11} neutrons/cm^2/sec., in the thermal column of the UTR300 reactor. After a cooling off period of 1 week to allow decay of the induced radioactivity, theplates were etched for 48 hours at room temperature in 2.5m NaOH solution.

P-13



P-7-3

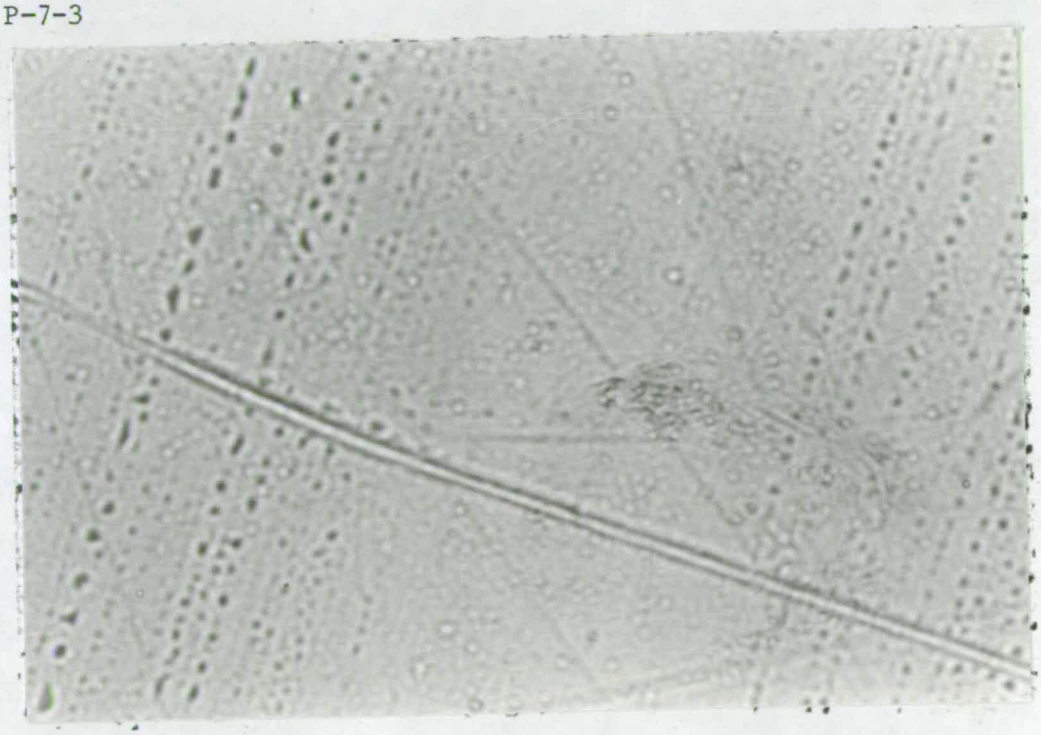


Fig. 12.9a) P-13. Fission Tracks representing Uranium distribution covering an area of 0.58cm^2

b) P-7-3. As above but also displaying "zoning effect".

Both photographs represent an area of 0.58cm^2 of the sample. This area is large compared to the α-particles range (of the order of microns)

The last is of great significance in the TL dating where such U microdistribution ("zoning effect") can upset the determination of the total dose (rads) experienced by the calcite sample due mainly to α-particle as well as to β- and γ- radiations.

Table 12.9 presents a "qualitative" distribution of the tracks. The irregular distribution of tracks makes any sort of quantitative interpretation difficult.

In almost all cases, the tracks were unevenly distributed and with some samples, marked concentration centres exist.

TABLE12.9

Qualitative Interpretation on the Distribution of Fission Tracks

(Inspection of the places at a magnification of x200 reveals a complex pattern of Fission Tracks)

Sample 1	Very low concentration. Less than 1 track per Field of View on microscope (FOV)
Sample 3	Tracks localised along one edge. About 100 tracks/FOV
Sample 4	Very low concentration. Less than 1 track/FOV
Sample 6	Fairly uniform distribution. 100-150/FOV
Sample 7	Three distinct density distributions: High: more than 1000 tracks/FOV Medium: about 200/FOV Low: about 50/FOV
Sample 8 21layer	Uniform distribution: about 400/FOV
Sample 8 4th layer	Uniform distribution: about 100/FOV
Sample 9	Fairly uniform: about 30/FOV
Sample 10	One localised high about 1000/FOV, otherwise uniform about 50/FOV
Sample 12	Fairly uniform: about 100/FOV
Sample 13	Highest density of all samples. Very uniform distribution - too high to count. Estimated more than 2000/FOV
Sample 15	Very low concentration. Less than 1/FOV

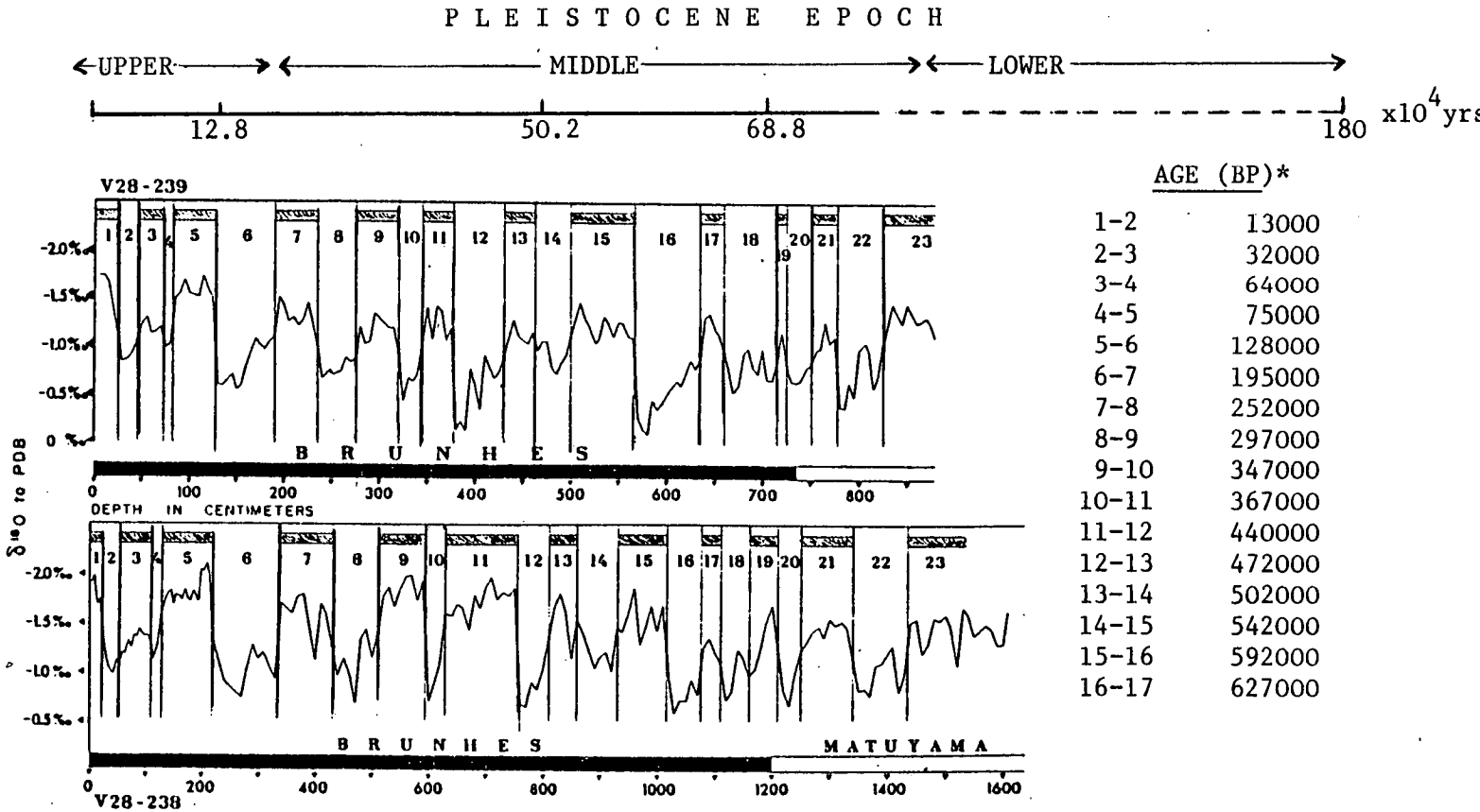
12.10 Possible Correlations Between Radiometric Data and Palaeoclimatic Changes

From Fig. 12.10 we can correlate the obtained ages with certain climatic features.

Therefore, the top travertine layers of the cave are identified with isotopic stage 4 - 5 (75Ka BP), or the Würm I/IIa epoch; the second and subsequent layers being of around 150Ka, 170ka, 200Ka, 250Ka, 450Ka and 600Ka, are identified with the other isotopic stages or epochs, Shackleton & Opdyke (1976), Lamb, (1977). The calcitic deposition and growth is a function of many parameters, eg., climatic changes, rate of water seepage and flow, CO_2 concentrations in the cave, geomorphology of the cave and the particular site, microorganism action, etc. On a world scale, cave deposits are laready being used to identify the warm and cold, wet and dry phases of the pleistocene, Fig. 12.10

In the Mediterranean, stalagmite and flowstone deposits are identified with wet conditions, occurring during interglacial periods. Deposits of "terra-rossa" are regarded as an indication of former warm conditions. The occurrence of cave breccia also is believed by some to be associated with a wet and frosty climate in the Mediterranean, possibly to be correalted with the cold phases of northern Europe, Sweeting, (1972). Concerning the last statement, we might relate the clastic sediementsof the excavated section $A_1 - A_2$ (Fig. 12.3) with the major presence of breccia and frosty rocks, with the cold period of Mindel, i.e. isotopic stage 10 or 347 — 367 Ka BP, Fig, 12.10.

However, such situations have to be delt with caution but a possible parallelism must not be excluded. Additionally, the observed



1. Wurm WIIc
2. " WIIb
3. " WIIa/b
4. " WIIa
5. " WI/IIa
6. " WI
7. Eamian E
8. Riss R
9. Holstenian
10. Mindel
11. Cromer
12. Gunz

	AGE (BP)*
1-2	13000
2-3	32000
3-4	64000
4-5	75000
5-6	128000
6-7	195000
7-8	252000
8-9	297000
9-10	347000
10-11	367000
11-12	440000
12-13	472000
13-14	502000
14-15	542000
15-16	592000
16-17	627000

Fig. 12.10 . Oxygen-isotope and peleomagnetic record from ocean cores, for all the Pleistocene Epoch. These climatic fluctuations imply Glacial/Interglacial events, identified with the stage numbers above left , and the time scale above right. * Dates were obtained by assuming a constant rate of sedimentation above the Brunhes-Matuyama Magnetic Reversal boundary at 1,200m. (after Shackleton, Opdyke, 1976).

"geochemical disturbance" for the lower part of the capping travertine in the section and for the 1.8m deep flowstone, seems also to be coinciding with the transitional stages from the Holstenian to Riss (i.e. 297Ka BP) and from Cromer to Mindel (i.e. 397Ka BP), interglacial to glacials, respectively.

During these times, leaching or enrichment or radioisotopes due to percolating waters can cause disturbances in the "close system " assumption.

However, in the light of this possible event, the observed relatively small time lapse between the top and the 1.8m deep travertines of the section A_1 - A_2 can be explained as a rapid accumulation of these deposits some time after 360Ka BP

Thus the quoted value of sedimentation rate by Kopper and Creer, (1976), of 29cm/1000 yrs for these sediments does harmonize with our dates and their interpretation.

Such a continuous rate would suggest a time laps of 6000 years.

Also the great "hiatus" which was found could well be related to the great Riss (Saale) glacial period (297 - 251Ka BP). Finally, minor temperature fluctuations leading to short periods of warm-cold phases (reported in Evans,1972) do esist, which duly participate in the creation of the zonal record of the calcitic and sedimentary growth and deposition (Schwarcz, Harmon, pers. comm).

12.10.1 From Wilderness to Metropolis in 15,000,000 years: The Unfolding Story of Human Evolution and the Human Conditions(a Resumé)

The ancestors of man arose 15million years ago in the slowly changing subtropics of the old world.

Geological changes certainly affected the movement of hominids and other

animals, and the last 2 million years or so mark not only the rise of man, but also one of the most unstable climatic periods in the earth's history.

Latterly, new studies have drawn attention to possible relationships between such changes and barriers to free migrations. Social forces, critical changes in evolving human behaviour patterns, may have been at least as important as geological forces in early migrations from Africa.

Regarding human migrations, it is not certain (from the number of fossils that have been found in different continents) where the crossing to the continents were made or when such transitions took place. Therefore, due to the complicated way of development and the evolutionary process of the early hominids, two theories have been developed. The Migration Theory holds that the predecessors of a particular species came from one p lace, eg. Near East and appeared in Europe, whilst opposing opinion rests on the notion of independant origins, the belief that evolution can proceed along parallel lines in different parts of the world. However, among the many changes of the environment and its constituents, more rapid changes took place amongst early hominids.

There are a number of ways of looking at these phenomena. The latter way concerns the cranial capacity which, together with chronological evolution, is summarized below.

i) from Ramapithecus (15,000,000 years ago) to the first Astralopithecus (5,000,000 years ago), there is 10,000,000 year span, during which body weight increased from perhaps 50 to 75 pounds and cranial capacity from 300 to 450cm^3.

ii) from the first Australopithecus (5,000,000 years ago) to more advanced forms as found at Olduvai and elsewhere (2,000,000 years ago) a time span of 3,000,000 years, during which body weight increased

from 75 - 100 pounds and cranial capacity increased from 450 - 700cm^3.

iii) from advanced forms (2,000,000 years ago) to fully fledged Homo Erectus (500,000 400,000 years ago), a time span of about 1500000 years, during which body weight increased from 100 to 125 pounds and cranial capacity increased from 700 to 1200cm^3.

iv) from Homo Erectus (400000 years ago) to Neanderthals (app130,000 yrs ago) there is a transitional period when these early Homo Sapiens present characteristic features between a progressive and a primitive type. (cranial capacity 1100 - 1250cm^3). We do not know where or when the transiton took place.

Skulls, such as Swanscombe (approx 250000 yrs ago) and Steinheim (approx 250000 yrs ago) represent this transitional stage. Because Homo Erectus consisted of a number of sub-species or races, oneof these sub-species could be theseearly Homo Sapiens which led to Neanderthals and subsequently to Cro-Magnons (approx 35,000 yrs ago), Pfieffer, (1972). In particular, for the Neandethalian type, many mysteries remain. His distinctive physical characteristics are widely different from other sub-species of those times, which reappeared in the sense that it was reminiscent of earlier human forms and that he seemsto have confined himself largely if not entirely to Western Europe (as far as recent excavations have revealed). One possibility was that he was cut off from his contemporaries. As a result, the partial separation, occassioned perhaps by geographical, climatological as well as social factors, may eventually have produced great differences so that theresult is distinction in species such as Australopithicus Africanus and Australopithicus Robustus .

The above notes place our Petralona skull (cranial capacity 1220 cm^3) in question to the Homo Erectus → Homo Sapiens transition, if not to an earlier Homo Sapiens, depending on how we relate the obtained age on artefacts and other cave materials to theoriginal burial position of the fossil, see also section 12.12 and Fig. 12.11.1.

Overall, a number of phylogenetic trees have been suggested attempting to represent the course of evolution leading up to modern man. From time to time proponents of one scheme or another, change our views so that no rigid formalisation is an accurate representation of any major school of thought. There are distinct differences in approach however, which are summarised below.

Scheme A (France)

There has been a tendency to reject, as a possible ancestor, any fossil that differs in form from modern man. There is an inclination, though, to suggest modern form for fossils which are too fragmentary or incomplete, eg. specimens of Stenheim, Swanscombe, (called pre-Sapiens). Ultimately, the question or origins is considered unanswerable, leaving the tree a collection of dead twigs with no truck.

Scheme B (Prof L S B Leakey)

There is a tendency to give non modern forms separate generic and/or specific designations and eliminate them from any role in the ancestry of modern man. He regards Kenyapithicus as the start of the true human being, separating Zinj and Neanderthals as being Astralopithicines and Pithicanthropines respectively.

Scheme C (Different Schools)

They regard Neanderthals and Astralopithicus Robostus (Zinj) as two separate groups different from the main line which leads from Ramapithicus through Homo Erectus to Homo Sapiens (modern man).

Scheme D (Different Schools)

It is a simplified picture where the course of human evolution is arranged in four broad stages: (Australopithicene- Pithicanthropine-Neanderthal-Modern), each of which is regarded as having evolved directly from the proceeding.

In general, the belief is that the course of human evolution has been too complicated and that the evidence is too incomplete to be represented by any simple scheme.

12.11 Critical Interpretation of the Age of Archanthropus Petraloniensis

We have isotopic data from many sites of the cave, which suggest a long history of deposition in this cave. These data indicates that the older Mausoleum site was the locus of travertine deposition as early as 600Ka BP, whereas travertine deposition at site $A_1 - A_2$ appears to have occurred more recently, at least down to 1.8m deep, sampled here.

Regarding the age of the Archanthropus Petraloniensis, the following criticims are made:

i) the skull at the Mausoleum site was found according to Prof Poulianos on a limestone bedrock covered by the stalagmite of P-6 sample (section 12.7i), Fig. 12.2. This was not covered completely by the stalagmitic material and that was the reason why it was spotted. Also from its present condition, Fig 12.11.1, one can see that only the front face was covered by stalagmitic materials. If this is the case, then a minimum age for the skull is at least 80Ka BP, i.e. the age of the sample, P-6.

ii) on the other hand, the associated skeleton, which has mysteriously disappeared, according to Prof Poulianos, was found under the sample P-12 or embedded in it, which is of course a very crucial point in the whole story (since P-12 has an extensive depositional history). The latter then is dealt with as follows:

iia) if the skeleton was covered by the P-12 and GR4-2-3 samples, then the age could well be at least as old as 750Ka BP

iib) if it was "sandwiched" between upper and lower layers of the Mausoleum travertine, with some of its parts being visible then the age lies between 350 and 750Ka BP (age span of the old Mausoleum). However, taking into account the possible hiatus over the period of ≈220Ka to 350 BP the "ancient man" could have been lying there since the last deposition or around 350Ka BP, subsequently dying and being covered by the stalagmitic material of the later deposition.

iii) in the 10th - 11th layers in the section, human activity was very high (from the stoney tools, traces of fire and teeth found there) and the cave seems to have been densely occupied, Fig. 12.11

This could imply a probable occupational time of the cave by this archanthropus before 350Ka BP This is also supported by the P-15A age of the travertine above the young boy's incomplete skull, of being at least 215Ka BP and the (iib) alternative above.

iv) the P-13 travertine covering a bone, nevertheless suggests a probable minimum age for the bone of ∿270Ka BP.
However, animal bones that have been found, by Prof. Poulianos around the former burial position of the archanthropus could well be associated directly with the activities of the archanthropus or its contemporaries earlier than 270Ka BP.

v) most of the calcitic samples incorporated small bones. Especially those lower flowstone layers above the sediments were very rich in such debris and the obtained ages as high as 400-600 Ka BP

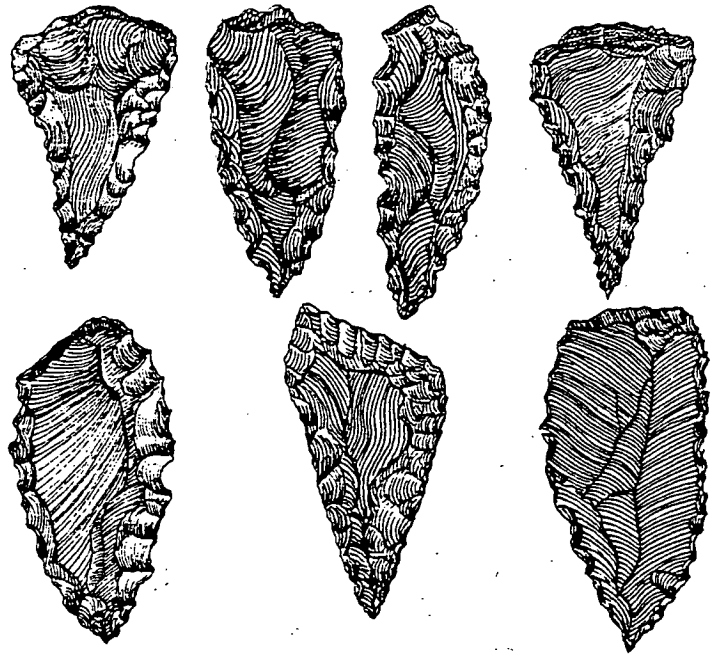


Fig.12.11 Some characteristic human tools found in Petralona cave by A Poulianos.

imply that the occupation in the cave by animals at least, was older than 600Ka BP.

The skull at the Mausoleum site represents, as noted a "link" between Homo Erectus and Neanderthal man, sections 12.1 and 12.10.1. While Homo Erectus species came into existance more than 10^6 years BP, (section 12.10.1), Stringer and Poulianos observed features resembling those of Neanderthal man, Poulianos, (1974). Nevertheless, the former suggested a pre-upper Pleistocene age for the skull and the latter stresses that that this has an even higher age, being an "ancient progressive" Homo Erectus (pre- Homo Sapiens).

In a comparative study involving other Neanderthal and related skulls, Stringer, (1974b), suggests a close relationship with the Homo Erectus skulls of Chou Kou Yien;and ages from 300Ka to greater than 500Ka BP have been suggested for the latter site, although no satisfactory geochronological data are yet available.

Fig12.11.1 shows a close comparison of the Petralona skull with other Neanderthal and Homo Erectus skulls. To our estimations, the "close resemblance" between them (in cranial measurements as well), is characteristic and the existing debate about the age for the Petralona skull is furthermore verified.

Furthermore, the section A_2 has yielded an extensive carnivoral fauna, which was studied by Kurten & Poulianos, (1977). These fossils are interpreted as being principally of Middle Pleistocene age (also suggested by Sickenberg, 1971).

The paper of Kurten & Poulianos quotes the earlier results for this site on sample 75022-2 (stalagmite above the section A_1 - A_2) as indicating an age of greater than 300Ka BP.

. 12.11.1 "Close Comparison" of the Petralona Skull with other
nderthal and Homo Erectus Skulls.

RO. Rhodesian Man. "Broken Hill", Homo Sapiens .. Neanderthalensis. Indirect dating evidence suggests an early Upper Pleistocene date of c 200,000 years BP or isotopic stage 7.

SH. Shanidar I. Homo Sapiens Neanderthalensis. Dating: Upper Pleistocene, Würm Glaciation, just under 50,000 years ago, (by C-14), i.e., isotopic stage 3.

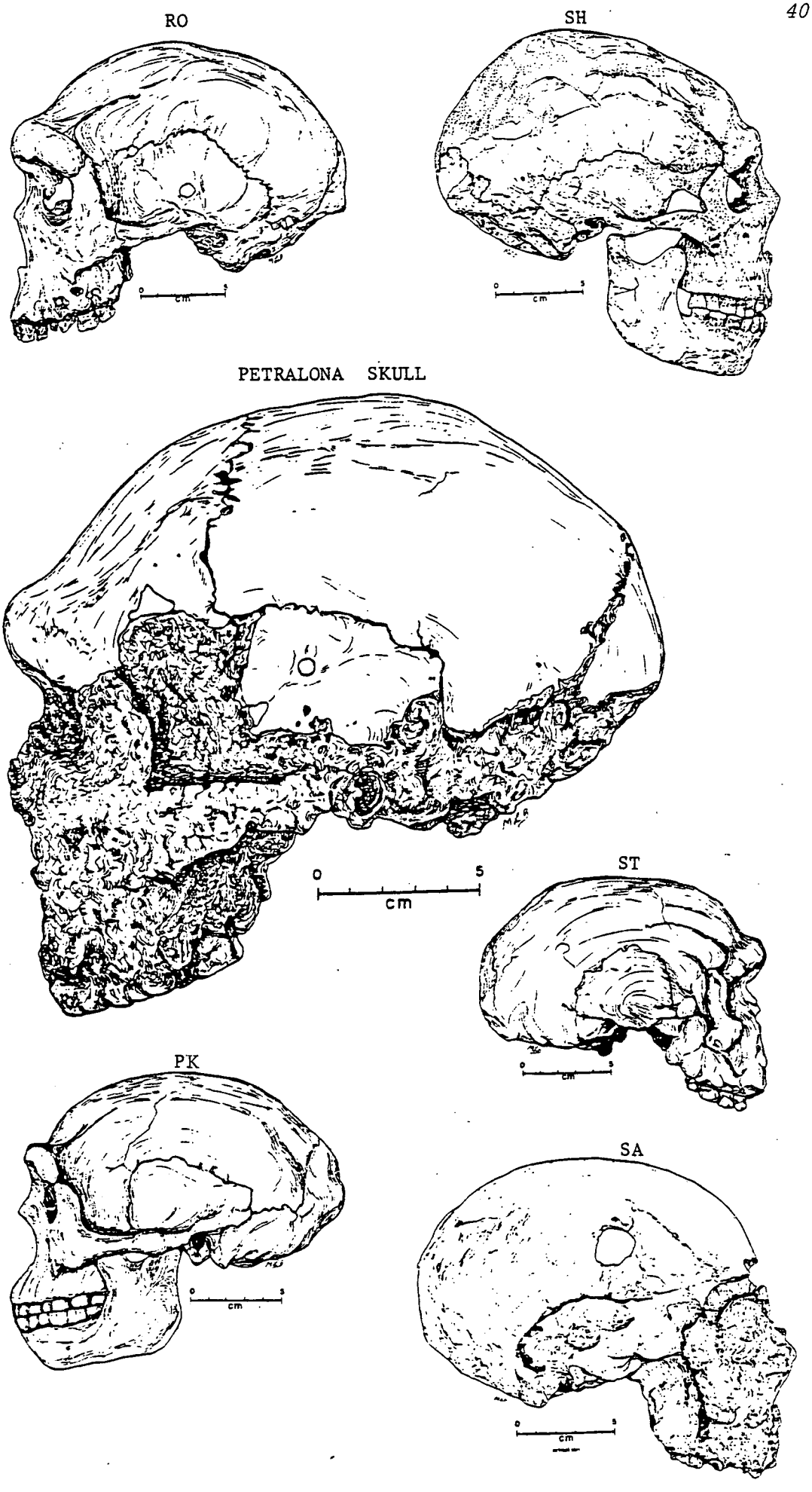
PK. Pekin Man. Homo Erectus. Middle Pleistocene at least 300,000 years old.

ST. Steinheim. Homo Sapiens. Middle Pleistocene, last second interglacial, approximately 250,000 years ago.

SA. Saccopastore. Homo Sapiens Neanderthalensis. Upper Pleistocene, end of 3rd (Riss - Würm) interglacial, approximately 150,000 years BP.

PETRALONA SKULL. Archanthropus Europeus Petraloniensis. Homo Erectus (Pre-Homo Sapiens). Middle Pleistocene, at least 270,000 years ago, (maximum age span 700,000 years).

Drawings reproduced from "Atlas of Fossil Man", by Brace et al, (1971).


RO
SH
PETRALONA SKULL
0
5
cm
ST
PK
SA

However, that sample was evidently found to be geochemically disturbed and an absolute age could not be reported for it.

As we have seen, otherwise, the radioisotopic data for samples from the section A_1 - A_2 do not permit assigning an exact age of these deposits, though they appear to be about 350KaBP old, or that the 1.8 deep flowstone represents the Cromer period (isotopic stage 11, i.e., 440 - 367 Ka BP).

Kurten & Poulianos, (1977) considered the fauna and the associated soil type from this layer to represent the Cromer interglacial (called Crenian) cycle prior to the onset of the Mindel glaciation, that is, isotopic stage 10, i.e. 367 Ka BP, while the age of the deposits between 2nd - 6th layers are considered to represent Mindel glaciation i.e. 367 - 347 Ka BP, which is within our age ranges and their associated error limits, but disturbingly close to the maximum.

This occurs because of the different timescale of glacial periods considered by the authors. We have, here, adopted the time vs δO scale by Shackleton, Opdyke (1976), whilst Kurten & Poulianos, (1977), another time scale based on palaeontological evidence general to European cave systems. We should point out, here, that animal bones found in a particular depositional layer do not necessarily represent the age of this layer. This depends on how the bones came to be there. Thus animals belonging, say, to the Cromer period, can be found in layers of the Riss glacial period, due to the washing down by percolating waters or sudden falls of sediments.

Therefore, it appears here, that our results do harmonize, otherwise, with the faunal data.

12.12. Epilogue

Overall, the age of the controversial Petralona skull and its mysteriously missing skeleton sways opinion towards the human species Homo Erectus.

Under the present circumstances, what is certain for this early human fossil is that it is definitely older than 270Ka BP. (The low part of the capping flowstone layer (Section A_2), and the upper travertine layers of the Mausoleum floor). If the findings in the 1.8m deep flowstone belong to this fossil, his age would be as old as 300 - 350Ka BP. Regarding the Mausoleum, its former burial spot, we can offer only age ranges (within $\pm 1\sigma$ error limits) due to the unknown former position of the skull and the skeleton, and the very slow calcitic growth in this site. Such time spans extend as high as 750Ka BP.

Until more findings related to this skull will come to light, we have to be, at present, very cautious when giving a final age. Nevertheless, our age estimates offer potential solutions to the burial age question, one of which may be selected by a later find.

INTENDED FUTURE WORK

The importance of the chronological speleothem studies to our understanding of human evolution and palaeoclimatic changes on the earth for the last one million years, prompts us to continue these studies in the near future.

This programme shall comprise of the dating of interstratified stalagmitic materials by dating each depositional layer separately by both the U/Th and Thermoluminescence dating techniques. Prior to dating, Fission Track analyses on these single layered calcitic episode will be carried out in order to check any"zoning effect", which could upset either of the above methods.

Also, further investigations will be carried out on Thermoluminescent dating of sediments (cave and oceanic) with the purpose of extending the TL method to other materials whose applications in palaeoanthropology are potentially very extensive.

In particular, it is anticipated that the radiation (TL) dose from sediments from an excavated section would be reduced by depth. This will occur if these sediments are authegenic , carrying almost the same U, Th concentrations each period of deposition. This can, however, be checked by radioisotopic analyses as well.

Preliminary results have shown a tendency to such a decrease of the total radioactivity, for alpha counted (ZnS) clay samples from Majorcan caves, Spain. Such a dose decrease would be the result of U, Th decay processes, and this principle could be applied to a single calcitic layer also Where only the determination of this total dose by TL means is needed, the aging factor being included in the radioisotopic decay equation of similar principles as for the U/Th dating.

The above studies will be applied mainly on the Petralona cave with extensions to other interesting cave materials.

APPENDIX A

Provinance of the samples for TL dating and Neutron Activation Analysis

1. Crete

Site			
Agia Triada	Sample No.	AT/7	Various fragments almost fused pieces.
		AT/8	Well fired clay from kiln wall.
		AT/9	Various fragments of well fired clay from kiln.
Kalo Horio Mirabelou	Sample No.	KH/5	Fired clay from kiln. Declination (magnetic compass) 270°, inclination 74°.
		KH/7	Well fired clay from kiln.
Faistos	Sample No.	FS(1)/5	Partially fused fragments of well fired clay
		FS(3)/8	Fragments of fired clay and pottery
		FS(3)/9	Fragments well fired clay and pottery
Stylos Hania	Sample No.	SH/2	Well fired clay from wall of kiln, near base.
		SH/5	Well fired clay from middle vent. Inclination 25°, declination (magnetic compass) 184°.
		SH/6	Well fired clay from middle vent. Inclination 59°, declination (magnetic compass) 40°.
		SH/11	Well fired clay from kiln.
Kato Zakros	Sample No.	KZ(1)/7	Fired clay.
		KZ(1)/9	Two pottery fragments from kiln base.
		KZ(2)/5	Well fired red clay.
		KZ(3)/1	Fragments of tile.
		KZ(3)/2	Two fragments of tile.

2. Thessaly

Site			
Sesklo	Sample No.	SK/1	Small fragment of pottery (Museum Ref. Sesklo 1963, T.2 layer 20).
		SK/2	Clay sample of aceramic period (Museum Ref. Sesklo 1962, clay sample, N.1).
		SK/3	Small fragment of pottery (Museum Ref. Sesklo 1962, Section , layer 0.40 - 0.65 under F, No.16)
		SK/4	Two small sherds of pot (Museum Ref. Sesklo 1968, Kerameos house 68).
		SK/5	Small sherd (Museum Ref. Sesklo 1968, under and south of house 31 - 1.20 under foundation stone and 1.20 beyond east end). Great trench 1966. Burnt clay).
		SK/6	Fragment of pottery (Museum Ref. Sesklo 1962, Trench A, Square 3, layer 68, No.80.
		SK/7	Two tiny pieces of burnt clay (Museum Ref. Sesklo 1962, A, 62/69).

SK/8	Three small red pieces of fired clay from Kerameos site. Possibly a kiln.
SK/9	A piece of well-fired clay (Museum Ref. Sesklo C72, C66, Trench 2 (passa 6) fired clay).
SK/10	A piece of well-fired clay. (Museum Ref. Sesklo 1972, Trench 2, p.p. C64, fired clay)
SK/11	A red piece of fired clay (Museum Ref. Sesklo C72, C117, Trench 2, N.ext, fired clay).
SK/12	A fragment of well-fired clay (Museum Ref. Sesklo C72, C74, Trench 2, p.p. fired clay).
SK/13	A piece of red, well-fired clay (Museum Ref. Sesklo C72 Trench 3, Level 15, C112, 175 - 180, fired clay).
SK/14	A piece of red, well-fired clay (Museum Ref. Sesklo C72, C89, Trench 3, Level 5, 90 - 100, fired clay).
SK/15	Two small red pieces of well-fired clay (Museum Ref. Sesklo C72, C16, Trench 3, Level 16, 100 - 105, 627 F, 5-10-76).
SK/16	Blue-yellow clay sample from about 300 metres north of the Acropolis.
SK/17	Blue-grey clay sample from the vicinity of the above site.
SK/18	Red clay sample from above.
SK/19	Red-yellow clay sample from above

SK B(I)	1972, p.22		
SK B(I)	18	well fired (1 - 2 cm	
SK B(I)	98	thick) pottery	
SK B(I)	27, 1972	Mixed samples of middle	
SK B(I)	1	or early neolithic?	
SK B(I)	2		
SK E1			
SK E2		well fired potsherds.	
SK E3		From early levels of	
SK E4		Sesklo excavations:	
SK E5		9/8/1972, 19.	
SK E6			

Dimini	Sample No.	DM(1)/1	Fragment of Pottery (Museum Ref. DM/1976 Megaron B, dtl).
		DM(1)/2	Fragment of pottery (Museum Ref. DM/1976, Megaron B, dtl).
		DM(3)/3	Sherd of pot (Museum Ref. DM/1975, House N, nd8).
		DM(2)/4	Sherd of pot (Museum Ref. DM/1975, nd8).
		DM/5	Three small sherds (Museum Ref. DM/1975, nd).
		DM(6)/6	Fragment of pottery (Museum Ref. DM/1976, Area B.A., Megaron B).
		DM(6)/7	Fragment of pottery (Museum Ref. DM/1976, Area B.A., Megaron B).
		DM(7)/8	Small piece of pottery (Museum Ref. DM/1975, Ne)

DM(7)/9 A piece of pottery (Museum Ref. DM/1975, Ne).

DM/10 Three small pieces of pottery (Museum Ref. DM/1975, House N, d5).

DM/11 Pieces of burnt and unburnt clay from the kiln. (Museum Ref. DM/1976).

DM(8)/12 A piece of pot (Museum Ref. DM/1976, House L).

DM(8)/13 A piece of pot (Museum Ref. DM/1976, House L).

DM/14 A fragment of well-fired clay (Museum Ref. DM/1976, 1/X.8.54 - 4.7.86, 13/7/76).

DM/15 A piece of fired clay from kiln in situ.

DM/16 Clay from Keramadico site.

DM(9)/17 A small piece of pottery (Museum Ref. DM/1975, House Nd2).

DM(9)/18 A small piece of pottery (Museum Ref. DM/1975, House Nd2).

DM/19 Fragment of pottery (Museum Ref. DM/1975, House Nd10).

DM(10)/20 A small piece of pottery (Museum Ref. DM/1975, House N cleaned up inside room.

DM(10)/21 Fragment of pottery (Museum Ref. DM/1975, House N)

DM(11)/22 Fragment of pottery (Museum Ref. DM/1975, Nd9).

DM(11)/23 Fragment of pottery (Museum Ref. DM/1975, Nd9).

DM(12)/24 Small piece of pottery (Museum Ref. DM/1975, Megaron B inside).

DM(12)/25 Small piece of pottery (Museum Ref. DM/1975, Megaron B inside).

DM(12)/26 Three small pieces of the same pottery (Museum Ref. DM/1975, Megaron B inside).

DM(13)/27 Fragment of pottery (Museum Ref. DM/1975, Nd1).

DM(13)/28 Fragment of pottery (Museum Ref. DM/1975), House Nd1).

DM/29 Two small pieces of pottery (Museum Ref. DM/1975, House L).

DM/30 Small piece of pottery (Museum Ref. DM/1975, Nd5, vasilikis).

APPENDIX B

BETA SOURCE CALIBRATION

The beta source was calibrated by means of specially annealed geological standard sand, which had been given an accurate dose of CO-60 gamma irradiation. Irradiated samples of this sand were treated and measured in exactly the same way as the archaeological quartz samples to determine the total dose.

CALIBRATION PROCEDURE

All beta irradiation (throughout this thesis) were performed with a Sr-90/Yt-90 disc source (SIP type, from the radiochemical centre at Amersham.)

The strontium is embedded in a 1mm thick layer of silver with a 0.1mm silver covering, with a gold coating to protect against corrosion. The nominal activity was 40mCi.

The source was used in two positions: 0.1" above the sample (5% spread of radiation) and 12cm above it, in a collar position, therefore low dose rates were used. The calibration was performed on geological sand of 90 - 150μ grain size, placed on to the heating strip.

The sand was initially annealed to 500°C, following irradiation of about 2000 rads and post annealing to 500°C.

The above amount of sand was divided into two equal portions, one of which was kept in the lab. (inside a black polyethene tube) and the other one was sent to Risø laboratories, in Denmark, where it was irradiated with a precise gamma source, depositing on them 809 rads, (Dr V Mejdahl, Risø, Denmark.)

(The quoted dose has taken into account corrections concerning gamma absorption and build up effects during gamma irradiation. Moreover,

the sand was irradiated in a quartz tube with an inner diameter of 2.4mm and a wall thickness of 2.4mm.)

This irradiated sand was treated identically as for archaeological dating, following the "additive procedure" to determine the Q and I intercepts, Fig. B shows its glowcurve.

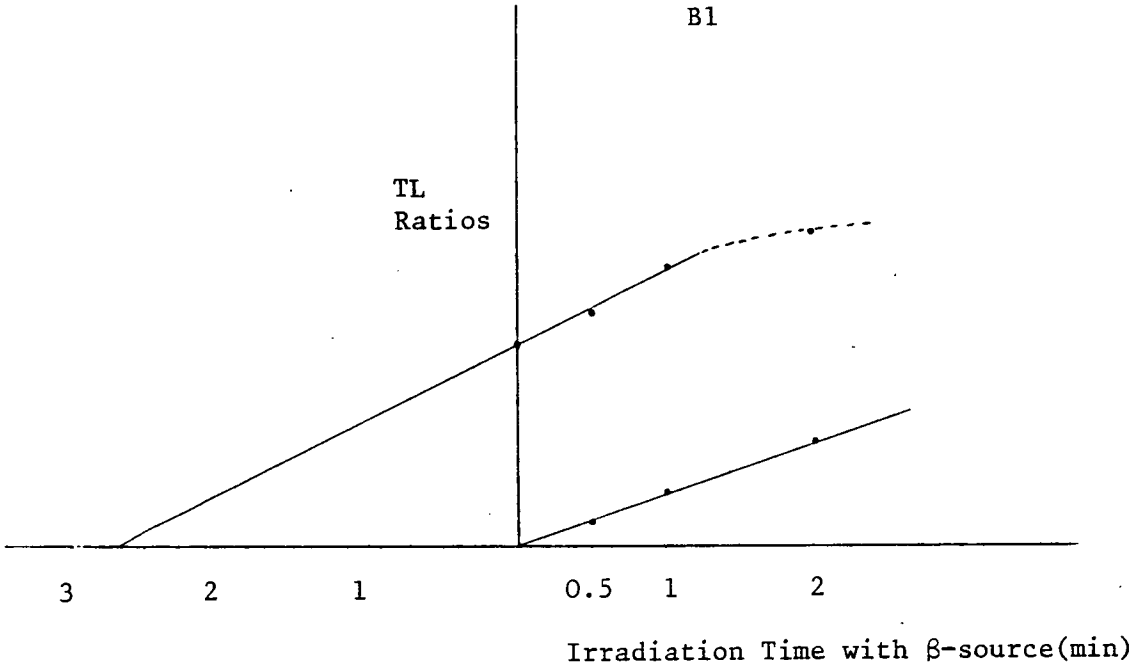
The two build-up curves are almost parallel, and the I-intercept is zero, Fig. B1

The total gamma dose of 809 rads was equivalent to 2.6 mins of beta irradiation or 312 rads/min. (Note that betas and gammas have the same TL efficiency.) The error involved is of the order of $\pm 3\%$ ($\pm 1\sigma$).

The above value of 2.6mins was also found to be within the statistical error, by plotting normalised ratios,by rad and mgr as well, of the annealed portion of the sand (which was kept in the lab) as three points;and the irriadiated sand (4th point) with 809 rads; against beta minutes of irradiation. The linear curve obtained for the fourth point gives the value of 2.75 of beta minutes of irradiating, or 293 ± 10 rads /min. Fig B2

The average value was taken as the best value for the dose rate which is 303 rads/min($\pm 3\%$). For the collar position, that is 12cm above the sample, the dose rate was 1.84 rads/min.

The remarkable agreement found implies that there is no predose effect for the peak used, nor was there any sensitivity change. Further the zero intercept could imply that the annealing-irradiation procedure for the geological sand sensitized the respective traps, (pre-dose sensitization effect) as to anneal small number of available centres which would be responsible for non-linear growth of TL sensitivity. Also such treatment seems to have destroyed high energy traps so that these traps saturate very quickly, Fig.B1



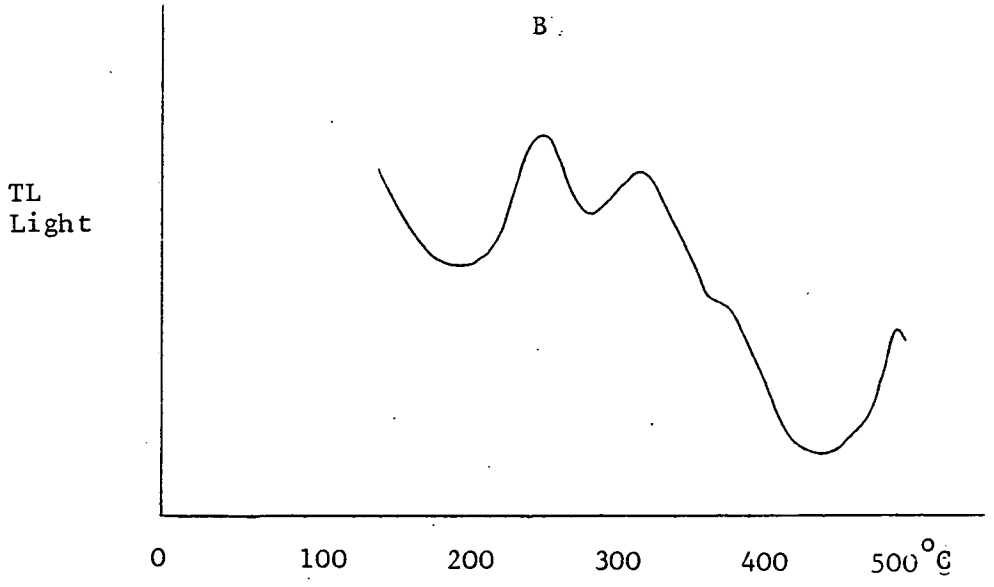


Fig. B Glow Curve of the Quartz used to calibrate the β-source
Fig. B1 First and Second Build-up curves for the same Quartz.

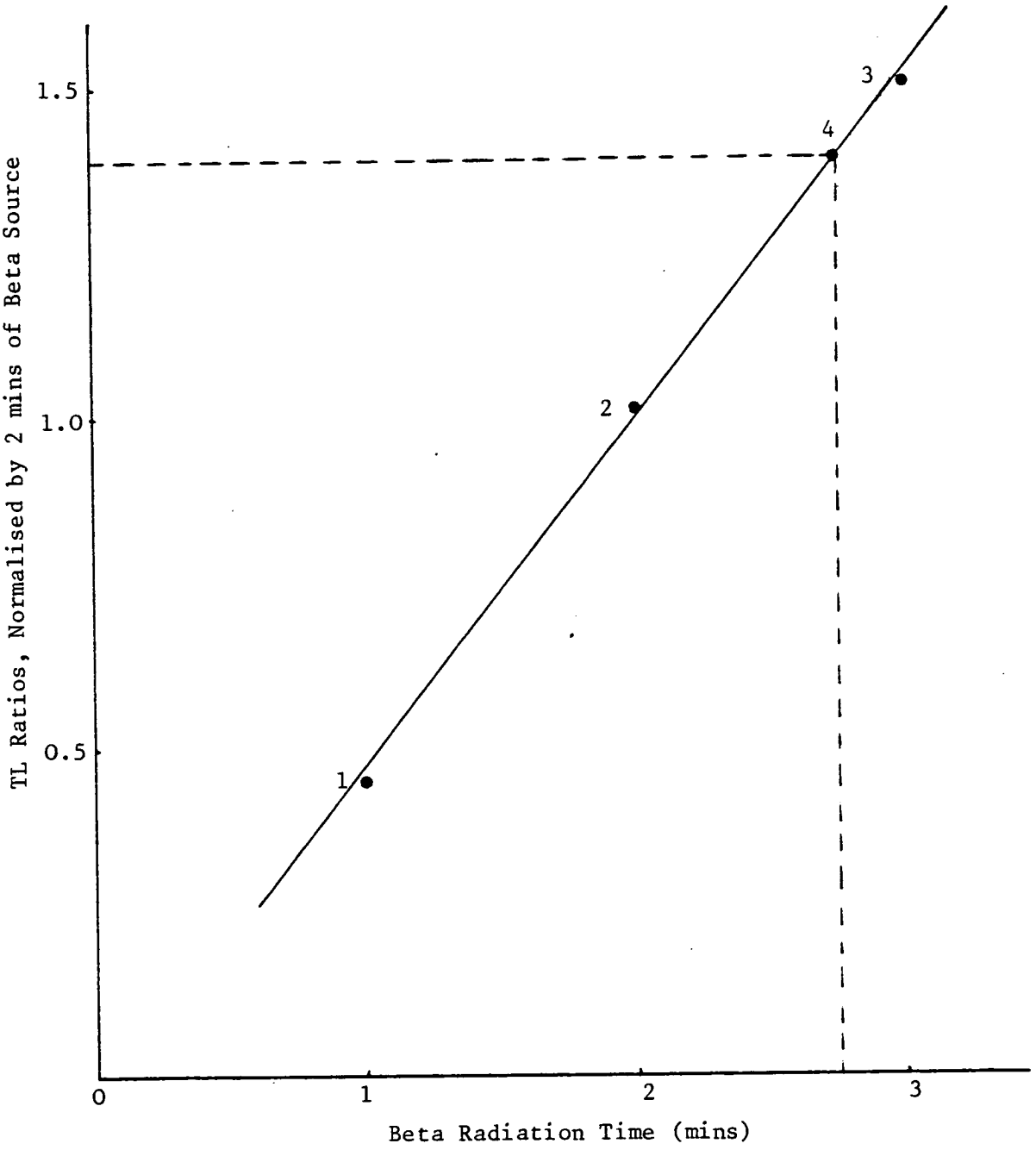


Fig. B2 Plotting of the TL Signal of Annealed Quartz, (1, 2, 3 points) and the specially γ-irradiated portion of Quartz (4th point) vs β mins. of irradiation. The TL Signal of the 4th point gives a corresponding β dose rate which is the calibrated dose rate of our source.

REMARKS

In the beta irradiation of grains, it should be worthwhile to consider the following phenomena:

i) the non-uniform irradiation on the samples. For that reason the sample must be evenly distributed on the heating place, in a small area and thinly. It is estimated that app. 5% (Ω=36°C) is spread over the sample for 0.1" distance between the sample and the source.

ii) backscattering from the nichrome plate and the surrounding aluminium of the vacuum chamber. The energy of the back-scattered electron will be about ½ that of the incident particles, Bothe, (1949).

APPENDIX C

STATISTICAL ERROR AS DERIVED FROM BUILD-UP CURVES - A TYPICAL EXAMPLE

A simple least-square programme was written to calculate the intercept and its error originated from the best straight line through three points in the dating procedure for the determination of the total archaeological dose which a potsherd has acquired. Fig. C illustrates the percentage scatter of the various readings per dose against the percentage final TL dose accuracy for particular cases.

In our typical example, we took three points averaging each one out of 3.5 and 10 readings of even scatter of 5 and 9 readings of gaussian scatter. The final conclusion is that three or four readings at three points gave a final TL accuracy almost equal to the scatter. Ten readings gave final TL accuracy equal to half the scatter accuracy. The gaussianas opposed to even scatter, only changes the accuracy by one percent or so.

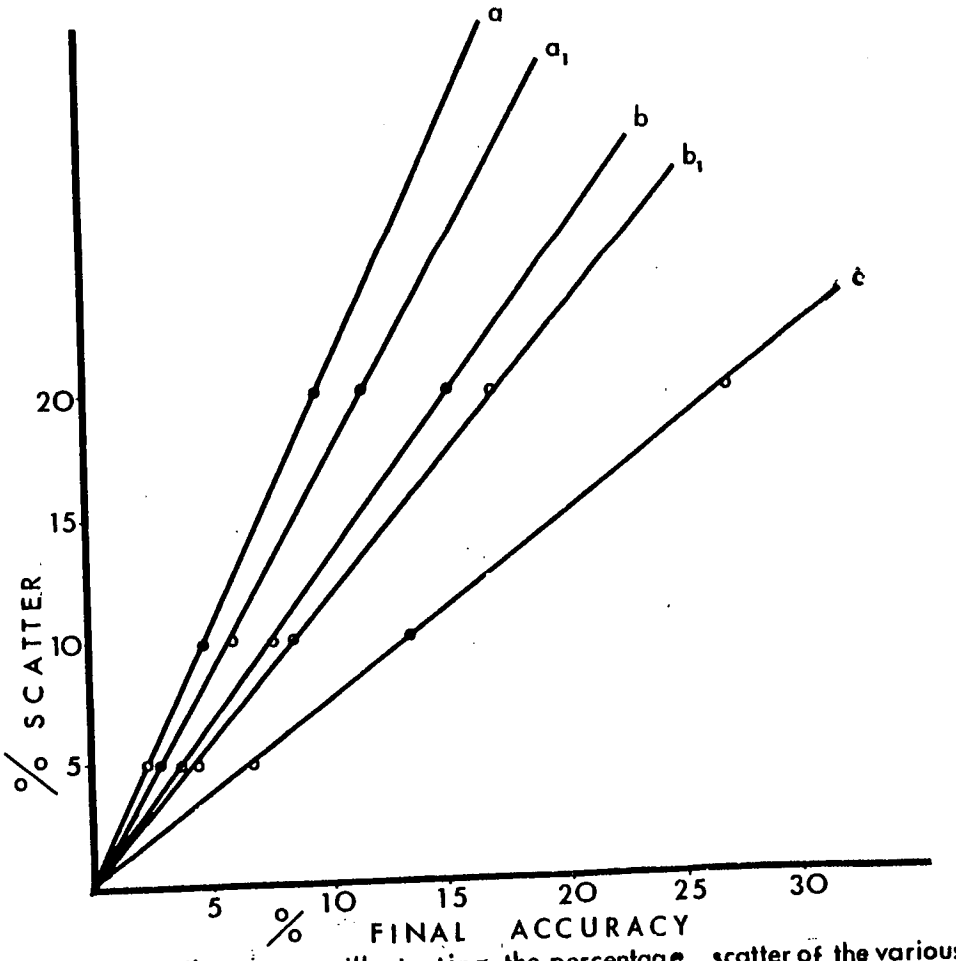


Fig.C Family of curves illustrating the percentage scatter of the various readings per dose against the percentage final TL dose accuracy, for:
(a) Nine points of gaussian distribution.
(a_1) Ten points of even scatter
(b) Five points of gaussian distribution
(b_1) Five points of even scatter
(c) Three points of even scatter

BIBLIOGRAPHY

Abrahamsen, N, (1976). Palaeomagnetic Methods and their Application in Archaeomagnetic Dating. Proc. of Conf. on TL Dating and other Archaeometric Methods, Uppsala University, Sweden, 26 - 25 Nov.

Adams, J, (1964). Laboratory Gamma Ray Spectrometer for Geochemical Studies. "Natural Radiation Environment", eds. Adams, J, Lowder, W. University of Chicago Press.

Adams, J, Lowder, W eds. (1964) The Natural Radiation Environment, Rice Univ., Semicentennial Series, The University Press, Chicago.

Adams, J, Osmond, J K, Rogers, J W, (1959). The Geochemistry of Thorium and Uranium. "Physics and Chemistry of the Earth". eds. Ahrans, L H, Press, F, Rankama, K, Runcorn, S. Pergamon Press, London, Vol. 3, 298 - 348.

Adams, J, Grasparini, P, (1970). Gamma-Ray Spectrometry of Rocks. Elsevier Bibl. Co., N. York.

Adams, Weaver (1958). Quoted in Adams, J, Osmond K J, Rogers, W J, (1959) see appropriate Ref.

Advances in Activation Analysis, I II, (1969). ed. Lenihan, A M J, Thomson, J S, Academic Press, London

Aitken, M J, Tite, M S, Reid, J, (1964). Thermoluminescent Dating of Ancient Ceramics. Nature 202, 1032 - 1033

Aitken, M J, Tite, M S, Fleming, S, (1967). Thermoluminescent Response to Heavily Ionizing Radiations. Lumin. Dosim. CONF-650637. NBS Springfield, Virginia. Proc. Inst. Conf., Stanford, 420 - 501.

Aitken, M J, Fleming, S, Reid, R, Tite, M S, (1968). Elimination of Spurious Thermoluminescence. "TL of Geological Materials" ed. D J McDougall, Academic Press, 133 - 142.

Aitken, M J, (1968). Evaluation of Effective Radioactive Content by Means of TL Dosimetry. "TL of Geological Materials" ed. D J McDougall, Academic Press, 463 - 470.

Aitken, M J, Zimmerman, D W, Fleming, S J, (1968). Thermoluminescent Dating of Ancient Pottery. Nature 219, 442.

Aitken, M J, Thompson, J, Fleming, S J, (1968d). Predose Effects in TL and in Luminescence during Irradiation. Proc Inter Conf Lumin Dosim 2nd. p 364. US Atom Energy Comm, CONF-680920.

Aitken, M J, (1969). Thermoluminescent Dosimetry of Environmental Radiation on Archaeological Sites. Archaeometry 11, 109.

Aitken, M J, Moorey, P R S, Ucko, P J, (1971). The Authenticity of Vessels and Figurines in the Haçilar Style. Archaeometry 13, (2).

Aitken, M J, Fleming, S, (1972). Thermoluminescent Dosimetry in Archaeological Dating. "Topics in Radiation Dosimetry - Supplement 1", ed. F H Attix, Academic Press, 1 - 78.

Aitken, M J, Alldred, J C, (1972). The Assessment of Error Limits in TL Dating. Archaeometry, 14, 257 - 267.

Aitken, M J, Huxtable, J, (1975). Thermoluminescence and Glozel: A Plea for Caution. Antiquity XLIX, 223 - 6

Aitken, M J, (1978). Radon Loss Evaluation by Alpha Counting. A Specialised Seminar on TL Dating, Oxford, July, 3 - 8.

Bailiff, I K, Bowman, S, Aitken, M J, (1974). Measurement of Internal Beta Dose-Rate by TLD: Utilisation in TL Dating. Proc. of 4th International Conf. on Lumin. Dosimetry. pp 1043 - 1052, Krakow, Poland.

Bangert, U, Hennig, G H, (1979). Studies on TL Dating of Calcite Cave Deposits. 19th Internal. Symp. on Arch. and Archaeol. Prospection. March (1979) British Museum.

Becker, K, (1973), Solid State Dosimetry. CRC Press Inc. Cleveland, Ohio.

Bell, W T, (1979). Problems and Uncertainties in the Dose and Dose-Rate Evaluation for TL Dating. 19th Internl. Symp. on Arch. and Archaeol. Prospection. March (1979) British Museum.

Belche J L, Cook, K, Cook, R M, (1963). British School Archaeol. 58, p8 (quoted by Davaras, C, in Μινωικη Καμινος εις Στυλου Χανιων Arch. Eph., 1978, p 75 - 80.

Bell, W T, (1976). The Assessment of the Radiation Dose Rate for TL Dating. Archaeometry 18 (1), 107 - 111.

Bell, W T, (1977). TL Dating: Revised Dose Rate Data. Archaeometry, 19 (1), 99 - 100.

Berger, M J, Seltzer, S M, (1964). Tables of Energy Losses and Ranges of Electrons and Positrons. Paper 10, NAS-NRC Publication 1133.

Berger, M J, Seltzer, S M, (1966). Additional Stopping Power and Range Tables for Protons, Mesons and Electrons. NASA SP-3036, National Bureau of Standards. Washington, DC.

Berger, R, Libby, W F, (1967). Radiocarbon, 9, 477.

Berger, R, (1978). Recent Advances in Radiocarbon Dating, Climatic Measurements and Source Analysis. 18th Interl. Symp. On Arch. and Archaeol. Prospection, Rheinisches Landesmuseum, Bonn, Germany, March, 1978.

Barbetti M, (1976). Archaeomagnetic Analysis of Six Glozelian Ceramic Artefacts. Jour. of Aracaeol. Sci. 3, 137 - 151.

Bothe, W, (1949). Zur Ruckdiffusion Schneller Electronen z. Naturfosch, 4a, 542 - 545

Bowman, S, (1975). Dependence of Supralinearity on Pre-dose: some Observations. Archaeometry, 17 (1), 129 - 132.

Bowman, S, Seeley, M A, (1978). The British Museum Flint Dating Project. A Specialist Seminar on TL Dating Oxford, July, 3 - 8.

Bieber, A M J, Brooks, D W, Harbottle, G, Sayre, E V, (1976). Application of Multivariate Techniques to Analytical Dating on Aegean Ceramics. Archaeometry, 18 (1), 59 - 74.

Brace L C, Nelson, H, Korn, N, (1971). Atlas of Fossil Man, Halt, Rinehart & Winston Inc. USA, p. 150.

Broecker, W S, (1963). A Preliminary Evaluation of the Uranium Series in Equilibrium, as a Tool for Absolute Age Measurements on Marine Carbonates. Journ. Geophys. Res. 68: 2817 - 34

Cameron, J R, Zimmerman, D, Bland, R W, (1967). Thermoluminescence vs roëntgens in Bithium Fluoride: A Proposed Mathematical Model. "Luminescence Dosimetry" ed. F H Attix, pp 45 - 56 US At. Ener. Comm, Washington, DC.

Cameron, J R, Suntharalingam, N, Kenney, G, (1968). Thermoluminescence Dosimetry. Univ. of Winsconsen Press.

Carriveau,G, (1978). Instrumental Neutron Activation Analysis for K, Rb, Th and U Determinations in TL Dating. A Specialist Seminar on TL dating. Oxford, (3 - 8 July, 1978)

Charlton, P E, (1970). Energy Dissipation near an Interface: A More Realistic Approach to Electron Range and Stopping Power. Radiation Effects, 44, 575 - 593.

Cherdynstev, V V, Kazacherskii, I V, Kuzmina, E A, (1965). Dating of Pleistocene Carbonate Formation by the Thorium and Uranium Isotopes. Geochem. Internatl,2, 794 - 801.

Chourmouziades, G, (1979). Το Νεολιθικο Διμινι, μια νεα Προσπαθεια για την αντιμετωπιση των Νεολιθικων υλικων, Athens.

Christodoulides, C, Fremlin, J H, (1971). TL of Biological Materials. Nature, 232, 257 - 258.

Claffy, E W, Klick, C C, Attix, F H, (1968). TL Processes and Colour centres in Lif:Mg. Proc. Int Conf Lumin Dom, p302. AEC CONF-680920

Coldztaub & Wey, (1955). Quoted in "Handbook of Geochemistry" Vol. II/5, p. 92-11- 1, ed. K H Wedepohl,(1978)
Curie, D, (1960). Luminescense in Crystals. trans. Garlick, G F J, London, Menthuen.

Cross W G, (1967). The Distribution of Absorbed Energy from a Point Beta Source. Canad. Journ. Phys. 45, 2021 - 2040.

Cross, W G, (1968). Variation of Beta Dose Attenuation in Different Media. Phys. Med. Biol, 13, 611 - 618.

Daniels, F, Boyd, C A, Saunders, D F, (1953). Thermoluminescence as a Research Tool. Science, 117, 343.

Daniels, F, (1967). Early Studies of TL Radiation in "Luminescence Dosimetry" 1.34 - 43, USAEC CONF-650637

Davidson, T E, McKerrell, H,(1976). Pottery Analysis and Halaf Period Trade in the Khabor Headwaters Region, Iraq, XXXVIII, 45 - 56.

Densgaard, W, Johusen, S J, Clausen, H B, Langway, G C, (1971). Climatic Record Revealed by the Camp Century Ice Vore, pp 37 - 56, "The Late Cenotoic Glacial Ages". ed. (K K Ture Kian, New Haven, Conn. Yale Univ Press.

Demon, P E, Long, A, Wallick, E E, (1973). Dendrochronological Calibration of the Carbon-14 Time Scale. Proc. 8th Int. Conf. Radiocarbon Dating, N. Zealand, A38 - A43.

Desai, V S, Aitken, M J, (1974). Radon Escape from Pottery: Effects of Wetness. Archaeometry 16, 95 - 97.

Desai, V S, (1975). Studies in Radon Emanation Relevant to TL Dating. Unpublished M.Sc. Thesis, Univ. of Oxford.

Elasser, W, Mey, E S, Winckler, J R (1958). Nature, 178, 1926.

Fremlin, J H, Srirath, S, (1964). Thermoluminescent Dating Examples of non-uniformityof Luminescence. Archaeometry, 7, 58.

Engelkemeir, D, (1956). Nonlinear Response of NaI (Tl) to Photons. The Review of Scientific Instruments. Vol. 27, No. 8.

Evans, P, (1972). Towards a Pleistocene Timescale, in "The Phanerozoic Timescale" Supplement - Geological Society special publication No 5, London

Evans, R D, (1955). The Atomic Nucleus. McGraw-Hill, N York.

Evans, M D, (1968). X-Ray and Gamma-Ray Interactions in Radiation Dosimetry. 2nd Edition. ed F H Attix and W Roesch, Academic Press, London.

Fagg, B E B, Fleming S J, (1970). TL Dating of a Terracotta of the Nok Culture, Nigeria. Archaeometry, 12 (1), 53-55.

Fano, U, (1954). Note on the Beta Ray - Gamma Ray Cavity Principle for Measuring Energy Dissipation. Radiation Research,1, 237 - 240.

Ferguson, W C, Gimbutas, M, Suess, E H, (1976). Historical Dates for Neolithic Sites of South East Europe. Science Vol. 19, 1170 - 1172.

Fiorella, O, Mangia, M, Olivieri, E, (1976). TL Isothermal Decay in Gamma-Irradiated $CaSO_4$ Dy Phosphors - Kinetics and Distribution of Trap Depths. Int. Journ. Radiat. Phys, Chem. 8, 441 - 447.

Fleming, S, (1966) Study of Thermoluminescence of Crystalline Extracts from Pottery. Archaeometry, 9, 170.

Fleming, S J, (1968). TL Age Studies in Mineral Inclusions Separated from Ancient Pottery. "Thermoluminescence of Geological Materials" ed. D J Dougall, pp 431 - 440, Academic Press, N York.

Fleming, S, (1969). The Acquisition of Radiothermoluminescence by Ancient Ceramics. Unpublished Ph. D. thesis, Oxford University.

Fleming, S J, Thompson, J, (1970). Quartz as a heat-resistant Dosimeter. Health Physics, 18, 567 - 568.

Fleming, S J, (1970). TL Dating: Refinement of the Quartz Inclusion Method. Archaeometry 12, 135.

Fleming, S J, (1971). New Techniques of TL Dating of Ancient Pottery. II The Predose Method. Proc. 3rd Int. Conf Lumin Dosim, Risø, Denmark, 895 - 929.

Fleming, S J, (1973). The Predose Technique: A New TL Dating Method. Archaeometry 15(1), 13 - 30.

Fleming, S J, Stoneham, D, (1973). The subtraction Technique of TL Dating. Archaeometry, 15 (2), 229 - 238.

Fleming, S J, (1975). Supralinearity corrections in Fine Grain TL Dating: A re-appraisal. Archaeometry 17(1), 122 - 129.

Fleming, S J, (1978). The Quartz Inclusion Method. A Specialist Seminar on TL Dating. Oxford, July, 3 - 8.

François, H, McKerrell, H, Mejdahl, V, (1977). TL Dating of Ceramics from Glozel. 5th Int. Conf. of Lumin. Dosim, San Paolo, Brazil.

Friedman, G M, (1957). Determination of Sieve Size Distribution from Thin Section Data for Sedimentary Petrological Studies. " Methods in Sedimentary Petrology". Vol. 1 G. Müller, trans. H Schwincke (1967).

Gabriel, A, Cox, E P, (1929). A Staining Method for Quantative Determination of Certain Rock Minerals. Amer Mineralogist, 14, 290 - 292.

Gabrysh, A F, Eyring, H, Bezirjiam O H, Merill, J H, (1968). Decay Products of Radium in Ceramics and Their Interaction with Matter. Materials. Res. Stand, 3, 902 - 905.

Garlick, G F, Gibson, A F, (1948). The Electron Trap Mechanism of Luminescence on Sulphide and Silicate Phosphors. Proc. Phys. Soc. A160, 587.

Gasgoyne, M (1977). Uranium Series Dating of Speleothems: An Investigation of Technique, Data Processing and Precision. Tech-Memo 77-4, McMaster Univ.

Gascoyne, M, Schqarcz, H, Ford, D C, (1978). Uranium Series Dating and Stable Isotope Studies of Speleothems: Part I Theory and Techniques McMaster University.

Gold, S, Barkhall, B S, Kahn, B (1964). Measurement of Naturally Occurring Radionuclides in Air. "The Natural Radiation Environment" Univ. of Chicago Press, 369 - 382.

Goksu, H Y, Fremlin, J H, Irwin, M T, Fryxell, R, (1974). Age determination of Burned Flint by a TL Method. Science, 183, 651 - 4.

Gorbics, S G, Nash, A E, Attix, E H (1969). Thermal Quenching of Luminescence in Sic Thermoluminescent Dosimetry Phosphors. II Intl. Journ. Appl. Radiat Osotopes, 20, 843.

Grogler, N, Houtermans, F G, Stauffer, H (1960). Veberdie Datierung von Keramik und Ziesel durch Thermolumineszenz. Helv. Phys. Acta. 33, 595.

Gustafson, P F, Brar, S S, (1964). Measurement of Gamma Emitting Radionuclides in Soil and Calculation of the Dose Arising Therefrom in the Natural Radiation Environment, eds. J Adams, W Lowder, Univ of Chicago Press, Chicago.

Halperin, A, Braner, A A, (1964), Phys. Review, 117, (2), 408.

Hammen, van der , Wijmstra, T A, Zagwija, W H, (1971). The Floral Record of the Late Cenozoic of Europe, pp 391 - 424, "The Late Cenozoic Glacial Ages". Proc. Yale Univ. Symp. Dec. 1969. ed., K K Turekian.

Harmon, R S, (1975). Late Pleistocene Palaeoclimates in North America as inferred from Isotopic Variations in Speleothems. Ph.D Thesis, McMaster University, Hamilton Canada.

Harmon, R S, Thompson, P, Schwarcz, H, Ford, D, (1975). Uranium Series Dating of Speleothems. Natl. Speleol. Soc. Bull. 27,21-33.

Hays, W C, (1970). "Cambridge Ancient History" 1, 175.

Hedges, R E M, McLellan, M, (1976). On the Cation Exchange Capacity of Fired Clays and its Effect on the Chemical and Radiometric Analysis of Pottery. Archaeometry 18 (2), 203 - 207.

Heyning. G., Bangert. U (1978) Dating of pleistocene limestone sinters by Disequilibrium in the Uranium Decay Series. 18th Intern. Symp. Archaeometry, Bonn, Rhein. Landes. museum. March 17 1978

Hill, C, (1976). Cave Minerals. NSS Huntsville Alabama, 35810, Cave Avenue, USA.

Houtermans, F G, (1960). Thermoluminescence Glow Curves. Summer Course in Nuclear Geology, Varenna, Laboratorio de Geologia Nucleare, Pisa, p233.

Huntley, D J, Wintle, A G, (1978). Some Aspects on Alpha Counting. A Specialist Seminar on TL Dating, Oxford, July 3 - 8.

Hutchison, R (1962). Prehistoric Crete. Harmondsworth.

Huxtable, J, Aitken, M J, Weber, J L, (1979). TL Dating of Baked Clay Balls of the Poverty Point Culture, Archaeometry, 14(2), 269 - 275

Hyde, E K, Perlman, I, Seaborg, G I, (1964). The Nuclear Properties of the Heavy Elements. II Detailed Radioactive Properties, Prentice Hall, Englewood Cliffs, N J.

Ichikawa, Y, (1965). Dating of Ancient Ceramics by Thermoluminescence Bull. Inst. Chem. Res. Kyoto Univ, 43.

Ikeya, M, (1979). ERS Age of the Trace of Fire at Petralona. Anthropos, vol 6, p44 - 47

Isabaev,E N, Usatov, E, Cherdynstev, W, (1960). The Isotopic Composition of Uranium in Natural Minerals. Radiokhimiya,2,94.

Jasiska, M, Niewiadomski, T, (1970). TL of Biological Materials, Nature, 227, 1159 - 1160.

Kaisar, W C, Barker, S I, MacKay, A J, Sherdman, S I, (1962), Response of NaI(Tl) to X-Ray and Low Energy Gamma Rays. IRE Trans. Nuclear Sci. NS - 9, No3,22

Kanelis, A, Savas, A, (1964). Craniometric Study of Homo Neaderthalensis in Petralona. University of Thessalonika, Sco. Bull. of Physics Mathematics Depts.v 9, p 65 - 83.

Kaufman, A, (1964). Th-230/U-234 Dating of Carbonates from Lakes Lahontan and Bonneville. Ph.D Thesis, Columbia Univ.

Kaufman, M I, Rydell, H S, Osmond, J K, (1969). U-234/U238 Disequilibrium as an Aid to Hydrologic Study of the Florida Acquifer. Journ. Hudrol., 9, 374 - 386.

Kennedy, G C, Knopff, L, (1960). Dating by Thermoluminescence , Archaeology, 13, 1947.

Kendall, A C, Broughton, P C(1978). Origin of Fabrics in Speleothems Composed of Columnar Calcite Crystals. Journ. Sedim. Petrol., vol 48, No. 2, pp 519 - 530.

Kigoshi, U, (1971). Alpha Recoil Th-234 Dissolution into Water and the U-234/U-238 Disequilibrium in Nature. Science 173, 47 - 48.

Kokkoros, P, Kannelis, A, (1960). Decouverte d'un Crane d'Homme Palaeolithique dans la Peninsule Chalkidique. L'Anthropologie, vol. 64, p438 - 446.

Koczy, F R, (1954). Radioactive Elements in Ocean Waters and Sediments: Geochemical Balance in the Hydrosphere. "Nuclear Geology", ed. H Faul. Wiley & Sons, N.Y., 120 - 127.

Kopper J, Creer K.M (1976). Paleomagnetic Dating and stratigraphic interpretation in Archaeology. MASCA Newsletter, Univ. Pennsylvania The Univ. Museum.

Koide, M, Goldberg, E D, (1965). Uranium-234/Uranium-238 Ratios in Sea Water. "Progress in Oceanography" H Sezrsed. Pergamon Press, 173 - 178.

Kolodny, Y, Kaplan, R F, (1970). Uranium Isotopes in Sea Floor Phosphorites. Geochim. Cosmochim. Acta, 34: 3 - 24.

Kraner, H W, Schroeder, G L, Evans, R D, (1964). Measurement of the Effects of Atmospheric Variables on Radon-222 Flux and Soil-Gas Concentrations. "The Natural Radiation Environment" Univ of Chicago Press, 191 - 218.

Kronfeld, J, (1971). Hydrolic Investigations of the Significance of U-234/U-238 Disequilibrium in the Ground Waters of Central Texas. "Development of Remote Methods for Obtaining Soil Information and Location of Construction Materials Using Gamma Ray Signatures for Project THEMIS, Semi- Annual Report to US Army Engineer, Dept. of Geol., Rice University.

Ku, T L, (1968). Prot actinium231 Method for Dating Corals from Barbados Island. Joun. Geophys. Res, 73, 2271 - 2275.

Ku, T L, Bull, N B, Freedman, S T, Knauss, K G, (1979). Th-230/ U1234 Dating of Pedogenic Carbonates in Gravelly Desert Soils of Vidal Valley, SE California. Geol. Soc. America Bull., in Press.

Kurten, B, Poulianos, A N, (1977). New Stratigraphic and Faunal Material from Petralona Cave, (with Special Refernce to the Carnivora, Anthropos vol 4, No 1 - 2, pp 47 - 130.

Lamb, H H, (1977). Climate (Present, Past and Future). Vol. 2. Climatic History and the Future. Menthuen.

Lapp, R B, Andrews, H C, (1972). Nuclear Radiation Physics, 4th ed. Englewood Cliffs, N J, Prentice-Hall.

Liritzis, Y, McKerrell, H, (1978). Some TL Dates and Neutron Activation Analysis of Greek Neolithic Pottery. Proc. of 18th Intern. Symp. of Arch. and Archaeol. Prospection, Archaeo Physika 10, Rheinisches Landesmuseum, Bonn, 486 - 498.

Liritzis, Y, Galloway, R B, Poulianos, A,(1979) Uranium Disequilibrium Dating of the Petralona Skull. 19th Inter. Symp Archaeom. and Archaeol. Prospection, British Museum, March 28

Liritzis, Y, Galloway, R B, (1979). Beta Dosimetry Evaluation of Ceramics. 19th Inter Symp Archaeom and Archaeol Prospection , British Museum, March, 28 - 3.

Liritzis, Y, Thomas, R, (1979). Archaeomagnetic Measurements and Thermoluminescence Dating of Cretan Kilns(to be published in Nature.).

Loe Vinger (1956). Radiology. 66. 55.

Løvborg, L, Kirkegaard, P,(1974). Response of "3 x 3" NaI(Tl) Detectors to Terrestrial Gamma Radiation. Nuclear Instruments and Methods, 121, 239 - 251.

Løvborg, L, Bøtter-Jensen, L, Kirkegaard, P, (1976). Experiences with Concrete Calibration Sources for Radiometric Field Instruments. Risø, DK-4 000, Roskilde, Denmark. Submitted to "Geophysics Journal".

McDougall, B J, ed. (1968). Thermoluminescence of Geological Materials, Academic Press, N York.

McKerrell, H, Mejdahl, V, François, H, Portal, G, (1971). Thermoluminescence and Glozel. Antiquity, 58, 265 - 272.

McKerrell, H, (1975). Correction Procedures for C-14 Dates. "Radiocarbon: Calibration and Prehistory" ed T Watson, Edinburgh Univ. Press, pp 47 - 100 and 110 - 127.

McKerrell, H, Mejdahl, V, (1976). Progress and Problems with Automated TL Dating. Proc. 1976 Symposium on Arch. and Archaeol. Prospection, Edinburgh, 24 - 27, March.

Mangia, M, Oliveri, E, Fiorella, O, (1977). TL Isothermal Decay in Supralinearity for Gamma Irradiated $CaSO_4$:Dy Phosphors. Behaviour of Distribution of Trap Depths. Proc. of the 5th Internal. Conf. on Lumin Dosimetry. San Paulo, p 29 - 39, ed. Scharman, Physikalishen Institut, Jugns - Liebig - Universitat Giessen.

Mazess, R B, Zimmerman, D, (1966). Pottery Dating by Thermoluminescence Science. 152, 347 - 348.

Meakins, R L, Dickson, B L, Kelly J C, (1978). The Effect on TL Dating of Disequilibrium in the Uranium Decay Chain. A Specialist Seminar on TL Dating, Oxford, July, 1978.

Mejdahl, V, (1969). TL Dating of Ancient Danish Ceramics. Archaeometry 11, 99.

Mejdahl, V, (1970). Measurement of Environmental Radiation at Archaeological Excavation Sites. Archaeometry, 12, 147 - 159.

Mejdahl, V, (1972) a Progress in TL Dating in Risø. Archaeometry, 14.

Mejdahl, V, (L972) b Dosimetry Techniques in TL Dating Risø. Report No. 261. Risø, DK-4000, Roskilde, Denmark.

Mejdahl, V, (1978). TL Dating: Beta Dose Attenuation in Quartz Grains. (to be published).

Mejdahl, V, (1979). Dating of Danish Ceramics by means of Quartz Inclusion Method (to be published).

Murray, A S, Aitken, M J, (1978). TL Evaluation of the Gamma Dose Rate Corresponding to a known Uranium Concentration. A Specialist Seminar on TL Dating, Oxford, July, 3 - 8.

Nambi, K V S, (1975). Evaluation of the Absolute TL Emission Spectrum and Intrinsic Efficiency for $CaSO_4$:Dy and CaF_2(natural) Phosphors. Nucl. Instr. & Methods, 130, 239 - 243.

Neustupny, E, (1968). Absolute Chronology of the Neolithic and Aneolithic Periods of Central and South-Eastern Europe. Slovenska Archaeologia, 16, 19 - 56.

Neustupny, E, (1969). Absolute Chronology of the Neolithic and Aneolithic Periods of Central and Southern Europe, II, Arch. Rozhledy, XXI, 783.

Oates, J, Davidson, T E, Kamili, D, McKerrell, H, (1977). Seafaring Merchants of Ur?. Antiquity, LI, 221 - 234.

Orlandos, A, (1955). The Ancient Greek Architecture, (Athens)

Parker, R (1960 - 7). Egyptian Astronomical Texts. Brown University Press (issued at intervals, completed 1967).

Papamarinopoulos, S, (1978). Limnomagnetic Studies on Greek Sediments Ph.D Thesis, Edinburgh University, p 67-72

Pfieffer J E (1972). The Emergence of Man, 2nd edition, Hamper & Row Publications, London, p550.

Perlman, I, Asaro, E, (1969). Pottery Analysis by Neutron Activation Analysis. Archaeometry 11, 21 - 52.

Pichler, H, Schiering, W, (1977). The Thera Eruption and Late Minoan IB Destructions on Crete. Nature, Vol 267, 819 - 822.

Picciotto, E, Wilgain, S, (1954). Thorium Determination in Deep Sea Sediments. Nature, 173, 632 - 633.

Pilcher, R J, (1979). Radiocarbon Calibration: Recent Progress . 19th Intern. Symp. on Arch. and Archaeol. Prospection. British Museum, London.

Piggott, S, (1965). Ancient Europe, Chicago Press.

Poulianos, A, (1971). Petralona - A Middle Pleistocene Cave in Greece. Archaeology, 24: 6 - 11

Poulianos, A N, (1972). Quelques caracteres Sapiens due Crane de Petralona (resume). Proceedings of the Paris Symposium of UNESCO, 1969, p55.

Poulianos, A, (1974). Η Μεταβατικη περιοδος απο το σταδιο του Νεαντερταλειου στο σταδιο του συγχρονου Ανθρωπου. Ανθρωπος vol 1, no 1 .

Poulianos, A, (1976). Ερευνες στο σπηλαιον πετραλωνων Ανθρωπος vol3, No 1, p195.

Poulianos, A, (1976b). Archanthropus Europeus Petraloniensis. Colloque de Taxonomie Anthropologique, Bordeaux I, Laboratoire d'Anthropolo

Poulianos, A N, (1977). Stratigraphy and Age of the Petralonian Archanthropus. Anthropos, vol 4, No. 1 - 2, 41 - 46.

Poulianos, A N (1978 - 1979) pers. comms.

Priler, R, Adams, J, (1962). The Distribution of Thorium, Uranium, and Potassium in the Mancos Shale. Geoch. Cosmoch. Acta, vol 26, pp 1115 - 1135 and 1137 - 1146.

Ralph, E K, Michael, H N, (1970). (in Press), quoted by Bucha in Phil. Trans. of Royal Soc, London, Vol. 269, p54.

Ralph, F K, Han , M C, (1969). Potential of TL in Supplementary Radiocarbon Dating. World Archaeol., 1, 157.

Randall, I J, Wilkins, M H F, (1965). Phosphorescence and Electron Traps. Proc. Roy. Soc., A, 184, 366.

Renfrew, C, (1970). The Tree-Ring Calibration of Radiocarbon: An Aracaeological Evaluation. Proc Prehistoric Soc. XXXVI, 280 - 311.

Renfrew, C, (1973). Before Civilisation: The Radiocarbon Revolution and Prehistoric Europe. London, Jonathen Cape.

Rogers, J J W, Adams, J A S, (1969). Abundance (of Uranium) in Canmon Sedimentary Rocks. Handbook of Geochemistry, H Wedepohl et al, II 92K.

Sackett, W M, (1958). Ionium - Uranium Ratios in Marine Deposited $CaCO_3$ and Related Materials, Ph.D Thesis, Washington Univ.

Salamang, H, (1961). Ceramics: Physical and Chemical Fundamentals, trans. M Francis, Butterworth & Co., London.

Schmidt, K, Lineman, Giessing, R, (1974). Influence of Preparation and Annealing on the Properties of $CaSO_4$:Dy Thermoluminescence Phosphor, Proc of the 4th Inter. Conf. on Lumin. Dosim., Krakow, p 237 - 253, ed T Niewiadomski, Inst. of Nuclear Phys, Krakow.

Schwarcz, H, Liritzis, Y, Dixon, A, (1979). Absolute Dating of Travertines from the Petralona Cave, Chalkidiki Peninsula, Greece. Anthropos, Vol.6. Greek Anth. Soc., Athens.

Schweiger, F, (1971). Chemical Analysis by Optical Spectroscopy. Appendix B. "The Authenticity of Vessels and Figurines in the Haçilar Style" by Aitken M, Moorey, P R S, Ucko, P J. Archaeometry 13 (2), 89 - 141.

Seigbahn, K, (1955), ed., Beta and Gamma Ray Spectroscopy. North Holland Publishing Co., Amsterdam

Shackleton, N J, Opdyke, N D, (1976). Oxygen-Isotope and Palaeomagnetic Stratigraphy of Pacific Core C28 - 239 Late Pliocene to Latest Pleistocene. Geol. Soc. America. Memoir 145, p 449 - 464.

Sickenberg, U, (1971). Revision der Wirbeltierfauna der Höhle Petralona (Greich Makedonien) Annales Geol de Pays Hellanique vol 23 230-264

Sneath, P H A, Sokal, R R, (1973). Numerical Taxonomy, Freeman, San Francisco.

Spencer, L V, (1959). Quoted in Cross, (1968),see appropriate reference

Stringer, C, (1974a) A Multivariate Study of the Patralona Skull. Journ of Human Evol. Vol. 3, p 397 - 404.

Sternheiner R.M (1952). The Density Effect of ionization Loss in various material. Phys.Rev,88,4,851.

" " (1956). Density effect for ionization Loss in

" " (1966). Density effect for the ionization loss of charged particles. Phys. Rev. 145,1,247.

Stringer, C, (1974b). Population Relationships of Later Pleistocene Hominids: A Multivariate Study of Available Crania. Journ Archaeol. Sci. Vol 1, 317 - 342.

Storm, E, Israel, H I, (1967). Photon Cross Sections from 0.601 to 100 Me for Elements 1 through 100, LA-3753, Univ. of California, Los Angeles

Suess, H E, (1969). Proc. XII Nobel Symp (in the Press), quoted in Bucha, Phil. Trans of Roy. Soc, London Vol. 269, 1970, p54.

Suess, H E, (1970). Bristle-cone Pine Calibration of the Radio-Carbon Timescale 5200BC to the Present. "Radiocarbon Variations and Absolute Chronology" ed I V Iksson, 303 - 12.

Suntharalingham, N, Cameron, J R, (1969). TL Response of Lithium Fluoride to Radiations with Different L.ET. Phys. Med. Boil 14, 394.

Sutton, S E, (1978). TL Dating of Lava Flows using Baked Soils: Application to the Idaho Rift System, USA. A Specialist Seminar on TL Dating, Oxford, 3 - 8.

Sutton, S E, Zimmerman, D, (1978). Attempts to Circumvent Anomalous Fading. A Specialist Seminar on TL Dating, Oxford, July 3 - 8.

Swanson, (1963). Quoted in "Handbook of Geochemistry" Vol II/5, p 92 - H - 1, ed., F H Wedepohl, (1978).

Sweeting, (1972). Karst Landforms, London.

Tanner, A B, (1964). Radon Migration in the Ground: A Review in "The Natural Radiation Environment", eds., J A S Adams, W M Lowder, pp 161 - 190, Univ of Chivago Press.

Theoharis, D, (1973). Neolithic Greece, ed. National Bank of Greece.

Thompson, G, (1973). Speleochronology and Late Pleistocene Climates inferred O, C, H, U and Th Isotopic Abundances in Speleothems, Ph.D Thesis, McMaster Univ., p 340.

Thompson, P, Ford, D C, Schwarcz, H P, (1975). U-234/U-238 Ratios in Limestone Cave Seepage Waters and Speleothems from West Virginia. Geochim. Cosmochim Acta, 39, 661 - 669.

Thurber, D L, (1962). Anamolous U-234/U-238 in nature. Journ. Geophys. Res 67, 4518 - 4520.

Thurber, D L, (1964). Natural Variations in the Ratio U-234/U-238 and an Investigation of the Potential of U-234 for Pleistocene Chronology, Ph.D Thesis, Columbia University.

Tite, M S, Waine, J, (1962). Thermoluminescent Dating: A Reappraisal Archaeometry, 5 53.

Tite, M S, (1966). Thermoluminescent Dating of Ancient Ceramics: A Reassessment. Archaeometry, 9, 155.

Valladas, G, Gillot, P Y, Guerin, G, (1978). Dating Plagioclases? A Specialist Seminar of TL Dating, Oxford, July, 3 - 8.

Waine, J (1964). Measurement Techniques for TL Dating. Unpublished Ph.D. Thesis, Oxford.

Warren, P, (1975). The Making of the Past. TheAegean Civilisations. Elsevier-Phaidon,Phaidon Press Ltd., London.

White, W B, Sweet, J, (1970). Fluorescence and Phosphorescence of Cave Minerals (abstr). Bull. Nat. Speleo. Soc., 32, 120 - 121.

Whittle, E H, Arnaud, J M, (1975). TL Dating of Neolithic and Chalcolithic Pottery from Sites in Central Portugal. Archaeometry 17(1), 5 - 24.

Whittle, E H, (1975). TL Dating of Egyptian Predynastic Pottery from Hemamieh and Quarna-Tarif. Archaeometry 17, (1), 119 - 122.

Wintle, A G, Oakley, K P, (1972). TL Dating of Fired Rock Crystal from Bellan Bandi Palassa, Ceylon. Archaeometry , 14, 271 - 279.

Wintle, A G, Aitken, M J, Huxtable, J, (1971). Abnormal Thermoluminescence Fading Characteristics. Proc. 3rd Int. Conf. Lumin. Dosim., Risø, Denmark, 105 - 131.

Wintle, A G (1973). Anomalous Fading of TL in Mineral Samples. Nature, 245, 143 - 144.

Wintle, A G, (1975). Thermal Quenching of TL in Quartz, Geophys. J R Astr. Soc, 41, 107 - 113.

Wintle, A G, (1975). Effects of Sample Preparation on the TL Characteristics of Calicite Modern Geology, 5, 165 - 167.

Wintle A G, (1977). Detailed Study of a Termoluminescent Mineral Exhibiting Anomalous Fading. Journ. of Luminescence 15, 385 - 393.

Wintle, A G, (1978). Thermoluminescence Dating Study of some Quaternary Calicite: Potential and Progress. Phys. Dept, Simon Fraser Univ., Canada (to be published).

Wintle, A G, Huntley, (1978). TL Dating of Ocean Sediments. A Specialist Seminar on TL Dsting, Oxford, July, 3 - 8.

Wijmstra, T A, (1969). Palynology of the First 30 metres of a 120m Deposition in Northern Greece. Acta Bot. Neerl. 18(4).

Wunderlich, H G, (1976). The Secret of Crete. Trans. by R Winston. Fontana. p. 319.

Yamashita, T, Nada, N, Onishi , H, Kitamura, S, (1968). Calcium Sulphate Phosphor Activated by Rare Earth. Proc. Int. Conf. Lumin Dosim, p4. US Energy Comm, Conf - 680920.

Yamashite, T, Nada, N, Onishi, H, Kitamura, S, (1971). Calcium Sulphate Activated by Thalium or Dysprosium for Thermoluminescence Dosimetry. Health Phys. 21, 245 - 300.

Zimmerman, D, Ryner, C R, Cameron, J R, (1966). Health Phys, 12, 525.

Zimmerman, D, (1967). TL from Fine Grains from Ancient Pottery. Archaeometry, 10, 26.

Zimmerman, D, Huxtable, J, (1969). Recent Applications and Developments in TL Dating. Archaeometry, 11, 105 - 107.

Zimmerman, D, (1970). The Dependance of TL Energy and Type of Ionizing Radiation and its Significance for Archaeologic Age Determination. Unpublished Ph.D. Thesis, Oxford Univ, Oxford.

Zimmerman, D, Huxtable, J, (1971). TL Dating of Upper Palaeolithic Fired Clays from Dolni Vestonice. Archaeometry, 13(1), 53 - 57.

Zimmerman, D, (1972). Relative Effects of Alpha and Beta Radiation in Inducing Thermoluminescence. Radiation Effects, 14, 81.

Zimmerman, D, Yuhas, M P, Meyers, P, (1974). Thermoluminescence Authenticity Measurements on Core Materials from the Bronze Horse of the New York Metropolitan Museum of Art. Archaeometry 16(1), 19 - 30.

Zimmerman, D, (1978). Introduction to Basic Procedures for Sample Preparation and TL Measurements of Ceramics. A Specialist Seminar of TL Dating, Oxford, July, 3 - 8.

Zimmerman, D, (1971a). Thermoluminescent Dating using Fine Grains from Pottery. Archaeometry, 13, 29.

Zimmerman, J., (1971b). The Radiation Induced Increase of TL Sensitivity of the Dosimetry Phosphor LiF (TLD-100). Journ Phys (Solid State Physics 4, 3277.)

Zimmerman, J., (1971c). The Radiation Induced Increase of the 100°C Thermoluminescence Sensitivity of Fired Quartz. J. Phys C: Solid State Phys 4, 3265.